

**Junction Jigsaw:
Reconstructing the plate tectonic puzzle
from the Panthalassa to the Tethys Realm**

Suzanna van de Lagemaat

Utrecht Studies in Earth Sciences No. 288

ISBN: 978-90-6266-659-1

Author contact: suzannavdl@gmail.com

Cover image: Aoraki/Mount Cook (New Zealand). Design: Margot Stoete

Copyright © 2023 S.H.A. van de Lagemaat. All rights reserved. No part of this publication may be reproduced in any form, by print or photo print, microfilm or any other means, without written permission by the author.

Printed in The Netherlands by Ipskamp

Junction Jigsaw: Reconstructing the plate tectonic puzzle from the Panthalassa to the Tethys realm

**Knooppuntkwestie:
Reconstructie van de plaattektonische puzzel
van de Panthalassa naar het Tethys domein
(met een samenvatting in het Nederlands)**

Proefschrift

ter verkrijging van de graad van doctor aan de Universiteit Utrecht op gezag van de
rector magnificus, prof. dr. H.R.B.M. Kummeling, ingevolge het besluit van het college
voor promoties in het openbaar te verdedigen

op vrijdag 13 oktober 2023 des ochtends te 10:15 uur

door

Suzanna Henderijne Aleide van de Lagemaat

geboren op 14 januari 1991 te Utrecht

Promotor: Prof. dr. D. J. J. Van Hinsbergen

Members of the dissertation committee:

Prof. dr. Suzanne Baldwin
Syracuse University - Syracuse, USA

Prof. dr. Carmen Gaina
University of Oslo - Oslo, Norway

Prof. dr. Manuel Pubellier
French National Centre for Scientific Research - Paris, France

Prof. dr. Bernhard Steinberger
GFZ Potsdam - Potsdam, Germany

Dr. Jonny Wu
University of Houston - Houston, USA
Now at University of Arizona - Tucson, USA

This thesis was accomplished with financial support from NWO Vici grant 865.17.001.

Contents

9	Summary	
11	Introduction	
21	Chapter 1	Southwest Pacific absolute plate kinematic reconstruction reveals major Tonga-Kermadec slab-dragging S.H.A. van de Lagemaat, D.J.J. van Hinsbergen, L.M. Boschman, P.J.J. Kamp & W. Spakman (2018). <i>Tectonics</i> 37(8), 2647-2674.
61	Chapter 2	Subduction initiation in the Scotia Sea region and opening of the Drake Passage: When and why? S.H.A. van de Lagemaat, M.L. Swart, B. Vaes, M.E. Kusters, L.M. Boschman, A. Burton-Johnson, P.K. Bijl, W. Spakman & D.J.J. van Hinsbergen (2021). <i>Earth-Science Reviews</i> 215, 103551.
101	Chapter 3	Reconciling the Cretaceous breakup and demise of the Phoenix Plate with East Gondwana orogenesis in New Zealand S.H.A. van de Lagemaat, P.J.J. Kamp, L.M. Boschman & D.J.J. van Hinsbergen (2023). <i>Earth-Science Reviews</i> 235, 104276.
139	Chapter 4	Causes of Cretaceous subduction termination below South China and Borneo: Was the Proto-South China Sea underlain by an oceanic plateau? S.H.A. van de Lagemaat, L. Cao, J. Asis, E.L. Advokaat, P.R.D. Mason, M.J. Dekkers & D.J.J. van Hinsbergen. <i>Geoscience Frontiers</i> , submitted.
181	Chapter 5	A critical reappraisal of paleomagnetic evidence for Philippine Sea Plate rotation S.H.A. van de Lagemaat, D. Pastor-Galán, B.B.G. Zanderink, M.J.Z. Villareal, J.W. Jenson, M.J. Dekkers & D.J.J. van Hinsbergen (2023). <i>Tectonophysics</i> 863, 230010.
205	Chapter 6	Plate tectonic cross-roads: Reconstructing the Panthalassa-Neotethys Junction Region from Philippine Sea Plate and Australasian oceans and orogens S.H.A. van de Lagemaat & D.J.J. van Hinsbergen. <i>Gondwana Research</i> , submitted.

311	Appendix 1	Post-remagnetisation vertical axis rotation and tilting of the Murihiku Terrane (North Island, New Zealand) S.H.A. van de Lagemaat, L.M. Boschman, P.J.J. Kamp, C.G. Langereis & D.J.J. van Hinsbergen (2018). <i>New Zealand Journal of Geology and Geophysics</i> 61(1), 9-25.
339	Appendix 2	Geochemistry of syntectonic carbonate veins within Late Cretaceous turbidites, Hikurangi margin (New Zealand): Implications for a mid-Oligocene age of subduction initiation S.H.A. van de Lagemaat, J.A. Mering & P.J.J. Kamp (2022). <i>Geochemistry, Geophysics, Geosystems</i> 23(5), e2021GC010125.
378	Supplementary information to chapters	
379	References	
432	Summary in Dutch (Samenvatting in het Nederlands)	
435	Acknowledgements (Dankwoord)	
439	Curriculum vitae	
440	Bibliography	



Mount Alpha, New Zealand

Summary

Reconstructing Earth's past tectonic plate motion is vital for understanding its geological history, with implications for geodynamics, paleogeography, paleoclimatology, and resource exploration. However, many challenges exist in the reconstruction of subducted plates. While existing ocean basins can be reconstructed using marine magnetic anomalies and fracture zone data, the reconstruction of subducted plates lacked a clear framework due to varying interpretations of geological and geochemical data. Recently, however, a reconstruction protocol was developed to limit input data of a reconstruction to quantitative geological constraints. This approach avoids geodynamic interpretations, and yields transparent, reproducible, and adaptable reconstructions. In this thesis, this reconstruction protocol is applied to the southwest and west Panthalassa realm, resulting in kinematic reconstructions spanning from Patagonia to Japan, culminating in the complex reconstruction of the Junction Region between the Panthalassa and Tethys realms.

The new reconstructions presented in this thesis have implications for both regional and global tectonics and geodynamics. The Cenozoic reconstruction of the SW Pacific region in a mantle reference frame shows that since subduction initiation, the Tonga-Kermadec slab was dragged laterally through the mantle for over 1200 km, including its lower-mantle portion. The most important finding of the Mesozoic SW Pacific reconstruction is that subduction along the East Gondwana margin continued until at least 90 Ma, and possibly until 79 Ma, which is 10 to 25 Ma longer than the generally accepted 100-105 Ma age for the end subduction there.

In the southeast of the Panthalassa domain, the reconstruction of the Scotia Sea region shows that the South Sandwich subduction zone originates from Late Cretaceous (~80 Ma) subduction initiation below South Orkney continental crust, which is part of Antarctica. Subsequently, this subduction zone propagated northwards by delamination of South American lithosphere, transferring the crustal lithosphere to the upper plate. The opening of the Drake Passage started at c. 50 Ma when South America started moving towards the west and initial opening was thus related to upper plate retreat. Oceanic spreading centers formed in the Scotia Sea ~35–25 Ma, reducing dynamic coupling between the down-going slab and the escaping overriding plate, allowing slab roll-back to contribute to back-arc extension.

In the northwest Panthalassa domain, new paleomagnetic, biostratigraphic, geochemical and geochronological data were obtained from Sabah, Borneo. These data suggest that the plate that subducted below Borneo in the Late Cretaceous was a newly recognized plate (the Pontus Plate) that was separated from the paleo-Pacific plates by a subduction zone. Moreover, these data suggest that Mesozoic subduction cessation in the Proto-South China Sea region possibly resulted from an obstructed trench, likely due to the arrival thickened, buoyant oceanic lithosphere.

The reconstruction of the Junction Region, in between the Panthalassa and Tethys realms, suggests that the preserved latest Jurassic oceanic crust in the Philippines originated from the northern Australian Plate margin, where continental margin subduction was active in the Permian and Triassic. In addition, the reconstruction shows there is no requirement for spontaneous subduction initiation at the Izu-Bonin Mariana trench, which initiated along the pre-existing Mesozoic subduction zone.



The sun sets over the Philippine Sea, Guam

Introduction

Reconstructing the past motions of tectonic plates provides the foundation for the analysis of Earth's history and dynamics. Plate tectonic reconstructions provide a critical context for research, including geodynamics, paleogeography, paleoclimatology, and the search for the Earth's resources. However, developing reproducible, quantitatively described restorations is challenging, particularly for reconstructions of plates that have been lost to subduction, and interpretations vary widely.

The reconstruction of changing paleogeography through time started in the early 20th century with Alfred Wegener's theory of continental drift (Wegener, 1912) and became kinematically understood in the 1960s when seafloor spreading was demonstrated through marine geophysical data. Early paleogeographic reconstructions were qualitative sketches based on general geological evidence. Marine geophysics-based restorations of ocean basins allowed the quantitative description of plate kinematic history (McKenzie and Parker, 1967), but restoration of crustal deformation became only available to mainstream Earth Science with the development of the freely available plate tectonic reconstruction software GPlates (Boyden et al., 2011; Müller et al., 2018). This allowed developing and using quantitatively described, adaptable plate reconstructions that have reached a wide Earth scientific community. But GPlates is only a software package: the reconstructions of lost lithosphere based on sparse geological remains are still widely varying between authors (see e.g., Clennett et al., 2020 vs. Vaes et al., 2019 for intra-oceanic subduction in the NW Pacific; Van Hinsbergen et al., 2019 vs. Müller et al., 2019 for the India-Asia collision; Boschman et al., 2014 vs. Montes et al., 2019 for the Caribbean region; Zahirovic et al., 2014 vs. Advokaat and Van Hinsbergen, 2023 for the SE Asian region).

The problem that underlies the poor reproducibility of reconstructions of lost lithosphere is that there is a wealth of geological and geochemical data that reflect processes that are directly and indirectly linked with subduction history (Seton et al., 2023). The classical plate reconstructions based on still-existing ocean basins apply a universal approach, which uses marine magnetic anomalies and fracture zone data. The universal approach to ocean basin restoration enables the construction of a global plate circuit that describes the relative plate motions of all major plates separated by ocean basins back in time, using data sets from different authors. This global plate circuit is thus easily updated when improved magnetic anomaly interpretations become available. The approach to restoring completely subducted ocean basins, on the other hand, lacks a universally-used framework. The loss of lithosphere through subduction leads to geological and geophysical expressions such as deformation, metamorphism, magmatism with differing geochemical signatures, and subducted slabs that may be resolved using seismic tomography (Seton et al., 2023). All these different data types may be used as input for plate kinematic reconstructions. The problem, however, is that the interpretation of these geological indicators in relation to subduction heavily

relies on a series of geodynamic interpretations regarding subduction zone dynamics. For instance, the geochemical signature of magmatic rocks is often used to interpret whether volcanism occurred during active subduction or during continental extension in the absence of subduction (Rollinson and Pease, 2021). Such inferences are based on a series of interpretations concerning chemical dynamics in the presence or absence of subducting slabs. As another example, subducted slabs are sometimes used as input into a reconstruction, but this requires making inferences about the motions of subducted slab in the mantle (Van der Meer et al., 2012; Sigloch and Mihalynuk, 2013). However, there are many different models on mantle dynamics and subduction zone dynamics (e.g., Seton et al., 2023), which have led to plate kinematic reconstructions that are model-dependent and therefore non-unique and highly variable. This makes comparing the reconstructions and integrating them into a global model difficult.

To overcome the problem of non-unique and non-reproducible reconstructions, a reconstruction protocol has been developed to kinematically reconstruct subducted plates and their past motions that limits the data that is used as input to geological data that demonstrate relative displacements, and that quantify timing of juxtaposition (Boschman et al., 2014; Van Hinsbergen et al., 2020a). This reconstruction protocol avoids geodynamic interpretations to prevent circular reasoning within the reconstruction. Kinematic data that are used in these reconstructions are:

1. Marine magnetic anomaly and fracture zone data of existing oceans to form a plate circuit that quantifies net lithosphere loss through time.
2. Faults and fault zones, which provide information about the direction and the (minimum) amount of extension, strike-slip, or shortening motion.
3. Timing of geological events based on cross-cutting relationships, stratigraphy, and geochronology (for example, the stratigraphic cover on faults constrains the minimum age of motion on the fault).
4. Paleomagnetic data, which provide information about paleolatitudinal motion and vertical-axis rotations.
5. Geometric consistency, which means that the reconstruction should not introduce large overlaps or gaps when there is no geological record of large-scale extension or convergence, and that it should follow the basic rules of plate tectonics of Cox and Hart (1986).

Recently, the reconstruction protocol was expanded with an approach to reconstructing lost oceanic plates and their plate boundaries (Boschman et al., 2021b; Van Hinsbergen and Schouten, 2021). This approach uses geological data from accreted sequences of oceanic crust and overlying deep-marine and foreland basin sediments (Ocean Plate Stratigraphy (OPS); Isozaki et al., 1990) and paleomagnetism to reconstruct the evolution of the oceanic crust from its birth at a mid-ocean ridge to its demise at a subduction zone.

The reconstructions using this reconstruction protocol start with the present-day geology and are made back in time. This ensures that it is clear how a geological record

is restored in the past and eventually where it paleogeographically originated. This allows for critical assessment of such restorations against independent data. This protocol thus provides reconstructions that are transparent, reproducible, and easily adaptable when new kinematic data become available. Moreover, these reconstructions may serve as independent input for geodynamic models, devoid of circular reasoning, as they do not rely on geodynamic interpretations.

The reconstruction protocol for lost-plate reconstructions has been applied to the Tethyan and northern and eastern Pacific realms (e.g., Boschman et al., 2014, 2019; Vaes et al., 2019; Van Hinsbergen et al., 2019, 2020a; Advokaat and Van Hinsbergen, 2023), which has resulted in detailed and reproducible reconstructions as basis for paleogeography and geodynamic modelling. This paved the way for restoring the most challenging of former plate boundary zones: the Junction Region between the Pangea-Tethys domain in the west and the Panthalassa domain in the east: the subject of this thesis (Figure 1).

The Tethys oceans were the internal oceanic basins enclosed by the Pangea continents, while the Panthalassa domain is the ocean that surrounded the Pangea continents. The plate tectonic Junction Region in between these domains was predominantly occupied by oceanic plates and intra-oceanic plate boundaries and reconstructing these plates and their plate boundaries presents one of the biggest challenges to develop a reproducible plate kinematic model from geological observations. This is mostly because the plates themselves subducted, and the geological remains of those subducted plates, in the form of accretionary prisms, are sparse, displaced, and reformed when they were incorporated in other orogens. This makes reconstructing their past motion much more challenging than the reconstruction of continental paleogeography from their orogenic remains (e.g., Van Hinsbergen and Schouten, 2021). As a result, plate tectonic reconstructions of oceanic domains in general, and of the Junction Region specifically, lack detail or come with a high uncertainty in the configuration of plate boundaries.

The present-day Junction Region (Figure 1) is centered around the Philippine Sea Plate, which separates the Pacific (Panthalassa) realm in the east from the Tethys realm in the west. The (former) plate boundaries and orogens surrounding the Philippine Sea Plate continue all the way south to the North Island of New Zealand, where a series of oceanic basins form the Junction Region between the Tethyan Australian Plate and the Panthalassic Pacific Plate. The entire region spanning from Japan to New Zealand is thus considered as the plate tectonic junction between the Tethys and Panthalassa realms in this thesis (Figure 1).

One of the main challenges in reconstructing the Junction Region is the absence of direct connections, through ocean floor records, with the plates of the Panthalassa or Pangea-Tethys realms. The current plate boundary of the Philippine Sea Plate, which forms part of the Junction Region, with the Pangea-Tethys realm is the Manila Trench, that connects southward with a thrust system within the Philippines. Farther south, the boundary between the Pangea-Tethys and Junction regions is the highly complex double-sided subduction zone that consumed the Molucca Sea Plate. The reconstruction of the



Figure 1. Present-day tectonic map showing the Panthalassa and Pangea-Tethys realms separated by the Junction Region

interaction between these realms is complicated by the complex evolution of Tethys closure in the SE Asian region. The SE Asian region consists of several small oceanic basins that have displaced fragments of continental lithosphere that were derived from South China as well as from Gondwana. The youngest Gondwana-derived fragments, which ultimately broke off northwestern Australia in the Jurassic, are collectively known as Argoland, and their collision with Sundaland (another Gondwana-derived fragment that already collided with South China in the Triassic (Metcalf 2011, 2017)) resulted in a mosaic of continental fragments with intervening (now-subducted) oceanic basins. Recently, the above-described reconstruction protocol was used to make a systematic kinematic reconstruction of Argoland and the SE Asian region back to the Triassic (Advokaat and Van Hinsbergen, 2023), which is used as a boundary condition to the kinematic reconstruction of the Junction Region and its interaction with the Pangea-Tethys realm. This recent reconstruction, and previous ones,

have shown that before opening of the South China Sea, the region between South China and Borneo was occupied by an enigmatic, now-subducted oceanic basin (the Proto-South China Sea), which was lost to subduction when the South China Sea opened (Hall, 2002; Zahirovic et al., 2014; Advokaat and Van Hinsbergen, 2023). The oceanic lithosphere that was underlying the Proto-South China Sea is generally thought to have been derived from the Panthalassa realm (Hall and Breithfeld, 2017), but its subduction below South China, Sundaland, and Argoland ceased in the Late Cretaceous. Which plate subducted or why subduction stopped is so far unknown, but it is widely thought that it was a Panthalassic Plate, and it is therefore included in the reconstruction of the Junction Region.

On the Panthalassa side, the Junction Region is bounded by subduction zones from the Pacific Plate, and for older times with the Izanagi and/or Phoenix plates, which have both been completely lost to subduction but whose reconstruction is still possible with marine magnetic anomalies preserved on the Pacific Plate (Nakanishi et al., 1992). The Phoenix Plate (in the south) and the Izanagi Plate (in the northwest) were major tectonic plates that occupied vast regions in the Panthalassa Ocean (Larson and Chase, 1972). Together with the Farallon Plate (in the northeast), they bordered the growing Pacific Plate that formed mid-ocean ridge boundaries with all three plates. The Izanagi Plate was lost to subduction below the Eurasian continent, where its evolution and interaction with the overriding plate was relatively straightforward and has been studied extensively (e.g., Vaes et al., 2019; Boschman et al., 2021a; Wu et al., 2022). However, the study of the Izanagi Plate has been limited to its interaction with the Eurasian margin and was mostly studied based on Japanese geology, but its western extent and western plate boundary type in the Junction Region are unknown. The evolution of the Phoenix Plate is much less well-known. Reconstructing its history is complex because magnetic anomalies preserved on the Pacific Plate show that the Phoenix Plate fragmented in the tens of millions of years prior to its final subduction below east Gondwana (Nakanishi et al., 1992; Chandler et al., 2012), and the orogens that formed during its subduction have been deformed by extensive overriding plate deformation after the Cretaceous cessation of subduction of the Phoenix Plate and its daughters (Seton et al., 2012).

Given that the Izanagi and Phoenix plates no longer exist makes it difficult to infer any relative plate motions with and within the Junction Region. For this reason, previous reconstructions have mostly focused on the Panthalassa or Tethys realms separately, focusing on the interaction of the respective oceans with the continents rather than studying the interaction between the two oceanic domains. Global plate tectonic reconstructions (e.g., Seton et al., 2012; Müller et al., 2019) do include plate boundaries in the Junction Region, but it is not always clear what the observations were that inspired the plate boundary configuration.

Based on high wave-speed anomalies imaged by seismic tomography in the lower mantle below the western Pacific region, Van der Meer et al. (2012) suggested that a major intra-oceanic subduction zone may have existed within the Panthalassa Ocean separating

the well-known Panthalassa plates from the unknown plate system of the Junction Region. However, while seismic tomography does provide some insight into the former existence of subduction zones, these lowermost mantle anomalies provide little quantitative data for the kinematic reconstruction of these subduction zones or the plates they bounded. Moreover, the absence of resolution in the tomographic model below the Pacific Ocean for the upper 2000 km of the mantle makes it impossible to trace how these lowermost mantle anomalies may relate to the tomographically better-imaged active subduction systems of the Junction Region (Hall and Spakman, 2002, 2003; Wu et al., 2016, 2022; Van der Meer et al., 2018).

This thesis aims to develop a quantitative kinematic reconstruction of the Junction Region between the Panthalassa and Tethys realms back to the Early Mesozoic. The basis of the reconstruction is the well-constrained plate circuit that links Australia to Eurasia (Seton et al., 2012; Müller et al., 2019), and the detailed reconstruction of the eastern Tethyan realm from the orogenic records of SE Asia to the west of the Philippines (Advokaat and Van Hinsbergen, 2023). This thesis therefore approaches the Junction Region problem from the Panthalassa side (Figure 2). This thesis first reconstructs the evolution of the southern orogenic systems that relate to the Junction Region plates, with a focus on the Phoenix Plate that subducted below a continental margin that spanned from New Zealand to New Caledonia. To this end, Chapter 1 restores Cenozoic deformation of the marginal basins of the SW Pacific region. For completeness, Chapter 2 restores the upper plate deformation in the Antarctic Peninsula, Scotia Sea region, and Patagonia, and serves as a boundary condition for the restoration of the Phoenix Plate. Subsequently, Chapter 3 restores the fate of the Phoenix Plate in the southern Panthalassa Ocean, and links the subduction history to orogenic records of eastern Gondwanaland. The thesis subsequently shifts to the northwest of the Junction Region, and Chapter 4 focuses on the remains of Mesozoic oceanic lithosphere preserved in the Proto-South China Sea suture of Borneo. Finally, the thesis dives deep into Junction territory. First, Chapter 5 re-evaluates the quality of paleomagnetic data that is frequently used as input for the Cenozoic reconstruction of the Philippine Sea Plate. And then, at last, with all boundary conditions set, Chapter 6 presents a kinematic reconstruction of the Junction Region back to the Jurassic, based on an exhaustive review of existing geological data and orogenic architecture from southwest Japan in the north to the Melanesian region in the south. Finally, this thesis contains two appendices with detailed field-based analyses of the geology of North Island, New Zealand, that provided temporal and spatial constraints as background for the reconstructions, but that have a more regional geological character.

Chapter 1: Reconstructing the Late Cretaceous – Cenozoic evolution of the SW Pacific to restore the East Gondwana margin that consumed the Phoenix Plate

The SW Pacific region contains the geological archives of the Phoenix Plate, and the plate is thought to have been subducted below East Gondwana in the Mesozoic. Moreover, this region also contains records of pre-Oligocene subduction systems, in the form of

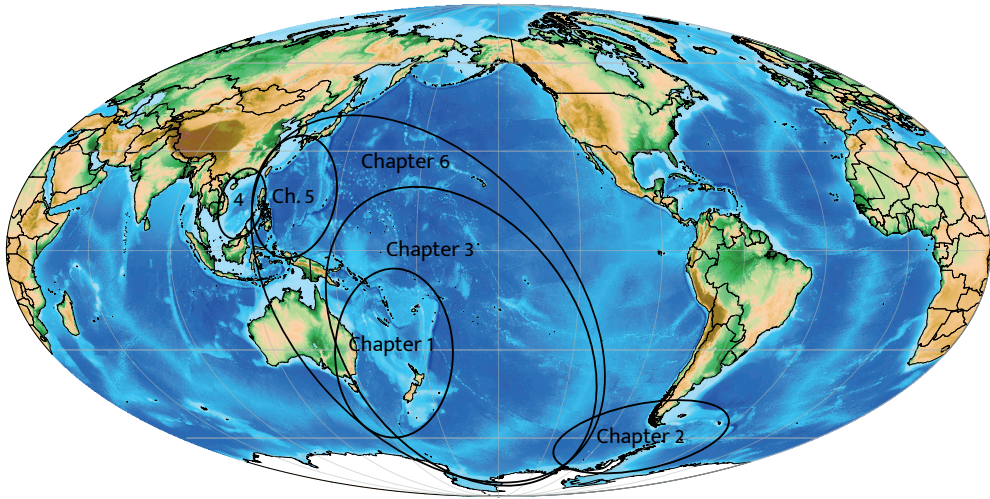


Figure 2. Map centered around the Pacific Ocean, showing the different regions of the respective thesis chapters

ophiolites exposed in New Zealand and New Caledonia, that connect to the Junction Region. These plate margin records have been subject to major Late Cretaceous-Cenozoic extensional deformation. Therefore, to reconstruct the Mesozoic evolution of this region, the Cenozoic tectonic evolution needs to be reconstructed first. Chapter 1 develops a kinematic reconstruction of the SW Pacific region, back to the Late Cretaceous formation of the Pacific-Antarctic Ridge. It closes the Cenozoic marginal and back-arc basins to the east of the Australian continent, and restores Australia, Zealandia, and Antarctica in their Mesozoic East Gondwana configuration. While this chapter restores plate tectonic motions in the Pacific Ocean, it is focused on the evolution of the overriding plate system. The reconstruction is subsequently used to constrain novel insights into the absolute motions of the Tonga-Kermadec slab, which is helpful when interpreting subduction histories of slabs imaged by mantle tomography.

Chapter 2: Reconstructing the Scotia Sea region and the Antarctic Peninsula as boundary condition for the reconstruction of the Phoenix Plate

Chapter 2 develops a kinematic reconstruction of the Scotia Sea Region, including Patagonia and the Antarctic Peninsula, that both formed the upper plate of the subducting Phoenix Plate. The Scotia Plate forms a relatively small plate in the junction region of the South American, Antarctic, and Pacific plates. Despite the wealth of marine magnetic anomaly data, it remained unknown when and why subduction started at the South Sandwich subduction zone and its possible connection with Phoenix Plate subduction, and when and why lithosphere of the South American Plate, which subducts below the Scotia Plate today, also became incorporated within upper plate Scotia Sea extension. This chapter

tries to answer these questions by making a kinematic reconstruction according to the reconstruction protocol. In addition, this chapter provides a geodynamic interpretation that explains the existence of continental fragments within the Scotia Plate that are derived from both South America and Antarctica. Moreover, it answers the question of when the Drake Passage opened, which is of major importance for paleoceanography and paleoclimate studies.

Chapter 3: The Mesozoic evolution and break-up of the Phoenix Plate

Chapter 3 builds upon the SW Pacific reconstruction of Chapter 1 and expands it back to the Late Jurassic, when the Phoenix Plate occupied the southern Panthalassa Ocean. Where Chapter 1 focuses on the overriding plate system, Chapter 3 focuses on the oceanic domain. The Late Cretaceous plate tectonic configuration of Chapter 1 is the starting point of this reconstruction. For the Mesozoic, a quantitative plate reconstruction is complicated by the absence of polarity reversals during the Cretaceous Normal Superchron (CNS). Coincidentally, there was a lot of plate tectonic action in the SW Pacific during this ~40 Ma interval, with the break-up of the Phoenix Plate into several daughter plates. These plates were subsequently captured by the Pacific Plate and Chapter 3 reconstructs the relative motion of Phoenix Plate's daughter plates back to their break-up configuration in the Early Cretaceous using fracture zone and geochronological data recovered from the Pacific Plate. The motion of the Phoenix Plate relative to the Pacific Plate back to the Late Jurassic is reconstructed using marine magnetic anomaly data preserved on the Pacific Plate. The reconstruction in this chapter focuses on the interaction of the Phoenix Plate and its daughter plates with the East Gondwana margin, as the northern limit of the Phoenix Plate is so far unknown.

Chapter 4: Restoring the Proto-South China Sea and its relation to the Junction Region with new data from Borneo

In search of the interaction between Tethys continents and Panthalassa plates, Chapter 4 presents new data from an accreted Cretaceous ocean plate stratigraphy sequence in Borneo. Most previous reconstructions assumed that the Izanagi Plate subducted below South China and Northwest Borneo. However, why subduction of the Izanagi Plate continued below Japan, while subduction ceased below South China has so far been unexplained. This chapter presents geochemical and paleomagnetic data from the oceanic crust, radiolarian biostratigraphy and paleomagnetic data from the overlying deep-marine sediments, and geochemical and detrital zircon geochronological data from the foreland basins clastics incorporated in the accretionary prism. With this new data this chapter tries to resolve whether it was the Izanagi Plate that subducted below NW Borneo. In addition, the aim is to unravel why subduction below the South China and NW Borneo margins ceased in the Late Cretaceous. The new data presented in this chapter therefore provide valuable new data about the plate boundary configurations in Junction Region.

Chapter 5: Re-evaluating the Cenozoic rotation of the Philippine Sea Plate as boundary condition for the reconstruction of the Junction Region

Restoring the Cenozoic kinematic history of the Philippine Sea Plate is essential for the reconstruction of the Junction Region further back in time. As the Philippine Sea Plate was surrounded by subduction zones for most of its history, previous reconstructions of this plate have strongly relied on paleomagnetic data. Chapter 5 critically re-evaluates the paleomagnetic data that are often used to infer major clockwise vertical-axis rotation of the entire Philippine Sea Plate. To establish whether these data are representative for whole-plate rotations or instead may reflect local, deformation related, rotations, this chapter presents new paleomagnetic data from Guam and a compilation of previously published paleomagnetic data, which are assessed using recently defined quality criteria.

Chapter 6: Reconstructing the plate tectonic Junction Region between the Panthalassa and Tethys realms


With chapters 1-5 as boundary conditions, Chapter 6 finally presents a plate kinematic reconstruction of the Junction Region that spans from southern Japan to New Zealand. The reconstruction is based on an exhaustive review of geological data from the Australasian and Philippine Sea Plate regions and subsequent stepwise kinematic restoration. The reconstruction is connected with the SW Pacific reconstructions of Chapters 1 and 3, and with recent reconstructions of SE Asia (Advokaat and Van Hinsbergen, 2023) and the NW Pacific (Vaes et al., 2019; Boschman et al., 2021a) and integrates the new data of Chapters 4 and 5. This final chapter thus presents a kinematic reconstruction of the entire plate tectonic evolution of the Junction Region since the Late Jurassic. The new reconstruction is used to make inferences about the cause of subduction initiation at the extensively studied Izu-Bonin Mariana trench. Additionally, it sheds light on the origin of the oceanic crust that makes up the Philippines and the now-subducted Molucca Sea.

Appendices 1 and 2: Plate boundary evolution in New Zealand

Appendices 1 and 2 provide new geological data for the reconstruction of the evolution of the SW Pacific. These studies are regional in character, which is why they are appendices and not thesis chapters. Appendix 1 presents new paleomagnetic data from a Late Triassic – Jurassic forearc terrane of an intra-oceanic subduction zone, now exposed in the North Island of New Zealand. With the new data it is aimed to determine possible locations of this intra-oceanic subduction zone in the Panthalassa Ocean when subduction was active. Appendix 2 presents new geochemical and geochronological data from calcite veins in a Late Cretaceous turbidite succession, exposed in the North Island of New Zealand. It has been interpreted that the Late Cretaceous turbidites were incorporated into an allochthon that was emplaced during Cenozoic subduction initiation at the Hikurangi subduction zone. The new data provide constraints on the age of subduction initiation at the Hikurangi subduction zone.



The Tasman Sea meets the Pacific Ocean at Cape Reinga, New Zealand



Southwest Pacific absolute plate kinematic reconstruction reveals major Cenozoic Tonga-Kermadec slab dragging

This chapter has been published as:

Van de Lagemaat, S. H. A., Van Hinsbergen, D. J. J., Boschman, L. M., Kamp, P. J. J. & Spakman, W. (2018). Southwest Pacific absolute plate kinematic reconstruction reveals major Cenozoic Tonga-Kermadec slab dragging. *Tectonics* 37(8), 2647–2674.

Abstract

Tectonic plates subducting at trenches having strikes oblique to the absolute subducting plate motion undergo trench-parallel slab motion through the mantle, recently defined as a form of “slab dragging.” We investigate here long-term slab-dragging components of the Tonga-Kermadec subduction system driven by absolute Pacific plate motion. To this end we develop a kinematic restoration of Tonga-Kermadec Trench motion placed in a mantle reference frame and compare it to tomographically imaged slabs in the mantle. Estimating Tonga-Kermadec subduction initiation is challenging because another (New Caledonia) subduction zone existed during the Paleogene between the Australia and Pacific plates. We test partitioning of plate convergence across the Paleogene New Caledonia and Tonga-Kermadec subduction zones against resulting mantle structure and show that most, if not all, Tonga-Kermadec subduction occurred after ca. 30 Ma. Since then, Tonga-Kermadec subduction has accommodated 1,700 to 3,500 km of subduction along the southern and northern ends of the trench, respectively. When placed in a mantle reference frame, the predominantly westward directed subduction evolved while the Tonga-Kermadec Trench underwent ~1,200 km of northward absolute motion. We infer that the entire Tonga-Kermadec slab was laterally transported through the mantle over 1,200 km. Such slab dragging by the Pacific plate may explain observed deep-slab deformation and may also have significant effects on surface tectonics, both resulting from the resistance to slab dragging by the viscous mantle.

1. Introduction

By its definition, lithosphere subduction operates by a trench-normal influx of lithosphere into the mantle. Deep subduction is considered to be primarily driven by slab pull (Conrad and Lithgow-Bertelloni, 2002; Turcotte and Schubert, 2002), which may tend to force the trench to be normal to subduction. Perhaps for these reasons the investigation of subduction kinematics and dynamics is frequently focused on slab motion orthogonal to trenches (e.g., Heuret and Lallemand, 2005; Schellart et al., 2008). Tectonic plates, however, often subduct along trenches with varying orientations relative to their subducting plate motion in an absolute plate motion frame of reference (Goes et al., 2011; Philippon and Corti, 2016). The gravitational pull acting on the subducting parts of a plate contributes to the overall plate motion, but as a rheologically strong plate undergoes one average motion about an Euler pole at a particular time, by implication slabs may undergo trench-parallel motions through the mantle. The Pacific plate, being the largest plate on Earth, serves as a prime example of a plate having subducting slabs of varying orientations at present. The Tonga-Kermadec and Mariana trenches roughly strike N-S, Japan and the Kuril trenches strike NE-SW and the Aleutian Trench strikes roughly E-W (Figure 1). When placed in a mantle reference frame (e.g., the moving hot spot reference frames of O'Neill et al., 2005, Torsvik et al., 2008, or Doubrovine et al., 2012), the Pacific plate has an overall NW-ward absolute plate motion, from which it follows that slabs of the Pacific plate must undergo trench-parallel motion

where a trench is oriented oblique to the local direction of absolute Pacific plate motion. This trench-parallel slab motion is a form of “slab dragging” (Chertova et al., 2014) and comprises in general any lateral slab transport through the mantle that results from the absolute surface motion of the subducting plate (Spakman et al., 2018). Slab dragging also includes any trench-normal slab advance that is caused by the subducting plate motion and which acts against slab rollback, as has been observed in laboratory experiments (Schellart, 2005). Slab dragging includes the exceptional cases where entire subduction systems are being dragged laterally through the mantle in directions independent of trench orientation (Spakman et al., 2018). Previous examples of slab dragging are the northward trench-parallel dragging of the Burma slab as part of the India plate (Le Dain et al., 1984), the NNE-ward transport of the entire Banda slab by the Australian plate (Spakman and Hall,

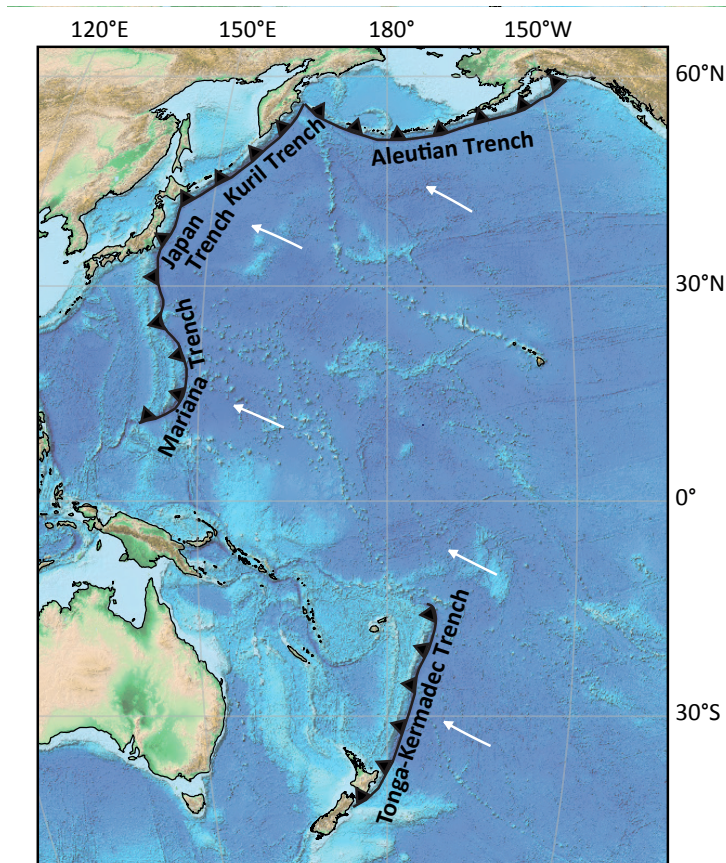


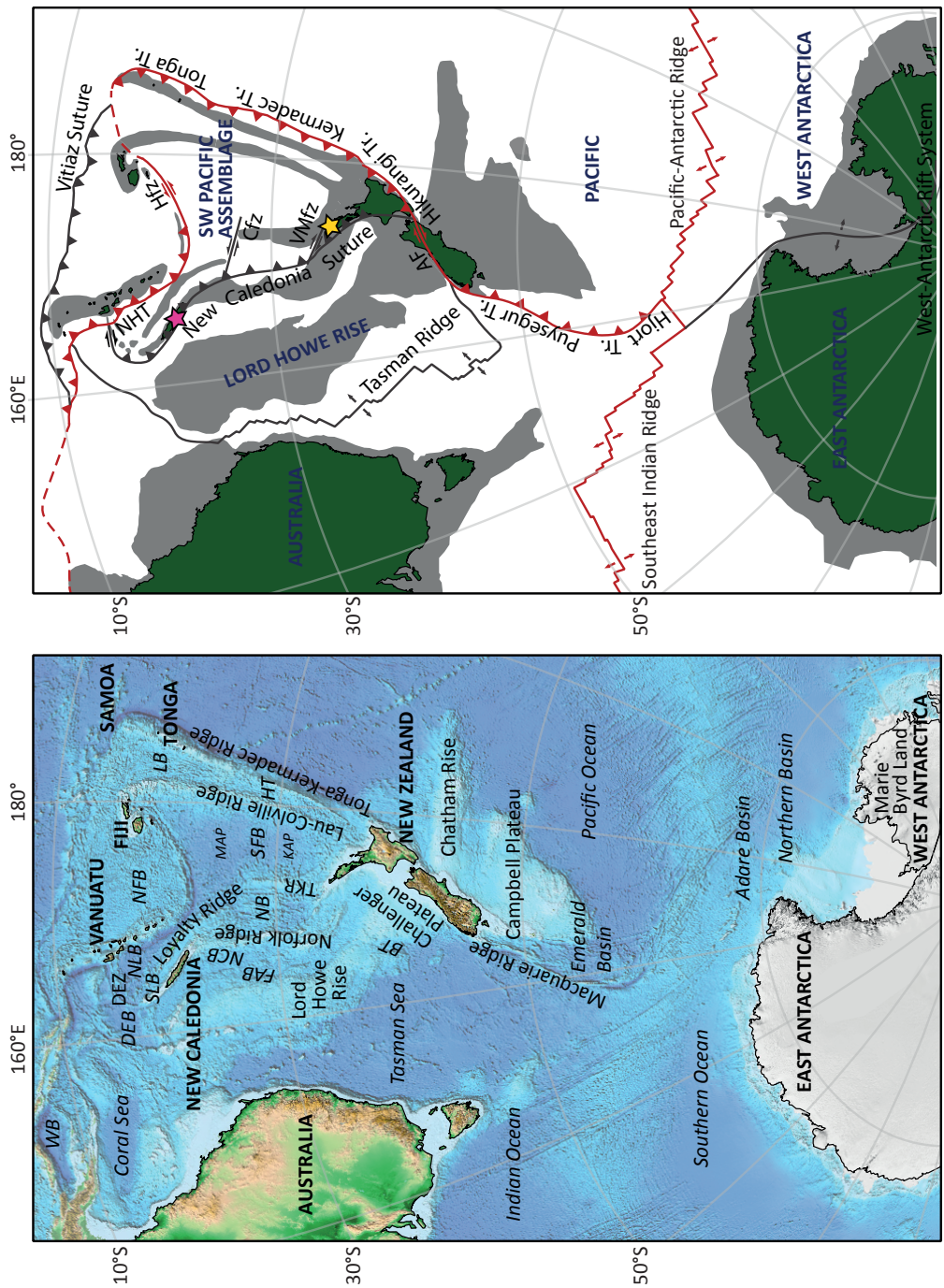
Figure 1. Present-day trenches in the western Pacific realm. White arrows indicate absolute Pacific plate motion for the last 10 Myr (based on our model, see Table 3 and the supporting information). The varying degrees of obliquity at Pacific subduction zones requires that during the last 10 Myr, the slabs subducting at these trenches must have undergone a component of trench-parallel absolute motion defined as “slab dragging.” Background map from Amante and Eakins (2009).

2010), slab “stumps” under western North-America that are laterally dragged by the Pacific plate (Furlong and Govers, 1999; Pikser et al., 2012; Wang et al., 2013), and the NNE-ward dragging of the entire Gibraltar slab by African plate motion (Spakman et al., 2018). The last example, which is particularly pertinent here, is that of Giardini and Woodhouse (1986), who attributed the strong horizontal deformation of the Tonga-Kermadec slab to horizontal shear interaction with the mantle. They proposed that the shear interaction is possibly induced by roughly northward trench-parallel transport of the slab through the mantle.

By reconstruction of the SW Pacific tectonic evolution during the Cenozoic, we here analyze the extent to which the Tonga-Kermadec subduction zone in the southwest Pacific may have been dragged northward through the mantle. At present, the Tonga-Kermadec subduction zone extends for approximately 2,700 km from the east coast of North Island, New Zealand, to south of Samoa (Figure 2). This subduction zone accommodates convergence between the Pacific and Australian plates and is the location of the highest rates of Pacific plate subduction and overriding plate extension (Bevis et al., 1995). The Tonga-Kermadec subduction zone is associated with a long, westward dipping subducted slab located below the present-day SW Pacific region that is well imaged by seismic tomography (Bijwaard et al., 1998; Fukao et al., 2001; Fukao and Obayashi, 2013; Gorbатов and Kennett, 2003; Hall and Spakman, 2002, 2003; Schellart et al., 2009; Schellart and Spakman, 2012; Van der Meer et al., 2018; Van der Hilst, 1995). This slab has penetrated the lower mantle along most of its length and reaches depths of at least ~1,200 km. In the northern part of the Tonga-Kermadec subduction system and at the 660-km discontinuity between the upper and lower mantle, the slab is flat lying to shallow dipping, whereas in the south, it is steeply dipping into the lower mantle (Figure 3).

In the context of relative Australian-Pacific plate convergence, the dynamics and structure of the Tonga-Kermadec subduction zone and its slab are well known, whereas the motion of the system in an absolute plate motion frame of reference remains less extensively explored. The moving hot spot reference frame (e.g., Doubrovine et al., 2012; O'Neill et al., 2005; Torsvik et al., 2008) suggests that the Australia and Pacific plates have shared a component of rapid northward absolute plate motion of up to ~7 cm/year during the Cenozoic. This shared absolute plate motion component is invisible in a relative plate

Figure 2 ►. Topography and bathymetry (left) and tectonic map (right) of the SW Pacific. Tectonic map is based on our model (see Table 3 and the supporting information): continents in green, submerged continental fragments and volcanic arcs in gray. Present-day plate boundaries in red, former plate boundaries in dark gray. Pink and yellow stars are locations of New Caledonia and Northland ophiolites, respectively. (Former) plate names in dark blue. SW Pacific assemblage consists of multiple smaller plates. BT = Bellona Trough; DEB = D'Entrecasteaux Basin; DEZ = D'Entrecasteaux Zone; FAB = Fairway-Aotea Basin; HT = Havre Trough; KAP = Kupe Abyssal Plain; MAP = Minerva Abyssal Plain = NB, Norfolk Basin; NCB = New Caledonia Basin; NFB = North Fiji Basin; NLB = North Loyalty Basin; LB = Lau Basin; SFB = South Fiji Basin; SLB = South Loyalty Basin; WB = Woodlark Basin; NHT = New Hebrides Trench; Cfz = Cook fracture zone; Hfz = Hunter fracture zone; VMfz = Vening Meinesz fracture zone; Tr = Trench.



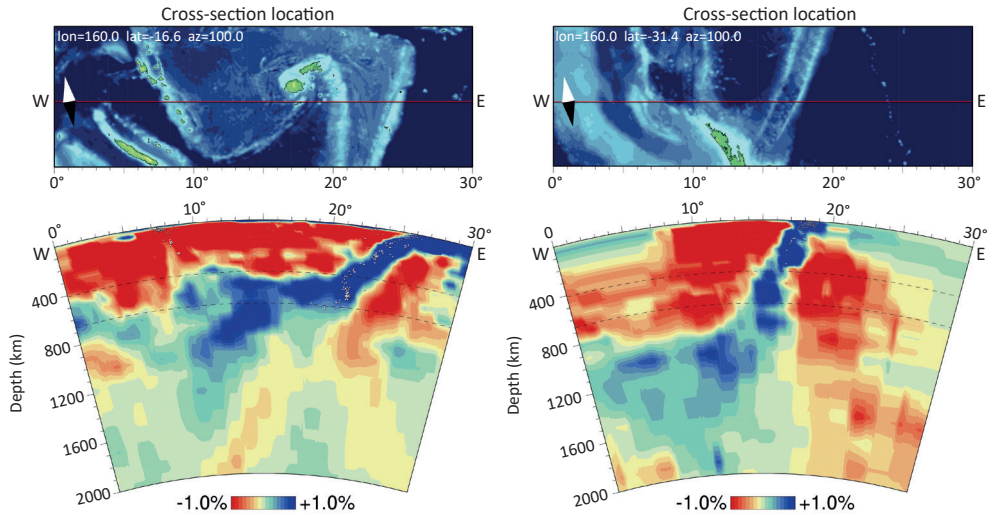


Figure 3. W-E tomographic cross sections of the Tonga-Kermadec slab at the northern (left) and southern (right) ends of the trench, based on the UU-P07 tomographic model (Amaru, 2007). In the north, a significant portion of the slab is flat lying before it continues into the lower mantle, whereas in the south the slab penetrates straight into the lower mantle.

motion reconstruction of Tonga-Kermadec subduction but must strongly influence the motion of the Tonga-Kermadec Trench relative to the mantle. Plate tectonic indications that such motion may actually have occurred are suggested by previous reconstructions presented by Sdrolias and Müller (2006), or Faccenna et al. (2012), for example, although left uninterpreted in terms of subduction zone dynamics. Here we investigate in particular the scale at which slab dragging may have affected the Tonga-Kermadec subduction zone and whether such influence may be evident from the position of the associated subducted slabs.

To this end, it is first necessary to estimate when subduction along the Tonga-Kermadec Trench started. Despite being one of the most spectacular subduction zones on Earth today, the age of its initiation proves to be difficult to assess and different ages have been suggested in the past. A widely held view is that subduction started around 45–50 Ma (e.g., Matthews et al., 2015), correlating it to an Eocene global-scale plate reorganization (e.g., Whittaker et al., 2007). This age corresponds to interpretations made by Bloomer et al. (1995) based on $^{40}\text{Ar}/^{39}\text{Ar}$ dated samples of a quartz gabbro and a tholeiitic basalt from the island of ‘Eua, Tonga (46.6 and 46.1 Ma, respectively; Ewart et al., 1977). However, other reconstructions have suggested ages of subduction initiation ranging from 90 Ma or even earlier (Schellart et al., 2006), to as young as 27 Ma (Yan and Kroenke, 1993).

One of the main reasons for uncertainty around the age of the Tonga-Kermadec subduction system is that it is not possible to make a Cenozoic closed plate circuit involving the Tonga-Kermadec subduction zone as the area between eastern Australia and the Pacific

Ocean hosted two Cenozoic subduction systems: the modern Tonga-Kermadec system and a former New Caledonia subduction system that led to Late Cretaceous-Paleogene formation and Early Miocene emplacement of an ophiolite belt on New Caledonia (Figures 2 and 4; e.g., Cluzel et al., 2012b; Schellart et al., 2009). The area between these two trenches (here referred to as the SW Pacific assemblage) underwent a complex Cenozoic history of back-arc spreading. While it is possible to reconstruct how much net convergence occurred and how much additional subduction must have occurred to accommodate the opening of the well-known extensional back-arc basins between the Tonga-Kermadec Trench and Australia, it is less straightforward to reconstruct how and when this convergence was distributed between the New Caledonia and Tonga-Kermadec subduction zones. Prior tectonic reconstructions of the SW Pacific assemblage have included a New Caledonia subduction zone (e.g., Matthews et al., 2015; Schellart et al., 2006; Yan and Kroenke, 1993), but how Pacific-Australia convergence was distributed between the two subduction zones has never been addressed and what it means for the age of the Tonga-Kermadec subduction system.

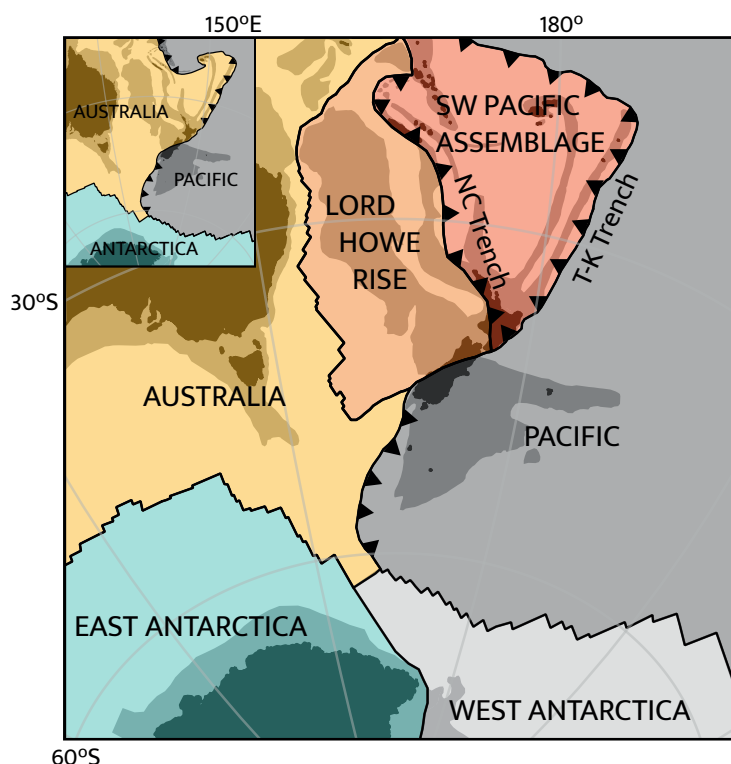


Figure 4. Plate tectonic setting of the SW Pacific region during the Late Cretaceous to Cenozoic (based on our model, see Table 3 and the supporting information). Inset: Present day plate configuration. The SW Pacific assemblage is surrounded by subduction zones that may have been active contemporaneously, which makes it difficult to make a definitive closed plate circuit for the Paleogene.

Our approach to resolving how subduction at the Tonga-Kermadec Trench responded to rapid absolute plate motion with a strong trench-parallel component is as follows: (i) development of a plate kinematic reconstruction of the SW Pacific region cast within the Australia-Pacific plate circuit; (ii) testing partitioning of plate convergence across the New Caledonia and Tonga-Kermadec subduction zones against resulting mantle structure inferred from tomography; (iii) making inferences about the possible age range of Tonga-Kermadec subduction initiation and its subduction rate through time; and (iv) assessing how the Tonga-Kermadec Trench and slab responded to absolute plate motions of the Pacific and Australian plates.

2. Seismic tomographic constraints on SW Pacific mantle structure

Seismic tomography has revealed several anomalies in the SW Pacific region that are interpreted to reflect subducted slabs. Here we use tomographic model UU-P07 (Amaru, 2007) of which slab interpretations for this region were made by Hall and Spakman (2002), Schellart et al. (2009), Schellart and Spakman (2012, 2015), and Van der Meer et al. (2018; Figure 5). In Figures 5 and 6 the percentage limits defined in the legends and applied in the map plots of the P wave velocity anomalies vary with depth. These limits are depth dependent following the relationship between P wave velocity and temperature as a function of depth, as established by Goes et al. (2004). The scaling is such that the contour limits

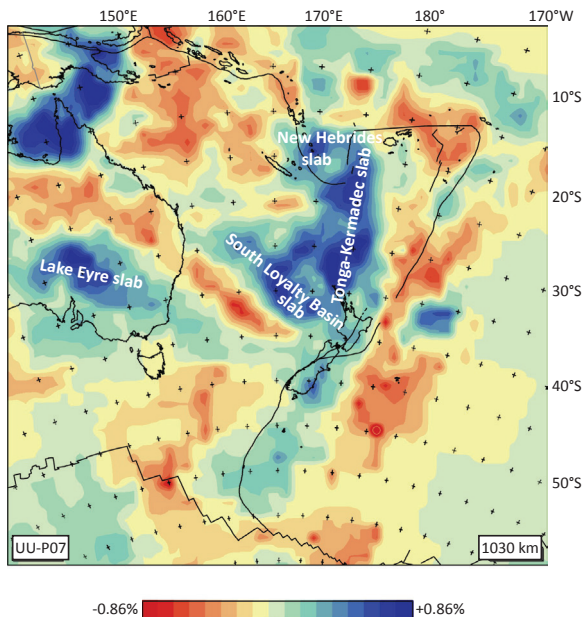


Figure 5. Tomographic image from the southwest Pacific region at a depth of 1,030 km, revealing the Tonga-Kermadec, South Loyalty Basin, Lake Eyre, and New Hebrides slabs, based on the UU-P07 tomographic model (Amaru, 2007). See section 2 for description of the contour parameters in the legend scale bar.

always correspond to an estimated temperature anomaly of -250 K (for the positive limit) and $+250$ K (for the negative limit). Thus, implicitly, the tomography map-view images also provide an estimate of the mantle temperature anomaly. This also emphasizes that while P wave velocity percentages in the lower mantle are generally small ($<1\%$), the corresponding temperature anomaly can be on the order of 10% of the ambient lower mantle temperature.

The most prominent anomaly in the SW Pacific is related to the Tonga-Kermadec slab (Hall and Spakman, 2002; Van der Hilst, 1995). The slab is west dipping, and located west of the present-day subduction zone, up to a depth of $\sim 1,200$ km along the whole length of the trench (Figure 6; Schellart and Spakman, 2012). In the south, the slab penetrates almost straight through the 660-km discontinuity into the lower mantle, whereas in the north, a significant portion of the slab lies horizontally over the 660-km discontinuity before it dips into the lower mantle at its western end (Figure 3). This leads to a N-S striking anomaly below the 660-km discontinuity and a clockwise rotation of the anomaly at successively shallower depths to its present-day NNE-SSW configuration.

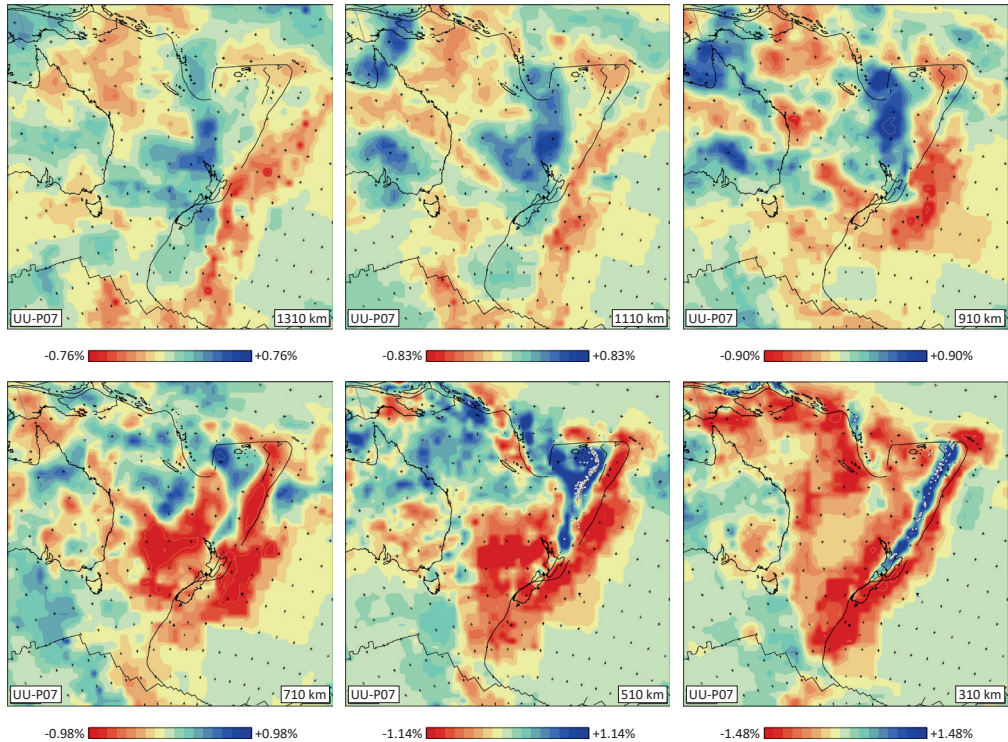


Figure 6. Seismic tomographic images of the SW Pacific regions at successive shallower depths, based on the UU-P07 tomographic model (Amaru, 2007). See section 2 for description of the contour parameters in the legend scale bars. These images illustrate that the entire Tonga-Kermadec slab is located west of the present-day trench along the entire length of the trench, and no southward deflection relative to the present-day trench is visible. The upper mantle portion of the slab is also located west of the present-day trench.

The anomaly considered to be related to the New Caledonia subduction zone was first identified by Schellart et al. (2009) and is referred to as the South Loyalty slab (Cluzel et al., 2001; Schellart, 2007; Schellart et al., 2006, 2009). It is located $\sim 1,500$ km south of New Caledonia, currently below the Tasman Sea, in the upper part of the lower mantle at ~ 950 to $1,350$ km depth and is best resolved at $\sim 1,000$ – $1,200$ km (Figure 5). The slab trends NW-SE and is flat lying with a lateral extent of $\sim 2,200$ by 600 – 900 km (Figures 5 and 7; Schellart et al., 2009). In the southeast, the South Loyalty slab is difficult to distinguish from the southern end of the Tonga-Kermadec slab, as the bases of both slabs are located at approximately the same depth (Figure 5).

A third anomaly is located in the SW Pacific, related to ongoing northeast dipping subduction at the New Hebrides subduction zone (Figure 5). This slab is well imaged and reaches the base of the upper mantle (Fukao et al., 2001; Fukao and Obayashi, 2013; Hall and Spakman, 2002, 2003; Obayashi et al., 2013; Schellart and Spakman, 2012; Wu et al., 2016).

A fourth anomaly, not located in the SW Pacific, that is of interest to this study is located below the Lake Eyre region in Australia and is interpreted as an ENE-WSW trending slab that subducted northwards at the New Guinea-Pocklington trough (Schellart and Spakman, 2015). The slab is currently located in the upper part of the lower mantle at 800 – $1,200$ km depth (Figure 5). Timing of slab break-off is interpreted from the final obduction of the ophiolite on New Guinea and in the Pocklington area at about 50 Ma (Schellart and Spakman, 2015).

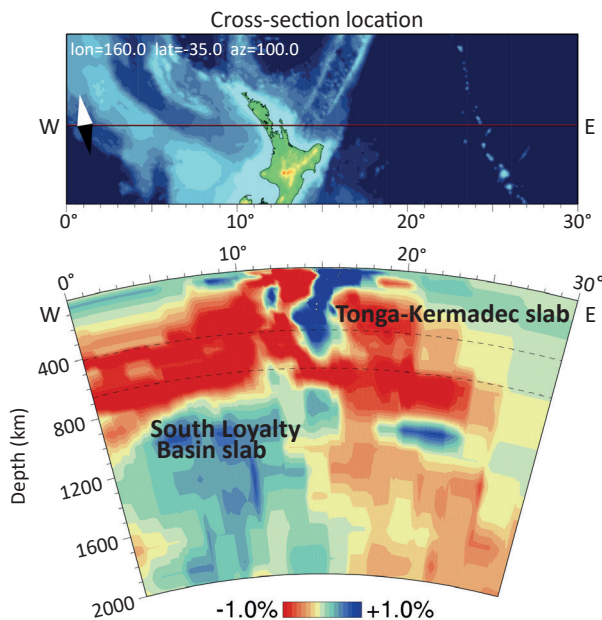


Figure 7. W-E tomographic cross section of the South Loyalty Basin slab, based on the UU-P07 tomographic model (Amaru, 2007).

Interestingly, the emplaced ophiolites associated with the end of subduction at the New Caledonia and Papua New Guinea subduction zones are presently located ~1,500 and ~2,800 km north of the New Caledonia and Lake Eyre slabs, respectively. The Australian plate overrode these detached slabs evidencing its northward absolute plate motion (Schellart and Spakman, 2015).

3. Australia-Pacific plate circuits

A relative plate circuit using a kinematic reconstruction needs to be constructed to study the convergence history between the Pacific and Australian plates. Such a circuit includes five major (former) tectonic plates: Lord Howe Rise (including the northern part of the New Zealand continent, hereafter abbreviated to LHR), Australia (AUS), East Antarctica (eANT), West Antarctica (wANT), and Pacific (PAC; Figure 4). Motion at the plate boundaries between AUS-eANT, AUS-LHR, and PAC-wANT is constrained by marine magnetic anomalies and transform faults/fracture zones of oceanic crust produced by former or active ridges (e.g., Croon et al., 2008; Gaina et al., 1998; Tikku and Cande, 1999, 2000; Whittaker et al., 2007, 2013; Wright et al., 2015, 2016). The boundaries between LHR and PAC in New Zealand (e.g., Alpine Fault) and between eANT and wANT (the West Antarctic Rift system) are, however, less well defined (Figure 2). Motion along these plate boundaries can be partly constrained by magnetic anomalies occurring in adjacent oceanic lithosphere, but typically only for brief intervals (Granot et al., 2013a, 2013b; Keller, 2004).

Motion between eANT and wANT is constrained between ~40 and 26 Ma by marine magnetic anomalies in the Adare Basin and adjacent Northern Basin (Cande et al., 2000; Cande and Stock, 2004a; Granot et al., 2013a). However, it has been tentatively suggested that extension in the Adare Basin started around 60 Ma (Cande and Stock, 2004a) and, additionally, apatite fission track thermochronology suggests that the West Antarctic Rift system was actively extending between ~100 and 60 Ma (Spiegel et al., 2016). Consequently,

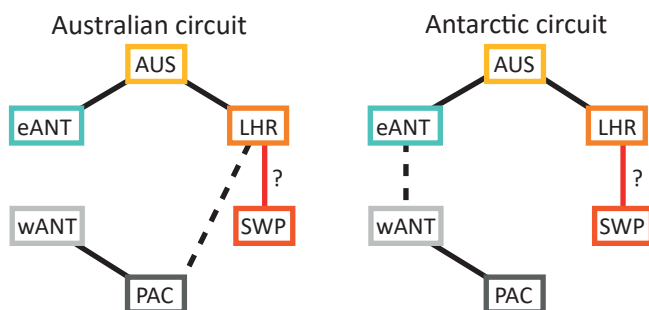


Figure 8. Australian and Antarctic plate circuits. Dashed lines indicate poorly constrained boundaries within each circuit. The plate motion chain to connect LHR and the southwest Pacific assemblage (SWP) is uncertain in both plate circuits due to the existence of the New Caledonia subduction zone in the Cenozoic.

marine magnetic anomalies do not provide sufficient constraints on the eANT-wANT plate boundary evolution.

Motion between LHR and PAC is constrained by marine magnetic anomalies of the Macquarie spreading center between ~40 and 24 Ma (Keller, 2004). The uncertainty ellipses of these rotation poles are relatively large as a result of the short strike-length of the anomalies mapped in Emerald Basin and southern Tasman Sea. Also, part of this original seafloor west of Macquarie Ridge has been consumed by subduction at Puysegur Trench (Keller, 2004) and hence the age structure of this former seafloor cannot be reconstructed. Post-28 Ma dextral bending of seafloor and fracture zones adjacent to the AUS-PAC plate boundary between Hjort and Puysegur trenches also contributes to the size of the Keller (2004) uncertainty ellipses (Hayes et al., 2009).

Because there are two poorly constrained plate boundaries in the circuit, two alternative plate motion circuits have been previously proposed (Figure 8): an Australian circuit, in which LHR is attached to PAC until 45 Ma and the eANT-wANT boundary is left unconstrained, and an Antarctic circuit, in which the LHR-PAC boundary is left unconstrained, while motion within the West Antarctic Rift system is incorporated (e.g., Doubrovine et al., 2012; Doubrovine and Tarduno, 2008a, 2008b; Matthews et al., 2015; Schellart et al., 2006; Steinberger et al., 2004).

Matthews et al. (2015) recently provided an extensive review and analysis of SW Pacific plate circuits. They tested a total of six Antarctic circuit scenarios and four Australian circuit scenarios. These scenarios differ in rotation poles used for the eANT-AUS and wANT-PAC spreading ridges. In the Antarctic circuit, different eANT-wANT rotations are also tested, while in the Australian circuit PAC is attached to LHR until 45 Ma (i.e., throughout their reconstruction period). In all scenarios, AUS-LHR motion is described using the finite rotation poles provided by Gaina et al. (1998). The different scenarios are used to explore the implications of the two plate circuits for the amount and type of deformation

Table 1. References for the finite rotation poles used in our reconstruction (Antarctic circuit)

Plate boundary	References
Lord Howe Rise – Australia	Gaina et al. (1998); Seton et al. (2012)
Australia – East Antarctica	Cande and Stock (2004a); Whittaker et al. (2013)
West Antarctica – East Antarctica	Granot et al. (2013a, 2013b ^a); Matthews et al. (2015)
Pacific – West Antarctica	Croon et al. (2008); Wright et al. (2015, 2016)
Challenger Plateau (LHR) – Campbell Plateau (PAC)	Keller (2004)

^a We chose to omit the finite rotation pole for chron 16y, because it leads to unrealistic back-and-forth movement within the Antarctic continent between ~40 and 34 Ma. This rotation pole is subject to a greater uncertainty due to difficulty in the identification of magnetic picks of this anomaly (explained in Granot et al., 2013a).

predicted within New Zealand and in the West Antarctic Rift system, and to the north of New Zealand. Matthews et al. (2015) proposed that after 55 Ma, the Antarctic circuit, using rotation poles of Whittaker et al. (2013), Granot et al. (2013a, 2013b), and Larter et al. (2002) for AUS-eANT, wANT-eANT, and PAC-wANT motions, respectively, produces the best fit with geological observations from both New Zealand and the West Antarctic Rift system. This plate circuit has been incorporated into the global plate model of Müller et al. (2016). Additionally, in the global plate model of Müller et al. (2016), PAC-wANT motion is updated using the finite rotation poles of Wright et al. (2015, 2016).

Because the models of Matthews et al. (2015) and Müller et al. (2016) produce fits that reasonably satisfy geological constraints for both the plate boundary through New Zealand and the West Antarctic Rift system, we adopt their (Antarctic) plate circuit as a basis for our SW Pacific restoration. However, we do not directly follow the reconstruction of Müller et al. (2016) but use it as a framework. We choose to use all finite rotation poles as published in the original papers (Table 1), whereas Müller et al. (2016) used only a selection of chrons, leading to greater detail in our reconstruction. Additionally, we updated the ages of the chrons to the timescale of Ogg (2012).

A set of Euler poles for the 40- to 24-Ma motions on the plate boundary through New Zealand was proposed by Keller (2004) that differ in details from those of the Müller et al. (2016) plate circuit. The discrepancy may have been accommodated on the poorly constrained Bellona Trough between Challenger Plateau and Lord Howe Rise where a plate boundary may have existed (e.g., Cande and Stock, 2004a; Gaina et al., 1998; Van de Beuque et al., 2003). To satisfy both the Müller et al. (2016) plate circuit and the Keller (2004) constraints, our reconstruction accommodates the difference at Bellona Trough. At 24 Ma, shortly after inception of the Alpine Fault (Kamp, 1986), the unconstrained boundary is relocated from Bellona Trough to the Alpine Fault.

4. SW Pacific plates and kinematics

In this section we provide a review of geological data from the SW Pacific region between LHR in the west and the Tonga-Kermadec Trench in the east. This part of the SW Pacific consists of a series of basins and ridges comprising oceanic, continental, and arc crust, and we will review their formation age and history. Because this area is surrounded by active and fossil subduction zones, these basins and ridges are reconstructed using a separate plate motion chain (Figure 9). To this end, we first review studies based on marine geophysical constraints on the opening history of the various extensional basins and subsequently summarize geological constraints from ophiolites in New Caledonia and in New Zealand bearing on evolution of the western subduction system. This review focuses on the basins and ridges between LHR and Tonga-Kermadec Trench. The northern part of the SW Pacific region, including the Coral Sea, d'Entrecasteaux, and Woodlark Basin provide no constraints on evolution of this trench and are not reconstructed in detail here.

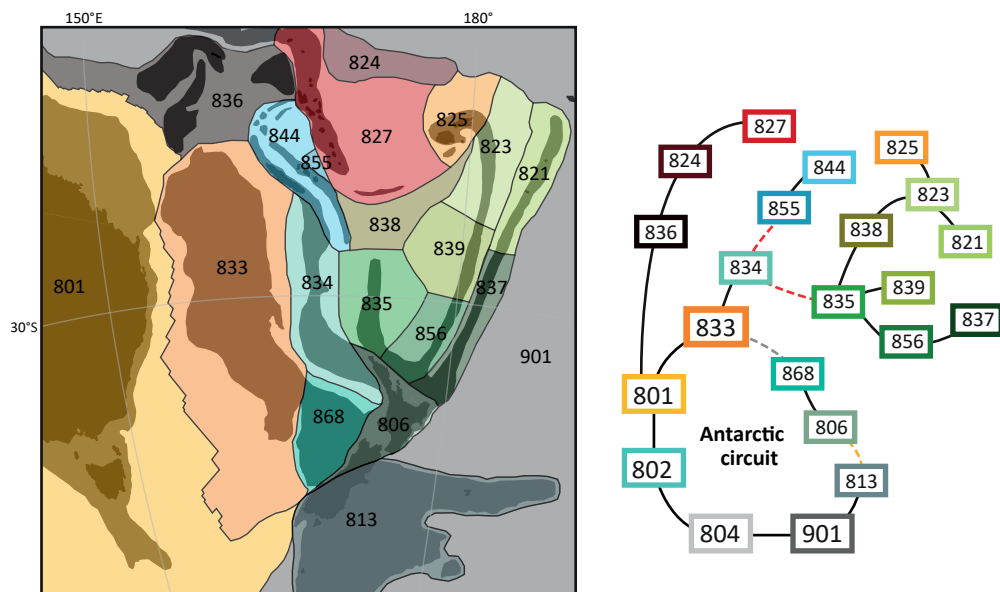


Figure 9. Tectonic units (left) and plate motion chain (right) for the SW Pacific realm. List of codes and their associated plates are found in Table 2. The unconstrained boundary between LHR and PAC is located between LHR (833) and Challenger Plateau (868) until 24 Ma (dashed gray line), and then relocated to the Alpine Fault (dashed yellow line), which marks the boundary between North New Zealand (806) and Campbell Plateau (813). Dashed red lines indicate the uncertain connection between LHR/Norfolk Ridge and the SW Pacific assemblage. These plates were separated by the New Caledonia subduction zone during its existence. LHR = Lord Howe Rise; PAC = Pacific.

4.1. Extensional basins

4.1.1. Fairway Aotea and New Caledonia basins

Between LHR and Norfolk Ridge, thus west of the New Caledonia ophiolite and the inferred paleo-subduction zone that led to its obduction, lie two basins separated by the Fairway Ridge: the western Fairway Basin and the eastern New Caledonia Basin. The Fairway Basin extends southward into Aotea Basin, commonly otherwise known as the southern part of the New Caledonia Basin (Figure 2).

Klingelhoef et al. (2007) reported wide-angle and reflection seismic data showing that the crust of Fairway Ridge is continental and that Fairway Basin is underlain by thinned continental crust. That study also showed that New Caledonian Basin is underlain by oceanic crust in its central part. The crust in the northern part of the basin is atypical and its origin remains unknown (Klingelhoef et al., 2007).

Owing to the difficulty of identifying the oceanic versus continental nature of crust in this part of the SW Pacific, contrasting tectonic models have been proposed. Lafoy et al. (2005) suggested that 85- to 65-Ma continental thinning in the Fairway and New Caledonia basins coincided with seafloor spreading in the southern Tasman Sea. They presume that

Table 2. Plate IDs and their associated plate names as used in the reconstruction

Plate ID	Plate name
801	Australia
802	East Antarctica
804	West Antarctica
806	New Zealand north of Alpine Fault
813	Campbell Plateau, including New Zealand south of Alpine Fault
821	Tonga Ridge
823	Lau Ridge
824	Suture Vitiaz Trench
825	Fiji
827	New Hebrides Trench and North Fiji Basin
833	Lord Howe Rise
834	Norfolk Ridge
835	Three Kings Ridge
836	Coral Sea
837	Kermadec Ridge
838	Northwest South Fiji Basin
839	East South Fiji Basin
844	North Loyalty Basin, including Loyalty Ridge and New Caledonia
855	Southeast North Loyalty Basin
856	Colville Ridge
868	Challenger Plateau
901	Pacific

subsequently, spreading in New Caledonia Basin occurred during the Paleocene, between ~62 and 56 Ma, concurrent with spreading in the Coral Sea Basin. Collot et al. (2009), on the other hand, suggested that extension in the Fairway and New Caledonia Basin predates Tasman Sea spreading and that these basins are early-Late Cretaceous (Cenomanian) or even older in age.

Any extension in the Fairway-Aotea and New Caledonia basins that occurred during the Late Cretaceous and later would increase the overall convergence that must have been accommodated by the subduction zones between LHR and PAC. We incorporate the scenario of Lafoy et al. (2005) and our reconstruction should thus be considered as a maximum-convergence and subduction scenario. Using 3-D modeling of satellite gravity data, approximately 30% crustal thinning is estimated for the New Caledonia Basin (Wood and Woodward, 2002). According to Lafoy et al. (2005), however, the basin studied by Wood and Woodward (2002) structurally corresponds to the South Fairway Basin.

4.1.2. Norfolk Basin

Norfolk Basin lies between Norfolk Ridge and Three Kings Ridge (Figure 2); the age and crustal nature of which have been debated. Proposed opening ages of Norfolk Basin include Late Cretaceous (Launay et al., 1982), Eocene-Oligocene (Sdrolas et al., 2003) and Early Miocene (Mortimer et al., 1998). Deep regions within Norfolk Basin show age-bathymetry curves that would be consistent with oceanic crust that formed during the Late Oligocene to Late Miocene (Sdrolas et al., 2004a). A Miocene age of spreading initiation would be consistent with a 23 ± 0.1 Ma $^{40}\text{Ar}/^{39}\text{Ar}$ age of a dredged seafloor tholeiite (Meffre et al., 2001; Bernardel et al., 2002, both cited in Sdrolas et al., 2004a). Cessation of spreading in the Norfolk Basin is poorly constrained but is thought to have occurred as late as 10 Ma (Sdrolas et al., 2004a).

The amount of divergence within the Norfolk Basin is estimated from displacement along the Cook and Vening Meinesz fracture zones (Figure 2). The Cook Fracture Zone is a left-lateral transform fault that offsets Three Kings Ridge from Loyalty Ridge by ~420 km (Sdrolas et al., 2004a). Motion at the southern boundary of Three Kings Ridge was accommodated along the Vening Meinesz Fracture Zone. This fault offsets Three Kings Ridge dextrally from Northland Plateau and accommodated about 170 km of seafloor spreading in the southern Norfolk Basin (Herzer and Mascle, 1996). The Three Kings Ridge migrated southeastward, causing transpressive motion on the Vening Meinesz Fracture Zone (Herzer and Mascle, 1996). Motion on the Vening Meinesz Fracture Zone ended around 15 Ma, based on radiometric $^{40}\text{Ar}/^{39}\text{Ar}$ ages for two linear seamounts interpreted as mini-hot spot trails (Herzer et al., 2009; Mortimer et al., 2007). This age coincides with waning tectonism on Northland Plateau (Herzer et al., 2009, 2011).

4.1.3. North Loyalty Basin

Loyalty Ridge and North Loyalty Basin are located to the northeast of New Caledonia (Figure 2). North Loyalty Basin is a remnant of a once larger basin and is located in a triangle formed by Loyalty Ridge, New Hebrides Trench, and d'Entrecasteaux Basin (Weissel et al., 1982). Weissel et al. (1982) identified clear magnetic anomaly lineations that they tentatively correlated with chrons 23–18 (~50–40 Ma). Later reinterpretation by Sdrolas et al. (2003) reassigned these to chrons 20–16 (~44.5–36 Ma). The identified magnetic anomaly lineations were generated on the north side of a ridge. Their southern counterparts are thought to have been subducted at the New Hebrides Trench (Sdrolas et al., 2003).

4.1.4. South Fiji Basin

The South Fiji Basin extends from Fiji Islands in the north to the Northland Plateau of New Zealand in the south (Figure 2). Its eastern boundary is defined by the, now extinct, Lau-Colville volcanic arc and the western boundary is defined by the Loyalty Ridge and the Three Kings Ridge. The basin is divided into the northern South Fiji Basin or the Minerva Abyssal Plain, and the southern South Fiji Basin or Kupe Abyssal Plain (Packham and

Terrill, 1975), separated by an E-W-oriented central ridge region. This ridge region is not the remnant of an actual mid-ocean ridge, but appears to be the eastward extension of the Cook Fracture Zone (Malahoff et al., 1982; Figure 2).

Anomalies 7–12 (24–31 Ma) were identified in the South Fiji Basin by Watts et al. (1977) and Malahoff et al. (1982). A complete set of anomalies from both sides of a N-S-oriented mid-ocean ridge was identified in the Minerva Abyssal Plain. A set of anomalies was identified in the Kupe Abyssal Plain by Malahoff et al. (1982), which they interpreted as younging westward. This would require that the western flank has been subducting beneath the Three Kings Ridge along a west-dipping subduction zone (Malahoff et al., 1982). Sdrolias et al. (2001), however, reinterpreted the anomalies as younging eastward, in contrast to that proposed by Malahoff et al. (1982). The absence of anomalies on the eastern half of the spreading system in the Kupe Abyssal Plain may be due to asymmetric spreading (Sdrolias et al., 2003). Sdrolias et al. (2003) computed finite rotations for both the Minerva and Kupe Abyssal Plains, based on their magnetic anomaly identifications.

More recent constraints from $^{40}\text{Ar}/^{39}\text{Ar}$ ages of abyssal tholeiites by Mortimer et al. (2007) suggest that South Fiji Basin formed during the Early Miocene, rather than during the Oligocene. The magnetic anomaly profiles are difficult to match to geomagnetic polarity reversal patterns and therefore are unsuitable to provide age constraints (Herzer et al., 2011). These authors reinterpreted the magnetic anomalies of the South Fiji Basin based on revised ages for crustal rocks from sites DSDP 205 and DSDP 285 from Mortimer et al. (2007) and concluded that the magnetic anomalies represent chrons 9 to 6B (27.4–21.9 Ma). This would mean that South Fiji Basin formed during Late Oligocene to Early Miocene, in tandem with Norfolk Basin spreading. The cessation of spreading in both basins is not well constrained but is thought to be around 15 Ma (Herzer et al., 2011; Mortimer et al., 2007).

4.1.5. Lau Basin – Havre Trough

The Lau Basin-Havre Trough is a Y-shaped active back-arc basin, immediately west of Tonga-Kermadec Trench (Figure 2). Seafloor spreading is propagating southwards and different stages of basin opening have been interpreted.

Ocean spreading currently occurs in the Lau Basin along Central and Eastern Lau spreading centers (Parson and Wright, 1996). A sequence of aeromagnetic profiles was obtained by Malahoff et al. (1994). Magnetic anomaly lineations J (C1r.1n, Jaramillo event, ~1 Ma) through 3 (4.6 Ma) were identified, indicating that seafloor spreading started around 5–7 Ma. The magnetic anomaly lineations have short lengths and spreading in the northern Lau Basin is irregular and disorganized, with multiple triple junctions and overlapping rifts (Malahoff et al., 1994). Farther south, spreading in Lau Basin more closely resembles steady state.

Extension in Havre Trough is currently in the rift phase and probably became active concurrent with extension in Lau Basin (Ruellan et al., 2003). A detailed study by Wysoczanski et al. (2010) using multibeam mapping suggested that Havre Trough is

currently in an incipient phase of distributed and disorganized spreading. Because there is no magmatic spreading in Havre Trough, magnetic anomaly data do not record accretion of oceanic crust. Linear magnetic anomalies in Havre Trough, as identified by Malahoff et al. (1982), are instead interpreted as the result of pseudo-linear emplacement of magnetic sheeted dikes into arc basement rocks (Wright, 1993). Yan and Kroenke (1993) used the magnetic anomaly identifications of Malahoff et al. (1982) to compute finite rotations for Lau Basin and Havre Trough.

4.1.6. North Fiji Basin

North Fiji Basin is a Late Miocene oceanic basin currently part of the Pacific plate. It lies as overriding plate above the east-dipping New Hebrides subduction zone (Figure 2) and has a complex spreading pattern. North Fiji Basin is considered to have opened after a subduction polarity switch that followed Early Miocene (Knesel et al., 2008) or Middle Miocene (Auzende et al., 1995; Crawford et al., 2003; Petterson et al., 1997; Quarles van Ufford and Cloos, 2005) arrival of Ontong Java Plateau at Vitiaz Trench (Figure 2). New Hebrides Trench would have formed as a result of this switch and rolled back with a clockwise rotation into its current north-south orientation.

Malahoff et al. (1994) identified two spreading centers and interpreted anomalies J (C1r.1n, Jaramillo event, ~1 Ma) through 4 (1–7.6 Ma), which Yan and Kroenke (1993) used to compute finite rotation. An additional spreading center is present in northern North Fiji Basin with anomalies 2 – 3Ar (1.95–7.14 Ma) identified by Lagabriele et al. (1996). In addition, Taylor et al. (2000) showed from paleomagnetic evidence that the Fiji Islands underwent a 135° counterclockwise rotation between 10 and 3 Ma.

4.2. Ophiolites and volcanic arcs

In addition to the mainly marine geophysical data listed above, key information on the location, timing, and duration of subduction between the SW Pacific region and Norfolk Ridge comes from geological constraints provided by New Caledonian and Northland ophiolites, as well as the d'Entrecasteaux Zone, Loyalty Ridge, and Three Kings Ridge (Figure 2). Here we review key constraints on the evolution of these ophiolites and associated accretionary prisms

4.2.1. Northland ophiolite

The Northland Ophiolite of New Zealand, also referred to as Tangihua Complex, represents the highest structural unit of the Northland Allochthon and is composed of minor upper mantle and oceanic crustal rocks (e.g., Nicholson et al., 2007). Because of similarities in lithology and structural settings with the New Caledonia ophiolite (see below), it is thought that both ophiolites once formed at a formerly contiguous plate boundary (Malpas et al., 1992).

The age of formation of oceanic crust of the Northland ophiolite was originally thought

to be of Late Cretaceous to Paleocene age (Nicholson et al., 2000b). An early Paleocene age (58–62 Ma) was also suggested by Hollis and Hanson (1991) based on the presence of Paleocene radiolarian species within inter-pillow limestone. Brothers and Delaloye (1982) applied K/Ar dating to igneous rock samples from different ophiolite massifs, reporting a wide age range between 102 and 20 Ma. They therefore suggested that the Northland ophiolite complex had a long and multistage history of igneous accretion.

The older ages are confirmed by $^{40}\text{Ar}/^{39}\text{Ar}$ dating of two volcanoclastic samples that yielded ages of ca. 108 Ma (Whattam et al., 2005). Their study also suggested that at least part of the oceanic crust of the Northland Ophiolite cooled during the Oligocene. Step heating $^{40}\text{Ar}/^{39}\text{Ar}$ techniques on tholeiitic basalt samples produced ages between 25 ± 0.8 and 29.6 ± 1 Ma, and $^{206}\text{Pb}/^{238}\text{U}$ dating of zircons from a plagiogranite sample gave an age of 28.3 ± 0.2 Ma (Whattam et al., 2005). These authors thus suggested that at least two distinct groups of igneous rocks are present in the Northland Ophiolite and attributed the c. 100 Ma ages to formation of the Mt. Camel Terrane that forms the basement onto which the ophiolite was emplaced (Whattam et al., 2004, 2005, 2006).

Northland Ophiolite was emplaced during a short period during the latest Oligocene, approximately at the Oligocene-Miocene boundary. This is indicated by the Late Oligocene age of the youngest rocks in the ophiolite versus the Early Miocene age of the oldest rocks overlying the ophiolite (Ballance and Spörli, 1979). Shear sense indicators indicate that emplacement was from the northeast (Malpas et al., 1992, and references therein).

Malpas et al. (1992) reported a MORB geochemical signature in the Northland ophiolite and suggested that it was generated at a major spreading center or in a mature back-arc basin. More recent work, however, has shown that tholeiitic rocks of the ophiolite have a negative Nb anomaly and are enriched in large ion lithophile elements, which are both consistent with a suprasubduction zone signature (Nicholson et al., 2000a; Whattam et al., 2004, 2005).

4.2.2. New Caledonia ophiolite

The New Caledonia archipelago consists of several islands that are part of Norfolk and Loyalty ridges (Figure 2). The main island is part of continental Norfolk Ridge. Loyalty Ridge to the north most likely represents an Eocene island arc (see below), with North Loyalty Basin interpreted as its associated back-arc basin (Cluzel et al., 2012a).

New Caledonia exposes the Peridotite Nappe, an ophiolite complex that was emplaced onto Norfolk ridge during the Eocene. Preceding this emplacement, a north or northeast dipping subduction zone was present, as indicated by the structural history of the ophiolite and its sole (Cluzel et al., 2012a; Quesnel et al., 2016).

The age of formation of the Peridotite Nappe is debated. Due to a complex history of the upper mantle and lower crustal section, the system became ultradepleted, making accurate dating difficult. K-Ar dating of dolerite veins, plutonic rocks (hornblendites and diorites), and of amphibole separates from a dolerite yielded an age range of 120–50 Ma (Prinzhofer,

1981, as cited in Collot et al. (1987) and Cluzel et al. (2012b)). Lower Eocene (55–50 Ma) mafic dykes, dated by the U/Pb zircon system, crosscut the ophiolite at all levels (Cluzel et al., 2006). This indicates a minimum Late Paleocene age for formation of oceanic crust of the Peridotite Nappe. The oceanic ridge that produced the ophiolite was likely oriented E-W (in present-day coordinates), based on N-S-oriented stretching lineations measured in the mantle section of the Peridotite Nappe (Prinzhofer, 1981, as cited in Cluzel, et al., 2012a).

The Peridotite Nappe is in places associated with a metamorphic sole consisting of meta-basalt at amphibolite grade with subordinate metasediments. These are generally interpreted to form during subduction initiation at or near a spreading ridge (Cluzel et al., 2012b; Van Hinsbergen et al., 2015). Hornblende $^{40}\text{Ar}/^{39}\text{Ar}$ and zircon U-Pb dating of metamorphic sole amphibolites yielded ages of ~56 Ma (Cluzel et al., 2012b). The closure temperature for Ar in hornblende is lower than for typical temperatures in amphibolite-facies sole rocks and thus the 56 Ma age dates cooling during sole exhumation, which is likely intrinsically related to the subduction initiation process (Van Hinsbergen et al., 2015). The subduction zone below the Peridotite Nappe therefore probably initiated within a few million years before 56 Ma.

Upon arrival of Norfolk Ridge at the trench and consequent obduction of the ophiolite, the western SW Pacific subduction zone terminated on New Caledonia. Timing of obduction initiation during the Late Eocene is constrained by the age of the youngest sediment on which the ophiolite was thrust (34.7–35 Ma, Cluzel et al., 2001). The end of obduction is constrained by postobduction plutons intruded into the Peridotite Nappe and its autochthonous basement. Ages of 27.5 and 24 Ma were obtained through U-Pb dating of magmatic zircons of these postobduction granitoids (Paquette and Cluzel, 2007).

Extensive geochemical analysis by Ulrich et al. (2010) suggested that the mantle section of the Peridotite Nappe underwent two melting stages. The Peridotite Nappe consists of highly depleted harzburgites with U-shaped bulk-rock rare-earth element patterns, indicative of a forearc environment. However, lherzolites are enriched with spoon-shaped light rare earth elements and melts from these lherzolites are geochemically similar to some of the mid-ocean ridge basalts from the underlying Poya Terrane that were offscraped from the oceanic crust that subducted below the Peridotite Nappe prior to its obduction. Therefore, it is inferred that the Peridotite Nappe formed in the same oceanic basin as the Poya Terrane (Ulrich et al., 2010). A second melting stage in a forearc environment led to the ultradepletion of harzburgites that now form the bulk of the nappe. The geochemical signature of the Peridotite Nappe and overlying gabbro-norite cumulates are indicative of a suprasubduction zone history (Marchesi et al., 2009; Ulrich et al., 2010).

4.2.3. D'Entrecasteaux zone

The D'Entrecasteaux zone is an arch-shaped ridge connecting northern New Caledonia to central New Hebrides and its northeastern extension is currently subducting along the New Hebrides Trench (Figure 2). The ridge separates D'Entrecasteaux Basin to the northwest

from North Loyalty Basin to the southeast. Bougainville Guyot is a seamount located at the eastern end of the South D'Entrecasteaux chain. The oldest rock dredged from this guyot is a volcanic breccia of Middle Eocene age (42–40 Ma), based on age determination from planktonic nanofossil content in the chalky matrix (Collot et al., 1992). K/Ar dating of volcanic rocks of the guyot yielded an age of 37 ± 0.1 Ma (Baker et al., 1994). Extensive geochemical analysis indicate an island arc tholeiite signature, with a negative Nb anomaly indicative of subduction-related magmatism (Baker et al., 1994). Based on these data, the D'Entrecasteaux zone is generally viewed as an Eocene island arc and the northward, intraoceanic, continuation of Loyalty Ridge (Crawford et al., 2003).

4.2.4. Loyalty Ridge

Seismic reflection and swath bathymetry data indicate that Loyalty Ridge is composed of spaced seamounts that are covered by a thick carbonate layer (Cluzel et al., 2012a; Lafoy et al., 1996). The size and spacing (~70 km, Eissen et al., 1998) of the seamounts are typical of an island arc, but due to lack of basement outcrop the geology of the ridge is still poorly known (Cluzel et al., 2012a; Lafoy et al., 1996). Despite the lack of data, most authors consider Loyalty Ridge to be an Eocene Island arc (e.g., Baker et al., 1994; Cluzel et al., 2001; Crawford et al., 2003; Maillet et al., 1983; Paquette and Cluzel, 2007; Schellart et al., 2006), partly based on continuity of the submarine structure and evidence from the Bougainville guyot as described above.

4.2.5. Three Kings Ridge

Three Kings Ridge is considered to represent a remnant of a volcanic arc, but both west-facing (e.g., Kroenke and Eade, 1982) and east-facing (e.g., Davey, 1982) arcs have been proposed. More recent work based on forearc boninites dredged to the immediate west of Three Kings Ridge suggests that it was the volcanic arc above an east-dipping subduction zone. $^{40}\text{Ar}/^{39}\text{Ar}$ ages between 37 and 30 Ma were obtained from plagioclase separates of these dredge samples (Bernardel et al., 2002). The 37 Ma boninite is interpreted to mark the start of subduction along Three Kings Ridge (Whattam et al., 2006, 2008). A 26 Ma $^{40}\text{Ar}/^{39}\text{Ar}$ age of biotite in volcanic breccia recovered from the western slope of Three Kings Ridge (Mortimer et al., 1998) is interpreted to represent the last stages of east-dipping subduction (Whattam et al., 2006).

5. Reconstruction

5.1. Reconstruction protocol

We now integrate the geological constraints described above into our plate kinematic restoration, which we made in the freely available software package GPlates (www.gplates.org; Boyden et al., 2011). GPlates-format shape and rotation files that contain this restoration are available in the supporting information.

The reconstruction presented here provides relative plate motions in the southwest Pacific realm and is based purely on spreading directions and rates from published

interpreted marine magnetic anomaly data and fracture zone-transform fault directions. We adopt the reconstruction hierarchy of data types of Boschman et al. (2014). This hierarchy defines the order in which quantitative data types are used, from lowest to highest levels of uncertainty. This reconstruction consists of the following two data types in decreasing order of certainty:

1. Ocean basin restorations. Magnetic anomaly data and transform faults/fracture zones provide the best constraints on relative plate motions. Spacing of magnetic anomalies quantifies the amount of movement and the direction of movement is quantified by the orientation of fracture zones.
2. Additional geological data, used in the following order: continental extension records, strike-slip faults, continental shortening records, and paleomagnetism. Dredge samples are used to identify offshore crustal type. Paleomagnetic analysis is used for rotations of continents that cannot be defined by magnetic anomalies. Rock samples that are dated by radiometric methods are used to obtain crustal ages of lithosphere that lacks magnetic anomalies.

The bulk of this reconstruction is based on ocean basin restorations from published magnetic anomaly and transform faults/fracture zone data. Geological data are only used for areas where magnetic anomaly data are not available, for example, for the Alpine Fault history of New Zealand and the New Caledonia subduction zone. Ages of marine magnetic anomalies are based on the timescale of Ogg (2012).

The Antarctic circuit as described in section 2 is used as a starting point for our SW Pacific reconstruction. Plate motions between the five major tectonic plates (AUS, eANT, wANT, PAC, and LHR) in the Antarctic circuit are based on previously published rotation poles (Table 1) most of which are used in the global plate model of Müller et al. (2016). All plate motions east of LHR are based on the geological and kinematic constraints described in section 4 (see Table 2 for plate names and IDs). We use previously published finite rotation poles where possible. A few rotations are computed within GPlates, about which our choices are explained in section 4.2.

5.2. Tectonic model of the Southwest Pacific

A summary of the reconstruction is found in Table 3 and snapshots at selected times are provided in Figure 10. Time slices are chosen based on proposed or observed important events in the SW Pacific kinematic history. At the start of our reconstruction (83 Ma) the five major tectonic plates (AUS, eANT, wANT, LHR, and PAC) were still assembled, but Gondwanaland breakup had commenced. Australia had started moving away from Antarctica around 90 Ma, but spreading was still very slow (Tikku and Cande, 1999, 2000; Whittaker et al., 2007, 2013; Williams et al., 2011). Also, some extension has taken place in the West Antarctic Rift system (Matthews et al., 2015; Spiegel et al., 2016).

Based on the finite rotation poles of Wright et al. (2015, 2016), there is an overlap between Campbell Plateau and the Marie Byrd Land sector of Antarctica. Because we put

the unconstrained boundary between PAC and LHR between Challenger Plateau and LHR, the poles of Wright et al. (2015, 2016) also cause an overlap between Challenger Plateau and LHR. With spreading along Tasman Ridge and Pacific-Antarctic Ridge since 83.6 Ma, the overlap between Challenger Plateau and LHR is removed by a short transtensional phase (83.6–80 Ma). The transtensional phase is also predicted by Gaina et al. (1998) and Van de Beuque et al. (2003).

Following the age interpretation of Lafoy et al. (2005), extension is adopted in Fairway-Aotea Basin and New Caledonia Basin between 85 and 56 Ma. Based on the 30% crustal thinning estimated for the Fairway Basin (Lafoy et al., 2005; Wood and Woodward, 2002), we speculatively use a total of 50% extension in the combined Fairway-Aotea and New Caledonia basins.

Based on the 56 Ma age of the metamorphic sole of the ophiolite (Cluzel et al., 2012b), we infer that northeast-directed subduction along the New Caledonia subduction zone started at 60 Ma (Figure 10). This age corresponds to a change in Australia absolute plate motion from north to east-northeast (using the global moving hot spot reference frame of Doubrovine et al., 2012), changing relative plate motion between Pacific and Norfolk Ridge from strike-slip to convergent.

Subduction along the New Caledonia Trench led to back-arc extension in the North Loyalty Basin between 44 and 35 Ma. We used the finite rotation poles of Sdrolias et al. (2003) for the opening of this basin and restored the northern part of the basin (i.e., D'Entrecasteaux zone) relative to the southern part of the basin. This leads to northwestwards directed trench rollback and arc-parallel extension at Loyalty Arc in the reconstruction, which is also predicted by the tectonic model of Sdrolias et al. (2003). Subduction along the New Caledonia Trench ended with final obduction of the New Caledonia ophiolite at around 30–25 Ma (Paquette and Cluzel, 2007). Slab break-off is thought to have occurred around 25 Ma in the New Caledonia, Three Kings Ridge and Northland regions (Schellart, 2007; Schellart et al., 2009; Sevin et al., 2014). A 30-Ma age for the end of New Caledonia subduction is incorporated in our model.

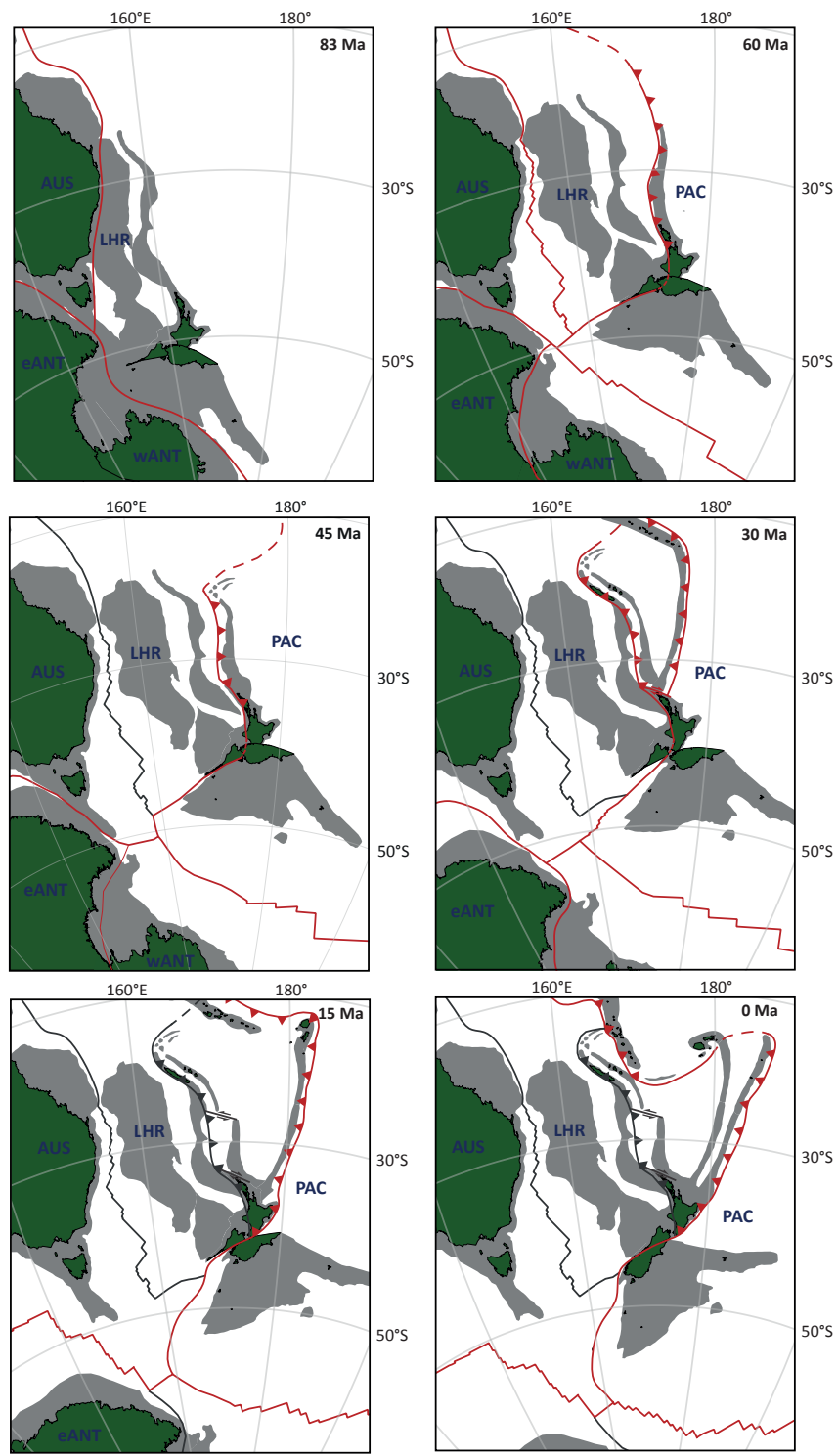
Subduction at the New Caledonia Trench consumed the South Loyalty Basin. The geometry of the South Loyalty Basin is modeled by assuming that the basin was part of PAC until New Caledonia was partially subducted. This means that in our Gplates plate circuit the Three Kings Ridge is attached to PAC until 60 Ma, as Three Kings Ridge forms the plate boundary between PAC and South Loyalty Basin during subduction at New Caledonia subduction zone. Subduction at the New Caledonia subduction zone is subsequently modeled to have occurred at a constant rate from the position of Three Kings Ridge at 60 Ma until the arrival of the Norfolk Ridge at 30 Ma (Figure 10).

During the final stages of obduction at the New Caledonia subduction zone, extension commenced in South Fiji Basin (~28 Ma, Herzer et al., 2011) and Norfolk Basin (~24 Ma, Sdrolias et al., 2004a). Opening of South Fiji Basin is modeled using finite rotations of Sdrolias et al. (2003), using the reinterpreted ages of Herzer et al. (2011). Opening of the

Table 3. Summary of constraints and amount of motion predicted by our model

Timing	Observation	Type of data used	References	Amount of motion predicted by our model
83.6–52.0 Ma	Tasman Sea spreading	Magnetic anomalies, fracture zone data	Gaina et al. (1998); Seton et al. (2012)	Ranging from 800 km in the northernmost Tasman Sea to 1,200 km in the southernmost Tasman Sea
83.6 Ma to present	Southeast Indian Ridge spreading	Magnetic anomalies, fracture zone data, continent-ocean boundary constraints	Cande and Stock (2004a); Whittaker et al. (2013)	3,000 km
83.6 Ma to present	Pacific-Antarctic Ridge spreading	Magnetic anomalies, fracture zone data	Croon et al. (2008); Wright et al. (2015, 2016)	Ranging from 1,500 km in the west to 1,900 km in the east northeast-southwest extension between 83.6 and 45 Ma, and an additional 1,500 km to 2,200 km northwest-southeast extension between 45 Ma and present
100–26.3 Ma	West Antarctic Rift system extension	Magnetic anomalies, fracture zone data	Cande and Stock (2004a); Granot et al. (2013a); Matthews et al. (2015)	100 km
83.6–56.0 Ma	Extension in Fairway-Aotea and New Caledonia Basins	Bathymetry, magnetic anomalies, gravity data and multichannel seismics	Wood and Woodward (2002); Lafoy et al. (2005); This study	160 km
63.0–52.0 Ma	Coral Sea spreading	Magnetic anomalies, fracture zone data	Gaina et al. (1999)	Ranging from 330 km in the west to 500 km in the east
60.0–30.0 Ma	New Caledonia subduction	Geologic data of the New Caledonia ophiolite (metamorphic sole and postobduction plutons)	Paquette and Cluzel (2007); Schellart (2007); Schellart et al. (2009); Cluzel et al. (2012b); This study	Ranging from 670 km at the northernmost part of the subduction zone to 300 km in the south

Timing	Observation	Type of data used	References	Amount of motion predicted by our model
43.4–35.0 Ma	Back-arc extension in North Loyalty Basin	Magnetic anomalies, fracture zone data	Sdrolias et al. (2003)	750 km
40.0–24.0 Ma	Macquarie Ridge Spreading	Magnetic anomalies, fracture zone data	Keller (2004)	Ranging from 550 km in the west to 250 km east, followed by 600 km dextral strike-slip motion since 24 Ma.
45.0 to 30.0 Ma to present	Tonga-Kermadec subduction	Kinematic reconstruction	This study	Total amount of subduction until present day ranges from 1,700 km in the south to 3,500 km in the north
27.4–15.0 Ma	Back-arc extension in South Fiji Basin	Magnetic anomalies, fracture zone data, Ar/Ar dating of dredge samples	Sdrolias et al. (2003); Mortimer et al. (2007); Herzer et al. (2009, 2011)	Ranging from 950 km in the northernmost South Fiji Basin to 350 km in the southernmost South Fiji Basin
24.0–15.0 Ma	Back-arc extension in Norfolk Basin	Fracture zone data, bathymetry, Ar/Ar dating of dredge samples.	Sdrolias et al. (2004a); Mortimer et al. (2007); Herzer et al. (2009, 2011); This study	270 km in the north and 170 km in the south of Norfolk Basin
10.0 Ma to present	New Hebrides subduction	Geological data	Crawford et al. (2003)	Total amount of subduction ranges from 400 km at the northern end of the subduction zone to 1,000 km at the southern end.
10.0 Ma to present	Spreading in North Fiji Basin	Magnetic anomalies, fracture zone data	Yan and Kroenke (1993)	Ranging from 400 km in the northwest to 1,000 km in the southeast of North Fiji Basin
10.0–3.0 Ma	Counterclockwise rotation of Fiji	Paleomagnetism	Taylor et al. (2000)	135° degree of counterclockwise rotation
7.0 Ma to present	Back-arc extension in Lau Basin	Magnetic anomalies	Yan and Kroenke (1993)	Ranging from 500 km in the north to 200 km in the south of Lau Basin



◀ **Figure 10.** Paleogeographic snapshots of the kinematic reconstruction at selected time slices in an Australia fixed frame. 83 Ma: Start of the reconstruction; 60 Ma: start of New Caledonia subduction; 45 Ma: oldest possible, and frequently mentioned, age of Tonga-Kermadec subduction zone; 30 Ma: end of New Caledonia subduction, youngest possible age of Tonga-Kermadec subduction zone initiation and start of Norfolk and South Fiji Basin back-arc spreading; and 15 Ma: end of Norfolk and South Fiji Basin back-arc spreading.

South Fiji Basin occurred in a back-arc setting to the Tonga-Kermadec subduction zone, where subduction had initiated by that time.

Spreading in Norfolk Basin was concurrent with spreading in South Fiji Basin and resulted in eastward migration of Three Kings Ridge. We restore Three Kings Ridge back to its original position by lining it up with the present-day position of Loyalty Ridge, along strike of the Cook Fracture Zone. This results in a 270-km southeastwards displacement of northern Three Kings Ridge between 24 and 15 Ma. Some 170 km of extension is predicted in southern Norfolk basin, and transpressive motion occurs on the Vening Meinesz Fracture Zone, which is in agreement with Herzer and Mascle (1996).

The 15 Ma end of extension in both basins is based on age interpretations of Mortimer et al. (2007) and Herzer et al. (2009, 2011). The rollback of the Lau-Colville Ridge associated with concurrent back-arc spreading in Norfolk and South Fiji basins is estimated to be about 500 km at the southern Colville Ridge and up to 700 km at the northern Lau Ridge.

The Ontong Java Plateau arrived at the Vitiaz Trench during the Early to Middle Miocene, resulting in a subduction polarity reversal (Auzende et al., 1995; Knesel et al., 2008; Petterson et al., 1997; Quarles van Ufford and Cloos, 2005). This led to spreading in North Fiji Basin from 10 Ma, clockwise rotation of New Hebrides arc (Yan and Kroenke, 1993) and anticlockwise rotation of the Fiji Plateau (Taylor et al., 2000).

Soon after 7 Ma, the Lau Basin-Havre Trough back-arc basin started opening (Ruellan et al., 2003), which led to splitting of the Tonga-Kermadec Ridge from the Lau-Colville Ridge. Extension in the Lau Basin is reconstructed using the finite rotation poles of Yan and Kroenke (1993). Motion in Havre Trough is reconstructed by closing the basin at 7 Ma and aligning the Kermadec Ridge with the position of the Tonga Ridge at that time. Constant spreading since 7 Ma is assumed, which leads to a good fit with the reconstructed motion of the southern end of the Tonga Ridge.

Rollback of Tonga Ridge since 7 Ma occurred in a clockwise fashion, which means that the amount of rollback is greatest in the north. There the amount of rollback exceeds 550 km, while it is only about 250 km at the southern Tonga Ridge. Rollback of the Kermadec Ridge, on the contrary, is reconstructed to have occurred parallel to Colville Ridge, with approximately 230 km of rollback along the entire length of the ridge.

Altogether, SW Pacific underwent several stages of basin opening and southeastward-directed trench rollback since 28 Ma. Our reconstruction predicts a total amount of trench rollback of approximately 1,300 km at the northern end of the subduction system, decreasing southwards to about 700 km just northeast of North Island, New Zealand.

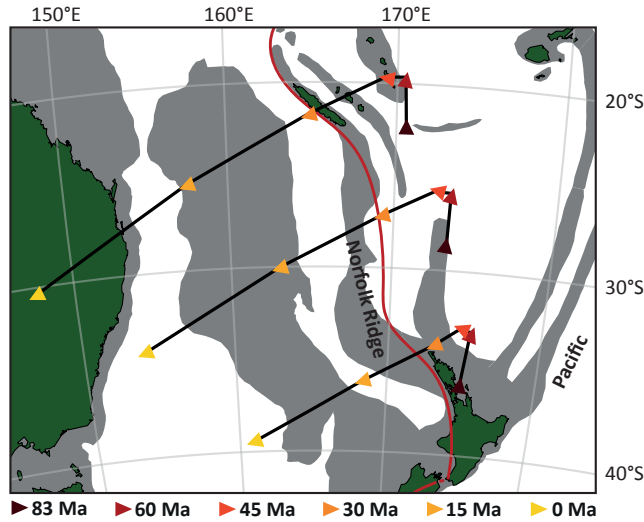


Figure 11. 83 Ma - Present day motion paths of three points on the Pacific plate relative to Norfolk Ridge, yielding maximum convergence during opening of the Tasman Sea between 83 and 52 Ma. Between 83 and 45 Ma, there is only minor relative plate motion. Around 45 Ma, there is a sharp increase in overall convergence, whereby convergence rates are less in the south than in the north.

5.3. Pacific-Norfolk Ridge convergence

Based on our choice of the Antarctic plate circuit and its associated finite rotations, our reconstruction yields a prediction of the amount of convergence between Pacific plate and Norfolk Ridge. Norfolk Ridge is chosen as a reference, as it is the most easterly element that moves independent of Australia until the Late Oligocene back-arc spreading in Norfolk and South Fiji basins started. Therefore, relative motion between Pacific plate and Norfolk Ridge yields the maximum amount of convergence.

Before onset of subduction at the New Caledonia trench (60 Ma), motion between Pacific plate and Norfolk Ridge is mainly strike-slip (Figure 11). Relative motion between 83 and 60 Ma is mainly left lateral, except for an interval between 72 and 65 Ma, when motion is right lateral with a divergent component. At 60 Ma, the relative motion becomes convergent, but this motion remains small (Figure 11). Between 60 and 51 Ma the total amount of net convergence along Norfolk Ridge is estimated to be about 100 km, which corresponds to an average convergence rate of ~14 mm/year. Between 51 and 45 Ma, relative motion is again predicted to be mainly left-lateral strike slip, with a diverging component southward of 30°S.

At 45 Ma, absolute Pacific plate motion changed from north-northeast to northwest, which caused rapid convergent motion between the Pacific plate and Norfolk Ridge (Figure 11), by this time part of the Australian plate. Since 45 Ma, relative Pacific-Australian plate motion has been fairly constant in both direction and rate. Relative motion has been directed mainly west to southwestwards, with a small interval between 34 and 30 Ma of more south to

southeastwards directed motion at southern latitudes (south of $\sim 30^\circ\text{S}$). Rate of convergence increased at 26 Ma from an average of ~ 30 mm/year between 45 and 26 Ma (~ 575 km in 19 Myr, latitude 20°S to 22°S), to an average of ~ 68 mm/year since 26 Ma ($\sim 1,775$ km in 26 Myr, latitude 22°S to 28°S). From 60 Ma onwards, our plate circuit predicts a total amount of Pacific-Norfolk Ridge convergence of $\sim 3,000$ km at the northernmost end of the Tonga-Kermadec subduction system and $\sim 1,500$ km at the southern end. Convergence estimates since 30 Ma are $\sim 2,200$ km and $\sim 1,000$ km for the northern and southern ends of the Tonga-Kermadec Trench, respectively. This means that, including trench-rollback of the Lau-Colville and Tonga-Kermadec ridges, a total of at least 3,500 and 1,700 km of subduction are predicted for the northern and southern ends of the Tonga-Kermadec Trench, respectively.

6. Discussion

6.1. South Loyalty Basin extension and implications for Tonga-Kermadec Trench evolution

For analysis of the onset of subduction along the Tonga-Kermadec Trench, the history of the oceanic lithosphere consumed by the New Caledonia subduction zone, referred to as South Loyalty Basin oceanic lithosphere (e.g., Cluzel et al., 2001; Cluzel et al., 2012b; Matthews et al., 2015; Schellart et al., 2006), is of importance. The opening history of this basin needs to be discussed as it may have influenced evolution of the Tonga-Kermadec Trench. We acknowledge that the age and geodynamic context of spreading within the inferred South Loyalty Basin is uncertain. Small relics of the South Loyalty Basin occur in the small basin nestled between Grande Terre and Loyalty Islands (Figure 2), and data from this basin are scarce. The only direct observations come from the Poya Terrane that was accreted below the New Caledonia ophiolite. Poya Terrane rocks are thought to have once floored South Loyalty Basin (e.g., Cluzel et al., 2001; Cluzel et al., 2012b).

The occurrence of radiolarian faunas in pelagic red chert and siliceous siltstone interbedded with Poya Terrane basalt (Cluzel et al., 2001) has led many authors to assume a Late Cretaceous to earliest Eocene (85–55 Ma) opening history of South Loyalty Basin (e.g., Matthews et al., 2015; Schellart et al., 2006). On the other hand, based on geodynamic modeling combined with geological and geophysical observations, Matthews et al. (2011) postulated that the Panthalassic Trench during the Mesozoic was likely located approximately 1,000 km east of the eastern Gondwana margin. They thus implied that South Loyalty Basin would have been in a back-arc position at that time, consistent with the geochemical fingerprint of some of Poya basalt as back-arc basin tholeiite (Cluzel et al., 2001; Eissen et al., 1998) and would have had an age of 140–120 Ma. This basin would then have opened during rollback of the southwest Panthalassa subduction zone that consumed the Phoenix plate (Matthews et al., 2012; Seton et al., 2012).

Opening of South Loyalty Basin is not included in our reconstruction due to an absence of direct kinematic constraints. However, its opening history has significant implications

for tectonic history of the SW Pacific region and evolution of the Tonga-Kermadec Trench. Two timeframes for opening of this basin has led to two different models of SW Pacific tectonic evolution.

If we assume for the moment that South Loyalty Basin opened between 140 and 120 Ma as a back-arc basin to the southwest Panthalassic Trench, it would have opened above the long-lived subduction zone that must have existed along the eastern margin of Gondwana and consumed Phoenix plate's oceanic crust beneath Panthalassa Ocean (Matthews et al., 2012; Seton et al., 2012). Competing models for the timing of subduction cessation exist, and both 105 and 100 Ma (e.g., Davy et al., 2008; Matthews et al., 2012; Sutherland and Hollis, 2001) and 86- to 80-Ma ages have been inferred (e.g., Seton et al., 2012; Worthington et al., 2006). Both suggested timeframes for cessation of subduction allow opening of South Loyalty Basin as a back-arc basin to the Panthalassic Trench between 140 and 120 Ma. In this scenario no subduction zone is required by the plate circuit or the geological record of the SW Pacific region between the cessation of subduction (sometime between 105 and 80 Ma) and onset of New Caledonia subduction around 60 Ma. In this case, there is no reason to assume that the Tonga-Kermadec Trench was active during the Early Cenozoic.

The alternative, in which South Loyalty Basin opened between 85 and 60 Ma, would allow a scenario where its spreading ridge became inverted around 60 Ma to form the New Caledonia Trench. Schellart et al. (2006) estimated that the South Loyalty Basin had a minimum east-west width of 750 km. In the absence of net PAC-LHR convergence, opening of South Loyalty Basin would require subduction of PAC and rollback of its trench over the 750 km width of the South Loyalty Basin, which, logically, would be accommodated along the former Panthalassic Trench (e.g., Cluzel et al., 2012a; Schellart et al., 2006; Ulrich et al., 2010).

There is no geological evidence for any significant extension in the SW Pacific region between 60 and 30 Ma, and there was barely any plate convergence until 45 Ma. What little plate convergence did occur between the ~60-Ma initiation of subduction recorded by the New Caledonia ophiolite and the 45 Ma onset of significant Pacific-Australia convergence must have been accommodated along the New Caledonia Trench. If there had been subduction at the former Panthalassic Trench until 60 Ma, we consider it most likely that the slab broke off at 60 Ma and subduction restarted at a later date. Seismic tomographic images reveal anomalies in the mantle deeper than the Tonga-Kermadec slab below the SW Pacific and Australian regions that likely represent subducted Phoenix plate lithosphere, but these have not been interpreted in detail given general lack of field observations of geological records associated with Mesozoic Phoenix subduction north of New Zealand (Van der Meer et al., 2018).

In summary, in both scenarios of opening of South Loyalty Basin, it is very unlikely that the current Tonga-Kermadec Trench has been continuously active since the Cretaceous. In the 140- to 120-Ma opening scenario, subduction ceased before 80 Ma (e.g., Seton et al., 2012). In the 85- to 60-Ma opening scenario subduction continued, entirely driven by

rollback in absence of plate convergence (Matthews et al., 2015; this study), followed by stagnation of subduction and slab break-off. We therefore consider scenarios inferring the occurrence of subduction at the Tonga-Kermadec Trench throughout the Late Cretaceous to Paleogene (e.g., Schellart et al., 2006) as unlikely. The present extent of slab subducted at the Tonga-Kermadec Trench must date from subduction initiation during the Cenozoic.

6.2. Age of Tonga-Kermadec subduction initiation versus New Caledonia subduction termination

We now combine our kinematic reconstruction with seismic tomographic constraints on mantle structure to estimate the age of initiation of subduction at the Tonga-Kermadec Trench as a function of evolution of the New Caledonia Trench.

In our reconstruction, the amount of Pacific-Norfolk ridge convergence before 45 Ma is minimal (~100 km between 60 and 45 Ma, which is within typical uncertainties of marine magnetic anomaly reconstructions). We consider it unlikely that this small amount of convergence was partitioned between two subduction zones. Recently, Sutherland et al. (2017) suggested that thrusting inferred from seismic sections from the Tasman Sea (Reinga Basin, Lord Howe Rise, New Caledonia Trough and Tasman Abyssal Plain) and dated 53–48 Ma resulted from subduction initiation at the Tonga-Kermadec Trench, assuming that initiation there occurred simultaneously with subduction initiation below the Philippine Sea Plate at the Marianas Trench. Such Eocene shortening was also reported from Fairway Basin located west of New Caledonia (Rouillard et al., 2017). Both Lord Howe Rise and Fairway Basin were part of the Australian plate, separated from the Tonga-Kermadec Trench by a plate boundary (the New Caledonia Trench) and from the Marianas Trench by another plate boundary (Melanesian Trench). Therefore, interpreting the shortening in Tasman Sea basins as an indication of subduction initiation along either trench (e.g., Rouillard et al., 2017; Sutherland et al., 2017) is not straightforward. This Eocene shortening may instead more likely reflect upper crustal processes emanating from the New Caledonia plate boundary and subduction there, or be related to termination of Australia plate subduction at Papua New Guinea and subsequent slab break-off following obduction (see Schellart and Spakman, 2015). Furthermore, the kinematic rationale why subduction initiation of the Pacific Plate beneath the Philippine Sea Plate at 52 Ma (e.g., Ishizuka et al., 2011a) should be contemporaneous with Pacific plate subduction below the Australia plate is unclear, particularly because Australia-Philippine Sea Plate motions are essentially unconstrained. As existence of the New Caledonia subduction zone since 60 Ma has been inferred from geological evidence, the maximum feasible age of the Tonga-Kermadec subduction zone is 45 Ma, corresponding to the onset of significant PAC-LHR convergence.

After the end of subduction at the New Caledonia Trench, all plate convergence must have been accommodated at the Tonga-Kermadec Trench. Schellart (2007) and Schellart et al. (2009) suggested a 30-Ma age for subduction cessation at New Caledonia and a 25-Ma age for final slab detachment (Sevin et al., 2014). This suggests that subduction at the

Tonga-Kermadec Trench started at earliest between 30 and 45 Ma.

During the existence of the New Caledonia subduction zone (60–30 Ma), our reconstruction predicts about 700, 450, and 225 km of Pacific-Norfolk Ridge convergence at New Caledonia, at northern Three Kings Ridge and at Northland, respectively (Figure 11). Based on seismic tomography, Schellart et al. (2009) interpreted the South Loyalty slab to contain 600–900 km of lithosphere. Our analysis of the UU-P07 tomographic model (Amaru, 2007) shows that the current anomaly has a length of about 300 km from bottom to top (Figure 7), but it may well have been thickened during its transition into the lower mantle (Schellart et al., 2009). Typical thickening factors of 2–3 for slabs in the upper 1,000 km of the lower mantle (Hafkenscheid et al., 2006; Van der Meer et al., 2018) bring our observation in line with the interpretation of Schellart et al. (2009). This means that the 700 km of 60- to 30-Ma Pacific-Norfolk Ridge convergence inferred from our reconstruction may have been completely accommodated at the New Caledonia subduction zone, which then consumed the entire, ~700 km E-W width of the South Loyalty Basin (Schellart et al., 2006).

Comparison of our kinematic reconstruction with constraints from seismic tomography thus implies that subduction at the Tonga-Kermadec Trench probably started as late as ~30 Ma. Subducted lithosphere volumes from seismic tomography are obviously subject to uncertainty and hence we cannot rule out occurrence of some subduction at the Tonga-Kermadec Trench between 45 and 30 Ma. Nonetheless, our study indicates that if Tonga-Kermadec subduction started sometime between 45 and 30 Ma, it accommodated no more than a few hundred kilometers of subduction. Even if the New Caledonia slab has not experienced any thickening, which is highly unlikely (Van der Meer et al., 2018), the Tonga-Kermadec subduction zone could only have accommodated the remaining 400 km of predicted convergence. The bulk of the present Tonga-Kermadec slab must therefore have formed after ~30 Ma. An implication is that back-arc spreading in Norfolk and South Fiji basins since 28 Ma occurred above the Tonga-Kermadec subduction zone.

Additional constraints on the timing and evolution of the New Caledonia and Tonga-Kermadec subduction zones comes from New Zealand, where both subduction zones terminate in the south, and its geological record also helps to constrain the age of initiation of these systems. Schellart et al. (2006) proposed that the southern end of the New Caledonia Subduction Zone lay immediately northeast of northern North Island from about 40 Ma and subsequently rolled back, leading to emplacement of Northland Allochthon during 25–21 Ma. While there are no data about which we are aware to constrain a 40-Ma age of subduction initiation northeast of Northland and a ~60 Ma initiation consistent with New Caledonia would hence be more likely, substantial Late Eocene-Early Oligocene shortening occurred in Reinga Basin and margins of New Caledonia Basin to the west of northern Northland (Bache et al., 2012). It is possible, therefore, that the shortening required from kinematic data to be expressed in the Northland region (225 km, see above) was partitioned across a wide area associated with the emplacement of Northland Allochthon—in part into

the southern end of the subduction zone and in part into continental crust immediately to the west beneath Reinga Basin. Taranaki Basin lies south of Reinga Basin and recent analysis shows that the Middle to Late Eocene-Early Oligocene sedimentary section beneath northern Taranaki Basin, including Taranaki Peninsula, accumulated in a foredeep, the subsidence having been caused by westward over-thrusting of basement on Taranaki Fault (Kamp et al., 2017). Thus, it appears that Eocene-Early Oligocene shortening expressed as

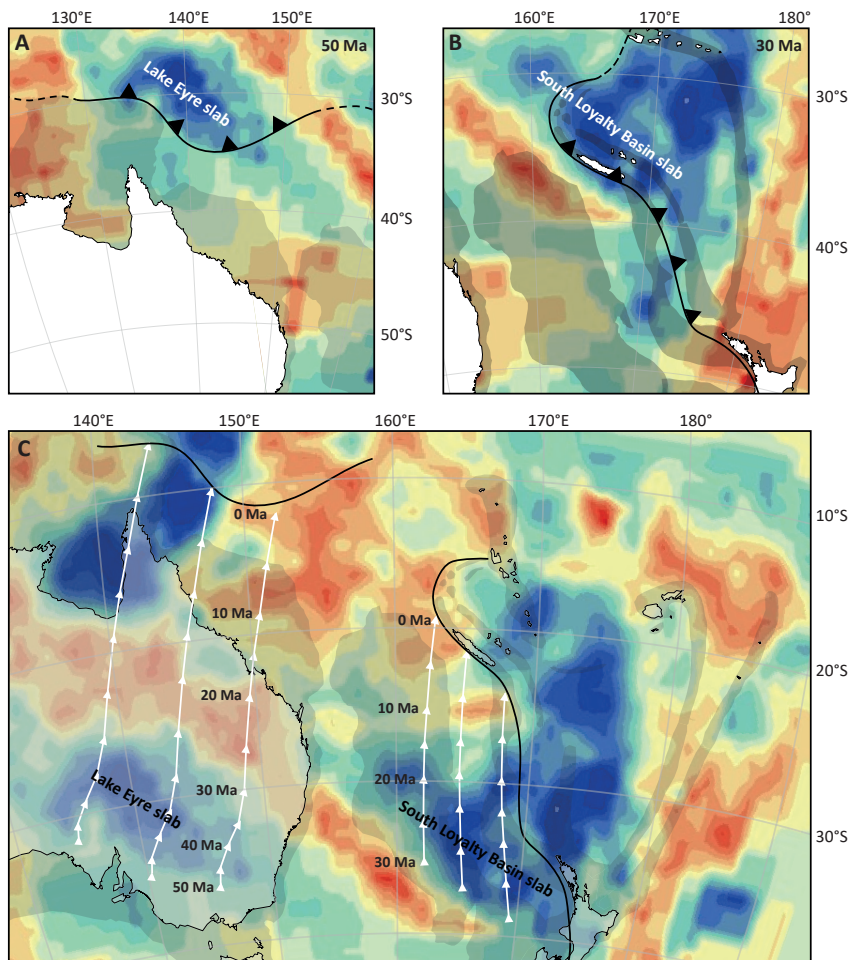


Figure 12. Reconstruction snapshots in the absolute plate motion frame of Doubrovine et al. (2012) and tomographic images at a depth of 1,050 km, based on the UU-P07 tomographic model (Amaru, 2007). The limits of the color scale used in this figure are the same as for Figure 5. The 1,050 km depth is selected as it reveals the extent of all three slabs very clearly. (a) Reconstructed location of the New Guinea-Pocklington subduction zone at 50 Ma above the Lake Eyre slab. (b) Reconstructed location of the New Caledonia subduction zone at 30 Ma above the South Loyalty Basin slab. (c) Present-day configuration of the SW Pacific. White lines indicate motion paths of the respective trenches relative to the mantle since inferred detachment of their associated slabs. White arrows indicate 5-Myr intervals.

subduction in the New Caledonia system transitioned into continental crust of northern New Zealand, initially via a zone of distributed deformation, before narrowing farther south into a paired thrust belt and foredeep in Taranaki Basin, where the shortening ended. The region south of Taranaki Peninsula, including South Island, lay south of the contemporary pole of rotation and hence Late Eocene-Early Oligocene plate boundary kinematics were manifest as continental rifting (Kamp, 1986; Furlong and Kamp, 2013) that then passed southward into Emerald Basin where seafloor spreading occurred during the Late Eocene-Oligocene (Keller, 2004).

The stratigraphy and structure of eastern North Island provide strong evidence for Early Miocene initiation of subduction along the Hikurangi Subduction Zone, which represents the southern part of the Tonga-Kermadec system. A comparatively thin (several hundred meters thick) Late Cretaceous and Paleogene succession, capped by Oligocene marl (Weber Formation), accumulated as bathyal deposits on a quiescent continental margin in eastern North Island (Field and Uruski, 1997). This sedimentation pattern changed dramatically during the Early Miocene with the emplacement of thrust sheets of the East Coast Allochthon (Stoneley, 1968) and with formation of localized basins (accretionary slope basins) in which thick (1–4 km) mud-dominated sequences accumulated (e.g., Field and Uruski, 1997; Mazengarb and Speden, 2000). The Early Miocene (23 Ma) initiation of subduction at the Hikurangi Margin is part of the development of a through-going Australia-Pacific plate boundary in New Zealand after about 23 Ma, including the Alpine Fault sector in South Island and the Puysegur subduction margin offshore to the southwest (Kamp, 1986; King, 2000; Sutherland, 1999). This 23-Ma timing of initiation of subduction at the Hikurangi margin constrains the minimum age of initiation of subduction along the southern Tonga-Kermadec system with which it is continuous.

6.3. Absolute plate and trench motion compared to tomography

We illustrate absolute plate motions in the SW Pacific region using the global moving hot spot reference frame of Doubrovine et al. (2012) and test the resulting positions of the reconstructed trenches against seismic tomographic constraints on slab locations. We compared the location of the New Caledonia subduction zone when subduction there ended at 30 Ma to the current location of the South Loyalty Basin slab in the mantle as identified by Schellart et al. (2009). Our reconstruction predicts a location of the New Caledonia subduction zone during slab detachment that corresponds very well to the present-day location of the slab. At 30 Ma the trench is located just south of the slab, consistent with north-east dipping subduction at the New Caledonia subduction zone (Figure 12). Since 30 Ma, the suture of the New Caledonia trench, including the associated ophiolites and extinct volcanic arc, moved ~1,400 km northwards relative to the mantle to its current location, leaving the detached slab behind in the mantle (Figure 12). This offset of the New Caledonia Ophiolite from the South Loyalty Basin slab is thus consistent with the absolute plate motion predictions of Doubrovine et al. (2012). Similarly, Schellart and Spakman

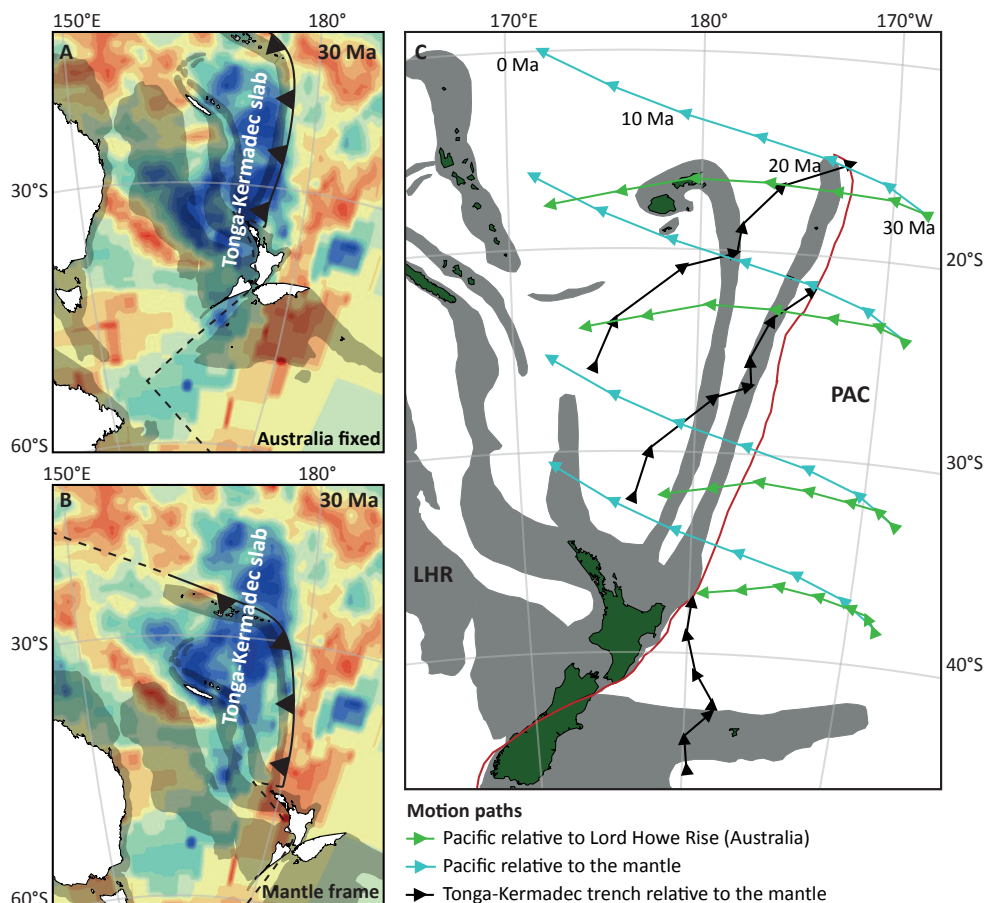


Figure 13. 30 Ma reconstruction in an (a) Australia-fixed reference frame and (b) mantle-reference frame, both with seismic tomographic images at 1,050 km depth, based on the UU-P07 tomographic model (Amaru, 2007). The limits of the color scale used in this figure are the same as for Figure 5. Whilst the image of Figure 13b shows the actual position of the Tonga-Kermadec Trench at 30 Ma, the fit between the tomography and the trench in Figure 13a is much better (see also Figure 6). This suggests that the Tonga-Kermadec slab must have moved northward through the mantle during its subduction history. This is illustrated in Figure 13c: Motion paths of Pacific plate relative to Lord Howe Rise (part of Australian plate; green), Pacific plate relative to the mantle (blue) and the Tonga-Kermadec Trench relative to the mantle (black) since 30 Ma (arrows in 5-Myr intervals) using the reconstruction shown in this paper placed in a mantle reference frame (Dobrovine et al., 2012).

(2015) showed that the Lake Eyre slab below southern Australia is also consistent with the predictions of the Dobrovine et al. (2012) global moving hot spot reference frame. In the same absolute motion frame, the Tonga-Kermadec analysis shows, however, no offset between the present-day trench and the associated anomaly imaged by seismic tomography because it is still attached to the Pacific plate. The entire slab is located to the west of the present-day trench along the full length of the trench (Figure 6). The location of the slab is

one that is to be expected when viewed in an Australia-fixed reference frame (Figure 13), or, by implication, the Tonga-Kermadec slab must essentially have shared all or a large part of the northward absolute plate motion component of the Australian and Pacific plates. Such a shared component is not evident at all in a local relative plate motion frame (Spakman et al., 2018) and puts a novel constraint on Pacific absolute plate motion independent of the data and assumptions that determined the GMHRF frame of Doubrovine et al. (2012).

6.4. Trench-parallel slab dragging component of Tonga-Kermadec subduction

The lack of offset between the Tonga-Kermadec Trench and the imaged deep portions of Pacific plate slab has important implications. Subduction at the Tonga-Kermadec Trench is the result of E-W (normal) convergence between Australia and Pacific plates. Concurrently, both plates underwent rapid (~ 7 cm/year) northwards absolute plate motion over the course of the 30 m.y. existence of the Tonga-Kermadec subduction zone. The northernmost part of the Tonga-Kermadec Trench thus moved $\sim 1,850$ km northeastwards relative to the mantle since 30 Ma, of which the northward absolute motion component was $\sim 1,200$ km. The southernmost Kermadec trench has moved $\sim 1,200$ km northward since 30 Ma. As seismic tomography reveals that the entire slab is located west (and not southwest or south) of the present-day trench, the slab, while subducting, must have been subjected to lateral dragging by the Pacific plate through the mantle, nearly parallel to the strike of the trench, by at least 1,200 km, along with northward motion of the trench (Figure 13). Even more spectacularly, seismic tomography suggests that slab dragging was not only restricted to the upper mantle, but that the portion of the slab located in the upper part of the lower mantle also shows no southward offset relative to the present-day trench (Figures 6 and 13).

The occurrence of slab dragging on such a large scale is a noteworthy discovery, especially considering the large volume of the slab and must result from the sum of dynamic processes forcing Pacific and Australian plate motions, in which northward motion at the edge of both plates plays an important role. The potential role of long-term slab-parallel mantle flow exerting viscous coupling to the slab can be limited as long as slab dragging by the Pacific plate occurred predominantly trench-parallel. A preliminary modeling study (Chertova et al., 2018) suggests that 25 Myr of slab-parallel upper and lower mantle flow of 3 cm/year may not have a very large effect on slab morphology, except for thickening of the slab edge on which the flow impacts, while if mantle flow is oblique to the slab larger slab deformation may occur such as strong out-of-plane deflections. The tomography image of the slab is too blurred to assess any slab morphology change due to internal deformation of the slab or to detect appreciable lateral shifts in lower mantle slab position of the order of a few hundred km. The observations from focal mechanisms of strong upper-mantle slab deformation made by Giardini and Woodhouse (1986) suggest, however, a significant effect of mantle resistance against slab dragging at least in the more recent evolution of subduction.

Our study shows that a very large slab that has penetrated the lower mantle has been

subjected to rapid slab dragging. In the case of this Tonga-Kermadec subduction zone, slab dragging may have been facilitated by interaction of the slab with the relatively hot mantle surrounding the Samoan plume, visible as the hot colors in tomographic images (Figure 7) below and east of the slab, that may have weakened the mantle regionally (Chang et al., 2016; Druken et al., 2014). Nevertheless, our study demonstrates that even at fast and long subduction zones, slabs may undergo trench-parallel absolute motion that must be far-field driven. Slab dragging alters the force balance of subduction via mantle resistance against lateral slab transport, which may lead to slab deformation, buildup of mantle seismic anisotropy and unexpected slab-plate interactions. Slab dragging and its effects on deformation of lithosphere opens new avenues for geodynamic and tectonic research (Chertova et al., 2014; Spakman et al., 2018).

7. Conclusions

We report here a kinematic reconstruction of the SW Pacific region for the Late Cretaceous to Present Day to estimate when Tonga-Kermadec subduction started and to study how the Tonga-Kermadec slab responded to a dominant component of northward absolute plate motion of the down-going Pacific plate that was partly shared by the overriding plates. Our conclusions are summarized as follows:

1. There was no demonstrable Pacific-Lord Howe Rise plate convergence between ~85 and 60 Ma. If subduction occurred at a Tonga-Kermadec Trench during this interval, it must have balanced divergence in South Loyalty Basin that is assumed by some to have opened during this period. If so, this subduction zone did not accommodate convergence between 60 Ma and ~30 Ma despite major absolute plate motion in this window and must thus have terminated at ~60 Ma by slab break-off. If, alternatively, South Loyalty Basin opened between 140 and 120 Ma, as has also been proposed, there is no reason to infer a subduction zone between the Pacific and Australian plates between ~85 and 60 Ma.
2. East-dipping New Caledonia subduction started at ~60 Ma. Subduction was initially very slow but rates increased markedly at ~45 Ma, leading to back-arc extension in North Loyalty Basin. South Loyalty Basin, which had an east-west width of approximately 750 km, was consumed by the New Caledonia subduction zone through to ~30 Ma, consistent with seismic tomographic constraints.
3. Subduction at the Tonga-Kermadec subduction zone started sometime between 45 and 30 Ma. A 30 Ma age of initiation of Tonga-Kermadec subduction is consistent with the results of seismic tomography of the subducted slabs of both the New Caledonia and Tonga-Kermadec subduction zones, but an older age up to 45 Ma cannot be excluded. However, if subduction initiated between 45 and 30 Ma, it was restricted to no more than a few hundred kilometers of slab subduction.
4. When viewed in an absolute plate motion frame, our reconstruction predicts the locations of the New Guinea-Pocklington and New Caledonia subduction zones

during their respective 50 Ma and 30 Ma slab detachments that correspond to the present-day location of their associated slabs. Absolute plate motions resulted in 2800 km and 1200 km of northward motion of the New Guinea-Pocklington and New Caledonia sutures relative to the present locations of the Lake Eyre and South Loyalty slabs in the mantle, respectively. This is in agreement with earlier findings by Schellart and coworkers. On the contrary, the Tonga-Kermadec slab, which is still attached to Pacific plate at the surface, does not show any southward offset related to the northward component of absolute plate motion.

5. Since the 30 Ma initiation of subduction, the entire Tonga-Kermadec slab, eventually including its lower-mantle portion, has been dragged laterally through the mantle by some 1,200 km to the north. The effects on slab deformation, mantle anisotropy, seismicity, and focal mechanism, as well as on surface deformation, require further investigation. Particularly, numerical modeling is required to distinguish between the trench-normal and trench-parallel components of slab dragging.



Perito Moreno Glacier, Patagonia

2

Subduction initiation in the Scotia Sea region and opening of the Drake Passage: When and why?

This chapter has been published as:

Van de Lagemaat, S. H. A., Swart, M. L., Vaes, B., Kusters, M. E., Boschman, L. M., Burton-Johnson, A., Bijl, P. K., Spakman, W. & Van Hinsbergen, D. J. J. (2021). Subduction initiation in the Scotia Sea region and opening of the Drake Passage: when and why? *Earth-Science Reviews* 215, 103551.

Abstract

During evolution of the South Sandwich subduction zone, which has consumed South American Plate oceanic lithosphere, somehow continental crust of both the South American and Antarctic plates have become incorporated into its upper plate. Continental fragments of both plates are currently separated by small oceanic basins in the upper plate above the South Sandwich subduction zone, in the Scotia Sea region, but how fragments of both continents became incorporated in the same upper plate remains enigmatic. Here we present an updated kinematic reconstruction of the Scotia Sea region using the latest published marine magnetic anomaly constraints, and place this in a South America-Africa-Antarctica plate circuit in which we take intracontinental deformation into account. We show that a change in marine magnetic anomaly orientation in the Weddell Sea requires that previously inferred initiation of subduction of South American oceanic crust of the northern Weddell Sea below the eastern margin of South Orkney Islands continental crust, then still attached to the Antarctic Peninsula, already occurred around 80 Ma. Subsequently, between ~71–50 Ma, we propose that the trench propagated northwards into South America by delamination of South American lithosphere: this resulted in the transfer of delaminated South American continental crust to the overriding plate of the South Sandwich subduction zone. We show that continental delamination may have been facilitated by absolute southward motion of South America that was resisted by South Sandwich slab dragging. Pre-drift extension preceding the oceanic Scotia Sea basins led around 50 Ma to opening of the Drake Passage, preconditioning the southern ocean for the Antarctic Circumpolar Current. This 50 Ma extension was concurrent with a strong change in absolute plate motion of the South American Plate that changed from S to WNW, leading to upper plate retreat relative to the more or less mantle stationary South Sandwich Trench that did not partake in the absolute plate motion change. While subduction continued, this mantle-stationary trench setting lasted until ~30 Ma, after which rollback started to contribute to back-arc extension. We find that roll-back and upper plate retreat have contributed more or less equally to the total amount of ~2000 km of extension accommodated in the Scotia Sea basins. We highlight that viewing tectonic motions in a context of absolute plate motion is key for identifying slab motion (e.g., rollback, trench-parallel slab dragging) and consequently mantle-forcing of geological processes.

1. Introduction

Subduction zones form during plate motion reorganizations, either by breaking a single plate into two independently moving plates, or by inverting a transform or ridge (e.g., Auzemery et al., 2020; Gurnis et al., 2004; Maffione et al., 2015; Stern, 2004). Interestingly, in the case of the South Sandwich subduction zone, which now forms an isolated trench in the South Atlantic Ocean, it is difficult to assess which of these mechanisms played a role. The overriding plate, to the west of the South Sandwich subduction zone, contains continental fragments that rifted from both the Antarctic Peninsula, part of the Antarctic

Plate, as well as from Tierra del Fuego (southern Patagonia), part of the South American Plate. These continental fragments are currently separated by small oceanic basins (Civile et al., 2012; Dalziel et al., 2013; Eagles and Livermore, 2002; Vuan et al., 2005). Interestingly, continental blocks derived from both the Antarctic and the South American Plate were part of the same upper plate, above the South Sandwich subduction zone. Since its formation, this subduction zone has been consuming South American oceanic lithosphere that formed the conjugate of the lithosphere underlying the Weddell Sea, which is part of the Antarctic Plate. Explaining the presence of Antarctica-derived lithospheric fragments in the upper plate of the South Sandwich subduction zone thus merely requires finding when the South American and Antarctic plates may have converged in the Drake Passage region (Figures 1 and 2). Different scenarios have been proposed to explain this (Barker, 2001; Dalziel et al., 2013; Eagles, 2016b; Lagabrielle et al., 2009; V  rard et al., 2012). What remains puzzling is that South American Plate fragments also ended up in the upper plate of the South Sandwich subduction zone.

In the search for causes of subduction initiation, previous studies have looked for evidence for convergence in the Drake Passage region. Two causes for subduction initiation have been proposed. The first is that westward motion of Tierra del Fuego relative to the Antarctic Peninsula led to the development of an active margin to the east of South Orkney Islands continental crust, then still part of the Antarctic Peninsula, and the westward subduction of oceanic crust of the South American Plate (Barker, 2001; Eagles and Jokat, 2014; Lagabrielle et al., 2009; V  rard et al., 2012). The proposed timing of this event varies from latest Cretaceous (~70 Ma; V  rard et al., 2012) to Eocene (~46 Ma; Lagabrielle et al., 2009; ~50 Ma; Eagles and Jokat, 2014). This does not explain, however, how South American oceanic lithosphere subduction below the Tierra del Fuego region began. The second hypothesis is that such subduction within South America may somehow be linked to the mid-Cretaceous closure of the South American Rocas Verdes Basin (Barker, 2001; Dalziel et al., 2013), unrelated to subduction below the Antarctic Peninsula.

The aim of this study is to develop a geodynamic scenario for the origin and evolution of the Scotia Sea that addresses: 1) when and why a subduction zone first formed between South America and the Antarctic Peninsula and 2) when and why this subduction zone may have propagated, or initiated, into the South American Plate, and how South American continental lithosphere transferred to the upper plate of the South Sandwich subduction zone. To this end, we have developed a kinematic restoration back to the time of Gondwana break-up embedded in a global plate reconstruction framework. We use a plate circuit through Africa, by restoring the opening of the South Atlantic and Southwest Indian oceans based on previously published marine geophysical constraints. We first restore the extensional history of the Scotia Sea recorded by the small oceanic basins using published marine magnetic anomaly data. Then, to assess the amount of pre-drift extension (i.e., the continental rifting phase before oceanic spreading), we use the plate circuit and published marine magnetic anomalies in the Weddell Sea ocean floor to approximate the location of

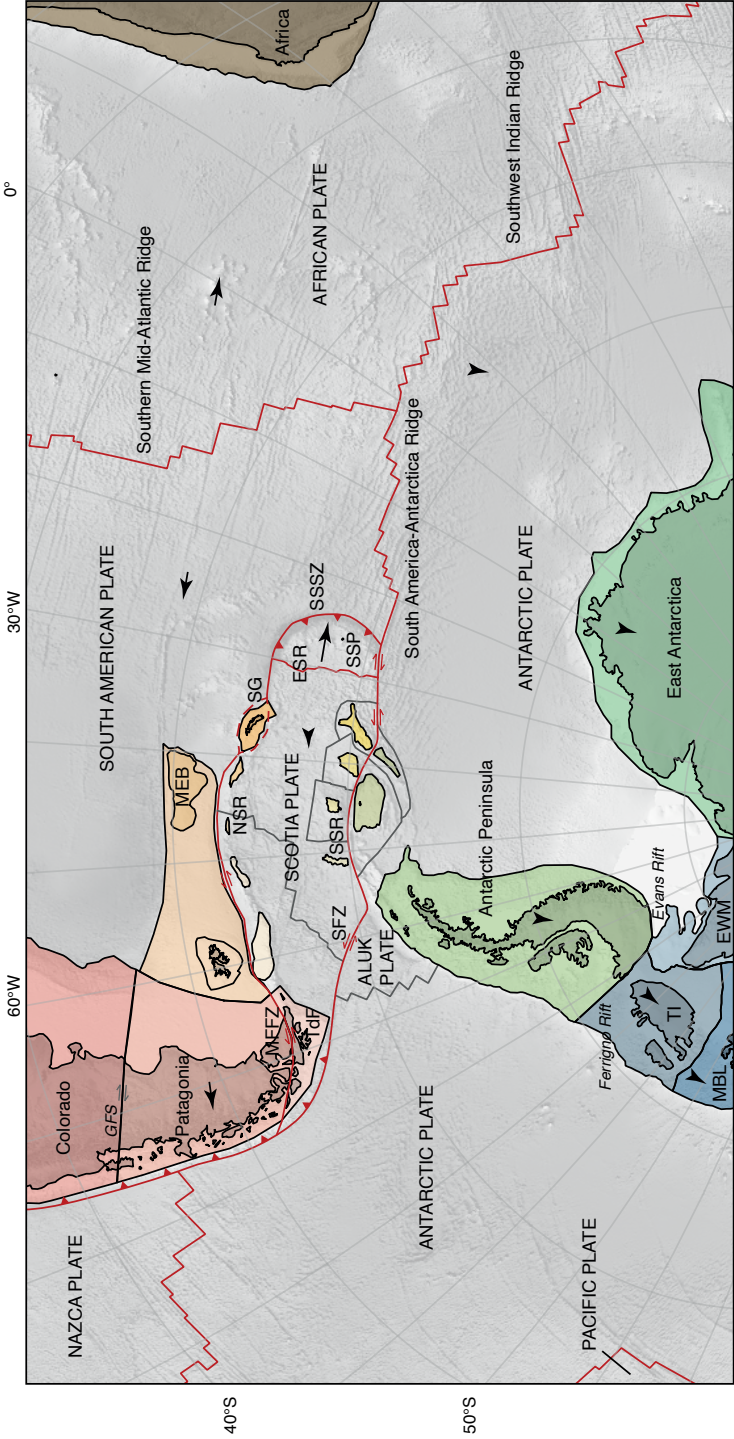


Figure 1 . Tectonic map of the Scotia Sea Region. The map shows the main faults, plate boundaries and tectonic blocks (colored polygons) discussed in this paper. Major plates are given in capital letters. Active plate boundaries are indicated with red lines. The plate boundary around South Georgia is dashed, as it is being transferred from the north to the south of the microcontinent (Smalley Jr. et al., 2019). Former plate boundaries of the Scotia Sea region in gray. Coastlines of West Antarctica tectonic blocks are based on present-day continental lithosphere that rises above sea-level. Black arrows represent plate motions relative to the mantle in the last 5 Myr in the reference frame of Doubrovine et al. (2012). Abbreviations: ESR = East Scotia Ridge; EWM = Ellsworth –Whitmore Mountains; NSR = North Scotia Ridge; SG = South Georgia; SSP = South Sandwich Ridge; SSSZ = South Sandwich subduction zone; TdF = Tierra del Fuego; TI = Thurston Island.

the South American ocean-continent transition to the Weddell Sea conjugate ocean floor. To assess the Antarctic Peninsula-Patagonia convergence in driving subduction initiation, we also correct for intracontinental deformation within South America and Antarctica and test this against a new compilation of paleomagnetic data. Based on our reconstruction, which we study in both relative and absolute plate motion context, we propose a new view on the timing and geodynamic forcing for the initiation and evolution of subduction, its propagation into the South American Plate, the transition to upper plate extension in the Scotia Sea region, and its subsequent evolution that led to opening of the Drake Passage.

2. Modern geological architecture of the Scotia Sea Region

The Scotia Sea is underlain by the Scotia and South Sandwich plates (Figure 1). Major tectonic plates that surround both plates are the South American Plate in the north and east and the Antarctic Plate in the south and west (Figure 1, Figure 2, Figure 3). To the southeast of the South Sandwich subduction zone, there is a short segment of the South American-Antarctica plate boundary that ends in a triple junction with the South America-Africa and Africa-Antarctica spreading ridges (Figure 1; Barker and Lawver, 1988; DeMets et al., 2010). In the Pacific Ocean to the west-northwest of the Scotia Sea, the South American and Antarctic plates are converging, which leads to the subduction of oceanic lithosphere of the Antarctic Plate below southern South America (Figure 1).

The Scotia Plate is separated from the South Sandwich Plate in the east by an active spreading ridge; from South America in the north by the left-lateral Magallanes-Fagnano and North Scotia Ridge transform system; from the small remnant of the Aluk (or Phoenix, or Drake) Plate in the west by the sinistral Shackleton fracture zone; and from Antarctica in the south by a diffuse plate boundary characterised by distributed left-lateral transpression (Figure 1) (Thomas et al., 2003). The South Sandwich Plate is separated from the South American Plate in the east by the South Sandwich trench, and from Antarctica in the south by a diffuse, dextral transform plate boundary (Thomas et al., 2003).

The Scotia Plate hosts three main oceanic basins characterised by different magnetic anomaly orientations: The East, Central, and West Scotia basins (Figure 3, Figure 4). Microcontinents, arc remnants, and intervening small oceanic basins to the south of the main Scotia Sea basins collectively form the South Scotia Ridge. These comprise, from east to west: 1) the Discovery Bank, separated by the Scan Basin from 2) the Bruce Bank, separated by the Dove Basin from 3) the Pirie Bank, separated by the Protector Basin from 4) the Terror Rise (Figure 3, Figure 4). The southernmost part of the Scotia Sea, along the diffuse plate boundary with Antarctica, hosts from east to west the Jane Bank separated by the Jane Basin from the South Orkney microcontinent, separated by the Powell Basin from the Antarctic Peninsula (Figure 3). Based on seismic data and dredge samples, Terror Rise and the Bruce and Pirie banks are considered to be underlain by extended continental crust (Eagles et al., 2006; Lodolo et al., 2010; Udintsev et al., 2012; Vuan et al., 2005). Dredging of the Discovery and Jane Banks have returned samples with a continental affinity (Lodolo et

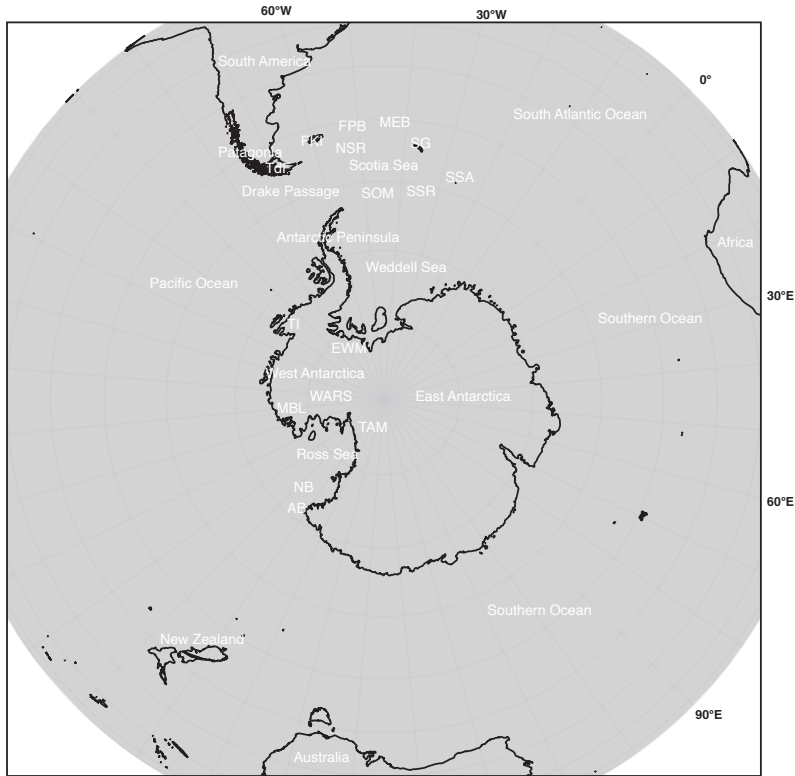


Figure 2. Geographic map of the Circum-Antarctic region. Abbreviations: AB = Adare Basin; EWM = Ellsworth-Whitmore Mountains; FKI = Falkland Islands; FPB = Falkland Plateau Basin; MEB = Maurice Ewing Bank; MBL = Marie Byrd Land; NB = Northern Basin; NSR = North Scotia Ridge; TdF = Tierra del Fuego; TI = Thurston Island; SG = South Georgia; SOM = South Orkney Microcontinent; SSR = South Scotia Ridge; WARS = West Antarctic Rift System.

al., 2010), as well as arc-type magmatic rocks of unknown age (Barker et al., 1984; Barker et al., 1982). The geology of South Orkney Islands shows that they consist of continental crust that likely formed in Paleozoic time by accretion at the Panthalassa margin (Matthews and Maling, 1967; Tanner et al., 1982). East of the Antarctic Peninsula and south of the South Scotia Ridge lies the Weddell Sea, with an ocean floor that is part of the Antarctic Plate (Figure 1, Figure 2, Figure 3).

The northern margin of the Scotia Plate is referred to as the North Scotia Ridge, comprising the Burdwood and Davis banks, Barker (previously named Aurora) Plateau, and Shag Rocks Bank, as well as the South Georgia microcontinent (Figure 3, Figure 4). Based on field investigations of South Georgia, and geochemistry and geochronology of dredge samples of the North Scotia Ridge banks, they are interpreted as continental fragments that share a geological affinity with the Fuegian Andes (Carter et al., 2014; Dalziel et al., 1975; Mukasa and Dalziel, 1996; Pandey et al., 2010; Riley et al., 2019; Storey and Mair, 1982;

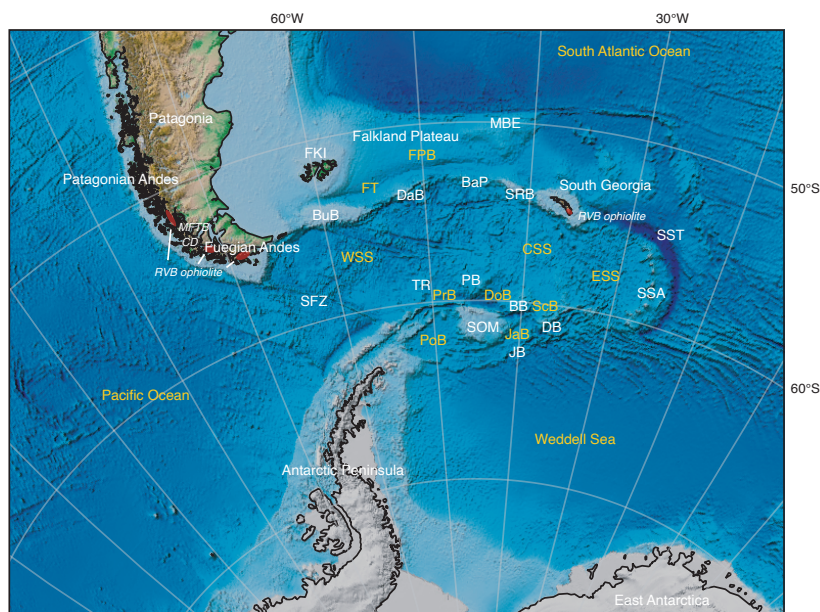
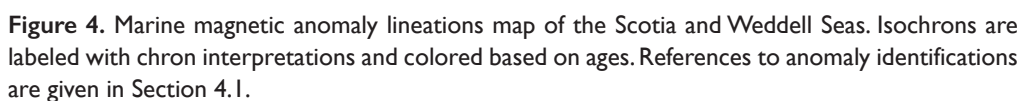


Figure 3. Geographic map of the Scotia Sea region. Basin names in yellow, abbreviations: CSS = Central Scotia Sea; DoB = Dove Basin; ESS = East Scotia Sea; FT = Falkland Trough; FPB = Falkland Plateau Basin; JaB = Jane Basin; PoB = Powell Basin; PrB = Protector Basin; ScB = Scan Basin; WSS = West Scotia Sea. Other names in white, abbreviations: BaP = Barker Plateau; BB = Bruce Bank; BuB = Burdwood Bank; CD = Cordillera Darwin; DaB = Davis Bank; DB = Discovery Bank; JB = Jane Bank; FKI = Falkland Islands; MBE = Maurice Ewing Bank; MFTB = Magallanes Fold-and-Thrust-Belt; PB = Pirie Bank; RVB = Rocas Verdes Basin; SFZ = Shackleton Fracture Zone; SRB = Shag Rocks Bank; SSA = South Sandwich Arc; SST = South Sandwich Trench; TR = Terror Rise.

Storey et al., 1977). The ridge is separated from the Falkland Plateau to the north by the Falkland Trough, a bathymetric depression that formed as part of the South American–Scotia transform plate boundary (Figure 1, Figure 3).

The Falkland Plateau, located east of Patagonia in the South Atlantic Ocean (Figure 2), forms a large promontory of extended South American crust (Ewing et al., 1971; Tankard et al., 2012). The Falkland Islands and Maurice Ewing Bank are emergent portions of the Falkland Plateau, underlain by continental crust (Schimschal and Jokat, 2019). They are separated from each other by the oceanic Falkland Plateau Basin (Schimschal and Jokat, 2018).

The transition from the N–S trending Patagonian Andes to the E–W trending Fuegoian Andes and Falkland Plateau (Figure 3) is known as the Patagonian Orocline (Carey, 1955). This region consists of five main geological provinces. From west to east, these are: 1) an Upper Jurassic – Miocene magmatic arc (Patagonian Batholith) related to (paleo-)Pacific subduction (Guillot, 2016; Herve et al., 2007; Hervé et al., 1984; Pankhurst et al., 2000); 2) thrust and uplifted, uppermost Jurassic to lowermost Cretaceous ocean floor volcanics and



68

1994a; Pelayo and Wiens, 1989; Smalley Jr. et al., 2007; Smalley Jr. et al., 2003).

Antarctica is characterised by two different crustal realms, separated by the Transantarctic Mountains (Goodge, 2020) (Figure 2). East Antarctica, facing the Atlantic and Indian Oceans, is a craton that formed during Precambrian and Cambrian times (Fitzsimons, 2000; Harley, 2003; Tingey, 1991). West Antarctica, facing the Pacific Ocean, comprises continental and arc crust of early Paleozoic age, divided into four major crustal blocks divided by fault or rift zones (Dalziel and Elliot, 1982; Gohl et al., 2007; Holt et al., 2006; Jordan et al., 2010): Thurston Island, Marie Byrd Land, Ellsworth-Whitmore Mountains, and the Antarctic Peninsula (Figure 1, Figure 2; Dalziel and Elliot, 1982). Deformation within West Antarctica formed intracontinental basins and transform zones, most prominently in the West Antarctic Rift System. This rift system is the deepest in the world (LeMasurier, 2008) and accommodated extension in Cretaceous to Cenozoic time (Granot and Dymant, 2018).

The Antarctic Peninsula, including the South Orkney microcontinent, evolved since the Late Paleozoic as a long-lived active continental margin related to (paleo-)Pacific subduction, and hosts a discontinuous record of Jurassic-Paleogene arc magmatism intruding continental rocks that were autochthonous to the Gondwana margin (Burton-Johnson and Riley, 2015; Jordan et al., 2020; Navarrete et al., 2019, and references therein). The western margin dominantly consists of convergent margin successions, including a Lower Jurassic to Lower Cretaceous accretionary complex (Doubleday et al., 1993; Suárez, 1976), overlain by an Upper Jurassic to mid-Cretaceous fore-arc succession (Butterworth et al., 1988). The eastern margin of the Antarctic Peninsula is characterised by Jurassic-Cretaceous magmatism, including the 188–153 Ma Chon Aike silicic Large Igneous Province (Pankhurst et al., 2000; Riley and Knight, 2001), and volcanic and sedimentary successions related to continental and ocean basin extension during Gondwana break-up (Hathway, 2000; Willan and Hunter, 2005). The mid-Cretaceous to Cenozoic geology of Antarctic Peninsula is characterised by subduction-related arc magmatism that ended before the Late Neogene, followed by extension-related Neogene to recent intraplate alkaline volcanic rocks (Burton-Johnson and Riley, 2015).

3. Approach

3.1. Methods

We review deformational records from Patagonia and the Antarctic Peninsula to build a geometrically consistent reconstruction using the freely available software package, GPlates (www.gplates.org; Boyden et al., 2011), based on published quantitative kinematic constraints. All reconstruction files are provided in the Supplementary Information (rotation files and shapefiles). We apply a reconstruction hierarchy for active margin reconstructions previously used for the Caribbean (Boschman et al., 2014), SW Pacific (Chapter 1), NW Pacific (Vaes et al., 2019), and Mediterranean regions (Van Hinsbergen et al., 2020a). This hierarchy ensures that the philosophy behind all regional reconstructions is identical

and can be integrated into a global model, and that reconstructions are reproducible and adaptable when new data become available. We only use input data that provide direct information on relative (plate) motion, with uncertainty increasing at every step of the hierarchy (Boschman et al., 2014; Van Hinsbergen et al., 2020a): first, extensional records are used, which are the most complete at the end of a tectonic event and thus provide the most reliable source of information for kinematic evolution. The primary data type used in our reconstruction is Euler rotations computed from marine magnetic anomalies and fracture zones. Our preferred data type thus comes from oceanic basins with active seafloor spreading. GPlates interpolates motion between constrained stages assuming constant rotation rate, thus allowing use of all available anomaly picks for the various ocean basins. Our reconstruction uses the timescale of Gradstein et al. (2012) that intercalibrated ages of the marine magnetic anomaly isochrons with biostratigraphy. Second, we use geological and geophysical data that allow estimating the timing and magnitude of rift records. These records are predominantly derived from intracontinental extensional settings but in some cases come from intra-oceanic rift settings. Third, intracontinental strike-slip and transform records are used. These accurately constrain the motion direction, but the amount of displacement may have higher uncertainty. Fourth, we use shortening records, which provide only a minimum estimate of convergence because part of the deformation record may be lost (e.g., Schepers et al., 2017).

The geometries of our tectonic blocks were drawn based on the approximate present-day locations of continent-ocean transitions, using a digital elevation model. The geometries of the tectonic blocks are shown in Figure 1. Our boundaries may differ slightly from the recently mapped block boundaries that Beniest and Schellart (2020) defined. However, because the continental fragments of the Scotia Sea have all been extended during rifting preceding oceanic spreading, their shapes and areas have been strongly deformed and the modern shapes will overlap in the reconstruction.

3.2. Reconstruction approach

To restore where the (proto-)South Sandwich subduction zone(s) initiated, we first restore motion along the Magallanes-Fagnano shear zone, shortening in the Magallanes fold-and-thrust-belt, and extension documented from marine magnetic anomalies in the Scotia Sea oceanic basins (Figure 1, Figure 4). This reconstruction will provide the tectonic configuration of the Scotia Sea region at the onset of oceanic crust formation in the latest Eocene (~36 Ma). Assessing intracontinental extension preceding oceanic spreading ('pre-drift extension') is challenging given the paucity of geological and geophysical data. We estimate the amount of pre-drift extension within southern South America by reconstructing the area that was occupied by South American oceanic lithosphere conjugate to the Weddell Sea prior to South Sandwich subduction. The locations of the restored anomalies on the South American Plate are based on the relative motion between the East Antarctic and South American plates. This follows from a plate circuit through Africa that we develop

by reconstructing spreading at the South Atlantic and Southwest Indian mid-ocean ridges based on constraints reviewed in section 4.2. The overlap between the South American conjugate lithosphere of the Weddell Sea on the one hand, and the restored latest Eocene configuration of Scotia Sea continental fragments on the other hand then provides an estimate of the amount of pre-drift extension. We use this estimate to restore the continental fragments to a location closer to Tierra del Fuego to avoid overlap of these fragments with South American oceanic crust that formed the conjugate to Weddell Sea.

Next, we use the plate circuit through Africa to evaluate whether convergence occurred between Tierra del Fuego and the Antarctic Peninsula in the Drake Passage region that may have started (proto-)South Sandwich subduction. However, this first requires restoring any intra-South American deformation between Tierra del Fuego and the South Atlantic margin and between the Antarctic Peninsula and East Antarctica. The Antarctic Peninsula is geographically part of West Antarctica, and it has been suggested that the West Antarctic Rift System, forming the plate boundary between East and West Antarctica, continues into the Weddell Sea (Dalziel, 2006). This would render the Antarctic Peninsula also tectonically part of West Antarctica. Based on paleomagnetic studies, however, most authors interpret the Antarctic Peninsula as rigidly attached to East Antarctica since at least the mid-Cretaceous (Bakhmutov and Shpyra, 2011; Gao et al., 2018; Grunow, 1993; Milanese et al., 2019; Milanese et al., 2017; Poblete et al., 2011; Watts et al., 1984).

3.3. Paleomagnetic data selection

We use a newly compiled paleomagnetic database (provided in the Supplementary Information) for the Antarctic Peninsula and southern South America to test, and if necessary, iteratively improve, our kinematic reconstruction. To this end, we use the online paleomagnetic analysis platform Paleomagnetism.org (Koymans et al., 2020; Koymans et al., 2016). This platform includes a tool that allows to predict the Global Apparent Polar Wander Path (for which we use the version of Torsvik et al. (2012) in the coordinates of any restored block in GPlates (see Koymans et al., 2020; Li et al., 2017). We compiled paleomagnetic data derived from Lower Jurassic to Eocene volcanic and sedimentary rocks of the Antarctic Peninsula, and southernmost South America. We use the criteria for data selection defined by Lippert et al. (2014) and Li et al. (2017), by which we exclude data that 1) are not used in the original publication if the reason for this exclusion was provided; 2) are (likely) remagnetised according to the original authors; 3) contain lava sites of mixed polarity, as spot readings cannot record reversals; 4) consist of less than 3 samples sedimentary sites or less than 3 lava sites for igneous rocks; 5) do not adequately sample paleosecular variation, using the criteria of Deenen et al. (2011).

To include as much information from the sparse record of paleomagnetic data as possible, published data is included in the database if at least 3 lava sites are present in close contact and these were interpreted by the original authors as primary magnetic directions. We thereby apply somewhat less stringent quality criteria compared to those of Meert et

al. (2020), who argue for a minimum of 8 sites. We color-coded the paleomagnetic data based on the quality of the paleomagnetic dataset. Mean directions based on 8 sites or more are plotted in green, unless the Fisher (1953) precision parameter of the distribution of VGPs falls outside of $10 \leq K \leq 70$ (following the quality criteria of Meert et al., 2020), in which case the mean direction is plotted in orange. Mean directions based on fewer than 8 sites are plotted in red. Datasets obtained from (clastic) sedimentary rocks are known to be prone to inclination shallowing (e.g., King, 1955; Tauxe and Kent, 2004) and are thus not suitable to provide estimates of the inclination and paleolatitude, unless corrected for the effects of inclination shallowing (e.g., Vaes et al., 2021). We used the available sedimentary

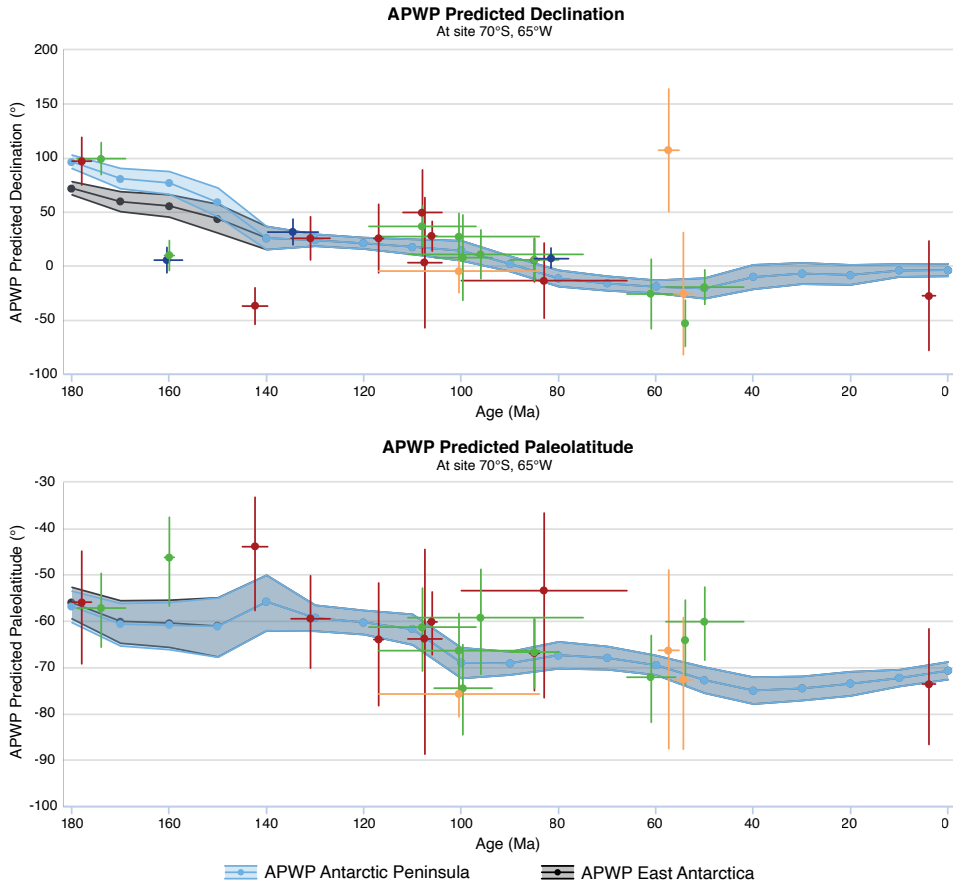


Figure 5. Paleomagnetic declination (top) and predicted paleolatitude (bottom) data from the Antarctic Peninsula plotted against our reconstructed declination/paleolatitude curves for East Antarctica (black line) and the Antarctic Peninsula (blue line) relative to a reference point on the Antarctic Peninsula (70°S, 65°W). The color of the volcanic data point represents their quality, based on the quality criteria of Meert et al. (2020). Green = $N \geq 8$ and $10 \leq K \leq 70$; Orange = $N \geq 8$ and $K < 10$ or $K > 70$. Red = $N < 8$. Blue data points are from sedimentary sites which all have $N \geq 8$ and $10 \leq K \leq 70$. Due to the potential effects of inclination flattening we only use sedimentary sites for declination (see also section 3.3).

datasets only to test the paleomagnetic declination as predicted by our reconstruction (plotted in blue; Figure 5, Figure 7). The only published inclination shallowing-corrected dataset for these regions is from a magnetostratigraphic study of Upper Cretaceous clastic sediments from Ross Island, by Milanese et al. (2019). We evaluated the reliability of their two results (NW and SE Ross Island) using the recently defined reliability criteria of Vaes et al. (2021). The anomalously large scatter of the individual directions ($K < 8$) suggests that the distribution of directions, even after the application of a data cut-off, is contaminated by a significant contribution of noise that is unrelated to paleosecular variation. Consequently, the application of the reliability criteria yields a quality grade 'C' for these datasets, indicating that the datasets do not provide a robust estimate of the inclination and associated paleolatitude (Vaes et al., 2021).

4. Review

We present here an overview of the quantitative kinematic constraints that are used as input for our reconstruction. First, we review the Scotia Sea region itself, delineated by the Shackleton Fracture Zone, the Magallanes-Fagnano Fault Zone and North Scotia Ridge, the South Sandwich Trench, and the South Scotia Ridge (Figure 1). The Scotia Sea region is mainly underlain by oceanic crust, which means that these data come from marine magnetic anomalies, corresponding to step 1 of our reconstruction hierarchy, as outlined in section 3.2. Second, we review constraints on the South America-Africa-Antarctica plate circuit from the South Atlantic and Southern oceans and the Weddell Sea, corresponding to steps 1 (oceanic spreading) and 2 (pre-drift extension) of our reconstruction hierarchy. Third, we review geological and paleomagnetic constraints on deformation within Antarctica and South America to tie Tierra del Fuego and the Antarctic Peninsula to the plate circuit. This part includes data from steps 3 (strike-slip and transform motion), 4 (intracontinental compression), and 5 (paleomagnetic constraints) of the reconstruction hierarchy.

4.1. Scotia Sea

Seafloor spreading in the East Scotia Basin is recorded by marine magnetic anomalies that are mirrored either side of the East Scotia Ridge (Figure 4). West of the ridge, anomalies go back to C5C (17 Ma; Larter et al., 2003), but on the eastern side, the oldest identifiable magnetic anomaly is C4A (9.1 Ma; Larter et al., 2003). The South Sandwich Arc has likely intruded and overlain the older anomalies (Vanneste and Larter, 2002). The Central Scotia Basin hosts E-W trending anomalies (Figure 4) suggesting N-S paleo-spreading of unknown age, either related to Cenozoic Scotia Sea extension (Livermore et al., 2007), or representing a relic of Mesozoic South American conjugate lithosphere of Weddell Sea (Eagles, 2010). Since there is no fossil spreading ridge identified (Dalziel et al., 2013), we will evaluate both possibilities in the reconstruction section. The West Scotia Basin occupies most of the Scotia Plate and hosts an extinct mid-ocean ridge with a well-defined, symmetric set of magnetic anomalies (Eagles et al., 2005). The identification of marine magnetic anomalies

C8–C5 (Figure 4) indicates that spreading started before ~26.0 Ma and ceased during chron C3An (~6.1 Ma; Eagles et al., 2005). However, some studies postulated the existence of older anomalies in the western part of the basin, with ages corresponding to chrons C10 or C12 (~28–30.5 Ma; Livermore et al., 2005; Lodolo et al., 2006). The identified anomalies older than C8 are of low amplitude and are interpreted as disorganised early stages of seafloor spreading that started around 32–30 Ma (Eagles et al., 2005; Livermore et al., 2005; Lodolo et al., 2006).

In the South Scotia Ridge, the Scan Basin between the Discovery and Bruce Banks contains NNW-SSE anomalies from chrons C16n.1n–C11n.2n, with ages ranging from ~35.7–29.5 Ma (Schreider et al., 2017). The Dove Basin between the Bruce and Pirie Banks contains a NNE-SSW elongated ridge that is close to the axis of the basin flanked by marine magnetic anomalies corresponding to chrons C6Cn.2n–C6Ar (23.0–20.7 Ma; Schreider et al., 2018), in correspondence with 20.4 ± 2.6 to 22.8 ± 3.1 Ma whole-rock $^{40}\text{Ar}/^{39}\text{Ar}$ ages of dredged MORB samples (Galindo-Zaldívar et al., 2014). Schreider et al. (2018) tentatively interpreted additional anomalies located in the eastern part of the Dove Basin as C8n.1n–C6Cr (23.3–25.3 Ma). These presumably formed during an earlier phase of slow spreading, after which the spreading ridge jumped westwards (Schreider et al., 2018). The Protector Basin between the Pirie Bank and the Terror Rise contains north-south oriented marine magnetic anomalies corresponding to chrons C5Dn–C5ABr (17.5–13.6 Ma; Galindo-Zaldívar et al., 2006; Schreider et al., 2018). To the south, the narrow Jane Basin between the Jane Bank and the South Orkney microcontinent has marine magnetic anomalies interpreted to have formed during chrons C5Dn–C5ADn (17.5–14.2 Ma; Bohoyo et al., 2002). Finally, the Powell Basin between the Antarctic Peninsula and the South Orkney microcontinent contains an extinct spreading ridge with NW-SE striking marine magnetic anomalies corresponding to chrons C11–C6AA (29.5–21.2 Ma; Figure 4; Eagles and Livermore, 2002).

4.2. South America – Africa – East Antarctica plate circuit

The oldest identified anomaly in the South Atlantic Ocean that records spreading between South America and Africa north of the Falkland Plateau (Figure 3) is M4 (e.g. König and Jokat, 2006), indicating that seafloor spreading has been active since at least ~131 Ma (Gradstein et al., 2012). Cretaceous opening of the South Atlantic in our reconstruction follows Gaina et al. (2013), but converted to the timescale of Gradstein et al. (2012). There are several pre-breakup fits for the South Atlantic region that differ by a few degrees, and these variably advocate for strike-slip fault zones cutting South America into several tectonic blocks, which were active during pre-drift extension before the onset of seafloor spreading (Heine et al., 2013; Moulin et al., 2010; Pérez-Díaz and Eagles, 2014; Torsvik et al., 2009). Recently, Owen-Smith et al. (2019) tested the different full-fit reconstructions of Africa and South America against paleomagnetic data of the Paraná (South America)-Etendeka (Africa) Large Igneous Province that is thought to have sparked the South Atlantic opening.

They concluded that the reconstruction of Torsvik et al. (2009) provides the best fit to the paleomagnetic data, and therefore we use the deformation zones and finite rotation poles for the pre-breakup fit from Torsvik et al. (2009), with the exception of the Gastre Fault, which we review separately in section 4.3. The fit of Torsvik et al. (2009) contains ~50–180 km pre-drift extension between southern South America and Africa, and ~120–600 km between northern South America and Africa, occurring from 138 Ma, before true seafloor spreading established at ~131 Ma (whereby we converted ages to the Gradstein et al. (2012) timescale).

Antarctica, as part of East Gondwana, broke away from Gondwana in the Jurassic, which preceded the break-up of West Gondwana into Africa and South America. The separation of East Gondwana from West Gondwana is constrained by marine magnetic anomalies of the Southwest Indian Ridge (Figure 1) identified by Royer and Chang (1991), Bernard et al. (2005), Cande et al. (2010), and Mueller and Jokat (2019). The oldest marine magnetic anomaly between Africa and East Antarctica was interpreted as M38n2n (~164 Ma; Mueller and Jokat, 2019). Pre-drift extension between East and West Gondwana was estimated to have started at ~182 Ma, coincident with the initial emplacement of flood basalts of the Karoo-Ferrar Large Igneous Province on both margins (Mueller and Jokat, 2019).

The combined South Atlantic and Southern Ocean reconstructions constrain relative motion between East Antarctica and South America. Direct constraints on this motion are also available, in the Weddell Sea. However, the remote conditions, thick sedimentary cover, and the fact that only half of the ocean crust remains (the South American conjugate has largely subducted), means that the anomaly data are of lesser quality than for the South Atlantic and Southern Oceans. The oldest marine magnetic anomaly of the South America–Antarctica Ridge preserved on the South American Plate to the east of the South Sandwich trench is C31y (~68.4 Ma; Eagles, 2016a; Livermore et al., 2005). Older marine magnetic anomalies are only preserved on the Antarctic Plate in the Weddell Sea (Figure 4). These are interpreted to become younger towards the north, but their age is debated (Barker and Jahn, 1980; Barker et al., 1984; LaBrecque and Barker, 1981; Livermore and Woollett, 1993). Eagles (2016a) identified M14o (~138 Ma) as the oldest isochron, while Jokat et al. (2003) proposed an onset of seafloor spreading at M24 (~154 Ma). Ghidella et al. (2002) suggested an even older but tentative start of seafloor spreading at ~160 Ma based on adjusting synthetic isochrons to seafloor spreading lineations and flow lines. Previously proposed pre-drift extension ages include ~167 Ma based on the extrapolation of spreading rates derived from subsequent marine magnetic anomalies (König and Jokat, 2006). These rates are used to restore pre-drift extension between South America and Antarctica back into the Gondwana fit (König and Jokat, 2006). An Early Jurassic onset of pre-drift extension has also been proposed based on arc extension in the Antarctic Peninsula (Storey et al., 1996). The most recent estimate, and the one used in our reconstruction, is of Mueller and Jokat (2019) who dated the start of pre-drift extension at ~182 Ma, based on ship-borne magnetic data, immediately following the emplacement of the Ferrar Large Igneous Province.

4.3. Deformation within South America

At present, deformation in southern South America is focused along the Magallanes-Fagnano fault zone (Figure 1). About 20–80 km of left-lateral strike-slip motion was estimated, with a minor (up to ~10 km) normal slip component (Klepeis, 1994a; Lodolo et al., 2003; Pelayo and Wiens, 1989; Torres-Carbonell et al., 2008a). Field observations and seismic data reveal that structures related to left-lateral strike-slip motion consistently crosscut contractional structures of the Magallanes fold-and-thrust belt (e.g. Betka et al., 2016; Klepeis, 1994a; Klepeis and Austin Jr., 1997). The onset of strike-slip motion is thought to be related to either the start or end of West Scotia Sea spreading; i.e. late Oligocene (Klepeis and Austin Jr., 1997) or late Miocene (Lodolo et al., 2006). Based on balanced cross-sections, the latest phase of contractional deformation in the Magallanes fold-and-thrust belt occurred in the latest Oligocene to early Miocene (Torres-Carbonell et al., 2011; Torres-Carbonell et al., 2008b). A maximum early Miocene age is therefore inferred for the onset of strike-slip motion along the Magallanes-Fagnano fault system (Betka et al., 2016), which corresponds to widespread uplift and exhumation in the region measured through low-temperature thermochronology (Fosdick et al., 2013). Based on displaced markers, Torres-Carbonell et al. (2008a) estimate ~50 km of sinistral strike-slip motion since the late Miocene. This age corresponds to the ~7 Ma onset of folding in the Falkland Trough, the offshore continuation of the South America-Scotia plate boundary (Esteban et al., 2020).

Shortening in the Magallanes fold-and-thrust belt occurred between mid-Cretaceous and early Miocene time (Klepeis et al., 2010; Torres-Carbonell et al., 2013; Torres-Carbonell et al., 2014). The onset of shortening in the mid-Cretaceous is related to the final closure of the Rocas Verdes Basin (Klepeis et al., 2010). The youngest rocks infilling the Rocas Verdes Basin are Albian (Dott et al., 1977), and the oldest flysch related to closure was deposited during the Albian to Cenomanian (Scott, 1966; Wilson, 1991). Foreland basin deposits following closure are dated at ~101–88 Ma based on U-Pb detrital zircon analysis (Fildani et al., 2003; Fosdick et al., 2011; McAtamney et al., 2011), although the initiation of thrusting probably occurred earlier (Calderón et al., 2007). During the Late Cretaceous and into the Cenozoic convergence continued and the deformation front migrated towards the foreland (Fosdick et al., 2011; Torres-Carbonell and Dimieri, 2013; Torres-Carbonell et al., 2013; Torres-Carbonell et al., 2011; Torres-Carbonell et al., 2008b). The Cenozoic phase of shortening was restored using balanced cross-sections, and here we follow the reconstruction of Schepers et al. (2017). Those authors restored a total of 50–80 km of Cenozoic shortening in the southern Patagonian and the Fuegian Andes based on estimates of Kley et al. (1999), Kraemer (1998), Ghiglione et al. (2014), Fosdick et al. (2011), Betka (2013), and Klepeis et al. (2010). In addition, based on a structural restoration of a deformed geological cross section, Fosdick et al. (2011) infer that 32–40 km of pre-Cenozoic shortening occurred in the Magallanes fold-and-thrust belt following the final closure of Rocas Verdes Basin around 100 Ma, of which about 27 km occurred between 88 and 74 Ma.

Quantifying the amount of shortening related to Rocas Verdes Basin closure is more

difficult due to absence of markers and loss of lithosphere through subduction related to closure of the basin (Klepeis et al., 2010). South directed subduction led to the consumption of oceanic crust of the Rocas Verdes Basin below the Pacific margin of Patagonia, which hosts the Patagonian batholith (Klepeis et al., 2010). The width of the basin is debated, and estimates mostly range between 100 and 300 km based on field, geochemical, and paleomagnetic arguments (Burns et al., 1980; Dalziel, 1981; De Wit, 1977; de Wit and Stern, 1981). Winn Jr (1978) proposed a maximum width of 300 km in Tierra del Fuego as the basin was filled with moderately coarse deep-sea fan sediments, which are unlikely to have been deposited if the basin edges were farther away. Kraemer (2003) estimated a minimum of 300 km and a maximum of 600 km of shortening across the entire southern Andes orogen since the Cretaceous. He attributed a maximum amount of 430 km to mid-Cretaceous shortening, of which 230 km was considered to be related to the mid-Cretaceous closure of the Rocas Verdes Basin, and 200 km to thick-skinned tectonics in the Cordillera Darwin (Kraemer, 2003). The age of opening of the Rocas Verdes Basin is estimated to be Late Jurassic to Early Cretaceous based on zircon U-Pb geochronology of ophiolitic rocks. These yielded ages of 139 ± 2 Ma in Patagonia (Stern et al., 1992) and 150 ± 1 Ma on South Georgia (Mukasa and Dalziel, 1996; Figure 3). Additionally, Calderón et al. (2007) used magmatic and detrital zircon U-Pb geochronology to date volcanism and rifting in the basin, which occurred between at least ~152 to 142 Ma.

For South America north of the southernmost Andes, we adopt the finite rotation poles of Schepers et al. (2017) for Cenozoic deformation in the Andes, and of Torsvik et al. (2009) for strike-slip deformation related to South America-Africa pre-drift extension. A controversial element in the latter reconstruction is the ~500 km of dextral strike-slip motion that is proposed to be accommodated on the Gastre Fault between initial breakup (182 Ma) and the onset of oceanic spreading (134 Ma). The Gastre Fault System (Figure 1) as a major Jurassic tectonic boundary was first proposed by Rapela and Pankhurst (1992), based on significant changes in geology across the shear zone, and scattered outcrops of mylonites and cataclasites with a NW-SE striking foliation that are thought to confirm the existence of a shear zone. Several kinematic reconstructions include dextral motion on this fault to create space for the Antarctic Peninsula outboard of Patagonia in Gondwana reconstructions (Dalziel et al., 2000; König and Jokat, 2006; Macdonald et al., 2003). Additionally, Schimschal and Jokat (2019) recently used seismic data to identify Jurassic extension in the Falkland Plateau between Maurice Ewing Bank and the Falkland Islands, which occurred between ~178 and 154 Ma. This extension requires almost 500 km of dextral motion on the Gastre Fault during the same period to avoid crustal gaps and overlaps of continental crust. However, whether the Gastre Fault System served as a major dextral shear zone remains debated (e.g., González et al., 2020) as unequivocally demonstrating its presence in the field proves challenging (Von Gosen and Loske, 2004; Zaffarana et al., 2010; Zaffarana et al., 2017).

4.4. Deformation within Antarctica

To use the South Atlantic plate circuit to constrain relative motion between southern South America and the Antarctic Peninsula, it is crucial to establish whether the Antarctic Peninsula was tectonically part of East Antarctica or West Antarctica. The Antarctic Peninsula is bounded in the south by the Ferrigno Rift that separates it from Thurston Island (Bingham et al., 2012), and in the southeast by the Evans Rift that separates it from the Ellsworth-Whitmore Mountains (Jones et al., 2002; Figure 3). There are no estimates on the magnitude and timing of displacement along these rifts, but one of these rifts may have served as the continuation of the West Antarctic Rift System (WARS), which formed the plate boundary between East and West Antarctica.

It is commonly accepted that the continuation of the WARS was located between the Antarctic Peninsula and Thurston Island and that the Antarctic Peninsula has been tectonically part of East Antarctica since at least the Early Cretaceous (Bingham et al., 2012; Eagles et al., 2009; Gohl et al., 2007; Jordan et al., 2010; Müller et al., 2007). Dalziel (2006), however, proposed that the WARS connects the Ross Sea with the Weddell Sea, which would imply that the Antarctic Peninsula is tectonically part of West Antarctica. In this setting, relative motion between the Antarctic Peninsula and East Antarctica may have occurred until the Miocene, based on marine magnetic anomalies from the Northern and Adare Basins that constrain motion in the WARS (Cande et al., 2000; Fitzgerald and Baldwin, 1997; Granot et al., 2013; Granot and Dymant, 2018; Luyendyk et al., 2001).

We use paleomagnetic data from the Antarctic Peninsula to evaluate whether the peninsula was tectonically part of West Antarctica or East Antarctica in the Mesozoic and Cenozoic. We plotted the declination and paleolatitude of these sites (Figure 5), rotated to East Antarctic coordinates for a reference point on the Antarctic Peninsula (70°S, 65°W), against the Global Apparent Polar Wander Path (GAPWaP) of Torsvik et al. (2012). The paleomagnetic data of the Antarctic Peninsula are in good agreement with the predicted GAPWaP for the last ~145 Ma (Figure 5). Based on these paleomagnetic constraints, there is no reason to assume any relative motion between the Antarctic Peninsula and East Antarctica since the Early Cretaceous. In our reconstruction the Antarctic Peninsula is tectonically part of East Antarctica, which is in agreement with earlier conclusions (Bakhmutov and Shpyra, 2011; Gao et al., 2018; Grunow, 1993; Milanese et al., 2019; Milanese et al., 2017; Poblete et al., 2011; Watts et al., 1984).

5. Reconstruction

5.1. Early Jurassic – Late Cretaceous

Our reconstruction (see Supplementary Information for GPlates files) starts at 182 Ma (Figure 6a), when East Gondwana (Antarctica, Australia, Zealandia, India) started to separate from West Gondwana (South America, Africa; Mueller and Jokat, 2019). Shortly after the onset of pre-drift extension between Africa and Antarctica, extension started at 178 Ma between the Falkland Islands and Maurice Ewing Bank, creating the Falkland

Plateau Basin (Schimschal and Jokat, 2019). During this time, the Maurice Ewing Bank remained in a fixed position relative to Africa, and we restore 450 km of extension in the Falkland Plateau that is accommodated by right-lateral strike-slip motion in South America along the Gastre Fault (Schimschal and Jokat, 2019). Both the extension in the Falkland Plateau Basin and strike-slip motion along the Gastre Fault ceased at 154 Ma (Figure 6b; Schimschal and Jokat, 2019).

After 300–500 km of pre-drift extension, seafloor spreading between Antarctica and Africa was established around 160 Ma (Mueller and Jokat, 2019) and caused an increase in divergence rates between East and West Gondwana. The increase in relative plate motion was concurrent with extension on the western margin of Gondwana. Subsequently, at 154 Ma, the Rocas Verdes Basin started opening (Calderón et al., 2007) and simultaneously, clockwise rotation of the Antarctic Peninsula relative to East Antarctica commenced (Figures 6b and 5c). This rotation is consistent with paleomagnetic data and is required to avoid overlap between the Antarctic Peninsula and Patagonia in the Gondwana reconstruction (Grunow, 1993; Longshaw and Griffiths, 1983; Figures 5a and 6a). The restoration of the Antarctic Peninsula outboard of Patagonia provides a straightforward explanation for why there is widespread pre-Late Jurassic arc magmatism due to Phoenix subduction below Gondwana on the Antarctic Peninsula and north of the Rocas Verdes Basin, but not in southern Patagonia (Navarrete et al., 2019). Following opening of the Rocas Verdes Basin, extension occurred along the eastern margin of Antarctica (Storey et al., 1996). Meanwhile, extension was also accommodated in the Weddell Sea between Antarctica and South America, where seafloor spreading was established around 140 Ma (Eagles, 2016a). This time marks the end of opening of the Rocas Verdes Basin (Calderón et al., 2007; Figure 5c). The end of rotation of the Antarctic Peninsula in our reconstruction coincides with the end of Rocas Verdes Basin opening at 140 Ma (Figure 6c).

Pre-drift extension between South America and Africa preceding the opening of the South Atlantic Ocean started around 135 Ma (Torsvik et al., 2009), and the onset of seafloor spreading was around the time of magnetic anomaly M4 (~131 Ma; König and Jokat, 2006). A clockwise rotation of Antarctica relative to South America and Africa occurred during the mid-Cretaceous. The exact timing is uncertain due to lack of polarity reversals during the Cretaceous Normal Superchron (~125.9–83.6 Ma; Gradstein et al., 2012), but is evidenced from a bend in fracture zones of the Weddell Sea (König and Jokat, 2006) and Southwest Indian Ocean (Mueller and Jokat, 2019). In the western Weddell Sea region, the rotation of Antarctica caused a change in relative motion between Tierra del Fuego and the Antarctic Peninsula: from the extensional phase since Gondwana break-up, to a period of transcurrent motion (~125–113 Ma), and then to a phase of convergence between ~113–102 Ma. The timing of these changes in relative plate motion is based on synthetic flowlines to fit fracture zones of the Southwest Indian Ridge, as marine magnetic anomalies are absent (Mueller and Jokat, 2019). The change in relative plate motion led to oblique convergence between the Antarctic Peninsula and the Pacific margin of the Rocas Verdes

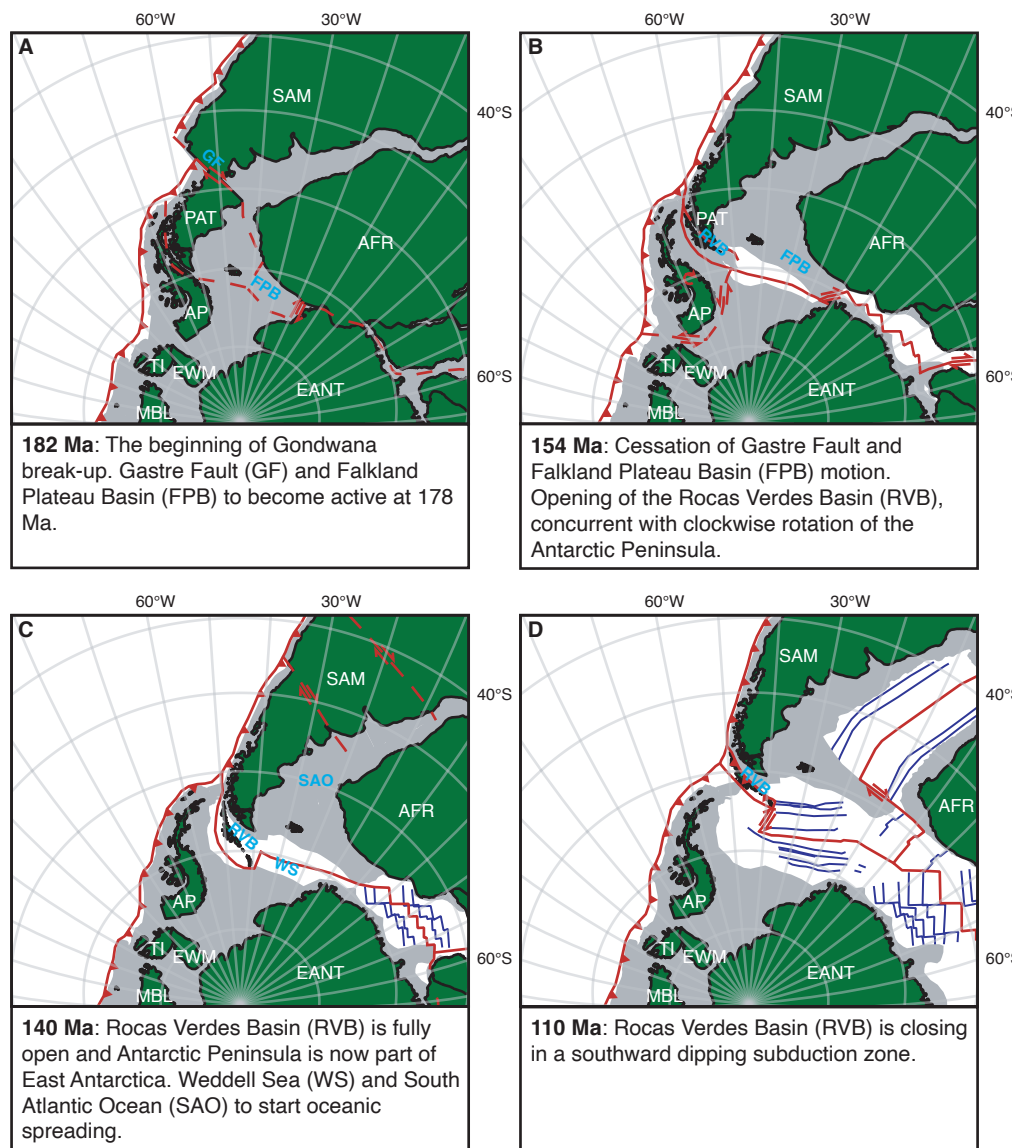


Figure 6. Snapshots of the kinematic reconstruction at selected time slices in an East Antarctica fixed reference frame. Dark green areas represent present-day coastal boundaries of the polygons, dark gray areas represent stretched and transitional continental crust. Red lines represent active plate boundaries, red arrows represent motions on the active plate boundaries. Dashed red lines are plate boundaries that are to become active soon after the reconstruction snapshot. Dark blue lines are marine magnetic anomaly lineations. The oceanic basins west of South America and Antarctica are not reconstructed, and therefore no marine magnetic anomalies are shown, plate boundaries in this region are given for reference and are based on the reconstruction of Müller et al. (2019).

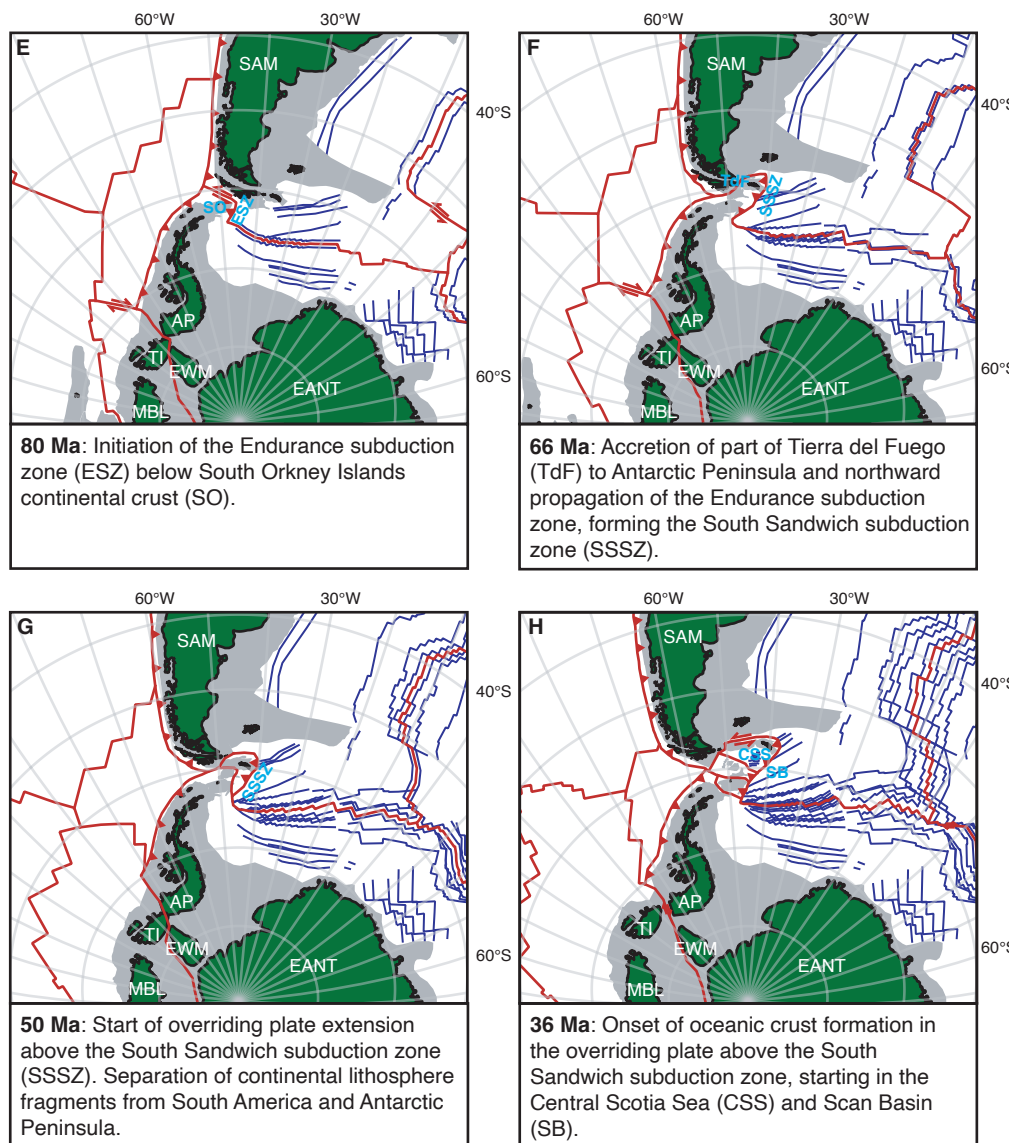


Figure 6 (continued).

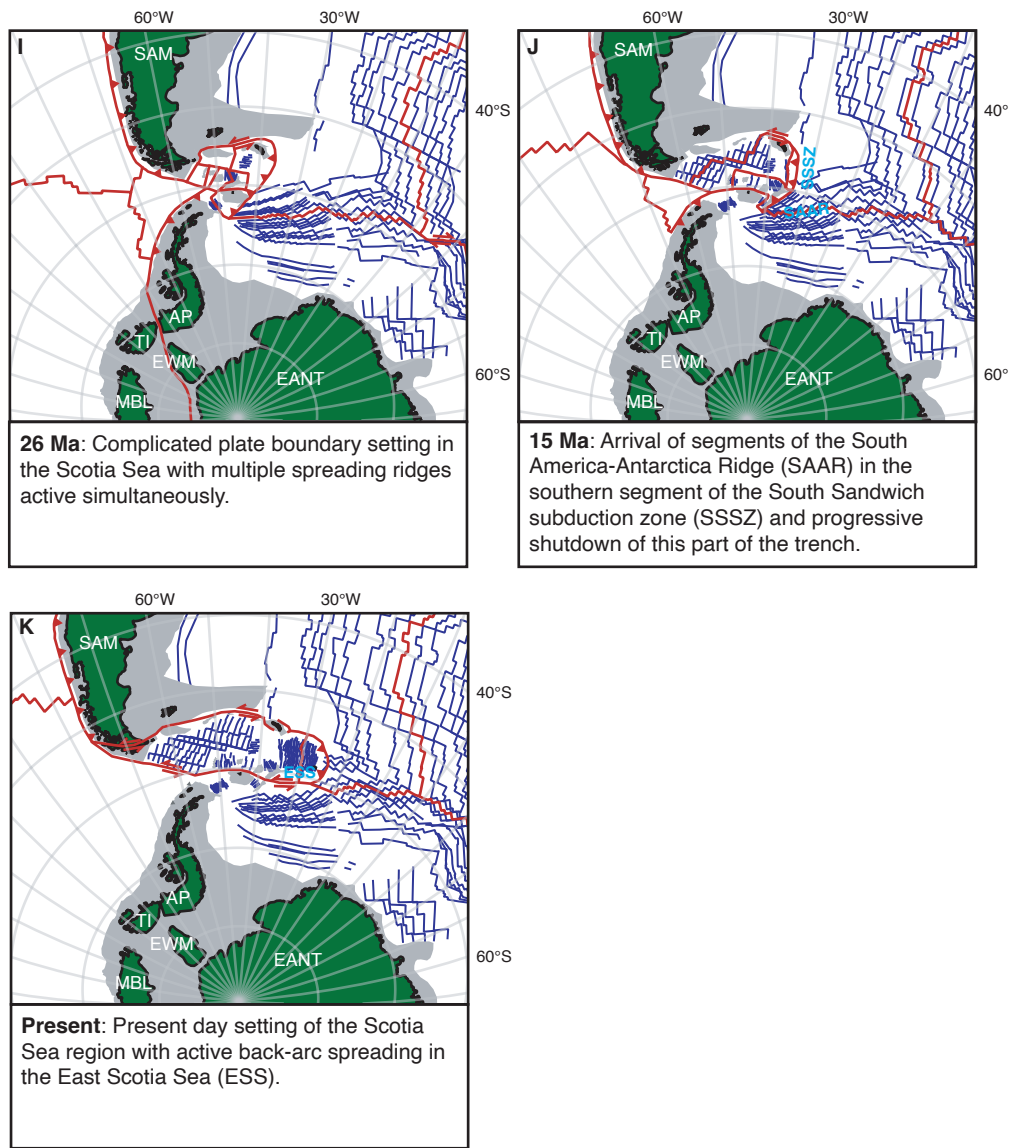


Figure 6 (continued).

Basin, which is thought to have led to closure of the Rocas Verdes Basin (Eagles, 2016a). In addition, this change in plate motion is proposed to have led to closure of a whole series of back-arc basins that were present along the western margin of South America south of 5°S (Dalziel, 1986). The change in plate motions allows for closure of the Rocas Verdes Basin between 113 and 102 Ma, in line with the ages of overlying flysch sediments (Scott, 1966; Wilson, 1991) and the formation of the fold-and-thrust belt (Fosdick et al., 2011), which we adopt in our reconstruction (Figure 6d).

5.2. Width of the Rocas Verdes Basin

The width of the Rocas Verdes Basin is difficult to constrain, as no quantitative kinematic constraints are available. To assess the effects of minimum and maximum basin widths, we created two end-member scenarios (Figure 7). We tested these against paleomagnetic data, as the closure of the Rocas Verdes Basin may be related to the formation of the Patagonian orocline (Burns et al., 1980; Carey, 1955; Cunningham et al., 1991; Maffione, 2016; Maffione et al., 2010; Marshak, 1988). Declinations from the Tierra del Fuego region in southern Patagonia show counterclockwise rotations up to ~100° between ~110 and 60 Ma, relative to the Global Apparent Polar Wander Path (GAPWaP) of Torsvik et al. (2012) in coordinates of the stable Amazonia Craton of South America, rotated into a reference point (55°S, 65°W) in southern South America (Figure 7). These rotations have been associated with the Late Cretaceous closure of the Rocas Verdes Basin (Poblete et al., 2016) based on the systematic pattern of ~90° counter-clockwise rotated rocks of Early Cretaceous age (although paleomagnetic data is scarce) and ~35–50° counter-clockwise rotated rocks of Late Cretaceous and early Eocene age (Figure 7). This would call for a ~40–55° rotation related to the closure of the Rocas Verdes Basin, and subsequent local rotations related to large sinistral strike-slip fault zones in the Tierra del Fuego region. Alternatively, the total rotations have been ascribed to strike-slip related deformation (Cunningham, 1993; Rapalini et al., 2015).

In the minimum width scenario, the basin is closed by the 113–102 Ma convergent motion between the Antarctic Peninsula and Tierra del Fuego only (Figure 7a). This means that the south-western margin of the basin is rigidly attached to the Antarctic Peninsula during closure, which results in a 100–150 km wide basin. This scenario does not involve counter-clockwise rotation of the southwest margin of the Rocas Verdes Basin, thus suggesting that the paleomagnetic rotations are completely the result of local rotations related to strike-slip tectonics (Figure 7a).

In the maximum width scenario, we open the Rocas Verdes Basin by the maximum clockwise rotation of the southwest margin of Patagonia relative to stable South America that does not lead to convergence between this margin and Antarctica. The resulting Rocas Verdes Basin in our reconstruction is up to 500 km wide (Figure 7b). Subsequent closure leads to ~50° counterclockwise rotation of the southwest margin of the Rocas Verdes Basin, which has a better fit with the Early Cretaceous paleomagnetic poles (Figure 7b). The

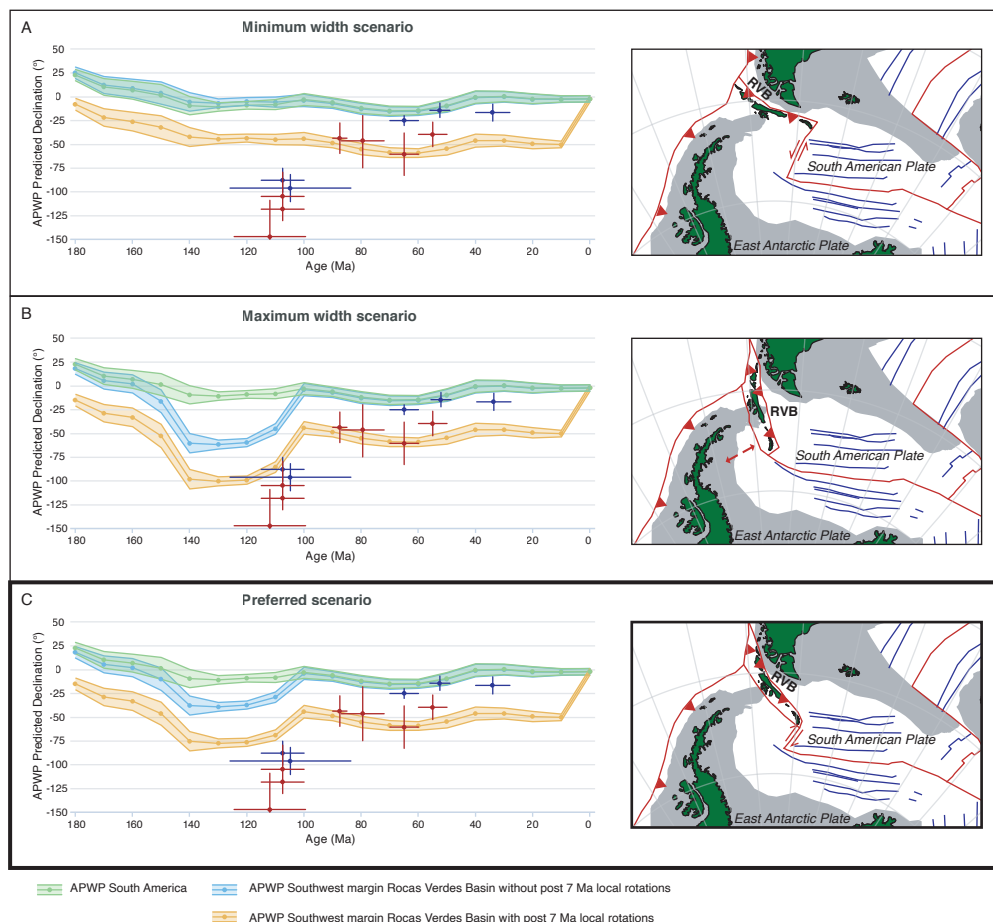


Figure 7. Paleomagnetic declination data from Tierra del Fuego plotted against declination curves of South America (green line) and the southwest margin of the Rocas Verdes Basin (blue line) relative to a reference point in Tierra del Fuego (55°S, 65°W). The yellow line is the APWP of the southwest margin of the Rocas Verdes Basin that includes post 7 Ma rotations related to strike-slip tectonics (see Section 5.2). Red data points are from igneous sites with less than 8 samples, blue data points are from sedimentary sites. The different plots show the declinations curves of the different width scenarios of Rocas Verdes Basin, as explained in Section 5.2. On the right: snapshots at 113 Ma of the different scenarios for the maximum width of the Rocas Verdes Basin just prior to closure.

implication of the rotation, however, is that it results in up to 600 km extension between the eastern margin of the Antarctic Peninsula and the south-western margin of the Rocas Verdes Basin. In addition, the maximum width scenario causes overlap with South Orkney Islands continental crust. Because the minimum width scenario does not include the paleomagnetic rotations, we prefer a mixed model (Figure 7c). In this model we reconstruct the closure of the Rocas Verdes Basin with the maximum counterclockwise rotation that does not lead to overlap between the southwest margin of the Rocas Verdes Basin and South

Orkney Islands continental crust. This mixed scenario involves a ~ 250 km wide Rocas Verdes Basin and accommodates about 25° counterclockwise rotation during closure of the basin.

The Apparent Polar Wander Path (APWP) of the southwest margin of the Rocas Verdes Basin (blue line; Figure 7) lies north of all paleomagnetic data points in all scenarios, which suggests additional counterclockwise rotation after closure of the Rocas Verdes Basin. These post-Early Cretaceous rotations cannot be the result of a whole-block rotation of the southwest margin, however, as this does not fit geometrically. The additional rotation is therefore interpreted as the result of local rotations related to post 7 Ma counter-clockwise rotation associated with left-lateral strike-slip motion of the Magallanes-Fagnano fault zone. To illustrate how this fits better with paleomagnetic data, we plotted the APWP of a block that is part of the southwest margin of the Rocas Verdes Basin (Figure 7c, yellow line), which underwent an additional 50° counterclockwise rotation since 7 Ma. We note that there is only a very limited amount of paleomagnetic data available from Tierra del Fuego, and the quality of data available is generally poor. There is a need for more paleomagnetic data to get better constraints on the timing and amount of rotation in this region.

5.3. Late Cretaceous subduction initiation in the Scotia Sea region

After closure of the Rocas Verdes Basin, the Magallanes fold-and-thrust belt started forming in the Late Cretaceous, where shortening continued into the Neogene. Meanwhile seafloor spreading remained active in the Weddell Sea. Around 80 Ma, South America started moving westwards relative to Antarctica (Figure 6e). This led to transcurrent motion in the future Drake Passage, where the Antarctica-Tierra del Fuego motion was accommodated along a transform system (Figure 6e). Concurrently, shortening was renewed in the Magallanes fold-and-thrust belt (Klepeis et al., 2010; Fosdick et al., 2011). The Weddell Sea mid-ocean ridge, separating East Antarctica (including the Antarctic Peninsula) and South America, was still located southeast of the northern tip of the Antarctic Peninsula and South Orkney Islands continental crust. The mid-ocean ridge and the transform fault north of the Antarctic Peninsula were connected by a NE-SW striking plate boundary along the eastern margin of the Antarctic Peninsula and South Orkney Islands continental crust. This boundary was a transform fault during pre-80 Ma N-S extension in the Weddell Sea (Figures 6d, 8a). The change in relative plate motion between South America and Antarctica at 80 Ma caused convergence on this boundary between the South American oceanic lithosphere of the North Weddell Sea, and the Antarctic Peninsula/South Orkney Islands continental crust (Figures 6e, 8b). As noted by many authors before us (Barker, 2001; Lagabrielle et al., 2009; V  rard et al., 2012; Eagles and Jokat, 2014), this change in relative plate motion caused the initiation of subduction of South American oceanic lithosphere below the Antarctic Peninsula/South Orkney Islands continental crust along the former transform fault (Figure 8b). Following Ghidella et al. (2002) who called this region the Endurance collision zone, we refer to this as the Endurance subduction zone. Previous authors inferred initiation ages

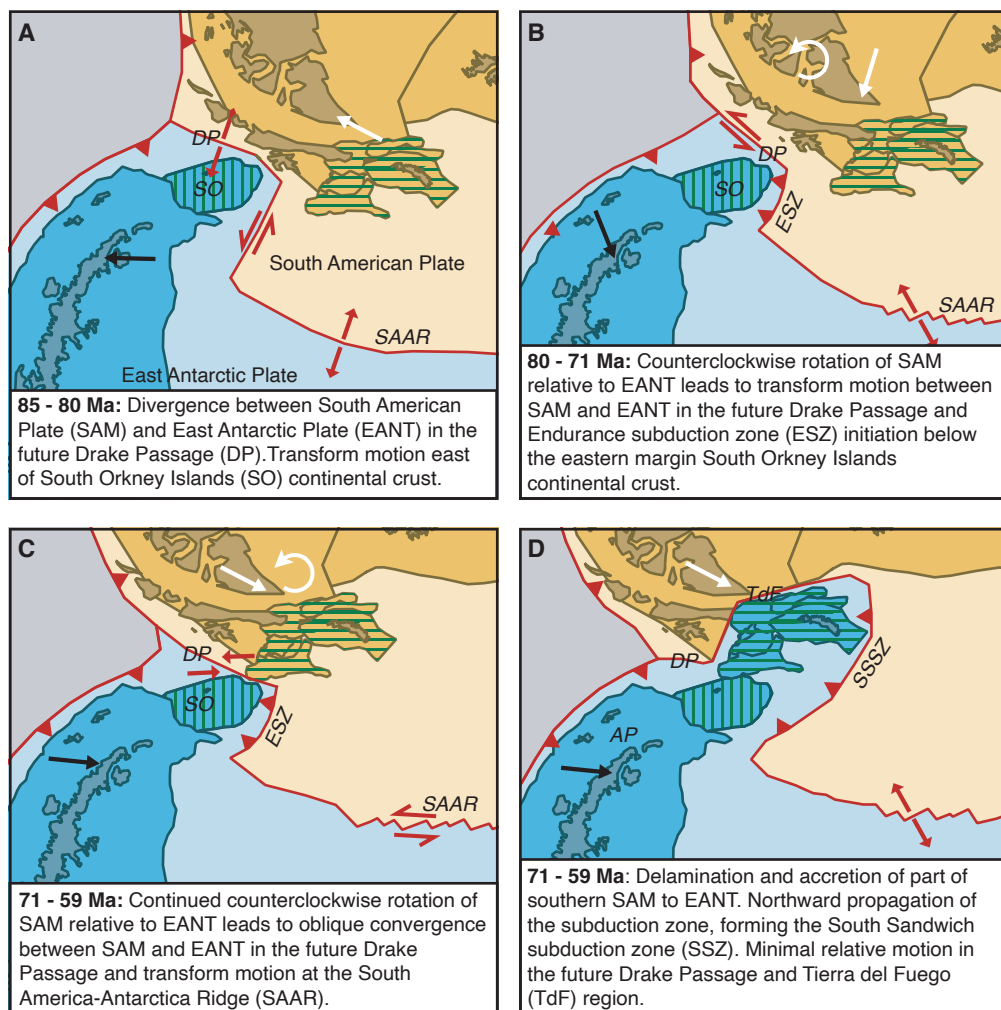


Figure 8. Snapshots of the kinematic reconstruction (Antarctica fixed) that serve to highlight the delamination and subsequent accretion of part of South America to the Antarctic Plate. Different plates have different colors, where darker shades represent continental crust and lighter shades represent oceanic crust: Yellow = South American Plate (SAM); Blue = Antarctic Plate and Antarctic Peninsula (AP); Green = Scotia Plate; Gray = (Paleo-)Pacific plates. Horizontal/vertical hatching: Continental crust that originates from the South American/Antarctic Plate; White and black arrows represent absolute plate motion of the South American and Antarctic Plates respectively. Snapshots G and H are at a smaller scale as these encompass a larger area.

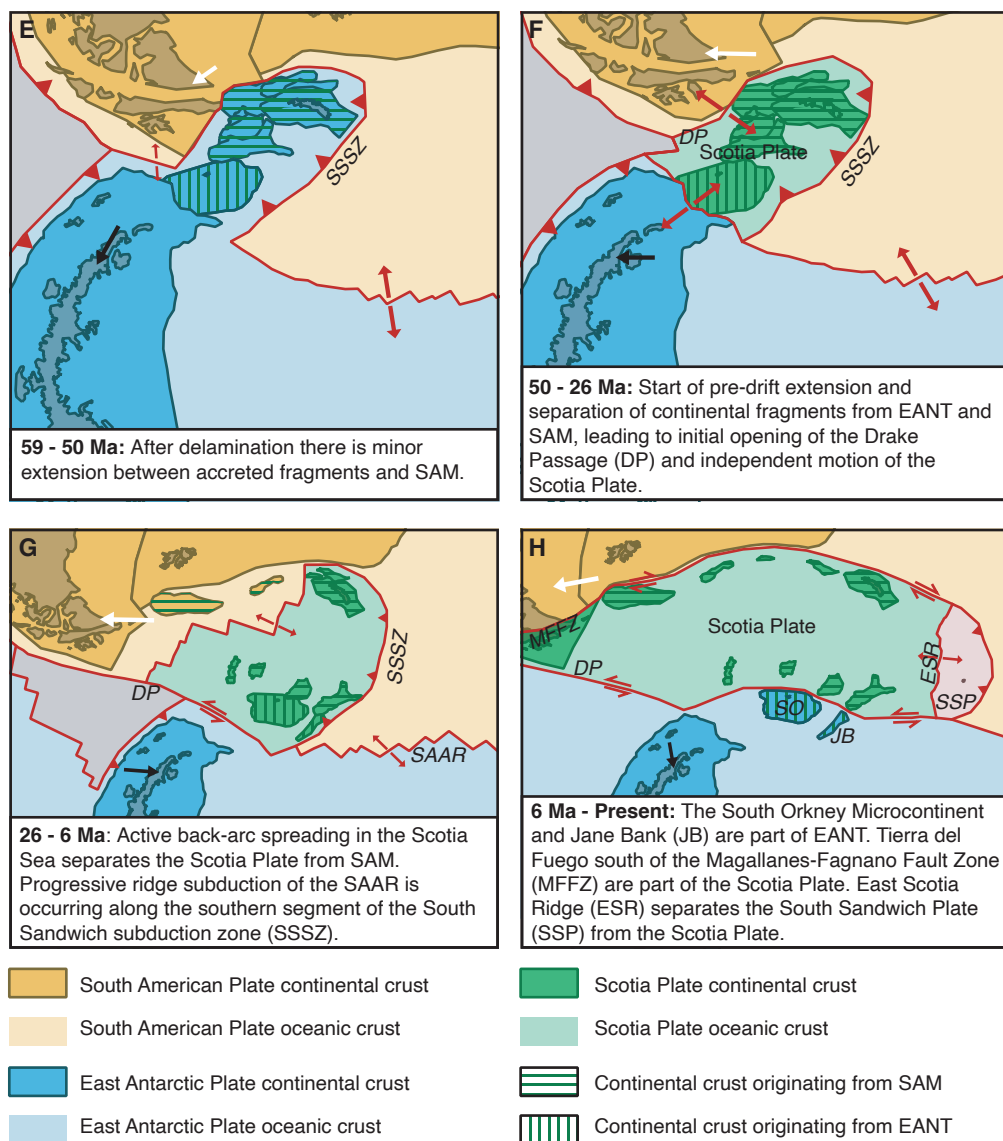


Figure 8 (continued).

of the Endurance subduction zone varying from 70 to 46 Ma (Barker, 2001; Lagabriele et al., 2009; V  rard et al., 2012; Eagles and Jokat, 2014). However, the anomalies of the Weddell Sea (Ghidella et al., 2002; Eagles, 2016a; K  nig and Jokat, 2006) reveal that the sharp change in spreading direction from N-S to NW-SE, accommodated by Endurance subduction, already occurred between chrons C34y and C33y, around 80 Ma (Figures 4; 8a and b).

5.4. Northward propagation of Endurance subduction and delamination of lithospheric mantle

Magnetic anomalies and fracture zones of the Weddell Sea may thus straightforwardly identify the onset of Endurance subduction, but do not explain why subduction also occurred below continental crust originally belonging to South America. In particular, the previously inferred closure of the Rocas Verdes Basin (Barker, 2001; Dalziel et al., 2013) does not offer a straightforward driver for the evolution of the South Sandwich subduction zone: the Rocas Verdes Basin was lost to south-dipping subduction or underthrusting with a suture in Tierra del Fuego (Klepeis et al., 2010). The South Sandwich subduction zone had an initial orientation at high angles to the Rocas Verdes one, had an opposite polarity, and does not logically follow from Rocas Verdes Basin closure. Others assume that the oldest dated arc volcanic rocks dredged from the Scotia Sea floor (~28.5–33 Ma; Barker, 1995; Dalziel et al., 2013) indicate that subduction initiated in the Scotia Sea region around 34 Ma (Crameri et al., 2020; Pearce et al., 2014). Because there is no plate convergence at that time, Pearce et al. (2014) assumed that subduction initiated spontaneously and immediately led to ocean basin formation in the upper plate. But absence of evidence for older arc volcanism from such a scarcely sampled and poorly accessible region does not provide a conclusive argument against older subduction. We therefore explore scenarios that explain the formation of the wide South Sandwich subduction zone by northward, lateral propagation of the Endurance subduction zone. Such propagation should have ruptured South American lithosphere and transferred continental crust of South America into an upper plate position, while the trench propagated northward. Transfer of crustal units from a downgoing to an overriding plate in subduction zones is a common process and typically forms narrow belts of stacked upper crustal nappes that were decoupled from their original mantle and lithospheric underpinnings forming the subducted slab (Van Hinsbergen and Schouten, 2021), such as in the Aegean region, Alps, or Himalaya (e.g., Capitanio et al., 2010; Handy et al., 2010; Van Hinsbergen et al., 2005). But the South American crust that transferred to the upper plate of the South Sandwich subduction zone occupied a wide region and there is no evidence that it ever formed a narrow fold-and-thrust belt. Moreover, such accretionary orogens are not associated with lateral propagation of the trench. Perhaps a better analogy is the evolution of the Sula Spur and Banda Sea region in SE Asia (Figure 9; Spakman and Hall, 2010). There, the Java trench, consuming Australian Plate lithosphere, came into contact with a continental promontory of Australia, the Sula Spur. Australian Plate subduction continued by propagating into the Australian Plate through delamination

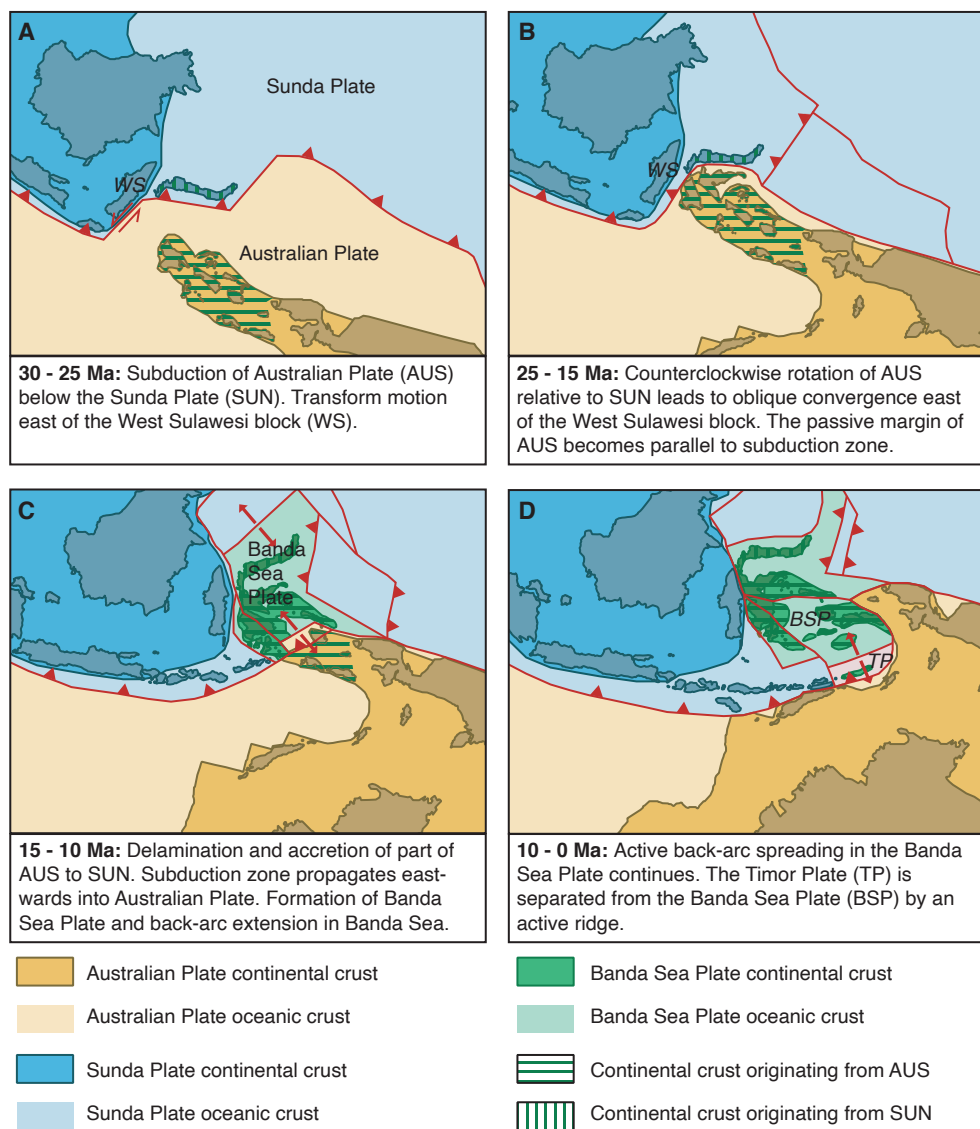


Figure 9. Snapshots of a kinematic reconstruction showing the subduction of the Australian Plate below the Sunda Plate and the formation of the Banda Sea Plate to illustrate the analogy with the formation of the Scotia Plate. Figures are based on the reconstruction of Hall (2002).

of mantle lithosphere from the Sula Spur, leaving the Sula Spur crust as fragments separated by extensional and partly oceanic basins in the upper plate (Figure 9; see also Spakman and Hall, 2010; their Figure 3).

We propose that the evolution of the Scotia Sea region has strong parallels with the evolution of the Banda region. This is best explained in a mantle reference frame, for which we take the modern moving hotspot reference frame of Doubrovine et al. (2012). This is possible because we embedded our regional reconstruction within the global framework of plate motion evolution. The Endurance slab had a free edge in the north where it was bounded by a transform (Figure 8b). A lateral, northward propagation of the Endurance subduction zone to the full width of the South Sandwich subduction zone may occur by delamination of the South American continental lithosphere (Figure 10), in analogy to the Sula Spur and the invasion of the Java subduction zone into the Banda embayment (Figure 9; Spakman and Hall, 2010).

It is interesting to note that between 70 and 50 Ma, the absolute plate motion direction of South America was southward (Figure 11; Doubrovine et al., 2012). This means that the northwestward subducting Endurance slab was dragged southward through the mantle by the subducting plate (for slab dragging see Chertova et al., 2014; Spakman et al., 2018; Chapter 1). Such slab dragging is resisted by the mantle and leads to northward indentation of South American lithosphere by the slab edge. An analogy of such geodynamic process is the indentation of the north African margin by the edge of the Gibraltar slab (Spakman et al., 2018). We propound that this indentation may have increased the propensity for the Endurance subduction zone to propagate northward

Delamination allowed for transfer of the crustal blocks, comprising the future Terror Rise, Bruce Bank, Pirie Bank, Discovery Bank, the North Scotia Ridge and South Georgia microcontinent, to the upper plate (Figure 8, Figure 10). The reconstructed South American continental blocks of the Scotia Sea region came close to the Endurance trench from ~71 Ma onwards, and delamination may have started then, but must have been underway by 50 Ma when extension in the Scotia Sea likely started (Figure 10). In this scenario, it is kinematically feasible that during this northward widening of the subduction zone the Central Scotia Sea formed between South Georgia and Discovery Bank due to N-S extension (Figure 6h; see section 5.6).

As a result, post ~50 Ma subduction occurred along the entire width of the North Weddell Sea oceanic lithosphere, from the ridge with Antarctica to the southern margin of Patagonia (Figures 6f; 8f, 10). This new trench connected in the north to the transpressional Magallanes fold-and-thrust belt that roughly followed the suture of the Rocas Verdes Basin, and transferred the plate boundary to the trench along the Fuegian Andes.

5.5. Extension in the Scotia Sea

Following formation of the South Sandwich-Endurance subduction system, pre-drift extension in the overriding plate started at 50 Ma (Livermore et al., 2005; Figure 6g). This

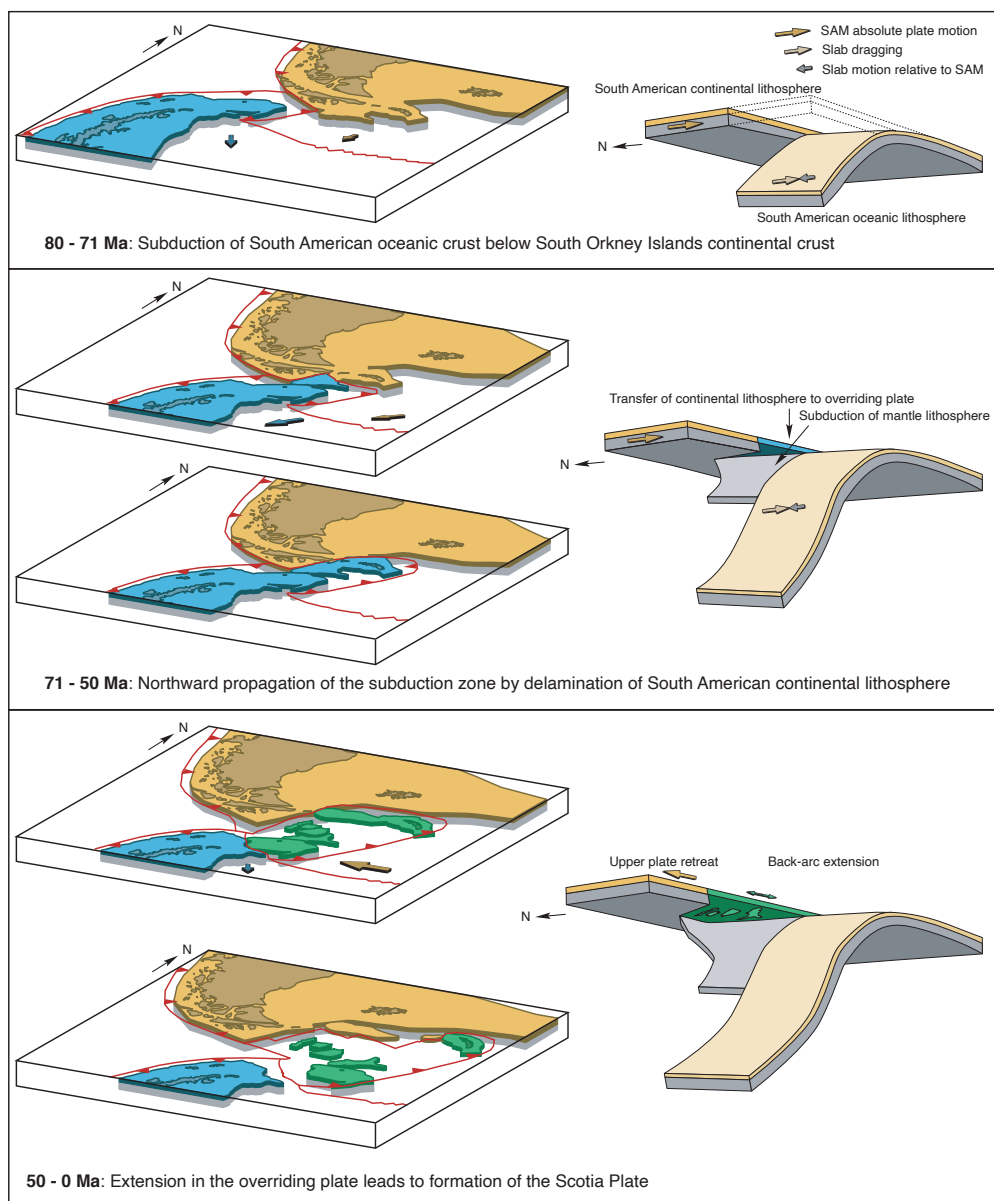


Figure 10. 3D snapshots of the kinematic reconstruction in a mantle reference frame (see also Figure 11) and 3D sketches showing the process of delamination and northwards propagation of the Endurance subduction zone and the subsequent transfer of South American continental crust to the overriding plate.

caused the South American margin to break up in multiple microplates and the separation of the South Orkney microcontinent and Jane Bank from the Antarctic Peninsula around 40 Ma (Eagles and Livermore, 2002; Figures 6h, 5i, j). We used the South America-Africa-East Antarctica plate circuit to determine the location of the northern ocean-continent transition conjugate to the southern Weddell Sea margin of Antarctica. This original South American ocean-continent transition was located 150–250 km north of the restored position of the Scotia Sea microcontinents at the onset of oceanic spreading at 36 Ma (Figure 6h). Such values for pre-drift continental extension are similar to those estimated for passive margins elsewhere (Torsvik et al., 2008). We restored the Scotia Sea microcontinents to the north and west of the reconstructed South American ocean-continent transition (Figure 6g). We assume a 50 Ma onset for pre-drift extension as widely inferred (Eagles et al., 2006; Livermore et al., 2007; Livermore et al., 2005; Mao and Mohr, 1995).

Following pre-drift extension, oceanic spreading first occurred in the Scan Basin between 35.7 and 29.5 Ma (Schreider et al., 2017; Figure 6h), followed by the Powell Basin between 29.5 and 21.2 Ma (Eagles and Livermore, 2002). Next, seafloor spreading started in the West Scotia Sea around 26 Ma, in a WNW-ESE direction (Eagles et al., 2005; Figure 6i). While this spreading ridge remained active, first the Dove Basin opened between 25.3 and 23.3 Ma (Schreider et al., 2018). Around 17.5 Ma, oceanic spreading started in two basins simultaneously, with spreading continuing until 14.2 Ma in the Jane Basin (Bohoyo et al., 2002) and until 13.6 Ma in the Protector Basin (Galindo-Zaldívar et al., 2006; Schreider et al., 2018; Figure 6j). Finally, spreading started in the East Scotia Basin around 17 Ma and remains active today (Larter et al., 2003; Figure 6k).

Shortly after formation of anomaly C6 (~19.7 Ma), segments of the South America-Antarctica spreading ridge started to arrive in the South Sandwich subduction zone that bordered the South Scotia Ridge (Figure 6j). The arrival of the ridge segments in the trench propagated east due to the obliquity of subduction. In absence of net plate convergence, with subduction being balanced by upper plate extension, the arrival of the spreading ridge led to the arrest of subduction, which propagated eastwards along the South Scotia Ridge (Barker et al., 1984). After complete shut-down of the southern segment of the trench, only the ~N-S striking portion of the subduction zone in the east remained, with E-W oriented back-arc spreading in the East Scotia Sea (Larter et al., 2003). At 7 Ma, transform motion started in the north, forming the Magallanes-Fagnano Fault Zone, and thereby the Scotia Plate (Torres-Carbonell et al., 2008a; Esteban et al., 2020). Shortly after, seafloor spreading in the West Scotia Basin ceased, at ~6 Ma (Eagles et al., 2005). Subduction continued in the eastern segment of the trench, where South American lithosphere is currently subducting below the South Sandwich Plate, with active E-W back-arc spreading restricted to the East Scotia Basin (Larter et al., 2003; Figure 6k).

Our reconstructed subduction evolution thus suggests that the Endurance-South Sandwich subduction system involved a single slab during its Late Cretaceous to early Cenozoic evolution. This is consistent with the interpretations of Van der Meer et al. (2018),

but we note that the tomography in the Scotia region is of poor resolution. It has been proposed that the eastern part of the slab is related to ongoing South Sandwich subduction, while a more westerly located high velocity zone represents a fossil part of the slab that formed at an Ancestral South Sandwich subduction zone (Beniest and Schellart, 2020). In this interpretation, the Ancestral South Sandwich subduction zone became inactive in the Miocene after the arrival of the South America-Antarctica Ridge in the southern segment of the trench (Pearce et al., 2014), which led to slab tearing and the onset of oceanic spreading in the East Scotia Basin, separating the South Sandwich arc from the Ancestral South Sandwich arc (Govers and Wortel, 2005; Pearce et al., 2014). The Ancestral South Sandwich subduction zone is the equivalent of our Endurance-South Sandwich subduction zone and these interpretations of the tomography are consistent with our reconstruction.

5.6. Age of the Central Scotia Sea

For the reconstruction of the Central Scotia Sea, with present-day E-W trending magnetic anomalies (Figure 4; Barker, 1970) two scenarios have previously been proposed. On the one hand, De Wit (1977) suggested that the Central Scotia Sea represents a piece of trapped Mesozoic oceanic crust, as the basin lacks a fossil ridge axis (De Wit, 1977) leading to various scenarios involving a Mesozoic Central Scotia Sea (e.g. Dalziel et al., 2013; Eagles and Jokat, 2014; Pearce et al., 2014). On the other hand, Hill and Barker (1980) speculated an Oligocene-Miocene age and many subsequent reconstructions have assumed a Cenozoic Central Scotia Sea opening (e.g. Barker et al., 1991; Carter et al., 2014; Livermore et al., 2007; Nerlich et al., 2013; V  rard et al., 2012). Here we discuss the implication of our reconstruction for both options.

If we assume a Mesozoic age for the Central Scotia Sea, we restore its position with the opening of the West Scotia Sea until 26 Ma, and with the South Georgia microcontinent before that time. In this reconstruction, the orientation of the Central Scotia Sea anomalies become parallel to the Weddell Sea anomalies. In this case the Central Scotia Sea oceanic crust formed part of the overriding plate above the subduction zone that consumed the Rocas Verdes Basin, which means the width of the Rocas Verdes Basin has implications for the age of the Central Scotia Sea. Our preferred Rocas Verdes Basin model predicts that the anomalies of the Central Scotia Sea formed as part of the Weddell Sea spreading system from ~132–125.9 Ma (chrons M7 – M0).

If we assume that the Central Scotia Sea opened in the Cenozoic, it must be younger than the 50 Ma onset of pre-drift extension (Livermore et al., 2007). The E-W trending lineations imply a N-S opening direction of the basin. In this case the Central Scotia Sea accommodates the northward motion of South Georgia from its 50 Ma position south of Burdwood Bank towards the North Scotia Ridge. To avoid overlap with the marine magnetic anomalies of the West Scotia Sea (Eagles et al., 2005), this northward motion must have occurred before 26 Ma. The bulk of the northward motion occurs before opening of the Scan Basin, and we reconstruct the opening of the Central Scotia between 48.5 and 36.9 Ma,

corresponding to chrons C22-C17.

Although both a Mesozoic and Cenozoic Central Scotia Sea are feasible within our reconstruction, we prefer a Cenozoic age for the Central Scotia Sea. Delamination of the South American lithosphere is most likely to have occurred along the passive margin at the transition from continental to oceanic crust. In the case of a Mesozoic Central Scotia Sea, however, part of the oceanic crust was trapped, which means delamination occurred intra-ocean. This may have occurred along a transform fault, but we find the passive margin a more likely location. Moreover, the northward motion of South Georgia that is required by the reconstruction and Cenozoic opening of the Central Scotia Sea fits exactly in the gap that forms when South Georgia separates from Discovery Bank. In addition, the extensive data review by Beniest and Schellart (2020) of currently available geological and geophysical data from the Scotia Sea region advocates for a Cenozoic Central Scotia Sea.

6. Discussion

6.1. Causes for the time lag between subduction initiation and back-arc extension

The onset of Scotia Sea extension started around 50 Ma (Livermore et al., 2005), based on subsidence in the Patagonia-Antarctic Peninsula land bridge around 49–47 Ma (Mao and Mohr, 1995), long after initiation of Endurance subduction. Why did it take so long for upper plate extension to start? To find an explanation, we first explore the contributions of the two potential drivers of upper plate extension: roll-back, i.e., the retreat of the subducting slab through the mantle in the direction of the down-going plate; and upper plate retreat, i.e., the absolute motion of the overriding plate away from the trench (Lallemand et al., 2005; Lallemand et al., 2008; Schepers et al., 2017; Van Hinsbergen et al., 2015). We investigate this in the mantle reference frame of Doubrovine et al. (2012) (Figure 11).

In the mantle frame of reference, Scotia Sea extension since 30 Ma has had a greater contribution from eastward slab roll-back than WNW-ward upper plate retreat. Of the total post-30 Ma extension, ~600 km resulted from WNW-ward upper plate retreat, and ~1250 km from slab rollback (Figure 11e, f, g). But between 50 and 30 Ma, the South Sandwich trench is almost mantle-stationary in the mantle reference frame (Figure 11c, d, e), suggesting that most, if not all, extension was the result of WNW-directed upper plate retreat (Figure 11c, d, e).

Interestingly, this WNW-ward motion of the South American Plate started around 50 Ma following a period of ~20–30 Ma of south-directed absolute plate motion (Figure 11). As noted in the previous section, the pre-50 Ma southward absolute motion of South America (Figure 11) was oblique to the NE-SW-striking trench and the NW-dipping Endurance slab, whose southward dragging was resisted by ambient-slab mantle (Figure 11 a-c). This would have increased the propensity for northward propagation of the subduction zone. We thus infer that the ~50 Ma onset of extension is a reflection of an absolute plate motion change of South America from southward to WNW-ward. Initially, the trench remained almost mantle stationary. This led to pre-drift extension within the delaminated South

American crustal blocks (Figure 10 c-d). The mantle-stationary trench continued until 30–25 Ma, during which the dragging of the subducted slab (extended by then to ~500 km) to the west-northwest was largely compensated by east-southeast rollback. Such interaction between advancing plate motion and rollback has been observed in laboratory experiments (Schellart, 2005).

Finally, accelerating ESE-ward slab roll-back started around 30–25 Ma when spreading ridges had formed across the upper plate (Eagles et al., 2005). This reduced the dynamic coupling between the down-going South Sandwich slab and the escaping South American Plate, which allowed the slab to roll back more freely. The direction of back-arc basin opening can be related to the changes in slab pull that control slab rollback. The oldest back-arc basins open in a WNW-ESE direction, in the same direction as the absolute plate motion of the South American Plate. When segments of the South America-Antarctica Ridge of the Weddell Sea started to arrive in the southern trench, subduction stopped there. As the existing slab lacked a strong connection to the surface, and slab pull was gradually concentrated to the north where the influence of slab-rollback on back-arc basin opening becomes dominant. This led to a change in the direction of overriding plate extension, from WNW-ESE in the West Scotia Sea to E-W in the East Scotia Sea.

Our analysis illustrates that placing a kinematic reconstruction in a mantle reference frame can reveal the slab motions and controlling geodynamic processes that determine the style of regional subduction and basin evolution, previously also shown by e.g., Spakman et al. (2018) and in Chapter 1. Relative reconstructions cannot provide such insights in case subduction is involved. Our reconstruction, placed in a mantle frame of reference, indicates that the onset of Scotia Sea extension and the opening of Drake Passage (Section 6.2) relate to the far-field driven absolute plate motion change of the South American Plate. This started to drive South America WNW-ward relative to the mantle around 50 Ma (Figure 11) while the slab assumed a near-stationary position in the mantle for a 20–25 Ma period. Slab roll-back, which was previously inferred to be the sole driver of Drake Passage opening in the Eocene, probably did not start until 30–25 Ma when slab pull started to dominate the forcing of subduction in concert with back-arc basin opening (Figure 11).

6.2. Opening of the Drake Passage and onset of circumpolar ocean flow in a global plate kinematic context

The opening of the Drake Passage occurred after the 50 Ma onset of overriding plate extension in a time interval of global geodynamic and climatic change. The onset of westward absolute South American Plate motion that is thought to have driven the rise of the Andes (Faccenna et al., 2017; Schellart, 2017) occurred in a time of global plate reorganization that also affected the Indian, Australian, and Pacific Plates (Müller et al., 2016; Torsvik et al., 2017; Vaes et al., 2019; Whittaker et al., 2007). It also coincides with first throughflow of ocean water through the Tasmanian Gateway between Australia and Antarctica (Bijl et al., 2013). Long-term global cooling started around the same time (Cramwinckel et al.,

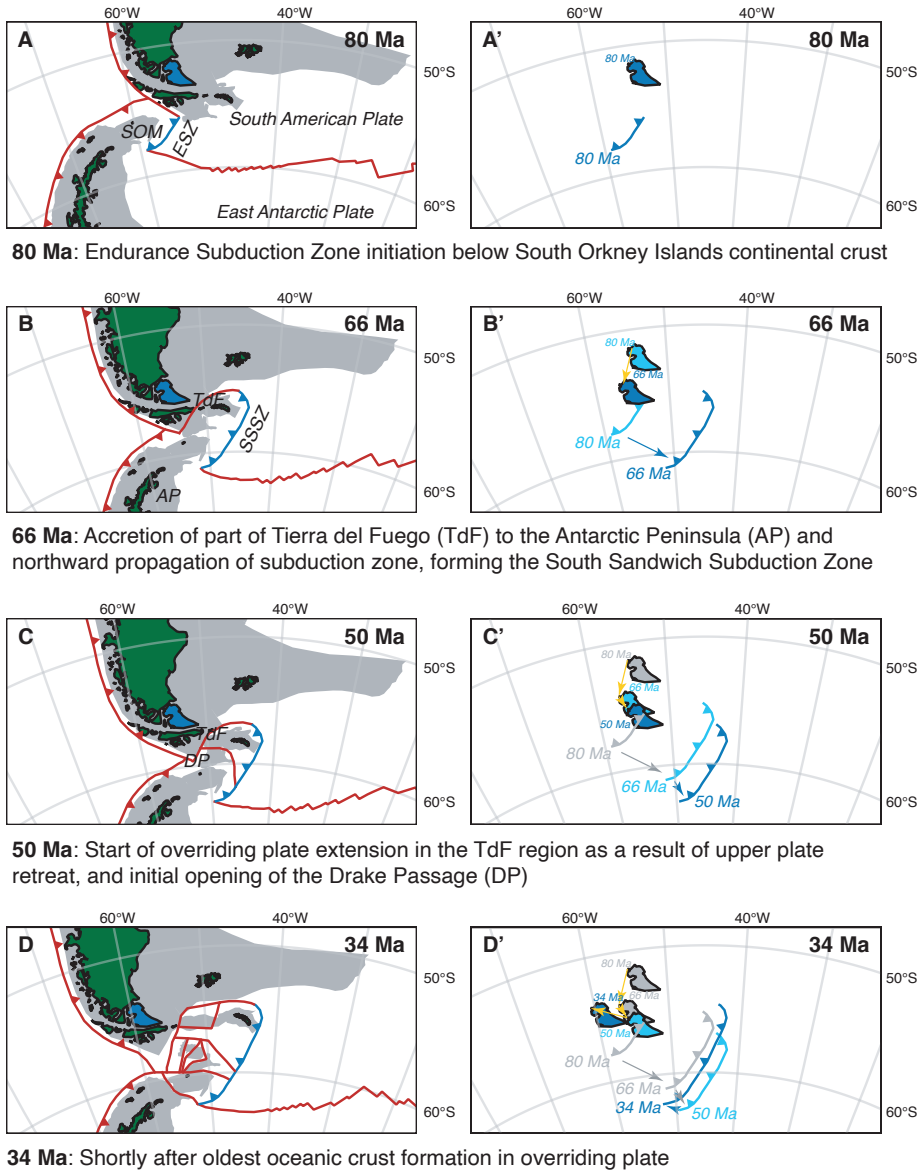


Figure 11. Snapshots of the kinematic reconstruction of the Scotia Sea region since subduction initiation at 80 Ma in a mantle reference frame (Dobrovine et al., 2012). A-H show major plate boundaries, present-day coastlines, and continental polygons, while A'-H' show the positions of Isla Grande de Tierra del Fuego and the South Sandwich trench relative to the mantle through time. A'-H' serve to illustrate the respective contributions of overriding plate escape and slab rollback to overriding plate extension through time. The locations of the South Sandwich trench and Isla Grande de Tierra del Fuego that correspond to the snapshot are shown in dark blue, while the location of the previous snapshot is light blue. Earlier locations are in gray.

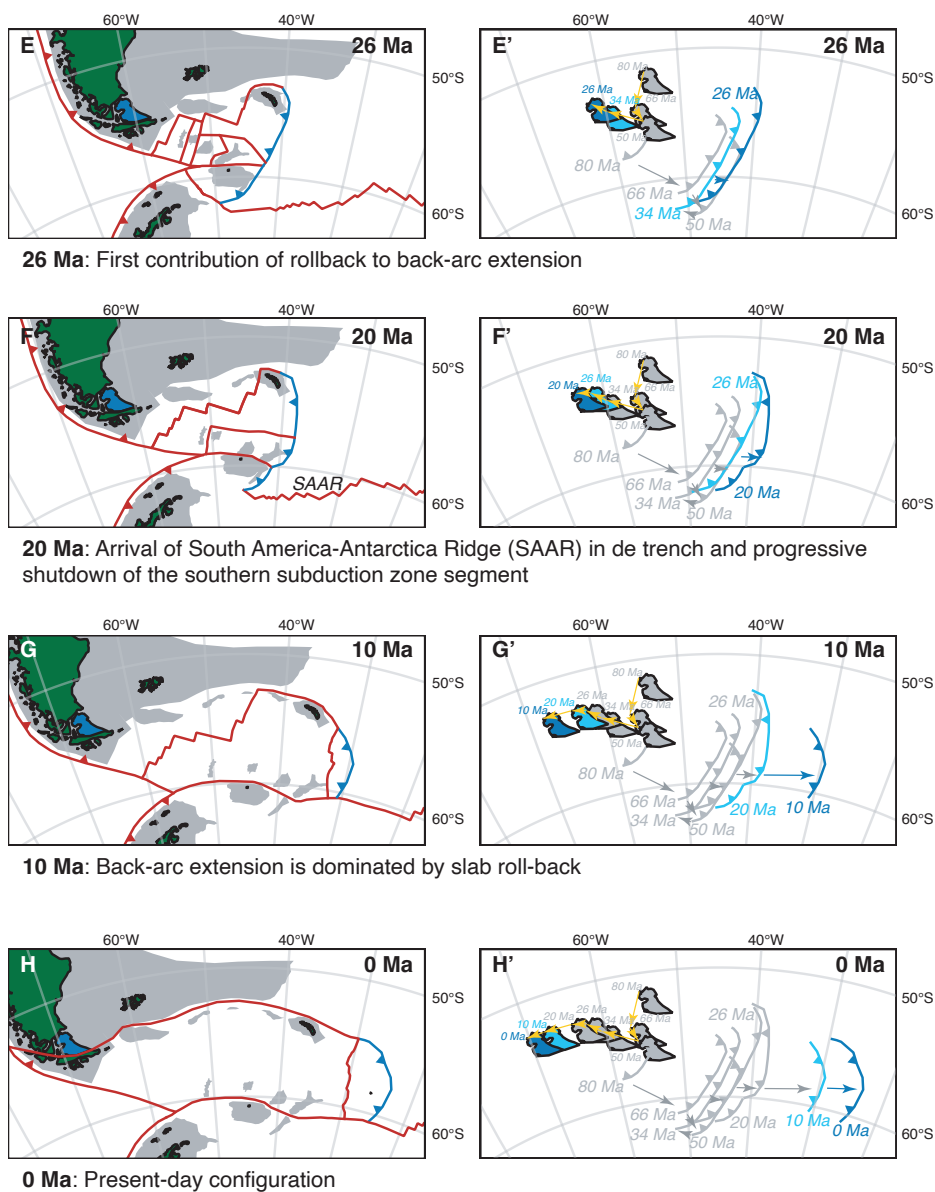


Figure 11 (continued).

2018) and is thought to be related to global atmospheric CO₂ decline through enhanced weathering, stimulated by enhanced silicate rock exposure from uplift of the Himalaya and Andes (Kump et al., 2000). This study shows that the same major plate reorganization responsible for the mid-Eocene tectonic development of climate-cooling mountain ranges also initiated the opening of the Drake Passage, clearing a major barrier for circumpolar flow of ocean water (a proto-Antarctic Circumpolar Current (ACC); e.g., Hill et al., 2013; Houben et al., 2019). Independent of CO₂ decline, this paleogeographic change promoted further regional cooling of Antarctica (Sijp et al., 2014), which preconditioned Antarctica for glaciation. This study thus demonstrates the influence of geodynamic changes in critical areas on the sensitivity of Antarctic climate and cryosphere to radiative forcing in the Cenozoic. Our reconstruction shows that a deep oceanic connection between the Pacific and the Atlantic started sometime between 50 and 36 Ma, in line with the 41 Ma onset of deep-water throughflow through the Drake Passage shown in geochemical records (Scher and Martin, 2006). However, it also shows this ocean connection was not unique: Cretaceous deep-water connections may have existed, and connections may have closed post-41 Ma as well. Ocean connections remained strongly constricted until <26 Ma, by obstruction through continental blocks and narrow deep-ocean passageways. This agrees with interpretations of a weak ACC and relatively flat latitudinal sea surface temperature gradients across the Southern Ocean during the Oligocene (Bijl et al., 2018; Evangelinos et al., 2020; Hartman et al., 2018; Salabarnada et al., 2018), which continued into the Miocene (~10 Ma; Sangiorgi et al., 2018). Although this may not be all due to the development of the Scotia Sea and other factors may have contributed (climate deterioration and ice sheet expansion), the Drake Passage was strongly constricted for most of the late Paleogene-early Neogene, and strengthening of the ACC coincides with major tectonic widening of the Scotia Sea (Figure 11g; see also Supplementary Figure 1).

7. Conclusions

Here we present a new kinematic reconstruction of the Scotia Sea region since the Early Jurassic (182 Ma). The aim of this study was to assess when and why subduction initiated that led to the formation of the South Sandwich subduction zone, and to explain the overriding plate position of both the Antarctic and South American plates. Our reconstruction results from systematic integration of available quantitative kinematic constraints, derived from marine geophysical, geological and paleomagnetic data, and the implementation of a global plate circuit, and enables the following conclusions:

1. The present-day South Sandwich subduction zone has its origin in the formation of a Late Cretaceous (~80 Ma) subduction zone below South Orkney Islands continental crust: the Endurance subduction zone. The occurrence of convergence along the South Orkney continental margin follows from the South American-Africa-Antarctica plate circuit and marine magnetic anomalies and fracture zones in the Weddell Sea. We suggest that delamination of the South American

continental lithosphere led to the northward propagation of the Endurance subduction zone to form the South Sandwich subduction zone. Delamination allowed for transfer of part of South American continental crust to the upper plate. Delamination was underway by 50 Ma when extension in the Scotia Sea started, but may have started around 71 Ma, when the South American continental margin came close to the Endurance trench.

2. Our kinematic reconstruction predicts that the Rocas Verdes Basin was up to 250 km wide. Cretaceous (~113–102 Ma) closure of the basin was accompanied by 25° counter-clockwise rotation of its southwestern margin. Excess rotations within Tierra del Fuego are ascribed to local block rotations related to post 7 Ma left-lateral strike slip motion of the Magallanes-Fagnano Fault Zone.
3. Overriding plate extension and subsequent opening of the Drake Passage started at 50 Ma. The time lag between subduction initiation and overriding plate extension is explained by the absolute plate motions of South America and Antarctica. Between Late Cretaceous subduction initiation and 50 Ma the absolute plate motion of South America was to the south, dragging the Endurance subduction system southward, and not contributing to lithosphere subduction. Around 50 Ma, the absolute plate motion of South America changed to west-northwest. The length of the slab was sufficient to provide a temporal balance between advancing motion and rollback, which led to the onset of upper plate extension as a result of motion of South America away from the trench. Our analysis thus suggests that early extension in the Scotia Sea region was the result of far-field changes in absolute plate motions.
4. The formation of oceanic spreading centres in the Scotia Sea around 35–25 Ma reduced the dynamic coupling between the down-going slab and escaping overriding plate, allowing the slab to roll-back freely. Subsequently, overriding plate extension resulted from both upper plate retreat and slab roll-back, dominated by the latter mechanism. The direction of back-arc basin opening is related to the relative influence of upper plate retreat and slab rollback. These inferences of slab evolution can only be made when using a mantle frame of reference, which our global circuit approach allows.
5. We deduce that the closely spaced micro-continental blocks in the Drake Passage Region must have initially limited throughflow of the Antarctic Circumpolar Current. Strengthening of the Antarctic Circumpolar Current in the Miocene coincides with major tectonic widening of the Scotia Sea.



Gertrude Valley, New Zealand

3

Reconciling the Cretaceous breakup and demise of the Phoenix Plate with East Gondwana orogenesis in New Zealand

This chapter has been published as:

Van de Lagemaat, S. H. A., Kamp, P. J. J., Boschman, L. M. & Van Hinsbergen, D. J. J. (2023). Reconciling the Cretaceous breakup and demise of the Phoenix Plate with East Gondwana orogenesis in New Zealand. *Earth-Science Reviews* 236, 104276.

Abstract

Following hundreds of millions of years of subduction in all circum-Pacific margins, the Pacific Plate started to share a mid-ocean ridge connection with continental Antarctica during a Late Cretaceous south Pacific plate reorganization. This reorganization was associated with the cessation of subduction of the remnants of the Phoenix Plate along the Zealandia margin of East Gondwana, but estimates for the age of this cessation from global plate reconstructions (~86 Ma) are significantly younger than those based on overriding plate geological records (105–100 Ma). To find where this discrepancy comes from, we first evaluate whether incorporating the latest available marine magnetic anomaly interpretations change the plate kinematic estimate for the end of convergence. We then identify ways to reconcile the outcome of the reconstruction with geological records of subduction along the Gondwana margin of New Zealand and New Caledonia. We focus on the plate kinematic evolution of the Phoenix Plate from 150 Ma onward, from its original spreading relative to the Pacific Plate, through its break-up during emplacement of the Ontong Java Nui Large Igneous Province into four plates (Manihiki, Hikurangi, Chasca, and Aluk), through to the end of their subduction below East Gondwana, to today. Our updated reconstruction is in line with previous compilations in demonstrating that as much as 800–1100 km of convergence occurred between the Pacific Plate and Zealandia after 100 Ma, which was accommodated until 90–85 Ma. Even more convergence occurred at the New Zealand sector owing to spreading of the Hikurangi Plate relative to the Pacific Plate at the Osborn Trough, with the most recent age constraints suggesting that spreading may have continued until 79 Ma. The end of subduction below most of East Gondwana coincides with a change in relative plate motion between the Pacific Plate and East Gondwana from westerly to northerly, of which the cause remains unknown. In addition, the arrival of the Hikurangi Plateau in the subduction zone occurred independent from, and did not likely cause, the change in Pacific Plate motion. Finally, our plate reconstruction suggests that the previously identified geochemical change in the New Zealand arc around 105–100 Ma that was considered evidence of subduction cessation, may have been caused by Aluk-Hikurangi ridge subduction instead. The final stages of convergence before subduction cessation must have been accommodated by subduction without or with less accretion. This is common in oceanic subduction zones but makes dating the cessation of subduction from geological records alone challenging.

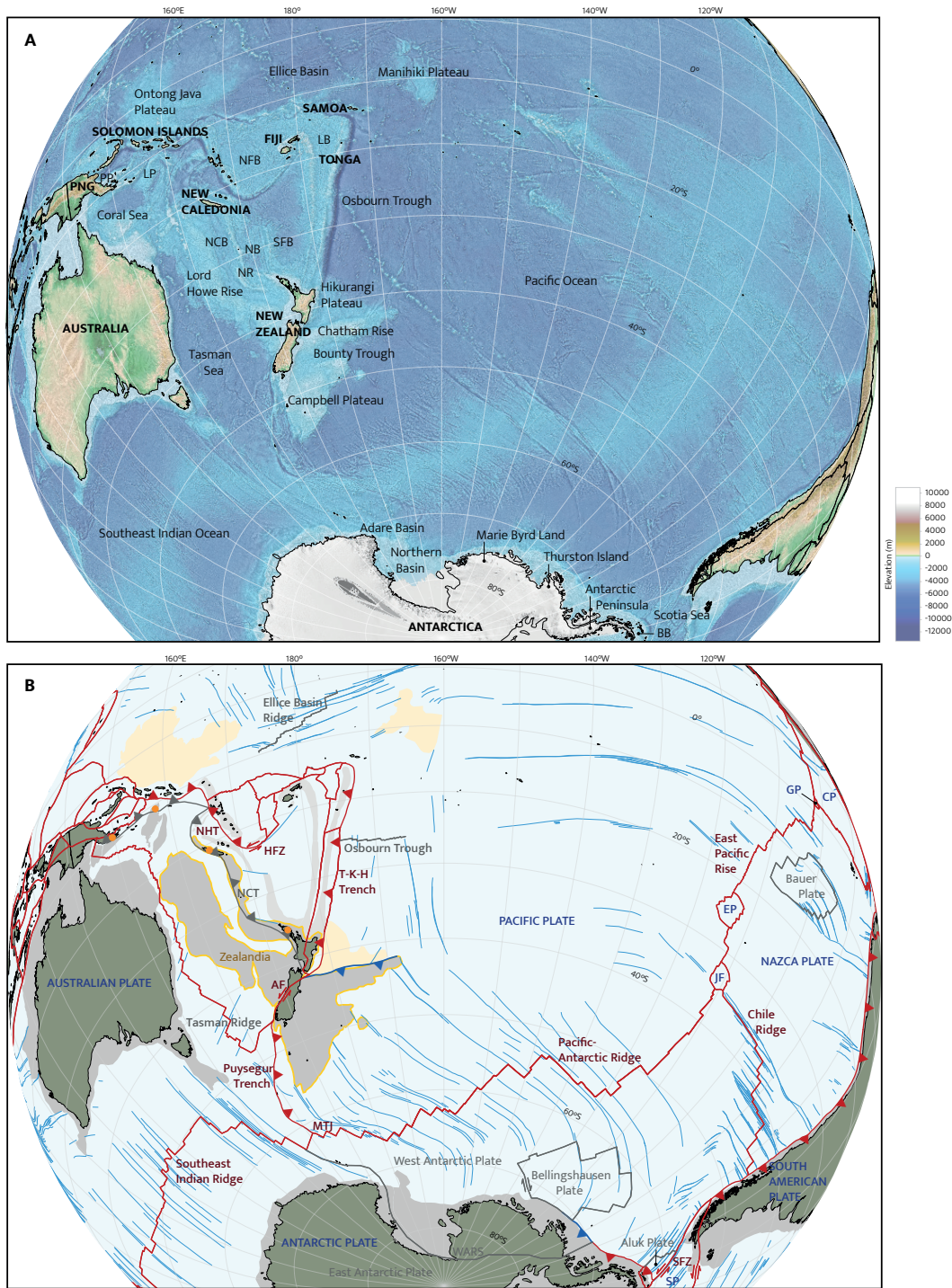
1. Introduction

During the Late Cretaceous, an important tectonic change occurred in the southern Pacific realm. For hundreds of millions of years, including most of the Mesozoic, the Panthalassa (or Paleo-Pacific) Ocean was surrounded by subduction zones that consumed oceanic lithosphere of the Farallon (NE), Izanagi (NW), and Phoenix (S) plates (e.g., Engebretson et al., 1985; Seton et al., 2012; Wright et al., 2016; Müller et al., 2019; Torsvik et al., 2019; Boschman et al., 2021a). During the Cretaceous, however, subduction ended along

the Zealandia sector of the East Gondwana continental margin (e.g., Bradshaw, 1989; Luyendyk, 1995; Davy et al., 2008; Matthews et al., 2012). Sections of the suture of the Mesozoic subduction zone are located along the northern margin of the Chatham Rise and along the Thurston Island sector of Antarctica, which are presently separated from each other by the Pacific-Antarctic Ridge (Figure 1). This implies that when Pacific-Antarctic spreading started, the ridge did not simply replace the former East Gondwana subduction zone. Instead, it cut through the subduction zone suture and formed partly intra-oceanic and partly intra-continental within East Gondwana lithosphere (Larter et al., 2002; Wobbe et al., 2012). Around the time of subduction cessation, several oceanic plates that formed after breakup of the Phoenix Plate, as well as part of Zealandia, merged with the Pacific Plate. Since then, the Pacific Plate has been diverging from West Antarctica, accommodated by oceanic spreading at the Pacific-Antarctic Ridge (Figure 1B). But despite its importance in the plate tectonic history of the Panthalassa/Pacific domain, the southwest Pacific-East Gondwana plate reorganization is surrounded with uncertainty.

The uncertainty surrounding the southwest Pacific-East Gondwana plate reorganization results from a discrepancy in the age of subduction cessation between different studies. On the one hand, geologists studying the magmatism and deformation in the orogen located at the overriding plate margin of New Zealand have found no conclusive evidence that shows that subduction must have continued beyond 105–100 Ma (e.g., Bradshaw, 1989; Luyendyk, 1995; Mortimer et al., 2019; Crampton et al., 2019). A 105–100 Ma age estimate for subduction cessation is commonly inferred from a change in deformation within New Zealand from largely compression to a regime dominated by extension (e.g., Bradshaw, 1989; Luyendyk, 1995; Crampton et al., 2019), coeval changes in the geochemical signature of magmatism (Muir et al., 1997; Waight et al., 1998; Tulloch and Kimbrough, 2003; Tulloch et al., 2009; Van der Meer et al., 2016, Van der Meer et al., 2017, Van Der Meer et al., 2018), and angular unconformities in the New Zealand forearc (Laird and Bradshaw, 2004; Crampton et al., 2019; Gardiner et al., 2021, Gardiner et al., 2022). On the other hand, global plate reconstructions suggest that convergence across the Zealandia margin of New Zealand continued until at least the end of spreading in the Osbourn Trough, of which estimates vary from ~101 Ma to 79 Ma, based on dredge samples and tentative marine magnetic anomaly identification (Billen and Stock, 2000; Worthington et al., 2006; Seton et al., 2012; Zhang and Li, 2016; Mortimer et al., 2019), with widely-used global plate reconstructions (Seton et al., 2012; Matthews et al., 2016; Müller et al., 2019) inferring an 86 Ma age that follows Worthington et al. (2006). This age, however, is based on interpretations of the New Zealand geological record that is disputed by many geologists that study New Zealand (e.g., Crampton et al., 2019; Mortimer et al., 2019). Reconciling the geological and plate kinematic estimates of the age of subduction cessation therefore requires using kinematic data from the oceanic and continental domain that are independent from interpreted ages of subduction cessation to avoid circular reasoning in making reconstruction choices.

To do so, we analyse the end of East Gondwana subduction along the Zealandia margin



◀ **Figure 1.** Present-day geographic and tectonic maps of the South Pacific region.

A) Geographic map.

BB: Bransfield Basin; LB: Lau Basin; LP: Louisiade Plateau; NB: Norfolk Basin; NCB: New Caledonia Basin; NFB: North Fiji Basin; NR: Norfolk Ridge; PNG: Papua New Guinea; PP: Papuan Peninsula; SFB: South Fiji Basin. Background image is ETOPOI 1 Arc-Minute Global Relief Model. (Amante and Eakins, 2009; NOAA National Geophysical Data Center, 2009).

B) Tectonic map. Current tectonic plate names in blue. Current plate boundaries (Bird, 2003) and plate boundary names in red, former plate names and plate boundaries in grey, suture of East Gondwana subduction zone in blue. Continental crust of Zealandia is outlined in yellow. Northland, New Caledonia, Louisiade, and Papuan Peninsula ophiolites are indicated by orange dots. Ontong Java Nui Large Igneous Provinces in light yellow. Lightblue lines are digitalized fracture zones, obtained from the GSFML database (Matthews et al., 2011; Wessel et al., 2015)

AF: Alpine Fault; CP: Cocos Plate; EP: Easter Plate; GP: Galapagos Plate; HFZ: Hunter Fracture Zone; JF: Juan Fernandez Plate; MS: Manihiki Scarp; MTJ: Macquarie Triple Junction; NHT: New Hebrides Trench; NCT: New Caledonia Trench; SFZ: Shackleton Fracture Zone; SP: Scotia Plate; T-K-H: Tonga-Kermadec-Hikurangi; WARS: West Antarctic Rift System.

by reassessing both the plate kinematic and orogenic perspectives. First, we evaluate whether the age for the end of convergence suggested by global plate models changes by using the latest, and most detailed published marine magnetic anomaly-based isochrons, and by using the range of estimates for the arrest of Osborn Trough spreading based on magnetic anomalies or dredge samples. Our reconstruction includes the evolution and fragmentation of the Phoenix Plate into its several daughter plates. We use the recent study of Torsvik et al. (2019) who revisited and modified absolute Pacific Plate models and updated earlier global plate reconstructions. We consider relative motions across the East Gondwana continental margin as a function of absolute plate motion models to evaluate when convergence may have ended, and which process may have been responsible for this cessation. Furthermore, we review aspects of the architecture and evolution of the Cretaceous New Zealand orogen, and attempt to reconcile the timing of the end of subduction with the available geological evidence. We will use our results as a basis for the reconstruction of the demise of the Phoenix Plate's daughters, which resulted from their capture by the Pacific Plate after cessation of subduction along the Gondwana margin and the enigmatic transition to the Pacific-Antarctic spreading ridge.

2. Plate tectonic setting

The south Pacific Ocean today is underlain by the Pacific, Antarctic, and Nazca plates, separated by trenches from the South American, Antarctic, and Australian plates (Figure 1). The oceanic plates of the Pacific Ocean are separated from each other by mid-ocean ridges: the Pacific-Antarctic Ridge, the East Pacific Rise between the Pacific and Nazca plates, and the Chile Ridge between the Antarctic and Nazca plates (Figure 1). Three microplates are present along the East Pacific Rise: The Juan Fernandez, Easter, and Galapagos microplates.

In the west, the Pacific Plate is currently subducting below the Australian Plate at the

Tonga-Kermadec-Hikurangi subduction zone. To the west of this subduction zone is a series of Cenozoic back-arc basins (e.g., Lau Basin, South Fiji Basin, Norfolk Basin; e.g., Yan and Kroenke, 1993; Sdrolias et al., 2003; Herzer et al., 2011), bounded in the west by the extended continental crust of Zealandia that underlies the Lord Howe Rise and Norfolk Ridge (e.g., Mortimer et al., 2017). Zealandia is separated from the Australian continent by the Upper Cretaceous-Paleogene Tasman Sea and New Caledonia basins (e.g., Gaina et al., 1998; Grobys et al., 2008). The Norfolk Ridge was overthrust from the east during the Oligocene (c. 30 Ma) by the Paleocene New Caledonia ophiolite (Cluzel and Meffre, 2002; Cluzel et al., 2012a). Ophiolite obduction occurred during cessation of a northeast-dipping intra-oceanic subduction zone that formed around 60 Ma. At this time other ophiolites also formed that were emplaced during the Late Oligocene onto Northland, New Zealand, and northward towards the Louisiade Plateau and the eastern Papuan Peninsula (Figure 1) (Chapter 1; Whattam et al., 2006; Cluzel et al., 2012a; Maurizot et al., 2020a; McCarthy et al., 2022).

At its northern end, southwest of Samoa, the Tonga-Kermadec-Hikurangi subduction turns sharply to the west (Figure 1). Here the plate boundary changes to a SW-trending, diffuse transform system around the Fiji Islands, southwest of which it continues as the Hunter fracture zone that connects to the New Hebrides Trench. At this trench the Australian Plate is subducting below the North Fiji back-arc basin that hosts spreading ridges with the Pacific Plate. The southern end of the Tonga-Kermadec-Hikurangi subduction zone connects via the right-lateral Alpine Fault to the Puysegur Trench where subduction of the Australian Plate below the Pacific Plate is occurring (e.g., Collot et al., 1995; House et al., 2002; Gurnis et al., 2019). The plate boundary ends at the Macquarie Triple Junction, where the Australian, Pacific, and Antarctic plates meet, and where the Macquarie microplate formed c. 7 Ma (Cande and Stock, 2004b; Choi et al., 2017). Kinematic reconstructions of Cenozoic tectonic history of the SW Pacific realm differ in the timing and distribution of convergence over the New Caledonia and Tonga-Kermadec subduction zones (Chapter 1; Hall, 2002; Schellart et al., 2006; Whattam et al., 2008), but mostly agree on the pre-late Cretaceous position of Zealandia against the Australian continent, and on the location of the subduction zone along the eastern Zealandia margin that consumed the Phoenix Plate and its daughters (Figure 2).

The southern boundary of the Pacific Plate is the Pacific-Antarctic Ridge (Figure 1B). This plate boundary formed c. 89 Ma, based on the extrapolation of spreading rates from the oldest identified marine magnetic anomaly (C34y; 83.7 Ma) towards the continental margin (Wobbe et al., 2012). This age is in correspondence with the 83.9 ± 0.1 Ma age of the Erik seamount, obtained from Ar/Ar dating of K-feldspar of a trachyte sample, which provides a minimum age of the oceanic crust (Mortimer et al., 2019). The Pacific-Antarctic Ridge accommodated the divergence of the Campbell Plateau (part of the Zealandia continent, located on the Pacific Plate) from Marie Byrd Land (located on the West Antarctic Plate) (e.g., Wobbe et al., 2012). Before break-up, the Campbell Plateau and West

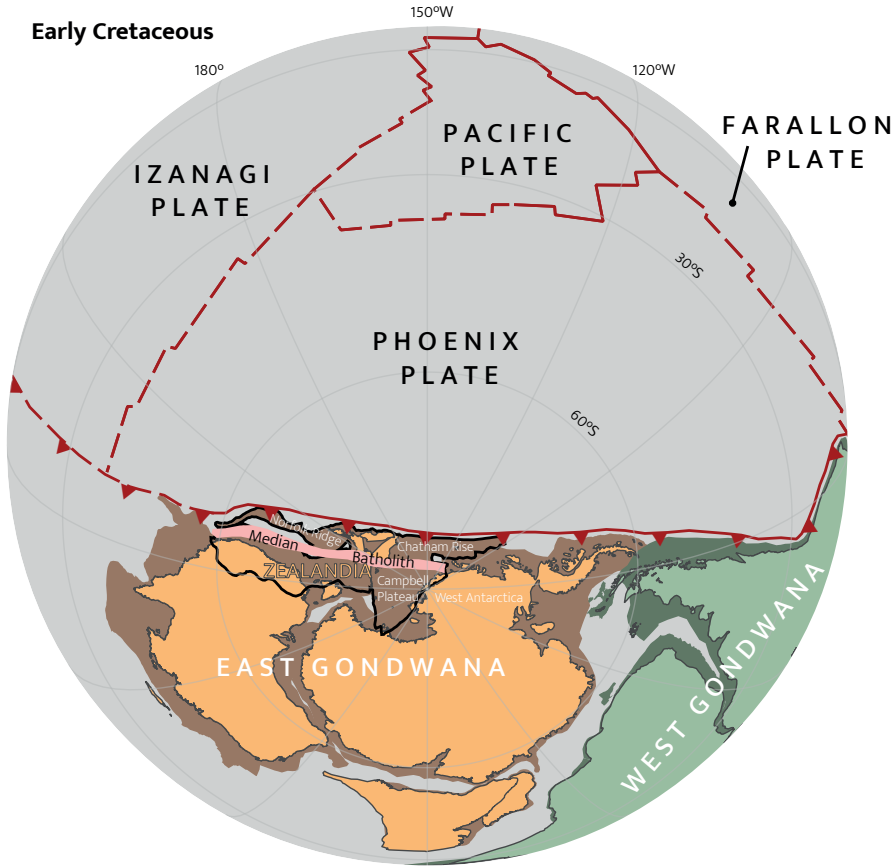


Figure 2. Early Cretaceous (c. 140 Ma) reconstruction of the paleo-Pacific/Panthalassa realm showing the approximate extent of the Phoenix Plate. Continental crust of future Zealandia is outlined in black, highlighting the Zealandia margin of East Gondwana. Plate boundaries are only shown in the Panthalassa domain, dashed where the location of the plate boundary is estimated.

Antarctica formed part of the upper plate adjacent to the Mesozoic active margin of East Gondwana (Figure 2) (e.g., Larter et al., 2002). This margin was contiguous with the active margins of the Antarctic Peninsula and South America, where subduction remains active today. Presently, subduction of a small remnant of the last of the Phoenix Plate's daughters, the Aluk Plate (Herron and Tucholke, 1976), is ongoing below the northern part of the Antarctic Peninsula (Figure 1) (e.g. Eagles, 2004). The Aluk Plate is often also referred to as Phoenix Plate, but we prefer the name Aluk Plate to make the distinction with the original parent Phoenix Plate. Subduction below Antarctica progressively ceased with the arrival of different segments of the Aluk-Antarctica Ridge. A small segment of this ridge remains in the Southeast Pacific Ocean, which became extinct c. 3.3 Ma (Eagles, 2004), effectively merging the Aluk Plate with the Antarctic Plate. Subduction below the Antarctic Peninsula

is currently accommodated by opening of the Bransfield Basin within the upper Antarctic Plate (Figure 1; Galindo-Zaldivar et al., 2004). The eastern boundary of the Aluk Plate is the Shackleton Fracture Zone, separating it from the West Scotia Sea. Opening of the Scotia Sea oceanic basins was not related to plate motions of the paleo-Pacific realm (Chapter 2) and the Shackleton Fracture Zone is thus the eastern boundary of our reconstruction. To the north of the Shackleton Fracture Zone, the Antarctic Plate, Chile Ridge, and Nazca Plate are subducting below South America.

Mesozoic subduction of Phoenix Plate lithosphere was accommodated along the Antarctica and Zealandia margins of East Gondwana (Figure 2). Breakup of these continents from each other and from Australia led to oceanic spreading around 84 Ma in both the Tasman Sea and South Pacific Ocean (Gaina et al., 1998; Wobbe et al., 2012; Mortimer et al., 2019), but continental rifting between Zealandia and Antarctica and between Zealandia and Australia has been considered to date back to c. 105–100 Ma (Bradshaw, 1989; Luyendyk, 1995; Laird and Bradshaw, 2004). Earliest extension between Australia and Antarctica started at c. 136 Ma (Whittaker et al., 2013).

A prominent record of Mesozoic subduction is present in New Zealand. The Eastern Province consists of Permian intra-oceanic arc sequences and a long-lived Mesozoic accretionary wedge (Figure 3) (Mortimer, 2004; Mortimer et al., 2014a). It is possible that the Eastern Province hosts the records of two subduction systems, one along the Gondwana margin and one intra-oceanic (Appendix 1; Adams et al., 2007; Campbell et al., 2020), but these have been juxtaposed since at least the latest Jurassic (Tulloch et al., 1999), i.e., throughout the window of interest of this paper. The western and eastern provinces are separated by the Median Batholith that represents a long-lived Paleozoic to Mesozoic magmatic arc (Figure 2, Figure 3) (Mortimer, 2004). The accretionary wedge of the Eastern Province consists of ocean plate stratigraphy (OPS; Isozaki et al., 1990) comprising pillow lavas, oceanic pelagic and hemipelagic sediments, and trench fill clastics (Caples, Waipapa and Torlesse terranes; Mortimer et al., 2014a). These OPS sequences accreted to the Gondwana margin from Permian to Early Cretaceous times and were intruded by magmatic arc plutons and overlain by forearc basin clastics (Adams et al., 1998; Adams et al., 2013; Mortimer, 2004; Boschman et al., 2021a). The geology of New Caledonia shares broad similarities with that of New Zealand: The Boghen Terrane of New Caledonia has been correlated to the Torlesse Complex of New Zealand; both Jurassic-Cretaceous accretionary complexes, and the Teremba Terrane of New Caledonia to the Murihiku Terrane of New Zealand; both forearc terranes consisting of late Permian to Jurassic island-arc derived strata (Cluzel and Meffre, 2002; Maurizot et al., 2020b). Cretaceous sedimentary sequences that overlie the Torlesse accretionary complex from 100 Ma onwards in New Zealand (Laird and Bradshaw, 2004; Crampton et al., 2019) provide important arguments for interpreting the end of subduction: they are widely seen as signaling a transition from a subduction margin to a passive margin (e.g., Field and Uruski, 1997; Laird and Bradshaw, 2004; Crampton et al., 2019). However, others have considered these Late Cretaceous sequences to be accretionary

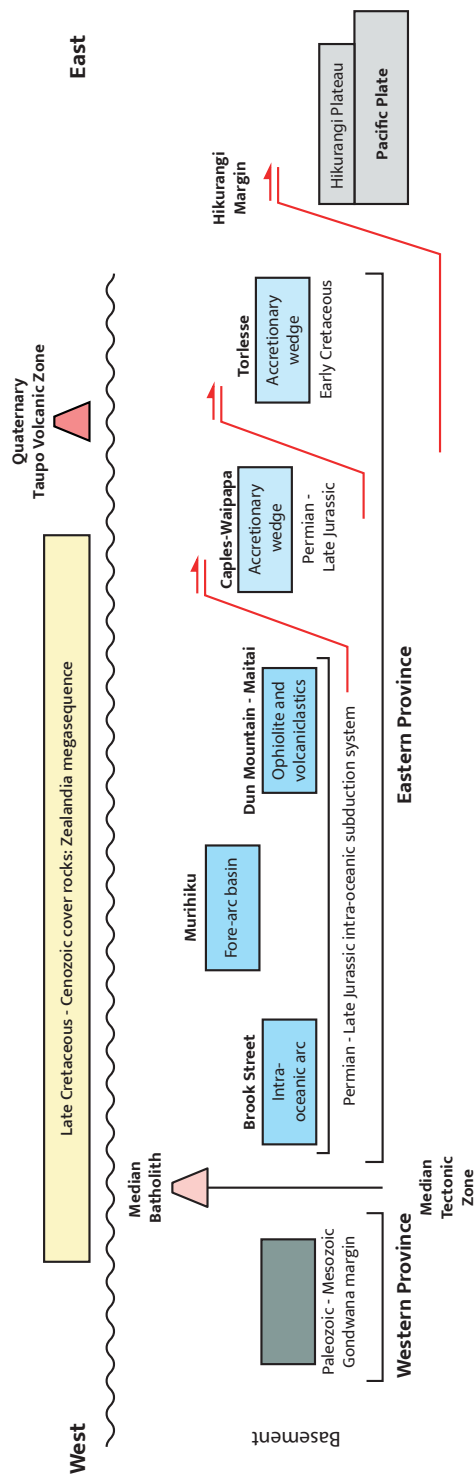


Figure 3. Schematic cross-section of the present-day geology of the North Island of New Zealand, based on Mortimer et al. (2014a).

shelf and slope basin fill that accumulated during outbuilding of the accretionary wedge and that subduction continued until c. 84 Ma (Mazengarb and Harris, 1994; Kamp, 1999, Kamp, 2000; Gardiner and Hall, 2021). Deposition of subduction-related volcanoclastic greywackes continued until c. 90 Ma in New Caledonia (Cluzel et al., 2010; Maurizot et al., 2020b).

The oceanic lithosphere of the modern Pacific Plate contains three prominent oceanic plateaus interpreted to have formed as a single ~120 Ma Large Igneous Province (LIP): the conceptual Ontong Java Nui LIP (Taylor, 2006; Chandler et al., 2012). The three oceanic plateaus that are thought to have once formed as Ontong Java Nui are currently separated by post-120 Ma Cretaceous oceanic basins. These oceanic plateaus are the Ontong Java Plateau, located to the north of the Solomon Islands; the Manihiki Plateau, located to the northeast of Samoa; and the Hikurangi Plateau, located offshore the North Island of New Zealand (Figure 1). The Manihiki Plateau is separated from the Ontong Java Plateau by the Ellice Basin, and the Hikurangi Plateau is separated from the Manihiki Plateau by the Osborn Trough (Figure 1).

3. Reconstruction approach, plate circuits, and reference frames

Quantitative constraints on the convergence history between the plates of the Panthalassa realm and the Zealandia margin of East Gondwana follows from the kinematic reconstruction of the South Pacific region. The reconstruction presented here includes a compilation of the most recent kinematic data and the new Pacific reference frame of Torsvik et al. (2019). For the analysis in this paper, we focus on the history of the South Pacific region back to the Early Cretaceous. Our reconstruction is made in GPlates, a freely available plate reconstruction software (www.gplates.org; Boyden et al., 2011; Müller et al., 2018).

We restore spreading along the different mid-ocean ridges that existed in the southern Panthalassa realm based on published marine magnetic anomaly data of ocean floor presently underlying the south Pacific Ocean (Figure 4), reviewed in section 4. The ages of the polarity chrons in our reconstruction are updated to the timescale of Ogg (2020). We incorporate all rotation poles as published, even though on short time intervals (<1 Myr) these are likely subject to some noise (Iaffaldano et al., 2012). Our conclusions, however, are not affected by the short time-scale noise and we prefer to see the effect of all interpreted isochrons rather than an arbitrary selection of these.

In the absence of polarity reversals during the Cretaceous Normal Superchron (121.4–83.7 Ma), the restoration of oceanic basins for this time interval is based on previously published radiometric data from dredged and cored samples as well as published interpretations of seafloor fabric (Figure 4; see section 4). Magnetic anomaly picks and fracture zone data were obtained from the Global Seafloor Fabric and Magnetic Lineation (GSFML) Database (Matthews et al., 2011; Seton et al., 2014; Wessel et al., 2015). We restore intra-continental deformation within East Gondwana applying a reconstruction hierarchy that uses quantitative kinematic constraints on continental extension, transform motion, or

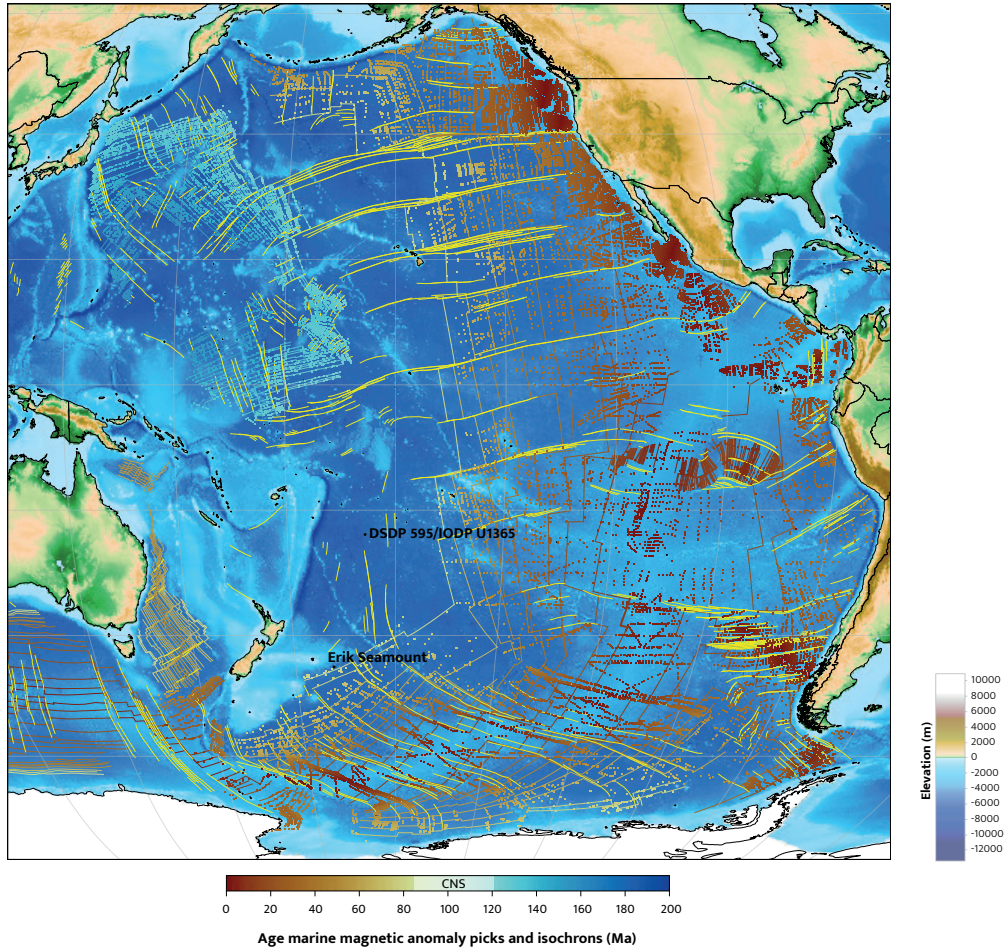


Figure 4. Geographic map of the Pacific and Southeast Indian oceans, showing the data used for the reconstruction of the oceanic domain. Marine magnetic anomaly picks (colored by age) and fracture zone data (in yellow) were obtained from the GSFML database (Matthews et al., 2011; Seton et al., 2014; Wessel et al., 2015, and references therein). Interpreted isochrons are from Seton et al. (2012), Wright et al. (2016), and from this study. Background image is ETOPO1 1 Arc-Minute Global Relief Model (Amante and Eakins, 2009; NOAA National Geophysical Data Center, 2009). Marine magnetic anomaly picks are colored using a colour bar of Crameri (2018); Crameri et al. (2020).

crustal shortening (see Boschman et al., 2014 and Chapter 1 for details).

Plate convergence can best be quantified when a plate circuit is present that connects the two converging plates through a series of active or fossil spreading ridges (Cox and Hart, 1986). For times after the formation of the Pacific-Antarctic Ridge (Chron C34y, c. 83.7 Ma; see section 4), plate convergence in the region can be reconstructed through a plate circuit that constrains the motion of the Australian Plate relative to the Antarctic Plate based on the record of oceanic spreading at the Southeast Indian Ridge (SEIR), and the

motion of the Pacific Plate relative to the Antarctic Plate by restoring spreading at the Pacific-Antarctic Ridge (PAR) (Figure 5). The Late Cretaceous and Cenozoic opening of marginal and back-arc basins east of Australia are reconstructed relative to the Australian Plate, that adds Zealandia-Australia, and Tonga-Kermadec-Hikurangi trench-Zealandia motion to the plate circuit. In addition, the relative motion of oceanic plates flooring the Pacific Ocean are reconstructed relative to the Pacific Plate (Figure 5). For the period of activity of the New Caledonia subduction zone in Paleocene to Oligocene time, it is not possible to quantify partitioning of convergence over the Tonga and New Caledonia trenches – only net convergence between Zealandia and the Panthalassa plates can be quantified (Chapter 1). However, for the interval of interest of this paper, this problem is of no consequence.

For times after the Cretaceous Normal Superchron, i.e. at C34y (post-83.7 Ma), we use the ‘Antarctic’ plate circuit Zealandia – Australia – East Antarctica – West Antarctica – Pacific (Figure 5). Due to uncertainties in relative motion between West Antarctica and East Antarctica before 45 Ma, some studies use a plate circuit for these times that ties the Lord Howe Rise to the Pacific Plate directly before c. 45 Ma instead (i.e., the Australian circuit) using magnetic anomalies in the Tasman Sea basin (e.g., Steinberger et al., 2004; Torsvik et al., 2019). In the Australian circuit it is assumed that there is no plate boundary between the Pacific Plate and Zealandia between 83 and 45 Ma. However, geological data from New Caledonia provides evidence for the existence of a subduction zone between the Pacific Plate and the Norfolk Ridge between c. 60 and 30 Ma (e.g., Chapter 1; Cluzel et al., 2012a; Maurizot et al., 2020b), which means that the Pacific Plate should not be reconstructed relative to Zealandia after 60 Ma. Combined with recently improved constraints on deformation within Antarctica (e.g., Granot et al., 2013; Granot and Dymant, 2018) leads us to prefer the Antarctic circuit for our reconstruction, similar to Seton et al. (2012), Matthews et al. (2015), and Müller et al. (2019). There is a c. 150 km difference in location of the Pacific relative to the Gondwana plates between the Antarctic and Australian circuits at chron C34y (83.7 Ma).

Before the onset of Pacific-Antarctic Ridge spreading, the plate circuit is broken, as the Panthalassa and Gondwana plates are connected through a subduction zone only (Seton et al., 2012; Wright et al., 2016). The reconstruction of pre-chron C34y (83.7 Ma) relative motions across the East Gondwana margin then relies on placing the Gondwana continents and the Panthalassa plates in mantle reference frames that were developed for each of the two systems separately (Figure 5). For this reason, we put our reconstruction in a mantle reference frame for the entire reconstruction period. The Gondwana continents are part of the Indo-Atlantic realm, whose relative motions are constrained by the reconstruction of the Indian and Atlantic Oceans. Several mantle reference frames are available for the Indo-Atlantic realm, from different approaches and iterations. We will illustrate the sensitivity of the choice of reference frame for convergence across the Zealandia margin, using the moving hotspot reference frames of O’Neill et al. (2005), Torsvik et al. (2008), and Doubrovine et al. (2012), and the semi-quantitative slab-fitted reference frame of Van

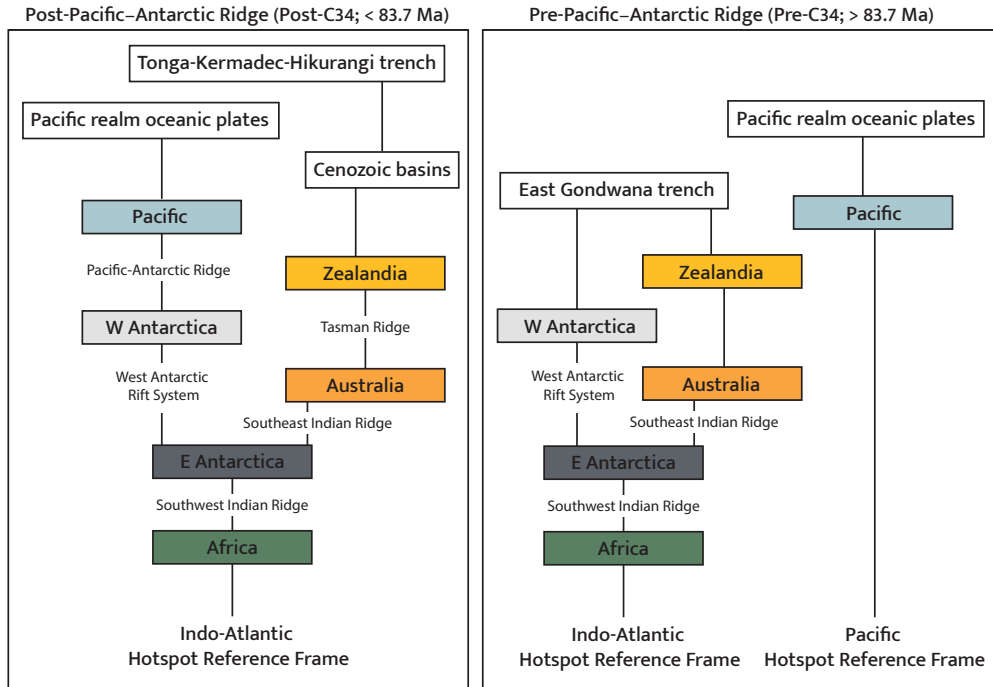


Figure 5. Plate circuits used in our reconstruction, highlighting the differences in the plate circuit before and after formation of the Pacific-Antarctic Ridge.

der Meer et al. (2010). These reference frames are given in African coordinates, requiring reconstructing the eastern Gondwana continents circuit to the African Plate. For the period after the Cretaceous Normal Superchron, we also use the Indo-Atlantic reference frame for the Panthalassa domain, as it is connected to the plate circuit. For the period before chron C34y (83.7 Ma), when the plate circuit is broken, we use the Pacific reference frame of Torsvik et al. (2019), who updated a fixed hotspot frame that constrains absolute Pacific Plate motion back to 150 Ma. We incorporate the ‘Earthbyte Model R’ of Torsvik et al. (2019), which corresponds to the Antarctic circuit as explained above.

4. Review of kinematic data

4.1. Post-Cretaceous Quite Zone plate reconstruction of ocean basins, and East Gondwana fit

The onset of spreading at the Pacific-Antarctic Ridge marks a major break in the plate tectonic history of the Panthalassa-Pacific realm, as it formed the first passive margin that connected the oceanic domain to the Indo-Atlantic plates after hundreds of millions of years (e.g., Molnar et al., 1975; Seton et al., 2012; Wright et al., 2016; Müller et al., 2019). The oldest magnetic anomaly that records spreading between the Campbell Plateau and Marie Byrd Land (West Antarctica) is chron C33 (79.9 Ma; Wobbe et al., 2012), the

oldest crust having formed after the end of chron C34y, i.e., after 83.7 Ma. Farther east, however, the marine magnetic anomaly of chron C34y (83.7 Ma) was identified just south of Chatham Rise and its conjugate margin off the coast of Thurston Island (Larter et al., 2002; Eagles et al., 2004a; Wobbe et al., 2012). There is no evidence for the existence of a plate boundary between the oceanic crust that formed south of the Chatham Rise and the Campbell Plateau and oceanic crust of the Pacific Plate, and it is therefore assumed that the Chatham Rise and Campbell Plateau have been part of the Pacific Plate since the formation of the Pacific-Antarctic Ridge (Molnar et al., 1975; Luyendyk, 1995). The set of marine magnetic anomalies of chron C34y (83.7 Ma) that formed south of Chatham Rise and off the coast of Thurston Island is therefore the oldest marine magnetic anomaly constraint for Pacific-West Antarctica spreading (Wobbe et al., 2012; Wright et al., 2016). As these marine magnetic anomalies are located close to the continental margins of Chatham Rise and West Antarctica, it is thought that true seafloor spreading started shortly before the end of the Cretaceous Quiet Zone (Wobbe et al., 2012). Based on the extrapolation of seafloor spreading rates, Wobbe et al. (2012) suggested that the first oceanic crust between Chatham Rise and Thurston Island (West Antarctica) formed around 84 Ma, which is in accord with the minimum age for the oceanic crust between Chatham Rise and West Antarctica, based on a 83.9 ± 0.1 Ma Ar/Ar age of K-feldspar in a trachyte sample from Erik Seamount (Mortimer et al., 2019), while rifting is thought to have started around 89 Ma (Wobbe et al., 2012). The oldest oceanic crust between Chatham Rise and West Antarctica may have formed during extension in the Bounty Trough (between 92 and 84 Ma; Grobys et al., 2008), before Chatham Rise was captured by the Pacific Plate. The timing of the capture of Chatham Rise by the Pacific remains uncertain, although it must have occurred in the 90–83.7 Ma interval: the location of the Pacific Plate is constrained at either end of this time interval: 90 Ma is the youngest age in the Pacific hotspot reference frame of Torsvik et al. (2019) and 83.7 Ma (i.e., chron C34y) is the oldest marine magnetic anomaly constraint (Wright et al., 2016). Between those times (90–83.7 Ma), the Pacific Plate may have started to diverge from West Antarctica, but we reconstruct the start of Pacific-Antarctic spreading based on the oldest marine magnetic anomaly constraint (i.e., C34y; 83.7 Ma; Wobbe et al., 2012), similar to other reconstructions (e.g., Seton et al., 2012; Wright et al., 2016; Müller et al., 2019). Any extension in the region (i.e., between Chatham Rise and Campbell Plateau and West Antarctica) before that time is considered to not have involved the Pacific Plate (Figure 6D and Figure 7C). We reconstruct the motion between the Pacific Plate and West Antarctica using finite rotation poles of Croon et al. (2008) (present–C20; 43.5 Ma) and Wright et al. (2016) (C21–C34y; 47.8–83.7 Ma). This is similar to the reconstruction of Müller et al. (2019), although we incorporate all published rotation poles whereas Müller et al. (2019) only used rotation poles for selected polarity chrons.

Shortly before the start of chron C33 (79.9 Ma) a piece of lithosphere broke off of West Antarctica to form the Bellingshausen Plate (Stock and Molnar, 1987). The Bellingshausen Plate started to rotate clockwise relative to West Antarctica and acted as an independent

plate until chron C27 (62.5 Ma; Stock and Molnar, 1987; Cande et al., 1995; Eagles et al., 2004b; Wobbe et al., 2012; Wright et al., 2016). During this time window, the northern margin of the Bellingshausen Plate was formed by a spreading ridge with the Pacific Plate and its western margin was defined by a short transform margin with the Marie Byrd Land sector of West Antarctica, close to the Euler pole of Bellingshausen-West Antarctica motion (Wright et al., 2016). To the east, the Bellingshausen Plate was bounded by a right-lateral transform fault from the Aluk Plate (Larter et al., 2002; Eagles et al., 2004b). To the south, the Bellingshausen Plate was converging with the Thurston Island sector of West Antarctica, although the maximum total amount of convergence was <250 km and no mature subduction zone developed (Wright et al., 2016). Like the reconstruction of Müller et al. (2019), we reconstruct the 79.9–62.5 Ma motion of the Bellingshausen Plate relative to the Pacific Plate using the finite rotation poles of Wright et al. (2016), which are based on marine magnetic anomalies of chrons C33–C27.

We tentatively suggest that friction at the transform fault that formed the eastern plate boundary of the West Antarctic Plate (Heezen Fracture Zone) led to the partial coupling of West Antarctica with the Aluk Plate. After the formation of the Pacific–Antarctic ridge, the Pacific–West Antarctica spreading and Pacific–Aluk spreading ridges were parallel, but Pacific–Aluk spreading occurred at a higher rate (~3.5 and ~7 cm/yr half-spreading rate, respectively). This resulted in lengthening of the transform fault that formed the plate boundary between the West Antarctic and Aluk plates. The partial coupling of part of West Antarctica with Aluk caused the formation of the Bellingshausen Plate, which was being dragged along by the Aluk Plate. This dragging resulted in clockwise rotation of Bellingshausen relative to West Antarctica. This suggestion is similar to what was proposed by Eagles et al. (2004b), who also suggested that the independent motion of Bellingshausen was related to the lengthening of the West Antarctica–Pacific transform plate boundary. A similar process was responsible for the formation of e.g. the Bauer microplate, which moved independently between c. 18–6 Ma, partitioning strain between the Pacific and Nazca plates (Eakins and Lonsdale, 2003).

Before C34y (83.7 Ma), pre-drift extension had already started to separate the Campbell Plateau from Marie Byrd Land and Chatham Rise from the Campbell Plateau (Molnar et al., 1975; Stock and Cande, 2002; Riefstahl et al., 2020) (Figure 6D and 7C). We reconstruct c. 180 km of pre-drift extension between the Campbell Plateau and Marie Byrd Land between 95 and 83.7 Ma, based on the estimated 90 km of extension in both margins based on crustal thickness calculations (Wobbe et al., 2012). We reconstruct c. 200 km of extension in the Bounty Trough (between Chatham Rise and the Campbell Plateau) between 92 and 84 Ma, based on the reconstruction derived from crustal thickness calculations of Grobys et al. (2008). This reconstruction also leads to extension between Chatham Rise and the Thurston Island sector of West Antarctica, where plate boundary activity may have started around 89 Ma (Wobbe et al., 2012).

A long-lived volcanic arc and accretionary prism on the Antarctic Peninsula shows

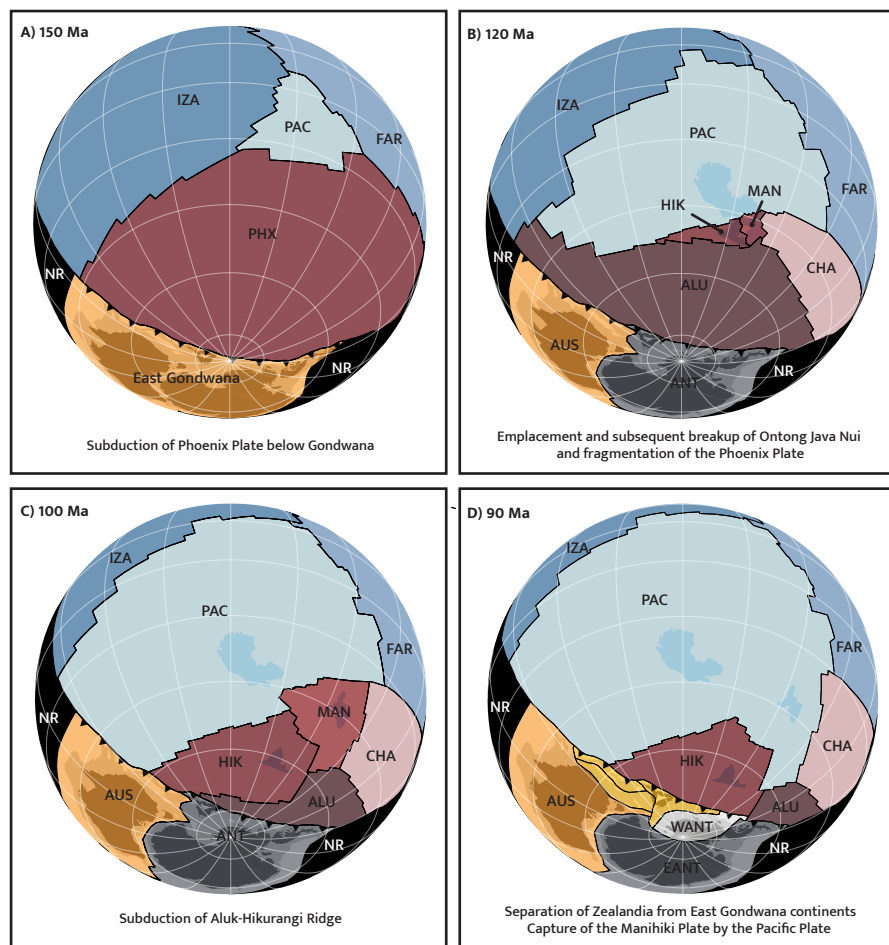


Figure 6. Snapshots of our kinematic reconstruction in the Van Der Meer et al. (2010) reference frame, highlighting key events in the evolution of the Phoenix Plate and East Gondwana subduction zone. These events are discussed in the main text. Present-day coastlines and outline of continental crust are shaded behind the plate colors and shown for reference. The Ontong Java Nui Large Igneous Provinces are also outlined, where the outline of the Hikurangi Plateau does not include the parts that were subducted below Chatham Rise and the North Island. Plate names: ALU: Aluk Plate; ANT: Antarctic Plate (EANT: East Antarctic Plate; WANT: West Antarctic Plate); AUS: Australian Plate; CHA: Chasca Plate; FAR: Farallon Plate; HIK: Hikurangi Plate; IZA: Izanagi Plate; MAN: Manihiki Plate; NAZ: Nazca Plate; PAC: Pacific Plate; SAM: South American Plate; ZEA: Zealandia. NR = Not Reconstructed.

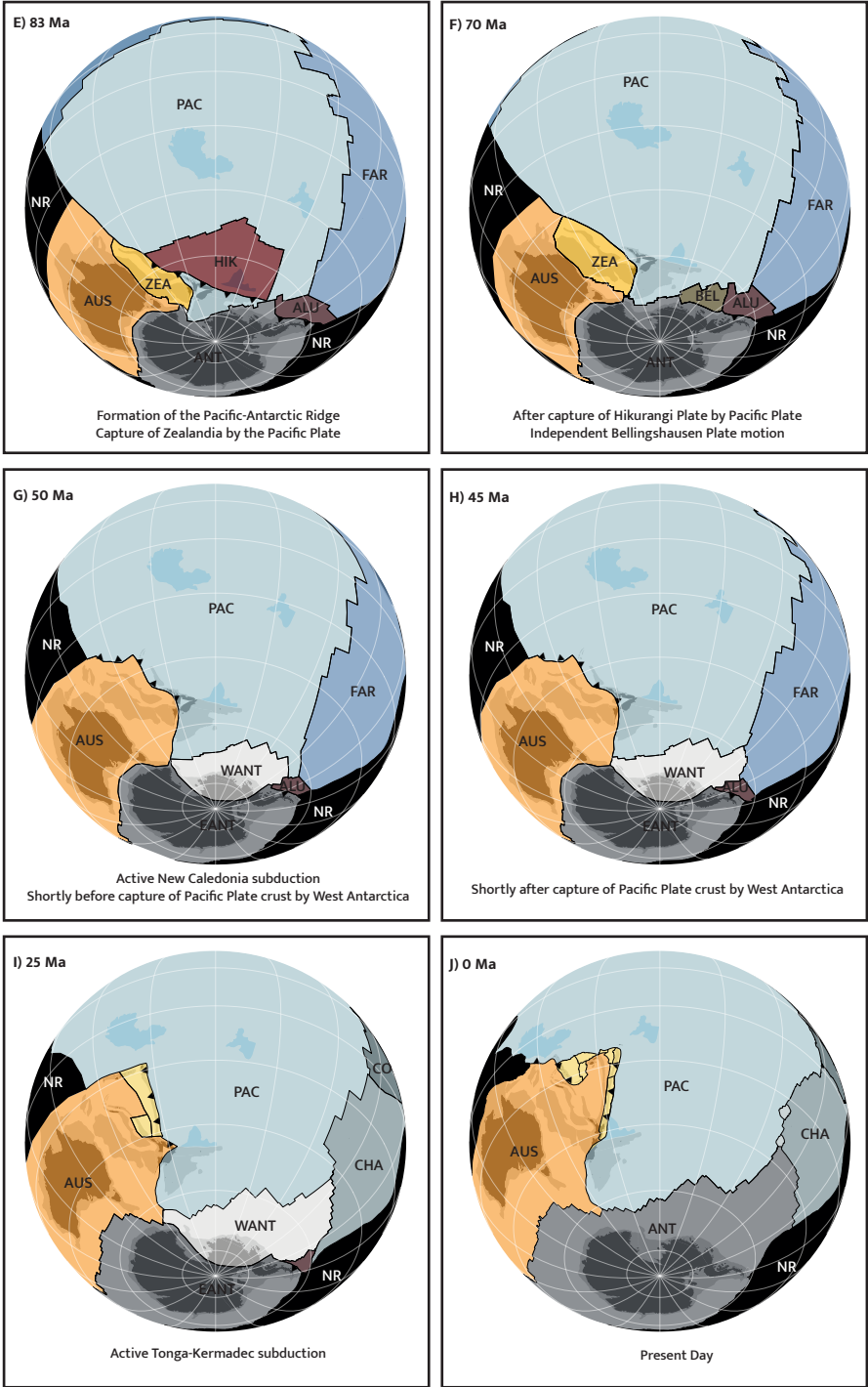


Figure 6 (continued).

that subduction continued throughout the Mesozoic and Cenozoic until the present-day (e.g., Burton-Johnson and Riley, 2015; Jordan et al., 2020). The plate that is subducting below the Antarctic Peninsula, the Aluk Plate, is therefore thought to be a descendent of the Phoenix Plate (Figure 1; e.g., Barker, 1982; Eagles, 2004). Interestingly, however, for much of the Cenozoic, and until the cessation of spreading around 3.3 Ma, the Aluk Plate has not been spreading relative to the Pacific Plate, but relative to oceanic lithosphere of West Antarctica (Eagles, 2004). Marine magnetic anomalies that formed along the Aluk-West Antarctica Ridge are preserved on the Aluk Plate back to C6A (21.32 Ma; Larter and Barker, 1991; Eagles, 2004), and on conjugate West Antarctica oceanic lithosphere back to C27 (62.52 Ma) (Cande et al., 1982). To the northwest, West Antarctica also contains a set of magnetic anomalies from C21 (47.8 Ma) and younger that record spreading between West Antarctica and the Pacific Plate (Cande et al., 1982; Cande et al., 1995; Croon et al., 2008). This spreading was near-parallel to West Antarctica-Aluk spreading, showing simultaneous and near-parallel spreading of West Antarctica with both the Pacific and Aluk plates (Wright et al., 2016).

Around the time of chron C21 (c. 47 Ma), part of the Pacific Plate that formed through Pacific-Aluk spreading was captured by the West Antarctic Plate (Cande et al., 1982; McCarron and Larter, 1998; Eagles et al., 2004a). Shortly before capture, the transform plate boundary between the West Antarctic and Pacific plates was lengthening due to the higher Pacific-Aluk compared to Pacific-West Antarctic spreading rates, similar to the situation that resulted in the formation of the Bellingshausen Plate. During capture, the Pacific-Antarctic ridge propagated into oceanic crust of the Pacific Plate that formed around C27 (c. 62.5 Ma) (Cande et al., 1982). At the southern end of the captured crust, the Pacific-Aluk ridge was replaced by the West Antarctic-Aluk ridge.

To the northeast, West Antarctica shared a spreading ridge with the Farallon Plate and its daughter Nazca Plate (Figure 6H-J) (Wright et al., 2016). However, before C21 (47.3 Ma), there was no Antarctic oceanic crust that separated the Aluk Plate from the Pacific Plate (Figure 6G): instead, the Aluk Plate was spreading directly with the Pacific Plate, recorded by marine magnetic anomalies back to C34y (83.7 Ma) on the Pacific Plate (Cande et al., 1982; Cande et al., 1995; Larter et al., 2002; Eagles et al., 2004a; Croon et al., 2008). In our reconstruction we use rotation poles of Aluk-West Antarctica and Aluk-Pacific motion back to C34y (83.7 Ma) of Eagles (2004), Eagles and Scott (2014) and Wright et al. (2016), similar to Müller et al. (2019). The tectonic history of the Aluk Plate prior to C34y (83.7 Ma) cannot be constrained by magnetic anomalies due to the Cretaceous Quiet Zone.

In the East Pacific, the Nazca Plate is spreading along the East Pacific Rise from the Pacific Plate and along the Chile Ridge from West Antarctica, while subducting below South America (Figure 1). The Nazca Plate formed c. 22 Ma (chron C6B), as the southern remnant of the broken up Farallon Plate (Barckhausen et al., 2001, Barckhausen et al., 2008; Wright et al., 2016). The East Pacific Rise records spreading between the Pacific and Nazca plates (and its predecessor the Farallon Plate) back to chron C23 (51.7 Ma) on the

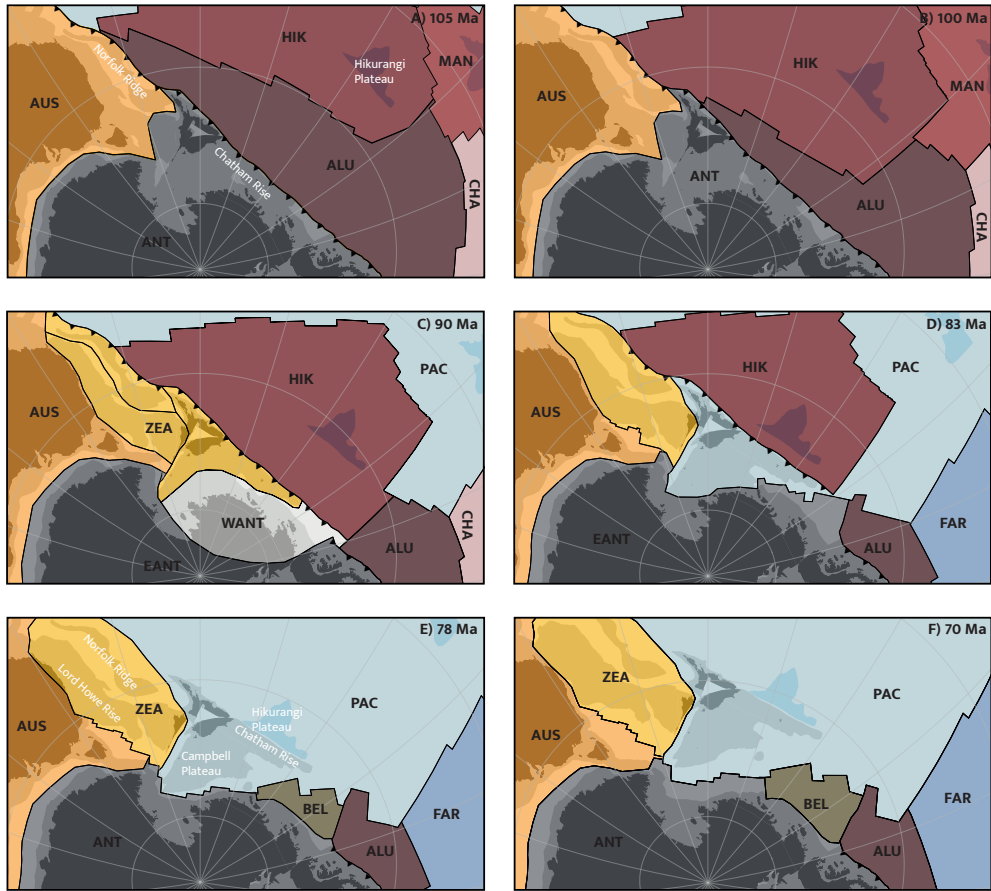


Figure 7. Detailed snapshots of our kinematic reconstruction in an East Antarctica fixed reference frame, highlighting the transition from the East Gondwana subduction zone margin to a passive margin. Extension within East Gondwana started in multiple locations before subduction of the Hikurangi Plate ended and this plate as well as Zealandia became part of the Pacific Plate. Present-day coastlines and outline of continental crust are shaded behind the plate colors and shown for reference. The Ontong Java Nui Large Igneous Provinces are also outlined, where the outline of the Hikurangi Plateau does not include the parts that were subducted below Chatham Rise and the North Island. Plate names: ALU: Aluk Plate; ANT: Antarctic Plate (EANT: East Antarctic Plate; WANT: West Antarctic Plate); AUS: Australian Plate; HIK: Hikurangi Plate; MAN: Manihiki Plate; NAZ: Nazca Plate; PAC: Pacific Plate; ZEA: Zealandia.

Nazca Plate (older magnetic anomalies have been lost to subduction below South America) and back to chron C34y (83.7 Ma) on the Pacific Plate (Atwater and Severinghaus, 1989; Barckhausen et al., 2008; Wilder, 2003; Handschumacher, 1976). Spreading between the Nazca Plate and West Antarctica is recorded at the Chile Ridge back to chron C24 (53.9 Ma) on West Antarctica and back to chron C5E (18.5 Ma) on the Nazca Plate (Cande et al., 1982; Tebbens et al., 1997). We reconstruct the Nazca Plate relative to the Pacific Plate, using

the finite rotation poles based on marine magnetic anomalies back to chron C6B (22.3 Ma) of Tebbens and Cande (1997), as published in Wright et al. (2016), similar to Müller et al. (2019). We include the Bauer Microplate that formed in Miocene times at the Nazca-Pacific ridge using magnetic anomalies C5E-C3A (18.5–6.7 Ma) identified by Eakins and Lonsdale (2003), with rotations computed in GPlates. We do not include the Galapagos, Easter and Juan Fernandez microplates in our reconstruction, which formed about 5 Ma (Tebbens and Cande, 1997; Wright et al., 2016). The Farallon Plate is reconstructed relative to the Pacific Plate between 22.3 (chron C6B) and 83.7 Ma (chron C34y) using the finite rotations poles of Wright et al. (2016), like in Müller et al. (2019). The record of Farallon-Pacific spreading during and before the Cretaceous Quiet Zone will be discussed in section 4.2.

Cenozoic relative motion between East Antarctica and West Antarctica is constrained by marine magnetic anomalies that formed in the Adare and Northern basins between chrons C5 and C27 (11.1–62.5 Ma) (Cande and Stock, 2004a; Granot et al., 2013; Granot and Dymant, 2018). We incorporate the finite rotation poles of Granot and Dymant (2018), Granot et al. (2013), and Cande and Stock, 2004b, Cande and Stock, 2004a for chrons C5-C8, C12-C18, and C20-C27, respectively. Mesozoic extension in the West Antarctic Rift System (WARS) between West Antarctica and East Antarctica is poorly constrained, but a main phase of extension was proposed to have occurred in the mid-Late Cretaceous, based on low temperature geochronology studies (Lawver and Gahagan, 1994; Fitzgerald, 2002; Spiegel et al., 2016; Veevers, 2012). Based on crustal thickness estimates (An et al., 2015; Llubes et al., 2018; Shen et al., 2018), we reconstruct c. 100 km of extension in the West Antarctic Rift System between 95 and 84 Ma (Figure 7).

Australia-East Antarctica motion is based on marine magnetic anomalies back to chron C34y (83.7 Ma), although seafloor spreading was slow before chron C17o (~38 Ma) (Cande and Stock, 2004a; Whittaker et al., 2007, Whittaker et al., 2013). Pre-drift extension between East Antarctica and Australia started at 136 Ma (Whittaker et al., 2013), and we base the East Gondwana fit of East Antarctica and Australia on the reconstruction of the extended conjugate continental margins of Williams et al. (2011) and Gibbons et al. (2012). Our Australia-East Antarctica reconstruction is similar to that of Müller et al. (2019).

The Late Cretaceous to early Eocene separation of Lord Howe Rise (North Zealandia) from Australia is recorded by marine magnetic anomalies C24-C34y (53.9–83.7 Ma) in the Tasman Sea (Gaina et al., 1998). We use the finite rotation poles of Gaina et al. (1998) in our reconstruction, like Seton et al. (2012) and Müller et al. (2019). Pre-drift extension is thought to have started c. 95 Ma, concurrently with extension in the New Caledonia Basin, between the Norfolk Ridge and Lord Howe Rise (Figure 6D-E and 7C) (Grobys et al., 2008). The back-arc basins between Lord Howe Rise and the Tonga-Kermadec-Hikurangi subduction zone are reconstructed as in Chapter 1, using marine magnetic anomaly constraints from Yan and Kroenke (1993), Sdrolias et al. (2003), and Herzer et al. (2011).

We connect the plate circuit of our reconstruction to Africa by reconstructing East Antarctica-Africa motion through the South Atlantic Ocean. This is based on finite rotation

poles based on marine magnetic anomalies back to chron M38 (c. 164 Ma) of DeMets et al. (2021) (C1-C23; 0–51.7 Ma), Cande et al. (2010) (C23-C29; 51.7–64.9 Ma), (Bernard et al., 2005) (C29-C33; 64.9–79.9 Ma), and Mueller and Jokat (2019) (C34y-M38; 84.7–162.9 Ma).

4.2. Pre-C34y plate reconstruction of the Paleo-Pacific realm

4.2.1. Evolution of the Phoenix Plate

Direct kinematic constraints on the evolution of the Phoenix Plate come from marine magnetic anomalies preserved on the Pacific Plate (Nakanishi et al., 1992). The oldest of these anomalies, preserved in the west Pacific Ocean, formed at the Pacific-Phoenix Ridge (Larson and Chase, 1972), and were identified as M29n.2n – M1n (Nakanishi et al., 1992), indicating that Pacific-Phoenix spreading was active from at least 155.9 to 123.8 Ma. We reconstruct the motion of Phoenix for this time interval using GPlates, by mirroring the marine magnetic anomalies that are preserved on the Pacific Plate, assuming symmetric spreading (Figure 6A-B). We reconstruct Pacific-Phoenix spreading until 120 Ma, the timing of Ontong Java Nui break-up (see section 4.2.2) (Taylor, 2006; Chandler et al., 2012).

While Pacific-Phoenix spreading was active, the Pacific Plate was also spreading with the Farallon and Izanagi plates (or Izanami Plate; see Boschman et al., 2021b). Marine magnetic anomalies that formed during chrons M29 – M0 (156.9–121.4 Ma) were identified on the eastern side of the Pacific triangle (Nakanishi et al., 1992), which constrain spreading between the Pacific and Farallon plates. Pacific-Izanagi spreading is constrained by marine magnetic anomalies that formed during chrons M35 – M5 (160.9–127.5 Ma) (Nakanishi et al., 1992). We reconstruct Farallon-Pacific and Izanagi-Pacific spreading in this time interval based on the marine magnetic anomalies (Nakanishi et al., 1992), using the reconstruction poles of Boschman et al. (2021a).

Marine magnetic anomalies that formed in the southeast corner of the Pacific triangle suggest the formation of two microplates (the Trinidad and Magellan microplates) around the Pacific-Farallon-Phoenix triple junction (Nakanishi and Winterer, 1998). The Trinidad microplate formed around chron M21 (146.6 Ma) and stopped acting as a separate plate around chron M14 (136.9 Ma) (Nakanishi and Winterer, 1998). The Magellan microplate formed around chron M15 (138.5 Ma) and remained active until chron M9 (129.9 Ma), when it merged with the Pacific Plate (Nakanishi and Winterer, 1998). We incorporate the independent motion of the Magellan microplate between chrons M15 and M9 (138.5–129.9 Ma) in the reconstruction. We computed finite rotation poles for this reconstruction in GPlates, based on the magnetic anomaly picks of Nakanishi and Winterer (1998). We do not reconstruct the Trinidad microplate, because there are not enough marine magnetic anomaly identifications for a reliable reconstruction of this microplate.

From reconstruction of Pacific-Farallon and Pacific-Izanagi spreading, it follows that the Phoenix Plate also formed mid-oceanic ridges with the Farallon and Izanagi plates (Figure 6A). The location of these spreading ridges relative to the Pacific triangle is unknown, but undated marine magnetic anomalies in the Caribbean plate have orientations

that are consistent in direction with those that would have formed at the Farallon-Phoenix ridge, and ages of ocean floor exposed in western Costa Rica are consistent with a Jurassic age of spreading of this lithosphere (Boschman et al., 2019). This suggests that prior to the Cretaceous Quiet Zone, the Farallon-Phoenix ridge was located at the longitude of (and subducting below) northern South America. The Izanagi-Phoenix ridge is generally assumed to have remained north of Australia (e.g., Seton et al., 2012). The Phoenix Plate and its Cretaceous to Cenozoic daughters were therefore lost along a continuous subduction margin that spanned from the Caribbean region, down along the westcoast of South America, continuing along the West Antarctic and Zealandia margins to northeast Australia and possibly into Southeast Asia (Figure 2, Figure 6A).

4.2.2. Ontong Java Nui breakup

The Phoenix lineations on the Pacific Plate are overlain in the west by the Ontong Java Plateau (Larson, 1997). South of the Phoenix lineations is the oceanic Ellice Basin, which is devoid of marine magnetic anomalies due to its formation during the Cretaceous Normal Superchron, but has east-west trending fracture zones (Benyshek et al., 2019). According to the ‘superplateau’ hypothesis, the Ontong Java Plateau, together with the Manihiki and Hikurangi plateaus was emplaced as a single Large Igneous Province, known as Ontong Java Nui, around 125–120 Ma (Figure 6B; Taylor, 2006; Chandler et al., 2012). Shortly after emplacement, Ontong Java Nui broke up into the three modern plateaus through spreading in the Ellice Basin and Osbourn Trough (Taylor, 2006; Chandler et al., 2012; Hochmuth et al., 2015). The Ontong Java Nui LIP erupted on either side of the already existing Pacific-Phoenix spreading ridge: the Ontong Java Plateau represents the part of the LIP that formed on the Pacific Plate, whereas the Manihiki and Hikurangi plateaus formed on the former Phoenix Plate (Larson, 1997; Seton et al., 2012). After separation, the Manihiki and Hikurangi plateaus became part of independent tectonic plates, which grew larger than the original LIPs through the formation of new oceanic crust at their bounding mid-ocean ridges (Figure 6B-C) (Seton et al., 2012). We refer to these plates as the Manihiki and Hikurangi plates. When we discuss the actual LIPs, we will refer to them as Manihiki and Hikurangi plateaus. Restoration of spreading in the Ellice Basin and Osbourn Trough reconstructs the Hikurangi Plate via the Manihiki Plate relative to the Pacific. The emplacement and subsequent break-up of Ontong Java Nui also resulted in the fragmentation of the Phoenix Plate (e.g., Seton et al., 2012). The spreading history of the Ellice Basin and Osbourn Trough is thus of key importance in the search of the Phoenix Plate and for reconstructing the convergence history between the Pacific realm plates and the Zealandia margin of East Gondwana.

The Ontong Java Nui fit of the three plateaus is based on the interpretation of conjugate rifted margins (Taylor, 2006; Chandler et al., 2012). The general absence of marine magnetic anomalies in the Cretaceous Quiet Zone makes the opening history of these basins challenging to reconstruct in detail. The start of opening of the basins postdated the main

formation phase of Ontong Java Nui, which occurred at 125–120 Ma. This age is based on $^{40}\text{Ar}/^{39}\text{Ar}$ dating of tholeiitic basalts dredged from the three plateaus (Mahoney et al., 1993; Hoernle et al., 2010; Timm et al., 2011) and on the age of sediments directly overlying pillow basalts (Winterer et al., 1974; Sliter et al., 1992). Spreading at the Osbourn Trough started before 115 Ma, based on 115 ± 1 Ma U-Pb zircon ages from dredged lavas and volcanoclastic sandstones from the West Wishbone Ridge (Mortimer et al., 2006). Dating of rift-related structures revealed a c. 120 Ma age of separation between the Hikurangi and Manihiki plateaus (Davy et al., 2008). The onset of rifting in the Ellice Basin between the Manihiki and Ontong Java plateaus is thought to have occurred concurrently with the onset of spreading at the Osbourn Trough, although this is not confirmed by radiometrically dated dredge samples (e.g., Chandler et al., 2012; Hochmuth et al., 2015).

A tectonic reconstruction for the final stages of opening of the Ellice Basin was presented by Benyshek et al. (2019), based on detailed bathymetric data from the center of the basin. They tentatively suggested ages for their rotation poles, based on estimated spreading rates, but these await confirmation by radiometric dating of basement samples (Benyshek et al., 2019). The end of spreading in the Ellice Basin most likely occurred before the end of the CNS, i.e., before 83.7 Ma.

Because no marine magnetic anomalies have been confidently identified, spreading at the Osbourn Trough is also widely interpreted to have occurred entirely during the Cretaceous Normal Superchron (e.g., Chandler et al., 2012). The age of arrest of the Osbourn Trough opening is important for the age of cessation of subduction at the Gondwana margin of New Zealand. The age of 86 Ma incorporated in the widely used global plate models (Seton et al., 2012; Matthews et al., 2016; Müller et al., 2019) came from Worthington et al. (2006), who interpreted the age of arrest of spreading from an age for arrest of subduction based on geological interpretations from New Zealand: occurrence of calc-alkaline volcanism until 89 Ma (Smith and Cole, 1997), the interpreted ongoing outbuilding of an accretionary wedge (Mazengarb and Harris, 1994; Kamp, 1999, Kamp, 2000) and an 86 Ma episode of metamorphism (Vry et al., 2004), all recognized in New Zealand. But because this young age of subduction arrest is widely disputed by the geological community of New Zealand who prefer a 105–100 Ma (e.g., Bradshaw, 1989; Luyendyk, 1995; Crampton et al., 2019; Mortimer et al., 2019; Gardiner et al., 2021), and it is this debate that we aim to reconcile, our reconstruction of Osbourn Trough should remain independent from the interpretations of the geology of New Zealand. Billen and Stock (2000) tentatively identified anomalies C33 and C32 (79.9 and 73.6 Ma) in the Osbourn Trough. Because the magnetic anomalies are not obvious lineations, they called for more magnetic data and dredge samples. The magnetic anomalies have thus far not been independently confirmed, but Mortimer et al. (2019) reported an 84.4 ± 3.5 Ma $^{40}\text{Ar}/^{39}\text{Ar}$ age of plagioclase in a basalt flow recovered from bore hole DSDP595, which is located c. 200 km north of the former Osbourn Trough spreading center (Figure 4). Through extrapolation of spreading rates, they proposed that Osbourn Trough spreading may have continued until ~79 Ma (Mortimer et al., 2019),

implying that spreading may indeed have continued after the Cretaceous Quiet Zone as suggested by Billen and Stock (2000). However, the 84.4 Ma age is a tentative age, as the effects of seawater alteration could not be entirely ruled out (Mortimer et al., 2019). On the other hand, Zhang and Li (2016) suggested that spreading at the Osbourn Trough ceased around 101 Ma, which would require ultrafast spreading rates of 19 cm/yr. This is based on a 103.7 ± 2.3 Ma Resingle bondOs isochron age of basalts recovered from bore hole U1365 (Figure 4), adjacent to bore hole DSDP595, which contradicts the 84.4 Ar/Ar age of Mortimer et al. (2019).

We reconstruct the start of spreading in both basins at 120 Ma (Figure 6B), following Chandler et al. (2012), similar to Seton et al. (2012) and Müller et al. (2019). For the Osbourn Trough, we use rotation poles of Chandler et al. (2012) to reconstruct the spreading history, but we incorporate the new constraints from Mortimer et al. (2019) of spreading until 79 Ma rather than the contested, New Zealand geology-based 86 Ma estimate of Worthington et al. (2006) that is used in Seton et al. (2012) and Müller et al. (2019). We note that the age for the end of Osbourn Trough spreading may change in the future if more reliable radiometric dating of the Osbourn Basin becomes available, and we will discuss below what difference a different age would make for the estimate for subduction arrest at the New Zealand margin. For the Ellice Basin, we use the Chandler et al. (2012) rotation pole for the Ontong Java-Manihiki fit at 120 Ma and the rotation poles of Benyshek et al. (2019) for subsequent opening, with spreading ending at 90 Ma.

The contemporaneous opening of the Ellice Basin and Osbourn Trough requires that a mid-ocean ridge existed between the Hikurangi and Pacific plates (Figure 6B-E). The rate and direction of spreading along this ridge follows from the Pacific-Manihiki and Manihiki-Hikurangi reconstructions. This spreading ridge, as well as the Pacific-Manihiki-Hikurangi triple junction was lost to subduction at the Tonga-Kermadec-Hikurangi subduction zone during the Cenozoic (Figure 6E-J).

4.2.3. Seafloor fabric

To the east of the Manihiki and Hikurangi plates, Seton et al. (2012) identified two more daughter plates of the Phoenix Plate: Chasca and Catequil. We continue using the name Chasca Plate, but the Catequil Plate of Seton et al. (2012) is the same as the Aluk Plate in our reconstruction. We prefer the name Aluk Plate, because it is the established name for the remnant of this plate whose lithosphere remains in the southeast Pacific today. As with Seton et al. (2012), we derive the former existence of the Chasca and Aluk plates from seafloor fabric and marine magnetic anomaly identifications.

The pre-83.7 Ma existence of the Aluk Plate follows from trends in the seafloor fabric east of the Osbourn Trough. The extinct Osbourn Trough spreading center can be followed eastwards until longitude 165°W, where it suddenly stops (Figure 8). North and south of the Osbourn Trough abyssal hill trends are WNW-ESE for the older part of the basin, and E-W for the youngest part (Downey et al., 2007, see also their Figure 6). These abyssal

hill trends, together with NNE-SSW trending fracture zones constrains the NNE-SSW to N-S spreading direction of the Hikurangi Plate relative to the Manihiki Plate. This trend in seafloor fabric that formed at the Osbourn Trough is delineated by the NNE-SSW trending Manihiki Scarp and the West Wishbone Ridge, clear traces in the ocean floor (Figure 8). East of the Manihiki Scarp and West Wishbone Ridge, abyssal hills are trending ENE-WSW (Downey et al., 2007, their Figure 6) and fracture zones are trending NNW-SSE (Figure 8). This suggests that the oceanic crust here formed at a different spreading center, between different plates (Downey et al., 2007). We suggest here that this part of oceanic crust formed through spreading between the Manihiki and Aluk plates, both daughters of the Phoenix Plate. There is no remnant of an extinct spreading ridge preserved in this part of the Pacific Plate, which suggests that all oceanic crust preserved here formed as part of the Manihiki Plate (e.g., Seton et al., 2012). As Manihiki was incorporated into the Pacific Plate at c. 90 Ma (Benyshek et al., 2019), the Manihiki-Aluk ridge became the Pacific-Aluk ridge at this time. The location of the Pacific-Aluk Ridge is constrained after 83.7 Ma by marine magnetic anomalies preserved on the Pacific Plate (Figure 4, Figure 6E; see also section 4.1) (Cande et al., 1995; Larter et al., 2002; Eagles, 2004; Wobbe et al., 2012). The direction of spreading between the Manihiki/Pacific and Aluk plates follows from the NNW-SSE directed fracture zones that are preserved on the Pacific Plate (Figure 8). The average rate of Manihiki-Aluk spreading follows from the 120 Ma break-up configuration of the Phoenix Plate into these plates and the chron C34y (83.7 Ma) location of the Aluk-Pacific ridge, which is constrained by marine magnetic anomalies on the Pacific Plate (Larter et al., 2002; Eagles, 2004). We reconstruct a constant spreading rate in this 120–83.7 Ma period.

The nature of the plate boundary between the Aluk and Hikurangi plates follows from the reconstruction of the Hikurangi and Aluk plates relative to the Manihiki Plate. In our reconstruction, Aluk-Manihiki spreading occurred at a higher rate than Hikurangi-Manihiki spreading (~8.5 cm/yr and ~4.5 cm/yr half-spreading rate, respectively) (Figure 6B-D). As a result, between 120 and 110 Ma, the plate boundary between the Aluk and Hikurangi plates was a right-lateral transform fault northeast of the Hikurangi Plateau, forming the West Wishbone Ridge. After 110 Ma, some extension occurred between the Aluk and Hikurangi plates east of the Hikurangi Plateau, accommodated by a mid-ocean ridge. South of the Hikurangi Plateau, the plate boundary between the Hikurangi and Aluk plates was a mid-ocean ridge from 120 Ma until its subduction below the Zealandia margin around 100–90 Ma (Figure 6B-C and 7).

From the northeast corner of the Manihiki Plateau towards the south, there is a clear trace in the seafloor fabric (Figure 8). This feature has been identified as a trace of a former triple junction (Larson and Chase, 1972), and was named the Tongareva triple junction (Larson et al., 2002). It was previously suggested that the Tongareva triple junction formed the junction between the Pacific, Farallon, and Phoenix plates (e.g., Larson et al., 2002; Viso et al., 2005; Hochmuth and Gohl, 2017). We instead infer that the Tongareva triple junction formed the junction between Manihiki, Chasca and Aluk plates, until c. 90 Ma,

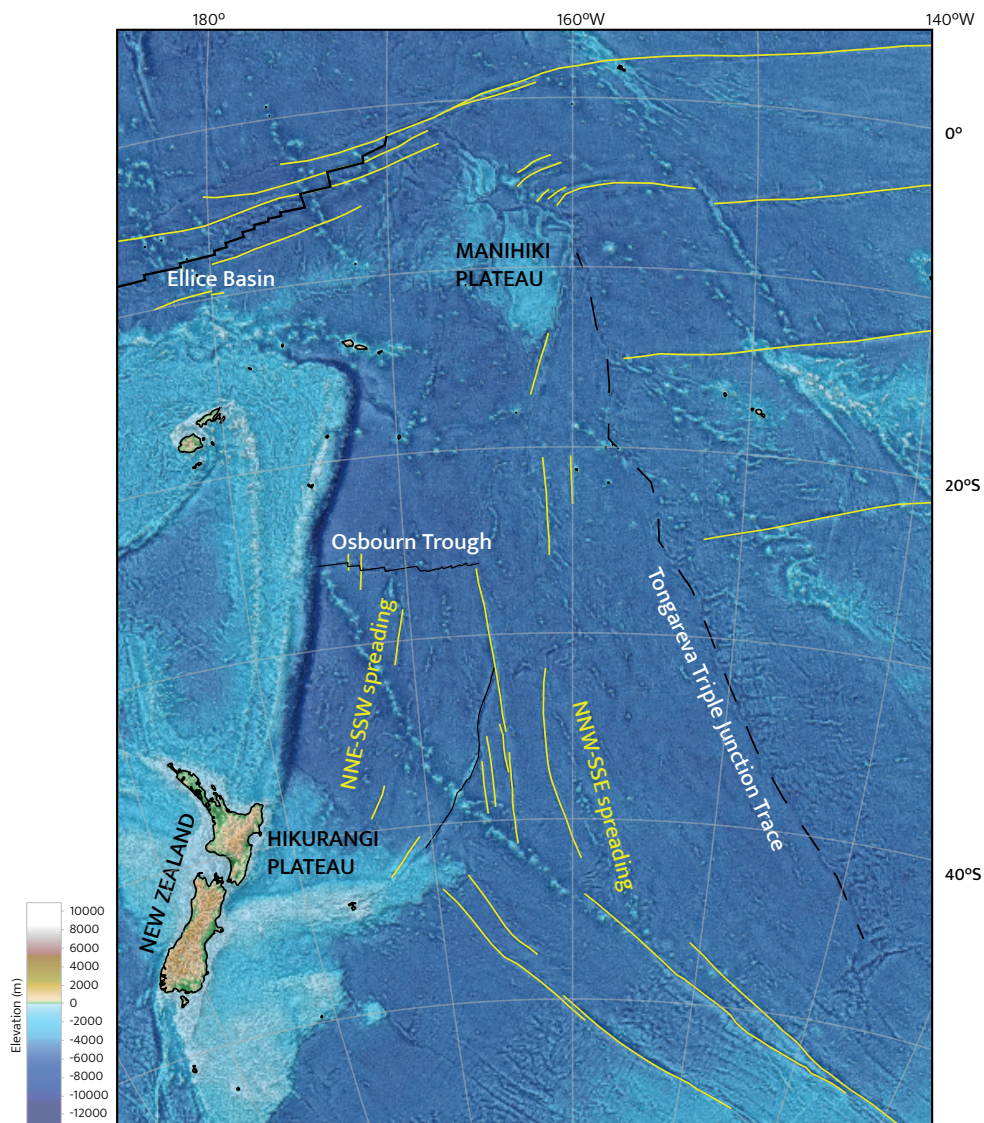


Figure 8. Bathymetry of the region to the northeast of New Zealand, highlighting features of the seafloor fabric. Digitalized fracture zone data (in yellow) were obtained from the GSFML database (Matthews et al., 2011; Seton et al., 2014; Wessel et al., 2015). Background image is ETOPO1 1 Arc-Minute Global Relief Model (Amante and Eakins, 2009; NOAA National Geophysical Data Center, 2009).

when Manihiki merged with the Pacific Plate. Between 90 and 83.7 Ma, the Tongareva triple junction was the junction of the Pacific, Chasca and Aluk plates, after which it became the triple junction between Pacific, Farallon and Aluk plates when Chasca was captured by Farallon (Figure 6B-F).

The existence of the Chasca Plate follows from rift structures on the northeast margin of the Manihiki Plateau (Figure 8) (Larson et al., 2002; Viso et al., 2005). It was previously suggested that this fragment was incorporated into the Farallon Plate at 110 Ma (Hochmuth and Gohl, 2017). The location of the Farallon Plate relative to the Pacific Plate is constrained by marine magnetic anomalies of chrons C34y (83.7) and M0 (121.4). Attaching a fragment of oceanic crust that formed east of the Manihiki Plateau to the Farallon Plate at 110 Ma, however, leads to convergence along the southeast margin of the Manihiki Plateau. This convergence is contradicted by the existence of the Tongareva triple junction trace, as described above. Instead, we reconstruct independent motion of the Chasca Plate until 83.7 Ma. The capture of the Chasca Plate by the Farallon Plate, which resulted from the inactivation of the transform fault (Clipperton Fracture Zone) that separated the Chasca and Farallon plates, may have occurred a few millions of years earlier. This would require higher Chasca – Manihiki/Pacific spreading rates, but these are unknown. We therefore choose to reconstruct the capture at the time of C34y (83.7 Ma), as this marine magnetic anomaly provides the first positive evidence that the Chasca plate was captured. Seton et al. (2012) and Chandler et al. (2012) incorporate the Chasca Plate into the Farallon Plate a few million years earlier at 86 Ma, contemporaneous with the cessation of Osbourn Trough spreading in their model (see section 4.2.2).

We reconstruct the start of Chasca – Manihiki motion at 120 Ma, the same time as the onset of spreading between the other daughters of the Phoenix Plate (Chandler et al., 2012). Rotation poles of the Chasca Plate relative to the Manihiki Plate are calculated in GPlates. In our reconstruction, we ensure that early motion of the Chasca Plate follows the trend of the curved rift structures at the NE Manihiki margin (Figure 8). In addition, we assume that the Pacific-Farallon ridge at 83.7 Ma formed at the location of the Pacific-Chasca ridge, after Manihiki was captured by the Pacific Plate at 90 Ma (Benyshek et al., 2019) and Chasca was captured by Farallon.

The rotation poles for the reconstruction of the Ellice Basin include a rotation of the Manihiki Plate relative to the Pacific Plate between 102 and 98 Ma, based on a change in fracture zone orientation in the Ellice Basin from ~E-W to WNW-ESE (Taylor, 2006; Chandler et al., 2012; Benyshek et al., 2019). As the Chasca Plate is reconstructed relative to the Manihiki Plate in our plate circuit, the rotation modeled by Benyshek et al. (2019) also results in a rotation of the Chasca Plate. This in turn leads to convergence at the Chasca-Farallon plate boundary that at that time was still located at the latitude of northern South America. This rotation of the Chasca Plate coincides with the estimated timing of subduction initiation at the western Caribbean plate boundary of modern Central America (Whattam and Stern, 2015; Boschman et al., 2019), which at 100 Ma was still located far west within the eastern Panthalassa realm (e.g., Pindell and Kennan, 2009; Boschman et al., 2014). Rotation of the Manihiki Plate may thus have resulted in subduction initiation at the future western Caribbean plate boundary.

5. Discussion

The kinematic constraints reviewed in section 4 lead to a plate kinematic evolution from 150 Ma onward as portrayed in Figure 6, and in snapshots highlighting the final stages of subduction in Figure 7. We provide GPlates reconstruction files and an animation of the reconstruction in the supplementary information. Below, we discuss uncertainties in our reconstruction, offer interpretations of possible dynamic drivers of plate reorganizations, and evaluate until when convergence along the Gondwana margin must have continued. Finally, we discuss how differences between plate kinematics and geology-based interpretations may be reconciled, and what opportunities our reconstruction provides for future geological research.

5.1. Dating the end of convergence across the Gondwana margins

During the Paleozoic and Mesozoic, the vast Phoenix Plate occupied large parts of the south Panthalassa Ocean. After the birth of the Pacific Plate around 190 Ma (Seton et al., 2012; Boschman and Van Hinsbergen, 2016), the Phoenix Plate formed spreading ridges with the Pacific, Izanagi/Izanami and Farallon plates. Subduction at the Gondwana margin of South America, Antarctica, and Australia/Zealandia is not controversial, although more plates may have been involved between the Phoenix Plate and the Gondwana margin (e.g., Boschman et al., 2021a). Our reconstruction from 150 Ma until the 125–120 Ma emplacement of the Ontong Java Nui LIP, placed in the Pacific hotspot reference frame of Torsvik et al. (2019) and the Indo-Atlantic slab-fitted frame of Van Der Meer et al. (2010) straightforwardly shows convergence of Phoenix in the west, south, and east, consistent with geological records from South America, Antarctica, and Zealandia (Mortimer et al., 2014a; Burton-Johnson and Riley, 2015; Pepper et al., 2016; Jordan et al., 2020; Maurizot et al., 2020b). Along the eastern margin of the southern Pacific, convergence and subduction continue today (Figure 1). Conversely, convergence ceased along the southern and western margins in the Late Cretaceous, which was followed by re-initiation of subduction in the west during the Cenozoic (e.g., Seton et al., 2012; Chapter 1). In this section, we establish until when, according to plate kinematic constraints, subduction continued. In addition, we examine whether the choice of mantle reference frame is of influence on this age estimation.

It is well agreed upon that a subduction zone was present along the entire East Gondwana margin, from the Antarctic Peninsula to New Caledonia, until 105 Ma (Bradshaw, 1989; Luyendyk, 1995; Maurizot et al., 2020b; Gardiner et al., 2021). In addition, our plate reconstruction shows that convergence at the Zealandia and Antarctic margins continued, until at least 90 Ma and possibly until 85 Ma (Figure 9). This is well beyond 105–100 Ma, when some models that are based on onshore geology (e.g., the onset of continental extension and the change in geochemistry of magmatism) argue for the cessation of subduction along the Zealandia sector of East Gondwana (Bradshaw, 1989; Davy et al., 2008; Crampton et al., 2019; Mortimer et al., 2019). In our updated plate kinematic model, the timing of the end of convergence is dependent on two variables: the reconstruction of Osborn Trough

spreading and the choice of Indo-Atlantic mantle reference frame for East Gondwana. We only use the Pacific mantle reference frame of Torsvik et al. (2019), because they showed that previous implementations of Pacific reference frames are flawed. Furthermore, the correctly implemented Pacific hotspot reference frame of Wessel and Kroenke (2008) only leads to more convergence across the Gondwana margin than the model of Torsvik et al. (2019). In all Indo-Atlantic mantle reference frames, convergence continues until the cessation of Osborn Trough spreading; that is, until 79 Ma in our reconstruction following Mortimer et al. (2019). This reconstruction of the Osborn Trough leads to c. 1500–2000 km of convergence between the Hikurangi Plate and the Gondwana margin between 100 and 79 Ma, depending on the reference frame (Figure 9). If future radiometric dating of dredge samples would suggest an older age for the end of Osborn Trough spreading, the convergence between the Hikurangi Plate and the East Gondwana margin would simply be accommodated by higher rates of spreading and subduction between 120 Ma and any new and reliable date suggested. Even if Osborn Trough spreading had already ceased by

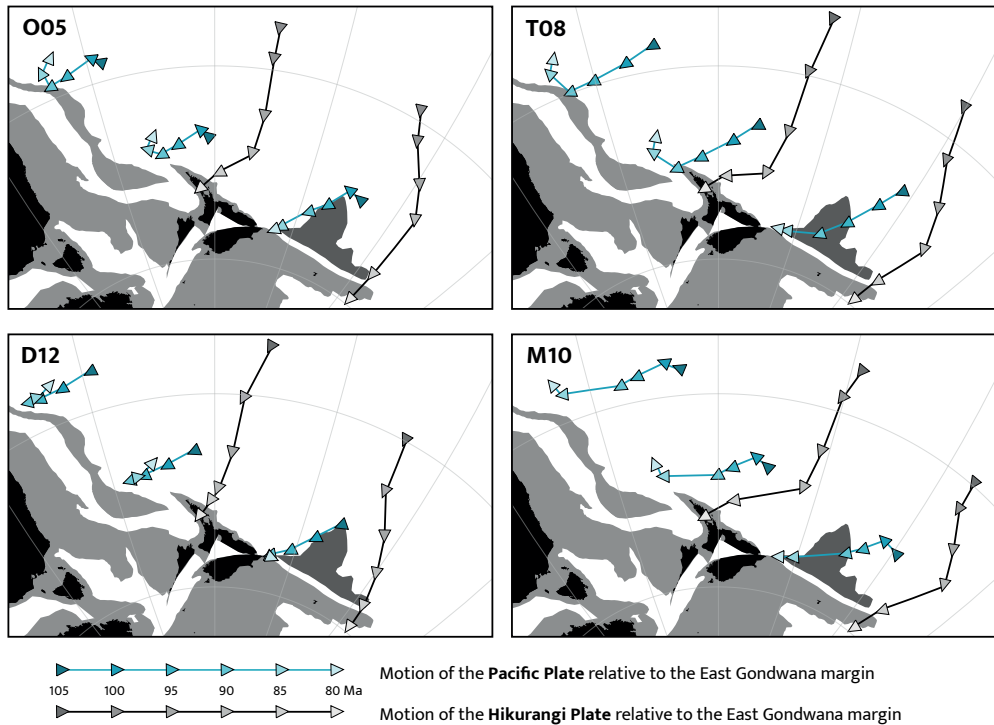


Figure 9. 80 Ma reconstruction in an East Antarctica fixed reference frame showing the motion of the Pacific Plate and Hikurangi Plate relative to the East Gondwana margin in different mantle reference frames (O05: O'Neill et al., 2005; T08: Torsvik et al., 2008; D12: Doubrovine et al., 2012; M10: Van Der Meer et al., 2010). This figure shows that convergence between the Pacific oceanic plates and the East Gondwana margin continued until at least 90 Ma in all reference frames, and until 79 Ma if Osborn Trough spreading was still active.

101 Ma, as interpreted by Zhang and Li (2016), there would still have been 800–1100 km of post-100 Ma convergence between the Pacific Plate and the Zealandia margin (Figure 9). In this scenario, convergence at the Zealandia margin continued until c. 90 Ma, applying the reference frames of Torsvik et al. (2008) or Doubrovine et al. (2012), or continued until c. 84 Ma (when the Campbell plateau became incorporated in the Pacific Plate) in applying the slab frame of Van Der Meer et al. (2010) or the hotspot reference frame of O'Neill et al. (2005).

The Hikurangi-Pacific ridge formed a triple junction with the subduction zone located along the margin of East Gondwana, in the vicinity of the Norfolk Ridge (Figure 6, Figure 7). North of this Hikurangi-Pacific-Gondwana triple junction, the rate and amount of convergence at the East Gondwana margin were not influenced by spreading at the Osborn Trough, as the Pacific Plate directly subducted below the Norfolk Ridge. The precise location of this triple junction, where the Pacific-Hikurangi ridge subducted below eastern Gondwana, is uncertain, as it has subsequently been consumed at the Cenozoic Tonga-Kermadec and New Caledonia trenches. In our reconstruction, after 95 Ma we place this triple junction just south of New Caledonia (Figure 6, Figure 7), which results from the assumption of symmetric spreading between the Pacific and Hikurangi plates between 120 and 79 Ma (see section 4.2.2). The relative motion between the Pacific Plate and the Norfolk Ridge north of the Pacific-Hikurangi-Gondwana triple junction is convergent in all reference frames until at least 90 Ma. In the hotspot reference frames of O'Neill et al. (2005), Torsvik et al. (2008), and Doubrovine et al. (2012), convergence north of the Hikurangi-Pacific-Gondwana triple junction ends at 90 Ma (Figure 9). In the slab-fitted mantle reference frame of Van Der Meer et al. (2010), convergence between the Pacific Plate and the Norfolk Ridge continues until 85 Ma. Subduction south of the New Caledonia sector of the East Gondwana margin thus continued until 90–85 Ma (Figure 9).

In an attempt to reconcile geological (on-land) interpretations of cessation of subduction in New Zealand with oceanic plate reconstructions, Mortimer et al. (2019) proposed a solution to avoid convergence beyond 100 Ma at the Zealandia margin. In this scenario, the Hikurangi Plateau arrives in the trench at 100 Ma, and the Manihiki and Ontong Java plateaus move northwards relative to the margin between 100 and 79 Ma. However, this model places the Pacific plate mosaic ~2250 km farther to the South at 100 Ma than suggested by the hotspot frame of Torsvik et al. (2019) (Figure 10), which is well beyond the 3° uncertainty assigned to the hotspot model. The solution of Mortimer et al. (2019) therefore does not work in our kinematic reconstruction that combines relative and absolute plate motions; it would require an absolute hotspot wander between 100 and 90–85 Ma of 10–20 cm/yr, for all hotspots below the Pacific Plate, for which there is no evidence, and which is two orders of magnitude faster than typical hotspot motions (e.g., Doubrovine et al., 2012). In addition, we tested whether the latest and highest-detail published isochron sets from the South Pacific realm change the age for the end of convergence across the Gondwana margin that followed from widely used global plate models (e.g., Seton et al.,

2012; Müller et al., 2019). And while our updated model differs in detail, for instance in the reconstruction of plates and plate motions in lithosphere that was lost to subduction, the conclusions from those global models are robust: Plate kinematic models leave no room for a cessation of subduction along the Zealandia margin at 100 Ma or before; instead, convergence between the Phoenix Plate's daughters and the East Gondwana margin must have continued until at least 90–85 Ma. Below the New Zealand margin, convergence likely continued even longer if spreading in the Osbourn Trough continued beyond 85 Ma (e.g., 79 Ma according to Mortimer et al., 2019).

100 Ma reconstruction

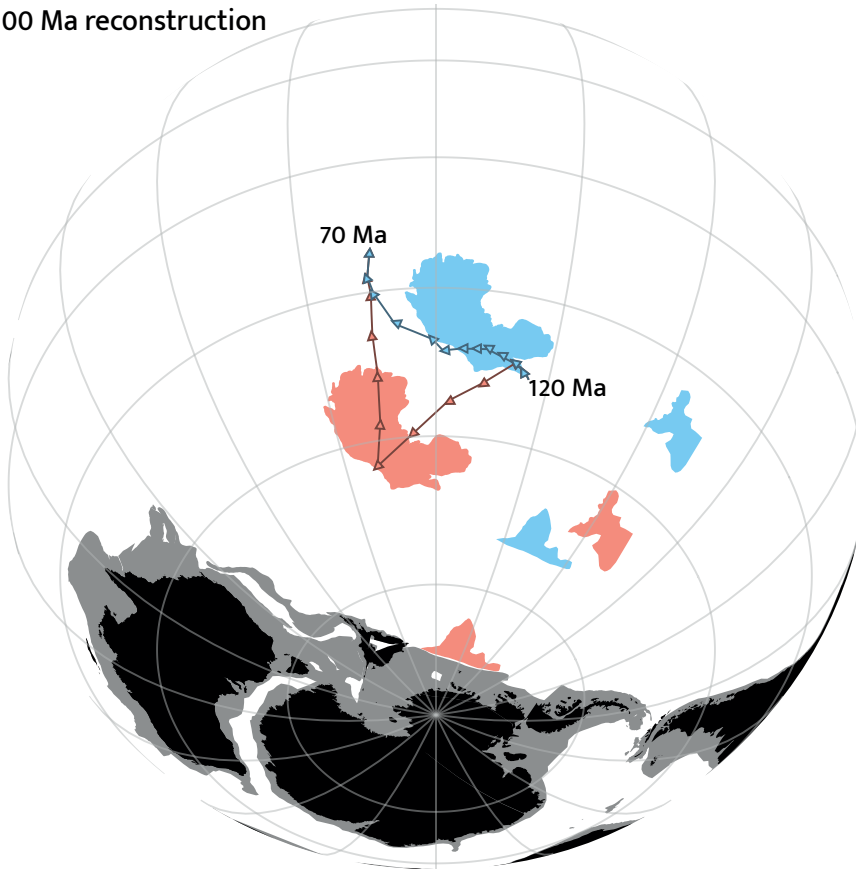


Figure 10. 100 Ma reconstruction that shows the difference in the location of the Pacific Plate between the hotspot reference frame of Torsvik et al. (2019) and the model of Mortimer et al. (2019) in which the Hikurangi Plateau arrives in the East Gondwana trench at 100 Ma. The difference is shown by the location of the LIPs, of which the Ontong Java Plateau has always been part of the Pacific Plate. In blue is the location of the LIPs as constrained by Torsvik et al. (2019), and in pink is the location of these plateaus in the model of Mortimer et al. (2019). Also shown are the 120–70 Ma motion paths of the Pacific Plate that result from the two models.

5.2. Reconciling ongoing convergence after 100 Ma with the geology of Zealandia

Our plate kinematic reconstruction requires that convergence, and by inference subduction, continued until at least 90 Ma along the entire East Gondwana margin, and possibly until 79 Ma below New Zealand and Chatham Rise. While our reconstruction is easily reconciled with the geology of New Caledonia, where subduction-related accretion and magmatism continued until c. 90 Ma (Cluzel et al., 2010; Maurizot et al., 2020b), it conflicts with the common interpretation based on geological observations from New Zealand that subduction there ceased at 105–100 Ma. The observations from New Zealand thus require an alternative explanation.

The first often-cited argument for subduction cessation at 105–100 Ma is the timing of the onset of extension that is recognized in the geology of New Zealand (Bradshaw, 1989; Tulloch and Kimbrough, 1989; Field and Uruski, 1997; Laird and Bradshaw, 2004; Crampton et al., 2019), for example in the Canterbury Basin (Barrier et al., 2020). However, extension in the upper plate above an active subduction zone is common, as evidenced by many intra- and back-arc basins across the world. In fact, extension is presently occurring within the Taupo Volcanic Zone in North Island New Zealand, above the Hikurangi subduction zone (e.g., Villamor and Berryman, 2001). In addition, neither numerical models (e.g., Van Hunen and Allen, 2011; Duretz et al., 2014) nor geological observations (Wortel and Spakman, 2000; Webb et al., 2017; Qayyum et al., 2022) suggest a systematic relationship between slab break-off and upper plate extension. It is even questionable whether the onset of extension in East Gondwana, which is recorded from the West Antarctic Rift System to the Tasman Sea region (Gaina et al., 1998; Behrendt, 1999; Fitzgerald, 2002; Raza et al., 2009; Cluzel et al., 2012a; Spiegel et al., 2016; Jordan et al., 2020), is directly governed by subduction termination, or related to the intra-continental forces that governed Gondwana breakup. In any case, extension in the Gondwana margin does not necessitate slab break-off and does not exclude ongoing subduction.

A cessation of subduction around 105–100 Ma is also interpreted from the unconformity between deformed accretionary prism rocks and overlying sedimentary sequences that are then interpreted as ‘passive margin’ sediments (e.g., Adams et al., 2013; Crampton et al., 2019; Field and Uruski, 1997; Gardiner et al., 2021; Gardiner et al., 2022). However, this transition from accretion to undisturbed sedimentation is only evidence for the cessation of subduction accretion locally, whereby the age of the overlying undeformed rocks dates the accretion of the rocks below the unconformity, but it does not exclude ongoing subduction (Figure 11; e.g., Kamp, 1999; Kamp, 2000; Mazengarb and Harris, 1994). The accretionary system in New Zealand is younging from west to east; while the youngest part of the accretionary system that is subaerially exposed in New Zealand may be 105–100 Ma, younger parts of the former subduction are located offshore, closer to the paleo-trench. This is also illustrated by the geology of New Caledonia, where the minimum age of the oldest ‘cover’ sediments is Cenomanian (~100–94 Ma), while subduction is considered to have continued until c. 90 Ma (Maurizot et al., 2020b). Kamp, 1999, Kamp, 2000 also suggested

that accretionary wedge accumulation occurred contemporaneously with the deposition of cover sequences in New Zealand, based on interpretations from apatite and zircon fission track dating of Torlesse accretionary wedge rocks. Furthermore, the overlying sequences are clastic sediments derived from the New Zealand orogen, and these sediments may represent forearc basin sediments deposited during ongoing subduction rather than passive margin sequences. For example, Mazengarb and Harris (1994) previously suggested that the formation of the accretionary wedge in New Zealand continued until 84 Ma, based on the interpretation that sedimentation in eastern North Island occurred within and in front of an active thrust system. Similarly, Gardiner and Hall (2021) suggested that sedimentary successions on the northern South Island were deposited in a trench-slope basin during ongoing subduction rather than in a passive margin setting. These interpretations are supported by apatite and zircon fission track thermochronology, which suggest that uplift and erosion migrated eastward until c. 85 Ma, resulting from the outbuilding of the accretionary wedge Kamp, 1999, Kamp, 2000. Nevertheless, even if the oldest accretion in New Zealand is truly 105–100 Ma, the geology of New Zealand itself illustrates the conclusion of (Isozaki et al., 1990, Isozaki et al., 2010) that accretion of OPS is episodic, intervened by long periods of wholesale subduction or even subduction erosion, which are the default modes of oceanic subduction (e.g., Van Hinsbergen and Schouten, 2021). Hence, the youngest accretion in New Zealand provides a maximum age for the end of subduction but does not preclude a younger age.

The geological interpretation of the cessation of subduction around 105–100 Ma is further inferred from interpretation of the geodynamic setting that caused a change in geochemical signature of magmatism in New Zealand. Although the youngest age of ‘normal’ subduction-related I-type magmatism in New Zealand was dated as 128 Ma (Tulloch and Kimbrough, 2003), the 131–105 Ma adakitic magmatism is also considered to be related to ongoing subduction (Tulloch et al., 2009). The subsequent onset of A-type magmatism around 100 Ma is widely regarded as signaling the end of subduction (Tulloch et al., 2009). However, the increase in A-type magmatism is interpreted as the result of thinning of the continental crust of Zealandia during extension, which caused less crustal contamination of the igneous rocks (Tulloch et al., 2009), indicating that these interpretations were made under the assumption that subduction ended around 100 Ma, and no alternative causes were explored.

While A-type magmatism is generally interpreted as occurring in the absence of subduction (Loiselle and Wones, 1979), such magmas have also been found in active margin settings, for example related to the arrival of a spreading ridge and the influx of sub-slab mantle to the former wedge (e.g., Zhao et al., 2008; Karsli et al., 2012; Li et al., 2012). We here suggest that the transition to A-type magmatism in New Zealand may also be explained by arrival of a spreading ridge. As explained in section 4.2.3, the plate boundary between the Hikurangi and Aluk plates was likely a spreading ridge south of the Hikurangi Plateau. Our reconstruction predicts that this spreading ridge subducted around 100 Ma below New

Zealand (Figure 7, Figure 11). The progressive arrival of successively younger oceanic crust before arrival of the spreading ridge may then explain the 128–105 Ma adakitic magmatism, which is often related to the subduction of young oceanic crust (Tulloch and Rabone, 1993).

In summary, geological and geochemical interpretations made for New Zealand do not require that subduction ended during c. 105–100 Ma (Figure 7, Figure 11). Alternative structural and stratigraphic arguments for the forearc region of New Zealand (Mazengarb and Harris, 1994; Kamp, 1999, Kamp, 2000; Gardiner and Hall, 2021) are straightforwardly reconciled with ongoing subduction, along with geochemical arguments for the composition of magmatic rocks, which do not exclude ongoing subduction.

5.3. Causes for the end of subduction

Why subduction stopped at the margin of East Gondwana in the Cretaceous is puzzling. Explanations for this cessation have so far mostly focused on regional geological features, such as the arrival of a mid-ocean ridge in the trench (Luyendyk, 1995; Bradshaw, 1989; Matthews et al., 2012). The arrival of a mid-ocean ridge in a subduction zone may indeed change the nature of a plate boundary and trigger slab break-off. The nature of the plate boundary that follows upon ridge arrival commonly depends on the relative motion between the original overriding plate and the plate that was formerly spreading with the original down-going plate. For example, west of the active trench below the Antarctic Peninsula, marine magnetic anomalies young from the ocean towards West Antarctica. This shows that subduction below the Antarctic Peninsula indeed ceased due to the arrival of the Aluk-West Antarctica ridge at the trench below West Antarctica, after which relative motion ceased (Eagles, 2004). However, the Hikurangi-Pacific ridge did not subduct parallel to the trench but subducted at an angle to it (Figure 6C-E and 7A-D). Moreover, until the ~84 Ma change in absolute plate motion of the Pacific Plate, the whole Panthalassa mosaic was converging with the East Gondwana margin, which means that subduction continued after the arrival of the Hikurangi-Aluk spreading ridge. More importantly, the newly formed Pacific-Antarctic Ridge did not replace the former subduction zone but cut through the suture and formed at a completely different location (Figure 6D-E and 7C-D). Ridge arrival is thus not a likely candidate to explain the end of subduction.

A second hypothesis for the end of subduction below the Zealandia margin of East Gondwana is the arrival of the Hikurangi Plateau in the trench (e.g., Billen and Stock, 2000; Davy et al., 2008, Davy, 2014; Reyners et al., 2017; Mortimer et al., 2019). In this hypothesis, the plateau choked the subduction zone after about 150 km of subduction (Riefstahl et al., 2020). However, the Hikurangi Plateau only represents a small portion of the Pacific Plate and only a short length of the trench. If a transform fault could be demonstrated to have bounded the western side of the Hikurangi Plateau, subduction could have continued below the North Island and New Caledonia sections. Moreover, while plateau arrivals at intra-oceanic trenches may cause a polarity reversal (and ongoing subduction), e.g., during the arrival of the Ontong Java Plateau at the Vitiaz trench triggering the formation of the New

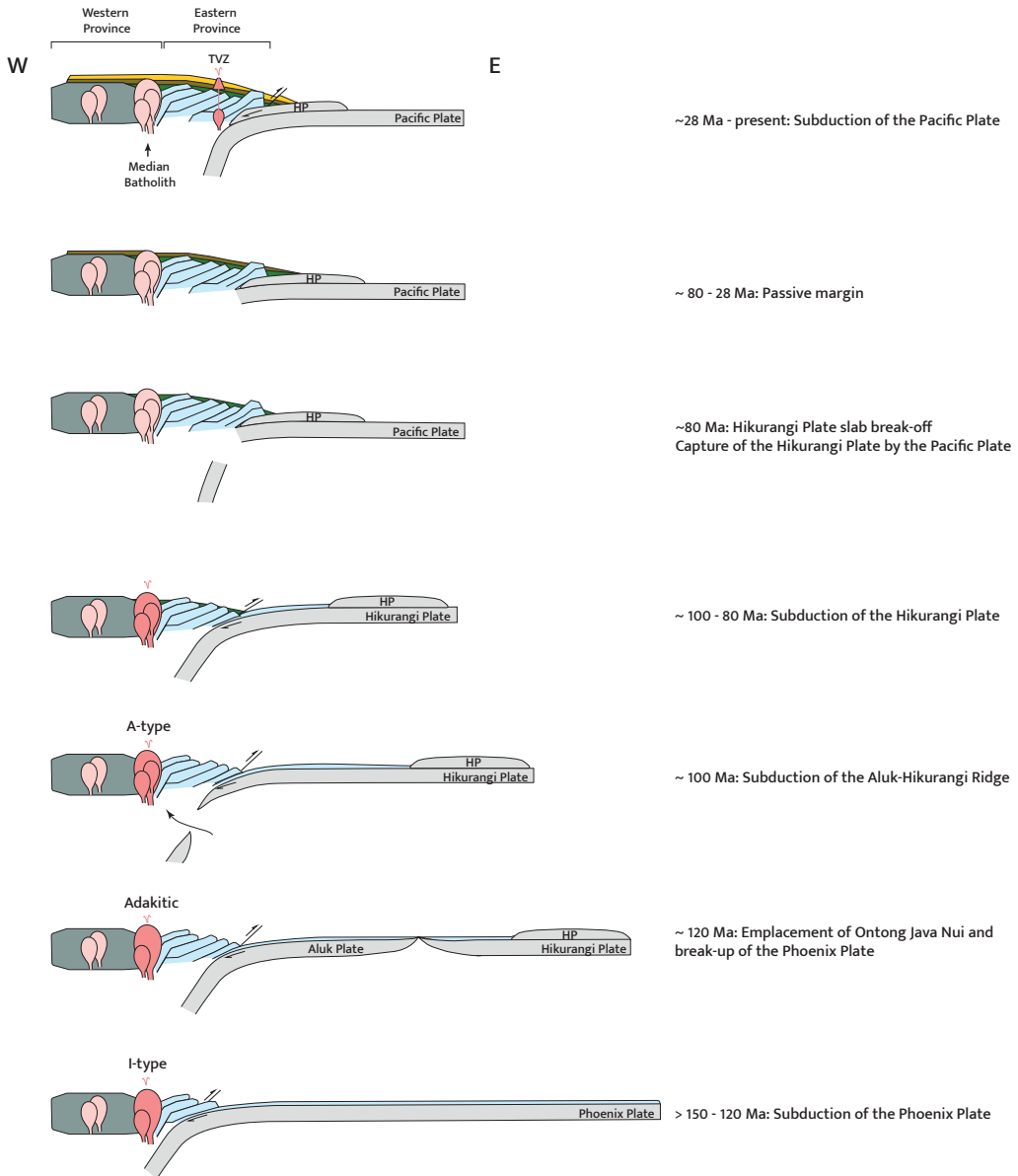


Figure 11. Schematic cross-sections along the Zealandia margin to highlight the 150 Ma to present tectonic history between the continental margin and the Pacific domain. The 28 Ma-present day cross-section is across North Island, New Zealand, where the Hikurangi Plateau is presently subducting, whereas older cross-sections are across the Chatham Rise where the Hikurangi Plateau entered the trench in the Cretaceous. TVZ refers to the active volcanism of the Taupo Volcanic Zone, which lies between the Waipapa and Torlesse terranes.

Hebrides trench and the South Solomon trench (Auzende et al., 1995; Petterson et al., 1997; Quarles van Ufford and Cloos, 2005; Knesel et al., 2008; Lallemand and Arcay, 2021), there is no record of LIP arrival at a trench causing subduction cessation or a plate reorganization on the scale as observed here. Instead, LIP subduction is physically straightforward, even though it may cause shallow dipping slabs (e.g., Yang et al., 2020; Liu et al., 2021). LIP subduction has, for example, been ongoing in the Maracaibo trench of the southern Caribbean region for more than 50 Ma (White et al., 1999; Boschman et al., 2014), and even the Hikurangi Plateau itself is subducting today at the Hikurangi trench (Collot and Davy, 1998; Reyners et al., 2011, Reyners et al., 2017; Timm et al., 2014; Figure 1), where subduction initiated in the Oligocene (Furlong and Kamp, 2009; Appendix 2). Therefore, while the preservation of the Hikurangi Plateau at the Gondwana margin may suggest that it played a role in determining where the slab broke, it is an unlikely trigger for the cessation of subduction along the entire East Gondwana margin.

Instead, we consider it most likely that the end of subduction in the Zealandia sector of East Gondwana was governed by a change in relative plate motion between the Pacific Plate and East Gondwana (Rey and Müller, 2010). More analysis of the driving forces of the Pacific Plate and the Pacific plate mosaic as a whole, not only of local features on the southernmost Pacific Plate could usefully be undertaken. In the East Asia region, below South China, we note that subduction along the continental margin suddenly stopped at around 90–80 Ma (e.g., Cui et al., 2021). Also, in the North Pacific realm there were prominent changes in plate boundary configuration around 90–85 Ma, including the formation of the Kula Plate (Engelbreton et al., 1985; Wright et al., 2016), and initiation of intra-oceanic subduction below the Olyutorsky and Kronotsky arcs (Konstantinovskaia, 2001; Shapiro and Solov'ev, 2009; Domeier et al., 2017; Vaes et al., 2019). An analysis of the causes of plate motion change that formed the prelude to the end of subduction below eastern Gondwana requires a detailed kinematic restoration of the plate boundary reorganization, particularly in the enigmatic transition between the Panthalassa and Tethyan domains of SE Asia, which is beyond the scope of this paper.

6. Conclusions

We have developed a kinematic reconstruction of the South Pacific and East Gondwana realms back to the Late Jurassic (150 Ma). Our aim was to reconstruct the evolution and destruction of the Phoenix Plate, and to reconcile the geological record of New Zealand with the end of Mesozoic subduction along the East Gondwana margin. From our reconstruction we conclude the following:

1. Resulting from the emplacement of Ontong Java Nui around 125–120 Ma, the Phoenix Plate broke into at least four plates: The Manihiki, Hikurangi, Chasca, and Aluk plates. During the Late Cretaceous, the Manihiki and Hikurangi plates were captured by the Pacific Plate, while Chasca was captured by the Farallon Plate. Only the Aluk Plate remained an independent tectonic plate into the Cenozoic.

2. Convergence occurred along the East Gondwana margin until 90 or 85 Ma, depending on choice of mantle reference frame. This convergence occurred independent from spreading at the Osbourn Trough and required the presence of a subduction zone along the entire Zealandia margin until at least 90 Ma and possibly until 85 Ma.
3. Subduction in the New Caledonia region ceased at c. 90 to 85 Ma, but convergence of the Hikurangi Plate with the Chatham Rise must have continued until the cessation of spreading at the Osbourn Trough, recently tentatively estimated at 79 Ma.
4. The cessation of subduction of the Hikurangi Plate along the entire East Gondwana margin was probably a result of a change in Pacific-Gondwana relative plate motion. This was not due to the arrival of the small Hikurangi Plateau compared with the East Gondwana subduction system.
5. The 105–100 Ma structural and magmatic changes within the crust of the overriding New Zealand continental plate may have resulted from subduction of the Aluk-Hikurangi ridge, rather than from the cessation of subduction at the East Gondwana margin.
6. Geological expressions in the overriding plate may be misleading when used to interpret subduction zone dynamics. While a geological record in the overriding plate may provide evidence for the presence of subduction, absence of such evidence should not be interpreted as conclusive evidence for the absence of subduction.



Cretaceous Radiolarian cherts in the Baliojong River, Borneo

4

Causes of Cretaceous subduction termination below South China and Borneo: Was the Proto-South China Sea underlain by an oceanic plateau?

This chapter has been submitted for publication in Geoscience Frontiers as:

Van de Lagemaat, S. H. A., Cao, L., Asis, J., Advokaat, E. L., Mason, P. R. D., Dekkers, M. J.
& Van Hinsbergen, D. J. J. Causes of Cretaceous subduction termination below South
China and Borneo: Was the Proto-South China Sea underlain by an oceanic plateau?

Abstract

The South China, Indochina, and Borneo margins surrounding the South China Sea contain long-lived arcs that became inactive at approximately 85 Ma, even though an embayment of oceanic crust (the ‘Proto-South China Sea’) remained in the intervening region. This oceanic crust eventually subducted in the Cenozoic below Borneo and the Cagayan arc, while the modern South China Sea opened in its wake. To investigate the enigmatic cessation of Mesozoic subduction below South China and Borneo, we studied a fragment of oceanic crust and overlying trench-fill sediments that accreted to NW Borneo during the final stages of subduction. Based on radiolarian biostratigraphy of cherts overlying the pillow basalts and detrital zircon geochronology of the trench-fill, we constrained the minimum age of the oceanic crust during accretion to 40 Ma. This shows that subduction cessation was not related to ridge subduction. Geochemical analysis of pillow basalts revealed an enriched mid-ocean ridge basalt signature comparable to oceanic plateaus. Using paleomagnetism, we show that this fragment of oceanic crust was not part of the Izanagi Plate but was part of a plate (the ‘Pontus’ Plate) separated from the Izanagi Plate by a subduction zone. Based on the minimum 40 Ma age of the oceanic crust and its geochemistry, we suggest that Mesozoic subduction below South China and Borneo stopped when an oceanic plateau entered the trench, while the eastern plate margin with the Izanagi Plate remained active. We show how our findings offer opportunities to restore plate configurations of the Panthalassa-Tethys junction region.

1. Introduction

For the last hundreds of millions of years, the East Asian margin of Japan has been accommodating subduction of paleo-Pacific (or ‘Panthalassa’) lithosphere (Isozaki et al., 1990; 2010). Today, the subduction zone along the east Asian margin continues as far as Taiwan, where it connects to plate boundaries of the Philippines. However, geological records of arc magmatism and accretionary complexes show that until the Late Cretaceous (~80 Ma) a subduction zone was active along the southeast China margin as far as Vietnam (e.g., Jahn et al., 1990; Lapierre et al., 1997; Xu et al., 1999; Shellnut et al., 2013; J. Li et al., 2014; Z. Li et al., 2014; Cao et al., 2021; Nong et al., 2021, 2022). Then, around 80-70 Ma, subduction at the SE China and Indochina margin appears to have ceased, the South China and Vietnamese margins became passive, Paleogene rift basins formed, and after the Eocene, the South China Sea extensional basin opened (C. Li et al., 2014; Morley, 2016; Wu et al., 2016; Ye et al., 2018). Why Cretaceous subduction stopped, and where the ensuing convergence between the plates from the Pacific realm and Eurasia was accommodated, is poorly known.

Clues as to why subduction ceased come from rock units of the subducted paleo-Pacific plates (Ocean Plate Stratigraphy (OPS); Isozaki et al., 1990) preserved in accretionary prisms. Relics of Late Cretaceous and older prisms are found on Taiwan (Yui et al., 2012), along the South China margin west of Taiwan (D. Zhou et al., 2006), and to the south of

the South China Sea in Palawan (e.g., Holloway, 1982; Shao et al., 2017; Figure 1). The Palawan record concerns a fragment of the South China margin that became separated from its original position by opening of the South China Sea basin within the SE China continental margin during the latest Eocene to middle Miocene (Briais et al., 1993; Li et al., 2015; Shao et al., 2017; Larsen et al., 2018). These records reveal that during the final stages of subduction, lithosphere with seamounts as old as 154.1 ± 1.8 Ma accreted (Xu et al., 2022). There are also relics of the lithosphere that remained in front of the former subduction zone after Late Cretaceous cessation (e.g., Moss, 1998). The Eocene to Miocene opening of the South China Sea basin was accommodated by a southward-dipping subduction zone below Borneo and the Cagayan arc (Hall, 2002; Hall and Breitfeld, 2017) (Figure 1C), at which an accretionary prism formed that on Palawan includes OPS sequences with mafic rocks of ~ 100 Ma (Keenan et al., 2016; Dycoco et al., 2021). This shows that after subduction cessation at the South China margin, oceanic lithosphere remained in the foreland embayment of the former subduction zone. This oceanic embayment that remained after Cretaceous subduction cessation and that was consumed during Eocene to Miocene subduction below Borneo and the Cagayan arc is referred to as the 'Proto-South China Sea' (Hinz et al., 1994; Hall and Breitfeld, 2017). Why this embayment formed while old oceanic lithosphere was still available to subduct (and eventually subducted in the Eocene to Miocene) is puzzling.

Obtaining new geological data to decipher the enigmatic tectonic history of the Proto-South China Sea from the deformed, poorly exposed, and largely submerged records of the South China margin, Taiwan, and Palawan accretionary prisms is difficult due to their poor preservation and accessibility. However, the Proto-South China Sea was also bordered by a former subduction zone to the south, of which accretionary records are preserved in North Borneo. There, an accretionary complex expose OPS sequences consisting of pillow basalts, radiolarian cherts, and trench-fill clastics (Jasin, 2000, 2018). These OPS sequences form the youngest part of a Mesozoic accretionary prism adjacent to a Jurassic to Cretaceous volcanic arc exposed in Kuching Zone (Breitfeld et al., 2017), and in the Schwaner Mountains of the SW Borneo Mega-Unit (Breitfeld et al., 2020). This prism and arc formed during northward motion of Borneo, as part of plate carrying continental fragments known as Argoland from the Gondwana margin towards Eurasia (Hall, 2012; Advokaat and Van Hinsbergen, 2023). Intriguingly, Borneo's northward motion towards Eurasia stopped in the Late Cretaceous (Advokaat and Van Hinsbergen, 2023), around the time of subduction cessation at the South China margin, 'trapping' oceanic crust in the Proto-South China Sea embayment.

In this study, we investigate the age of the crust of the youngest OPS nappes exposed in the Baliojong Complex in Sabah, North Borneo, using radiolarian biostratigraphy of the chert to determine the minimum age of the oceanic crust, and detrital zircon geochronology of the trench-fill deposits to constrain the age of its accretion. This allows us to determine the minimum age of oceanic crust when it entered the subduction zone. We use major and trace element geochemistry of pillow basalts to investigate the tectonic setting of formation of the ocean floor. Finally, we use paleomagnetism of the pillow basalts and radiolarian

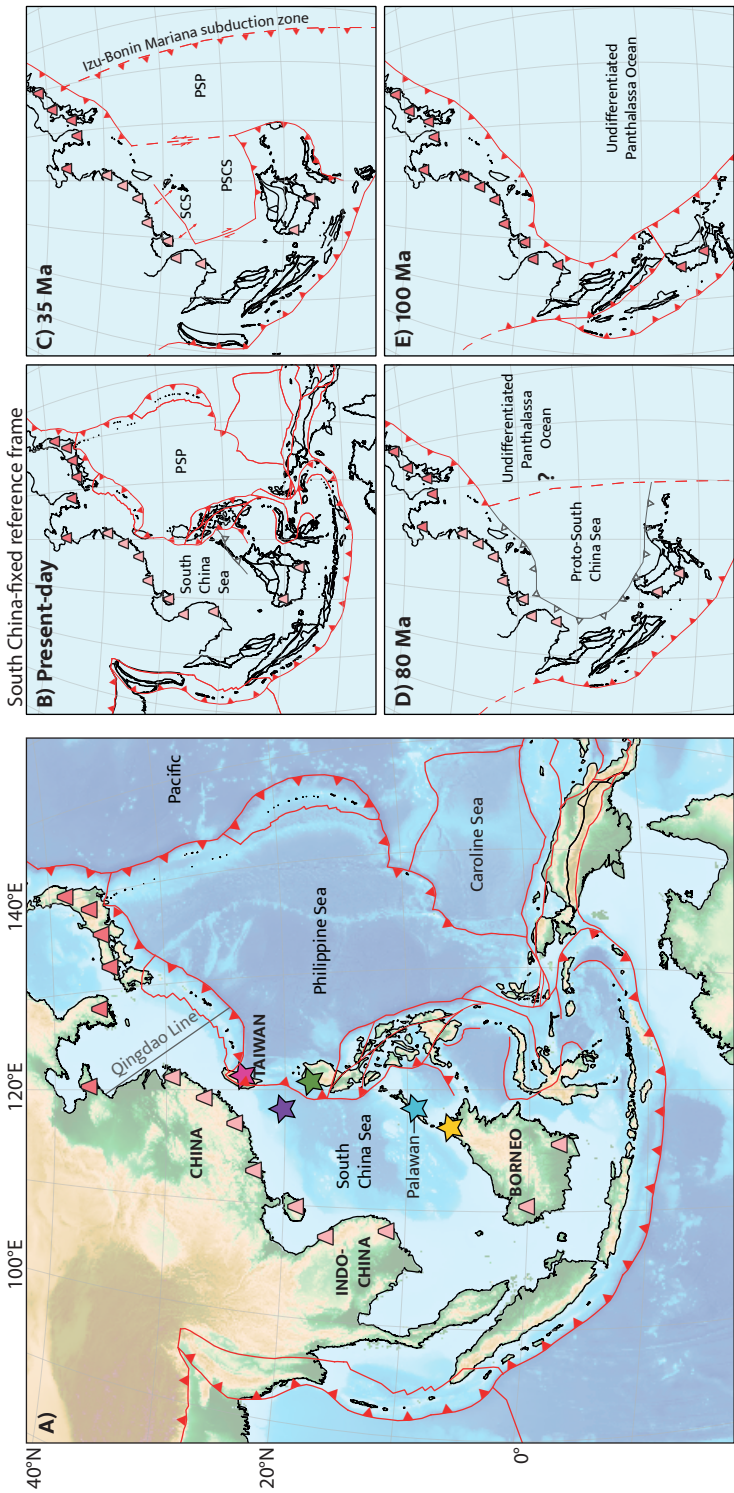


Figure 1. A) Present-day map of the (Proto-)South China region. Stars mark locations of geological data from the Proto-South China Sea: Yellow: Baliojong River (this study); Blue: South Palawan Ophiolite; Green: Dos Hermanos Mélange; Purple: Accreted seamounts; Pink: Tailuko Belt. Dark pink cones indicate active arc magmatism, light pink cones indicate extinct arc magmatism. Arc magmatism has been continuously active northeast of the Qingdao Line, whereas it went extinct in the Late Mesozoic to the southwest of this line. B-E) Simplified Late Mesozoic - Cenozoic tectonic evolution of the proto-South China region, based on the reconstruction of Advoikaat and Van Hinsbergen (2023), in a South China-fixed reference frame. Active plate boundaries are shown in red, former plate boundaries in gray. Dark pink cones indicate active arc magmatism, light pink cones indicate extinct arc magmatism. Background image is ETOPO 2022 15 Arc-Second Global Relief Model. (NOAA National Centers for Environmental Information, 2022).

chert to constrain the paleolatitude of formation of the oceanic crust. This allows us to test possible connections of the Proto-South China Sea crust to the Tethyan or Paleo-Pacific paleo-plates. In combination with available constraints from Palawan, the South China margin, and Taiwan, we will evaluate possible reasons for the enigmatic cessation of long-lived subduction at the South China-Sundaland margin, and the origin and destruction of the Proto-South China Sea.

2. Geological setting

2.1. Records of arcs surrounding the Proto-South China Sea

A Mesozoic paleo-Pacific subduction zone below SE China, Indochina and Borneo has been interpreted based on evidence arc magmatism and accretionary complexes. Granitoid emplacement in SE China occurred throughout the Mesozoic (e.g., X. Zhou et al., 2006; Ji et al., 2017). For the suite of granites and related volcanics emplaced during the Late Jurassic and Cretaceous it is generally accepted that they formed as a magmatic arc that formed during subduction of paleo-Pacific oceanic lithosphere (Jahn et al., 1976; Lapierre et al., 1997; Zhou and Li, 2000; Li and Li, 2007; Zhou et al., 2006; H. Li et al., 2012; J. Li et al., 2014; Zhu et al., 2017; Jiang et al., 2015; Liu et al., 2020; Sun et al., 2021). Most magmatism in SE China had ceased by c. 90 Ma, after which limited A-type magmatism occurred until 80 Ma, which was interpreted to reflect extension (Li et al., 2012; Z. Li et al., 2014; J. Li et al., 2014; Liu et al., 2020). The youngest granite intrusion, with a 73 Ma zircon U-Pb age is exposed on Hainan Island (Jiang and Li, 2014).

The youngest arc magmatism interpreted to be related to paleo-Pacific subduction below Indochina is most prominent in the Dalat Zone of Vietnam (e.g., Nguyen et al., 2004; Thuy et al., 2004; Shellnut et al., 2013; Nong et al., 2022). Radiometric dating of these plutons using zircon and titanite U-Pb geochronology revealed ages from 118 to 87 Ma (Nguyen et al., 2004; Shellnutt et al., 2013; Nong et al., 2021). Younger plutons, emplaced between 75 and 79 Ma, are exposed to the southwest of the Dalat Zone in SW Vietnam and SE Cambodia (Nong et al., 2022). Based on the geochemistry of the igneous rocks in Vietnam and Cambodia, the older magmatic stage (110-91 Ma) that produced calc-alkaline I-type granitic batholiths, is thought to have formed during active subduction. The younger magmatic stage (83-75 Ma) that produced A-type granites may instead relate to extensional deformation after subduction cessation (Shellnutt et al., 2013; Nong et al., 2022).

Westernmost Borneo (west Sarawak and NW Kalimantan) has been part of Sundaland since at least the Triassic (e.g., Breiffeld et al., 2017) and was likely derived from South China (e.g., Metcalfe, 1985). Triassic magmatism and metamorphism in this part of Borneo was interpreted to be related to Triassic westward subduction of a paleo-Pacific plate (Breiffeld et al., 2017) predating accretion of the Proto-South China Sea. This sequence is unconformably overlain by Upper Jurassic shallow marine limestone (Kakizaki et al., 2013), Upper Jurassic mudstone and radiolarian chert, and Cretaceous deep marine volcanics (Breiffeld et al., 2017; Jasin and Said, 1999; Schmidtke et al., 1990; A. Zhang et al., 2022).

This sequence was interpreted to record the transition from a passive margin in the Jurassic to a forearc basin in the Late Jurassic to Late Cretaceous (Breitfeld et al., 2017). The sequence is unconformably overlain by Upper Cretaceous (Maastrichtian) to Eocene continental clastics that post-date arc magmatism (Breitfeld et al., 2018).

SW Borneo, which was derived from Gondwana, preserves evidence of Jurassic magmatism that was interpreted as being related to rifting of the SW Borneo block (as part of 'Argoland') from Gondwana (Davies et al., 2014; Breitfeld et al., 2020; Batara and Xu, 2022). Subsequent magmatism related to paleo-Pacific subduction below Gondwana-derived Borneo is well-exposed in the Schwaner Mountains of SW Borneo (e.g., Hennig et al., 2017; Breitfeld et al., 2017, 2020), and was underway by c. 132 Ma (Breitfeld et al., 2017, 2020), and perhaps already by 154–150 Ma (Batara and Xu, 2022). In North Borneo, arc magmatism was already active during the Triassic and Jurassic (Burton-Johnson et al., 2020), when the SW Borneo block was still part of the Gondwana margin (Advokaat and Van Hinsbergen, 2023). The youngest magmatism that may be related to paleo-Pacific subduction exposed in the Schwaner Mountains has ages of c. 77 Ma (Breitfeld et al., 2017, 2020; Qian et al., 2022), but as in South China and Vietnam, A-type granite geochemical signatures in the post-80 Ma plutons in SW Borneo have also been interpreted as extensional magmatism that followed subduction cessation (Breitfeld et al., 2017, 2020).

2.2. OPS records of the Proto-South China Sea

Information about the oceanic lithosphere that was subducting below SE China and Borneo comes from the accretionary prisms exposed in Taiwan, the northern South China Sea margin, Palawan, and Borneo. There is no accretionary prism related to paleo-Pacific subduction exposed onshore in China or Vietnam.

Based on gravimetric, magnetic, and wide-angle seismic data, an accretionary complex was interpreted in the NE margin of the South China Sea (Zhou et al., 2006). In this area, relics of two seamounts have been found, which were originally interpreted as Miocene features (e.g., Wang et al., 2012; Xu et al., 2020), but recently yielded plagioclase $^{40}\text{Ar}/^{39}\text{Ar}$ plateau ages of 154.1 ± 1.8 Ma and 93.2 ± 5.0 Ma (Xu et al., 2022). These seamounts have ocean island basalt (OIB) geochemistry and are interpreted as intraplate basalts that formed on paleo-Pacific lithosphere (Xu et al., 2020, 2022). The oldest seamount thus provides a minimum age for the oceanic crust (~ 154 Ma) of the paleo-Pacific lithosphere that was subducting below SE China. The youngest seamount provides a maximum age of accretion (~ 93 Ma), i.e., not long before the end of subduction. Xu et al. (2022) suggested that these seamounts may have formed as part of an oceanic plateau.

The submerged accretionary complex in the northern South China Sea may be contiguous with the Tailuko Belt of Taiwan, which is interpreted as a Late Jurassic to Early Cretaceous accretionary complex that formed during paleo-Pacific subduction below the South China margin (Yui et al., 2012). Here, upper Jurassic to lowermost Cretaceous terrigenous trench-fill clastic sediments overlie Permian greenschist facies interlayers

of marble, chert, and metabasite (Yui et al., 2012), interpreted as an OPS sequence. The massive marbles are interpreted as platform deposits, possibly deposited on seamounts or an oceanic plateau (Jahn et al., 1992; Yui et al., 2012). The accretionary prism is intruded by Late Cretaceous granitic plutons, for which ages of 87–90 Ma were obtained (Yui et al., 2009, 2012). The Tailuko Belt is unconformably overlain by Eocene syn-rift sediments, which are interpreted as the passive margin sediments of the northern South China Sea margin (Ho, 1986; Conand et al., 2020).

To the south of the South China Sea, the Palawan Continental Terrane is exposed on the Palawan and Calamian Islands, in the Philippines. This ‘continental’ terrane is also interpreted to have formed as an accretionary prism along the SE China Margin (e.g., Holloway, 1982; Shao et al., 2017). After subduction ceased, the Palawan Continental Terrane formed part of the SE China passive margin and was subsequently transported southwards during opening of the South China Sea and became accreted in the Cenozoic accretionary fold-thrust belt that formed north of the Cagayan arc during southward subduction (e.g., Cao et al., 2021). The Palawan Continental Terrane exposed on the Calamian Islands comprises Permian to Upper Jurassic radiolarian chert, middle Permian to Upper Jurassic limestone, and Middle Jurassic to Lower Cretaceous trench-fill clastic sediments (Zamoras and Matsuoka, 2001, 2004). Based on the lithologic transition from chert to limestone to terrigenous clastic sediments, it was interpreted that these accreted units define a north-to-south younging accretionary prism, which formed during three distinct accretion events in the Middle Jurassic, Late Jurassic, and Early Cretaceous (Zamoras and Matsuoka, 2001, 2004). A Middle Jurassic to Late Jurassic accretionary prism is also exposed on the island of Palawan (Faure and Ishida, 1990) and on the Buruanga Peninsula of Panay (Zamoras et al., 2008). Detrital zircons in the trench-fill turbidites of the Palawan Continental Terrane suggest a South China magmatic arc provenance (Cao et al., 2021). The Palawan Continental Terrane is overlain by Upper Cretaceous continental clastic sediments with arc-derived detrital zircons interpreted to have been deposited over the prism after subduction ceased. The Upper Cretaceous continental clastics are overlain Eocene syn-rift turbidites with a South China provenance, which are interpreted to reflect the early opening stages of the South China Sea basin. These are overlain by Upper Oligocene–Lower Miocene limestones that formed during the drift of the Palawan Continental Terrane towards the Palawan subduction zone. Finally, the Early Miocene trench-fill clastic sediments date the arrival of the Palawan Continental Terrane in the trench along the Cagayan arc (Steuer et al., 2013; Aurelio et al., 2014; Suggate et al., 2014; Shao et al., 2017; Cao et al., 2021).

Sarawak exposes OPS-mélange with blocks of Upper Jurassic to Upper Cretaceous radiolarian chert and Cretaceous trench-fill clastics (e.g., Jasin, 2000). U–Pb zircon detrital zircon geochronology on the trench-fill sediments revealed maximum depositional ages between 119 Ma and 88 Ma (Wang et al., 2021; Zhao et al., 2021). Similar mélange complexes are also present in northern Sabah, where they comprise gabbro, plagiogranite, pillow basalt, Cretaceous radiolarian chert, and trench-fill clastics (Jasin, 2000, 2018).

Zircon U-Pb dating of gabbro samples from these North Borneo accretionary complexes, of which the (tectono-)stratigraphic context is not well known, yielded mean ages between 112 ± 2 and 123 ± 1 Ma and basalt samples yielded $^{40}\text{Ar}/^{39}\text{Ar}$ plateau ages of $\sim 134.5\pm 2.8$ and 135.9 ± 2.2 Ma (Wang et al., 2023). Trench-fill sandstones yielded maximum depositional ages of ~ 114 Ma, based on detrital zircon geochronology (Wang et al., 2023). The OPS mélanges in North Borneo are unconformably overlain by Middle Eocene sandstones (Hutchison, 1996; Jasin and Tongkul, 2013; Van Hattum et al., 2013; Rahim et al., 2017) that farther to the north were incorporated into a north-vergent fold-thrust belt known as the Rajang-Crocker accretionary prism that formed during southward subduction below north Borneo along-strike of Palawan (Van Hattum et al., 2006, 2013; Lambiase et al., 2008).

Information about the Proto-South China Sea, which is the oceanic lithosphere that was preserved after Mesozoic subduction cessation, comes from the OPS sequence exposed in Palawan. These sequences are found thrust over the Palawan continental terrane, and, in turn, are overthrust by supra-subduction zone ophiolites with latest Eocene metamorphic soles showing that they accreted in a late Eocene and younger subduction zone before the arrival of the Palawan Continental Terrane in the trench (Schlüter et al., 1996; Aurelio et al., 2014; Dycoco et al., 2021). These ophiolites were interpreted to have formed by inversion of a mid-oceanic ridge (Keenan et al., 2016), but regional kinematic restoration makes it more likely that they formed in the forearc of a subduction zone along the northern SW Borneo continental block, which includes the basement of the Cagayan arc (Advokaat and Van Hinsbergen, 2023).

The OPS sequences that are tectonically sandwiched between the Palawan Continental Terrane and the Palawan Ophiolite, are somewhat confusingly known as the ‘Southern Palawan Ophiolite’ (Gibaga et al., 2020; Dycoco et al., 2021), but are not associated with metamorphic sole rocks and are instead interpreted as off-scraped relics of a subducted, oceanic lithosphere. The Southern Palawan Ophiolite was assigned a Mesozoic age based on the presence of Early Cretaceous nannoplankton in calcareous red clay associated with pillow basalts (Muller, 1991) and Upper Cretaceous radiolarian cherts (Wolfart et al., 1986). In addition, float samples of gabbro and syenite, interpreted to have been derived from the Southern Palawan Ophiolite, yielded 100.7 ± 1.2 Ma and 103.0 ± 1.1 Ma zircon U-Pb ages (Dycoco et al., 2021). Whether these samples are derived from the gabbroic section of the South Palawan Ophiolite or from intrusions into it is unknown, but the obtained ages provide minimum ages of the oceanic lithosphere of the Proto-South China Sea (Dycoco et al., 2021), which thus must already have existed prior to the arrest of subduction at the south China Sea margin. The volcanic section and the gabbroic float samples of the South Palawan Ophiolite have an ocean island basalt geochemical affinity, while a mafic dike has an island arc signature (Gibaga et al., 2020; Dycoco et al., 2021). Peridotites of the South Palawan Ophiolite have signatures transitional between Mid-Ocean Ridge Basalt (MORB) and Island Arc Tholeiite (IAT) and are interpreted to have formed in a supra-subduction zone environment (Labis et al., 2021).

The Proto-South China Sea was also lost to oblique eastward subduction below northern Luzon (e.g., Hall, 2002) and fragments of its oceanic crust may be preserved in the Philippines (Yumul et al., 2020). In western Luzon, a highly sheared *mélange* with a serpentinite matrix and blocks of Lower Cretaceous radiolarian cherts is exposed to the west of the Zambales Ophiolite, referred to as the West Luzon Shear Zone (Karig, 1983). A similar serpentinite-matrix *mélange* (the Dos Hermanos *Mélange*), with Uppermost Jurassic to Lower Cretaceous radiolarian chert is exposed in the northwest of Luzon, in the Ilocos Norte region (Queaño et al., 2017a). Geochemical signatures of the Dos Hermanos *Mélange* ultramafic and mafic rocks display MORB and island arc signatures and are interpreted to have formed in a supra-subduction setting (Pasco et al., 2019).

3. Methods, results, and interpretation

We collected samples from OPS sequences in the Cretaceous accretionary prism of Sabah, north Borneo. We performed fieldwork along the well-exposed section along the Baliojong River, northeast of Kota Marudu (Figure 2 and 3). The rocks in this section form the structurally deepest and hence presumably youngest parts of the Mesozoic accretionary prism exposed in Borneo. We studied five sequences of OPS (B2-B5) that are exposed in thrust fault-bounded, coherent stratigraphic sections comprising pillow basalts with overlying radiolarian chert and trench-fill turbidites consisting of fine- to coarse-grained sandstone (Jasin and Tongkul, 2013). In a few instances, the oldest part of the deep marine sediments consist of a rhythmic alternation between radiolarian chert and red siltstone. We documented five sections from fault-bounded thrust slices. Each section is overturned with dips typically between 25 and 50° (115-140°), but with local variation due to folding. In sections 2 and 3, the trench-fill clastic sediments were truncated from the OPS sequence along footwall cutoffs. Based on field relationships, it was not possible to conclusively demonstrate whether all thrust slices represent a duplexed series of a single accreted OPS sequence, or whether there are multiple OPS sections that accreted at different times. From four sections (B2-B5) we collected samples for geochemical analyses from pillow lavas, for radiolarian stratigraphy from chert sections, for paleomagnetic analyses from both pillow lavas and red clays intercalated in the basal chert sections, and finally, from two sections (B2 and B5) we collected turbiditic sandstones for sediment provenance and maximum depositional age analysis. Below, we describe the results and first-order interpretation per data type.

3.1. Basalts: major and trace element geochemistry

3.1.1. Sampling and methods

We collected 22 samples of basaltic pillow lavas from sections 2, 3, 4, and 5. Samples were crushed using a steel jaw crusher and ground in a tungsten carbide mill. Loss on ignition (LOI) was measured at 1000°C by thermo-gravimetric analysis. Fusion beads were prepared for whole rock x-ray fluorescence (XRF) major element analysis using 0.6 g

sample and 6g of flux consisting of 66% lithium tetraborate, 34% lithium metaborate and 0.5% lithium iodide. Wavelength dispersive XRF measurements for major elements were done sequentially with a Thermo Scientific ARL Perform'X 4200W instrument at Utrecht University, the Netherlands. Results were reported on a loss-free basis.

Trace elements were measured by laser ablation inductively coupled plasma-mass spectrometry (LA-ICP-MS) on the fusion beads using a GeoLas 200Q 193nm ArF Excimer laser ablation system coupled to a Thermo Finnigan Element2 sector field ICP-MS at Utrecht University. Fusion beads were ablated with a fluence of 12 Jcm⁻², a pulse repetition rate of 10Hz and with a crater diameter of 120 μ m. Calibration was performed against NIST SRM 612 glass using standard data reduction protocols (Longerich et al., 1996) and accuracy was monitored using the USGS basaltic glass standard BCR2-G.

Three basaltic standard reference materials, BIR-1, JB-1B and JB-2 were treated as external standards and were measured in parallel with the basaltic rocks collected in this study. Results are reported alongside the samples in Table 1 and show excellent agreement with recommended values from the GEOREM database (Jochum et al., 2005), to within 10% of recommended values for the majority of elements measured.

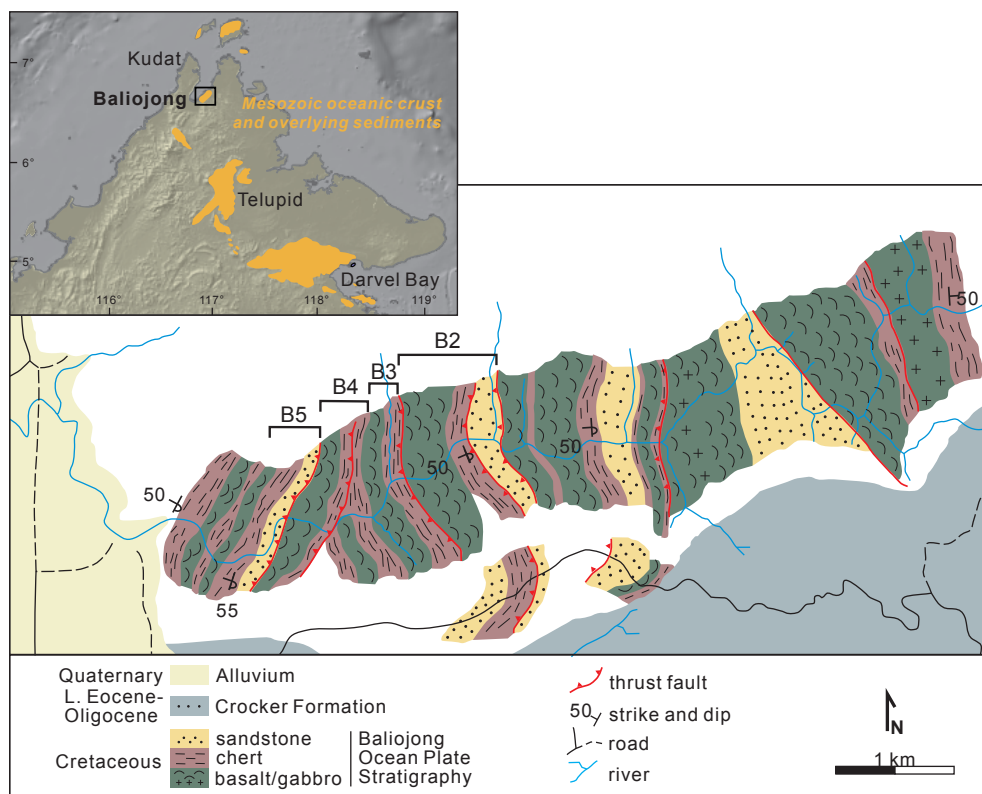


Figure 2. Geological map of the OPS sections of the Baliojong River showing the sampled sections (based on Jasin and Tongkul, 2013). Inset: Generalized geological map of Sabah, showing the distribution of Mesozoic ophiolite and OPS exposures.



Figure 3. Field photos from the Baliojong River OPS: A) Sandstone turbidite; B) Overturned contact (highlighted with yellow line) between pillow basalts and radiolarian cherts; C) Rhythmic alternation between radiolarian chert and red cherty siltstone; D) Pillow basalts.

3.1.2. Results and Interpretation

Eighteen samples plot as basalts on the total alkali-silica diagram (Le Bas et al., 1986) and four have slightly elevated SiO_2 , plotting in the basaltic andesite field. Major elements such as MgO , Al_2O_3 and CaO vary across this range in SiO_2 consistent with minor degrees of fractional crystallization (Table 1). Loss on ignition was typically below 5%, but some samples showed elevated LOI and/or an increase Na_2O and K_2O that reflects minor post-magmatic alteration (Table 1). Increased concentrations of alkalis compromise the use of these elements in tectonic discrimination diagrams. In contrast, immobile trace element ratios and relative abundances are consistent with a mid-ocean ridge basalt (MORB) origin, for example using Zr vs Ti , Ti/Y vs Zr/Y and Ti/1000 vs V (Rollinson et al., 2021; plots not shown here). Rare earth element abundances further constrain the tectonic setting and are consistent with a slightly enriched E-MORB origin, with Ce/YbN equal to or > 1 (Figure S1).

Table I. Major and trace element compositions of Baliojong River basalt samples

wt. %	PB 2.1	PB 2.8	PB 2.13	PB 2.35	PB 2.50	PB 3.15	PB 3.26	PB 3.4	PB 3.5	PB 3.6	PB 3.44	PB 4.7	PB 4.21	PB 4.23	PB 4.24	PB 4.38	PB 4.48	BB 5.1	BB 5.2	BB 5.3	BB 5.4	BB 5.5	BIR-1	JB-1B	JB-2
SiO ₂	4987	5359	4906	5224	5062	5012	4875	5289	5087	5103	4977	5182	5382	5075	4839	4934	5298	4988	4960	4572	4758	5072	4678	5151	5232
Al ₂ O ₃	1700	1495	1645	1484	1570	1670	1688	1638	1734	1750	1809	1538	1546	1578	1543	1633	1387	1655	1586	1444	1601	1527	1557	1459	1473
TiFe ₂ O ₃	824	933	1036	1019	994	900	965	795	779	765	810	973	842	1060	1323	916	970	996	1010	1042	1057	912	1142	908	1435
MnO	0.13	0.15	0.17	0.17	0.16	0.13	0.15	0.15	0.17	0.17	0.17	0.16	0.14	0.17	0.17	0.20	0.17	1.08	0.15	0.17	0.22	0.17	0.18	0.15	0.22
MgO	6.72	7.78	6.21	8.86	6.94	7.53	6.84	8.49	8.82	8.65	9.04	7.84	7.07	7.91	6.91	7.16	7.72	7.37	6.32	6.36	6.25	7.57	9.55	8.48	4.60
CaO	11.92	6.39	10.84	7.07	8.81	8.56	11.05	6.01	7.65	7.49	8.86	7.27	6.31	6.66	8.08	9.45	8.10	8.03	10.59	16.33	13.63	10.20	13.11	9.52	9.61
Na ₂ O	2.81	4.67	4.70	3.65	3.46	2.68	2.75	5.27	4.08	3.94	2.66	4.33	3.98	3.42	2.92	2.67	2.51	4.00	3.34	2.51	3.53	3.45	1.71	2.59	1.92
K ₂ O	0.99	0.62	0.14	0.66	1.87	2.78	1.43	0.43	0.94	1.13	0.88	1.06	1.62	1.94	2.05	2.67	2.07	0.61	1.76	1.89	0.45	1.33	0.01	1.32	0.41
TiO ₂	1.23	1.53	1.14	1.70	1.32	1.24	1.14	1.14	1.16	1.21	1.19	1.51	2.04	1.83	1.76	1.83	1.85	1.57	1.14	0.97	1.17	1.10	0.90	1.19	1.10
P ₂ O ₅	0.13	0.22	0.11	0.13	0.19	0.13	0.19	0.17	0.17	0.18	0.16	0.16	0.38	0.35	0.24	0.25	0.24	0.17	0.11	0.14	0.10	0.10	0.01	0.23	0.08
Total	99.04	99.23	99.18	99.51	99.01	98.87	98.83	98.88	98.99	98.95	98.92	99.26	99.24	99.41	99.18	99.06	99.21	99.22	98.97	98.95	99.51	99.03	99.24	98.66	99.34
LOI	2.92	3.00	4.42	3.66	3.84	3.92	5.87	3.56	3.99	3.85	3.74	2.87	3.18	3.65	3.75	4.77	3.10	7.59	3.73	7.53	5.20	3.00			
ppm																									
Sc	45.4	48.6	41.2	47.8	45.8	45.8	39.6	41.3	41.7	43.0	40.7	49.6	44.1	44.1	43.4	41	43.3	43.8	48	42.9	49.6	45	50	33	61
Ti	9628	12042	8833	13212	9970	9663	8830	8808	8982	9497	9473	11983	15983	14328	13832	14137	13980	11995	8692	7430	8947	8389	7262	9100	8499
V	279	240	268	259	276	289	279	241	276	278	283	289	227	258	288	265	265	191	259	286	258	270	375	228	643
Cr	388	254	457	139	374	405	403	430	443	436	409	264	87	239	228	312	183	357	422	407	463	438	485	532	59
Mn	985	1180	1330	1263	1174	1001	1169	1152	1302	1326	1364	1256	1022	1276	1276	1441	1236	8174	1114	1290	1646	1257	1401	1119	1685
Co	66.1	44.1	61.7	64.3	52.7	57.7	60.7	73.0	64.4	80.9	84.2	65.8	47.4	52.8	49.0	52	60.3	46.3	47	47.2	49.5	51.0	58.3	41	37
Ni	118	65	112	70	75	98	143	200	180	202	188	76	57	60	53	107	90	112	76	73	80	75	189	174	30
Cu	41	60	85	44	70	48	67	67	65	66	65	67	39	42	35	24	28	51	41.9	32	170	73	88	41	179
Zn	107	108	113	108	82	98	91	88	95	81	98	113	95	112	106	107	69	102	90	76	85	75	86	88	117
Ga	18	13	17	14	21	25	18	14	18	17	19	14	17	19	22	20	17	21	27	28	17	24	15	28.9	20
As	2.1	2.8	4.4	2.3	2.1	1.6	3.7	2.9	2.1	2.6	1.7	3.9	2.4	4.0	3.3	3.0	3.8	5.3	1.3	1.4	1.5	1.3	2.1	1.7	2.2
Rb	14	11	2	12	30	28	13	5	9	12	9	21	17	27	35	27	19	21	31	28	9	25	0.26	39	6.4
Sr	179	141	116	135	178	116	115	201	242	243	172	135	167	158	135	192	119	169	199	197	153	249	113	451	179
Y	25	30	23	33	29	25	25	22	23	25	25	28	34	31	28	31	32	28	24	25	25	24	15	20.8	22
Zr	78	104	70	114	92	79	80	76	76	81	81	96	162	118	125	135	132	112	65	56	69	63	15	119	43
Nb	5.1	9.2	4.8	9.4	6.4	6.3	13.3	14.0	14.1	14.2	12.2	9.7	21.9	14.8	15.6	16.5	16.2	11.0	4.3	3.4	4.6	4.3	0.55	25.6	0.59
Mo	1.3	1.8	1.6	1.6	2.2	2.0	1.8	2.1	2.6	1.6	1.3	1.6	1.8	1.8	1.5	1.6	1.3	1.8	6	2.3	2.9	1.5	1.3	6	2.1
Cs	0.71	0.32	0.06	0.29	1.15	1.14	0.40	0.19	0.51	0.78	0.49	0.70	0.49	0.92	1.3	0.96	0.51	0.93	1.43	1.92	0.25	2.2	0.02	0.84	0.80
Ba	92	83	64	66	282	389	151	140	227	217	175	70	113	141	144	153	113	240	466	495	182	443	8.7	540	219
La	48	85	4.7	7.0	6.7	5.8	8.9	7.0	8.1	8.1	7.6	8.1	18.0	14.4	12.7	12.7	11.8	8.7	4.3	5.1	4.2	4.2	0.64	40.4	2.3

Causes of Cretaceous subduction termination below South China and Borneo:
Was the Proto-South China Sea underlain by an oceanic plateau?

Ce	12.6	20.0	11.2	16.5	15.6	13.6	18.9	15.9	17.8	18.4	17.5	19.2	38.2	31.7	28.1	28.6	26.4	20.3	11.3	10.0	10.4	10.8	1.6	70	6.5
Pr	1.77	2.8	1.60	2.7	2.29	1.94	2.38	2.24	2.28	2.40	2.30	2.70	4.82	4.0	3.57	3.64	3.6	2.72	1.47	1.68	1.56	1.49	0.39	7.2	1.1
Nd	9.5	14.1	8.5	14.3	11.6	9.7	11.1	9.5	10.7	11.2	11.0	12.4	21.9	18.2	16.7	17.2	17.5	13.4	8.2	8.4	8.2	8.5	2.8	26.1	6.1
Sm	3.1	3.9	2.6	4.3	3.4	2.9	2.9	2.9	3.1	2.9	3.2	3.9	5.5	4.8	4.2	4.4	4.6	3.7	2.9	2.7	2.5	2.7	1.1	5.2	2.1
Eu	1.2	1.3	1.1	1.4	1.2	1.1	1.1	0.9	1.0	1.1	1.1	1.1	1.8	1.6	1.5	1.6	1.6	1.3	1.0	1.1	1.0	1.2	0.52	1.5	0.7
Gd	3.9	4.7	3.51	5.50	4.29	4.0	3.80	3.5	3.5	3.6	3.98	4.4	6.1	5.4	4.8	4.9	5.4	4.2	3.9	3.49	3.8	3.5	1.85	4.4	2.9
Tb	0.63	0.81	0.62	0.87	0.73	0.64	0.58	0.58	0.60	0.61	0.62	0.75	0.96	0.85	0.80	0.87	0.86	0.70	0.61	0.61	0.64	0.61	0.34	0.60	0.46
Dy	4.6	5.4	4.1	6.2	5.2	4.6	4.5	3.9	4.0	4.6	4.4	5.1	6.2	5.7	5.4	5.5	5.9	5.0	4.2	4.4	4.6	4.4	2.62	4.1	3.8
Ho	0.96	1.14	0.81	1.22	1.04	0.95	0.89	0.82	0.86	0.93	0.90	1.03	1.26	1.15	1.05	1.14	1.23	1.07	0.9	0.90	0.99	0.95	0.56	0.76	0.81
Er	2.77	3.19	2.43	3.43	3.1	2.68	2.51	2.41	2.46	2.73	2.77	3.1	3.52	3.18	2.98	3.28	3.2	3.2	2.8	2.56	2.69	2.6	1.76	2.1	2.4
Yb	2.7	3.08	2.2	3.36	2.95	2.60	2.75	2.2	2.40	2.6	2.64	2.7	3.4	3.1	2.71	3.18	2.97	3.0	2.4	2.60	2.81	2.7	1.68	1.9	2.9
Lu	0.35	0.43	0.32	0.46	0.44	0.39	0.37	0.34	0.35	0.41	0.38	0.43	0.48	0.44	0.41	0.46	0.44	0.47	0.40	0.37	0.40	0.40	0.26	0.27	0.33
Hf	2.0	2.6	1.8	2.73	2.29	2.13	2.05	1.86	1.83	2.1	2.05	2.6	4.05	3.0	2.92	3.2	3.21	2.9	1.9	1.58	1.82	1.7	0.60	3.0	1.4
Ta	0.77	1.04	0.70	0.96	0.82	0.88	1.27	1.31	1.24	1.33	1.15	1.1	1.82	1.47	1.38	1.43	1.41	1.19	0.80	0.73	0.80	0.72	0.55	1.9	0.48
Pb	0.80	1.01	0.73	1.4	1.44	0.7	0.84	0.56	0.68	1.9	0.39	0.8	1.4	1.14	1.1	1.18	1.11	3.3	0.9	0.67	1.2	0.8	3.6	5.3	4.3
Th	0.40	0.68	0.37	0.77	0.51	0.49	1.03	1.07	1.12	1.14	0.91	0.77	1.76	1.26	1.32	1.33	1.26	0.85	0.31	0.28	0.33	0.35	0.04	8.9	0.24
U	0.18	0.39	0.16	0.35	0.14	0.15	0.49	0.4	0.31	0.6	0.25	1.3	0.5	0.47	0.38	0.6	0.6	0.16	0.5	0.10	0.17	0.2	0.02	1.3	0.17

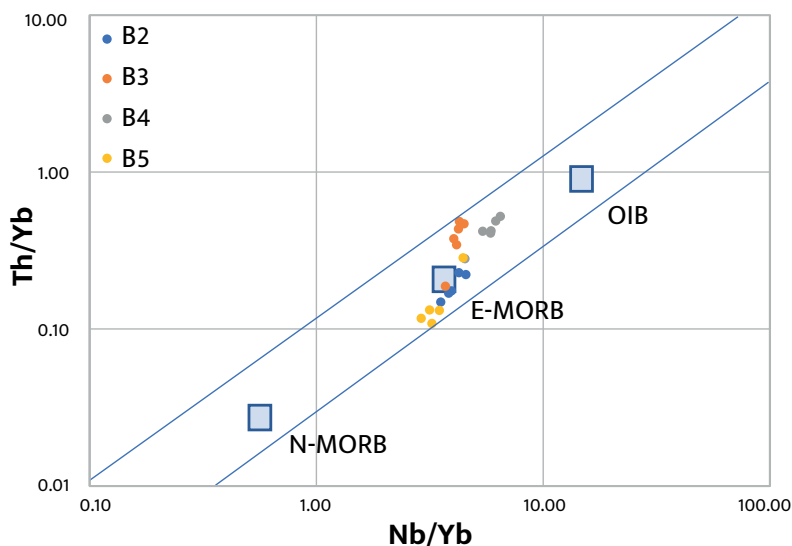


Figure 4. Th/Yb versus Nb/Yb diagram of the Baliojong River pillow basalt samples. Geochemical discrimination based on Pearce (2008).

Samples from the four thrust sheets show distinctive trace element compositions with variable degrees of enrichment seen between the sampled locations. This is shown most clearly on a plot of Th/Yb vs Nb/Yb where variable enrichment is seen around average E-MORB (Figure 4; Pearce, 2008). There is no evidence for fluid-modified melting or melting of more enriched OIB mantle sources in the source of the basalts that we sampled. In summary, the basalts were produced by melting of an enriched MORB source, coupled with minor degrees of fractional crystallization. These data would be consistent with an origin in an oceanic plateau, although a mid-oceanic ridge setting is not excluded.

3.2. Radiolarian cherts: biostratigraphy

3.2.1. Sampling and methods

We collected 29 samples of radiolarian chert and red cherty siltstone from the Baliojong River OPS, nine samples from section BC2, ten samples from section BC3, and ten samples from section BC5, to complement earlier biostratigraphic results for the Baliojong River section of Jasin and Tongkul (2013). All samples were crushed into small fragments (1cm to 2cm), which were subsequently dissolved using dilute hydrofluoric acid 5% and water, with a ratio of acid to water of 1:9 and soaked for about 24 hours (the concentration of acid and the time of treatment varied slightly, depending on the sample) (Pessagno and Newport, 1972). After that all samples were rinsed with fresh water and dried before they were examined under the microscope. Well-preserved specimens were photographed using scanning electron microscopy (SEM) for further examination.

3.2.2. Results and interpretation

The classification, taxonomy and biostratigraphic range of the radiolarian species are based on Sanfilippo and Riedel (1985), Thurow (1988), Vishnevskaya (1993) and O'Dogherty (1994). All samples collected contain radiolarian skeletons that are moderately to well-preserved. The amount of radiolarian skeletons in the red siltstone samples was much lower than in the radiolarian chert samples. We identified a total of 62 radiolarian species and some selected radiolarian species are portrayed in Figure S2.

The biostratigraphic analysis of the radiolarian species, which is described in detail in Supporting Information 1, reveals two assemblages of radiolarian species that are identified in all three sections (Figure 5). Assemblage I ranges in age from Barremian to Aptian (Early Cretaceous (i.e., 126.5-113.2 Ma) and is represented by samples BC2.9 to BC2.5 in Section BC2, samples BC3.10 to BC3.4 in section B3 and samples BC5.10 to BC5.3 in Section BC5. Assemblage II is indicative of Albion to Cenomanian age (Early to Late Cretaceous, i.e. 113.2-93.9 Ma) and is recorded in samples BC2.4 to BC2.1 in section BC2, samples BC3.3 to BC3.1 in section B3 and sample BC5.2 and BC5.1 in section BC5. This confirms previous biostratigraphic results of Jasin and Tongkul (2013) and shows that the E-MORB basalts of the Baliojong River section formed in Early Cretaceous times, and must have formed on an ocean floor that predated this age.

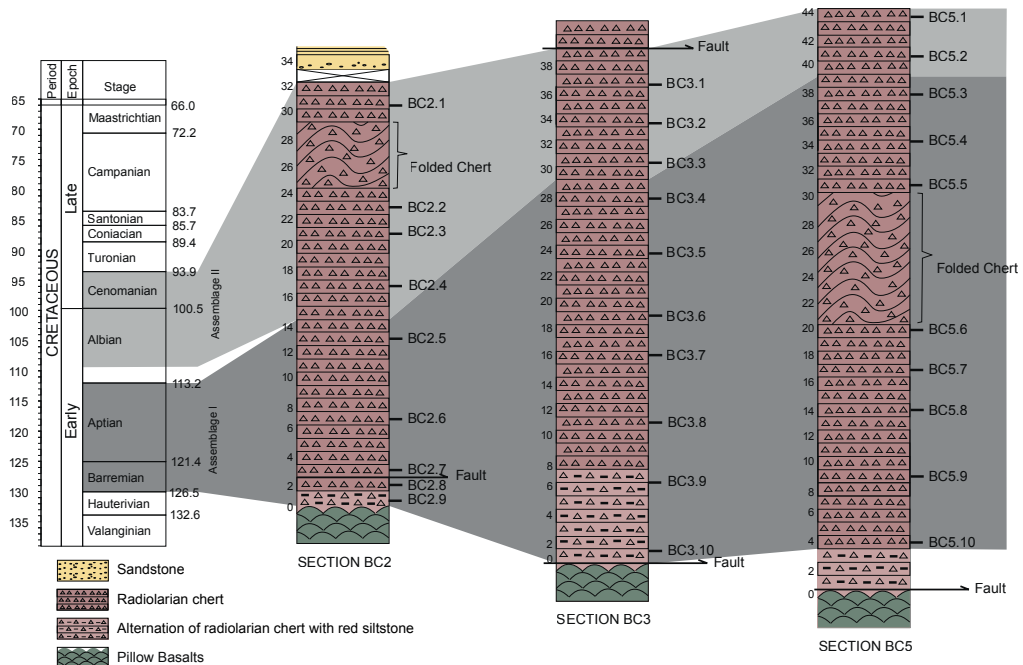


Figure 5. Correlations of radiolarian biostratigraphy in sections BC2, BC3, and BC5. Section length in meters. Time scale based on Gradstein et al. (2020).

3.3. Foreland basin clastics: Detrital zircon geochronology and provenance

3.3.1. Sampling and methods

We collected a total of twelve samples from turbiditic sandstones: seven samples (BF2.1 to BF2.7) from section B2 of and five samples (BF5.1 to BF5.5) from section B5; sections B3 and B4 do not contain sandstone. As shown in representative thin section photomicrographs (Figure S3), samples of section BF2 are quartzose sandstones composed of angular to sub-angular quartz with feldspar, sericite, and chert clast, whereas those of section BF5 are calcite-bearing lithic arenites. These samples were prepared for whole-rock geochemical analysis, heavy mineral analysis and detrital zircon single-grain geochronology using procedures described in Supporting Information 2.

3.3.2. Results

3.3.2.1. Whole-rock geochemistry

The results of major and trace element analyses of the sandstone samples are provided in Table 2. In the ternary diagram of relative proportions of Ca, Al, and Si (Figure 6A), samples of section BF2 plot near the Si apex, showing dominance of detrital silicates therein. In contrast, samples of section BF5 are separate from this cluster due to a varying degree of Ca dilution (31.8%–0.8%), which correlates with authigenic components therein. This compositional difference is also observed in the Upper Continental Crust (UCC; Rudnick and Gao, 2003)-normalized elemental distributions (Figure 6B). Samples of section BF2 display slight enrichment of Mn, Zr, and Hf and strong depletion of Ca and Na, whereas strong enrichment of Ca and Mn and slight depletion of Zr and Hf in samples of section BF5 confirm the dilution by authigenic components. In addition, samples of the two sections show a varying degree of depletion of large-ion lithophile elements (e.g., K, Rb, Sr, Cs, and Ba) and high field-strength elements (e.g., Nb, Th, and U). In the distribution of chondrite-normalized (Sun and McDonough, 1989) rare earth elements (REE), samples of the two sections are comparable in showing moderate light-REE enrichment and negative Eu anomalies, with average $\Sigma\text{LREE}/\Sigma\text{HREE}$ and $\delta\text{Eu} ((\text{Eu}/\sqrt{(\text{Sm} \cdot \text{Gd}))})/\text{N}$ values of 6.1 and 0.7, respectively (Figure 6C). The REE concentrations of section BF5 (average 131.3 ppm), because of relatively enriched middle and heavy-REEs, are systematically higher than those of section BF2 (average 88.7 ppm), which could be caused by the preferential adsorption of REEs in more fined-grained sediments of section BF5. Among all samples, sample BF5.1 features the largest REE concentration (240.2 ppm) and strong light-REE enrichment

Figure 6 ►. Geochemistry of sandstone samples. A) Ternary diagram showing the relative concentrations of Ca, Al, and Si of Baliojong sandstone samples. The sum of three components is normalized to 100 (wt.%); B-C) Major and trace element and REE spider diagrams, normalized to Upper Continental Crust (UCC; Rudnick and Gao, 2003) and Chondrite (Sun and McDonough, 1989), respectively. D-G) Element-based provenance discrimination diagrams of Baliojong sandstone samples. (D) Hf versus La/Th plot (Floyd and Leveridge, 1987). (E) Zr/Sc versus Th/Sc plot (McLennan et al., 1993). (F) Discriminant function diagram of major elements (Roser and Korsch, 1988). (G) Y/Ni versus Cr/V plot (McLennan et al., 1993).

Causes of Cretaceous subduction termination below South China and Borneo: Was the Proto-South China Sea underlain by an oceanic plateau?

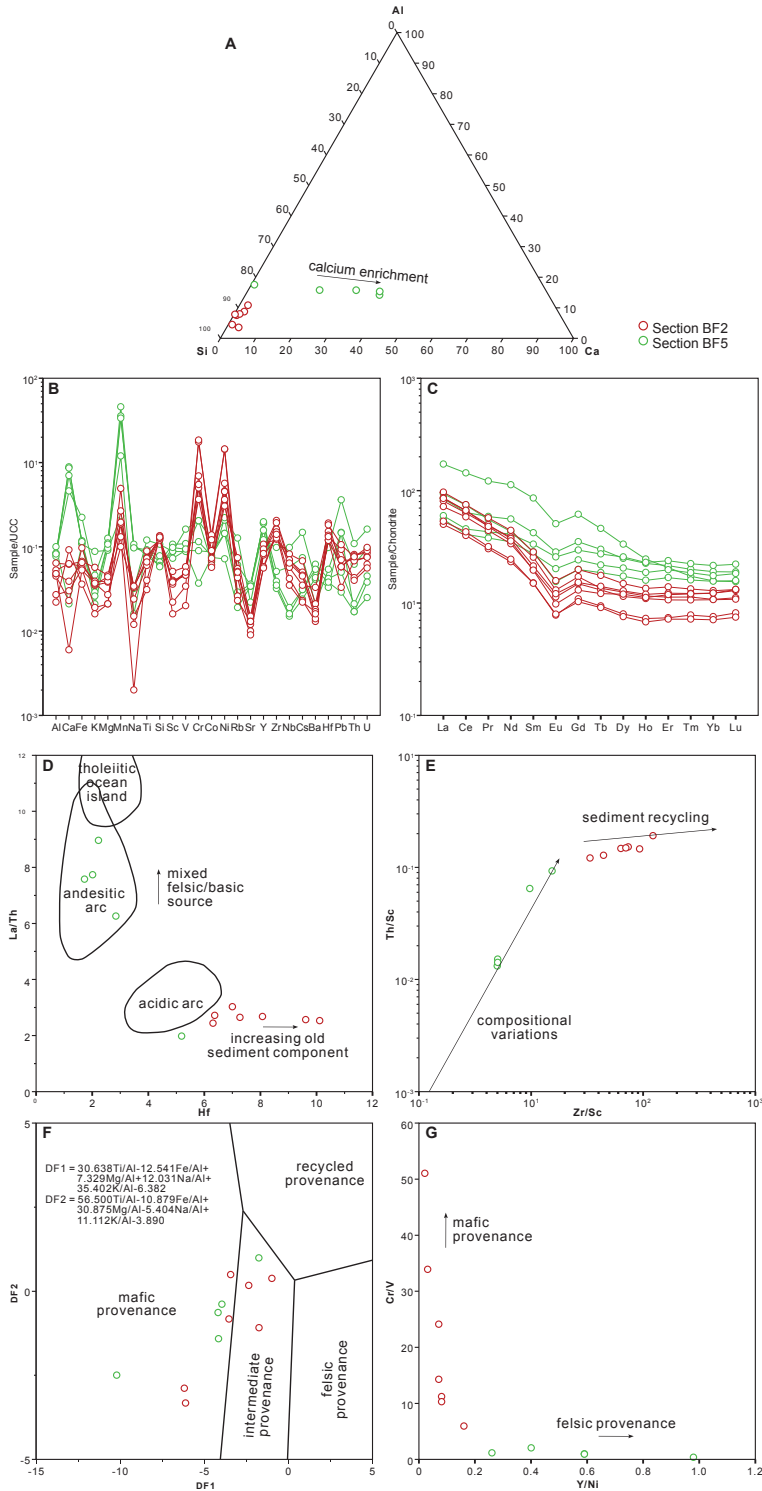


Table 2. Major and trace element compositions of Baliojong River sandstone samples

wt%	BF2.1	BF2.2	BF2.3	BF2.4	BF2.5	BF2.6	BF2.7	BF5.1	BF5.2	BF5.3	BF5.4	BF5.5
SiO2	81.10	75.94	79.69	88.01	81.01	85.57	84.16	44.40	68.18	35.35	31.05	29.67
TiO2	0.37	0.54	0.45	0.25	0.45	0.19	0.41	0.49	0.73	0.47	0.39	0.42
Al2O3	6.68	9.44	7.82	4.14	7.11	3.26	7.14	10.92	14.64	10.35	9.16	9.62
TFe2O3	4.73	3.22	2.84	2.72	3.18	1.72	2.62	9.59	5.20	4.75	4.27	4.43
MnO	0.26	0.18	0.13	0.18	0.19	0.47	0.10	1.02	0.22	2.85	2.60	3.49
MgO	0.91	1.09	0.92	0.51	1.06	0.51	0.66	2.65	2.15	2.20	1.85	2.03
CaO	0.78	2.13	2.16	1.07	1.36	3.15	0.21	14.04	0.73	20.15	24.65	23.54
Na2O	0.77	1.05	0.07	0.38	1.04	0.47	1.10	0.44	1.00	2.56	2.70	2.43
K2O	0.96	1.53	1.05	0.53	0.97	0.44	1.00	1.09	2.34	0.65	0.45	0.55
P2O5	0.07	0.08	0.08	0.04	0.06	0.03	0.06	0.50	0.08	0.82	0.31	0.25
Total	96.63	95.20	95.21	97.83	96.43	95.81	97.46	85.14	95.27	80.15	77.43	76.43
LOI	2.91	4.43	4.70	1.59	3.04	3.45	2.05	14.45	4.25	19.36	21.80	23.53
ppm												
Li	31.63	34.03	30.62	15.37	25.36	14.48	27.90	57.56	50.41	26.40	21.83	21.34
Be	0.69	1.31	0.87	0.51	0.87	0.50	0.89	1.29	1.71	0.81	0.61	0.62
Sc	4.97	7.08	5.57	3.12	5.41	2.22	5.35	10.28	12.36	15.02	12.26	13.76
V	47.36	56.48	44.49	33.26	44.52	19.03	48.96	87.96	156.99	105.65	85.72	91.39
Cr	1605.91	336.16	498.66	1696.31	636.57	458.78	503.95	82.36	186.99	105.70	33.79	188.08
Co	23.83	12.01	10.48	20.99	12.68	9.78	15.59	15.05	21.29	13.53	12.96	11.37
Ni	672.82	143.00	215.13	678.91	266.17	170.58	212.30	67.90	97.52	67.59	33.67	103.83
Cu	63.08	28.84	26.21	87.14	39.41	28.31	41.65	79.20	98.40	76.55	75.67	48.86
Zn	47.70	54.91	44.03	28.77	36.84	23.70	42.74	124.79	91.65	58.19	50.03	53.95
Ga	7.68	11.15	8.63	4.84	8.48	4.10	8.25	13.05	17.31	11.31	9.63	10.93
Rb	35.71	61.83	46.14	22.21	42.64	19.16	41.81	51.65	106.41	24.46	16.32	21.46
Sr	30.46	46.19	39.87	27.77	48.59	40.57	41.30	112.35	71.67	115.95	107.54	108.18

Causes of Cretaceous subduction termination below South China and Borneo:
Was the Proto-South China Sea underlain by an oceanic plateau?

Y	18.14	22.48	16.81	12.10	19.83	11.79	17.46	40.02	25.36	39.90	33.04	41.63
Zr	312.92	236.57	245.56	288.62	396.18	270.70	372.87	98.91	189.16	74.67	60.88	67.86
Nb	6.88	9.85	8.31	5.03	8.35	4.16	7.68	6.90	11.78	2.28	1.76	1.92
Sn	1.98	1.83	1.55	1.66	1.67	1.00	1.63	1.47	2.42	0.89	0.63	0.75
Cs	1.72	3.34	2.47	1.13	2.25	1.10	2.19	3.61	7.24	1.52	1.17	1.50
Ba	206.06	134.12	112.37	79.56	85.53	103.14	101.37	130.02	253.20	384.80	270.48	336.21
La	19.19	22.95	17.08	11.85	20.46	12.65	20.16	40.75	22.24	20.14	13.19	14.17
Ce	38.74	45.84	35.70	24.37	40.58	26.28	40.87	87.98	45.52	39.19	25.07	27.94
Pr	4.60	5.43	4.19	2.89	4.72	3.01	4.55	11.56	5.26	5.60	3.60	4.09
Nd	18.06	20.65	15.71	10.87	17.49	11.44	16.65	52.68	20.23	26.08	16.41	19.18
Sm	3.90	4.35	3.04	2.31	3.26	2.29	3.00	13.14	4.36	6.45	4.20	5.11
Eu	0.76	0.92	0.65	0.45	0.70	0.46	0.57	2.94	0.90	1.65	1.17	1.49
Gd	3.52	4.08	3.05	2.23	3.14	2.11	2.67	12.64	4.09	7.21	4.97	6.08
Tb	0.51	0.66	0.49	0.35	0.53	0.34	0.45	1.72	0.70	1.12	0.81	1.02
Dy	3.17	3.78	2.90	2.03	3.25	1.91	3.04	8.48	4.40	6.33	5.20	6.54
Ho	0.65	0.76	0.62	0.41	0.68	0.38	0.63	1.39	0.90	1.27	1.06	1.30
Er	1.87	2.30	1.76	1.22	2.02	1.19	1.96	3.43	2.78	3.56	3.27	3.94
Tm	0.29	0.34	0.27	0.20	0.31	0.18	0.31	0.44	0.41	0.51	0.48	0.57
Yb	1.83	2.19	1.82	1.28	2.08	1.20	2.08	2.68	2.66	3.24	2.98	3.66
Lu	0.28	0.33	0.27	0.21	0.33	0.19	0.33	0.39	0.40	0.48	0.46	0.56
Hf	8.08	6.38	6.32	7.28	10.12	7.01	9.62	2.86	5.20	2.24	1.74	2.03
Ta	0.55	0.74	0.64	0.36	0.65	0.34	0.61	0.51	0.91	0.18	0.12	0.14
Tl	0.34	0.56	0.31	0.16	0.28	0.17	0.60	0.31	1.06	0.18	0.16	0.18
Pb	11.88	9.94	5.60	9.92	9.88	15.89	18.06	25.21	61.15	8.46	24.78	4.90
Th	7.24	8.53	7.10	4.52	8.17	4.21	7.93	6.53	11.43	2.25	1.74	1.84
U	2.04	2.26	2.03	1.68	2.42	1.51	2.65	2.56	4.36	1.20	1.02	0.67

relative to heavy-REE with a (La/Lu)_N ratio of 11.1.

Geochemical data are also plotted in different diagrams for compositional discrimination (Figure 6D-G). The Hf-La/Th and Zr/Sc-Th/Sc plots show increasing old components and corresponding sediment recycling for samples of section BF2 (Figure 6D-6E), which is consistent with their slight Hf and Zr enrichment observed in the UCC-normalized curves (Figure 6B). In contrast, most samples of section BF5 have a geochemical affinity of an andesitic arc source with limited influence of sediment recycling. Samples between sections BF2 and BF5 are further discriminated by ferromagnesian elements with the former and the latter plotting towards more mafic and felsic source endmembers, respectively (Figure 6F-G). Likewise, Cr and Ni in samples of section BF2, compared to UCC, are highly enriched by a factor of up to 17.5 and 14.3, respectively (Figure 6B). The major element-based discriminant function diagram (Roser and Korsch, 1988) does not perform well in provenance discrimination and samples show a scattered distribution between the fields of mafic and intermediate sources (Figure 6F).

3.3.2.2. Heavy minerals

Samples of sections BF2 and BF5 show great difference in heavy mineral compositions (Figure 7, Table 3). The mineral assemblages in section BF2 are consistent, with dominant zircon (average 50.6%) and pyrite (average 23.3%) as well as a minor percentage of rutile, Cr-spinel, and leucoxene. Sample BF2.7 also contains abundant hematite-limonite. In contrast, the mineral compositions significantly vary in section BF5. While the mineral assemblage of sample BF5.2 is comparable to that of section BF2, sample BF5.1 and samples BF5.4 and BF5.5 are dominated by ilmenite (87.8%) and pyrite (average 80.1%), respectively. Compared to the zircon-tourmaline-rutile (ZTR; Hubert, 1962) index of 65.6–36.8 in section BF2, the commonly lower values in section BF5 (average 18.2) indicate lower compositional maturity due to the lack of detrital components therein.

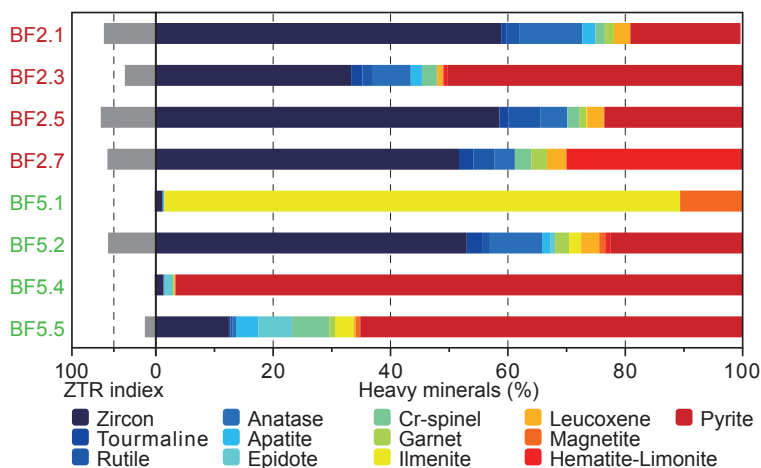


Figure 7. Relative abundance of heavy minerals and zircon-tourmaline-rutile (ZTR; Hubert, 1962).

Table 3. Relative abundance of heavy minerals and zircon-tourmaline-rutile

Sample	Zircon	Tourmaline	Rutile	Anatase	Apatite	Epidote	Cr-spinel	Garnet	Ilmenite	Leucoxene	Magnetite	Hematite-Limonite	Pyrite
BF2.1	58.86	0.94	2.11	10.77	2.24	0.00	1.59	1.54	0.00	2.75	0.04	0.09	18.70
BF2.3	33.29	1.91	1.64	6.61	1.90	0.01	2.54	0.04	0.00	0.93	0.17	0.72	50.24
BF2.5	58.55	1.57	5.47	4.49	0.10	0.00	2.04	1.10	0.18	2.80	0.09	0.10	23.50
BF2.7	51.67	2.43	3.57	3.52	0.00	0.00	2.82	2.63	0.00	3.31	0.03	29.42	0.59
BF5.1	1.16	0.03	0.08	0.06	0.08	0.00	0.00	0.10	87.79	0.05	10.61	0.00	0.04
BF5.2	52.99	2.74	1.20	8.89	1.37	0.85	0.00	2.39	2.05	3.08	1.03	0.85	22.56
BF5.4	1.29	0.05	0.10	0.07	0.07	1.19	0.18	0.13	0.03	0.10	0.20	0.02	96.58
BF5.5	12.46	0.28	0.28	0.65	3.81	5.76	6.32	0.98	3.16	0.37	0.70	0.14	65.09

3.3.2.3. Detrital zircon geochronology, geochemistry, and morphology

A total of 640 zircon grains from sections BF2 and BF5 were analyzed in this study. The results of zircon single-grain analyses of sandstone samples, including U-Pb geochronology, geochemistry, grain size and shape, are provided in Table S2. Detrital zircon age signals within each section show a varying degree of inter-sample variation (Figure 8). In section BF2, samples BF2.3 and BF2.5 consistently show strong age peaks at ca. 115 Ma and 240–235 Ma, a subordinate peak at ca. 450–430 Ma, as well as a scattered distribution of Proterozoic ages. The age signals of samples BF2.1 and BF2.7 are slightly different from the above pattern, with a larger percentage of Cretaceous ages and fewer Proterozoic ages in the former and an implicit peak of Caledonian (i.e., mid-Paleozoic) ages in the latter. Greater inter-sample variety of age signals is observed in section BF5. Samples BF5.2 and BF5.5 feature a near unimodal signal with dominance of Jurassic–Cretaceous ages and a scattered distribution of more ancient ages. The Jurassic cluster peaking at ca. 150 Ma is also seen in sample BF5.4, albeit with subordinate peaks at ca. 225 Ma, 435 Ma, and 1840 Ma. In contrast, sample BF5.1 features an Early Cretaceous cluster peaking at ca. 120 Ma and a weak Caledonian peak. Samples within each section are grouped to characterize their overall age signals. Along with the common occurrence of the Caledonian cluster and scattered Proterozoic ages, sections BF2 and BF5 are clearly discriminated by a moderate lull and a strong peak of Jurassic ages, respectively.

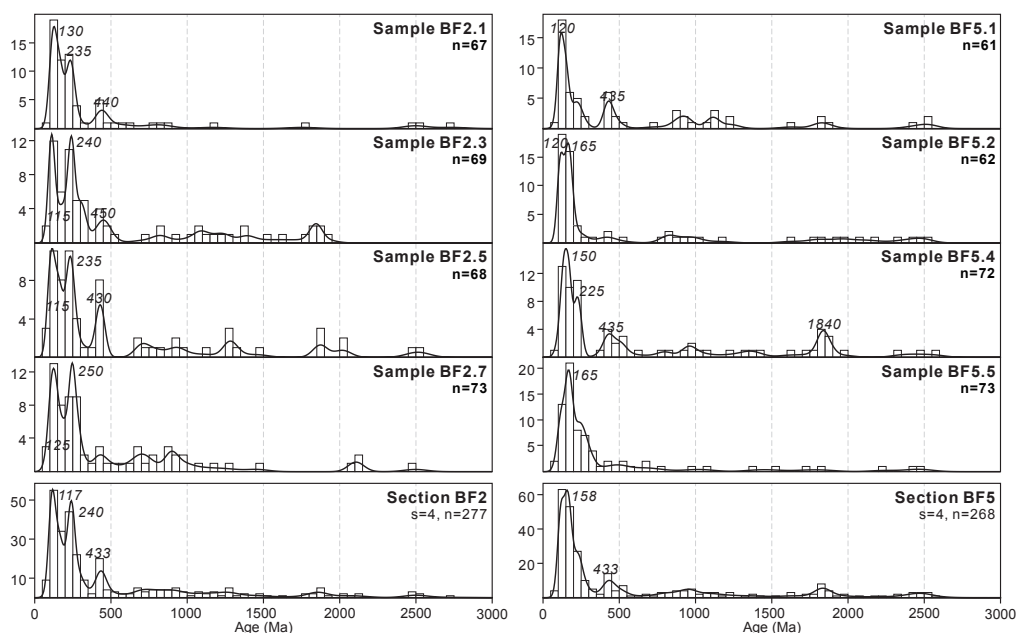


Figure 8. Histograms and kernel density estimation (KDE) spectra for detrital zircon U-Pb ages of Baliojong sandstone samples from sections BF2 and BF5. s—number of samples; n—number of concordant analyses.

3.3.3. Interpretation

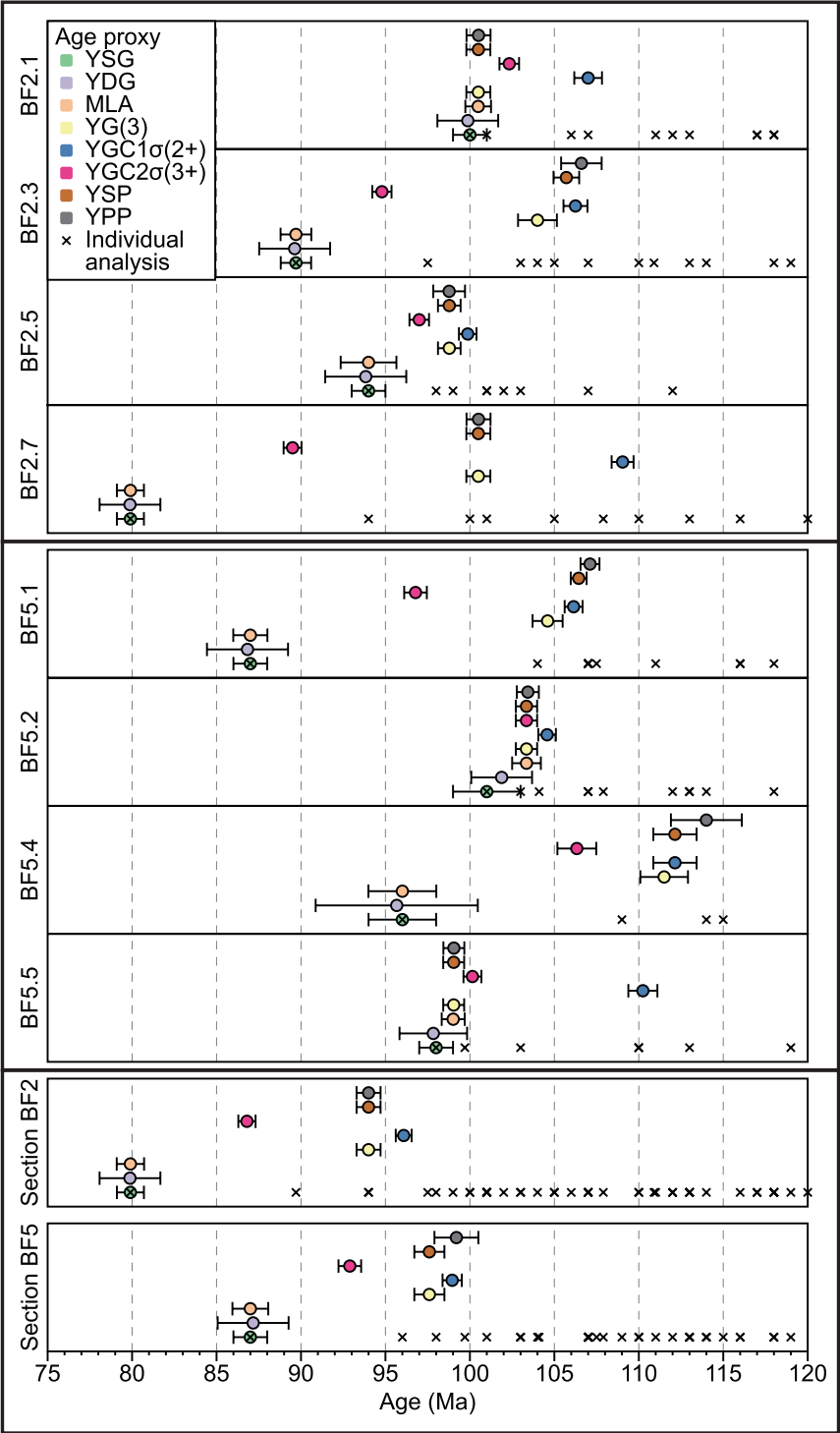
The radiolarian biostratigraphic ages of the Baliojong OPS reveal that the foreland basin clastics are younger than Albian–Cenomanian (Jasin and Tongkul, 2013; see section 3.2). We use the U-Pb detrital zircon ages to establish the maximum depositional age of the foreland basin clastics (Dickinson and Gehrels, 2009), which in accretionary orogens adjacent to active arcs are typically close to the depositional age (Cawood et al., 2012).

We calculate maximum depositional ages using eight proxies: (i) the youngest single grain age (YSG); (ii) the ‘youngest detrital zircon’ age calculated by Isoplot (YDG; Ludwig, 2003); (iii) the maximum likelihood age calculated by IsoplotR (MLA; Vermeesch, 2021); (iv) the weighted mean age of three youngest grains (YG(3); Zhang et al., 2015); (v) the weighted mean age of the youngest cluster with two or more grains overlapping in age at 1σ (YGC1 σ (2+); Dickinson and Gehrels, 2009); (vi) the weighted mean age of the youngest cluster with three or more grains overlapping in age at 2σ (YGC2 σ (3+); Dickinson and Gehrels, 2009); (vii) the weighted mean age of the youngest cluster with a mean square weighted deviation (MSWD) of ~ 1 (YSP; Coutts et al., 2019); (viii) the youngest graphic peak age of the kernel density estimation (KDE) spectrum (YPP).

Among 640 zircon grains analyzed in this study, two concordant grains (BF2.5-45 and BF5.5-45) are dated with Eocene ages (36.6 Ma and 41.6 Ma) with one containing a very high U concentration of 3056.3 ppm (Table S2). The rare existence of these abnormally young ages contrasts with the ages of the unconformably overlying Crocker Formation and cannot represent the sedimentary age of the foreland basin clastics (Hall and Breitfeld, 2017; Jasin and Tongkul, 2013). Moreover, the Crocker formation has a distinctly different mineralogical and geochronological signal including dominance of zircon and tourmaline and the absence of Neoproterozoic and Caledonian zircons (van Hattum et al., 2013) (Figure S4). We infer that these Eocene grains may potentially be influenced by Pb loss, and we excluded them in the calculation of maximum depositional ages.

Different proxies of maximum depositional ages of sandstone samples range from 109.0 Ma to 79.9 Ma in section BF2 and from 114.0 Ma to 86.3 Ma in section BF5, but they do not explicitly show a younging or aging trend within each section (Figure 9). Age proxies roughly cluster in samples BF2.1, BF5.2, and BF5.5 and the age estimates through the YSG, YDG, and MLA approaches are younger than the other proxies.

Following the data treatment strategy of Rinke-Hardekopf et al. (2021), regardless of the choice of age proxies, the calculated maximum depositional ages mostly belong to the Late Cretaceous and individual age proxies of section BF2 are about 6 Ma younger than those of section BF5. The interpretation of different depositional ages between the two sections is consistent with their different signatures of whole-rock geochemistry, heavy minerals, and zircon U-Pb ages (Figures 6, 7, 8). Considering the potential Pb loss effect for youngest single grains and the conservative nature of age proxies based on multiple grains, we select the YGC2 σ (3+) proxy to represent the maximum depositional age, which is 86.8 Ma in section BF2 and 92.9 Ma in section BF5 (Figure 9). Thus, Baliojong turbidites were



◀ **Figure 9.** Maximum depositional ages of Baliojong sandstone samples and grouped samples of sections BF2 and BF5, represented by a range of age proxies of detrital zircon U-Pb geochronology. Age proxies are calculated and visualized at 1σ and individual analyses of ≤ 120 Ma are also shown for comparison. YSG—the youngest single grain age; YDG—the age calculated by the ‘Youngest Detrital Zircon’ routine of Isoplot (Ludwig, 2003); MLA—the age calculated by ‘Maximum Likelihood Age’ algorithm of IsoplotR (Vermeesch, 2021); YG(3)—the weighted mean age of three youngest grains (Zhang et al., 2015); YGC1 σ (2+)—the weighted mean age of youngest cluster with two or more grains overlapping in age at 1σ (Dickinson and Gehrels, 2009); YGC2 σ (3+)—the weighted mean age of youngest cluster with three or more grains overlapping in age at 2σ (Dickinson and Gehrels, 2009); YSP—the weighted mean age of youngest cluster with a mean square weighted deviation (MSWD) of ~ 1 (Coutts et al., 2019); YPP—the youngest graphic peak age of kernel density estimation (KDE) spectrum.

likely deposited around the Turonian–Coniacian, which is reasonably younger than the underlying Albian–Cenomanian cherts and Early Cretaceous basalts (Jasin and Tongkul, 2013; Wang et al., 2023).

3.4. Paleomagnetism of basalts and pelagic sediments

3.4.1. Sampling and methods

We collected core samples with a standard diameter of 25 mm for paleomagnetism using a petrol-powered drill from pillow basalts and cherts. A total of 147 pillow basalt samples (coded PB) was collected from sections B2, B3, and B4, and 48 samples were collected from red siltstones (coded PC) intercalated in the basal parts of the chert sequence in sections B2, B3, and B5 (Figure 2 and 3C). The pillow basalt section of section B5 was of insufficient stratigraphic thickness to collect enough samples that would accurately sample paleosecular variation, while section B4 did not contain the rhythmic alternation of red siltstone and radiolarian chert. The orientation of the samples was measured in the field with a magnetic compass and inclinometer attached. Following sampling procedures for paleomagnetic poles recommended in Gerritsen et al. (2022), we collected a single core per basalt pillow or siltstone bed to optimize the chance of sampling individual spot readings of the paleomagnetic field with each core. The pillow basalt sections were generally sufficiently thick to collect about 50 samples over at least 100m of stratigraphy. Ten to twenty red siltstone samples were collected per section, from exposures of a few meters in thickness. Estimated bedding attitudes of pillow basalts are generally striking roughly N-S with a $\sim 45^\circ$ overturned dip. Our bedding estimates of the pillow basalts were similar to those measured in the directly overlying radiolarian cherts, although our estimation was somewhat steeper. As the bedding attitude of pillow basalts is difficult to measure, and as pillows may have a small primary dip, we will discuss how the use of the bedding attitudes of the radiolarian chert alters our results.

Paleomagnetic analyses were carried out at the paleomagnetic laboratory Fort Hoofddijk at Utrecht University, the Netherlands. The pillow basalt samples were subjected to stepwise alternating field (AF) demagnetization in a robotized setup (Mullender et al., 2016) and

the red siltstone samples were subjected to stepwise thermal (TH) demagnetization. The magnetization of all samples was measured on a 2G DC-SQUID magnetometer. During this process, the samples were kept in a magnetically shielded room.

We used the online portal Paleomagnetism.org (Koymans et al., 2016, 2020) for sample interpretation and statistical analysis. Demagnetization diagrams were plotted as orthogonal vector diagrams (Zijderveld, 1967) and magnetic components were determined using principal component analysis (Kirschvink, 1980). Components decaying towards the origin are not forced to the origin, except when demagnetization diagrams are noisy. We did not apply a maximum angular deviation cutoff, as it does not demonstrably influence the precision or position of a pole (Gerritsen et al., 2022), but the widely used cutoff of 15° would not have eliminated data. Site mean directions were calculated using Fisher (1953) statistics on virtual geomagnetic poles following statistical procedures described in Deenen et al. (2011). To support the paleomagnetic results, thermomagnetic analysis was carried out with a modified horizontal translation Curie balance (Mullender et al., 1993) on selected samples to shed light on the dominant magnetic minerals. In the thermomagnetic analysis samples were stepwise heated to 700 °C in air with intermittent cooling segments to distinguish thermochemical alteration from magnetic behavior. The Curie temperature is estimated with the two-tangent method (Grommé et al., 1969). The temperature sequence is as follows for the pillow basalts (in a cycling field between 200 and 300 mT): room temperature – 150 °C – 70 °C – 250 °C – 150 °C – 350 °C – 250 °C – 450 °C – 350 °C – 520 °C – 420 °C – 620 °C – 500 °C – 700 °C – room temperature. For the red silts it is (in a cycling field between 50 and 300 mT): room temperature – 250 °C – 150 °C – 350 °C – 250 °C – 450 °C – 350 °C – 520 °C – 420 °C – 620 °C – 500 °C – 700 °C – room temperature. To check for hematite behavior in a non-saturated applied field a second sample was stirred in the Curie balance sample holder after the 250 °C – room temperature partial run after which the complete stepwise thermomagnetic run was done (cf. De Boer and Dekkers, 1998).

3.4.2. Results and interpretation

In the thermomagnetic analysis, pillow basalts showed a gradual magnetization decay with minor removal of magnetic moment during the experiment, typical of maghemite that partly converts to less magnetic hematite (Figure 10A). The Curie temperature is estimated at ~610 °C. Sample PB2.11 has this behavior to a greater extent than sample PB3.18 which reveals more or less reversible magnetic behavior. This indicates that the maghemite (presumably thermally stabilized by some substituted Ti or Al) is probably formed in nature (i.e., not during the experiment itself). During the final cooling from 700 °C most maghemite converts to hematite as testified by the much lower final magnetization.

As expected, the red silts are much weaker (~10 to ~100 times) than the pillow basalts. The thermomagnetic behavior is dominated by hematite as indicated by the Néel temperature at 675 °C (Figure 10B). Because high-coercivity hematite is not magnetically saturated in a field of 300 mT, the cooling segments are above the corresponding heating segments (Figure

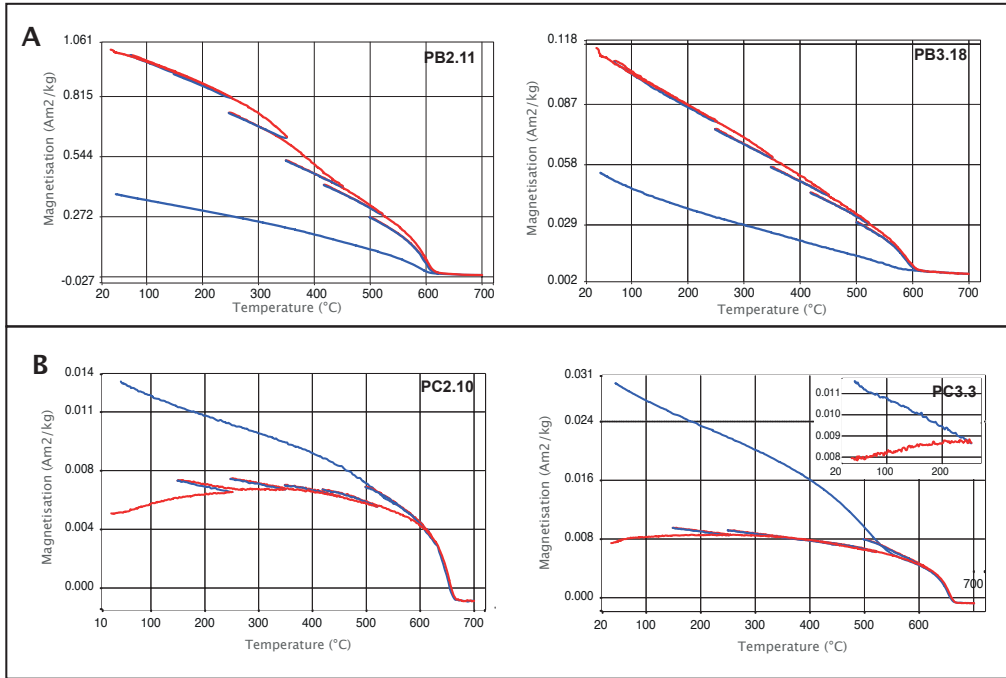


Figure 10. Thermomagnetic curves measured on a modified horizontal translation Curie balance (Mullender et al., 1993). Heating segments in red, cooling in blue. Inset in PC3.3 shows the first heating cycle to 250°C as part of the stirring experiment (see main text).

10B). This is an expression of acquisition of a magnetic moment and not of thermochemical alteration, as demonstrated by the stirring experiment in sample PC3.3. After the partial run to 250 °C, stirring of the sample when back at room temperature, the second run (again to 250 °C and then according to the full thermomagnetic experiment procedure) starts at approximately the same magnetic moment as at the beginning of the first run and not at the final magnetic moment of the first run. This indicates that the increase has a magnetic cause and is not induced by thermochemical alteration (De Boer and Dekkers, 1998). Rather surprisingly, magnetite – the carrier of the NRM signal – is below the limit of detection albeit that magnetite is formed during heating between 600 and 700 °C as manifested by marked increase in magnetic moment during cooling below 550 °C on the final cooling run. Sample PC3.3 shows this behavior to a larger extent than sample PC2.10 (Figure 10B).

The NRM of the red silt samples shows a fairly large secondary component up to ~200 °C (Figure 10B). We speculate that this may be associated with the relatively large increase during the cooling segments in the thermomagnetic experiments after 250 and 350 °C, while the increase after cooling at higher temperatures up to 520 °C is barely noticeable (Figure 10B). It would indicate a big proportion of very fine-grained hematite with low unblocking temperatures.

Samples from pillow basalts had initial NRM intensities ranging from 0.2 to 1.0 A/m,

whereas the red silts had much lower intensities ranging from 200 to 2000 $\mu\text{A}/\text{m}$. Alternating field (AF) demagnetization in the pillow basalt (PB) samples generally shows a low coercivity component, followed by linear demagnetization trends towards the origin on the Zijderveld diagram (Figure 11A). Maximum unblocking fields for the basalts mostly occur around 100 mT. In addition, at fields of 40-50 mT, a small component appears that deviates the trend away from the origin, which is interpreted as a laboratory-induced gyroremanent magnetization (GRM) (Dankers and Zijderveld, 1981). The datapoints influenced by GRM were not used to interpret the ChRM. ChRM directions were interpreted based on a minimum of four consecutive data points.

The Zijderveld diagrams of the cherty siltstone samples (PC) are noisier than those of the basalts, but it is in most cases possible to discern a low-temperature component that is distinct from a high-temperature component that decays towards the origin (Figure 12A). In the case of the pillow basalts, the high-coercivity component has northeasterly declinations (Figure 11B), while in the case of the cherty siltstones, the high-temperature component has southerly declinations (Figure 12B). We interpret these high-coercivity (PB sample set) or high-temperature (PC sample set) components as the Characteristic Remanent Magnetization (ChRM) directions. The ChRM directions of the pillow basalts were generally interpreted in the range of 30-50 mT. In some cases, the ChRM direction was already isolated from as low as 15 mT up to as high as 120 mT. ChRM directions of red siltstones were interpreted mostly in the range 250-510°C, but could sometimes be interpreted up to 580°C. It was possible to isolate a ChRM from most PB and PC samples, although a few samples were rejected due to erratic demagnetization behavior or strongly deviant paleomagnetic directions that we interpreted as the result of orientation errors or lightning strikes when a sample was almost completely demagnetized below 20 mT. Including these directions in the grand average would not have significantly shifted the computed paleomagnetic poles.

Mean paleomagnetic ChRM directions for all sites in geographic and tectonic (corrected for bedding tilt) coordinates are listed Table 4 and shown in Figure 11B and 12B. All interpreted pillow basalt (PB) samples indicate the same polarity and the mean ChRM directions of the PB sites are different from the present-day GAD field in both geographic and tectonic coordinates (Figure 11B). There is a slight variation in mean paleomagnetic direction between PB sites. In geographic coordinates, the directions of all three sections are significantly different (no Common True Mean Direction; CTMD; Tauxe et al., 2010) and vary by $\sim 15^\circ$ in declination and inclination. In tectonic coordinates, the different PB sites also do not share a CTMD, but the variation in declination is smaller, up to maximum 8° (Table 4), while the inclination of PB2 is significantly steeper than for PB3 and PB4 ($I = -26.9 \pm 6.9^\circ$ in PB2 versus $I = -4.9 \pm 7.2^\circ$ in PB3 and $8.9 \pm 7.1^\circ$ for PB4). Fold tests per section are inconclusive (Tauxe and Watson, 1994; implemented in Paleomagnetism.org). When PB2 and PB3 are combined, the fold test is negative, but PB2 and PB4, as well as PB3 and PB4 yield an optimal clustering at $\sim 90\%$ unfolding (Figure 11C). When all sites are combined,

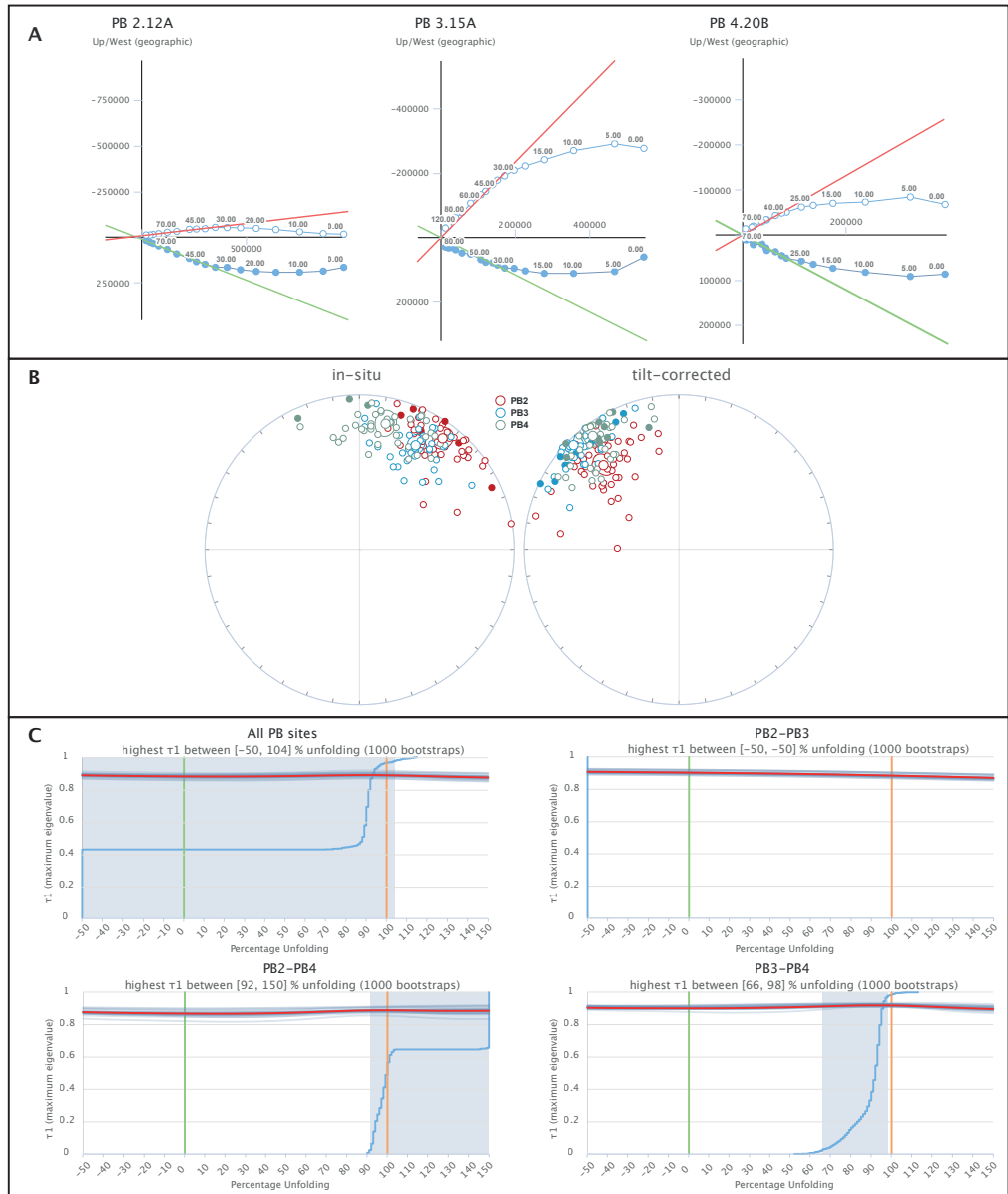


Figure 11. Paleomagnetic results from PB sections; A) Orthogonal vector diagrams of selected samples in geographic coordinates. Closed (open) symbols for declination (inclination). Numbers along axes are intensities in $\mu\text{A/m}$; B) Characteristic remanent magnetization (ChRM) directions, including means, per section in geographic (in-situ) and tectonic (tilt-corrected) coordinates; C) Results of bootstrapped fold tests for different combinations of sections.

the fold test is inconclusive (Figure 11C).

The red siltstone (PC) samples have an opposite polarity to the basalts (Figure 12B). In geographic coordinates, the three sampled sections yield similar direction clusters, with average declinations varying from $D=163.8\pm9.5^\circ$ in PC2 to $173.1\pm7.6^\circ$ in PC3, although the inclinations vary more, from $I=-0.2\pm14.8^\circ$ in PC2 to $I=-29.4\pm15.0^\circ$ in PC5. This overall southeasterly direction cluster differs significantly from the ChRM directions in geographic coordinates from the pillow basalts, that when corrected for the opposite polarity, have a declination difference in geographic coordinates of $\sim 40^\circ$ (Figure 11B and 12B; Table 4). This suggests that the ChRM directions of the red silts and the pillow lavas do not reflect the same paleomagnetic field, even though they are part of the same stratigraphic sequence, have similar bedding orientations, and are unlikely to be of significantly different age, since the red silts occur at the very base of the sedimentary sequence immediately overlying the pillow lavas. In tectonic coordinates, the magnetic directions of the cherts and pillows are also not antipodal (mean inclination of all PB and all PC sites is -14.4° and 5.9° , respectively, Table 4) and there is a rotation difference: mean declination of all PB and all PC sites is 319.0° and 159.2° , respectively. Between sites PC2 and 3 and the basaltic sections, this angle is approximately 20° . Locality PC5 has a bedding strike that is nearly 90° different from the other two PC sections as a result of local folding and thrusting. The mean paleomagnetic direction obtained from PC5 is also very different to those of localities PC2 and PC3 that have a similar bedding orientation: PC2 and PC3 give in tectonic coordinates declinations/inclinations of $164.0\pm6.2^\circ/0.99\pm12.4^\circ$ ($N=20$) and $148.2\pm7.6^\circ/16.5\pm14.2^\circ$ ($N=9$), while PC5 has a declination of $252.4\pm25.87^\circ$ and inclination of $-66.6\pm12.3^\circ$ ($N=12$). The fold test of the red silt sections, in any combination, is either negative or inconclusive (Figure 12C).

The magnetization of the pillow basalts in geographic coordinates is profoundly different from that of the remagnetized red siltstones, showing that they were magnetized at different times. In addition, the A95 values of the different PB localities all satisfy the criterion of Deenen et al. (2011, 2014), which suggests that the scatter that we obtained may be explained by paleosecular variation alone, and that paleosecular variation is adequately represented in our sample set. Moreover, the fold test of the basalt sections of PB2 and PB3 gives optimal clustering at $\sim 90\%$ unfolding. We therefore interpret the magnetization of the pillow basalts as primary. Because pillow lavas do not form strictly horizontal bedding and topography may be somewhat rugged during deposition, we consider this as a positive fold test, whereby we note that this test shows that the uncertainty in the bedding tilt correction, and hence in the estimated inclination and paleolatitude, is larger than for normal sediments.

Based on the negative fold test of the PC samples, we interpret that the magnetic directions obtained from the red siltstone samples represent a remagnetization of these samples that occurred after folding (i.e., after the late Cretaceous accretion of the Baliojong OPS sequences), but before or during a phase of counterclockwise rotation given the declinations preserved in the sequence that differ significantly from the recent field. Paleomagnetic data from Cenozoic successions have revealed that Borneo underwent $\sim 45^\circ$

of counterclockwise rotation between the late Eocene and early Miocene (Advokaat et al., 2018), during which time the Rajang-Crocker accretionary prism formed at the subduction zone that consumed the Proto-South China Sea below the Baliojong section (Hall et al., 2008). It seems plausible that the remagnetization occurred during this time period in a reverse magnetic field, possibly more or less halfway the rotation phase, i.e. sometime in the Oligocene, given the $\sim 15^\circ$ counterclockwise rotated overprint direction. Hence, we will not use the paleomagnetic results of the red siltstone samples for further tectonic interpretations.

We also tested what the effect on the interpreted inclination would be when the bedding attitude of the oldest overlying red beds would be used to estimate the bedding of the pillow basalts. In all sections, the inclination would become a few degrees shallower, suggesting a

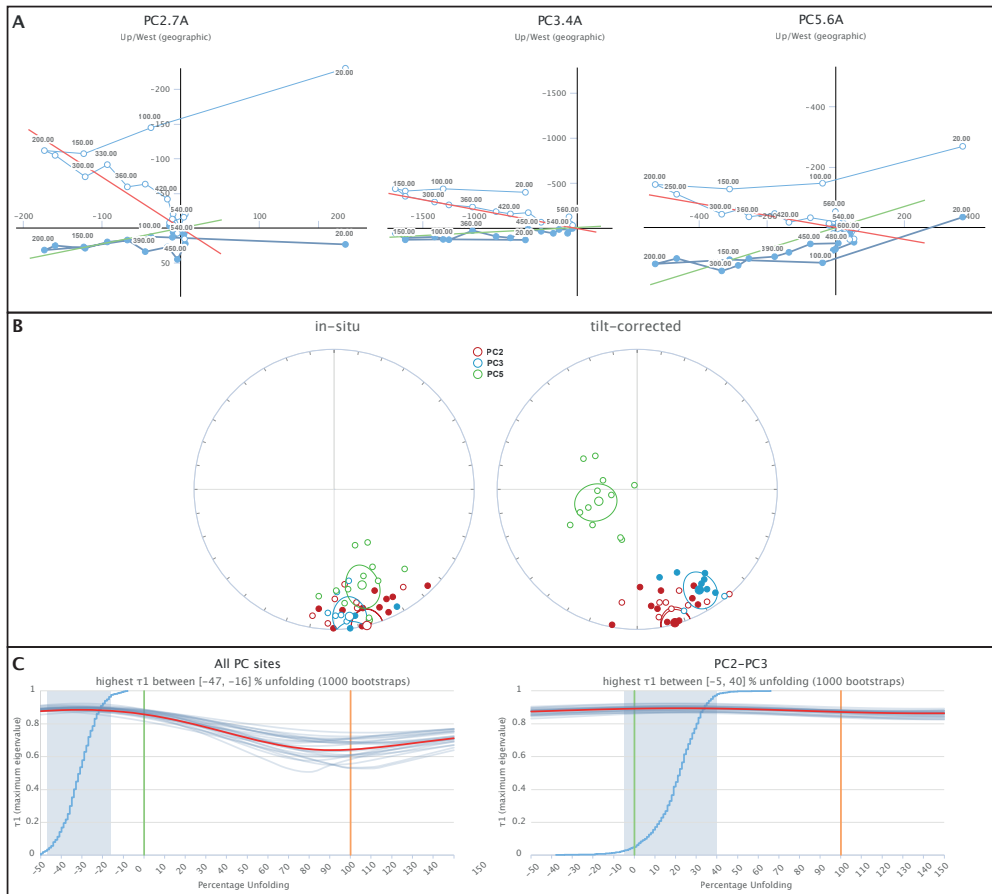


Figure 12. Paleomagnetic results from PC sections; A) Orthogonal vector diagrams of selected samples in geographic coordinates. Closed (open) symbols for declination (inclination). Numbers along axes are intensities in $\mu A/m$; B) Characteristic remanent magnetization (ChRM) directions, including means, per section in geographic (in-situ) and tectonic (tilt-corrected) coordinates; C) Results of bootstrapped fold tests for all PC sites and for PC2 and PC3.

Table 4. Paleomagnetic results

In-situ (geographic) coordinates														
Section	Lat (°N)	Lon (°E)	N	Dec (°)	Inc (°)	k	a95	K	A95	A95 _{Min}	A95 _{Max}	ΔDx (°)	ΔIx (°)	λ (°)
PB2	6.553786	116.888377	48	36.89	-11.09	19.93	4.73	27.91	3.96	2.55	7.16	3.98	7.71	-5.6
PB3	6.550320	116.883665	38	28.25	-24.26	27.72	4.49	35.87	3.93	2.8	8.29	4.03	6.87	-12.7
PB4	6.549018	116.881319	42	11.78	-17.88	19.43	5.13	23.45	4.65	2.69	7.78	4.71	8.64	-9.16
PB all	6.551192	116.884662	128	26.22	-17.54	15.4	3.29	18.98	2.94	1.72	3.86	2.98	5.48	-8.98
PC2	6.554266	116.888754	20	166.4	-0.24	16.07	8.4	25.92	6.54	3.62	12.42	6.54	13.07	-0.12
PC3	6.551292	116.883954	9	173.06	-9.68	23.25	10.9	47.3	7.56	4.98	20.54	7.59	14.81	-4.87
PC5	6.546785	116.874234	12	163.77	-29.37	17.11	10.8	23.56	9.13	4.44	17.14	9.49	14.97	-15.71
PC all	6.551423	116.883450	41	167.23	-10.82	12.72	6.52	22.96	4.76	2.72	7.9	4.78	9.27	-5.46
Tilt-corrected (tectonic) coordinates														
Section	Lat (°N)	Lon (°E)	N	Dec (°)	Inc (°)	k	a95	K	A95	A95 _{Min}	A95 _{Max}	ΔDx (°)	ΔIx (°)	λ (°)
PB2	6.553786	116.888377	48	318.28	-27.68	19.93	4.73	23.23	4.36	2.55	7.16	4.51	7.31	-14.7
PB3	6.550320	116.883665	38	314.92	-4.9	27.72	4.49	42.23	3.62	2.8	8.29	3.62	7.19	-2.45
PB4	6.549018	116.881319	42	322.76	-8.89	22.06	4.8	36.98	3.67	2.69	7.78	3.69	7.22	-4.47
PB all	6.551192	116.884662	128	318.75	-14.7	16.64	3.15	26.42	2.47	1.72	3.86	2.49	4.71	-7.47
PC2	6.554266	116.888754	20	163.98	0.99	16.07	8.4	28.53	6.22	3.62	12.42	6.22	12.43	0.49
PC3	6.551292	116.883954	9	148.17	16.53	23.25	10.9	47.18	7.57	4.98	20.54	7.66	14.23	8.44
PC5	6.546785	116.874234	12	252.43	-66.55	17.11	10.8	7.79	16.62	4.44	17.14	25.87	12.26	-49.05
PC all	6.551423	116.883450	41	168.77	-15.78	3.09	15.38	3.32	14.61	2.72	7.9	14.76	27.6	-8.04

N: number of samples; Dec: Declination; Inc: Inclination; ΔDx/ΔIx: uncertainty in declination/inclination; λ: paleolatitude

somewhat lower latitude. We thus consider the paleolatitudes that we computed using the in situ estimated bedding orientations of the pillows as maximum values.

Based on the interpretation that the pillow basalts carry a primary magnetic signal, we use the results in tectonic coordinates for our tectonic analysis. The declination data of the different sections suggest that they all underwent a similar rotation, of about 40° clockwise for a normal, southern hemisphere magnetization, or 140° counterclockwise for a reverse, northern hemisphere magnetization. The pillow basalts of a thrust slice below section 5 formed during the Early Cretaceous (c. 135 Ma; Wang et al., 2023), around which time the magnetic field underwent multiple polarity reversals, which means that the polarity of the magnetic field during magnetization is unknown. In addition, the Baliojong River section is a largely deformed accretionary prism, where large-scale rotations cannot be excluded. Hence, in our tectonic interpretation, we will discuss both the northern and southern hemisphere alternatives of formation of the pillow basalts. The inclination data suggest that the pillow basalts of section B2 formed at higher latitudes ($14.7 \pm 4.3^\circ$) than the pillow basalts of section B3 and B4 ($2.5 \pm 3.6^\circ$ and $4.5 \pm 3.7^\circ$, respectively), which may indicate that these sequences represent different tectonic nappes that accreted at a different time, whereby B2, with a significantly steeper inclination, may derive from a different nappe that accreted at a later time, because it is structurally deeper.

4. Discussion

Our data above suggest that the Baliojong OPS contains nappes that accreted in at least two events at the north Borneo margin. Based on maximum depositional ages of the foreland basin deposits, these events occurred around 92 and 86 Ma, i.e., shortly before the end of subduction inferred from the cessation of arc magmatism in the South China and Indochina regions, and the consequent trapping of the Proto-South China Sea lithosphere (Moss, 1998; Hall and Breitfeld, 2017; Advokaat and Van Hinsbergen, 2023). Our data show that at that time, an oceanic lithosphere with E-MORB geochemistry was subducting at the north Borneo margin that was then ~45-50 Ma old (and currently 135 Ma; Wang et al., 2023). Finally, we show that the ocean floor formed at a paleolatitude ranging from ~14° to ~2°, although we cannot directly infer from the data whether these formed on the northern or southern hemisphere. Placing the reconstruction of Borneo of Advokaat and Van Hinsbergen (2023) in the paleomagnetic reference frame of Vaes et al. (2023) reveals that the latitude of accretion of the OPS sequences at 92-86 Ma was ~3°N. This shows that the lithosphere that was underlying the Proto-South China Sea underwent a maximum net motion of up to 17° northwards or 11° southwards in the 45-50 Ma interval between its formation and its accretion in the Late Cretaceous. In the reconstruction of Zahirovic et al. (2014), accretion occurred at ~4°S, which would indicate a smaller northward motion of 10° or a larger southward motion of 18°S. As the southward drift scenario does not straightforwardly explain active subduction below the South China margin, we consider the northward drift scenario more likely. We first use this information, combined with

constraints from the accretionary prisms of the South China and Palawan margins to re-evaluate the plate kinematic history of the Proto-South China Sea and its motion relative to the Tethyan or Panthalassa plate systems. Next, we re-evaluate previously proposed causes of subduction cessation.

The lithosphere that was subducting below the SE China and Indochina margins prior to the late Cretaceous subduction cessation is typically loosely assigned to a paleo-Pacific plate of the Panthalassa tectonic realm (e.g., Hall and Breitfeld, 2017; Zheng et al., 2019; Zhang et al., 2019). The simplest plate tectonic interpretation is then to infer that this lithosphere formed part of the Izanagi Plate (e.g., Zahirovic et al., 2014; Zhu et al., 2022), whose conjugate spreading records are preserved on the Pacific Plate (Nakanishi et al., 1992). We use our paleomagnetic data to test this hypothesis. To this end, we reconstructed the Proto-South China Sea oceanic crust as part of the Izanagi Plate from 85 Ma (the inferred end of its subduction), backwards in time to 135 Ma, whereby we connect the Panthalassa plate system to the Indo-Atlantic plate system using the reference frames of Torsvik et al. (2019) for the Panthalassa, and of Van der Meer et al. (2010) for the Indo-Atlantic frame prior to 85 Ma, which was shown to best reconcile paleomagnetic and plate kinematic constraints for the eastern Panthalassa-Caribbean realm by Boschman et al. (2019). We then place this connected plate system into the paleomagnetic reference frame of Vaes et al. (2023) to predict the paleolatitude of the Proto-South China Sea for a coordinate coinciding with our sampling locations, using the reconstruction of the Izanagi Plate of Boschman et al. (2021b). This results in a predicted paleolatitude that is much farther south ($\sim 30^\circ\text{S}$) than what is obtained from paleomagnetism in this study (Figure 13). In other words, our data show that the oceanic crust that eventually floored the Proto-South China Sea embayment cannot have been part of the Izanagi Plate but must have been part of a plate with a slower northward motion component than the Izanagi Plate (Figure 13). Although the paleolongitudinal motion of this plate is unknown, we may infer that it also has a westward motion component relative to Eurasia to satisfy the observation that there was subduction between South China, Indochina, as well as Borneo, whereby Borneo converged with South China (Advokaat and Van Hinsbergen, 2023).

Because the Izanagi Plate was moving northwestward at a higher rate than the Proto-South China Sea lithosphere, a subduction zone must have existed between these two plates, whereby Izanagi must have been in a downgoing plate position. A magmatic arc may thus have formed on the eastern boundary of the Proto-South China Sea lithosphere. We infer that the island arc volcanics of c. 100 Ma found in the Cenozoic accretionary prisms of from West Luzon and South Palawan (Pasco et al., 2019; Dycoco et al., 2021), which formed when the Proto-South China Sea eventually subducted, are remains of this intra-oceanic island arc. Interestingly, Van der Meer et al. (2012) inferred such a scenario from lower mantle tomographic images, from which they inferred that in Jurassic to early Cretaceous time, the Panthalassa plates that surrounded the Pacific plate must have been subducting below an oceanic plate system to the west that was itself separated from the Neotethyan



Figure 13. Simplified tectonic reconstruction showing the reconstructed positions of the Baliojong River basalts as part of the Izanagi Plate and as part of a separate plate at 135 Ma. Reconstruction is made using the reconstructions of Advokaat and Van Hinsbergen (2023) and Boschman et al. (2021b), in the paleomagnetic reference frame of Vaes et al. (2023). The uncertainty in the reference frame is $\sim 1^\circ$, which is smaller than the star.

realm by subduction zones. They termed this plate system the ‘Pontus Ocean’ and named the intervening plate boundary the Telkhinia subduction zone. The relics of 100 Ma arc volcanoes found in the Palawan and west Luzon accretionary prisms may then be fragments of the Telkhinia arc. Because the tomographic resolution shallower than ~ 2000 km depth was too low for a meaningful interpretation, Van der Meer et al. (2012) were not able to reconstruct when and how the Telkhinia subduction zone came to an end. We infer that this plate boundary eventually evolved to the Philippines-Proto-South China Sea boundary, although detailed kinematic restoration is needed to systematically reconstruct its kinematic history. We infer, however, that the Proto-South China Sea lithosphere were actually the last remains of the Pontus Ocean and refer to it as the Pontus Plate. The existence of a plate such as the Pontus Plate was previously suggested by Seton et al. (2012), who postulated that a ‘Junction Plate’ separated from the Panthalassa plates existed between 140 and 70 Ma to

account for convergence.

We now evaluate why the Pontus Plate did not entirely subduct in the late Cretaceous, but first came to an arrest around 85 Ma, after which it finally subducted between ~40 and 15 Ma. There are several models that explain the end of subduction in the circum-Proto-South China Sea region. One model that explains the end of magmatism in SE China and Indochina infers that subduction continued beyond 85 Ma, but retreated southward, which resulted in the opening of the Proto-South China Sea as a back-arc basin analogous to e.g., the Sea of Japan (e.g., He and Xu, 2012; Li et al., 2012, 2014; Zahirovic et al., 2014; Yan et al., 2017). The model, however, does not explain the presence of a subduction record that ceased at the Borneo margin. Moreover, the ~100 Ma basalts accreted in Palawan during the Oligocene (Dycoco et al., 2021) show that the crust of the Proto-South China Sea formed before the end of South China arc magmatism: the Proto-South China Sea crust can therefore not have formed in a post-85 Ma back-arc basin. Finally, a back-arc basin scenario does not explain how an accretionary prism with Jurassic seamounts was preserved to the north of the Proto-South China Sea in the South China margin (Xu et al., 2022). We conclude that the back-arc basin model does not satisfy the geological data from the accreted OPS sequences in the South China, Palawan, and North Borneo margins.

Subduction thus ceased during the Late Cretaceous, even though oceanic crust remained in the foreland. Such an arrest of oceanic subduction may conceptually be explained by the arrival of a mid-oceanic ridge in the subduction zone, as occurred at the continental margin of Antarctica in the south Pacific (Eagles, 2004; Chapter 3), and in the eastern Pacific adjacent to California and Baja California (Atwater, 1989). However, a ridge arrival-scenario is readily excluded for the Proto-South China Sea, because the last subducted oceanic crust that left an accretionary record was at least ~40 Ma old in the Baliojong OPS (this study), and ~60 Ma old in the South China margin (Xu et al., 2022).

We therefore propose that subduction ceased because the resistance against subduction of the oceanic lithosphere increased, likely because of enhanced buoyancy. Such a scenario has been proposed before to explain the cessation of subduction below the SE China margin. Hall (2012) and Niu et al. (2015) speculated that subduction may have ceased by the arrival of a microcontinent. While such a scenario may explain subduction arrest, there is no geological evidence for the arrival of a microcontinent in the Cretaceous or its consumption during Eocene-Early Miocene subduction below Borneo and Palawan – on the contrary, all accreted records consist of OPS sequences that show no evidence that continental crust was involved in the subduction around the time of subduction cessation.

Xu et al. (2022) proposed that the arrival of an oceanic plateau led to the arrest of subduction, and this is a promising explanation. They based their interpretation on the discovery of two Lower Cretaceous seamounts in the south China margin west of Taiwan. The geochemical signatures that we obtained from the pillow basalts of the Baliojong OPS sequence give an E-MORB geochemistry (Figure 4). According to Xia and Li (2019), oceanic plateau basalts generally have a Transitional-MORB (T-MORB) to E-MORB geochemistry.

Samples from the Ontong Java and Caroline plateaus in the West Pacific, for example, display T-MORB to E-MORB geochemical affinities (Zhang et al., 2020). Our results may thus indicate that thickened oceanic lithosphere also arrived at the north Borneo margin shortly before the ~85 Ma of subduction arrest. Interestingly, however, very different ages were obtained from the magmatic rocks that accreted at the Proto-South China Sea margins: ~154 Ma in the north, at the SE China continental margin (Xu et al., 2022), ~135 Ma in NW Borneo (Wang et al., 2023), whereas ~100 Ma arc volcanoes remained in the eastern Proto-South China Sea that eventually ended up in the Palawan and west Luzon accretionary prisms (Pasco et al., 2019; Dycoco et al., 2021). These different ages suggest that it was perhaps not a single Large Igneous Province like the Ontong-Java Plateau that arrived in the trench, as those generally form within a few million years. Instead, the Proto-South China Sea embayment may have been underlain by a composite plateau that was thickened by multiple magmatic events. In the east, this included the ‘Telkhinia’ arc. Elsewhere, such thickened oceanic crust may have formed in a tectonic setting analogous to the “hotspot-highway” in the Pacific (Jackson et al., 2010) that comprises multiple seamount chains that formed from different hotspot sources in relatively close proximity, forming a region of thickened oceanic crust with different ages. Alternatively, the different ages may be related to a main event of oceanic plateau formation in the latest Jurassic, with secondary volcanism after the main stage of plateau formation. The Ontong Java Plateau, for example, had a main stage of formation at around 120 Ma, but minor magmatism also occurred at 90 Ma (Mahoney et al., 1993; Fitton et al., 2004; Korenaga, 2005). The c. 20 Ma age difference in the Pontus Plate volcanoes is therefore not unusual. Regardless of whether it was a true Large Igneous Province or a ‘hotspot-highway’, we suggest that end of subduction at the continental margin surrounding the Pontus Plate in the Proto-South China Sea embayment was related to the arrival of thickened oceanic crust, which we conceptually refer to as the Pontus Plateau (Figure 14).

Even though we infer that thickened crust initially blocked a major and long-lived subduction zone, this fragment of oceanic lithosphere was eventually lost to subduction during the Cenozoic, which suggests that such crust is subductable after all – which must be the case since records of ancient intra-oceanic plateaus are rare (Van Hinsbergen and Schouten, 2021). A similar history has been reconstructed from the Hikurangi Plateau in the SW Pacific. The Hikurangi Plateau is a fragment of the Ontong-Java-Nui Large Igneous Province (Taylor, 2006; Chandler et al., 2012), and its arrival in the New Zealand trench is thought to have caused the shutdown of local subduction at the East Gondwana subduction zone in the Late Cretaceous (e.g., Billen and Stock, 2000; Davy et al., 2008; Chapter 3). Nonetheless, that same plateau is subducting today at the Hikurangi Trench (Collot and Davy, 1998; Timm et al., 2014; Hoernle et al., 2021). It was probably able to stop subduction in the Late Cretaceous because it formed part of a relatively small plate (the Hikurangi Plate; Chapter 3). Today, it forms part of the major Pacific Plate, whose westward motion is forcing the Hikurangi Plate below the Australian Plate at the North Island of New Zealand.

Like the Hikurangi Plate, the Pontus Plate was by the Late Cretaceous reduced to a relatively small surface area (Figure 14). Moreover, it was surrounded by subduction zones. This suggests that the obstruction of the subduction caused by the arrival of an oceanic plateau on the Pontus Plate is geodynamically straightforward. Relative convergence at its eastern boundary that was already being accommodated simply increased to accommodate all Izanagi-Eurasia convergence after the Pontus Plate itself stopped subducting. Subsequently,

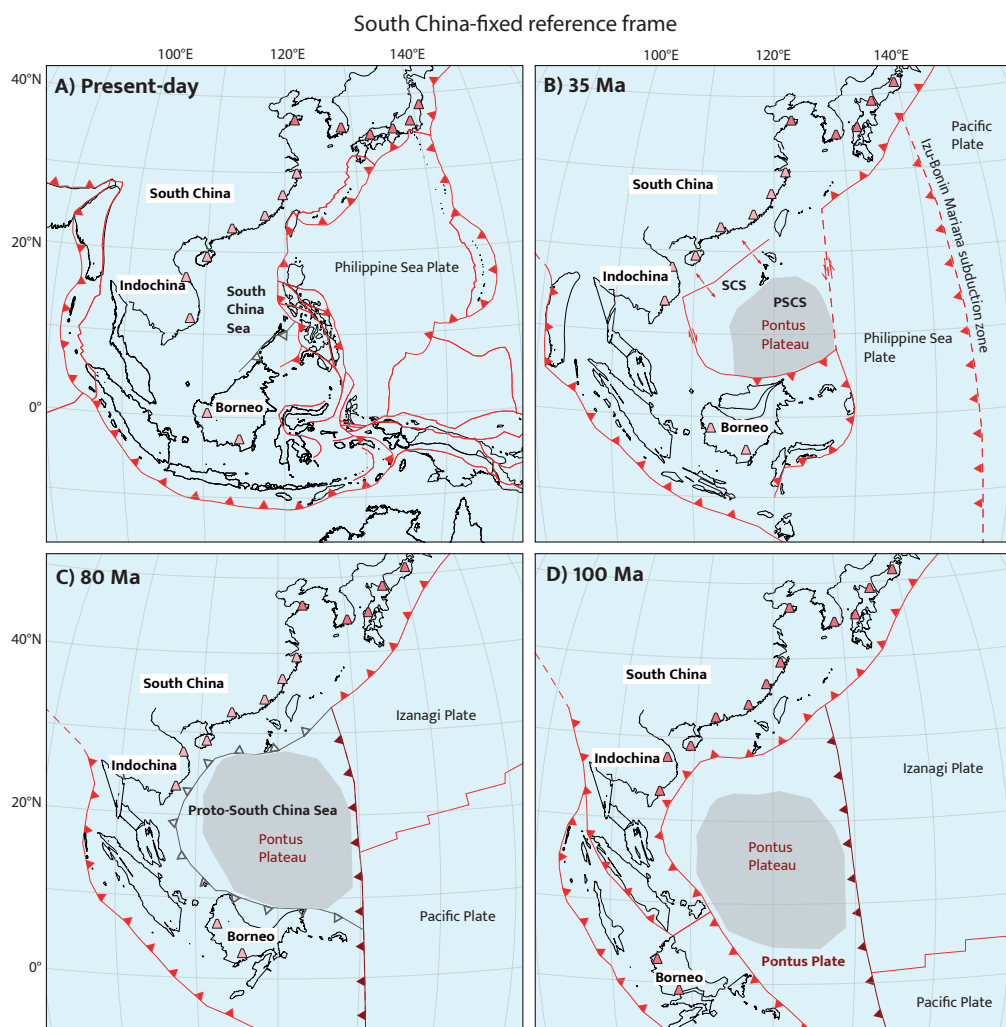


Figure 14. Simplified Late Mesozoic - Cenozoic tectonic evolution of the NW Panthalassa region, including the Pontus Plate and the Pontus-Izanagi subduction zone, in a South China-fixed reference frame. Reconstruction of SE Asia based on Advokaat and Van Hinsbergen (2023). Dark pink cones indicate active arc magmatism, light pink cones indicate extinct arc magmatism. Active plate boundaries in red, former plate boundaries in gray. New tectonic features based on this study in dark red.

in the Eocene, when it formed part of the much larger Eurasian Plate, it was ultimately forced to subduct below NW Borneo and the Cagayan arc, likely induced by the 45 Ma pulse of northward motion of the Australian Plate, that triggered a northward motion and counterclockwise rotation of Borneo (Advokaat et al., 2018). And when the Pontus Plate/Proto-South China Sea eventually subducted, it forced the opening of the South China Sea in its wake, in a downgoing plate position. We speculate that eclogitization of the thickened oceanic crust may have generated a slab pull that was so strong that it broke the former accretionary prism at the South China margin to form the South China Sea basin.

5. Conclusions

In this paper, we investigated the potential geodynamic causes of enigmatic subduction cessation along the South China Sea margin, which led to the formation of the Proto-South China Sea that from late Cretaceous to Eocene time intervened Borneo and South China, after which it subducted in the Oligocene-early Miocene. To this end, we studied the youngest accreted rocks that formed at the North Borneo margin during the latest stages of subduction of the Proto-South China Sea lithosphere below northern Borneo, just prior to late Cretaceous subduction arrest. This record is preserved as well-exposed, deformed Ocean Plate Stratigraphy (OPS) remains of the Baliojong River section in Sabah, NW Borneo. We report a detailed analysis of this OPS section. Based on our results from pillow basalt geochemistry, radiolarian biostratigraphy, and detrital zircon geochemistry, geochronology, and provenance, and paleomagnetism we conclude the following:

1. The Baliojong River exposes different thrust slices of OPS that were likely accreted in at least two events, inferred from the slight variation in basalt geochemistry, sediment provenance and maximum depositional ages, and the different paleolatitudes.
2. These thrust slices of oceanic crust accreted at different times in the Late Cretaceous, during the final stages of subduction in the Proto-South China Sea embayment, at c. 92 and 86 Ma.
3. The oceanic crust formed at near-equatorial latitudes around 135 Ma. This low latitude excludes that the lithosphere was part of the Izanagi Plate whose spreading history is reconstructed from Pacific Plate anomalies. Instead, the Proto-South China Sea lithosphere was part of a slower NW moving plate below which Izanagi subducted. Remnants of this subduction zone are identified in accretionary prisms on Palawan and western Luzon as ~100 Ma arc volcanic remains. Such a plate system was previously inferred from lower mantle slab remnants (Van der Meer et al., 2012), and following that work, we name the plate to which the Proto-South China Sea lithosphere belonged the Pontus Plate, and the arc remains on its eastern margin the Telkhinia Arc.
4. Our geochemical data are consistent with formation of the Baliojong basalts as part of an oceanic plateau. Combined with previously published evidence

for seamount accretion in the Late Cretaceous at the South China Sea margin and the Telkhinia arc remains, we infer that subduction cessation resulted from obstruction of the trench induced by thickened, buoyant oceanic lithosphere (the 'Pontus Plateau'), which may have been comparable to the Ontong Java plateau or, alternatively, a series of seamount chains such as the Hotspot Highway of the Central Pacific. Its arrival at the trench caused the end of subduction in the Proto-South China Sea embayment in the Late Cretaceous.

5. Final subduction of the Proto-South China Sea lithosphere and the conceptual Pontus Plateau below the Borneo and Palawan margins resulted from convergence between Borneo and South China that was likely induced by an Australia-Eurasia convergence pulse. We speculate that the opening of the South China Sea in the downgoing plate in the wake of the subducting Proto-South China Sea may have resulted from enhanced slab pull when the thickened subducting crust underwent eclogitization.



Aslinget Valley, Guam

5

A critical reappraisal of paleomagnetic evidence for Philippine Sea Plate rotation

This chapter has been published as:

Van de Lagemaat, S. H. A., Pastor-Galán, D., Zanderink, B. B. G., Villareal, M. J. Z., Jenson, J. W., Dekkers, M. J. & Van Hinsbergen, D. J. J. (2023). A critical reappraisal of paleomagnetic evidence for Philippine Sea Plate Rotation. *Tectonophysics* 863, 230010.

Abstract

The kinematic history of the Philippine Sea Plate (PSP) is crucial for interpreting its geological record related to subduction initiation processes and the paleogeography of the junction between the Paleo-Pacific and Tethyan oceanic realms. However, reconstructing PSP's kinematic history is difficult because the plate has been surrounded by subduction zones for most of its history. In absence of marine magnetic anomalies to constrain PSP's motion relative to its neighboring plates, paleomagnetic data may be used as quantitative constraints on its motion. Previous paleomagnetic studies interpreted easterly deflected declinations to infer clockwise rotations of up to 90° since the Eocene. However, rotations inferred from these datasets may also reflect local block rotations related to plate margin deformation. We here re-evaluate to what extent paleomagnetic data from the PSP unequivocally demonstrate plate motion rather than local rotation. To this end, we provide new data from Guam, in the Mariana forearc, and reassess published paleomagnetic data. Our new data from Guam come from two localities in the Eocene, two in the Oligocene, and two in the Miocene. Our compilation assesses data quality against recently defined criteria. Our new results demonstrate that on Guam, local rotation differences of up to 35° occurred since the Eocene. Our compilation identifies both clockwise and counterclockwise rotations from the plate margins, with little confidence which of these would reflect plate-wide rotation. We compiled paleolatitude data from igneous rocks, which we correct for microplate rotation constrained by intra-PSP marine magnetic anomalies and show a northward drift of the PSP of ~15° since the Eocene, but without a paleomagnetic necessity for major vertical axis rotation. Hence, with the currently available data, reconstructing rotations may be permitted, but are not required. Plate motion is currently better reconstructed from geological constraints contained in circum-PSP orogenic belts.

1. Introduction

For most of its tectonic history since the Eocene, the Philippine Sea Plate (PSP) and associated microplates have been surrounded by subduction zones (e.g., Hall, 2002; Gaina and Müller, 2007; Wu et al., 2016). Consequently, the reconstruction of the PSP relative to the surrounding major plates of the Pacific, Australia, and Eurasia cannot be determined from marine magnetic anomalies, and reconstruction of its past tectonic motions is challenging. In such cases, paleomagnetic data may provide quantitative constraints on paleolatitude evolution and vertical axis rotation of the plate (e.g., Fuller et al., 1989; Haston and Fuller, 1991; Hall et al., 1995a, 1995b), which may then be incorporated in reconstructions based on geological (e.g., Hall, 2002) or seismic tomographic data (Wu et al., 2016).

The paleomagnetic data from the PSP come from rocks exposed on the plate margins (Figure 1), i.e., on the Philippines and Halmahera in the west and the islands in the arc and forearc adjacent to the Marianas and Izu-Bonin trenches in the east, as well as from boreholes in the plate interior. Even though the database is extensive (e.g., Loudon, 1977; Kinoshita, 1980; Keating and Herrero, 1980; Keating, 1980; Bleil, 1982; Fuller et al., 1989;

Haston and Fuller, 1991; Haston et al., 1992; Koyama et al., 1992; Hall et al., 1995a, b; Queaño et al., 2007, 2009; Yamazaki et al., 2010, 2021; Balmater et al., 2015; Richter and Ali, 2015; Liu et al., 2021; Sager and Carvalho, 2022), these sampling locations come with challenges in providing firm constraints on plate motion evolution. The western plate margin is strongly deformed by distributed strike-slip faults and thrusts which makes it difficult to assess whether vertical axis rotations are local or plate-wide (e.g., Queaño et al., 2007). The eastern plate margin is also strongly deformed, e.g., by extensional processes opening forearc and back-arc basins (e.g., Yamazaki et al., 2003; Sdrolias et al. 2004a). The drill cores in the plate's interior yielded large paleomagnetic datasets (e.g., Loudon, 1977; Kinoshita et al., 1980; Keating and Herrero, 1980; Keating, 1980; Bleil, 1982; Yamazaki et al., 2010, 2021; Richter and Ali, 2015; Sager and Carvalho, 2022), but these are not azimuthally oriented and can only be used to constrain paleolatitude. As a result, declinations from the PSP vary widely and it is difficult to establish whether declination data may be interpreted as representative for rotation of the PSP in its entirety, and which represent local block rotations of the deformed plate margins. Despite the ambiguity in paleomagnetic data interpretation, most models include major clockwise rotation of up to 90° of the PSP, following paleomagnetic constraints (e.g., Haston and Fuller, 1991; Hall et al., 1995a; Deschamps and Lallemand, 2002; Sdrolias et al., 2004; Seton et al., 2012; Wu et al., 2016; Liu et al., 2023), sometimes despite questioning the reliability of paleomagnetic data (Wu et al., 2016). Others chose to not use paleomagnetic data as input for their reconstruction (e.g., Xu et al., 2014), or only to a limited extent (Zahirovic et al., 2014), and therefore those reconstructions include a much smaller rotation or no vertical-axis rotation at all.

While declination data of the PSP may be considered as ambiguous, paleomagnetic studies to obtain inclination data are still useful, as they provide insight into the paleolatitude evolution of the PSP. Published paleomagnetic data are often indicating Eocene paleolatitudes that are about 20° lower than today (e.g., Haston and Fuller, 1991; Hall et al., 1995b; Queaño et al., 2007; Yamazaki et al., 2010), although paleolatitudes obtained from sediments are subject to inclination shallowing. Taking the relative motions of the present and former microplates that together comprise the PSP into account that are reconstructed from marine magnetic anomalies (Hilde and Lee, 1984; Deschamps and Lallemand, 2002; Yamazaki et al., 2003; Sdrolias et al. 2004a), these paleolatitudes provide valuable information on PSP motions.

In this paper, we compile the current state-of-the art of the paleomagnetic database of the PSP and surrounding former and present microplates, and re-evaluate the paleomagnetic evidence for major vertical-axis plate rotation. We report newly collected paleomagnetic data from the island of Guam, located in the forearc of the southernmost portion of the Izu-Bonin Mariana (IBM) subduction zone, whose crust formed shortly after initiation of the present subduction zone in the Eocene (Ishizuka et al., 2011a, 2018; Reagan et al., 2010, 2013, 2019; Hickey-Vargas et al., 2018). We collected samples from Eocene, Oligocene, and Miocene volcanic and sedimentary rocks from Guam, whereby we collected samples from

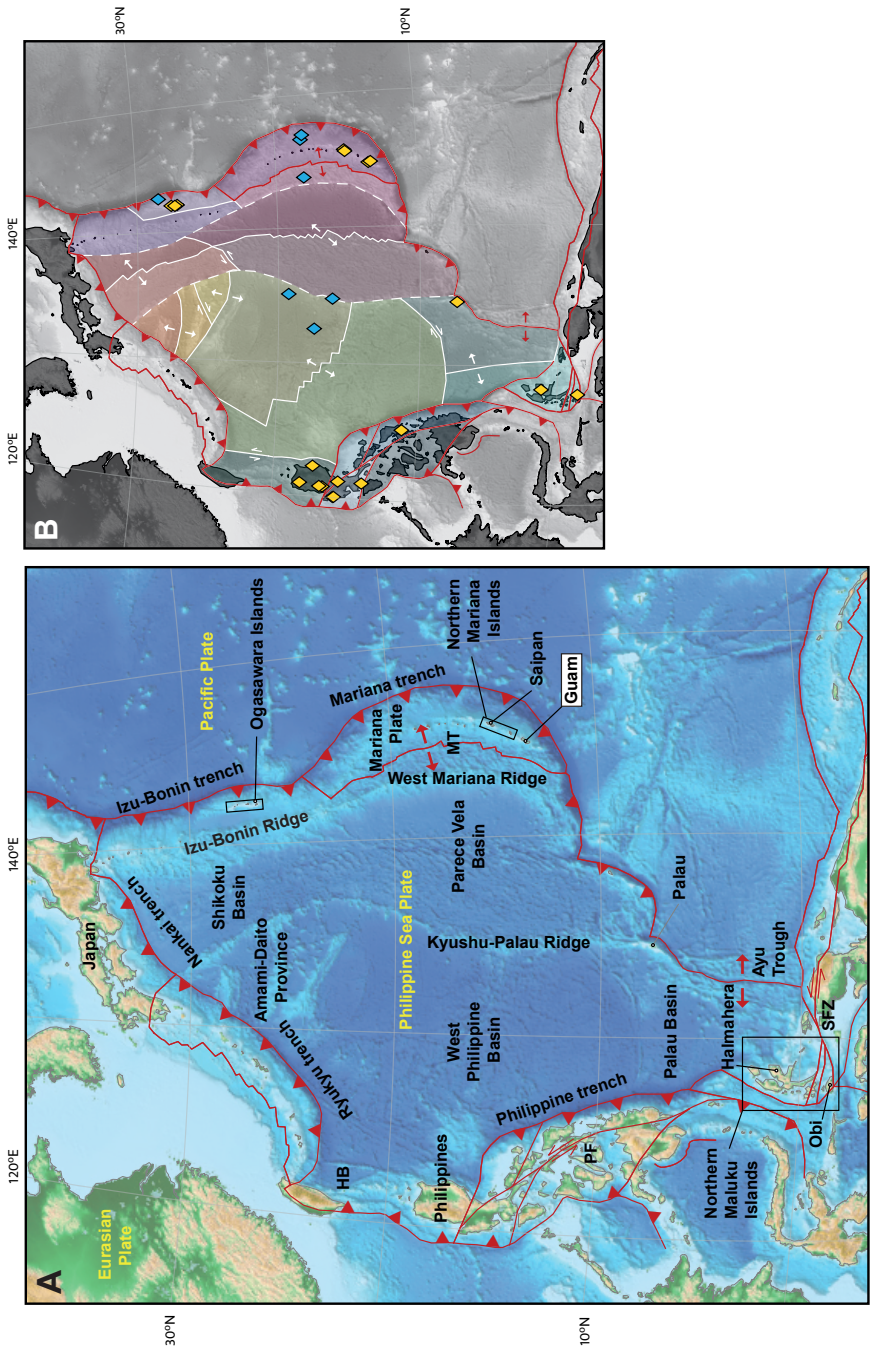


Figure 1. A) Geographic map of the Philippine Sea Plate region; B) Current and former microplates of the PSP. Current plate boundaries (based on Bird, 2003) in red, former plate boundaries in white. Yellow (blue) diamonds (blue diamonds) represent locations of previously published paleomagnetic data obtained from igneous rocks in field (borehole) localities. Base map is ETOPO 2022 15 Arc-Second Global Relief Model (NOAA National Centers for Environmental Information, 2022). HB: Huatung Basin; MT: Mariana Trough; PF: Philippine Fault; SFZ: Sorong Fault Zone.

two localities of each epoch to evaluate whether declinations are coherent on the scale of the island. We add these data to our compilation of previously published paleomagnetic data from the PSP. We evaluate the reliability of the available paleolatitude constraints using recently defined quality criteria (Meert et al., 2020; Vaes et al., 2021; Gerritsen et al., 2022). We will use these to critically re-evaluate the paleomagnetic constraints on vertical-axis rotation and paleolatitudinal evolution of the PSP.

2. Geological setting

The PSP is in the West Pacific realm and is separated from the Pacific Plate by the Izu-Bonin Mariana subduction zone, where the Pacific Plate is subducting westwards below the PSP (Figure 1). The PSP contains small remains of Jurassic and Cretaceous ocean floor and arc sequences (e.g., Dimalanta et al., 2020; Yumul et al., 2020; Ishizuka et al., 2022, and references therein), as well as several inactive spreading ridges where the plate's lithosphere grew at different times throughout much of the Cenozoic (Hilde and Lee, 1984; Deschamps and Lallemand, 2002; Sdrolias et al. 2004a). At present, one microplate (the Mariana microplate carrying the Mariana arc, including Guam) is diverging from the PSP, accommodated by oceanic spreading in the Mariana Trough (Figure 1). This separated the active arc from the now inactive West Mariana Ridge, a remnant volcanic arc that was active until the Miocene (e.g., Yamazaki et al., 2003). To the north, the Mariana Trough spreading center disappears and no oceanic spreading is currently active in the Izu-Bonin ridge region (Figure 1). The Izu-Bonin Ridge and West Mariana Ridge remnant arcs form the eastern margin of the Shikoku-Parece Vela Basin that hosts former oceanic spreading centers that were simultaneously active in the Oligocene-Miocene (c. 30–15 Ma; Sdrolias et al., 2004; Ishizuka et al., 2010), although different kinematic solutions have been proposed for the formation of each basin (Sdrolias et al. 2004a). The western boundary of the Shikoku-Parece Vela Basin is the Kyushu-Palau Ridge, another remnant volcanic arc with magmatic rocks that formed from c. 48 to 25 Ma (Ishizuka et al., 2011b). To the west of the Kyushu-Palau Ridge is the West Philippine Basin (Figure 1). This basin hosts a fossil spreading center that formed through N-S spreading (in present-day coordinates), between ~54 and 34 Ma (Hilde and Lee, 1984; Deschamps and Lallemand, 2002). In the north, in the Amamii-Daito Province, the PSP hosts a series of Cretaceous remnant arcs with intervening basins (e.g., Hickey-Vargas, 2005; Ishizuka et al., 2022; Hickey-Vargas et al., 2013; Morishita et al., 2018). Based on radiometrically dated dredged and drilled samples, it was interpreted that these basins opened in the Eocene, between c. 52 and 42 Ma (Hickey-Vargas, 1998; Ishizuka et al., 2013, 2018, 2022). The formation history of the different basins of the PSP thus indicates that the plate is a composite of about a dozen lithospheric fragments that formed at spreading centers in different orientations and at different times since ~54 Ma, within a Jurassic and Cretaceous lithosphere overlain by Cretaceous arc rocks.

Guam is the southernmost island exposed on the Mariana Ridge (Figure 1). Together with the Northern Mariana Islands (Rota, Tinian, and Saipan), it forms the subaerially

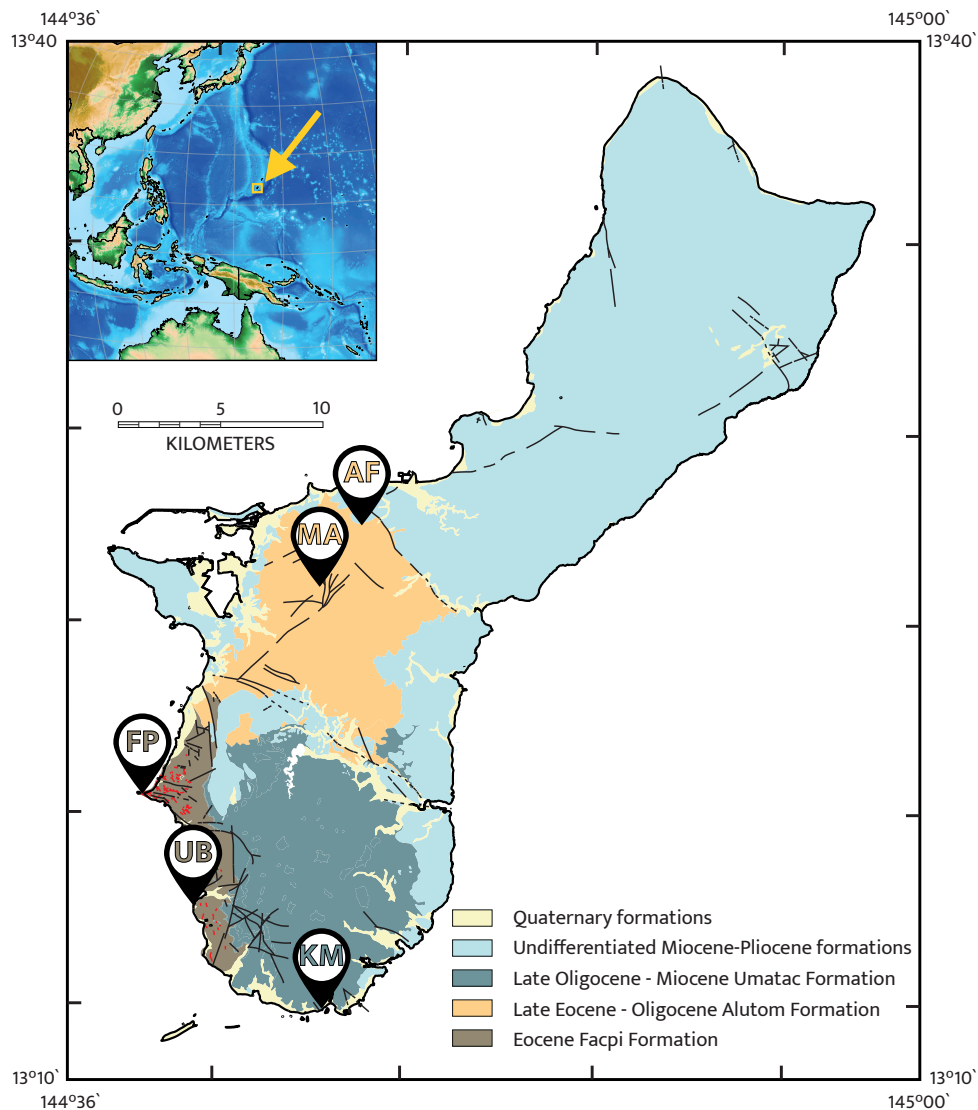


Figure 2. Simplified geological map of Guam (based on Siegrist and Reagan, 2008), showing the different sampling locations.

exposed forearc of the Mariana subduction zone. The currently active Mariana arc is located to the west and north of Guam and the Northern Mariana Islands. Guam exposes a stratigraphy spanning the Eocene to the Quaternary (Figure 2). The northern half of Guam is dominated by Neogene limestone formations, which are also exposed in a smaller area in the southeast of the island (Figure 2). The southern half of the island exposes Eocene to Miocene volcanics, volcanoclastic sediments, and minor limestones (Figure 2). The oldest rocks exposed on Guam, dated to 43.8 ± 1.6 Ma using K-Ar whole-rock dating (Meijer et al.,

1983), form the Eocene Facpi Formation, which comprises pillow basalts and andesite flows thought to have formed on the flanks of a strata-volcano (Reagan and Meijer, 1984; Siegrist and Reagan, 2008). The Facpi Formation is exposed in the southwest of the island, with fresh outcrops along the coastline. Apart from a small eastward tilt, there is no coherent structure within the pillow basalts, but the orientation of (sub)vertical dikes is predominantly NW-SE to roughly E-W. The Facpi Formation is cut by steeply dipping normal faults with similar orientations as the dikes (Reagan and Meijer, 1984; Siegrist and Reagan, 2008). Such normal faults do not occur in Miocene and younger formations, which suggests that they may have formed shortly after or during eruption of the Facpi Formation volcanics (Reagan and Meijer, 1984). Because of these faults, we interpret the 10-30° bedding tilts of the pillow basalts resulting from deformation.

The Eocene pillow basalts and dikes are overlain by Eocene-Oligocene sediments of the Alutom Formation, which comprises mostly volcanoclastics, including bedded breccias, conglomerates, turbiditic sandstones, and minor limestone (Reagan and Meijer, 1984; Siegrist and Reagan, 2008). It is exposed in the northern part of the southern half of island, to the north of the Facpi Formation. The Alutom formation is late Eocene to earliest most Oligocene as shown by the occurrence of late Eocene foraminifera in its base section (Tracey et al., 1964) and K-Ar whole rock ages between 35.6 ± 0.9 and 32.2 ± 1.0 Ma from its top (Meijer et al., 1983). Antiform and synform structures within the Alutom Formation are interpreted to be the result of volcano-tectonic collapse (Tracey et al., 1964), possibly related to paleotopography during deposition.

The Alutom Formation is overlain by the Oligocene to Miocene Umatac Formation, which is exposed in the south of Guam. The oldest, Oligocene, rocks of this formation are interbedded limestones, sandy and tuffaceous limestones, sandstones, and conglomerates (Siegrist and Reagan, 2008). The Miocene lithologies of the Umatac Formation consist of basaltic andesitic pillow lavas, volcanic sandstones, breccias, and conglomerates, and medium to coarse-grained andesite flows (Siegrist and Reagan, 2008). The volcanic members of the Umatac Formation are highly weathered and only sporadically exposed. Bedding dips are mostly sub-horizontal, although some steeper dips up to 35° have been recorded in the west, where the Umatac Formation is in direct structural contact with the Facpi Formation (Siegrist and Reagan, 2008). As most of the Neogene formations have (sub) horizontal bedding planes, we interpret the steeper bedding dips in the west as related to paleotopography of the eroded pillow basalts on top of which the sediments were deposited and not as the result of deformation.

3. Sampling and analytical methods

Paleomagnetic samples with a standard diameter of 25 mm were collected with a water-cooled, petrol-powered drill. The orientation of the samples was measured using a magnetic compass with an inclinometer attached. We collected samples from six localities on the island of Guam from volcanic and sedimentary rocks. We collected a single core per basalt



Figure 3. Field photos of the different sampling locations. A and B) Pillow basalts and cross-cutting dike of the Eocene Facpi Formation; C and D) Volcaniclastics of the Oligocene Alutom Formation. E) Coarse pyroclastics from the Miocene Umatac Formation.

pillow or per sedimentary bed to optimize the chance of sampling individual spot readings of the paleomagnetic field with each core, following sampling procedures for paleomagnetic poles recommended by Gerritsen et al. (2022).

We collected samples from two localities in the Eocene Facpi Formation, from two localities in the Eocene-Oligocene Alutom Formation, and from two localities in the Miocene Umatac Formation (Figures 2 and 3). We collected samples from pillow basalts and lava flows at Facpi Point (FP1 and FP2; 63 samples) and Umatac Bay (UB; 34 samples). From the Eocene-Oligocene Alutom formation we collected samples from fine to coarse-grained turbiditic sandstones with volcanic detrital material and volcanic ash deposits at Mount Alutom (MA; 71 samples) and the Lonfit River (AF; 64 samples). Collecting samples from Miocene rocks was complicated, as Miocene volcanic and volcaniclastic rocks exposed

in Guam are highly weathered and only sporadically exposed, while Miocene limestones are often recrystallized. We collected 40 samples from coarse volcanoclastics of the Umatac Formation, at two relatively small road-sections along Highway 4 in the southernmost part of the island (KM1 and KM2 samples).

We carried out the paleomagnetic measurements at the paleomagnetic laboratory Fort Hoofddijk, Utrecht University (Utrecht, The Netherlands). Samples were either demagnetized using stepwise alternating field (AF) demagnetization in a robotized setup (Mullender et al., 2016) or stepwise thermal (TH) demagnetization. The magnetization was measured on a 2G DC-SQUID magnetometer. Throughout the demagnetization process, samples were kept in a magnetically shielded room.

Sample interpretation and statistical analysis was done using the online portal Paleomagnetism.org (Koymans et al., 2016, 2020). All our data are provided in the supplementary information and will be made available in the Paleomagnetism.org database (Koymans et al., 2020) as well as the MagIC database (Jarboe et al., 2012). Demagnetization diagrams were plotted as orthogonal vector diagrams (Zijderveld, 1967) and principal component analysis was used to determine the characteristic remanent magnetizations (ChRM) component (Kirschvink, 1980). We used Fisher (1953) statistics on virtual geomagnetic poles following statistical procedures described in Deenen et al. (2011) to calculate site mean directions.

Thermomagnetic analyses were done with a modified horizontal translation Curie balance (Mullender et al., 1993) on selected samples from each locality to constrain the interpretation of the NRM components. The analysis was carried out in air and involved stepwise heating to 700 °C with intervened cooling to be able to discern potential thermochemical alteration due to the heating of the samples. The temperature sequence is as follows for most lithologies (in a cycling field between 200 and 300 mT): room temperature 150 °C – 70 °C – 250 °C – 150 °C – 350 °C – 250 °C – 450 °C – 350 °C – 520 °C – 420 °C – 620 °C – 500 °C – 700 °C – room temperature. Where deemed appropriate the 150 °C segment with corresponding cooling to 70 °C was omitted. Curie temperatures are determined with the two-tangent method (Grommé et al., 1969). Each ChRM is interpreted with a minimum of four consecutive demagnetization steps. AF demagnetization steps affected by gyroremanent magnetization (Dankers and Zijderveld, 1981) were not used for ChRM interpretation. Where two components unblocked simultaneously and decay did not trend towards the origin, we used great circle interpretation (McFadden and McElhinny, 1988). In general, we interpreted ChRM directions without forcing the component through the origin, unless demagnetization behavior was noisy. We did not apply a maximum angular deviation cut-off, because Gerritsen et al. (2022) showed that this makes no difference for the precision or position of the final paleomagnetic pole, but we note that the widely used MAD-cutoff of 15° would not have eliminated data. Finally, we applied a 45° cutoff to eliminate outliers, but this omitted <5% of the data.

4. Results and Interpretation

4.1. Thermomagnetic results

The Eocene Facpi Formation pillow lavas (FP2.8 and UB1.1, ~ 0.5 - 0.6 Am²/kg) are strongly magnetic, as expected for basaltic lavas (Figure 4a-b). On heating in air, they oxidize to a variable extent. Barely or no oxy-exsolution is observed; it would be manifested by a corresponding cooling segment above the previous heating segment pointing towards formation of iron-rich titanomagnetite. FP2.8 shows two Curie temperatures, at ~ 470 °C and ~ 560 °C indicating titanomagnetite with a variable amount of Ti substitution. On heating to 700 °C, oxidation to less magnetic material, presumably hematite, is noted because the final cooling curve is below the heating segments. UB1.1 only shows the higher Curie temperature, at ~ 560 - 570 °C indicating a very low level of Ti substitution. The Oligocene rocks of the Alutom Formation (~ 0.1 to 0.3 Am²/kg; MA1.20, MA1.69; AF1.12; Figure 4c-e) are less magnetic than the Eocene rocks. AF1.12 is essentially reversible up to 520 °C with only minute oxidation. Curie temperature is estimated at ~ 500 - 520 °C. Some oxy-exsolution appears in the next heating segment (and rises the Curie temperature). On further heating to 700 °C oxidation to less magnetic material is noted (Curie temperature remains at 500-520 °C). MA1.20 shows prominent oxy-exsolution across a large temperature interval: already after heating to 350 °C the behavior is visible which makes determination of the original Curie temperature tedious. MA1.69 is the weakest Oligocene sample; it behaves like FP2.8. The Miocene sample (KM1.15) is not that magnetic (~ 0.1 Am²/kg) and shows prominent oxy-exsolution from 350 °C upward (Figure 4). Oxidation at the highest temperature leads to a final cooling curve below the heating curves.

4.2. Paleomagnetic results

4.2.1. Facpi Formation

Paleomagnetic samples from the different sampling locations in the Facpi Formation basalts provided uniform demagnetization behavior. Thermal as well as AF demagnetization yielded small viscous overprints that were generally cleaned by 150°C, occasionally up to 270°C, or 10-15 mT, after which specimens decayed to the origin. Thermally demagnetized samples lost their signal after heating until ~ 510 - 580 °C, consistent with (titano-)magnetite as carrier, whereas AF demagnetization often started to deviate from the path towards the origin at fields of ~ 50 mT and higher. We interpret the latter behavior as gyroremanent magnetization (Dankers and Zijdeveld, 1981), which is common for (titano-)magnetite-bearing basalts (e.g., Van Hinsbergen et al., 2010). We interpreted the component decaying towards the origin as the ChRM, typically unblocking between ~ 180 and 580 °C, or between 15 and 50 mT (as at higher levels gyroremanent magnetization may interfere).

Thermal and AF demagnetization yielded similar directions (Figure 5a, b). We corrected our paleomagnetic results for bedding strikes and dips of $349/20^\circ$ E and $356/20^\circ$ E in the FP and UB sites, respectively. We report both geographic (in-situ) and tectonic (tilt-corrected) results in Table 1, but limit our analysis to the tilt-corrected results, as these are interpreted

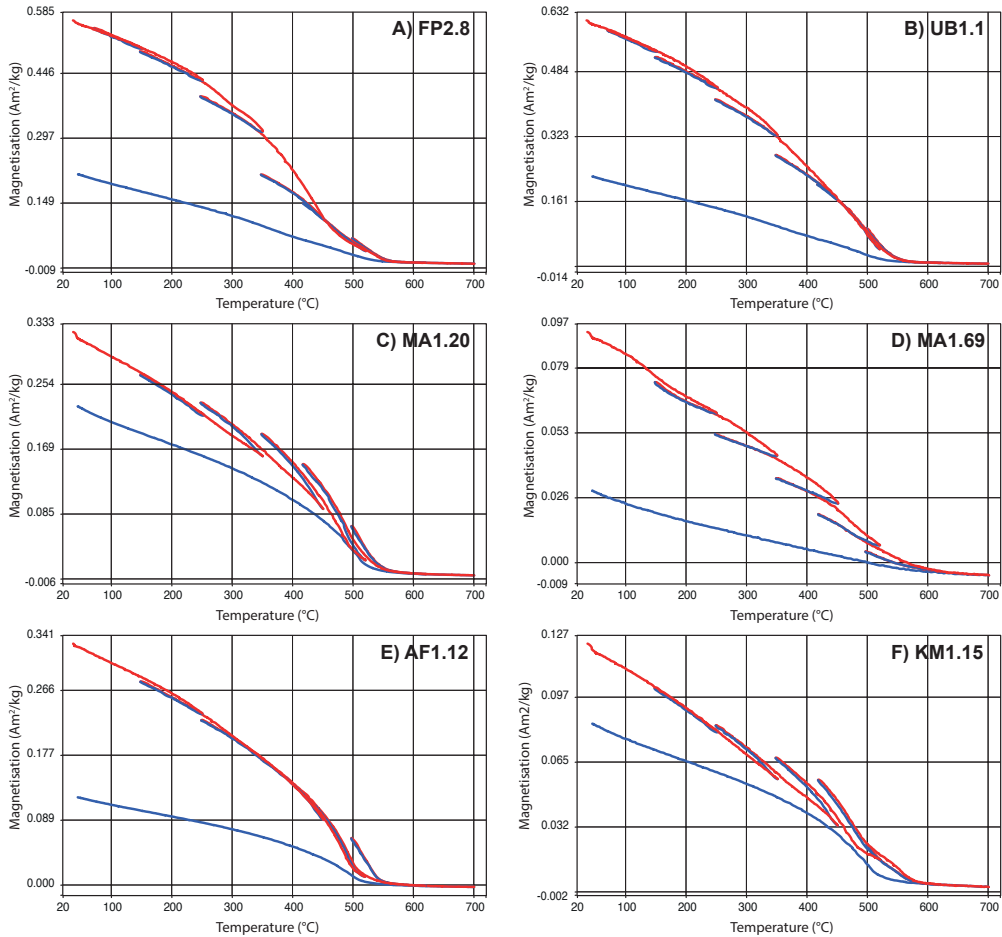


Figure 4. Results of thermomagnetic analysis. Heating segments are in red, cooling segments are in blue.

as being representative of the paleomagnetic signal at the time of formation of the rock. The majority of samples yielded magnetic directions with shallow inclinations, and with northeasterly declinations (Figure 5c, d). A small cluster of 7 stratigraphically consecutive samples in the UB locality has opposite polarity (Figure 5a, b; Figure 6b). We exclude outliers by applying a 45° cut-off, which eliminates a few directions. The opposite polarities ($N=28$ vs $N=7$) yield antipodal declinations, but the smaller dataset has a steeper inclination than the larger dataset (in geographic coordinates; Figure 6b) such that a reversals test (of Tauxe et al, 2010) as implemented in Paleomagnetism.org (Koymans et al., 2016) is negative. We interpret this as the result of insufficient averaging of paleosecular variation (PSV) in the small dataset and consider the presence of reversals in the sequence as a signal that the ChRM is primary. The FP sampling locations were cut by dikes with thicknesses up to ~5 m. To evaluate whether the intrusion of these dikes may have remagnetized the

surrounding pillow lavas, we collected 5-8 samples each from one dike cutting FP1 and three dikes cutting FP2. These dikes yielded K-values of 17-130. The K-values (between 17 and 57) of three of the dikes are consistent with PSV-induced scatter (Deenen et al., 2011), suggesting that they cooled gradually, and each sample represents a spot reading of the field, while the K-value (130) of the fourth dike suggests rapid cooling, which means that this dike represents a single spot-reading. In addition, while the average directions of the dikes and the lavas are northeasterly, they are not identical to the clusters from the pillow lavas (Figure 6a). The scatter within and difference between the average directions of the dikes and the pillow lavas is straightforwardly explained by the low number of samples underpinning these averages (see Vaes et al., 2022). These results therefore do not suggest that dike intrusion remagnetized the surrounding pillow lavas, but rather that the samples collected from the pillow lavas and dikes each may be considered a spot reading from the paleomagnetic field.

We computed a grand average for the FP locations and for the UB location (Figure 6c; Table 1), which are located 6 km apart. The FP locations yielded a direction of Dec/Inc = $37.3 \pm 4.5^\circ / -8.2 \pm 8.8^\circ$ (N=72, K=15.0, A95=4.5) and the UB location yielded a direction of Dec/Inc = $71.9 \pm 4.6^\circ / -15.0 \pm 8.7^\circ$ (N=35, K=29.1, A95=4.6). Both pass the Deenen et al. (2011) criteria, suggesting that their data scatter can be straightforwardly explained by PSV alone. The inclinations of both localities are very similar (paleolatitudes of 4.1° and 7.6° N or S; Figure 6c), but the declinations reveal a $\sim 35^\circ$ difference in vertical axis rotation. A southern hemisphere normal component would require clockwise rotations of 37° and 72° relative to the present-day GAD field, a northern hemisphere reversed component would require counterclockwise rotations of 147° and 108° , respectively. We consider the smaller rotations the most likely and use these in the data compilation.

4.2.2. Alutom and Umatac Formations

Demagnetization diagrams of the MA section display varying demagnetization behavior throughout the section that is characterized by consecutive samples with similar behavior that strongly differs from subsequent parts of the section. This is probably owing to the volcanoclastic nature of the section, whereby beds may represent volcanic events, as well as intra-volcanic sedimentary deposits. First, the magnetization intensity varies strongly, from several 10.000 to several million mA/m. Second, the magnetizations, typically showing decay towards the origin, display varying degrees of overprinting. South-directed (likely reverse) overprints occur on north-directed magnetizations and vice versa (Figure 5e, 5f). These may represent recent overprints of a normal field over a primary reverse magnetization, but also an overprint induced by a volcanic episode during a reverse polarity state of the field over a primary normal magnetization. In addition, the presence of volcanic events is suggested by the tight clustering of directions of consecutive samples in the section. For example, samples MA1.50-MA1.56 show a tightly clustered reverse magnetization (k=250, n=7), an overlying sequence of MA1.58-1.66 yield a nearly antipodal direction with a k-value of 133

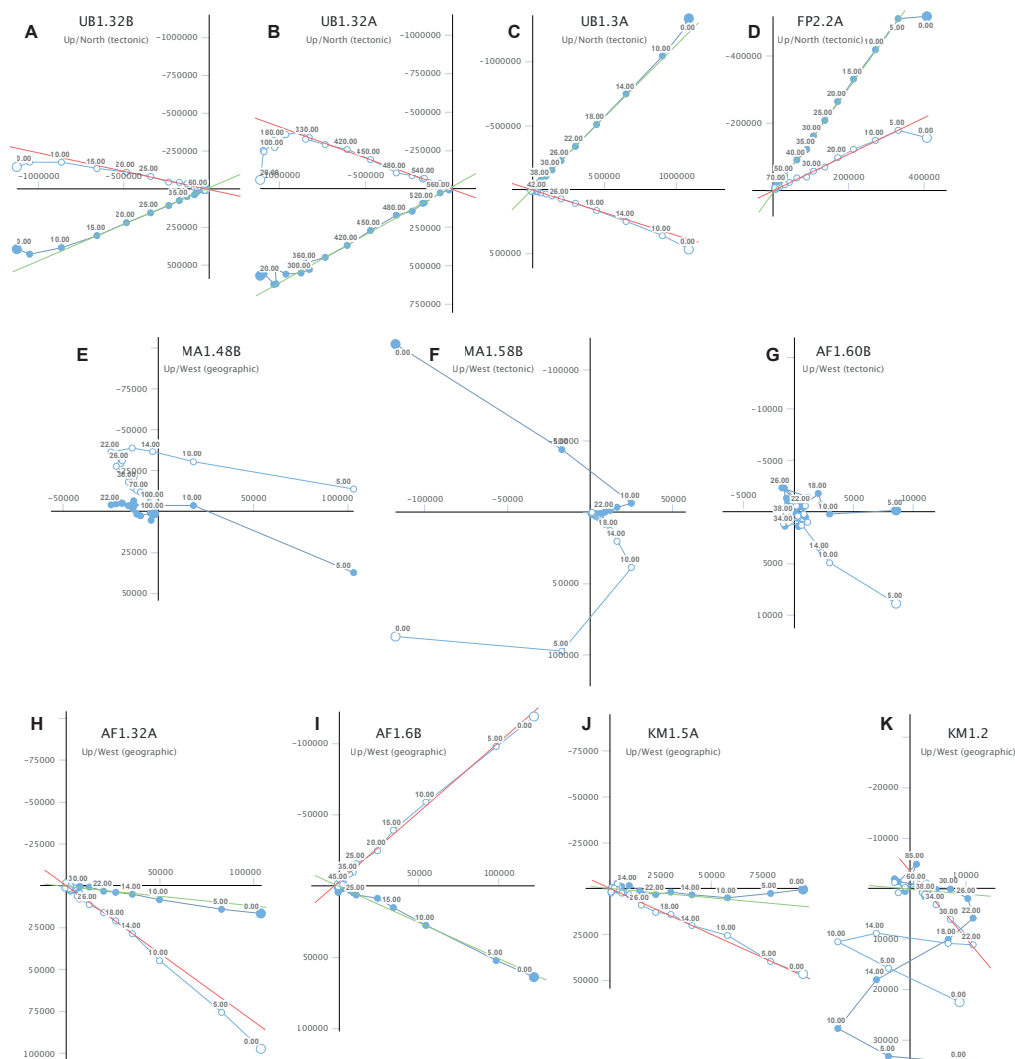


Figure 5. Zijdeveld demagnetization diagrams of selected samples. Closed circles for declination, open circles for inclination. Numbers along axes are intensities in $\mu\text{A/m}$.

($n=8$) (Figure 6d). Such tight clustering is much higher than may be expected from PSV (Deenen et al., 2011) and likely represent paleomagnetic spot readings recorded in discrete volcanic events.

When all dominant magnetizations, i.e., of the components that decay towards the origin, are combined into a single plot, it is evident that clusters of opposite polarity are present in the section, as well as a large cluster of data around the recent paleomagnetic field direction. We suspect that the magnetizations include recently remagnetized and primary magnetizations (Figure 6d). Because we cannot establish with certainty per sample which directions are overprints and which are primary, and because of the evidence that sets of

primary directions may represent single spot readings of the field, we do not consider the directions we determined as a reliable indicator of the paleomagnetic field. We refrain from using the paleomagnetic data from MA for further analysis.

Samples of section AF typically display gradual decay towards the origin defining single components with little overprint. In some cases, the magnetization is only carried by carriers that lost their magnetization by ~ 20 mT, after which only erratic behavior remains (Figure 5g). We interpret these samples as only carrying a recent overprint. The remainder of samples demagnetized typically until 50-60 mT or ~ 270 and 500°C , after which only erratic behavior of low-intensity magnetization remained (Figure 5h, 5i). Interpreting the components that decay towards the origin as the ChRM leads to a tight cluster of directions with $D = 352.2 \pm 2.0$; $I = 23.0 \pm 3.5$; $K = 47.5$, $A95 = 2.0$, $N=113$. The clustering of the data is tight (Figure 6e) but may still be explained by PSV ($A95_{\text{min}}$ sensu Deenen et al. (2011) for $N=113$ is 1.8). Because the bedding is changing orientation throughout the section, varying in dip by $\sim 25^\circ$, we performed a fold test, which is clearly negative (Figure 6g). The paleolatitude computed from the paleomagnetic direction in geographic coordinates is $\sim 12^\circ$, which corresponds to the latitude of the sampling location. This, combined with the solely normal magnetization leads us to interpret the magnetization of section AF as a recent overprint, whereby the small counterclockwise rotation may reflect the effects of e.g., land sliding or otherwise minor, recent deformation.

Finally, the Miocene sites of KM display demagnetization behavior that is similar to that of site AF. A minor viscous overprint is typically demagnetized by 10 mT (Figure 5j), although non-systematic overprint directions are occasionally demagnetized until ~ 20 mT (Figure 5k), after which demagnetization decays to the origin until ~ 50 mT. At higher demagnetization steps, decay becomes noisy. Thermal demagnetization diagrams are incomplete because the loose samples disintegrated during thermal demagnetization. Interpreting the magnetizations that decay towards the origin as the ChRM leads to a clustering of normal polarity, north-directed directions. The average direction is $D = 355.7 \pm 6.4^\circ$, $I = 21.4 \pm 11.4^\circ$, $K=15.3$, $A95 = 6.3$, $N=36$ (Figure 6f; Table 1). This is an insignificant difference with the recent GAD direction predicted for the sampling location. A fold test is permitted because there is bedding orientation variation. This fold test gives optimal clustering at $<0\%$ unfolding, which may suggest that some folding of an originally undulating sedimentary cover occurred prior to magnetization. The cluster of paleomagnetic directions may in principle be explained by PSV ($A95_{\text{min}}$, $\text{max} = 2.9, 8.6$ sensu Deenen et al., 2011). Nonetheless, the insignificant difference between the average direction in geographic coordinates with the recent field, combined with the negative fold test leads us to not consider this result as a primary magnetization from which we may infer tectonic motion of Guam since the Miocene. Combined, we do not interpret the samples from the two Oligocene sections or the Miocene sites to carry a resolvable primary magnetization, and where it may, it does not represent a long-term GAD direction with representative PSV scatter.

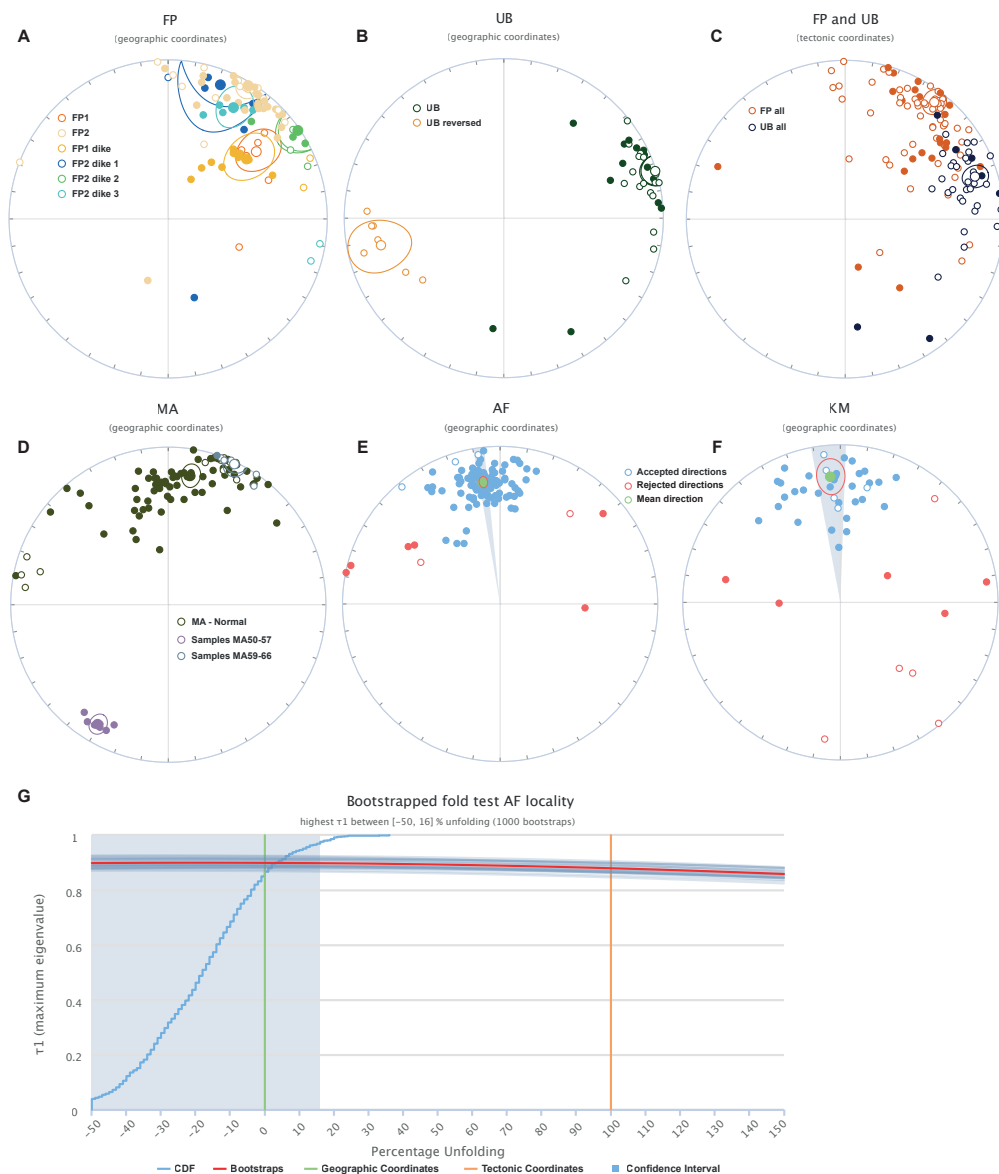


Figure 6. Paleomagnetic results from the different sections. A-F) Paleomagnetic directions and means of the different sampled sections. Open (closed) symbols are up (down) directions. G) Fold test of the AF locality.

Table 1. Paleomagnetic results

Geographic (in situ) coordinates															
Locality	Lat (°N)	Lon (°E)	N	Ns	Dec (°)	Inc (°)	k	a95	K	A95	A95 _{Min}	A95 _{Max}	ΔDx (°)	ΔIx (°)	λ (°)
FP	13.3419	144.6367	79	73	37.05	7.65	9.15	5.81	14.72	4.48	2.16	5.49	4.49	8.83	3.84
UB	13.2957	144.6597	38	36	73.52	3.94	15.9	6.18	23.7	5.01	2.86	8.58	5.01	9.99	1.97
AF	13.4590	144.7310	121	113	352.17	23.04	35.49	2.26	47.52	1.95	1.81	4.17	1.99	3.45	12.01
MA	13.4324	144.7129	79	69	9.98	18.08	13.9	4.75	18.52	4.08	2.21	5.69	4.13	7.57	9.27
KM	13.2492	144.7166	46	36	355.67	21.36	9.4	8.24	15.3	6.31	2.86	8.58	6.43	11.37	11.06
Tectonic (tilt-corrected) coordinates															
Locality	Lat (°N)	Lon (°E)	N	Ns	Dec (°)	Inc (°)	k	a95	K	A95	A95Min	A95Max	ΔDx (°)	ΔIx (°)	λ (°)
FP	13.3419	144.6367	79	72	37.26	-8.19	9.47	5.74	14.98	4.47	2.17	5.54	4.48	8.8	-4.12
UB	13.2957	144.6597	38	35	71.92	-14.96	18.14	5.85	29.14	4.57	2.89	8.73	4.61	8.68	-7.61
AF	13.4590	144.7310	121	113	335.05	40.45	23.14	2.82	24.13	2.76	1.81	4.17	3	3.78	23.09
MA	13.4324	144.7129	79	71	4.45	8.5	13.79	4.7	22.55	3.62	2.18	5.59	3.63	7.13	4.28
KM	13.2492	144.7166	46	33	346.1	21.77	8.65	9.03	14.11	6.9	2.96	9.06	7.04	12.38	11.29

N: number of samples; Ns: number of samples after 45° cut-off; Dec: Declination; Inc: Inclination; ΔDx/ΔIx: uncertainty in declination/inclination; λ: paleolatitude

5. Paleomagnetic data compilation

We compiled published paleomagnetic data from the PSP, to which we added our two sites from the Eocene Facpi Formation of Guam that were interpreted as primary directions. The database contains data from boreholes that drilled into igneous basement, and from field localities in the Philippines and the northern Maluku islands, from Palau, Guam, the Northern Mariana, and Ogasawara islands. We compiled site-level data as originally published, whereby we followed the authors' interpretations about magnetic field polarity and whether bedding tilt corrections were applicable. We subsequently calculated mean paleomagnetic directions from collections of similar age and locations, using the online portal Paleomagnetism.org (Koymans et al., 2016, 2020), whereby we assumed that each reported direction, i.e., a lava site, represents a spot reading of the magnetic field, regardless of its k -value. If an antipodal paleomagnetic direction is present within a locality, we flipped the polarity and combined the data into one collection before calculating the locality mean. Before calculation of the paleomagnetic mean direction, we excluded sites if they were rejected by the original authors. In addition, we did not calculate means for localities with fewer than 4 sites (spot readings). Our calculated means may differ from the originally published mean direction, for example when the authors mixed sedimentary sites with igneous sites, which we kept separate. We applied a 45° cut-off to exclude outliers and transitional directions before recalculation of mean directions. After recalculation of mean paleomagnetic directions, we excluded localities with K values (Fisher (1953) precision parameters on poles) below 10 (following Meert et al., 2020) or when means yielded an $A95$ outside the $A95_{\text{min-max}}$ confidence envelope of Deenen et al. (2011). Our recalculated means are provided in Table 2, while the site-level compilation is provided in Supplementary Table S1. A total of 20 paleomagnetic poles in our PSP compilation passed our quality criteria, obtained from lava flows, pillows, or dikes, as well as 7 paleolatitudes obtained from boreholes.

Paleomagnetic data obtained from sedimentary rocks were not added to the compilation, because it is unclear whether the reported sites represent spot-readings of the field or whether a site adequately averages PSV. In addition, the number of samples collected at the sedimentary localities is insufficient (i.e., <80–100, see Tauxe and Kent, 2004; Vaes et al., 2021) to properly apply the E/I inclination shallowing correction (Tauxe and Kent, 2004), prohibiting using these data to assess paleolatitudinal motion. In a few cases, paleomagnetic datasets obtained from sedimentary rocks of boreholes contain sufficient samples to correct for inclination shallowing, especially large magnetostratigraphic sections, but individual directional data is needed for the E/I correction. Also, these borehole data do not contain declination data because they are not azimuthally oriented. Recently, declination data from a borehole in the PSP were obtained from an oriented core (Yamazaki et al., 2021). However, the uncertainty on these data remains unknown and with their limited number of samples (13 samples from each of two cores of c. 30 cm), the data cannot be used for paleolatitude constraints. For these reasons, all sedimentary data are excluded from our compilation.

Table 2. Paleomagnetic data compilation (field sites only)

Location	Age (Ma)	Lat (°N)	Lon (°E)	N	Ns	Dec (°)	Inc (°)	k	a95	K	A95	A95 _{min}	A95 _{max}	ΔDx (°)	ΔIx (°)	λ (°)	Reference
C. Cordillera	2.6±2.6	16.672	120.822	6	6	349.88	30.59	23.71	14.04	20.87	15.01	5.86	26.52	15.67	24.19	16.46	Queaño et al. (2007)
Batangas	7.0±0.8	13.7	121.2	6	6	318.28	35.35	39.34	10.81	38.76	10.9	5.86	26.52	11.57	16.32	19.53	Fuller et al. (1991)
C. Cordillera	10.2±4.9	18.062	120.998	8	7	274.88	20.65	23.71	12.65	29.32	11.33	5.51	24.07	11.54	20.55	10.67	Queaño et al. (2007)
Obi*	11±1	-1.58	127.83	4	4	14.17	-41.89	452.72	4.32	368.69	4.79	6.89	34.24	5.25	6.38	-24.15	Ali and Hall (1995)
Obi	11.3±3.0	-1.52	127.95	9	9	327.78	-25.91	57.2	6.87	103.87	5.08	4.98	20.54	5.22	8.7	-13.65	Ali and Hall (1995)
Saipan	12±3	15.13	145.71	5	5	28.76	31.87	57.07	10.21	79.36	8.64	6.3	29.75	9.05	13.67	17.27	Haston and Fuller (1991)
C. Cordillera	14.2±8.9	16.45	120.8	4	4	315.49	7.73	39.8	14.74	50.46	13.06	6.89	34.24	13.09	25.76	3.88	Fuller et al. (1991)
Sierra Madre	16.04±4.41	15.368	121.24	5	5	297.55	19.14	17.96	18.55	18.31	18.37	6.3	29.75	18.65	33.77	9.85	Queaño et al. (2007)
Palau	20.1±0.5	7.37	134.52	5	5	54.48	3.48	20.31	17.39	32.69	13.58	6.3	29.75	13.59	27.09	1.74	Haston et al. (1988)
Guam	28.5±5.5	13.45	144.7	4	4	57.67	10.73	61.13	11.85	98.58	9.3	6.89	34.24	9.34	18.12	5.41	Haston and Fuller (1991)
Kasiruta	32.3±3.0	1.18	128.31	9	9	40.49	-24.68	27.64	9.97	29.61	9.62	4.98	20.54	9.87	16.72	-12.94	Hall et al. (1995)
Saipan	35.8±1.9	15.23	145.8	12	11	42.09	-8.68	13.2	13.05	21.31	10.12	4.6	18.1	10.15	19.9	-4.37	Haston and Fuller (1991)
Guam	43.8±2.6	13.296	144.66	38	35	71.92	-14.96	18.14	5.85	29.14	4.57	2.89	8.73	4.61	8.68	-7.61	This study
Guam	43.8±2.6	13.342	144.64	79	72	37.26	-8.19	9.47	5.74	14.98	4.47	2.17	5.54	4.48	8.8	-4.12	This study
Hahajima	45±7	27.08	142.16	7	7	32.69	2.86	11.24	18.82	19.43	14.04	5.51	24.07	14.05	28.03	1.43	Kodama et al. (1983)
Sierra Madre	45±11	17.216	122.313	7	7	230.18	-2.7	19.93	13.86	30.41	11.12	5.51	24.07	11.13	22.21	-1.35	Queaño et al. (2007)
Anijima	45±7	27.12	142.21	16	14	86.84	9.04	7.41	15.66	14.22	10.92	4.18	15.55	10.96	21.44	4.55	Keating et al. (1983)
Chichijima	45±7	27.08	142.21	27	25	104.96	9.98	6.77	12.04	10.54	9.37	3.31	10.79	9.4	18.31	5.03	Kodama et al. (1983)
Zambales	46.4±5.3	15.657	120.057	6	6	288.7	-0.1	17.64	16.4	49.39	9.63	5.86	26.52	9.63	19.25	-0.05	Fuller et al. (1989)
Zambales	46.4±5.3	15.56	120.08	13	13	235.29	-1.96	18.85	9.8	36.67	6.94	4.3	16.29	6.94	13.86	-0.98	Fuller et al. (1989)
C. Cordillera*	67±33	17.17	121.06	5	5	159.26	-12.47	162.46	6.02	400.54	3.83	6.3	29.75	3.85	7.39	-6.31	Queaño et al. (2009)
Samar	99.0±3.9	11.1	125.25	13	13	341.6	-26.6	14.69	11.19	25.88	8.3	4.3	16.29	8.56	14.11	-14.06	Balmater et al. (2015)

*A95 outside of Deenen et al. (2011) confidence ellipse
N: number of samples; Ns: number of samples after 45° cut-off; Dec: Declination; Inc: Inclination; ΔDx/ΔIx: uncertainty in declination/inclination; λ: paleolatitude

6. Discussion

Determining the vertical axis rotation of the PSP using paleomagnetic data is not straightforward. First, datasets are typically small ($N < 10$) and the dispersion of such datasets around the true pole is often larger than suggested by their A95 error margins, and the reliability varies with N (Vaes et al., 2022). Both easterly and westerly declinations have been obtained, generally westerly in the northern Philippines, and generally easterly on the islands in the south and east of the plate (Figure 7). However, which of these declinations, if any, are representative for the rotation history of the plate as a whole is difficult to assess given that all locations come from its deformed plate margins. The Philippine Mobile Belt, which comprises PSP's western boundary, is cross-cut by major left-lateral strike slip faults, including the 1200 km long Philippine Fault (Aurelio et al., 1991), which are bound to induce local block rotations (Queaño et al., 2007, 2009). Similarly, the northern Maluku islands, including Halmahera and Obi, are in the south crosscut by the Sorong Fault system and are in an upper plate position relative to the Halmahera trench (Figure 7). This position in a tectonically active region increases the likelihood of local block rotations, as shown by the strongly varying paleomagnetic declinations (Ali and Hall, 1995; Hall et al., 1995a). Moreover, a problem with paleomagnetic data from igneous rocks, often from stratovolcanoes of arcs, is that structural control on bedding tilt is generally poor, and the effect of small tectonic tilts on large primary bedding dips cannot be seen in the field.

Whether local deformation played a role in the paleomagnetic data obtained from the islands along the eastern margin of the PSP was less well-defined. The declination difference of 35° that we obtained from two Eocene localities in Guam shows that local block rotations also played a role in the forearc of the Mariana Trench. All paleomagnetic poles from the eastern PSP margin that pass our quality criteria have been interpreted as an easterly deflection of the magnetic field (Figure 7). However, due to their sub-equatorial paleolatitude, the polarity of these data, and hence the sense of rotation, is not well known (Kodama et al., 1983; Haston and Fuller, 1991). Moreover, most reliable paleomagnetic poles obtained from the eastern margin of the plate were obtained from the southern forearc regions, i.e., Saipan, Guam, and Palau. The curved shape of the Mariana and Palau arcs makes interpreting these data as unequivocal evidence of plate-wide rotations difficult to defend.

Despite the limited number and the questionable use of paleomagnetic data to infer whole-PSP motion, many plate motion models suggest that the Philippine Sea Plate underwent a large-scale clockwise rotation, of about 90° (e.g., Hall et al., 1995a; Yamazaki et al., 2010; Seton et al., 2012; Wu et al., 2016; Liu et al., 2023). This idea was originally proposed based on the first paleomagnetic results from the Philippine Sea Plate (Keating and Helsey, 1985; Haston et al., 1988; Haston et al., 1991), although some authors suspected that local vertical-axis rotations resulting from arc bending or forearc rotation were actually more realistic (McCabe and Uyeda, 1983; Keating et al., 1983; Kodama et al., 1983; Seno and Maruyama, 1984). Subsequently, based on data from the northern Maluku islands, Hall et

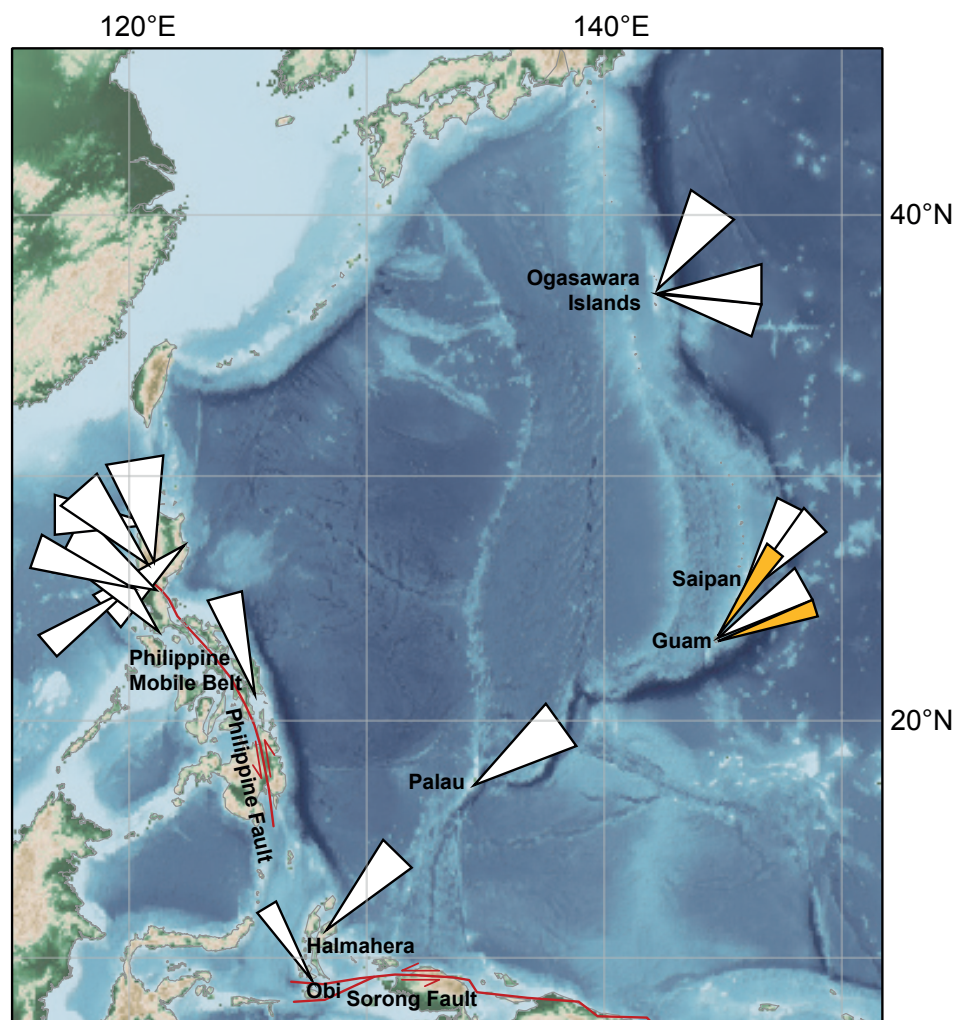


Figure 7. Map of the Philippine Sea Plate showing declinations in our paleomagnetic data compilation with A95 confidence parachutes. White parachutes mark previously published paleomagnetic data, yellow parachutes mark our new paleomagnetic data from Guam. Base map is ETOPO 2022 15 Arc-Second Global Relief Model (NOAA National Centers for Environmental Information, 2022).

al. (1995a) suggested that the PSP underwent a 50° clockwise rotation between 50 and 40 Ma, no rotation between 40 and 25 Ma, and an additional 35° clockwise rotation between 25 and 5 Ma. More recent studies compiled paleomagnetic data (e.g., Wu et al., 2016), and some studies questioned the validity of some of the existing paleomagnetic data, including the possibility of local block rotations and raised the issue whether some localities, such as Halmahera, have been part of the PSP throughout the Cenozoic (Xu et al., 2014; Zahirovic et al., 2014; Wu et al., 2016). However, the quality of the existing data was never assessed in detail using recent quality criteria (Meert et al., 2020; Vaes et al., 2021; Gerritsen et al.,

2022) and it was thus never quantitatively assessed whether the existing paleomagnetic data are reliable to infer PSP motions. Therefore, despite the suspicion of compromised data, the idea of a large-scale clockwise rotation of the entire PSP plate is still widely used, and recent plate tectonic reconstructions often assumed c. 90° clockwise rotation, citing paleomagnetic data (Seton et al., 2012; Wu et al., 2016; Liu et al., 2023).

Based on our new compilation of PSP paleomagnetic data, however, we find that the paleomagnetic data base is not of sufficient quality to form a basis to invoke rotation of the entire plate. Notably, the quality criteria that we used for the compilation in this paper are loose compared to those of Meert et al. (2020). If we were to apply the criterion of Meert et al. (2020) that each locality should include at least 8 sites (spot-readings), only nine paleomagnetic results would pass, of which two are from this study, and our data reveal strong local rotations. Applying additional criteria of Meert et al. (2020), one of the nine remaining poles would be discarded because of its K-value >70, even though it passes the Deenen et al. (2011) criteria, and our two new poles would be discarded because we did not take a minimum of 3 samples per individual lava flow (even though doing so cannot be demonstrated to significantly change the precision or position of paleomagnetic poles (Gerritsen et al., 2022), which is why we focused on maximizing the number of spot readings). This would leave only six datapoints; two from the Philippine Mobile Belt, with strongly varying declinations demonstrating that local block rotations must have occurred (e.g., Queaño et al., 2007, 2009), and two from the North Maluku islands that are also in the deformed plate margin (e.g., Wu et al., 2016; Pubellier et al., 1991). Hence, the declinations of the PSP paleomagnetic database should not be used as basis for plate reconstructions.

This does not mean, of course, that paleomagnetic data exclude such rotations. It may well be that the entire PSP underwent regional vertical axis rotation. However, this rotation should follow from the kinematic reconstruction of the region and existing paleomagnetic data should not be used as input for such reconstructions. The paleomagnetic data obtained by Yamazaki et al. (2021) from oriented drill-cores from the PSP's interior may be the first declination data that are representative for a vertical-axis rotation of the entire PSP. These data suggest a ~50° clockwise rotation of the PSP since the mid-Oligocene (c. 28 Ma), which is distinctly less than the ~90° rotation that is incorporated in many PSP models. However, the small number of samples and the unknown uncertainty in declination, makes the data insufficient as a basis for kinematic reconstruction. Yamazaki et al. (2021)'s study, however, shows that the large paleomagnetic datasets from the drill cores of the plate interior may provide a promising avenue towards obtaining quantitative constraints on plate rotation, but it is currently unknown what the uncertainty associated with the core-rotation correction is, and how this propagates into the final declination estimate. However, the mostly sedimentary rocks from the drill cores need to be corrected for inclination shallowing correction before also the inclination data can also be used for plate reconstruction.

We may use the data from igneous rocks in our compilation to infer PSP's paleolatitudinal motion. To this end, we compare the net paleolatitudinal displacements of the sampling

sites between their moment of formation and the present, in a ‘Huatung Basin-fixed’ frame. We chose the Huatung Basin because it is the oldest oceanic lithosphere of the PSP and therefore exists throughout the reconstructed period. We reconstructed opening of PSP’s oceanic basins using the available magnetic anomaly data (Hilde and Lee, 1984; Deschamps and Lallemand, 2002; Yamazaki et al., 2003; Sdrolias et al. 2004a, making a ‘Philippine plate motion chain’. The root of this plate motion chain is the Huatung Basin, and all motions are reconstructed relative to this microplate. We subsequently infer the paleolatitudinal correction that the Huatung Basin needs to get to fit with the paleomagnetic data in our compilation. The paleolatitude results show that a northward motion of about 15° since 45 Ma (Figure 8) is suggested by the paleolatitude data, although the scatter is quite large. Our $\sim 15^\circ$ estimate is $\sim 5^\circ$ less northward motion than previous estimates (Louden, 1977; Kinoshita, 1980; Hall et al., 1995b; Haston and Fuller, 1991; Queaño et al., 2007, Yamazaki et al., 2010). The c. 5° difference may be explained by the fact that most boreholes are from the northern half of the PSP (Figure 1), which underwent additional northward motion accommodated by spreading in the West Philippine Basin (Hilde and Lee, 1984). Without correction for the opening of the West Philippine Basin, a larger northward motion of up to 7° of the entire plate would be inferred. We find no systematic trend between paleolatitudinal mismatches and sampling location that would demonstrate a whole-plate vertical axis rotation. The single mid-Cretaceous pole obtained from the Philippine Mobile Belt (Balmater et al., 2015) suggests that the latitudinal position of the ‘proto-PSP’ at that

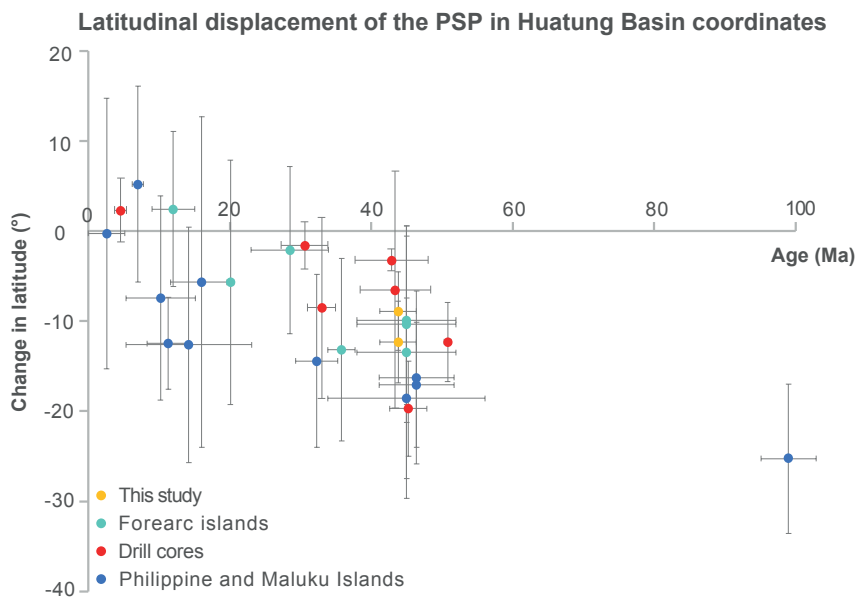


Figure 8. Graph showing the change in latitude versus age, showing a more southerly position (negative latitudes) of the PSP back in time. The data is plotted in a ‘Huatung Basin reference frame’ to correct for intra-PSP plate motions (see main text). Paleolatitudes are colored by general sampling location.

time was about 10° south of its mid-Eocene position (Table 2), although more paleomagnetic data is needed to confidently determine the pre-Eocene latitudinal evolution of the proto-PSP. This single pole, however, suggests that the Philippine arcs cannot have been part of the Izanagi Plate, which was moving considerably faster to the north (Seton et al., 2012; Boschman et al., 2021a; Wu et al., 2022). Instead, the proto-PSP formed part of a plate that was located in the junction region between the Tethyan and Panthalassa realms.

Finally, improved constraints on PSP motion may be obtained from the available drill-cores of the PSP, especially magnetostratigraphic data that contain large sample sets. These data are currently only useful for assessing general trends in paleolatitude evolution, but future efforts to correct for inclination shallowing may significantly improve their value. Subsequently, if the paleolatitude of different drill-cores is well-constrained, vertical-axis rotations may be deduced from well-dated paleolatitude-only data of drill locations spread throughout the plate.

7. Conclusions

We report new paleomagnetic data from Eocene, Oligocene and Miocene rocks from the island of Guam, located in the forearc region of the Izu-Bonin-Mariana subduction zone. These data include two Eocene poles that demonstrate rotation differences on Guam of as much as 35°, revealing that local rotations related to forearc deformation likely occurred. We include our new data into a compilation of previously published paleomagnetic data from the Philippine Sea Plate. Based on our paleomagnetic results and a critical re-evaluation of existing data we conclude that:

1. It cannot be established to which extent paleomagnetic declinations from the Philippine Mobile Belt, the northern Maluku Islands, and the Izu-Bonin-Marianas forearc provide evidence of plate-wide rotation. Regional rotations demonstrably play a role, and unequivocally robust data from the plate interior are currently not available.
2. The inclination-only data from igneous rocks are satisfied by a reconstruction in which all microplates of the Philippine Sea Plate are reconstructed relative to the Huatung Basin, and for the latter a c. 15° northward motion since the mid-Eocene is reconstructed.
3. Drill-core paleomagnetic data with large sample sets from the stable plate interior are promising for future efforts to constrain the motion history of the Philippine Sea Plate. However, inclination shallowing should be corrected for, and uncertainties with for instance using the present-day field to correct for drill core rotation should be propagated into the analysis.
4. The paleomagnetic database does not require vertical axis rotations but does not preclude them.
5. Kinematic reconstructions of the Philippine Sea Plate should, for now, develop from systematic restorations of the geological records accreted at plate boundaries.



Eocene turbidites in Gouaro Bay, New Caledonia

6

Plate tectonic cross-roads: Reconstructing the Panthalassa-Neotethys Junction Region from Philippine Sea Plate and Australasian oceans and orogens

This chapter has been submitted for publication in Gondwana Research as:

Van de Lagemaat, S.H.A. & Van Hinsbergen, D.J.J. Plate tectonic cross-roads: Reconstructing the Panthalassa-Neotethys Junction Region from Philippine Sea Plate and Australasian oceans and orogens.

Abstract

The plate tectonic history of the Junction Region, which separated the Panthalassa and Tethys realms, is notoriously challenging to reconstruct. The region has been dominated by intra-oceanic subduction zones, which has led to a sparsely preserved geological record because not only the down-going plates but also the overriding plates were lost to subduction. Even though most lithosphere that was present in the Junction Region during the Mesozoic has been lost to subduction, orogenic records preserve sparse geological data that provide information for a plate tectonic reconstruction. Here we present a kinematic reconstruction of the Junction Region back to the Jurassic, based on the present-day geological record of the circum-Philippine Sea Plate and Australasian regions, and sparse paleomagnetic data. We provide a comprehensive review of orogenic and oceanic architecture from Japan to the SW Pacific region and use a systematic reconstruction protocol for a plate kinematic restoration back to the Triassic. Based on our reconstruction, we propose that the Molucca Sea Plate formed as an Eocene back-arc basin behind a north-dipping subduction zone that consumed Australian oceanic lithosphere. We find that the Jurassic oceanic lithosphere preserved in the Philippines originated from the northern Australian margin when a back-arc basin formed. By placing our reconstruction in a mantle reference frame, we identify multiple cases of slab dragging and suggest that the lithospheric collapse that led to Izu-Bonin Mariana forearc extension may have been a trigger for the absolute plate motion change of the Pacific Plate that formed the Hawaii-Emperor Bend. Finally, we show that there is no need for spontaneous subduction initiation at the Izu-Bonin Mariana trench. Instead, subduction initiation was more likely forced through a change in Pacific-Australia relative plate motion around 62 Ma. Subduction started along a pre-existing Mesozoic subduction zone that had accommodated mostly transform motion since about 85 Ma.

1. Introduction

Kinematic reconstructions of the modern oceans and orogens have revealed how since the formation of the supercontinent Pangea in the late Paleozoic, the Earth's plate tectonic system has been organized in two main plate tectonic realms. In the Tethyan realm, enclosed by Pangean continents, oceanic lithosphere formed and subducted along predominantly E-W trending ridges and trenches, and in the Panthalassa realm, surrounding the Pangea continents, subduction occurred predominantly radially away from the ocean, below Pangean continental margins and marginal basins (e.g., Larson and Chase, 1972; Engebretson et al., 1985; Stampfli and Borel, 2002; Seton et al., 2012; Torsvik and Cocks, 2017). In the Junction Region between these two realms, located between Australia and Eurasia (Figure 1), these two plate systems interacted, forming a complex plate boundary system with long- and short-lived subduction zones and marginal basins (Seton and Müller, 2008; Hall, 2002, 2012; Zahirovic et al., 2014). The interaction between these plate systems holds many clues for the understanding of the drivers of plate tectonics and the formation and demise of oceans and subduction zones. However, much of these subduction zones

in the Junction Region were intra-oceanic, which has a much lower propensity to leaving geological records of subduction than active continental margins do, because not only the down-going, but also the overriding plates are eventually lost to subduction.

Kinematic restorations typically focus on regional tectonic problems of the Junction Region, such as the formation and evolution of the Philippine Sea Plate (e.g., Zahirovic et al., 2014; Wu et al., 2016; Liu et al., 2023). Such reconstructions give plate tectonic and paleogeographic context to present-day geological records of the region but focus less on the kinematic context of the wider region reconstructed in less detail. These reconstructions vary widely between authors and are difficult to connect to the global plate circuit. On the other hand, reconstructions that focused on hemispheric scales are schematic and conceptual and do not display in detail where modern geological records restore (e.g., Seton et al., 2012; Müller et al., 2019; Scotese, 2021). In this paper, we aim to bridge this gap, and provide a kinematic restoration of the Junction Region in which present-day geological records are reconstructed into the plate kinematic framework of the entire region back to Mesozoic times.

To this end, we provide a comprehensive review of the modern oceanic basins and orogenic architecture of the entire Junction Region, spanning from Japan to New Zealand (Figure 1), following the approach of Van Hinsbergen et al. (2020a) and Boschman et al. (2021a), and connected to the recent reconstruction of SE Asian orogenic and plate tectonic evolution of Advokaat and Van Hinsbergen (2023), and Pacific Basin evolution as summarized in Chapter 3. Based on this review, we systematically reconstruct the Junction Region in the context of the entire plate tectonic system of the west Panthalassa and eastern Neotethyan realms. Our reconstruction goes back to the oldest records of intra-oceanic subduction that are preserved in the Junction Region, on the Philippines, i.e., back to the latest Jurassic (Dimalanta et al., 2020). We will discuss the implications of our reconstruction for the formation and destruction of plate boundaries and interpretation of modern mantle structure.

2. Reconstruction approach

To kinematically restore the Junction Region, we thoroughly review the ocean floor structure and age of marginal basins and the surrounding orogenic architecture, of the Philippine Sea Plate, New Guinea, and their surroundings. We review previously published geological and geophysical data that provide kinematic information as input for our reconstruction. This reconstruction is made using GPlates, a freely available plate reconstruction software (www.gplates.org; Boyden et al., 2011; Müller et al., 2018). To ensure that our reconstruction is reproducible, we use a systematic reconstruction hierarchy (Boschman et al., 2014; Van Hinsbergen et al., 2020a), which also makes our reconstruction easily adaptable when new kinematic data become available.

The first step in the reconstruction hierarchy aims at establishing the relative motions of the major plates surrounding the Junction Region (Eurasia, Australia, Pacific) using the



Figure 1. Map of the Pangea-Tethys and Panthalassa plate tectonic realms separated by the Junction Region. Present-day plate boundaries are red (modified from Bird, 2003), relevant former plate boundaries are gray. Dark shaded areas behind colored realms are present-day subaerially exposed crust, the light shaded areas are submerged continental crust and thickened oceanic crust, i.e., oceanic plateaus and island arcs.

most recent marine magnetic anomaly and fracture zone data. For the age of polarity chrons (intervals of geologic time with a normal or reversed field) and magnetic field reversals, we use the geomagnetic polarity time scale of Ogg (2020). Marine magnetic anomaly and fracture zone data of marginal ocean basins within the Junction Region are reviewed, which provide information about the timing, amount, and direction of their opening.

Our plate reconstruction has its root in Africa, of which the motion can be described relative to an independent reference frame, i.e., the spin axis or the mantle. Prior to the formation of the Pacific-Antarctic Ridge (~84 Ma), there is no plate circuit connection between the Panthalassa and Indo-Atlantic realms. Following Boschman et al. (2019), we use the Pacific mantle reference frame of Torsvik et al. (2019) combined with the slab reference frame of Van der Meer et al. (2010) to reconstruct Panthalassa plate motions

before 84 Ma.

Next, we review the architecture of accretionary orogens that contain relics of now-subducted lithosphere and their overriding plates, and their subsequent deformation. We follow the reconstruction philosophy of Van Hinsbergen and Schouten (2021), by reconstructing upper/intraplate deformation and crustal accretion separately. Upper/intraplate deformation is reconstructed based on estimates of displacement accommodated by crustal extension, strike-slip faults, and tectonic shortening obtained from structural geology. This provides a plate kinematic model that must be geometrically consistent, without any large over- or underlaps when there is no geological evidence, and that follows the basic rules of plate tectonics, which means that all plates are surrounded by plate boundaries that end in triple junctions (Cox and Hart, 1986).

We then reconstruct the nature and geological history of the large portions of lithosphere that have been lost to subduction, based on information preserved in accretionary complexes and ophiolites. The analysis of the stratigraphy and metamorphic history of accreted ocean-plate derived units (Ocean Plate Stratigraphy (OPS); Isozaki et al., 1990; Wakita and Metcalfe, 2005; Wakita, 2015) allows us to determine the age and geological history of the subducted oceanic lithosphere. Similarly, accreted Continental Plate Stratigraphy (CPS) allows restoration of passive margins and microcontinents that were entrained in subduction zones (Van Hinsbergen and Schouten, 2021). Key constraints for the history of oceanic basins also comes from oceanic upper plate lithosphere preserved as ophiolites and overlying volcanic arcs. Because ophiolites provide key information for the study of subduction initiation and cessation (e.g., Guilmette et al., 2018; Stern and Gerya, 2018; Cramer et al., 2020; Lallemand and Arcay, 2021; Van Hinsbergen et al., 2021), we carefully include them in our reconstruction to provide regional kinematic context for these processes. In addition, the geochemical composition of ophiolites provides insight into the tectonic setting of formation of the oceanic lithosphere. We review tectonic interpretations based on geochemistry, to facilitate the interpretation of the reconstruction, but we do not use this information to build the reconstruction for which we only use kinematic data. Finally, we test our reconstruction against a compilation of paleomagnetic data from the Philippine Sea Plate (Chapter 5), using the paleomagnetic reference frame of Vaes et al. (2023), and iterate where necessary, to ascertain that the reconstruction is in accordance with paleomagnetic constraints.

3. Review of continental, oceanic, and orogenic architecture

To reconstruct the plate tectonic history of the Philippine Sea Plate and New Guinea region, we first define and review the boundaries of the region of interest for our reconstruction (Figure 1 and 2; A0 versions of the geographic and tectonic maps are provided in the Supporting Information as Figures S1 and S2). The Junction Region as we will use it throughout this study encompasses the following region: The Philippine Sea and Caroline plates and their plate boundaries, the Philippine archipelago and the northern Molucca

Islands, New Guinea and surrounding islands and intervening basins, the Melanesian borderlands, which includes the Solomon Islands, Vanuatu, Fiji, and oceanic basins such as the Bismarck Sea and the Solomon Sea, and the SW Pacific region, which comprises the series of ridges and oceanic basins to the east of Australia (Figures 3 – 7, S1 and S2).

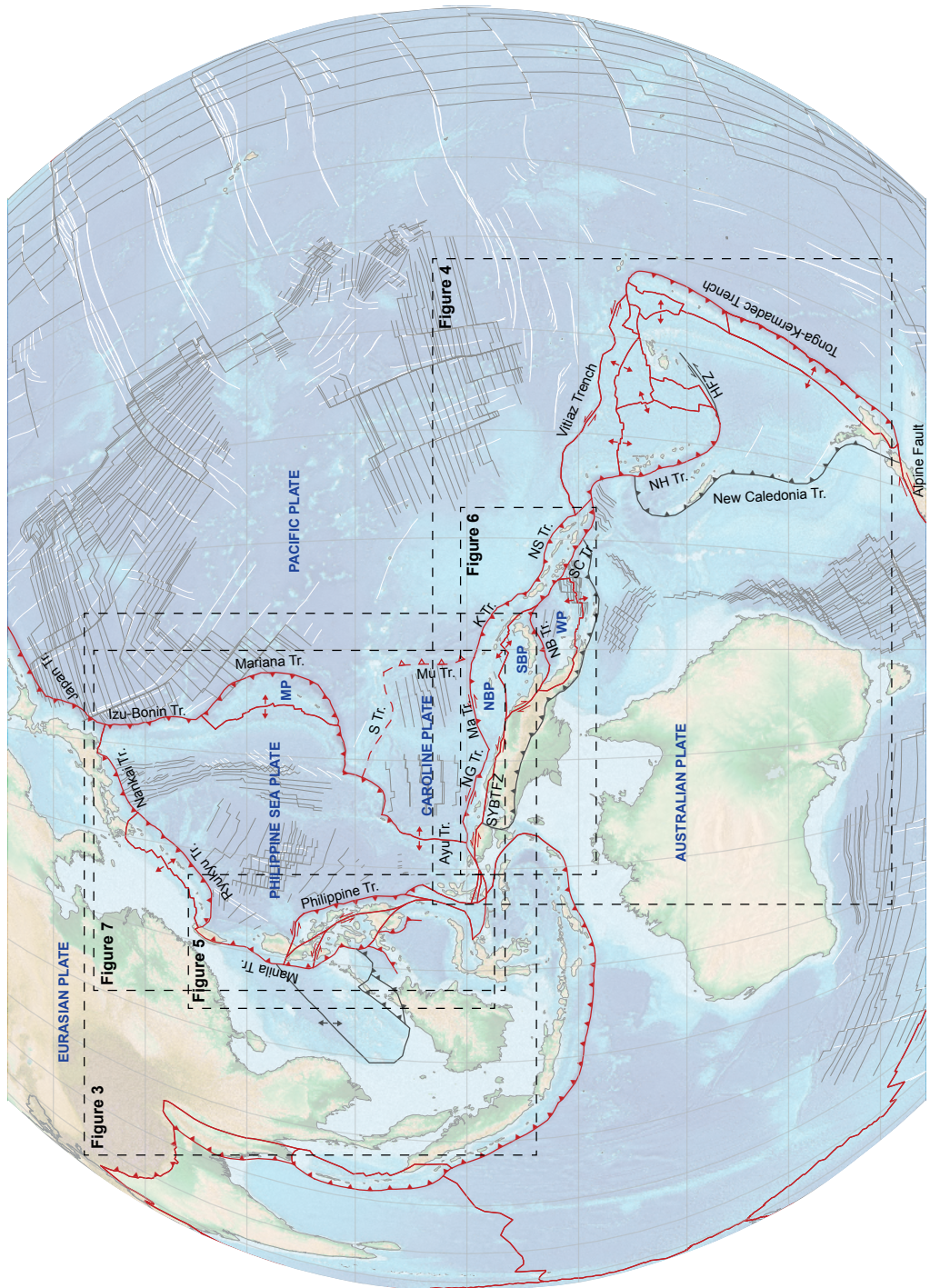
Surrounding the Junction Region are three major, mostly rigid tectonic plates: the Eurasian, Australian, and Pacific plates that are connected in a plate circuit (Figure 2). To also be able to use absolute plate motion frames, the plate circuit has its root in Africa, whose motion relative to the Earth's mantle or spin axis is available through e.g., hotspot and paleomagnetic reference frames (O'Neill et al., 2005; Torsvik et al., 2008, 2012; Doubrovine et al., 2012; Vaes et al., 2023). The plate circuit that we use in our reconstruction is Eurasia – North America – Africa – Antarctica – Australia/Pacific, whereby we follow the circuit described in Vaes et al. (2023).

In addition to these rigid plates, there are also deformed regions that border the Junction Region. These are the region west of the Philippine archipelago, i.e., the circum-South China Sea region, as well as the Sulu, Celebes, and Banda Sea, and surrounding islands (Figure 3). This part of SE Asia contains continental fragments that were derived from Gondwana and migrated to and collided with Eurasia during opening and closure of Tethyan ocean basins (Hall, 2012; Advokaat and Van Hinsbergen, 2023; Metcalf, 2013). We refer to this orogenic collage as the SE Asian Tethysides. The south of the study region is the SW Pacific realm, hosting extensional basins and fold-thrust belts east of Australia (Figure 4).

For the reconstruction of the rigid plates that are part of the global plate circuit and for the deformed SE Asian and Zealandia regions, we use previously published reconstructions, as reviewed below. The reconstruction of the circum-Junction Region provides a net area change of the Junction Region through time, which serves as the plate kinematic boundary condition of our new reconstruction of the Junction Region itself. Below, we first describe the plate circuit and the kinematic data that describe the relative motions that are incorporated in our reconstruction. Next, we give a short overview of the deformed regions adjacent to the Junction Region, and, finally, we provide an extensive review the orogenic architecture of the Junction Region itself.

Figure 2 ►. Map of the reconstructed region. A0 geographic and tectonic maps of the region are provided in the supporting information as Figure S1 and Figure S2. Present-day plate boundaries are red (modified from Bird, 2003), relevant former plate boundaries are gray. Marine magnetic anomalies are indicated by black lines, fracture zones are indicated by white lines (both based on the GSFML database, Matthews et al., 2011; Seton et al., 2014; Wessel et al., 2015, and references therein). Background image is ETOPO 2022 15 Arc-Second Global Relief Model (NOAA National Centers for Environmental Information, 2022).

HFZ = Hunter Fracture Zone; K Tr = Kilinailau Trench; Ma Tr = Manus Trench; MP = Mariana Plate; NB Tr = New Britain Trench; NBP = North Bismarck Plate; NG Tr = New Guinea Trench; NH Tr = New Hebrides Trench; NS Tr = North Solomon Trench; S Tr = Sorol Trough; SBP = South Bismarck Plate; SC Tr = San Cristobal Trench; SYBTfZ = Sorong-Yapen-Bewani-Torricelli Fault Zone; WP = Woodlark Plate.



3.1. Plate circuit

The upper plate to the Junction Region is the Eurasian continent. The Eurasian Plate is currently essentially rigid but is an amalgamation of formerly independently moving tectonic plates. The North and South China blocks have moved in unison since the Triassic, but relative motion between the China blocks and Siberia/Eurasia continued into the Cretaceous, until the closure of the Mongol-Okhotsk oceanic basin (Klimetz, 1987; Kravchinsky et al., 2002; Cogné et al., 2005; Van der Voo et al., 2015). For the motion of the China blocks relative to Eurasia before the Cretaceous, we incorporate the plate model of Torsvik and Cocks (2017), which builds on the reconstruction of Van der Voo et al. (2015).

Our reconstruction uses the global plate circuit used by Vaes et al. (2023) as basis for their paleomagnetic reference frame. In this plate circuit, the Eurasian Plate is reconstructed relative to the North American Plate, based on marine magnetic anomalies that formed in the North Atlantic Ocean. We use the rotation poles of DeMets et al. (2015), Vissers and Meijer (2012a, b), and Srivastava and Roest (1996). The North American Plate is reconstructed relative to Africa, also based on marine magnetic anomalies in the Atlantic Ocean. In our reconstruction, we use the rotation poles of DeMets et al. (2015), Müller et al. (1999), Gürer et al. (2022), and Van Hinsbergen et al. (2020a).

The other two rigid plates, the Australian and Pacific plates, are both reconstructed relative to Antarctica, which is in turn reconstructed relative to Africa. East Antarctica is reconstructed relative to Africa based on rotation poles derived from marine magnetic anomalies that formed along the Southwest Indian Ridge. We use the rotation poles of Bernard et al. (2005), Cande et al. (2010), Mueller and Jokat (2019), and DeMets et al. (2021) for this relative motion. The Australian Plate is reconstructed relative to East Antarctica based on marine magnetic anomalies that formed through spreading along the Southeast Indian Ridge. We incorporate the finite rotation poles of Cande and Stock (2004), Whittaker et al. (2007, 2013), and Williams et al. (2011). The Pacific Plate is reconstructed back to 83.7 Ma relative to West Antarctica based on marine magnetic anomalies that formed along the Pacific-Antarctic Ridge, for which we use the rotation poles of Croon et al. (2008) and Wright et al. (2015, 2016). The motion of West Antarctica relative to East Antarctica is based on marine magnetic anomaly constraints and continental extension estimates based on crustal thicknesses, for which we use the rotation poles of Cande and Stock (2004), Granot et al. (2013), Granot and Dymant (2018), and Chapter 3. Before the formation of the Pacific-Antarctic Ridge, the Pacific Plate is disconnected from the plate circuit, and is instead reconstructed in a separate Pacific absolute plate motion frame, for which we use the hotspot frame of Torsvik et al. (2019).

After its birth in the Panthalassa Ocean around 190 Ma, the Pacific Plate was surrounded by mid-ocean ridges and was actively spreading with three oceanic plates: the Farallon Plate in the east, the Phoenix Plate in the south, and the Izanami Plate and subsequently the Izanagi Plate in the west (Engebretson et al., 1985; Nakanishi et al., 1992; Nakanishi and Winterer, 1998; Seton et al., 2012; Boschman and Van Hinsbergen, 2016; Boschman et al.,

2021a). Marine magnetic anomalies that record spreading between the Pacific and Izanami/Izanagi plates between polarity chrons M5-M35 (127.5-160.9 Ma) are preserved on the Pacific Plate (Nakanishi et al., 1992). Spreading between the Pacific and Phoenix plates is recorded by marine magnetic anomalies that formed during chrons M1 and M29 (123.8 – 160.9 Ma; Nakanishi et al., 1992). The Pacific oceanic crust that is currently subducting at the Izu-Bonin-Mariana trench is oceanic crust that formed along the Pacific-Izanami/Izanagi ridges and is younging northwards. The oldest crust that is currently subducting at the Izu-Bonin-Mariana subduction zone in the south is Jurassic in age (c. 160 Ma), while Early Cretaceous (c. 130 Ma) oceanic crust is currently subducting below the northernmost Izu-Bonin Mariana subduction zone and below Japan. Pacific oceanic crust that formed through spreading with the Phoenix Plate is in the west overlain by the Ontong Java Plateau, a Large Igneous Province (LIP) that erupted at about 120 Ma (Mahoney et al., 1993; Larson, 1997; Chambers et al., 2004). The emplacement of the Ontong Java LIP led to the break-up of the Phoenix Plate around 120 Ma (Taylor, 2006; Chandler et al., 2012; Chapter 3). We incorporate the evolution of the western Panthalassa oceanic basin using the reconstruction of Chapter 3 for the Pacific and Phoenix plates, that of Boschman et al. (2021a, b) for the Izanami and Izanagi plates, and of Vaes et al. (2019) for the deformation of the Eurasian margin forming the Japan Sea between 23 and 15 Ma.

3.2. Deformed border regions

3.2.1. SE Asian Tethysides

We here briefly summarize the tectonic evolution and architecture of the SE Asian Tethysides that is overthrust westwards by the Cretaceous and Cenozoic ophiolites of the Philippine Mobile Belt (Rangin, 1991). We refer to Advokaat and Van Hinsbergen (2023) for a detailed review of the SE Asian Tethysides and its tectonic reconstruction since the Mesozoic, which we incorporate into our model.

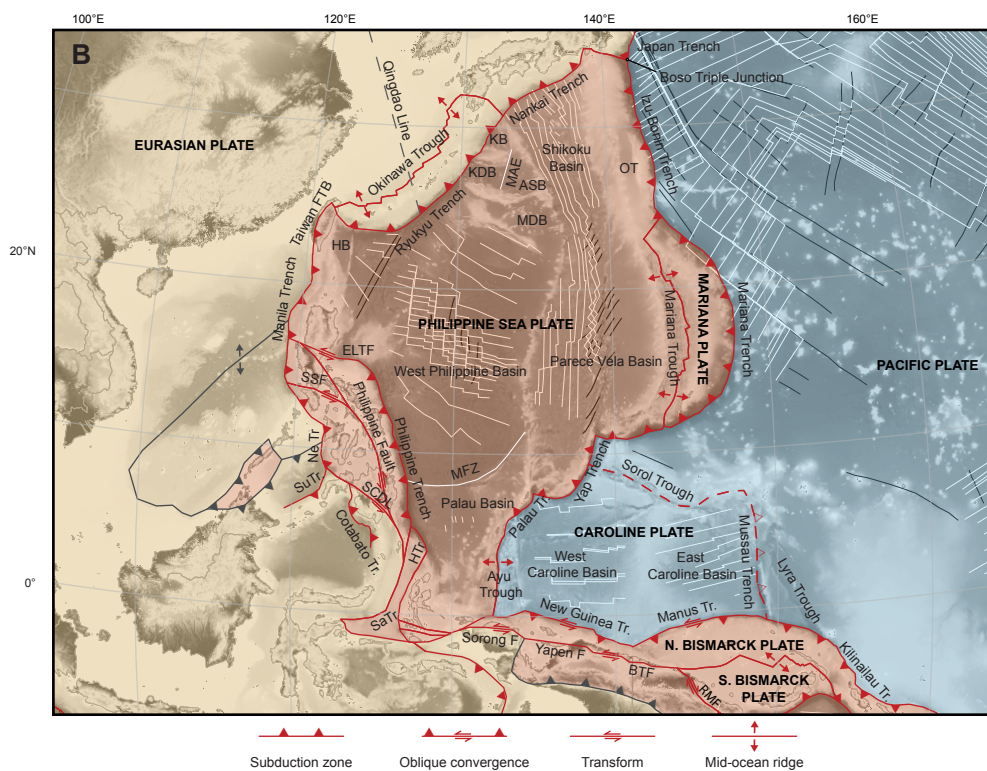
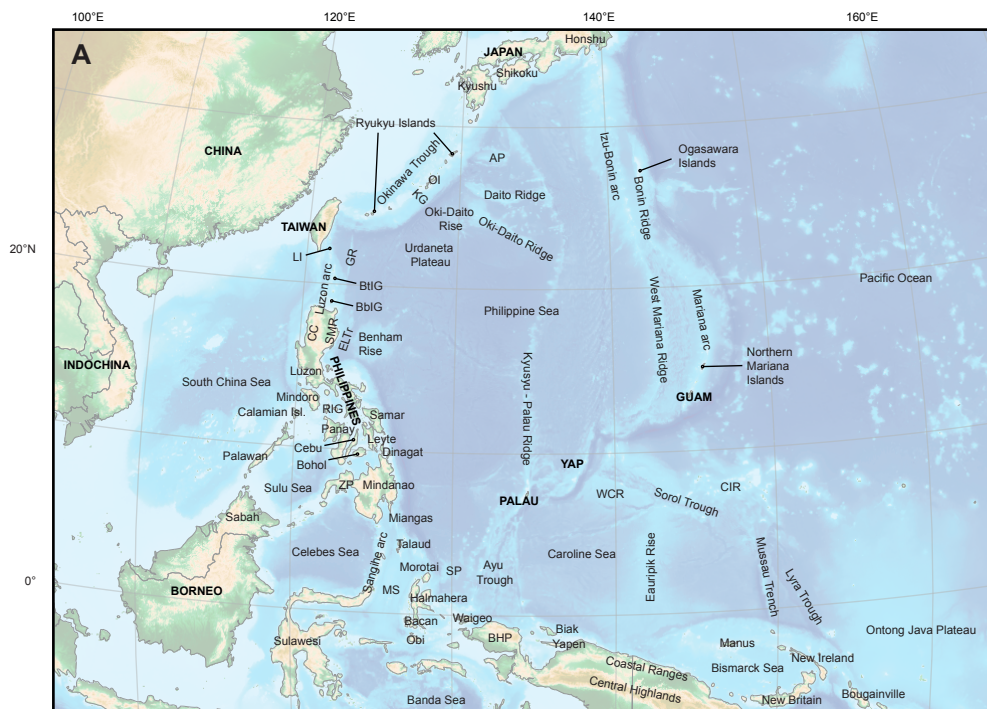
The northernmost basin of this region is the South China Sea, which is an uppermost Eocene to middle Miocene oceanic basin that formed after an Eocene phase of rifting that separated a Cretaceous and older accretionary prism from the South China Block (Faure and Ishida, 1990; Briaud et al. 1993, C. Li et al., 2014; Cao et al., 2021). The opening of the South China Sea basin occurred while Borneo was converging with South China (Advokaat et al., 2018), which was accommodated by southward subduction of a Cretaceous lithosphere that became trapped between Borneo and South China in the Late Cretaceous: the so-called proto-South China Sea (Chapter 4). On Palawan, this subduction zone was associated with the formation of a supra-subduction zone ophiolite (the Central Palawan Ophiolite; Figure 5) of which a plagiogranite was dated to 40.0 ± 0.5 Ma using U-Pb zircon geochronology (Dycoco et al., 2021) and basaltic flows were dated to 43.8 ± 2.2 Ma using K-Ar whole-rock dating (Fuller et al., 1991). $^{40}\text{Ar}/^{39}\text{Ar}$ and U-Pb dating of the metamorphic sole associated with the ophiolite yielded ages of c. 34 Ma (Schlüter et al., 1996; Aurelio et al., 2014; Keenan et al., 2016; Dycoco et al., 2021). The Central Palawan Ophiolite overlies an

accretionary prism that contains OPS of Cretaceous (c. 100 Ma) ocean island basalt (OIB) and island arc basalts (IAT), referred to as the Southern Palawan or Calatungas Ophiolite (Figure 5; Almasco et al., 2000; Aurelio et al., 2014; Dycoco et al., 2021) and a fragment of the Cretaceous accretionary prism that rifted off the South China margin, known as the Palawan Continental Terrane (Rangin, 1991; Zamoras and Matusoka, 2001, 2004; Aurelio et al., 2014; Shao et al., 2017; Cao et al., 2021; Advokaat and Van Hinsbergen, 2023).

The Palawan ophiolites are to the north of the Cagayan arc, and likely formed in its forearc (Advokaat and Van Hinsbergen, 2023). The Cagayan arc is a mostly submerged magmatic arc that formed on continental basement correlated to the SW Borneo mega-unit, that is thought to have broken off Australia in the early-mid Mesozoic (Advokaat and Van Hinsbergen, 2023, and references therein). The arc was active in Oligocene to Miocene time during and likely related to the subduction of the Proto-South China Sea lithosphere during the opening of the South China Sea (Bellon and Rangin, 1991; Silver and Rangin, 1991; Hutchison et al., 2000). The Cagayan arc and its underlying continental basement share a passive margin with the Sulu Sea oceanic basin to the south, a Miocene (~24-10 Ma) back-arc basin that formed by N-S extension behind the Cagayan arc (Roeser, 1991; Schlüter et al., 1996). The Sulu Sea ocean floor becomes younger southward, towards the Sulu Trench where a well-developed accretionary prism separates the Sulu Sea ocean floor from the Sulu arc, which is built on continental crust to the south (Schlüter et al., 1996; Advokaat and Van Hinsbergen, 2023, and references therein). The conjugate of the sea floor of the Sulu Sea is interpreted to have subducted at the Sulu Trench (Roeser, 1991). To the east, the Sulu Sea subducts eastward below the Philippine Mobile Belt along the Negros Trench (Figure 3).

The Sulu arc is built on continental crust that is also thought to correlate to the SW Borneo Mega-Unit (Advokaat and Van Hinsbergen, 2023). The available ages from the Sulu arc give Miocene-Pliocene ages, ~18-3 Ma, and stratigraphic ages indicate volcanism may have started in the late Oligocene (Bergman et al., 2000; Rangin et al., 1990). To the south, the Sulu arc shares a passive margin with the Eocene Celebes Sea oceanic basin. Oceanic crust of the Celebes Sea basin is being subducted towards the east below southwestern Mindanao at the Cotabato Trench (Figure 3). The Celebes Sea is underlain by oceanic crust with magnetic anomalies that young southward to the North Sulawesi Trench and were interpreted to have 46-36 Ma ages (Weissel, 1980; Beiersdorf et al., 1997; Gaina and Müller 2007). The conjugate seafloor to the south is likely represented by ophiolites that are exposed on eastern and southeastern Sulawesi and that underlie the volcanic arc of the Sulawesi North Arm (Monnier et al., 1995; Advokaat et al., 2017). The ophiolites are underlain by units accreted from northward subducted Australian plate-derived oceanic and continental units (Advokaat and Van Hinsbergen, 2023, and references therein). The North Sulawesi Trench formed at approximately 8.5 Ma (Smith et al., 1990; Nichols and Hall, 1999) and may have reactivated the former spreading ridge of the Celebes Sea (Advokaat and Van Hinsbergen, 2023).

The most important events in the kinematic reconstruction of the SE Asian Tethysides for the Junction Region occurred prior to the Late Cretaceous, when the SW Borneo Block and associated continental fragments were converging with Eurasia and diverging from Australia, and since the Eocene, when the SE Asian tectonic collage was deformed, oceanic back-arc basins opened, and the South China Sea formed (See Advokaat and Van Hinsbergen for details). During the Eocene, at c. 45 Ma, the northward motion of the Australian Plate accelerated which resulted in the interaction between the Australian Plate and southern Sundaland resulting in large-scale counterclockwise rotation of Borneo in the Eocene and Miocene (Advokaat et al., 2018). This rotation caused convergence between Borneo and South China that led to subduction of the proto-South China Sea below northern Borneo and the Cagayan arc, while the South China Sea opened in its wake (Rangin et al., 1990; Rangin and Silver, 1991; Hinz et al., 1994; Lee and Lawver 1994, 1995; Hall 1996, 2002; Hall and Breitfeld, 2017). In the Mesozoic, the proto-South China Sea region is thought to have been occupied by a paleo-Pacific Plate that subducted northwards, westwards, and southwards below the South China, Indochina, and northern Borneo margins (e.g., Jahn et al., 1990; Lapiere et al., 1997; Hall and Breitfeld, 2017; Nong et al., 2021). Evidence for this subduction zone is formed by arcs and accretionary prisms. Such prisms formed during the Jurassic to Late Cretaceous (~85 Ma) in a northwest dipping subduction zone below South China, exposed in Taiwan and on Palawan and the Calamian Islands (Zamoras and Matsuoka, 2001, 2004; Yui et al., 2012). In addition, evidence for extensive continental arc magmatism is found in South China, Vietnam, and SW Borneo (e.g., Li et al., 2012; Liu et al., 2020; Nong et al., 2022; Breitfeld et al., 2017; Batara and Xu, 2022). Mesozoic subduction of the paleo-Pacific Plate is thought to have ceased around 85 Ma, based on the end of magmatism (Breitfeld et al., 2017; Liu et al., 2020; Nong et al., 2022; Qian et al., 2022), and the widespread deposition of upper Cretaceous-Eocene synrift sediments (Shao et al., 2017; Breitfeld et al., 2018; Conand et al., 2020; Cao et al., 2021, 2023). Subduction continued below Japan (e.g., Isozaki et al., 1990; Vaes et al., 2019; Boschman et al., 2021a, b; Wu et al., 2022) and the boundary between the ongoing and ceased subduction is the so-called Qingdao Line (Wu et al., 2022). The Qingdao line represents the location of a hypothesized plate boundary that was located between the northern and southern Ryukyu islands (around the Kerama Gap; Figure 3) that separated ongoing Panthalassa oceanic plate subduction to the east from a Proto-South China Sea surrounded by passive margins to the west during the late Mesozoic and Early Cenozoic (Wu et al., 2022). It has been suggested that the end of subduction in the proto-South China Sea embayment was related to the arrival of an oceanic plateau in the subduction zone (e.g., Xu et al., 2022; Chapter 4), after which relative motion between Pacific realm plates and Eurasia must have been accommodated at a plate boundary to the east of the Proto-South China Sea, from the Qingdao Line southwards.



◀ **Figure 3.** Geographic (A) and tectonic (B) maps of the Philippine Sea Plate region. Present-day plate boundaries are red (modified from Bird, 2003), relevant former plate boundaries are gray. Marine magnetic anomalies are indicated by white lines, fracture zones are indicated by black lines (both based on the GSFML database, Matthews et al., 2011; Seton et al., 2014; Wessel et al., 2015, and references therein). AP = Amami Plateau; ASB = Amami-Sankaku Basin; BbIG = Babuyan Island Group; BHP = Bird's Head Peninsula; BTF = Bewani-Torricelli Fault; BtIG = Batan Island Group; CC = Central Cordillera; CIR = Caroline Islands Ridge; ELTF = East Luzon Transform Fault; ELTr = East Luzon Trench; GR = Gagua Ridge; HTr = Halmahera Trench; HB = Huatung Basin; KB = Kikai Basin; KDB = Kita-Daito Basin; KG = Kerama Gap; LI = Lanyu Island; MAE = Minami-Amami Escarpment; MDB = Minami-Daito Basin; MS = Molucca Sea; Ne Tr = Negros Trench; OI = Okinawa Island; OT = Ogasawara Trough; RIG = Romblon Island Group; RMF = Ramu-Markham Fault; Sa Tr = Sangihe Trench; SCDL = Sindangan-Cotabato-Daguma Linemaent; SMR = Sierra Madre Range; SP = Snellius Plateau; SSF = Sibuyan Sea Fault; Su Tr = Sulu Trench; WCR = West Caroline Rise; ZP = Zamboanga Peninsula.

3.2.2. SW Pacific extensional basins

The northeastern and eastern Australian margin is deformed by extensional basins resulting in a mostly submerged mosaic of basins and rises that consist of continental fragments separated from Australia, as well as fragments of arc and LIP crust (Figure 4). Below the Coral Sea are several oceanic plateaus separated by basins. The largest of these basins is the Coral Sea Basin, where oceanic spreading was active between 62.5 and 52.9 Ma, during polarity chrons C27-C24 (Gaina et al., 1999). Opening of the Coral Sea Basin led to the separation of the Papuan and Eastern plateaus from northeastern Australia (Figure 4). This opening may have been related to opening of the Tasman Sea to the south, where oceanic spreading had been propagating northwards since c. 84 Ma, after rifting had started c. 95 Ma (Gaina et al., 1998; Grobys et al., 2008). Opening of these basins separated various plateaus from the Australian margin, including the Eastern, Papuan, Louisiade, and Kenn plateaus and the Lord Howe, Pocklington, and Mellish rises (Gaina et al., 1999; Collot et al., 2012; Van den Broek and Gaina, 2020; Mortimer et al., 2017) (Figure 4).

The difference in spreading direction between the N-S opening Coral Sea and the E-W opening Tasman Sea was accommodated by extension, crustal thinning, and in places formation of oceanic crust in the northeastern part of the system. Short-lived oceanic spreading occurred in the Louisiade Trough between the Louisiade Plateau and Mellish Rise between 62.5 and 59 Ma (Gaina et al., 1999). The northeast Australian margin also contains evidence for even older extension: the Queensland Plateau, between the Coral Sea and Australia, rifted off Australia in the Cretaceous or possibly the Late Jurassic, accommodated by extension in the Townsville Basin (Falvey and Taylor, 1974; Struckmeyer and Symonds, 1996).

To the east of the Louisiade Plateau and Mellish Rise is an additional set of rises and troughs. The nature of the bathymetric highs is mostly unknown. The Rennell Ridge, West Torres Plateau, and Lapérouse rises (Figure 4) have been interpreted as continental fragments, remnant island arcs, oceanic crust, or LIPs (Landmesser et al., 1973; Weissel and

Watts, 1979; Yan and Kroenke, 1993; Schellart et al., 2006; Seton et al., 2016). Seton et al. (2016) obtained an $40\text{Ar}/39\text{Ar}$ ages of 42.8 ± 1.2 Ma from a dredged basalt sample from the Rennell Ridge, with an E-MORB geochemical signature. In addition, a low-quality 38 ± 5 Ma $40\text{Ar}/39\text{Ar}$ age was obtained from a primitive arc tholeiitic basalt sample dredged from the western margin of the Rennell Ridge (Mortimer et al., 2014b). Dredged basalt from the western margin of the West Torres Plateau had N-MORB geochemistry and a 26.2 ± 0.8 Ma $40\text{Ar}/39\text{Ar}$ age and a dredged basalt from the East Lapérouse Rise yielded a 39.1 ± 1.2 Ma $40\text{Ar}/39\text{Ar}$ age with E-MORB geochemistry (Seton et al., 2016).

The Rennell Ridge is separated from the Louisiade Plateau by the Rennell Basin. Direct age constraints for the Rennell Basin are lacking, but an Eocene to Miocene age was inferred from seismic reflection lines (Récy et al., 1977). Additionally, based on the structure of the basin, it was suggested that the basin formed an east-dipping trench of a subduction zone below the Rennell Ridge (Récy et al., 1977; Weissel and Watts, 1979).

The West Torres Plateau is separated from the Rennell Ridge by the Santa Cruz Basin (Figure 4). Seton et al. (2016) identified marine magnetic anomalies C20-C13 (43.5 – 33.7 Ma) in the Santa Cruz Basin. They infer that the basin opened between 48 and 28 Ma, based on the possible existence of marine magnetic anomaly C21 (47.8 Ma). The end of spreading is based on 29.3 ± 1.6 Ma and 28 ± 3 Ma $40\text{Ar}/39\text{Ar}$ plagioclase ages of dredged basalts from the ridge crest of the South Rennell Trough (Mortimer et al., 2014b), which is interpreted as the southern continuation of the Santa Cruz Basin spreading center (Seton et al., 2016). Based on this interpretation, spreading in the South Rennell Trough was also active between c. 48 and 28 Ma (Mortimer et al., 2014b; Seton et al., 2016). The South Rennell Trough is flanked by the West and East Lapérouse rises (Figure 4), and their elevated nature is thought to be the result of the interplay between magma supply and extension (Seton et al., 2016).

The East Lapérouse Rise and Lord Howe Rise are separated from the West Torres Plateau by the D'Entrecasteaux Basin. The age and geochemistry of the oceanic crust that underlies

Figure 4 ►. Geographic (A) and tectonic (B) maps of the Melanesian – SW Pacific region. Present-day plate boundaries in red (modified from Bird, 2003), relevant former plate boundaries in gray. Marine magnetic anomalies are indicated by white lines, fracture zones are indicated by black lines (both based on the GSFML database, Matthews et al., 2011; Seton et al., 2014; Wessel et al., 2015, and references therein). AR = Adelbert Range; BTF = Bewani-Torricelli Fault; BTPA = Bewani-Torricelli-Prince Alexander Mountains; BHP = Bird's Head Peninsula; DEB = D'Entrecasteaux Basin; DEI = D'Entrecasteaux Islands; DER = D'Entrecasteaux Ridge; DI = Deboyne Islands; ELR = East Laperouse Rise; East. Pl. = Eastern Plateau; FinR = Finisterre Range; Foja R = Foja Range; Guad. = Guadalcanal; HFZ = Hunter Fracture Zone; LA = Louisiade Archipelago; LP = Louisiade Plateau; LT = Louisiade Trough; MR = Mellish Rise; Mi = Misima Island; Mu = Muyua/Woodlark Island; NB Tr = New Britain Trench; NGG = New Georgia Group; NLB = North Loyalty Basin; OSF = Owen-Stanley Fault; Pap. Pl. = Papuan Plateau; PI = Pentecost Island; PR = Pocklington Rise; RMF = Ramu-Markham Fault; RB = Rennell Basin; RIR = Rennell Islands Ridge; SCB = Santa Cruz Basin; SoS = Solomon Sea; SF = Sorong Fault; SRT = South Rennell Trough; TrS = Trobriand Scarp; WLR = West Laperouse Rise; WTP = West Torres Plateau; WP = Woodlark Plate; YF = Yapen Fault.

CHAPTER 6



the D'Entrecasteaux Basin remains unknown. Lapouille (1982) interpreted Cretaceous marine magnetic anomalies, but this interpretation was rejected by Seton et al. (2016), as the interpreted anomalies cross-cut structural trends of the basin. No new interpretation of anomalies was made due to the lack of continuity of magnetic anomaly patterns between magnetic profiles. Instead, Seton et al. (2016) suggested that the D'Entrecasteaux Basin formed as part of the South Loyalty Basin, which is a hypothesized Cretaceous oceanic basin that was lost to subduction at the New Caledonia subduction zone in the Eocene-Oligocene (e.g., Cluzel et al., 2001).

To the east of the Lord Howe Rise are an additional set of ridges separated by oceanic basins (Figure 4). The tectonic history of these basins was reviewed and reconstructed by Chapter 1, and we incorporate their reconstruction with updates of Chapters 2 and 3 into our model. We here briefly summarize the formation history of these basins.

To the east of the Lord Howe Rise is the New Caledonia-Fairway-Aotea basin, which separates the Norfolk Ridge from the Lord Howe Rise (Figure 4). The Norfolk Ridge forms the easternmost part of Zealandia (Mortimer et al., 2017) and consists of Late Mesozoic and older accretionary complexes overlain by foreland basin clastics that can be traced into New Zealand and New Caledonia (Mortimer et al., 1998; Cluzel et al., 2012a; Maurizot et al., 2020b). The age of opening of the New Caledonia-Fairway-Aotea basin remains uncertain (e.g., Lafoy et al., 2005; Collot et al., 2009), but it likely opened in tandem with the Tasman Sea, between 85 and 56 Ma (Lafoy et al., 2005; Chapter 1).

East of the Norfolk Ridge is the Norfolk Basin. Due to the absence of marine magnetic anomalies, the age of the oceanic crust has been debated (Launay et al., 1982; Mortimer et al., 1998; Sdrolias et al., 2003), but a late Oligocene to late Miocene age of formation was inferred from a 23 ± 0.1 Ma $^{40}\text{Ar}/^{39}\text{Ar}$ age of a dredged seafloor tholeiite (Sdrolias et al., 2003). The opening direction of the Norfolk Basin is constrained by the Cook and Vening Meinesz fracture zones (Figure 4), which form the northern and southern limits of the basin (Herzer and Mascle, 1996; Sdrolias et al., 2004a). The Norfolk Basin is bounded in the east by the Three Kings Ridge, which is offset from the Loyalty Ridge by the Cook Fracture Zone. The Three Kings Ridge is interpreted as a remnant volcanic arc that formed during the Eocene-Oligocene above the east-dipping New Caledonia subduction zone (Kroenke and Eade, 1982; Whattam et al., 2006, 2008).

To the east of the Three Kings Ridge is the South Fiji Basin (Figure 4). This basin formed in the Oligocene-Miocene as a back-arc basin above the Tonga-Kermadec subduction zone (e.g., Sdrolias et al., 2003). The age of formation of the basin is constrained by marine magnetic anomalies, but different interpretations have been suggested (Watts et al., 1977; Malahoff et al., 1982; Sdrolias et al., 2003; Mortimer et al., 2007). Using additional age constraints obtained from $^{40}\text{Ar}/^{39}\text{Ar}$ dating, which yielded ages between 19.3 and 25.9 Ma, Mortimer et al. (2007) suggested that the marine magnetic anomalies formed during chrons C9 and C6B (27.4–21.9 Ma), which is younger than previous interpretations. Spreading in the South Fiji Basin is thought to have ceased around 15 Ma (Mortimer et al., 2007; Herzer

et al., 2009, 2011).

The South Fiji Basin is bounded in the east by the Lau-Colville Ridge (Figure 4), which formed part of the active arc above the Tonga-Kermadec subduction zone, until the arc split around 7 Ma when the Lau Basin and Havre Trough started opening (Ruellan et al., 2003; Yan and Kroenke, 1993). The Lau Basin-Havre Trough system is the currently active back-arc basin above the Tonga-Kermadec subduction zone, where westward subduction of the Pacific Plate is accommodated since the Eocene or Oligocene (Seton et al., 2012; Sutherland et al., 2017; Chapter 1; Appendix 2).

3.3. Junction Region oceanic domain

3.3.1. Philippine Sea Plate

The Philippine Sea Plate is an oceanic plate mostly surrounded by subduction zones, whose oceanic crust formed at multiple spreading ridges since the Cretaceous (Figure 6; Hilde and Lee, 1984; Deschamps and Lallemand, 2002; Yamazaki et al., 2003; Sdrolias et al., 2004b; Hickey-Vargas et al., 2013). In the east, the Philippine Sea Plate is in an upper plate position relative to the Pacific Plate that is subducting along the Izu-Bonin-Mariana Trench (Figures 2 and 6). The well-studied forearc above the Izu-Bonin-Mariana subduction zone reveals a magmatic stratigraphy with geochemical compositions ranging from MORB-like to arc-like that is widely interpreted as the product of catastrophic extension associated with foundering of the nascent slab shortly after Pacific subduction initiation below Izu-Bonin-Mariana (Stern and Bloomer, 1992; Stern, 2004; Stern et al., 2012). The oldest age of this sequence is dated at ~52 Ma (Ishizuka et al., 2011a; Reagan et al., 2013, 2019), which is often interpreted as the age of inception of subduction at the Izu-Bonin-Mariana trench (Stern et al., 2012; Arculus et al., 2015), although examples elsewhere showed that similar catastrophic extension may postdate incipient subduction by some 10 Ma (Guilmette et al., 2018).

To the west of the Izu-Bonin-Mariana trench lies the Izu-Bonin-Mariana magmatic arc. This arc is in places emergent and exposes a stratigraphy that goes back to the Eocene (e.g., on Guam and the Ogasawara Islands; Meijer et al., 1983; Reagan et al., 2008; Ishizuka et al., 2006). To the west of the active arc are remnant arcs that form submarine ridges and that are separated from the active arc by back-arc basins. Upper plate extension in the Izu-Bonin segment in the north is restricted to the Ogasawara Trough (Nishimura, 2011). This basin separates the Bonin Ridge, an uplifted section of the forearc, from the currently active Izu-Bonin arc (Figure 3). Based on the interpretation that volcanoclastics, dredged from the eastern slope of the Ogasawara Trough, were deposited before a c. 44-42 Ma episode of volcanism, Ishizuka et al. (2006) suggested that the Ogasawara Trough opened during the Eocene, as a narrow back-arc basin behind the Izu-Bonin-Mariana subduction zone. To the south, however, the Mariana Trough is an active back-arc basin that separates the West Mariana Ridge, a remnant arc, from the active Mariana arc (Figure 3). The Mariana Trough has been opening since magnetic anomaly chron C3 (~5 Ma) that was identified

in the northern half of the basin (Yamazaki et al., 2003), consistent with the youngest volcanic rocks known from the West Mariana Ridge remnant arc, which are 6–4 Ma based on biostratigraphy and $^{40}\text{Ar}/^{39}\text{Ar}$ whole-rock ages of dredged basalts (Karig, 1971; Kroenke et al., 1981; Ishizuka et al., 2010).

To the west of the West Mariana Ridge and Izu-Bonin arc are the Oligocene to Miocene Shikoku and Parece Vela basins (Figure 3). These basins separate the more recent Izu-Bonin and Mariana arcs from the Kyushu-Palau Ridge to the west, which forms another remnant arc (Figure 3). Sdrolias et al. (2004b) identified a conjugate set of marine magnetic anomalies in the Shikoku Basin mirrored in a mid-basin high that is interpreted as an extinct spreading ridge. These were interpreted in combination with radiometric ages of dredge samples as C7–C5B (24–15 Ma) (Sdrolias et al., 2004b). In the western portion of the Parece Vela Basin, marine magnetic anomalies interpreted as C9–C5D (27–15 Ma) were identified (Sdrolias et al., 2004b). Magnetic anomalies were not identified elsewhere in this basin, but clear fracture zones provide additional constraints for reconstructing its opening. These fracture zones are S-shaped and reflect a change in spreading direction within the basin from E–W to NE–SW (Figure 3; Sdrolias et al., 2004b). A 15.6 ± 0.1 Ma $^{40}\text{Ar}/^{39}\text{Ar}$ whole-rock age was obtained from a basalt lava that was dredged from the Parece Vela extinct ridge (Ishizuka et al., 2010), providing a constraint for the end of spreading.

In the south, the extinct mid-ocean ridge of the Parece Vela basin is continuous with the Yap Trench (Figure 3). To the west of the Yap Trench lies oceanic crust that is contiguous with the western Parece Vela Basin, younging eastwards towards the Yap Trench (Sdrolias et al., 2004b). There is currently no active volcanism and little seismicity at the Yap trench (Sato et al., 1997). The basement of Yap Island consists of a metamorphic igneous complex of greenschist to amphibolite-facies rocks (Shiraki, 1971; Hawkins and Batiza, 1977). Ages of metamorphism were obtained from dredged greenschists and amphibolites from south of the Yap Islands, which returned a titanite U–Pb weighted mean age of 21.4 ± 0.9 Ma and $^{40}\text{Ar}/^{39}\text{Ar}$ amphibole ages of 20.7 ± 0.1 Ma and 22.0 ± 2.1 Ma (Zhang and Zhang, 2020). Based on geochemistry, the protoliths of the metamorphic rocks are interpreted to be of fore-arc basin basalt, ocean island basalt, and island-arc tholeiite affinity, but the age of the protolith remains unknown (Zhang and Zhang, 2020). The metamorphic complex is underthrust by Miocene mélangé, which contains fragments of these metamorphic rocks as well as other volcanic and sedimentary rocks of unknown age (Shiraki, 1971; Rytuba and Miller, 1990). The metamorphic complex and mélangé are both overlain by Miocene andesitic lava flows and tuffs, which is the youngest volcanism on the Yap Islands (Shiraki, 1971; Rytuba and Miller, 1990). Collectively, these data show that contractional deformation, burial, and metamorphism at the Yap Trench must have been underway by ~ 21 Ma, i.e., while the Parece Vela Ridge to the north was still active. This suggests that during the opening of the Parece Vela basin in the north, the southern part was compressed, and the back-arc ridge inverted into a subduction zone that consumed the eastern forearc plate.

Plate tectonic cross-roads: Reconstructing the Panthalassa-Neotethys Junction Region
from Philippine Sea Plate and Australasian oceans and orogens

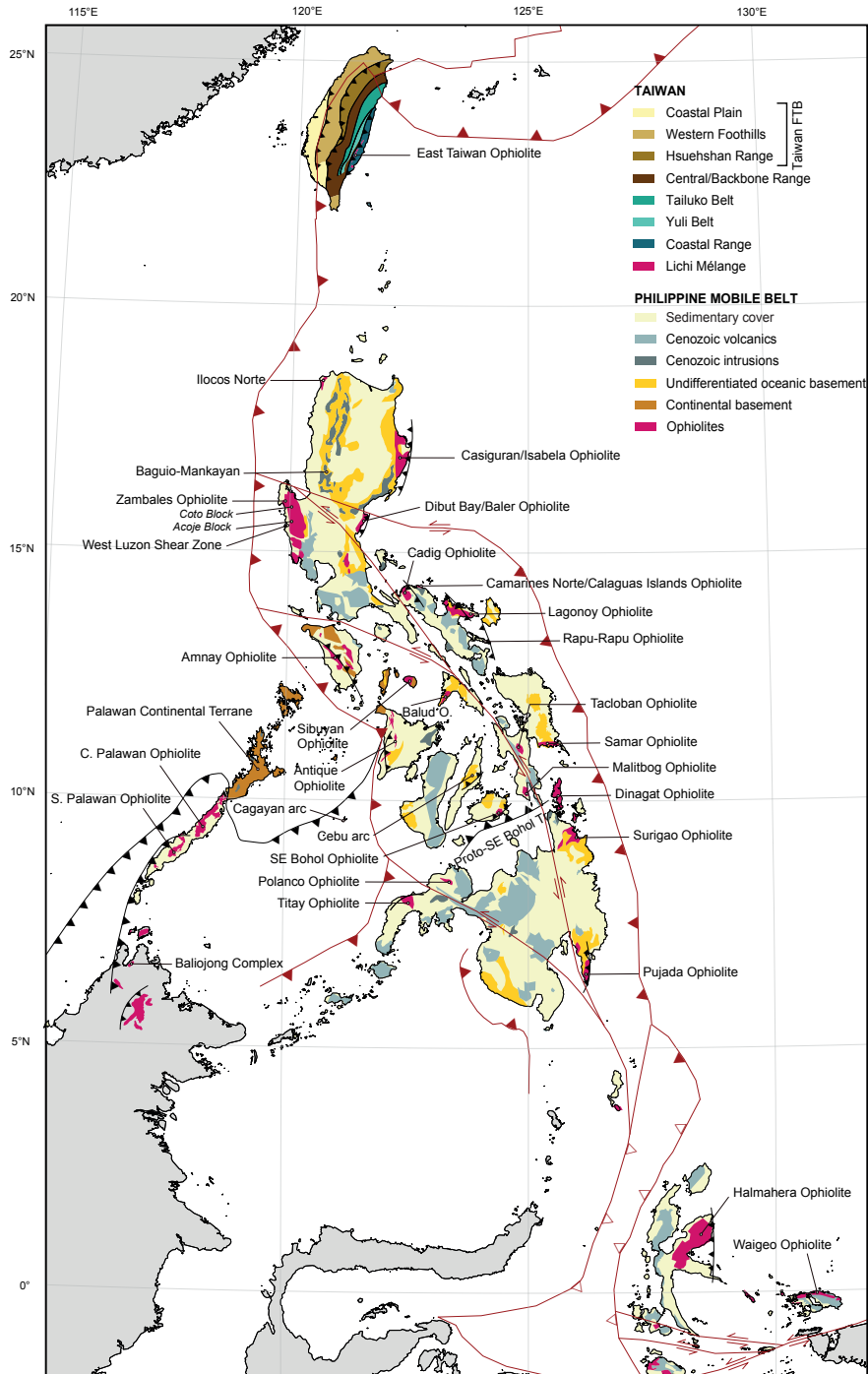


Figure 5. Geological map of Taiwan, the Philippines, and the northern Molucca Islands. Based on Ren et al. (2003). FTB = Fold-and-Thrust Belt.

The western boundary of the Shikoku and Parece Vela basins is the Kyushu-Palau Ridge, another remnant arc built on lithosphere of the eastern West Philippine Basin (Figure 3). Radiometric dating based on an extensive suite of $^{40}\text{Ar}/^{39}\text{Ar}$ ages of dredged and drilled samples along the length of the ridge shows that it was active from at least 48 to about 25 Ma (Ishizuka et al. 2011b), after which the Shikoku and Parece Vela Basins started opening. The southernmost extension of the Kyushu-Palau Ridge forms the Palau arc, immediately west of the Palau Trench. The arc is not associated with active volcanism, and subduction seismicity is shallow and weak (Kobayashi et al., 1997). The Palau Islands consist mostly of basalt and andesite lavas, flow breccias, and tuffs overlain by Mio-Pliocene lignite and limestones (Meijer et al., 1983; Rytuba and Miller, 1990; Hawkins and Ishizuka, 2009). Reported K-Ar whole-rock ages are mostly in the range of 30–34 Ma (Meijer et al., 1983; Cosca et al., 1998), with the oldest reliable K-Ar whole-rock age being 37.7 ± 3.1 Ma (Haston et al., 1988). A late Eocene age was also assigned based on foraminifera and nannofossils in interbedded tuffaceous marls and limestones (Cole, 1950; Meijer et al., 1983). The youngest age derived from volcanic rocks is a K-Ar whole-rock age of 20.1 ± 0.5 Ma (Meijer et al., 1983).

To the west of the Kyushu-Palau Ridge is the West Philippine Basin, the largest of the Philippine Sea Plate basins (Figure 3). Marine magnetic anomalies interpreted to have formed during polarity chrons C26 to C13 (~59–34 Ma) were identified by Hilde and Lee (1984). Deschamps and Lallemand (2002) revised the model for the oldest part of the basin based on improved bathymetric data and suggest spreading started at c. 54 Ma instead. Based on new marine magnetic anomaly interpretations, Sasaki et al. (2014) suggested that spreading in the basin already ceased around 36 Ma, and that formation of oceanic crust during the initial stages of the basin (south of anomaly C21; 48 Ma) was disorganized, which resulted in a lack of formation of clear marine magnetic anomalies. Nonetheless, the onset of spreading of the West Philippine Basin is likely older than, and spreading occurred more or less perpendicular to, the rapid extension of the Izu-Bonin-Mariana forearc and the associated formation of boninites at 52 Ma (Ishizuka et al., 2011a; Reagan et al., 2013, 2019).

Oceanic crust of the West Philippine Basin is overlain by the Benham Rise, Urdaneta Plateau and the Oki-Daito Rise. The Benham Rise and Urdaneta Plateau are located south and north of the extinct West Philippine Basin spreading center, roughly at equal distance. The Oki-Daito Rise is located north of the Urdaneta Plateau. $^{40}\text{Ar}/^{39}\text{Ar}$ dating yielded ages of 35.6 ± 0.4 Ma and 36.2 ± 0.5 Ma from the Benham Rise (Hickey-Vargas, 1998), and an average of 37.9 ± 0.1 Ma from the Urdaneta Plateau (Ishizuka et al., 2013). An older age of 40.5–44.4 Ma was obtained from the Oki-Daito Rise, which is further away from the extinct spreading ridge, north of the Urdaneta Plateau (Ishizuka et al., 2013). All three plateaus have OIB-like geochemistry, and based on this and the age progression, it was suggested that a mantle plume (referred to as the Oki-Daito Plume) triggered opening of the West Philippine Basin and that the West Philippine Basin spreading center remained fixed on the plume for about 10 Ma (Ishizuka et al., 2013). Similarly, Wu et al. (2016) suggested that

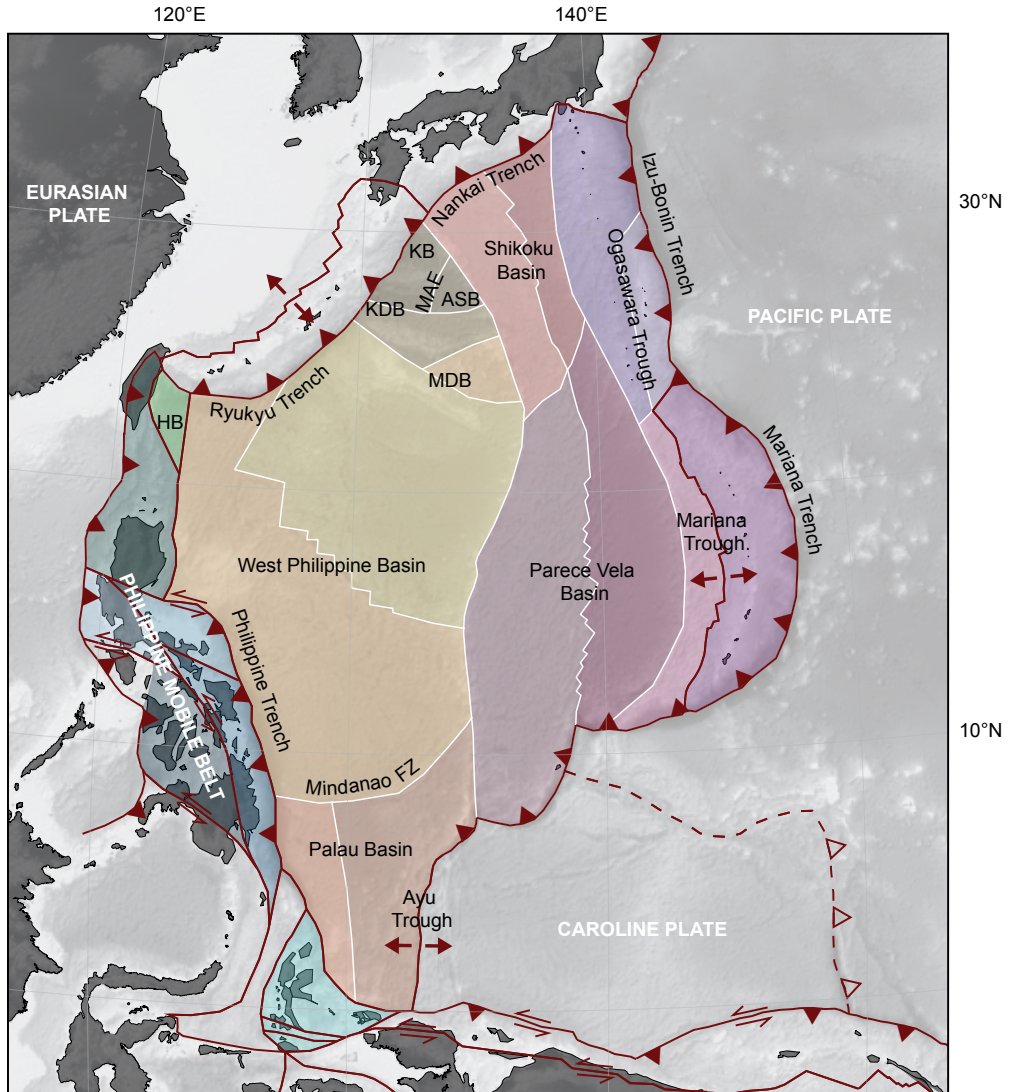


Figure 6. Tectonic map of the Philippine Sea Plate, highlighting the different microplates that formed as a result of oceanic spreading at different spreading centers. Present-day plate boundaries are red (modified from Bird, 2003), former plate boundaries are white. KB = Kikai Basin; KDB = Kita-Daito Basin; MAE = Minami-Amami Escarpment; ASB = Amami-Sankaku Basin; MDB = Minami-Daito Basin; HB = Huatung Basin.

the Cenozoic Philippine Sea Plate nucleated above the Manus Plume and as Ishizuka et al. (2013) do not link the Oki-Daito Plume to a mantle structure, their Oki-Daito Plume may reflect the Manus Plume.

To the north of the West Philippine Basin is a series of E-W trending ridges separated by basins. These are, from south to north, the Oki-Daito Ridge (which is different from the Oki-Daito Rise), the Minami-Daito Basin, the Daito Ridge, the Kita-Daito Basin, the Amami Plateau, and the Kikai Basin. The Amami Plateau and the Kita-Daito Basin are bound to the east by the Minami-Amami Escarpment that separates them from the Amami-Sankaku Basin (Figure 3). The age of the basement of southernmost ridge, the Oki-Daito Ridge, remains unknown, but dredged volcanics overlying the ridge yielded 40.5 ± 0.3 – 48.4 ± 0.1 $^{40}\text{Ar}/^{39}\text{Ar}$ whole-rock ages (Ishizuka et al., 2013). Dredged and drilled basalt samples showed that the Daito Ridge contains andesites, which yielded much older, 116.9–118.9 Ma $^{40}\text{Ar}/^{39}\text{Ar}$ ages (Ishizuka et al., 2011b). Eocene $^{40}\text{Ar}/^{39}\text{Ar}$ ages from the Daito Ridge were obtained by Hickey-Vargas et al. (2013), with a 49.3 ± 0.5 plagioclase age obtained from a basalt clast and ages between 44.7 and 48.0 of hornblende and biotite from volcanoclastic sediments. Basalts and tonalites dredged from the Amami Plateau, again gave Cretaceous, 115.8–117.0 Ma $^{40}\text{Ar}/^{39}\text{Ar}$ ages (Hickey-Vargas, 2005). Based on their geochemical signature, the Amami Plateau and Daito Ridge are interpreted as extinct Mesozoic arc remnants (Hickey-Vargas, 2005; Ishizuka et al., 2011b, 2022; Hickey-Vargas et al., 2013; Morishita et al., 2018). Even though the oldest volcanics and sediments recovered from the Oki-Daito Ridge are of Eocene age, based on a similar stratigraphy, it was inferred that the Oki-Daito Ridge is also a remnant Mesozoic arc (Ishizuka et al., 2022).

Dredged and drilled OIB-like basalt samples yielding 51.3–42.8 $^{40}\text{Ar}/^{39}\text{Ar}$ ages were recovered from the Minami-Daito Basin (Hickey-Vargas, 1998; Ishizuka et al., 2013). 45.8–41.0 Ma $^{40}\text{Ar}/^{39}\text{Ar}$ and 43 Ma U–Pb zircon ages were reported from andesites recovered from the Kita-Daito Basin (Ishizuka et al., 2022). Similar $^{40}\text{Ar}/^{39}\text{Ar}$ whole-rock ages, between 49.3 and 46.8 were obtained from drilled lava flows of the Amami-Sankaku Basin (Ishizuka et al., 2018). Collectively, these basins and ridges reveal that during the Eocene formation of the West Philippine Basin, smaller basins also formed to the north, within an oceanic lithosphere that contained ~118–116 Ma oceanic crust, or arc of that age built on even older crust. In other words, the West Philippine Basin formed by breaking oceanic lithosphere that was at least 60 Ma old at the moment of inception of extension.

In the northwest of the Philippine Sea Plate, east of Taiwan, lies the Huatung Basin, separated from the West Philippine Basin by the Gagua Ridge (Figure 3). Hilde and Lee (1984) originally interpreted marine magnetic anomalies identified in the Huatung Basin as C19 to 16 (41 – 36 Ma), younging northward, an interpretation recently repeated by Doo et al. (2015). However, Deschamps et al. (2000) showed that the ocean floor of the Huatung Basin has an Early Cretaceous age: they obtained 114.7 ± 4.0 and 124.1 ± 2.5 Ma $^{40}\text{Ar}/^{39}\text{Ar}$ ages from amphibole of dredged gabbros from the Huatung Basin. They consequently reinterpreted the anomalies as M10–M1 (130.6–123 Ma), younging towards

the south (Deschamps et al., 2000). These Early Cretaceous ages were confirmed by a mean U-Pb age of 130.3 ± 1.0 Ma obtained from 18 zircon grains from the same dredged gabbro sample (Huang et al., 2019). The Cretaceous marine magnetic anomaly ages correspond well to Lower Cretaceous (Barremian) radiolarian assemblages collected from the nearby Lanyu Island (Deschamps et al., 2000; Yeh and Cheng, 2001). The original extent of the Huatung Basin, as well as the timing of onset and cessation of spreading remains unknown, as no extinct spreading center has been identified. Much of the originally surrounding lithosphere must have been consumed by subduction, e.g., at the Ryukyu and East Luzon trenches (Deschamps et al., 2000). From the Gagua Ridge, Cretaceous lavas were recovered (Qian et al., 2021). These lavas yielded 124.06 ± 0.27 and 123.99 ± 0.24 Ma $40\text{Ar}/39\text{Ar}$ ages of plagioclase and have a subduction-related arc geochemical signature (Qian et al., 2021). The Gagua Ridge thus likely originally formed as a Cretaceous arc that was used in the Eocene to form a transform plate boundary that separated the Cretaceous Huatung Basin from the actively spreading West Philippine Basin.

The southern boundary of the West Philippine Basin is formed by the Mindanao Fracture Zone, which separates it from the southern part of the Philippine Sea Plate known as the Palau Basin (Figure 3). In this basin, Sasaki et al. (2014) identified short segments of N-S trending marine magnetic anomalies, roughly perpendicular to the anomalies of the West Philippine Basin. These anomalies were tentatively interpreted as the eastern flank of a spreading center that formed during chrons C18-C15 (40-35 Ma) (Sasaki et al., 2014). The correlation is based on a 40.4 Ma $40\text{Ar}/39\text{Ar}$ age of a dolerite sample from the Mindanao Fracture Zone, located north of the magnetic survey lines (Sasaki et al., 2014; Ishizuka et al., 2015). This N-S trending ridge must have ended against the Mindanao Fracture Zone. In the west, oceanic crust of the Palau Basin is subducting below the Philippines, which consumed at least part of the western conjugate lithosphere of the Palau Basin. The southeastern margin of the Palau Basin is the ultra-slowly spreading Ayu Trough mid-oceanic ridge that separates the Philippine Sea Plate from the Caroline Plate and that to the north transitions to the Palau Trench in the Caroline-Philippine Sea Plate Euler pole of rotation (e.g., Weissel and Anderson, 1978; Fujiwara et al., 1995). The total amount of rotation since the formation of the Ayu Trough is estimated at $\sim 25^\circ$ based on the angle between the Ayu Trough rift margins (Figures 3 and 6). A crude estimate for the age of onset of Ayu Trough spreading is 15-25 Ma based on the sediment thickness within the basin and estimated sedimentation rates that are extrapolated from a nearby borehole (Weissel and Anderson, 1978; Fujiwara et al., 1995). K-Ar whole rock dating of dredge samples recovered from 62 km east of the Ayu Trough rift axis yielded 19.9 ± 0.7 , 20.5 ± 1.5 and 25.2 ± 1.1 Ma ages (Kumagai et al., 1996). These dredge samples are high-alkali andesites with an island arc geochemical signature (Kumagai et al., 1996), which suggest that the eastern margin of the Ayu Trough was a subduction zone at least until c. 20 Ma.

3.3.2. Caroline Plate

The Ayu Trough forms the western boundary of the Caroline Plate, separating it from the Philippine Sea Plate (Figures 3 and 6). The Caroline Plate is bounded to the Pacific Plate in the north and east by the Sorol Trough and Mussau Trench. Whether the Caroline Plate is currently moving relative to the Pacific Plate is uncertain due to its poorly understood plate boundaries and scarce kinematic data (DeMets et al., 2010). The Mussau Trench may be the site of incipient subduction of the Caroline Plate below the Pacific Plate (Hegarty et al., 1983; Gurnis et al., 2004). The southern boundary of the Caroline Plate is formed by the New Guinea and Manus trenches, which separate the Caroline Sea from the New Guinea orogen and from the Bismarck Sea basin.

The Caroline Plate hosts an eastern and a western basin, both with E-W trending marine magnetic anomalies (Gaina and Müller, 2007), separated by the Eauripik Rise (Figure 3). Gaina and Müller (2007) interpreted marine magnetic anomalies in the eastern basin as chrons C15r to C8n (c. 35-25 Ma) and in the western basin as chrons 16n to 8r (c. 36-25 Ma). While the eastern basin contains a symmetric set of anomalies, mirrored in a single extinct spreading ridge, the extinct spreading ridge in the western basin is not located in the center but well to the north. Close to this extinct spreading ridge, a conjugate set of anomalies from chron C8 is interpreted (Gaina and Müller, 2007). To the north of the extinct spreading ridge, the next anomaly is interpreted to have formed during chron C15. To the south of the extinct spreading ridge, two marine magnetic anomalies from chron C10 are interpreted, then two anomalies from chron C11, and then the southern anomaly of chron C15, which is interpreted to be the conjugate of the C15 anomaly in the north of the basin (Gaina and Müller, 2007). This marine magnetic anomaly pattern is interpreted to be the result of several ridge-jumps during opening of the western Caroline Basin (Gaina and Müller, 2007).

The Eocene-Oligocene oceanic crust of the Caroline Plate is juxtaposed in the north and east with Jurassic oceanic crust of the Pacific Plate across the Sorol Trough and Mussau Trench (Figure 3). The northern boundary between the Caroline and Pacific plates is overlain by the West Caroline Rise and Caroline Islands Ridge, collectively known as the Caroline Ridge, separated from each other by the Sorol Trough (Altis, 1999). The Caroline Ridge is interpreted as a large igneous province, with an age-progressive seamount chain to the east, on the Pacific Plate (Zhang et al., 2020). K-Ar and $^{40}\text{Ar}/^{39}\text{Ar}$ ages from different sites on the Caroline Ridge yielded ages between 8.1 ± 0.8 Ma and $23.9 \text{ Ma} \pm 1.2$ Ma (Ridley et al., 1974; Zhang et al., 2020). Based on the emplacement of the Caroline Ridge onto the Caroline and Pacific Plates, it was inferred that there has only been minor motion between the two plates since at least the Miocene (Wu et al., 2016).

Based on its morphology, the Sorol Trough was interpreted as a transtensional feature, whereby extensional motion along the Sorol Trough was proposed to have split a once-contiguous, plume-related Caroline Ridge into the West Caroline Rise and Caroline Islands Ridge (Weissel and Anderson, 1978, Altis, 1999; Dong et al., 2018). The southern margin

of the Sorol Trough has large normal faults, but the northern margin is less distinctively faulted and the crust within the trough is highly disrupted (Weissel and Anderson, 1978). Bracey and Andrews (1974) suggested that the Sorol Trough formed as an interarc basin behind a north-dipping subduction zone that was interpreted from a bathymetric trough along the southern margin of the West Caroline Rise. If the Sorol Trough is an extensional feature, its modern width shows that it would have accommodated less than 100 km of extension since the early Miocene (Weissel and Anderson, 1978; Altis, 1999; Dong et al., 2018). A recent K-Ar age of 23.8 ± 0.7 Ma was obtained from basalt samples collected from a site that was interpreted to represent the age of extension in the Sorol Trough (Yan et al., 2022). We find it more likely, however, that this age represents volcanics from one of the Caroline ridges as the limited amount of extension that occurred in the Sorol Trough is unlikely to have formed new oceanic crust. At present, the Sorol Trough likely forms the current plate boundary between the Caroline and Pacific plates, with very minor relative transform motion (Weissel and Anderson, 1978; Dong et al., 2018).

The Mussau Trench represents the present-day eastern plate boundary between the Caroline and Pacific plates, where the Caroline Plate is starting to subduct below the Pacific Plate (Hegarty et al., 1983; Gurnis et al., 2004). The Lyra Trough, to the east of the Mussau Trench, however, may represent a former plate boundary (Hegarty et al., 1983; Gaina and Müller, 2007; Wang et al., 2022) and is thought to have been a transform fault during opening of the Caroline Sea basin (Hegarty and Weissel, 1988; Gaina and Müller, 2007).

3.4. Junction Region orogenic domain

Orogenic belts with accreted and deformed relics of now-subducted lithosphere, and remains of forearcs are located along the Eurasian margin, on the Philippines, and in the Melanesian and Polynesian regions. In this section, we review the orogenic architecture and the constraints they provide for the tectonic and geological history of the lithosphere that was lost to subduction.

3.4.1. Southwest Japan (Southwest Honshu, Shikoku, Kyushu, Ryukyu Islands)

At the Boso triple junction, the Izu-Bonin-Mariana trench meets with the Japan and Nankai trenches that accommodate subduction of the Pacific and Philippine Sea Plate below the islands of Japan, respectively (Figure 3). The islands of Japan comprise a long-lived accretionary orogen, where accretion of OPS occurred episodically during a subduction history of c. 500 million years (Isozaki et al., 1990, 2010). The southwestern part of Japan, west of the Boso triple junction, exposes foreland-younging thrust units that accreted in the late Permian the Middle-Late Jurassic, the Late Cretaceous, the Eocene (around 50 Ma), and during the Miocene, alternating with episodes of subduction without accretion, or with subduction erosion (Isozaki et al., 1990). Throughout this history, arc magmatism remained active (Isozaki et al., 2010). This accretion occurred at the continental margin of the South China Block, and within the accretionary orogen, the Japan Sea back-arc

basin opened in Early Miocene time (Jolivet et al., 1994; Martin, 2011; Van Horne et al., 2017). The accretionary orogen of southwest Japan is intersected by the Median Tectonic Line, a major E-W striking fault, juxtaposing the older Inner Zone against the younger Outer Zone. The Inner Zone comprises Permian-Jurassic accretionary complexes intruded by Cretaceous granitoids, while the Outer Zone is dominated by Jurassic-Paleogene accretionary complexes (e.g., Ito et al., 2009; Isozaki et al., 2010; Wallis et al., 2020). The Median Tectonic Line is currently a right-lateral strike-slip fault (Okada, 1973; Sugiyama, 2012), but is thought to have been the site of subduction during the Early to Late Cretaceous that may have consumed a former back-arc basin (Boschman et al., 2021a, and references therein).

Towards the west, the Nankai Trench connects with Ryukyu Trench and the accretionary complexes are traced from the main islands of Japan to the Ryukyu Islands (Kizaki, 1986; Wallis et al., 2020). There is a marked difference between the geology of the northern and southern Ryukyu Islands, which are separated from each other by the Kerama Gap (Figure 3). The youngest part of accretionary complex exposed on the northern Ryukyu Islands is exposed along the southeast coast of Okinawa Island and is composed of trench-fill turbidites of Eocene age (Kizaki, 1986; Miki, 1995; Ujiie, 1997, 2002; Hou et al., 2022). On the other hand, farther northwards, on southern Kyushu, the youngest part of the accretionary complex, also mainly composed of trench-fill turbidites, is of Early Miocene age (Taira et al., 1982; Kiminami et al., 1994; Raimbourg et al., 2014). The Eocene accretionary complex on the Ryukyu Islands does not expose OPS sequences, but Paleocene to early Eocene radiolarians were derived from blocks of OPS within an Eocene *mélange* complex in Shikoku (Taira et al., 1988) and lower middle Eocene mudstone associated with blocks of basalt are embedded in mid-middle Eocene terrigenous trench-fill deposits on Kyushu (Saito, 2008). The southern Ryukyu Islands, to the south of the Kerama Gap, on the other hand, have a basement of Late Paleozoic to Jurassic accretionary complexes correlated to the Inner Zone, overlain by Eocene limestones, sandstones, pyroclastics, and andesite lavas and Lower Miocene sandstones and limestones (Kizaki, 1986). The deposition of Upper Miocene to Pleistocene siltstones, sandstones and tuff is the first evidence of a shared geological history between the north and south Ryukyu Islands (Kizaki, 1986). This has been used to suggest that the Izu-Bonin-Mariana trench, and therefore the Boso trench-trench-trench triple junction, most likely migrated from a location in the central Ryukyu Islands, at or near the Kerama Gap, towards the northeast since the Miocene (e.g., Kimura et al., 2014).

The Ryukyu Islands are separated from continental crust of South China by the Okinawa Trough (Figure 3). The Okinawa Trough is a young, currently active, extensional back-arc basin underlain by thinned continental (Lee et al., 1980; Sibuet et al., 1987, 1995; Arai et al., 2017), or possibly in places oceanic crust (Liu et al., 2016). Extension in the Okinawa Trough is thought to have started in the late Miocene, based on the oldest sediments above an unconformity over basement and may amount c. 100 km (Lee et al., 1980; Letouzey and

Kimura, 1986; Sibuet et al., 1987; Fabbri et al., 2004; Tanaka and Nomura, 2009; Gungor et al., 2012).

3.4.2. Taiwan

The Ryukyu Trench ends in a complex plate boundary zone that surrounds the Taiwan orogen, where the polarity of subduction changes, and where continental crust of the South China margin is underthrust below oceanic lithosphere of the Philippine Sea Plate (Figure 3). The geology of Taiwan is divided into five roughly N-S trending tectonostratigraphic terranes, separated by major east-dipping faults (Figure 5; e.g., Huang et al., 2006; Brown et al., 2011, 2017; Camanni and Ye, 2022). The three western terranes (the Coastal Plain, Western Foothills, and the Hsuehshan Range) make-up the mostly non-metamorphic Taiwan fold-and-thrust belt, and together with the metamorphic Central Range that lies adjacent to the suture with the Philippine Sea Plate, forms a series of nappes that were accreted from the subducted South China margin. The Coastal Range in the east comprises Miocene volcanic and volcanoclastic rocks that are interpreted to be part of the Luzon arc built on the Philippine Sea Plate (Huang et al., 2018; Brown et al., 2022).

The Taiwan fold-and-thrust belt comprises westward-younging Eocene to upper Miocene clastic sediments interpreted to have formed on the South China passive margin, overlain by upper Miocene foreland basin sediments interpreted to derive from the approaching orogen (Huang et al., 1997; Alvarez-Marron et al., 2014; Brown et al., 2022). No crystalline basement rocks are exposed within the fold-and-thrust belt (Brown et al., 2022). Based on balanced cross-sections, shortening estimates for the fold-and-thrust belt vary from 10-30 km (Mouthereau et al., 2001; Yang et al., 2007, 2016; Mouthereau and Lacombe, 2006; Rodriguez-Roa and Wiltschko, 2010; Brown et al., 2022), to up to ~120 km (Suppe, 1980).

The fold-and-thrust belt underthrusts the Central Range, comprising of the Tananao metamorphic complex, which has been subdivided into the Tailuko and Yuli belts (e.g., Chen et al., 2016, 2017). The Tailuko Belt comprises a schist unit, a marble unit associated with metabasite, and a granitoid unit, which were metamorphosed to greenschist- to amphibolite-facies (Yui et al., 2012). Based on the occurrence of metabasite, marble, and chert, the Tailuko Belt is interpreted as metamorphosed OPS (Yui et al., 2012). Permian ages were obtained for the marbles, based on forams, corals, and Sr-isotope data (Jahn et al., 1984, 1992). The age of quartz-mica schist from the Tailuko Belt, interpreted as metaforeland basin clastics, was determined from dinoflagellate assemblages, which yielded Late Jurassic to Early Cretaceous ages (~155-120 Ma; Chen, 1989 in Yui et al., 2012). More recently, U-Pb detrital zircon ages yielded 120-110 maximum depositional ages for the schist formation in the Tailuko Belt (Chen et al., 2016). Based on these ages, as well as zircon-provenance data, it was inferred that the Tailuko Belt represents a Late Jurassic to Late Cretaceous accretionary complex, where Upper Permian oceanic crust was accreted at a northwest-dipping subduction zone below the South China continental margin (Yui et al.,

2012). The Tailuko Belt is locally intruded by Upper Cretaceous granitic intrusions, which may belong to the youngest magmatic suite southwest of the Qingdao Line/Kerama Gap (Wintsch et al., 2011; Yui et al., 2012; Wintsch and Li, 2014; Wu et al., 2022). The Tailuko Belt is overlain by syn-rift sediments, which comprises Eocene shallow-marine sandstones, conglomerates, and limestones and Miocene deep-marine argillite with thin layers of sandstones, now metamorphosed at lower greenschist facies because of the late Neogene Taiwan orogenesis. These are interpreted as passive margin sediments of the South China margin that formed after the Late Cretaceous end of subduction zone and formation of the Tailuko accretionary prism (Ho, 1986; Fisher et al., 2002; Conand et al., 2020). A similar stratigraphic sequence is known from the northern margin of the South China Sea to the west (Shao et al., 2017; Advokaat and Van Hinsbergen, 2023).

The Yuli Belt is to the east and structurally above the Tailuko Belt and comprises greenschist facies, carbonaceous, quartz-micaschists, with allochthonous blocks of blueschist facies metabasites (Zhang et al., 2020). Detrital zircon U-Pb geochronology showed that the Yuli Belt comprises a mixture of host-rocks with ages between the Cretaceous and Miocene (Chen et al., 2017). A middle Miocene maximum depositional age was inferred for the Yuli Belt from the mean 15.6 ± 0.3 Ma crystallization age of youngest zircons in blueschist samples (Chen et al., 2017). The age of peak metamorphic conditions was determined for a retrogressed blueschist sample to be 5.1 ± 1.7 Ma based on a Lu-Hf garnet age (Sandmann et al., 2015). Based on these constraints, the Yuli Belt was interpreted to have formed as the most distal part of the Miocene South China margin, which was subsequently incorporated in a Miocene accretionary prism (Sandmann et al., 2015; Chen et al., 2017).

To the east of and structurally above the Yuli Belt is the Lichi Mélange (Figure 5), the unmetamorphosed equivalent of the Yuli Belt (e.g., Chen et al., 2017). The Lichi Mélange comprises a Pliocene matrix with blocks of andesite volcanics derived from the Luzon arc to the east, Miocene turbidites, and oceanic crust sequences with overlying deep-marine sediments (Jahn, 1986; Lo et al., 2020). The blocks of oceanic crust are commonly referred to as the East Taiwan Ophiolite (Chung and Sun, 1992). Zircons from radiolarian cherts and gabbros of the East Taiwan Ophiolite yielded U-Pb ages of 14.7 ± 0.2 Ma and 17.8 ± 0.4 Ma, respectively (Lo et al., 2020). U-Pb zircon ages of 16.7 ± 0.2 Ma and 16.1 ± 0.6 Ma were obtained from blocks of pegmatitic gabbro and plagiogranite (Lin et al., 2019). A 14.8 ± 1.2 Ma $^{40}\text{Ar}/^{39}\text{Ar}$ whole-rock age was obtained from a pillow basalt sample (Lo et al., 2020). MORB geochemical signatures further support that the oceanic crust of the East Taiwan Ophiolite formed part of the South China Sea basin, which was subsequently accreted by nappe-stacking to the Luzon forearc during subduction along the Manila trench (Lin et al., 2019). U-Pb zircon crystallization ages of 17.4–16.9 Ma were derived from metaplagiogrinites in the Yuli Belt (Lo et al., 2022). These ages were interpreted to be derived from the forearc crust that formed in a supra-subduction zone environment, providing an estimate for the age of subduction initiation of the Eurasian Plate below the Philippine Sea Plate (Lo et al., 2022).

The easternmost, and uppermost, tectonostratigraphic terrane, the Coastal Range, is formed by the northernmost extension of the Luzon arc and forearc. Two Oligocene and early Miocene K-Ar ages have been reported from volcanics of the Coastal Range (Ho, 1969; Richard et al., 1986), but these have been considered unreliable due to scattered results and possible alteration (e.g., Lo et al., 1994). Therefore, the volcanism in the Central Range section of the Luzon arc is thought to have started around 16 Ma, based on 16.4–15.4 Ma zircon fission-track dating (Yang et al., 1995), and a 16.0 ± 0.2 $^{40}\text{Ar}/^{39}\text{Ar}$ whole-rock age of andesites (Lo et al., 1994). These ages correspond to the oldest volcanoclastic forearc sediments (c. 18 Ma; Suppe and Chi, 1985). The youngest volcanic activity in the Central Range was dated at $4.2 \text{ Ma} \pm 0.1$, obtained from $^{40}\text{Ar}/^{39}\text{Ar}$ groundmass dating (Lai et al., 2017), which corresponds to the earliest stages of underthrusting of the continental South China margin and the accretion of the western nappe systems of the Taiwan orogen.

3.4.3. The Philippines

Cretaceous ophiolites: Luzon; Mindoro; Romblon; Panay

The Luzon arc continues from Taiwan over Luzon southwards, associated with subduction of oceanic crust of the South China Sea basin at the Manila Trench (Figure 3). The Babuyan and Batan island groups, between Taiwan and Luzon, expose Late Miocene to recent volcanics (Defant et al., 1989, 1990). The Luzon arc on the island of Luzon comprises 14 Ma to recent calc-alkaline basalts and andesites, exposed in the Central Cordillera, the western mountain range of northern Luzon to the north of the Philippine fault (Maleterre et al., 1988; Defant et al., 1990).

Motion on the 1200 km long Philippine Fault is thought to have started in the Pliocene, around 4 Ma, contemporaneous with subduction initiation at the Philippine Trench (Aurelio et al., 1991; Barrier et al., 1991; Aurelio, 2000). Estimates for total displacement on the fault vary between 110 and 200 km (Mitchell et al., 1986; Cole et al., 1989).

The Luzon arc was built on oceanic crust. At the northern end of the Central Cordillera, in the Ilocos Norte region (Figure 5), a *mélange* is exposed that contains blocks of radiolarian cherts, peridotite, and subordinate metamorphic rocks in a serpentinite matrix (Queaño et al., 2017a). Based on radiolarian biostratigraphy, the chert was assigned an uppermost Jurassic to Lower Cretaceous age, the age of the matrix is unknown (Queaño et al., 2017a). Ultramafic and mafic clasts within the *mélange* have an island arc and MORB geochemical signature and are interpreted to have formed in a supra-subduction zone setting (Pasco et al., 2019). The *mélange* is thrust over an Eocene volcanoclastic unit, with at its base interbeds of sandstones and siltstones that conformably overly pillow basalts with an arc geochemical signature (Queaño et al., 2017a, 2020). Other occurrences of oceanic basement are exposed in the southern Central Cordillera, in the Baguio-Mankayan region (Figure 5), as pillow basalts and basaltic feeder dikes, sporadically intercalated with undated radiolarian chert, and unconformably overlain by epiclastic rocks, including volcanoclastics and turbidites (Ringebach et al., 1990; Encarnación et al., 1993; Queaño et al., 2008). The basement has

not been dated directly, but the oldest sedimentary formation overlying the basement in the Central Cordillera are volcanoclastics of Eocene age (Ringebach et al., 1990; Encarnación et al., 1993). The pillow basalts have a transitional MORB-IAT geochemical affinity and are therefore interpreted to have formed in a back-arc basin environment (Queaño et al., 2008).

The Central Cordillera is intruded by the Central Cordillera Diorite Complex, with active magmatism since the late Oligocene (e.g., Hollings et al., 2011; Deng et al., 2020). This complex intruded in several magmatic phases, of which a 26.8 ± 0.4 U-Pb zircon age from a quartz diorite (Encarnación et al., 1993) is the oldest reported age. Other ages from the Central Cordillera Diorite Complex are between 23 and 0.5 Ma (MMAJ-JICA, 1977; Bellon and Yumul, 2000; Imai, 2001; Waters et al., 2011). Late Oligocene-early Miocene (c. 20-27 Ma) magmatic rocks with an island-arc geochemical signature are also found to the east of the Central Cordillera Diorite Complex (MMAJ-JICA, 1977; Knittel, 1983; Hollings et al., 2011).

Along the east coast of Luzon, several complete ophiolite complexes are exposed (Figure 5), which include, from north to south, the Casiguran/Isabela, Dibut Bay/Baler, Montalban, Camarines Norte/Calaguas Islands/Cadig, Lagonoy, and the Rapu-Rapu ophiolites (e.g., Encarnación, 2004; Dimalanta et al., 2020). Major and trace element geochemistry revealed transitional MORB to IAT geochemical signatures in these ophiolites and a back-arc basin setting of formation is generally inferred (Geary, 1986; Geary et al., 1988; Geary and Kay, 1989; Billedo et al., 1996; Tamayo et al., 1998; Tejada and Castillo, 2002; Andal et al., 2005). Radiolarian biostratigraphy from the chert sedimentary carapace of the northernmost, Casiguran Ophiolite yielded Lower Cretaceous (upper Barremian-Albian) ages (Queaño et al., 2013), i.e., similar as the ages of cherts on Lanyu Island (Deschamps et al., 2000; Yeh and Cheng, 2001), the ages of the ocean floor of the Huatung Basin (Huang et al., 2019) and the Gagua Ridge arc lavas (Qian et al., 2021) to the north. For the other ophiolites, the sedimentary carapace is either absent or has not been dated (Encarnación, 2004; Dimalanta et al., 2020). However, radiometric ages have been reported for some of the ophiolites exposed in eastern Luzon, which in all cases are minimum ages. A 92.0 ± 0.5 40Ar/39Ar amphibole age was obtained from a foliated amphibolite from the metamorphosed Dibut Bay Ophiolite, which is interpreted as the age of metamorphism (Billedo et al., 1996). A similar metamorphic amphibole age of 99.9 ± 7.0 Ma was obtained from amphibolite of the structurally disrupted Camarines Norte ophiolite, using 40Ar/39Ar dating of a metagabbro (Geary et al., 1988). Ultramafic, metamorphic, and gabbroic rocks of the Camarines Norte Ophiolite are juxtaposed on east-dipping thrust faults (Geary and Kay, 1989). Estimates for the P-T conditions during formation of the amphibolites are 500-550° and 2-4 kbar (Geary and Kay, 1989). There are no interpretations about the cause of metamorphism, so it remains unknown whether the metamorphism occurred as seafloor metamorphism during extension of the ophiolite, in which case the metamorphic ages essentially represent the age of formation of the oceanic crust, or whether metamorphism occurred during a later phase of upper plate shortening, in which case the metamorphic ages may be much younger than

the formation of the oceanic crust.

In contrast to the Late Cretaceous metamorphic ages obtained from the Dibut Bay and Camarines Nortes ophiolites, the Lagonoy Ophiolite yielded $40\text{Ar}/39\text{Ar}$ ages of 150.9 ± 3.3 and 156.3 ± 2.0 Ma, obtained from amphiboles from a metagabbro and metaleucodibase sample (Geary et al., 1988), i.e., as much as 25–30 Ma older than the crust of the Huatung Basin. Whether these ages represent magmatic, metamorphic crystallization, or cooling ages remains unknown, and they were thus regarded as the minimum age of the ophiolite (Geary et al., 1998). No interpretations were made about possible causes of metamorphism. In addition, a 122.7 ± 4.0 Ma K-Ar whole-rock age was obtained from a gabbro of the Lagonoy Ophiolite (David et al., 1997), although this age may have suffered from Ar loss (Encarnación, 2004). Undated metamorphic rocks, interpreted as a metamorphic sole, are exposed on easternmost Rapu-Rapu island, below the (undated) Rapu-Rapu Ophiolite towards the west (Yumul et al., 2006). To the southwest, on the island of Masbate to the west of the Philippine Fault, lies another Early Cretaceous ophiolite: the Balud Ophiolite contains mafic magmatic rocks, including pillow lavas with subordinate isotropic gabbros and diabase dikes (Manalo et al., 2015), although no ultramafic rocks have been reported. The basalts are overlain by Lower-Upper Cretaceous (Aptian-Cenomanian) radiolarian chert and has a transitional MORB-IAT geochemistry (Manalo et al., 2015).

The ophiolites of southeastern Luzon and neighboring Calaguas and Rapu-Rapu islands are unconformably overlain by Upper Cretaceous sedimentary sequences. Unconformably overlying the Lagonoy Ophiolite are Upper Cretaceous volcanic sequences interpreted to be arc-related, consisting of andesitic volcanics including pillow basalts, volcanoclastics, and hemipelagic limestone interbedded with radiolarian chert (David et al., 1997). A 91.1 ± 0.5 Ma $40\text{Ar}/39\text{Ar}$ was obtained from amphibole separates of a basalt flow (David et al., 1997). Finally, a diorite pluton that intruded into the harzburgites of the Rapu-Rapu Ophiolite, yielded a 77.1 ± 4.6 Ma K-Ar whole-rock age and may represent a plutonic equivalent of the Upper Cretaceous arc sequence (David et al., 1997). The Camarines Norte Ophiolite to the north of the Lagonoy Ophiolite is unconformably overlain by a sedimentary sequence of graywacke, arkose, and mudstone, with minor spilite, which is possibly a distal equivalent of the Upper Cretaceous arc sequence overlying the Lagonoy Ophiolite (Encarnación, 2004).

The Upper Cretaceous arc sequences of the East Luzon ophiolites are overlain by middle to upper Eocene volcanics, volcanoclastics, limestones, and turbidite sequences, interpreted as an arc sequence that is separate from the Cretaceous sequence (David et al., 1997; Billedo et al., 1996; Encarnación, 2004; Queaño et al., 2020). The Eocene volcanoclastics are the equivalent of volcanoclastics exposed in the northernmost part of Central Cordillera in the Ilocos Norte region (Queaño et al., 2020). The Sierra Madre range of East Luzon is intruded by Eocene (49–43 Ma) and Oligocene-earliest Miocene batholiths (33–22 Ma; MMAJ, 1977, 1987; Billedo et al., 1996; Encarnación, 2004; Hollings et al., 2011). Also, the Balud Ophiolite of Central Luzon is overlain by Eocene volcanics that consist of basaltic and andesitic flows with minor sandstones and mudstones (MMAJ-JICA, 1986; Manalo et al., 2015). The Late

Cretaceous and the Eocene arc sequences of the Bicol region, to the south of the Sierra Madre range, are intruded by Oligocene plutons which yielded K-Ar and $^{40}\text{Ar}/^{39}\text{Ar}$ ages between 36 and 30 Ma (David et al., 1997; Encarnación, 2004).

Eocene ophiolites: Zambales; Angat; Sibuyan; Antique

In contrast to northern and eastern Luzon, western Luzon exposes Eocene ophiolites (Figure 5). These ophiolites are in the hanging wall of the eastward subduction zone that consumes the South China Sea crust, and the SE Asian tectonic mosaic including the Palawan accretionary prism and ophiolite. The northernmost of these ophiolites is the Zambales Ophiolite, which is subdivided into the Acoje and Coto blocks, which have transitional MORB-IAT and IAT geochemical signatures, respectively (Hawkins and Evans, 1983; Yumul, 1989), showing they were formed in or adjacent to the Eocene arc (e.g., Hawkins and Evans, 1983; Encarnación et al., 1993; Yumul et al., 2000a). The Acoje Block yielded a 44.1 ± 3 Ma K-Ar whole rock on sill cutting pillow lavas (Fuller et al., 1989) and 44.2 ± 0.9 Ma U/Pb zircon age on plagiogranite (Encarnación et al., 1993), whereas the Coto block gave a whole-rock K-Ar age of 46.6 ± 5.1 Ma from a diabase dike intruding gabbros (Fuller et al., 1989) and a plagiogranite 45.1 ± 0.5 Ma U/Pb zircon age (Encarnación et al., 1993). The Coto Block is overlain by Eocene pelagic limestone interbedded with tuffaceous turbidites (Garrison et al., 1979; Schweller et al., 1983). Emergence of the Zambales Ophiolite occurred prior to the Early Miocene, based on the presence of ophiolite clasts in a conglomerate and sandstone formation unconformably overlying the ophiolite, interpreted to result from activity of the Manila Trench and equivalents to the south (Yumul et al., 2020). Miocene sedimentary rocks overlying the Acoje Block rework Upper Jurassic to Lower Cretaceous radiolarian cherts (Queaño et al., 2017b).

To the west of the Zambales Ophiolite are isolated outcrops of a *mélange* with a matrix of sheared serpentinite containing blocks of Lower Cretaceous radiolarian chert and quartz-sericite-chlorite schist, referred to as the West Luzon Shear Zone (Karig, 1983). This was interpreted as a major left-lateral strike-slip fault zone that became inactive before the end of the Oligocene, based on the lack of shearing in unconformably overlying upper Oligocene sediments (Karig, 1983).

The incomplete and structurally disrupted Angat Ophiolite, to the southeast of the Zambales Ophiolite, yielded a 48.1 ± 0.5 zircon U-Pb age from a plagiogranite (Arcilla et al., 1989; Encarnación et al., 1993). The ophiolite comprises gabbros, a sheeted dike complex and pillow basalts. The Eocene Angat Ophiolite is in fault contact with pillow basalts associated with Upper Cretaceous radiolarian chert overlain by Eocene volcanoclastics, referred to as the Montalban Ophiolite (Encarnación et al., 1993). Similar to the Eocene ophiolites to the north, the Angat Ophiolite is overlain by arc-derived sediments (Karig, 1983) and has a geochemistry displaying MORB and IAT characteristics (Yumul, 1993).

To the southeast of Mindoro is the Sibuyan Ophiolite, on the Romblon Island Group. The Sibuyan Ophiolite is exposed as tectonic slices separated by west-dipping thrust faults

(Dimalanta et al., 2009). A 43.2 ± 2.5 K-Ar whole rock age was obtained from a diorite sample (Dimalanta et al., 2009). Jurassic to Cretaceous radiolarians were reported from cherts intercalated with pillow lavas (Maac and Ylade, 1988). However, these may be derived from a *mélange*, analogous to the West Luzon Shear Zone exposed to the west of the Zambales Ophiolite (Karig, 1983). The ophiolite is intruded by 18-20 Ma andesites and rhyolites (Bellon and Rangin, 1991). The ophiolite is structurally above a tectonic *mélange* to the northeast that comprises clasts of ophiolitic material and metasediment in a sheared serpentinite and red mudstone matrix (Dimalanta et al., 2009). In addition, the ophiolite is structurally above a metamorphic unit comprising mostly plagioclase-quartz-mica schist. K-Ar mica age determinations from a quartz-mica schist and a mica schist yielded ages of 12.3 ± 0.2 Ma and 12.2 ± 0.2 Ma (Dimalanta et al., 2009). U-Pb zircon dating of the protolith of the metamorphic unit yielded a c. 110 Ma maximum depositional age (Knittel et al., 2017).

South of the Romblon Island Group is the island of Panay, which exposes the Antique Ophiolite. The ophiolite comprises a mantle and crustal section and is exposed in thrust slices along SE dipping thrust faults (Tamayo et al., 2001). U-Pb ages constrain the crystallization age of the ophiolite to 44-42 Ma (Mesalles et al., 2018). Calcareenites with Early Eocene foraminifera conformably overly the pillow basalts (Rangin et al. 1991; Tamayo et al., 2001), but Late Jurassic to Early Cretaceous and Late Cretaceous radiolarians have also been found in the area, in unknown tectonic context (McCabe et al., 1982; Rangin et al., 1991). The geochemistry of the ophiolite is intermediate between MORB and IAT (Tamayo et al., 2001; Yumul et al., 2013). The ophiolite body is thrust towards the west over Middle Miocene clastic sediments, and these volcanoclastics, conglomerates, sandstones, and minor carbonates also unconformably cover the ophiolite. To the east of the ophiolite is a *mélange* with blocks of ophiolite material in a Middle Miocene matrix, but the contact between the *mélange* and the ophiolite is not exposed (Tamayo et al., 2001). The *mélange* underthrusts to the east an Oligocene-Early Miocene volcanic arc sequence (K-Ar ages of 30-21 Ma; Bellon and Rangin, 1991) with overlying marine sediments (Tamayo et al., 2001).

There is no evidence that the belt of Eocene ophiolites of the northwest Philippines is separated from the Cretaceous ophiolites by a major thrust fault that may represent a former subduction zone. Instead, they more likely represent Eocene oceanic crust that formed within the Cretaceous oceanic crust exposed on the eastern Philippines. Their geochemistry and overlying Eocene arc-derived sediments suggest that they formed above a subduction zone, that is related to the Eocene and younger arc rocks that unconformably overlie the Cretaceous ophiolites to the east. The associated trench was likely to the west, since no evidence exists that there was an Eocene trench between the Philippines and the Philippine Sea Plate.

Finally, to the west of the Eocene ophiolites, on Mindoro Island, lies the Amnay Ophiolite, on a ridge that forms the eastern continuation of Palawan orogenic belt (Figure 5). The Amnay Ophiolite has been interpreted to have formed in the forearc of the

subduction zone that consumed the proto-South China Sea oceanic lithosphere (Yu et al., 2020), and has been correlated to the Palawan Ophiolite (Advokaat and Van Hinsbergen, 2023). A Middle Oligocene age was assigned to the ophiolite based on foraminifera in siltstone intercalated with pillow basalts (Rangin et al., 1985; Sarewitz and Karig, 1986). Zircon U-Pb dating of two metagabbro samples yielded zircon ages of 23.3 ± 0.2 Ma and 23.6 ± 0.4 Ma (Yu et al., 2020). These ages are considered magmatic crystallization ages based on the structure and chemical composition of the zircon grains. A fresh gabbro sample, on the other hand, yielded a 33.0 ± 0.8 Ma zircon U-Pb age (Yu et al., 2020). The geochemistry of the ophiolite is dominantly MORB with a minor subduction-related component (Yumul et al., 2009). Structurally below the Amnay Ophiolite are Jurassic siltstones and Upper Cretaceous (Campanian-Maastrichtian) black shales that are unconformably overlain by Middle Eocene-Lower Oligocene syn-rift clastic sediments and Upper Oligocene-Lower Miocene post-rift clastic sediments and carbonates, correlated to the Palawan Continental Terrane (Marchadier and Rangin, 1990; Advokaat and Van Hinsbergen, 2023).

Southern Philippines ophiolites; Cebu arc, Southeast Bohol accretionary prism and trench; Mindanao; Halmahera

The central and southern Philippines are divided by the Philippine Fault Zone into an eastern belt with a NNW-SSE structural grain, and a western belt with a nearly perpendicular, ENE-SWS structural grain. The eastern zone contains several prominent ophiolite complexes, from north to south including the Samar, Tacloban, Malitbog, Dinagat, Surigao, and Pujada ophiolites. The western zone from north to south includes the Cebu arc, the SE Bohol Ophiolite and accretionary prism, the proto-SE Bohol Trench, and on Mindanao, the Polanco and Titay ophiolites (Figure 5).

The Samar Ophiolite is exposed on southernmost Samar Island (Figure 5). Based on radiolarian biostratigraphy of chert intercalating with pillow basalts, the Samar Ophiolite was assigned a Late Cretaceous or possibly Early Cretaceous age. This age is supported by K-Ar whole-rock dating of two basalt samples that yielded ages of 100.2 ± 2.7 Ma and 97.9 ± 2.8 Ma (Balmater et al., 2015). Based on its geochemistry, the Samar Ophiolite has a supra-subduction zone signature and is thought to have formed in an intra-arc or forearc setting (Guotana et al., 2017a, 2018). Unconformably overlying the ophiolite are Upper Oligocene to Lower Pliocene sediments that incorporate fragments of successively deeper parts of the ophiolitic sequence and that were likely deposited adjacent to an active arc (Pacle et al., 2017).

Just west of the Samar Ophiolite is the Tacloban Ophiolite, exposed on Leyte Island (Figure 5). Zircon U-Pb dating of a gabbro from the ophiolite complex yielded two very different ages: 145.1 ± 3.2 Ma and 124.7 ± 3.3 Ma (Suerte et al., 2005). The Tacloban Ophiolite is unconformably overlain by Upper Miocene to Lower Pliocene sediments with clasts derived from the ophiolite (Suerte et al., 2005). On southern Leyte Island lies the Malitbog Ophiolite (Figure 5). The different units of the ophiolite are separated by northeast

trending thrust faults (Dimalanta et al., 2006). An early Late Cretaceous age was assigned based on foraminifera in limestones that overlie the ophiolite (Florendo, 1987). Based on geochemistry of the mantle peridotites, the Tacloban and Malitbog ophiolites were inferred to have formed in a backarc basin setting (Guotana et al., 2018).

To the east of the Malitbog Ophiolite, on Dinagat Island lies the Dinagat Ophiolite, which is also exposed in northeastern Mindanao (where it is also known as the Surigao Ophiolite; e.g., Yumul, 2003, 2007). The Dinagat Ophiolite comprises a complete mantle-crustal section, and sporadically, the basalt flows are intercalated with tuffs, tuffaceous sandstones, siltstones, and shales (Dimalanta et al., 2020). The age of the ophiolite was inferred from an 84.4 ± 4.2 Ma K-Ar whole rock age (MMAJ-JICA, 1986), although the dated rock type is not clear. Geochemical analyses revealed a transitional MORB-IAT and supra-subduction zone affinity of the mantle and volcanic sections (Tamayo et al., 2004; Yumul et al., 1997). In the west, structurally below the ophiolite are metamorphic rocks consisting of amphibolite schist, quartzo-feldspathic schist, biotite schist, and metacherts, presumed by Santos (2014) to be Late Cretaceous in age, although no radiometric ages were reported. The ophiolite is unconformably overlain by Upper Eocene conglomerates interbedded with calcareous sandstone and mudstone (Santos, 2014). First clasts of the ophiolite appear in clastic sedimentary rocks of Upper Miocene age (Santos, 2014).

The Pujada Peninsula of southeastern Mindanao exposes the Pujada Ophiolite (Figure 5) of which zircon U-Pb geochronology from three gabbro samples yielded ages of 90.9 ± 2.7 , 90.2 ± 2.0 , and 88.4 ± 7.6 Ma (Olfindo et al., 2019). A back-arc basin setting was interpreted for the generation of the ophiolite, based on its geochemistry (Olfindo et al., 2019). The ophiolite is thrust eastwards over amphibolites, which are in turn thrust over greenschist-facies metamorphosed mafic rocks with an eastward decreasing metamorphic grade (Hawkins et al., 1985). This partly metamorphosed volcano-sedimentary section has a distinct island arc affinity (Olfindo et al., 2019). Based on radiolarian and foraminiferal content, a Late Cretaceous age was assigned to the island-arc volcano-sedimentary sequence (Yumul et al., 2003; Olfindo et al., 2019). Basalts of the ophiolite are unconformably overlain by Eocene limestones (Mitchell et al., 1986). Ophiolite clasts of the Pujada ophiolite first appear in an overlying Upper Miocene–Pliocene turbidite succession (Queaño, 2005).

In summary, the southeastern Philippines ophiolites to the east of the Philippine Fault systematically reveal Cretaceous ages, perhaps younging southward from ~100 to ~90 Ma although some outlying ages of 125 or 145 are reported (Tacloban Ophiolite; Suerte et al., 2005), with geochemical signatures suggesting arc, back-arc, or forearc chemistries. In places, these are thrust over metamorphosed volcano-sedimentary rocks with Cretaceous protoliths and presumably Late Cretaceous ages metamorphic ages that suggest a period of upper plate shortening above a subduction zone. There is no record of Eocene arc volcanism reported from the southeastern Philippines, in contrast to Luzon in the northern Philippines, but instead, this period is characterized by limestone sedimentation. The southeastern Philippine ophiolites became uplifted and emergent in the late Miocene.

To the west of the Philippine Fault Zone, the central Philippine island of Cebu exposes a metamorphic basement composed of metavolcanics, greenschists, amphibolite schists and siliceous metasediments consistent with metamorphosed ophiolitic mafic crust and overlying pelagic sediments (Diegor, 1996; Dimalanta et al., 2006; Rodrigo et al., 2020). This sequence is intruded and overlain by a Cretaceous volcanic arc sequence (Deng et al., 2015). Ages of the protoliths of the metamorphic rocks are unknown and were originally inferred to be Jurassic, but zircons extracted from amphibolite schist yielded a U/Pb mean age of 120.4 ± 0.3 Ma suggesting an Early Cretaceous age instead (Rodrigo et al., 2021). The metamorphic rocks are overlain by Lower Cretaceous limestones and arc volcanics, and an Upper Cretaceous succession of interbedded sandstone-siltstone, conglomerates, carbonaceous mudstones, and rare siliceous mudstones, which rework the deeper sequence (Rodrigo et al., 2020; Rodrigo and Schlagintweit, 2022). The volcanic arc sequence was dated through zircon U-Pb geochronology of a porphyritic andesite and a pyroclastic rock, yielding ages of 126.2 ± 2.4 Ma and 118.5 ± 1.2 Ma, respectively (Deng et al., 2015). In addition, U-Pb dating of zircons from diorite intrusions yielded weighted mean ages between 107.3 ± 1.0 Ma and 110.3 ± 4.1 Ma (Deng et al., 2017, 2019), consistent with K-Ar and U-Pb ages of 101–108 Ma and 109 ± 2 Ma (Walther et al., 1981). Moreover, detrital zircons from river sands vary in age between 100 and 140 Ma, with a peak at 118 Ma (Deng et al., 2015). Using zircon U-Pb dating on a variety of rocks interpreted to belong to the arc sequence, Gong et al. (2021) also yielded several Early Cretaceous crystallization ages (between 120.0 ± 4.7 Ma and 107.5 ± 1.6 Ma). In addition, a mean 89.1 ± 1.4 Ma crystallization age was obtained from two andesite samples (Gong et al., 2021) suggesting that arc magmatism may have continued for ~30 Ma. Cebu Island also contains Eocene-early Oligocene and Miocene volcanics: andesites and pyroclastics yielded ages between 43 and 30 Ma, as well as a 14.2 ± 0.7 Ma age (Gong et al., 2021). The Cebu Island arc samples contain Permian to Triassic xenocrysts in the Cretaceous samples and mainly Mesozoic with minor early Paleozoic and Archean xenocrysts in the Cenozoic samples, which suggest that the arc resurfaces continent-derived subducted sediments, perhaps from the SE Asian Tethysides (Gong et al., 2021).

To the south of the Cebu arc, the island of Bohol exposes the SE Bohol Ophiolite (Figure 5). The pillows of the ophiolite sequence are overlain with Upper Cretaceous radiolarian chert (Faustino et al., 2003; Dimalanta et al., 2020) which gives a minimum age for the ophiolite's crust. The ophiolite thrusts towards the southeast over non-metamorphosed *mélange*, comprising ophiolite-derived chaotically disrupted rock units in a serpentinite matrix (De Jesus et al., 2000). Structurally below the *mélange* are metamorphic rocks, including chlorite schists, quartz-sericite schists, and amphibolites (De Jesus et al., 2000). Collectively, these units were interpreted as a Late Cretaceous forearc and accretionary prism that formed at the proto-SE Bohol Trench, which forms a prominent, but tectonically inactive depression to the southeast of the island (Yumul et al., 2000b; Faustino et al., 2003). The Upper Cretaceous units are unconformably overlain by lower Miocene to Pleistocene

clastics, carbonates, and igneous units (Faustino et al., 2003). Clasts of the ophiolite are present in middle Miocene clastics of the overlying sedimentary sequences (Faustino et al., 2003). Zircon U-Pb dating from pyroclastics and andesites yielded ages between 42.5 ± 1.3 Ma and 30.7 ± 0.2 Ma (Gong et al., 2021), showing that Eocene-Oligocene magmatism also affected the Bohol region.

To the south of the SE Bohol Trench, on the Zamboanga Peninsula of western Mindanao are the Titay and Polanco ophiolites, both of unknown age. The Titay Ophiolite complex is thought to be emplaced onto continental basement that also underlies the Sulu arc (e.g., Pubellier et al., 1991; Tamayo et al., 2000; Yumul et al., 2004), correlated to the SW Borneo Mega-Unit of the SE Asian Tethysides (Advokaat and Van Hinsbergen, 2023). The Titay Ophiolite is in the north underlain by metamorphic rocks, including metagreywackes, amphibolites, and quartz-mica schists (Tamayo et al., 2000). A latest Oligocene to early Miocene age of metamorphism was inferred from 24.6 ± 1.4 and 21.2 ± 1.2 Ma K-Ar ages of amphibole separates from amphibolites (Tamayo et al., 2000; Yumul et al., 2004). This episode of metamorphism and associated Miocene volcanism may be related to the Miocene subduction of the Sulu Sea below the Zamboanga Peninsula along the Sulu Trench (Yumul et al., 2004).

The Zamboanga Peninsula is underlain by continental basement, correlated to the SW Borneo mega-unit (Advokaat and Van Hinsbergen, 2023). The Titay Ophiolite complex is separated from the Polanco Ophiolite to the east by the Sindangan-Cotabato-Daguma lineament, a transform fault that is referred to as the Siayan-Sindangan Suture Zone in the north, and that links to the Negros Trench at the eastern Sulu Sea margin (Pubellier et al., 1991; Yumul et al., 2004) (Figure 3). This zone is characterized by serpentinite-matrix mélange with ophiolite-derived clasts and a middle Miocene shale-matrix mélange with clasts of sandstone, andesite, and metamorphic rocks, interpreted as a Miocene subduction interface (Yumul et al., 2004). An upper Miocene formation comprising limestone, basalt lavas, and tuffaceous sediments, and a clastic sequence straddles the mélange and is also exposed on either side of it, providing a minimum age for the emplacement of the Polanco Ophiolite over the SE Asian continental basement (Yumul et al., 2004). To the southwest of the Siayan-Sindangan Suture Zone, southwestern Mindanao comprises oceanic crust of unknown age, which is suggested to have formed as part of the Eocene Celebes Sea (Honza and Fujioka, 2004).

Central Mindanao is underlain by oceanic basement and volcanics of unknown age, overlain by upper Oligocene to lower Miocene limestones, upper Miocene clastic sedimentary rocks, and Pliocene to recent volcanic rocks (Quebral et al., 1996; Sajona et al., 1997). K-Ar whole-rock dating of andesite samples from central Mindanao yielded ages of 19.9 ± 0.4 Ma and 16.3 ± 0.9 Ma (Sajona et al., 1997), related to the subduction of the Celebes Sea below Central Mindanao at the Cotabato Trench.

Towards the south, the Sindangan-Cotabato-Daguma lineament transitions southward into an east-dipping back-thrust to the west of the Sangihe arc (Figure 3). The Sangihe

arc formed above a west-dipping subduction zone that consumed the western part of the Molucca Sea Plate and that is dipping below the Eocene lithosphere of the Celebes Sea (e.g., Rangin et al., 1999). K-Ar dating of andesites of the Sangihe arc yielded ages between 15.6 and 0.9 Ma (Morrice et al., 1983) suggesting Miocene subduction, contemporaneous with the convergence between the Philippine Mobile Belt and the SE Asian Tethysides, but with opposite polarity. The forearc of the Sangihe subduction zone is exposed on Talaud Island (Figure 5) and consists of an ophiolite of unknown age (Moore et al., 1981) with a MORB-BABB geochemical signature (Evans et al., 1983). This ophiolite is thrust westwards over middle Miocene-Pliocene marine volcanoclastics and andesitic volcanics (Moore et al., 1981; Rangin et al., 1996), emplaced onto a *mélange* comprising blocks of ophiolitic rocks and marine sediments, including Eocene (Lutetian) radiolarian chert (Moore et al., 1981). The cherts are interpreted as accreted from subducted Molucca Sea Plate lithosphere, which therefore must have had an Eocene minimum age.

The Molucca Sea Plate was also subducted eastwards, below Halmahera. The forearc of the Halmahera subduction zone is currently being underthrust westwards below the forearc of the Sangihe subduction zone, which means that all oceanic lithosphere of the Molucca Sea has been consumed (Silver and Moore, 1978; McCaffrey et al., 1980). Arc magmatism related to the eastward subduction of the Molucca Sea Plate found on Halmahera is young, 8 Ma and younger, and slightly older on Obi to the south of Halmahera, dated at 11.8 ± 0.7 Ma using K-Ar whole rock dating (Baker and Malaihollo, 1996). On eastern Halmahera, and the islands of Morotai to the north, Obi to the south, and Waigeo to the east, ophiolitic rocks are exposed, including peridotites, gabbros, and few pillow basalts (Hall et al., 1988). From these ophiolitic rocks, $^{40}\text{Ar}/^{39}\text{Ar}$ ages of 87.3 ± 7.0 and 73.8 ± 1.5 Ma were obtained from hornblende minerals from diorite samples (Ballantyne, 1990, 1991). The ophiolitic rocks of the basement complex of Halmahera are tectonically intercalated with Upper Jurassic/Lower Cretaceous and carbonaceous turbidites, Upper Cretaceous (Campanian-Maastrichtian) volcanoclastics, and Eocene pelagic and shallow marine limestones (Hall et al., 1988). This sequence was interpreted as an east-facing forearc, with ophiolites of similar age and origin as on the southern Philippines (Hall et al., 1988), such as the Pujada Ophiolite (Olfindo et al., 2019). Oligocene-Miocene sedimentation on Halmahera is dominated by marine marls and limestones without evidence for magmatism, until the occurrence of volcanoclastics and lavas in the Miocene (Hall et al., 1988). On Waigeo, to the east of Halmahera, the ophiolites are deformed and intercalated with Lower Eocene radiolarian chert (Charlton et al., 1991; Ling et al., 1991) and unconformably overlain by sandstone with ophiolitic detritus, Lower Oligocene volcanoclastic sandstone, Upper Oligocene calc-alkaline island arc basalt, and Lower Miocene-Pliocene deep marine limestone (Charlton et al., 1991), showing that here arc magmatism was active since at least early Oligocene time.

The connection of the divergent subduction complexes of the Sangihe and Halmahera trenches to the trenches southwest and southeast of Mindanao is diffuse and complex. Pubellier et al. (1999) showed that the connections are essentially two relay ramps. The

thrust displacement on the Sangihe trench decreases northward, and between the islet of Miangas and southeast Mindanao connects to the Philippine Fault Zone. The convergent motion is northward increasingly accommodated by the east dipping Cotabato Trench below southwest Mindanao (Figure 3). The east-dipping subduction below Halmahera also decreases northward and is traced towards the Snellius Plateau, which may represent a submerged volcanic arc of Oligocene age (Pubellier et al., 1999) perhaps correlated to the Oligocene arc sequence of Waigeo (Pubellier et al., 2004). To the east of the Snellius Plateau, the Philippine Trench accommodates westward underthrusting of the Philippine Sea Plate, which gradually disappears southward towards northern Halmahera (Figure 3) (Pubellier et al., 1999).

To the south of Halmahera, metamorphosed continental basement of Australian affinity is exposed on southern Bacan and Obi islands. This basement consists of diorite with a U-Pb age of 329.8 ± 2.7 Ma, micaceous quartzites with a maximum depositional age of 159 Ma, and metasedimentary gneiss with a maximum depositional age of 87 Ma (Hall et al., 1988; Malaihollo and Hall, 1996; Decker et al., 2017). The continental basement was detached from the Australian continent and is now juxtaposed against the forearc basement of the Miocene Halmahera subduction zone by a splay fault of the Sorong Fault Zone (Saputra et al., 2014). This left-lateral fault system bounds the Sangihe and Halmahera trenches in the south and continues eastwards onto the Bird's Head Peninsula of New Guinea (Figures 3 and 4).

3.4.4. New Guinea

Southern New Guinea forms the northernmost margin of Australian continental basement, overthrust from the north by plates of the Junction Region (Figures 1, 4, and 7). In the southern part of central New Guinea, Precambrian and Paleozoic basement of the Australian foreland is exposed (Davies, 2012). This basement is overlain by a series of clastic sediments interpreted as a foreland basin to advancing nappes from the north. This foreland basin has been referred to as the Arafura and Fly Platforms (e.g., Pigram and Symonds, 1991). In the western part, on the Arafura Platform (Figure 7), the Precambrian basement is overlain by mostly conformable sedimentary sequences that span the upper Proterozoic or Cambrian to the mid to upper Cenozoic (Davies, 2012). These sediments show a history of shelf sedimentation up to the late Paleozoic or early Triassic, intruded by Permian-Triassic continental arc magmatism (Amiruddin, 2009; Crowhurst et al., 2004; Webb and White, 2016; Jost et al., 2018). This was followed by rifting of the continental margin, which led to the deposition of mudstones, sandstones, and conglomerate, associated with rift-related volcanism in the Middle Triassic to Early Jurassic (Home et al., 1990; Pigram and Symonds, 1991). Post-rift passive margin subsidence in the Late Jurassic to Early Cretaceous led to the deposition of marine shales interbedded with quartz-rich sandstones. The latest Cretaceous and most of the Cenozoic was dominated by the deposition of carbonates, with short intervals of clastic sedimentation interpreted to reflect periods of eustatic sea-level

fall (Cloos et al., 2005). Around 30 Ma, an influx of clastic sediments occurred, which was interpreted as the onset of foreland basin formation in response to an approaching active margin in the north (Pygram and Symons, 1991; Quarles van Ufford and Cloos, 2005). Since the late Miocene, thick packages of terrestrial continental clastic sediments were deposited related to uplift of an advancing Papuan and Irian Jaya fold-and-thrust belt from the north (Davies, 2012).

The Fly Platform in the east (Figure 7), where the basement is of Permian age, has a similar Mesozoic and Cenozoic stratigraphy as the Arafura Platform. However, a phase of uplift and erosion led to a widespread Upper Cretaceous to Eocene hiatus that is not seen in other parts of New Guinea (Davies, 2012). This uplift is thought to have occurred as a precursor to the opening of the Coral Sea Basin in the Paleocene (Pygram and Symonds, 1991; Davies, 2012).

Bird's Head Peninsula

The Sorong Fault that forms the plate boundary between the Philippine Sea Plate and northwestern New Guinea runs across the northwestern tip of the Bird's Head Peninsula (Figure 4 and 7). To the north of the Sorong Fault, the Bird's Head Peninsula exposes a similar Oligocene-Miocene oceanic island arc sequence as on Waigeo: basaltic-andesitic lava, agglomerate and volcanoclastics that yielded K-Ar ages of 31.5-10.5 Ma, sometimes intercalated with limestone and gabbro intrusions (Pieters et al., 1983; 1989). These island arc volcanics (known as the Tosem Block) are thrust along the Koor Fault over an allochthonous unit of Upper Jurassic to Lower Cretaceous age (known as the Tamrau Block; Figure 7), which consist of partly metamorphosed shales, siltstones, and sandstones, interpreted as continental slope deposits of the Australian passive margin. The Mesozoic passive margin sediments are unconformably overlain by Eocene to middle Miocene limestones (Webb et al., 2019). Both the Mesozoic and Eocene to Miocene sediments are intruded and overlain by Miocene granitoids and lavas, including andesitic, dacitic and basaltic tuffs and lavas, volcanoclastics and intercalated limestones, as well as middle Miocene calcareous mudstones and sandstones (Webb et al., 2019). K-Ar ages of 20-9 Ma and U-Pb zircon ages of 18-10 Ma were obtained from the Miocene volcanics (Bladon, 1988; Webb et al., 2020). Based on their dominantly calc-alkaline nature, it was interpreted that these volcanics formed as part of a continental arc (Webb et al., 2020). The Koor Fault is sealed by Plio-Pleistocene sediments, which constrains the timing of thrusting of the Philippine Sea Plate and overlying arc onto the northern Bird's Head to late Miocene to Pliocene (Webb et al., 2019). The Tosem and Tamrau blocks are separated from autochthonous Australian basement (Kemum Block) by the Sorong Fault (Figure 7). Correlations across the fault based on detrital zircon ages, stratigraphy, and structural data suggested that the northern tip of the Bird's Head Peninsula was displaced westwards by about 300 km along the Sorong Fault since the late Miocene-Pliocene (Webb et al., 2019).

South of the Sorong Fault, Bird's Head Peninsula exposes Paleozoic basement of the

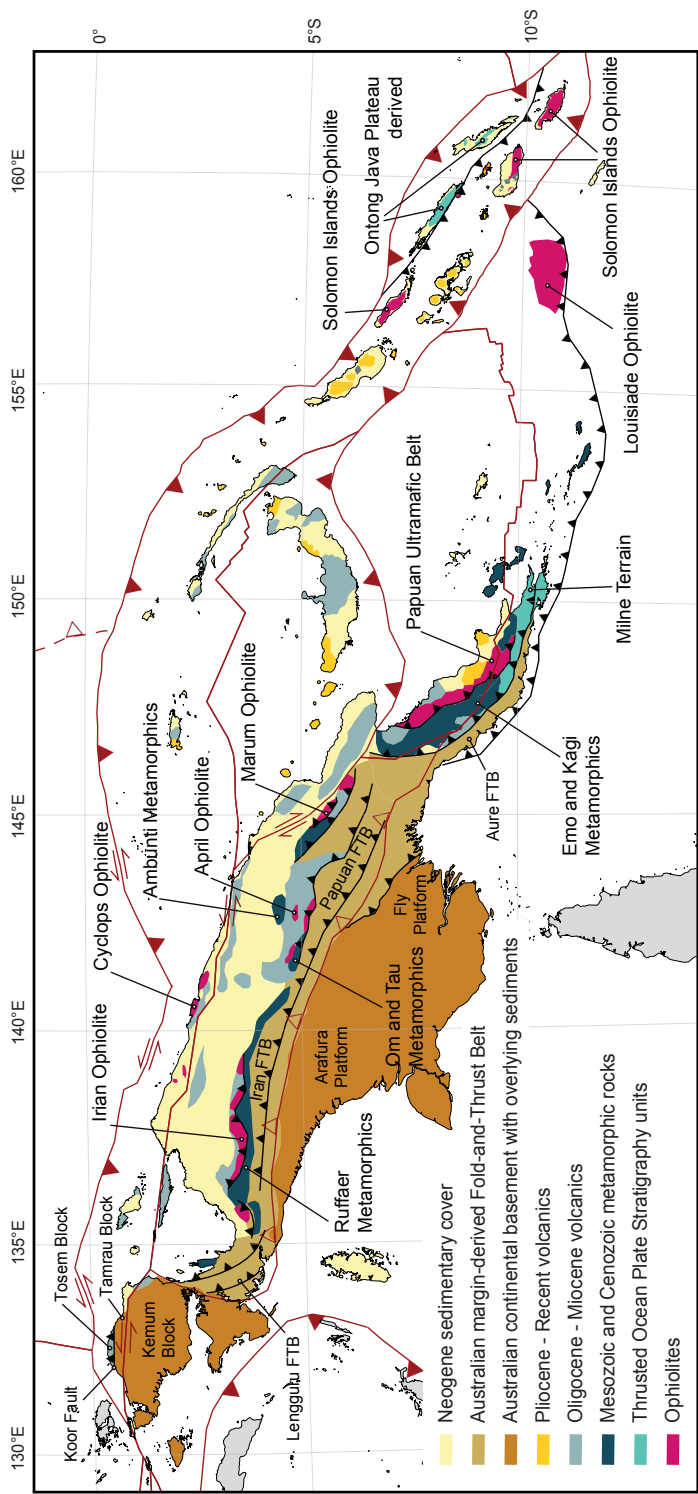


Figure 7. Geological map of New Guinea and the Solomon Islands, based on Davies (2012); Tejada et al. (1996); Petterson et al. (1999); Tapster et al. (2014). FTB = Fold-and-Thrust Belt.

Australian continent (the 'Kemum Block') intruded by plutons that yielded K-Ar biotite, muscovite, and hornblende ages between 225 and 295 Ma (Pieters et al., 1983), and overlain by Paleozoic turbidites, Permian and Mesozoic platform carbonates, Paleocene to Miocene limestone and Miocene to recent siliciclastics (Pieters et al., 1983; Davies, 2012). In the Bird's Neck isthmus to the southeast of the Bird's Head, this sequence is deformed and locally metamorphosed in the Lengguru fold-and-thrust belt (Figure 7), a west-verging, N-S striking fold-and-thrust belt that formed in a short time span of a few million years after 11 Ma, of which the total amount of shortening is uncertain (Bailly et al., 2009). During formation of the fold-and-thrust belt some of the transform motion on the Sorong Fault stepped southward towards a transform fault on Central New Guinea (see below). This was followed by Pliocene E-W extension leading to core complex exhumation (Bailly et al., 2009).

Central New Guinea

The Australian foreland of the Arafura and Fly Platforms is overthrust from the north by the roughly WNW-ESE trending fold-and-thrust belt, comprising north-dipping, south-verging thrust faults, referred to as the Papuan fold-and-thrust belt in Papua New Guinea and the Irian Jaya/Western fold-and-thrust belt in Indonesia (Figure 7). It comprises thrust sheets that incorporate Australian basement that is overlain by sediments of up to Late Miocene age (Hill, 1999; Cloos et al., 2005). The onset of deformation that formed the southern, continent-derived fold-and-thrust belt was in the Late Miocene, based on the incorporation of Miocene sediments in the entire fold-and-thrust belt and on fission-track thermochronology (Hill and Gleadow, 1989; Hill, 1991; Hill and Raza, 1999).

The continent-derived fold-and-thrust belt is underthrust to the north below a belt of metamorphic rocks, ophiolites (the Irian, April, and Marum ophiolites), and island arc volcanics and intrusives (Figure 7; Hill and Hall, 2002; Davies, 2012). Here we review the different ophiolites, which most likely formed part of a coherent oceanic lithosphere.

The Irian Ophiolite is exposed in the western part of Central New Guinea (Figure 7). It is mainly composed of serpentinized peridotites: crustal sections such as gabbros, sheeted dikes and pillow basalts have not been reported (Weiland, 1999). The ophiolite is thrust southwards over *mélange* that includes metamorphosed pillow basalt, amphibolites with greenschist and blueschist overprints, and rare eclogites (Weiland, 1999). The ophiolite and underlying oceanic crustal rocks that were likely accreted from now-subducted oceanic lithosphere that existed north of the Australian margin lie overthrust on continental metasedimentary rocks of the Ruffaer (or Derewo) unit that comprises slate and phyllites (Cloos et al., 2005), whose protoliths are likely the Jurassic and Cretaceous shales exposed in of the Irian fold-and-thrust belt and Arafura Platform to the south (Warren and Cloos, 2007). Radiometric ages from the structurally coherent ophiolite are lacking. However, K-Ar amphibole age of 57.9 ± 3.9 Ma from a gabbro float sample, and a 68.6 ± 1.1 Ma K-Ar white mica age from amygdules in a pillow basalt likely date the age of oceanic crust as they

were probably derived from the ophiolite (Weiland, 1999).

The amphibolites underlying the ophiolites yielded different age clusters. The only available U/Pb zircon age yielded 66.4 ± 0.3 Ma (Weiland, 1999), which is similar to K-Ar ages of 68.4 ± 2.4 Ma (Weiland, 1999) and K-Ar hornblende ages between 61.4 ± 1.5 and 68.3 ± 1.5 Ma and a K-Ar whole-rock age of 62.8 ± 1.5 Ma obtained from amphibolite float samples (Bladon, 1988; Permana, 1995 in Weiland, 1999). These ages were interpreted by Weiland (1999) as a metamorphic sole age suggesting incipient subduction around 68 Ma. On the other hand, K-Ar ages of hornblende obtained from the amphibolites of 182.8 ± 8.0 Ma, $40\text{Ar}/39\text{Ar}$ ages between 94.2 ± 0.9 and 171.3 ± 8.1 Ma (Weiland, 1999) and a 147 ± 3.7 Ma K-Ar whole-rock age obtained by Permana (1995) and reported by Weiland (1999), reveal a wider and much older age range. These Jurassic amphibolite ages were interpreted as recording dynamic metamorphism that occurred at mid-ocean ridge during sea floor hydration, thus dating the protolith age, whereby Cretaceous ages are interpreted as partly reset ages (Weiland, 1999). Such a Jurassic seafloor spreading age is consistent with the interpreted break-up age of northern Australia, based on the stratigraphy of the Arafura Platform (Davies, 2012).

High-pressure metamorphism occurred in the Eocene: an eclogite-facies sample yielded a 48.4 ± 0.8 Ma K-Ar white mica age and blueschist whole-rock K-Ar ages yielded an average age of 43.8 ± 2.2 Ma (Weiland, 1999). Permana (1995) reported K-Ar whole-rock ages from meta-gabbro and meta-dolerite of 49.5 ± 1.3 and 42.6 ± 1.4 Ma, showing that oceanic subduction continued through the middle Eocene. Lower grade metamorphism in the structurally underlying Ruffaer metamorphic belt to the south of the ophiolite yielded c. 35–20 Ma K-Ar whole-rock ages of metapelites and siliciclastic rocks (Weiland, 1999), indicating the Australian passive margin entered the trench below the ophiolites by latest Eocene to earliest Oligocene time.

To the north of, and likely overlying, the Irian Ophiolite are Oligocene-Miocene volcanic arc rocks that yielded K-Ar and U-Pb zircon ages of c. 35–24 and 12–10 Ma (Weiland, 1999). The older suite has an intra-oceanic arc geochemical signature, whereas the younger suite was interpreted as a volcanic arc that incorporated material derived from a continent (Weiland, 1999), consistent with the ages of the metamorphic rocks reported above.

The April Ophiolite (Figure 7), commonly referred to as the April Ultramafics, occurs as thrust slices of mainly peridotite with minor pyroxenite and gabbro and underlying partly metamorphosed sedimentary and volcanic rocks of up to middle to late Eocene age (Davies, 1982; Davies and Jaques, 1984). The ophiolitic crust is undated, but a Late Cretaceous age was assigned based on the presence of Upper Cretaceous (possibly Maastrichtian) foraminifera in limestone intercalated with pillow basalts (Ryburn, 1980). Similar to the Irian Ophiolite to the west, high pressure – low temperature metamorphic rocks (Om Formation and Tau Blueschists) are exposed south of and structurally below the ophiolite (Ryburn, 1980; Baldwin et al., 2012), with 40 – 45 Ma K-Ar ages obtained from sodic amphiboles from the Tau blueschists (Davies, 1982; Rogerson et al., 1987; Weiland, 1999). The Tau blueschists

are predominantly mafic schists with a northward increasing metamorphic grade (Ryburn, 1980). Two amphibolites that occur close to the April Ophiolite have been dated, yielding K-Ar hornblende ages of 27.2 ± 0.6 and 23.8 ± 2.8 Ma (Page, 1976). Blueschist samples that were collected in the vicinity of the April Ophiolite yielded K-Ar mica ages of 28.0 ± 0.6 and 24.9 ± 0.4 Ma (Davies, 1982; Rogerson et al., 1987). To the north, the ultramafic complex is intruded by Early to Late Miocene arc plutons comprising mostly granodiorite and diorite (Davies, 1980a).

The Marum Ophiolite forms the easternmost ophiolite complex of Central New Guinea (Figure 7). It consists mainly of peridotites and gabbros that to the south lie thrust on a thrust sheet that contains pillow lavas, lava breccia, volcanoclastics, and argillite (Davies and Jaques, 1984). Based on geochemical differences between the basalt sheet (enriched in LREE, Ti, Zr; transitional MORB; Jaques et al., 1978, 1983) and the ophiolite (depleted in LREE, Ti, Zr, Y) the basalt sheet is thought to derive from oceanic lithosphere that subducted below the ophiolite (Davies and Jaques, 1984). The only radiometric ages were reported by Jaques (1981), which are a K-Ar age of 173 Ma of plagioclase separates from cumulus gabbros and a 59 ± 2.5 Ma age from hornblende in a granophyric diorite in the upper gabbro sequence. No analytical details were provided, but these ages fall in the cluster of ages that may represent the protolith of the subducted lithosphere, and the age of the oldest metamorphism interpreted as metamorphic sole-related in the Irian Ophiolite. The pillow basalts are intercalated with argillites that contain poorly preserved radiolaria of probable Eocene age (Jaques, 1981). There is no extensive metamorphic sequence found below the ophiolite, although some low-grade metasediments are present (Jaques, 1981). These shales, siltstones and limestones are of Late Cretaceous to Eocene age and are thought to be derived from the Australian continental margin (Davies and Jaques, 1984).

The total amount of shortening in Papua New Guinea was recently estimated to be c. 500 km based on a cross section balancing analysis (Martin et al., 2023). This includes 220 km of shortening related to ophiolite emplacement over the Australian continental margin between roughly 35 and 21 Ma, 190 km of shortening within the Australian passive margin sequence underneath the ophiolite between 21 and 9 Ma (Martin et al., 2023), and c. 100 km of shortening within the Papuan fold-and-thrust belt to the south of the ophiolite since 9 Ma, consistent with earlier estimates (Hill, 1991; Hobson 1986).

The Central Highlands of New Guinea is separated from the coastal mountain ranges by prominent strike-slip fault zones that form part of the northern plate boundary zone of Australia (Figures 4 and 7). In the north, these strike-slip faults form the eastward continuation of the Sorong Fault Zone of the Bird's Head and include from west to east the Yapen Fault Zone and the Bewani-Torricelli Fault Zone. The Bewani-Torricelli Fault Zone connects eastwards to the ridge-transform plate boundary in the Bismarck Sea, which separates the North and South Bismarck microplates. The North Bismarck microplate is separated in the north and east from the Caroline and Pacific plates by the Manus and Kilinailai trenches (Figure 4). The Manus Trench continues westwards as the New Guinea

Trench. The South Bismarck microplate is separated from the Australian Plate by the onshore Ramu-Markham Fault Zone that connects eastwards with the New Britain Trench (Figure 4; e.g., Holm et al., 2015). The Ramu-Markham Fault Zone accommodates eastwards increasing convergent motion between the New Guinea orogen and the South Bismarck Microplate (Koulali et al., 2015).

The amount of left-lateral displacement on the Sorong-Yapen-Bewani-Torricelli Fault system after the late Miocene-Pliocene is estimated at ~300-370 km based on the similar U-Pb detrital zircon age spectra and lithological similarities of the Tamrau Block of the Bird's Head Peninsula and rocks in the Lengguru fold-and-thrust belt farther east (Dow and Sukanto, 1984; Webb et al., 2019).

The coastal ranges also expose ophiolites, intruding and overlying magmatic rocks, and sedimentary rocks. The geology of the westernmost range, the Foja Range, is poorly known, but includes ultramafics as well as andesites, basalts and volcaniclastic sediments, presumed to be of Paleogene age, unconformably overlain by Neogene sediments (Davies, 2012). Biak Island, north of the Sorong Fault between the Bird's Head Peninsula and the northern ranges of Central New Guinea (Figure 7), exposes an ophiolite overlain by Eocene to Lower Oligocene volcanics and Oligocene to recent shallow-marine carbonates and clastic erosion products thereof (Saragih et al., 2020). This stratigraphy is comparable to that of the northern Bird's Head Peninsula and Waigeo Island to the west.

The Cyclops Ophiolite, at the north coast of New Guinea (Figure 7), comprises peridotites, cumulate gabbros, dolerites, and lavas including pillow basalts and minor boninites (Monnier et al., 1999). The ophiolite is deformed by S-dipping thrust faults and is underthrust by undated greenschist to amphibolite facies metabasites (Monnier et al., 1999). The ophiolite is unconformably overlain by Miocene volcaniclastics and limestones. The geochemistry of the peridotites has been interpreted as supra-subduction zone affinity (Monnier et al., 1999; Zglinicki et al., 2020), and the crustal series have a geochemistry consistent with a back-arc basin origin (Monnier et al., 1999). K-Ar whole rock dating yielded a 43 ± 1 Ma age for the boninite sample, and 29.3 ± 0.7 and 29.5 ± 0.7 Ma ages of basalts with interpreted back-arc basin affinities (Monnier et al., 1999).

To the east of the Cyclops Ophiolite are the Bewani-Torricelli-Prince Alexander Mountains, which expose ultramafic, volcanic, and intrusive formations, unconformably overlain by Early Miocene to recent conglomerate, siltstone, and limestone formations (Hutchison and Norvick, 1978; Griffin, 1983; Doust, 1990). This mountain range has an ophiolitic basement, consisting of mafic and ultramafic rocks that returned an uncertain Jurassic K-Ar whole-rock age of a gabbro (188 ± 55 Ma; Hutchison and Norvick, 1978). The basement is overlain by a Paleocene to earliest Miocene volcanic complex (Bliri Volcanics) and intruded by gabbros, dolerites, and diorites (Torricelli Intrusive Complex), from which some Late Cretaceous (75-70 Ma), but mostly Eocene to Early Miocene (42-18 Ma) K-Ar ages were obtained (Hutchison, 1975; Hutchison and Norvick, 1980; Griffin, 1983; Doust, 1990). Towards the east, the basement consists of highly deformed amphibolite facies

orthogneiss and subordinate micaschist, intruded by andesite and pegmatite dikes (Griffin, 1983; Doust, 1990). K-Ar ages between 114 and 106 Ma were obtained from sheared granodiorite, while Upper Oligocene to Lower Miocene (25-20 Ma) ages were obtained from andesite and pegmatite dikes (Hutchison, 1975; Griffin, 1983). A metamorphosed sedimentary complex of unknown age is exposed to the south of the Bewani-Torricelli-Prince Alexander Mountains, referred to as the Ambunti Metamorphics (Doust, 1990). The complex consists of metapelites of mixed continental and oceanic origin (Crowhurst et al., 2004; Davies, 2012). The metamorphic grade is generally low to medium but increases northwards to locally high-grade amphibolite facies (Doust, 1990). The basement, the intrusives, and volcanics are, together with sediments of Early Miocene to Pleistocene age, exposed in top-to-the-south thrust sheets (Hutchison and Norvick, 1978, 1980).

Southeast of the Bewani-Torricelli-Prince Alexander Mountains and north of the Marum Ophiolite are the Adelbert and Finisterre ranges (Figure 4). These comprise Eocene pelagic and hemipelagic sediments with subordinate volcanics overlain by Lower Oligocene to Lower Miocene volcanics, including basalt and andesite flow breccia, pillow lavas and tuff, sometimes intercalated with argillite, micrite and radiolarian chert (Jaques, 1976; Jaques and Robinson, 1980). The Paleogene sediments and volcanics form shallow north-dipping thrust-sheets and are in the south overlying low-grade Mesozoic metasediments that are also known to the south of the Ramu-Markham Fault (Jaques 1974; Jaques and Robinson, 1980). Both the Paleogene formations and the metamorphosed Mesozoic sediments are unconformably overlain by middle Miocene to Pliocene siliciclastics and carbonates (Jaques and Robinson, 1976).

In summary, the geology of the northern mountain ranges of New Guinea is generally similar to the geology of the Central Highlands. These mountain ranges comprise Mesozoic (Jurassic to Cretaceous) oceanic crust overlain and intruded by mostly Eocene to early Miocene volcanics and intrusives, thrust towards the south over metamorphosed sediments. The exception is the Cyclops Ophiolite, which is exposed in south-dipping thrust sheets, and of which Eocene to Oligocene crystallization ages were obtained.

Papuan Peninsula

The geology of the Papuan Peninsula overall follows a similar logic as in central New Guinea. It exposes an ophiolite belt, underlain in the south by metamorphosed ocean- and continent-derived, accreted metasedimentary and meta-igneous thrust slices, and overlain by Paleogene and Neogene volcanics (Figure 7). However, the architecture of the accreted thrust slices differs from Central New Guinea.

The ophiolite exposed on the Papuan Peninsula is referred to as the Papuan Ultramafic Belt (e.g., Davies and Smith, 1971; Davies, 1980b; Davies and Jaques, 1984; Lus et al., 2004). The most complete sequence of this ophiolite is exposed as a NE-ward dipping unit containing tectonite and cumulate ultramafic rock, gabbroic rock, sheeted dikes, and pillow basalts that are interbedded with calcareous pelagic sediments. Less complete parts

of this ophiolite are found farther east on the D'Entrecasteaux and Louisiade islands, on the Moresby Seamount, and on Muyua/Woodlark Island (Davies and Smith, 1971; Davies and Warren, 1988; Monteleone et al., 2001; Little et al., 2011; Webb et al., 2014; Lindley, 2021). Geochemical signatures of basalts in the Papuan Ultramafic Belt are interpreted as varying between MORB and supra-subduction zone signature (Jaques and Chappell, 1980; Whattam et al., 2008; Whattam, 2009). A minimum age of the ophiolite is provided by 50–55 Ma K-Ar hornblende and plagioclase ages from plagiogranites and diorites that intrude the ophiolite (Davies and Smith, 1971). Late Paleocene (58.9 ± 1.1 Ma and 58.8 ± 0.8 Ma) $^{40}\text{Ar}/^{39}\text{Ar}$ whole rock ages were obtained from a tholeiitic lava and boninite from the Dabi Volcanics, which are exposed east of the main ophiolite body (Walker and McDougall, 1982). Others assigned a Late Cretaceous (Maastrichtian) age to the ophiolite based on the ages of foraminifera in sediments intercalated with basalts (Davies and Smith, 1971; Lus et al., 2004). The structural relationship between these stratigraphic units and the ophiolite is unclear, and as the age of the sediments is older than the crystallization ages of the crust of the ophiolite, we speculate that the basalts overlain by Maastrichtian sediments are from the unit that is structurally below the ophiolite. The ophiolite is overlain by Paleocene to Eocene carbonates, turbidites, and volcanics including pillow lavas, Upper Oligocene to middle Miocene platform carbonates, turbidites, submarine basalt and volcanoclastics and Miocene to recent continental clastics derived from contemporary volcanism (Davies and Smith, 1971).

The ophiolite nappe is thrust over a metamorphic sole along the Owen Stanley Fault Zone. The metamorphic sole grades downwards from granulite to amphibolite facies rocks (Lus et al., 2004). The cooling of the metamorphic sole is dated to 58.3 ± 0.4 Ma, obtained from the mean $^{40}\text{Ar}/^{39}\text{Ar}$ age of five samples (Lus et al., 2004), i.e., the same age as the age of the SSZ ophiolitic crust, as is commonly observed worldwide (e.g., Van Hinsbergen et al., 2015). The Owen Stanley Fault thus originally formed as a subduction interface, but currently forms the plate boundary between the Australian and Solomon Sea plates (Davies and Jaques, 1984). The current relative motion along the Owen Stanley Fault transitions from transtensional in the southeast to strike-slip and transpressional in the northwest (Benyshek and Taylor, 2021).

A unit of mafic schists is thrust below the metamorphic sole. This unit, referred to as the Emo Metamorphics, consists of metamorphic rocks ranging from prehnite-pumpellyite to greenschist facies, that locally overprint an older blueschist facies metamorphism (Pieters, 1978; Worthing and Crawford, 1996). Cooling of amphibolite minerals has been dated to ~34 Ma and ~14 Ma, based on $^{40}\text{Ar}/^{39}\text{Ar}$ ages (Worthing and Crawford, 1996). Protolith rock constituted gabbro, micro-gabbro and basalt, interbedded with minor volcanoclastic sediments (Davies and Jaques, 1984; Pieters, 1978; Worthing and Crawford, 1996; Smith, 2013). Basalts show a geochemical signature intermediate between E-MORB and N-MORB and were interpreted as back-arc basin-derived (Worthing and Crawford 1996; Smith, 2013; Österle et al., 2020). An age of the protolith has not been established.

A partly metamorphosed body of continent-derived clastic rocks with minor metavolcanics is underthrust below the Emo Metamorphics (Pieters, 1978; Worthing and Crawford, 1996). This unit, the Kagi Metamorphics, contains garnet-greenschist rock, which grade southwards to unmetamorphosed clastic sedimentary rock (Pieters, 1978; Johnson, 1979; Worthing and Crawford, 1996). The age of the protolith ranges from Middle Cretaceous to Early Eocene based on rare occurrences of planktonic foraminifera (Johnson, 1979; Worthing and Crawford, 1996; Davies, 2012).

The continent-derived Kagi Metamorphics are underlain by another unit of oceanic crustal rocks, known as the Milne Terrain, consisting of gabbro, dolerite, and basalt, with N-MORB to E-MORB geochemistry without a trace of arc or supra-subduction zone signature (Davies and Smith, 1971; Wai et al., 1994; Smith, 2013; Österle et al., 2020). Farther east, the Emo and Kagi metamorphics pinch out and the Milne Terrain is in direct structural contact with the Papuan Ultramafic Belt (Smith, 2013). Detrital zircons from metasediments intercalated with metabasalts yielded maximum depositional ages of ~103 and ~72 Ma for two different samples (Österle et al., 2020). These basalts are intruded by low-grade tholeiitic meta-grabbroic and tonalitic rocks that yielded zircon U-Pb ages between 67.1 ± 2.5 and 53.6 ± 1.2 Ma (Österle et al., 2020). In addition, K-Ar hornblende ages of 56.3 ± 0.5 and 55.7 ± 1.5 Ma were obtained from gabbroic rocks (Rogerson and Hilyard, 1990). The fault separating the Milne Terrain from the Kagi Metamorphics is covered by an Upper Miocene (~5.7 Ma) basalt flow (Davies and Smith, 1971; Pain, 1983), providing a minimum age for emplacement of the continent-derived series over the ocean-derived series.

The southernmost, and structurally lowest, tectonic unit of the Papuan Peninsula is the Aure-Moresby fold-and-thrust belt. The Aure-Moresby fold-and-thrust belt and associated foreland basin formed since the late Miocene (Ott and Mann, 2015). Here, the orogen of the Papuan Peninsula is thrust over thinned continental crust of the Papuan and Eastern plateaus (Ott and Mann, 2015). The Papuan and Eastern Plateaus comprise pre-Mesozoic basement that was separated from Australia during opening of the Coral Sea Basin (Gaina et al., 1998). The thinned continental crust of these plateaus is covered with Upper Cretaceous to Paleocene syn-rift clastics, Paleocene to Oligocene post-rift deep water carbonates and Oligocene to recent pelagic sediments (Rogerson and Hilyard, 1990; Ott and Mann, 2015).

3.4.5. Louisiade Archipelago and Louisiade Ophiolite

The elevated ridge of the Papuan Peninsula (Pocklington Rise) continues to the east, mostly submerged with small islands known as the Louisiade Archipelago, with a southward convex shape (Figure 4). The Pocklington Rise forms the southern margin of the Woodlark Basin and is in the east overthrust by the Solomon Islands at the San Cristobal Trench. Metamorphosed mafic volcanics and associated intrusives are exposed on the Deboyne Islands (Davies and Smith, 1971), and a mélange of ultramafic rocks is thrust towards the SW over a metasedimentary schist unit (Webb et al., 2014). The majority of the Louisiade

Archipelago comprises metasediments and intruding metagabbros, both of which underwent prehnite-pumpellyite to greenschist facies metamorphism (Webb et al., 2014). Based on detrital zircon U-Pb ages, it was inferred that the protoliths of the metasedimentary rocks are volcanoclastics derived from a Cretaceous silicic Large Igneous Province of the eastern Australian margin (Zirakparvar et al., 2013). This led to the interpretation that the metasediments of the Louisiade Archipelago represent a rifted fragment of the Australian passive margin that became separated from Australia during opening of the Coral Sea (Webb et al., 2014).

To the east of the Louisiade Archipelago, the Louisiade Ophiolite was recently identified based on dredging of the northern Louisiade Plateau (Figures 4 and 7). This returned serpentinized peridotites, basalt breccia, and lavas, together with sedimentary rocks, and geochemical data suggest it is a supra-subduction zone ophiolite (McCarthy et al., 2022). Based on a seismic reflection transect, the ophiolite was interpreted as obducted towards the south onto the Louisiade Plateau, analogous to the Papuan Ultramafic Belt (Davies and Jaques, 1982; McCarthy et al., 2022).

3.4.6. Woodlark microplate

The Woodlark Basin is bounded by the Pocklington Rise in the south and by the Woodlark Rise in the north and contains the N-S spreading ridge that separates the Woodlark Microplate from Australia. The oldest unit exposed on Muyua/Woodlark Island, on the Woodlark Rise, comprises metamorphosed sandstones and chert beds, including turbidite and shallow marine shelf deposits of unknown age, in the southeast sometimes intercalated with basalt (Lindley, 2021). Based on the age of the unconformably overlying Upper Oligocene to Middle Miocene platform carbonates, the age of the oldest unit is inferred to be Paleocene to Eocene (Joseph and Finlayson, 1991; Lindley, 2021). Middle Miocene (14–12 Ma) volcanism is not straightforwardly linked to subduction, and may be extension-related (Lindley, 2021). This episode of post-middle Miocene extension may be related to the early opening of the Woodlark Basin.

The Woodlark Ridge produced ocean floor with magnetic anomalies initially interpreted as dating back C2A (3.5 Ma; Weissel et al., 1982). Taylor et al. (1999) subsequently identified additional anomalies back to C3A (6.2 Ma) in the southeast of the basin. Reconstructed spreading rates of the Woodlark plate decrease westward and define an Australia-Woodlark Plate Euler pole on the eastern Papuan Peninsula. To the west of this pole, the Woodlark-Australia plate boundary is likely formed by the Owen Stanley Fault Zone that ends in a triple junction with the New Britain Trench and the Ramu-Markham Fault Zone. The New Britain Trench connects to the San Cristobal Trench, which consumes the Woodlark Ridge (Figure 4).

Towards the west, the amount of extension in the Woodlark Basin decreases and just east of the Woodlark-Australia Euler pole, on the D'Entrecasteaux Islands, the extension did not lead to oceanic spreading, but to extension of the orogen and exhumation of

previously buried orogenic units. The D'Entrecasteaux Islands expose one of the youngest metamorphic core complexes and the youngest exhumed ultrahigh-pressure rock on Earth, which were at a depth of more than 90 km at about 8 Ma based on U-Pb zircon dating from eclogites and host gneisses, and garnet Lu-Hf ages on coesite eclogite (Baldwin et al., 1993, 2004, 2008; Monteleone et al., 2007; Zirakparvar et al., 2011). The metamorphic core complexes, exposing mafic eclogites, are separated from non-metamorphosed mafic and ultramafic rocks by Pliocene ductile shear zones and brittle fault zones (Davies and Warren, 1988; Baldwin et al., 1993; Hill, 1994). Final exhumation of the rocks to the surface occurred since the Plio-Pleistocene and extension is still active (Baldwin et al., 1993, 2004; Hill and Baldwin, 1993).

Metamorphic grade decreases southeastwards. On Misima Island, to the southeast of the D'Entrecasteaux Islands, upper amphibolite-facies felsic to mafic gneisses are juxtaposed against greenschist-facies schist and unmetamorphosed sediments along a low angle normal fault (Zirakparvar et al., 2013). The Louisiade Archipelago exposes prehnite-pumpellyite to greenschist facies metasediments and metagabbros (Webb et al., 2014). Conversely, $^{40}\text{Ar}/^{39}\text{Ar}$ cooling ages become younger westwards, which is thought to be related to the westward propagation of the Woodlark Rift (Baldwin et al., 2008). Based on Nd and Hf isotopic, U-Pb zircon geochronologic, and trace element data, Zirakparvar et al. (2013) inferred that the (U)HP basement gneisses of the D'Entrecasteaux Island were derived from the Cretaceous Large Igneous Province of eastern Australia, akin to the metasediments exposed in the Louisiade Archipelago. This connection between these islands with the Australian continent led to a tectonic model in which the metamorphosed rocks exposed on the D'Entrecasteaux Islands are derived from the thinned Australian continental margin that was subducted northwards, below the Papuan Ophiolite, and subsequently exhumed from below the ophiolite during extension in the Woodlark Rift (e.g., Baldwin et al., 2008). A 68.0 ± 3.6 Ma Lu-Hf age was obtained from a garnet porphyroblast within a Pleistocene amphibolite facies shear zone, which was interpreted to record subduction of the Australian continental margin (Zirakparvar et al., 2011), but may instead mark the arrival of a microcontinent that rifted from the Australian margin. A similar age of 66.4 ± 1.5 Ma was obtained using U-Pb zircon dating of a diabase sample obtained from a drill site on the Moresby Seamount (Monteleone et al., 2001), which is interpreted to have formed part of the upper plate during northwards subduction (Monteleone et al., 2001; Zirakparvar et al., 2013).

To the north of the D'Entrecasteaux Islands is the Trobriand Scarp that forms a marked northward deepening of bathymetry towards the Solomon Sea basin (Figure 4). Marine magnetic anomalies were first identified in the Solomon Sea basin by Joshima et al. (1987). These authors developed different models that could fit the anomaly pattern, and then preferred a model in which the anomalies formed during chrons C12 to C9 (33–28 Ma), younging southwards. To explain the absence of a conjugate set of anomalies to the south (the ophiolites of the Papuan Peninsula and d'Entrecasteaux Islands are considerably older (~59

Ma; Davies and Smith, 1971; Walker and McDougall, 1982; Rogerson and Hilyard, 1990), they proposed that the Trobriand Scarp may have been a subduction zone that consumed the southern conjugate lithosphere. However, there is no clear fault or trench along the Trobriand Scarp, nor evidence for an accretionary prism. Later, Gaina and Müller (2007) reinterpreted the marine magnetic anomalies as chrons C19-C15 (41-35 Ma), younging northward. This would require that the northern conjugate lithosphere has subducted northward along the still-active San Cristobal and New Britain trenches. Extrapolating the spreading rates reconstructed from the Solomon Sea floor back in time could well explain the ages of the ophiolites on the Papuan Peninsula if these are part of the same oceanic lithosphere. Hence, in this scenario there is no need to invoke that subduction occurred along the Trobriand Scarp. Instead, this scarp likely represents the northern margin of the continental lithosphere of the Papuan and Eastern plateaus below the obducted Papuan ophiolites.

3.4.7. North and South Bismarck plates; New Britain; New Ireland

The Melanesian Borderlands occupy the zone of microplates that intervene the Australian and Pacific plates. This region includes the Bismarck Sea, the islands of Manus, New Britain, New Ireland, the Solomon Islands and Vanuatu (Figure 4).

The Bismarck Sea hosts the Manus spreading ridge that is estimated to have started around 3.5 Ma based on the identification of active spreading and marine magnetic anomalies back to C2A (3 Ma; Taylor, 1979). This spreading ridge links up towards the west with the Bewani-Torricelli-Yapen-Sorong fault system. The opening of this basin thus constrains the amount of left-lateral strike-slip on these faults, which is within the range of the estimated 300-370 km based on lithological constraints (Dow and Sukanto, 1984; Webb et al., 2019).

New Britain is part of the South Bismarck Plate and is likely contiguous with the Adelbert and Finisterre ranges of the eastern Coastal Ranges of central New Guinea (e.g., Abott, 1995). On the North Bismarck Plate are the islands of Manus and New Ireland together with some smaller islands (Figure 4). Prior to the late Neogene extension in the Manus Basin, all these islands were part of the same plate and the islands of the Bismarck plates have a similar tectono-sedimentary architecture. The oldest formations of these islands comprise Upper Eocene pillow basalts, andesite lavas, andesitic breccia and volcanics interbedded with coralline and tuffaceous limestone (Francis, 1988; Lindley, 1988, 2006; Stewart and Sandy, 1988; Davies, 2005) that overlie an unknown, but presumably oceanic crust. The age of these formations is based on paleontological evidence and radiometric ages, including 49.0 ± 5.0 and 45.8 ± 5.0 K-Ar ages from Manus Island (Francis, 1988), and a 37.4 ± 1.7 K-Ar age from a dike intruding the oldest volcanics on New Ireland (Stewart and Sandy, 1988). On all three islands, these oldest volcanic units are overlain by Oligocene to middle Miocene volcanics and limestone and intruded by upper Oligocene to lowermost Miocene arc plutons (Francis, 1988; Lindley, 1988; Stewart and Sandy, 1988; Davies, 2005;

Lindley, 2006). Subsequently, extensive platform carbonates were deposited during a lull in magmatism from the middle to late Miocene (Francis, 1988; Lindley, 1988; Stewart and Sandy, 1988). Regional-scale volcanism became active again in the early Pliocene (Francis, 1988; Lindley, 1988; Stewart and Sandy, 1988). Recent volcanism on New Britain and on islands to the north of the main island, as well as the West Bismarck arc, is suggested to be related to subduction at the New Britain Trench (e.g. Weissel et al., 1982; Woodhead et al., 2010; Baldwin et al., 2012; Holm et al., 2016), while the extensional opening of the Manus Basin may be responsible for recent volcanism on the islands northeast of New Ireland (Lindley, 2016).

3.4.8. Solomon Islands

The modern North Bismarck Plate continues eastward towards the island of Bougainville (politically part of Papua New Guinea) and the Solomon Islands (Figure 4 and 7). The Solomon Islands are in an upper plate position relative to the San Cristobal Trench that consumes the Woodlark microplate, and Australian Plate basins and ridges, such as the Santa Cruz Basin, along the southwestern margin of the archipelago. The northern boundary of the Solomon Islands is the North Solomon Trench which forms the continuation of the Manus and Kilinailai trenches (Tregoning et al., 1998). Oceanic crust of the Ontong Java Plateau on the Pacific Plate is being subducted below the Solomon Islands along this trench, although relative convergent motion is slow ($\sim 14\text{--}23$ mm/yr; Tregoning et al., 1998; Phinney et al., 2004; Taira et al., 2004).

The Solomon Islands expose two basement terranes and two generations of arc volcanism. The uppermost basement terrane is an ophiolite, exposed on the islands of Choiseul, southern Santa Isabel, Guadalcanal, and Makira (Figure 7). It comprises peridotites, some gabbro and dolerite, and abundant pillow lavas that are in places intercalated with cherts and pelagic limestones (Coulson and Vedder, 1986; Ridgway and Coulson, 1987; Berly, 2005; Tejada et al., 1996; Petterson et al., 1999, 2009). $^{40}\text{Ar}/^{39}\text{Ar}$ dating of basalt samples from Santa Isabel yielded five ages between 60.9 ± 1.2 Ma and 64.0 ± 1.1 Ma, as well as two ages of ~ 46.5 Ma (Tejada et al., 1996). A 46.5 ± 1.2 Ma zircon U-Pb age was obtained from a gabbro sample from Choiseul Island (Battan et al., 2022). The basalts display a wide range in geochemical signatures, but are generally MORB-like, with some lavas having characteristics of back-arc basin basalts (Tejada et al., 1996; Berly, 2005). A supra-subduction zone affinity was found in gabbros and periodites on San Jorge and Santa Isabel islands (Berly, 2005; Berly et al., 2006).

The ultramafic section of the ophiolite overthrusts to the northeast a unit of volcanic rocks and schists with a metamorphic grade up to amphibolite facies, exposed on Choiseul and Santa Isabel (Ridgway and Coulson, 1987; Berly, 2005). This unit may represent the metamorphic sole of the ophiolite that formed during subduction initiation. Radiometric ages that constrain the metamorphism are sparse, but K-Ar ages of ~ 36.5 Ma and 44.7 ± 2.1 Ma of tremolite-actinolite-amphibolite from Nggela Island were obtained by Neef and McDougall (1976), and Richards et al. (1966) presented K-Ar ages between 32.4 ± 6.8 Ma

and 51.5 ± 6.8 Ma, with a mean of 44 ± 18 Ma of amphibolite and schists from Choiseul.

Exposed on the islands of Santa Isabel, Malaita, and Maramasike, to the northeast of the ophiolite, and structurally underlying the metamorphic rocks, is an OPS sequence comprising mainly of tholeiitic pillow and flow basalts and some minor gabbro, overlain by Cretaceous-Pliocene pelagic cherts and limestones (Petterson et al., 1999). $^{40}\text{Ar}/^{39}\text{Ar}$ ages of 120.8 ± 2.4 and 121.8 ± 2.9 were obtained from basalts exposed on Malaita, and ages of 122.9 ± 1.5 and between 90 and 95 Ma were obtained from basalts on Santa Isabel (Tejada et al., 1996). These ages are very similar to the 120.6 ± 0.9 Ma and 88–93 Ma $^{40}\text{Ar}/^{39}\text{Ar}$ ages obtained from drill holes on the Ontong Java Plateau (Tejada et al., 1996; Mahoney et al., 1993). Based on these corresponding ages and identical isotopic ratios and geochemistry (transitional between tholeiitic N-MORB and E-MORB) of the Ontong Java Plateau (e.g., Kroenke et al., 1986; Mahoney et al., 1993; Tejada et al., 1996, 2002; Petterson et al., 1997; Phinney et al., 1999) this sequence is interpreted as accreted Ontong Java Plateau lavas (Petterson et al., 1999; Phinney et al., 2004). A 44.2 ± 0.2 Ma $^{40}\text{Ar}/^{39}\text{Ar}$ age obtained from basalts on Malaita was interpreted lavas that erupted onto the Ontong Java Plateau when it passed over the Samoan hotspot (Tejada et al., 1996). These accreted sequences are unconformably overlain by Upper Pliocene-Pleistocene clastic sedimentary formations (Petterson et al., 1997; Cowley et al., 2004), and accretion of Ontong Java Plateau rocks to the Solomon Islands thus occurred since c. 4 Ma (e.g., Mann and Taira, 2004; Phinney et al., 2004).

Overlying and intruding the Solomon ophiolite are arc complexes that formed during two periods separated by a lull. The older episode of arc volcanism occurred in the Oligocene–Early Miocene, the younger, currently active, episode started in the latest Miocene (Kroenke et al., 1986; Petterson et al., 1999). Tapster et al. (2014) reported 23.3–25.7 Ma U–Pb zircon ages from tonalite and diorites, in correspondence with the 24.4 ± 0.3 K–Ar age of a tonalite (Chivas and McDougall, 1978), both from Guadalcanal. The tonalite and diorite samples of Tapster et al. (2014) also include zircon xenocryst samples with c. 39–33 Ma and 71–63 Ma U–Pb ages, which may be recycled zircons from earlier arc volcanism or from the ophiolite. The oldest volcanoclastics in the Solomon Islands are of Late Oligocene age (Cowley et al., 2004). The oldest radiometric age reported for the younger volcanic arc sequence is a 6.4 ± 1.9 K–Ar age from Guadalcanal (Petterson et al., 1999).

3.4.9. Vanuatu; Vitiaz Trench; North Fiji Basin.

Towards the east, the WNW–ESE trending San Cristobal trench changes its orientation and connects with the NNW–SSE trending New Hebrides trench. The Vanuatu archipelago to the east of this trench forms an active intra-oceanic arc above the NE-dipping New Hebrides subduction zone (Figure 4). The active arc overlies an older arc basement, of which the oldest dated rocks returned 39 ± 5 and 36.7 ± 1 K–Ar ages of hornblende andesite (Taylor et al., 1985), a 35.4 ± 3.8 $^{40}\text{Ar}/^{39}\text{Ar}$ age of basaltic andesite and a 32.4 ± 0.57 U–Pb zircon age of dolerite (Buys et al., 2014). These ages are similar to the oldest zircon U–Pb ages reported

from Fiji (38.6 ± 0.5 Ma; Rickard and Williams, 2013), which formed part of the same arc before opening of the North Fiji Basin since c. 10 Ma (Yan and Kroenke, 1993; Malahoff et al., 1994; Chapter 1). In addition to these late Eocene ages, several late Oligocene and early Miocene ages have been reported from the western belt of Vanuatu (e.g. Mitchell and Warden, 1971; Crawford et al., 2003; Buys et al., 2014), whereas magmatism in Fiji was most prominent between c. 15 and 5 Ma (Cluzel and Meffre, 2019). Furthermore, a dismembered ophiolite suite is exposed on Pentecost Island in eastern Vanuatu, which comprises peridotites and gabbros with lenses of amphibolites and green schist in serpentinites (Mitchell and Warden, 1971; Parrot and Dugas, 1980). An $40\text{Ar}/39\text{Ar}$ age of 44.9 ± 3.0 was obtained from a dolerite dyke within the ophiolite, while an amphibolitic mylonite and a metadolerite of greenschist facies, yielded $40\text{Ar}/39\text{Ar}$ ages of 33.4 ± 0.8 and 35.5 ± 0.6 , respectively (Crawford et al., 2003).

The North Solomon Trench connects to the east with the Vitiaz Trench Lineament (Fairbridge and Stewart, 1960) that currently forms a transform plate boundary between Cretaceous crust of the Pacific Plate and Neogene crust of the North Fiji Basin (e.g., Pelletier and Auzende, 1996; Gill et al., 2022). Not much is known about this feature, but it is generally thought that it formed originally as a subduction zone, where the Pacific Plate was being subducted (south)westwards since the Eocene, until a polarity switch in the Miocene that was likely associated with the arrival of the Ontong-Java Plateau in the trench (Brocher, 1985; Pelletier and Auzende, 1996; Crawford et al., 2003).

3.4.10. New Caledonia; Northland Ophiolite

Finally, the obduction front of ophiolites that is traced from the Papuan Peninsula to the Louisiade Ophiolites continues from the D'Entrecasteaux Ridge to the south, over New Caledonia towards the North Island of New Zealand (Figure 4). The architecture and evolution of this belt was extensively described in Chapter 1, which we here summarize and update with recently published results. The New Caledonia Ophiolite (Figure S2), also referred to as the Peridotite Nappe, is interpreted to have formed in a supra-subduction zone setting (e.g., Maurizot et al., 2020a). The age of formation of the ophiolite's crust is not well constrained, as existing K-Ar ages are considered unreliable (Maurizot et al., 2020b). The age of the metamorphic sole is c. 56 Ma, based on $40\text{Ar}/39\text{Ar}$ hornblende and U-Pb zircon dating of amphibolites (Cluzel et al., 2012b). Timing of emplacement of the ophiolite is bracketed by 34 Ma age of the youngest sediments that are thrust below the ophiolite (Cluzel et al., 2001), and the c. 27 Ma age of post-obduction plutons that intrude into the Peridotite Nappe (Paquette and Cluzel, 2007; Sevin et al., 2020). Based on geophysical modelling from seismic and gravity data, the Peridotite Nappe may be contiguous with the oceanic lithosphere that underlies the North Loyalty Basin to the north of the main island of New Caledonia (Collot et al., 1987; Patriat et al., 2018).

The ophiolite is the highest structural unit that is exposed in New Caledonia. Below the metamorphic sole of the ophiolite occur several units that were incorporated in the

NE-dipping New Caledonia subduction complex (Maurizot et al., 2020a). The uppermost section comprises oceanic crust as well as a passive margin succession (Poya Terrane), which formed part of the South Loyalty Basin, the conceptual oceanic basin that was subducted at the New Caledonia subduction zone. Based on macro-fossils and detrital zircon provenance, the South Loyalty Basin likely opened in the Late Cretaceous (Campanian) - Paleocene, based on geochemistry as a back-arc basin (Cluzel et al., 2018). Structurally below the Poya Terrane is the Montagnes Blanches Nappe, which was derived from the sedimentary cover of passive margin of the Norfolk Ridge (Maurizot et al., 2020a, b) that forms the eastern margin of the extended continent Zealandia, the easternmost continental crust of the Australian Plate (Mortimer et al., 2017). A belt of HP-LT metamorphic rocks of oceanic and continental passive margin origin is exposed in the northeast of the main island of New Caledonia (Maurizot et al., 2020a). Syn-tectonic trench-fill sediments were deposited during the Eocene, and unconformably over a Cretaceous and older accretionary prism and overlying forearc basin, related to subduction below the entire East Gondwana margin (Maurizot, 2011; Maurizot and Cluzel, 2014).

The obduction front is inferred to continue submarine along the eastern margin of the Norfolk Ridge and western margin of the Three Kings Ridge to the southernmost exposures: the Northland Ophiolite in northernmost North Island, New Zealand (Figure S2). This ophiolite formed in a supra-subduction zone setting (Whattam et al., 2004, 2005) and its oceanic crust is thought to be of Paleocene age, based on radiolarians in limestones that are intercalated with pillow basalts (Hollis and Hanson, 1991). The ophiolite also returned Oligocene ages: between 25.1 ± 1.2 and 26.1 ± 1.0 based on $40\text{Ar}/39\text{Ar}$ dating of tholeiitic basalts and 31.6 ± 0.2 Ma 28.3 ± 0.2 based on U/Pb zircon dating of a gabbro and a plagiogranite (Whattam et al., 2005, 2006). The age of emplacement is constrained by the youngest upper Oligocene sediments that are part of the ophiolite and the lower Miocene age of the oldest sediments sealing the basal thrust (Ballance and Spörli, 1979).

The New Caledonia and Northland ophiolites thrust (south)westward over accretionary complexes that formed during long-lived, Mesozoic subduction below the East Gondwana margin (Mortimer, 2004; Mortimer et al., 2014a; Maurizot et al., 2020a, b). Westward Mesozoic subduction below the East Gondwana margin ended between 90 and 85 Ma at the New Caledonia margin and possibly ~79 Ma along New Zealand (Chapter 3).

4. Paleomagnetic data

We initially made the reconstruction based on marine geophysical and structural geological constraints without paleomagnetic data as input, after which we tested our reconstruction against paleomagnetic data. Where necessary, we then iterated the reconstruction within the previous constraints (see Van Hinsbergen et al. (2020a) for details on the approach).

There is only a limited amount of paleomagnetic data available in the Junction Region, and most of it was collected from the Philippine Sea Plate. We used the paleomagnetic data compilation of the Philippine Sea Plate of Chapter 5. In addition, paleomagnetic data

relevant for the reconstruction are available from the Baliojong accreted OPS units of Sabah, North Borneo (Chapter 4) from accreted rocks of the Southern Palawan/Calatugas Ophiolite (Almasco et al., 2000), and from the Eocene volcanic rocks of the Solomon Islands (Musgrave, 1990). (Supplementary Table S1).

As explained in Chapter 5, paleomagnetic data from the Junction Region either come from strongly deformed and uplifted plate margins, or from drill cores, and the declinations of those data that inform vertical axis rotations display strong regional differences owing to local deformation, or drill core rotation. We therefore only test our reconstruction against paleolatitude data computed from inclinations. In addition, we tested our reconstruction against paleolatitudes obtained from igneous data only, as the number of samples collected at sedimentary localities is insufficient to correct for inclination shallowing, which makes testing our reconstruction against sedimentary data problematic.

We use the global apparent polar wander path of Vaes et al. (2023) for the major plates surrounding the Junction Region (Eurasia, Australia, Pacific). For times prior to the 85 Ma connection of the Pacific Plate to Antarctica, we follow Boschman et al. (2019) in estimating the relative rotations of the Pacific Plate to South Africa using two mantle reference frames (Torsvik et al., 2019 for the Pacific, Van der Meer et al., 2010 for the Indo-Atlantic), and used this connection to predict the position of the Pacific and surrounding plates (e.g., Izanagi) in the paleomagnetic reference frame. The predicted paleolatitudes of the reconstruction that is described in section 5 compared to the paleomagnetic data in our compilation is given in Figure 8.

5. Reconstruction

This section presents our reconstruction, which in principle straightforwardly follows from the reconstruction protocol explained in section 2, and the kinematic and geological constraints reviewed in section 3 and summarized in Table 1. GPlates reconstruction files are available in the Supporting Information. Here, we provide a description of the reconstruction (see Figures 9 - 32) from the present back to the past, i.e., in order of increasing levels of interpretation. Each section describes a period back to a moment where we made a key choice or interpretation.

Our approach to the reconstruction of the Cenozoic Philippine Sea Plate differs fundamentally from previous reconstructions (Hall, 2002; Gaina and Müller, 2007; Seton and Müller, 2008; Zahirovic et al., 2014; Wu et al., 2016; Liu et al., 2023). The most important difference with most previous renditions is that we do not use paleomagnetic data as basis to infer vertical axis rotations of the Philippine Sea Plate. This is based on a critical re-appraisal of paleomagnetic data from the Philippine Sea Plate, which showed that the available datasets are small and do not unequivocally demonstrate whole-plate rotation, but may instead reflect regional deformation-associated rotations (Chapter 5).

Previous plate reconstructions that focus on the Junction Region generally only go back to the early Eocene (Hall, 2002; Gaina and Müller, 2007; Wu et al., 2016; Liu et al., 2023), as

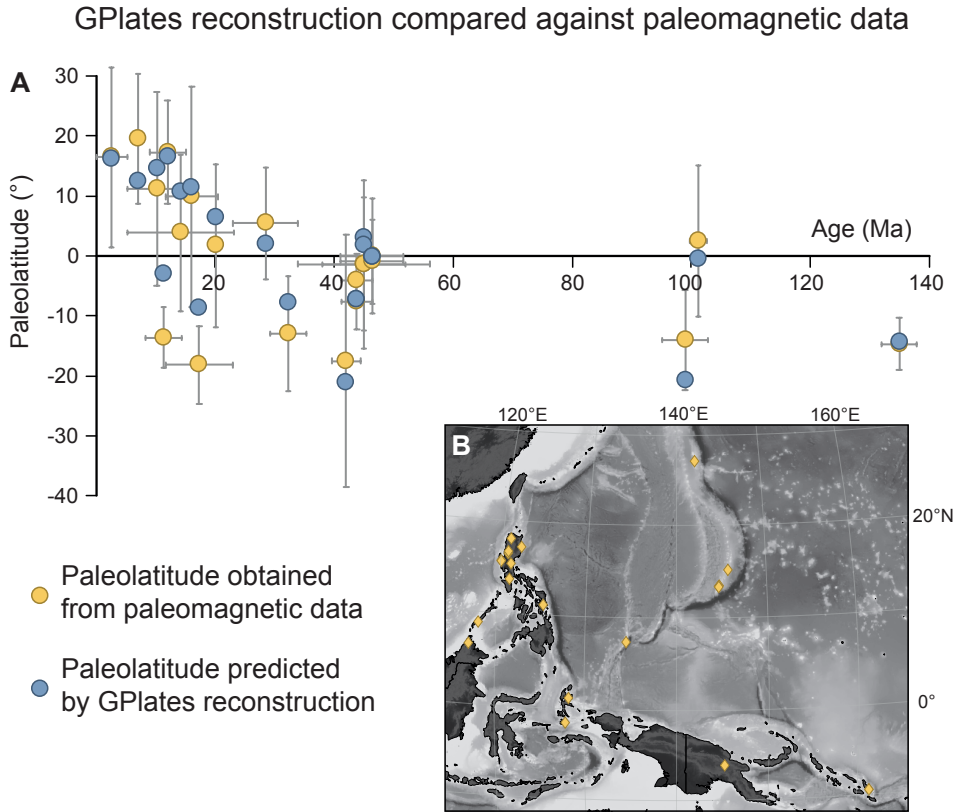


Figure 8. A) Graph that compares the paleolatitudes of paleomagnetic sampling locations predicted in our GPlates reconstruction against paleomagnetically obtained paleolatitudes. B) Paleomagnetic sampling locations. The paleomagnetic compilation is provided in the Supporting Information as Table S1.

this is the classically inferred age of subduction initiation at the Izu-Bonin-Mariana trench (Stern and Bloomer, 1992; Reagan et al., 2010). Of the regional reconstructions, only those of Seton and Müller (2008) and Zahirovic et al. (2014) extend back to the Early Cretaceous. Global plate and paleogeographic reconstructions (e.g., Seton et al., 2012; Müller et al., 2019; Scotese, 2021) do go back to the early Mesozoic, but these do not describe the data or rationale behind their reconstruction of the Junction Region. Hence, our reconstruction is the first to consider the entire western Pacific/Panthalassa Plate system, starting from modern geological architecture and developing the reconstruction back in time using systematic plate boundary continuation, assuming the simplest plate tectonic scenario that satisfies geological observations.

At the end of each reconstruction section, we compare our reconstruction with the reconstructions of Hall (2002), Gaina and Müller (2007), Zahirovic et al. (2014), model 1 of Wu et al. (2016), and Liu et al. (2023) back to the Early Cretaceous. We do not compare our

Table 1. Summary of kinematic data and predicted relative motions in our reconstruction

Location	Interpretation	Type of data used	Anomalies	Time (Ma)	Reference
Philippine Sea Plate					
Mariana trough	Back-arc extension	Marine magnetic anomalies	3n.3 - 0	4.8 - 0	Yamazaki et al. (2003)
Mariana trough	Start of extension	Magnetic vector analysis, DSDP Leg 60		6 - 4.8	Yamazaki and Stern (1997); Iwamoto et al. (2002); Hussong and Uyeda (1982)
Ogasawara trough	Back-arc extension	Stratigraphy		55 - 53	Ishizuka et al. (2006)
Shikoku Basin	Back-arc extension	Marine magnetic anomalies	C7.2n y - 5Dn y	24.47 - 17.24	Sdrolias et al. (2004); Seton et al. (2014)
Parece Vela Basin	Back-arc extension	Marine magnetic anomalies	C9n - C5Dn	27.44 - 17.24	Sdrolias et al. (2004); Seton et al. (2014)
Parece Vela and Shikoku basins	Beginning of extension	Age of arc magmatism along Kyushu - Palau ridge		30	Ishizuka et al. (2011)
Parece Vela and Shikoku basins	End of extension	15.6 ± 0.1 Ma basalt from extinct spreading ridge		15	Ishizuka et al. (2010)
Guam and Northern Mariana Islands	Back-arc extension	Geometry (line up with Palau Ridge)		28 - 20	This study
West Philippine Basin	Oceanic spreading	Marine magnetic anomalies	C22n.2n y - C14n y	53.20 - 35.29	Hilde and Lee (1984); Deschamps and Lallemant (2002)
Okinawa Trough	Back-arc extension	Crustal structures (refraction data)		10 - 6 and 2 - 0	Sibuet et al. (1995); Miki et al. (1995); Arai et al. (2017)
Kita Daito Basin	Back-arc extension	Crustal structures (refraction data)		46 - 41	Ishizuka et al. (2022)
Minami Daito Basin	Back-arc extension	51.3 - 42.8 Ma dredged basalts		52 - 48	Hickey-Vargas (1998); Ishizuka et al. (2013)
Amami Sankaku Basin	Back-arc extension	49.3 - 46.8 Ma drilled basalts		50 - 46	Ishizuka et al. (2018)
Palau Basin	Back-arc extension	Marine magnetic anomalies + Mindanao Fracture zone	C18n y - C16n. In y	38.4 - 35.58	Sasaki et al. (2014); This study
Palau Basin	Back-arc extension	Geometry (Line up with Philippine Mobile Belt)		55 - 45	This study
Ayu Trough	Ultra slow spreading	Crustal structures (sedimentation rate) + reconstruction		15 - 0	Weissel and Anderson (1978); Fujiwara et al. (1995)
Ayu Trough	Subduction	Dredged arc lavas		> 15	Kamasaki et al. (1996); This study
Huatung Basin	Back-arc extension	Marine magnetic anomalies + dredged samples		130 - 119	Deschamps et al. (2000)

Philippines				
Philippine fault zones	50-150 km left-lateral strike slip	Keep relative motion in north minimal, some subduction in the south	4 - 0	Aurelio et al. (1990); This study
Philippine Mobile Belt	Forearc spreading	Supra-subduction zone ophiolites	110 - 85	Dimalanta et al. (2020); This study. See main text for additional references
Proto-SE Bohol Trench	Subduction	Cebu arc lavas	130 - 110	This study. See main text for additional references
Lagonoy subduction zone	Subduction	Philippine ophiolites	157 - 85	Advokaat and Van Hinsbergen (2023); This study. See main text for additional references
Lagonoy subduction zone	Subduction initiation	Lagonoy ophiolite	156	Geary et al. (1988); This study
Tipuma-Jimi Basin	Back-arc extension	Philippine ophiolites and reconstruction of Argoland	157 - 110	Advokaat and Van Hinsbergen (2023); This study
Telkhinia subduction zone	Subduction	Paleomagnetic data	> 160 - 30 (?)	Chapter 4
Philippine Mobile Belt	Clockwise rotation	Double relay ramp	62 - 45	This study
Caroline Plate				
West Caroline Basin	Oceanic spreading	Marine magnetic anomalies	Cl 6n. In γ - Cl 1n. 2n	Gaina and Muller (2007)
East Caroline Basin	Oceanic spreading	Marine magnetic anomalies	Cl 6n. In γ - Cl 8n. 2n o	Gaina and Muller (2007)
Caroline Plate	Caroline Plate fixed to Pacific	Overlapping Caroline Ridges	> 15	Wu et al. (2016); This study
Sorol Trough	250 km subduction	To avoid shortening at the New Guinea and Manus trenches; Paleomagnetic data	15 - 7	This study
Molucca Sea				
Molucca Sea	Back-arc extension	Eocene ophiolites in Philippine and Talaud, contiguous with Solomon Sea	45 - 30	This study

Table I (continued)

Location	Interpretation	Type of data used	Anomalies	Time (Ma)	Reference
New Guinea					
Sorong-Yapen-Bewani Torricelli Fault	300 km left-lateral strike slip	Opening of Manus Basin		3.5 - 0	Taylor (1979); Webb et al. (2019); This study
New Guinea and Manus trenches	1200 km left-lateral strike slip	Avoid overlap with SE Asian Tethysides		15 - 3.5	This study
	210 km shortening related to ophiolite emplacement (no shortening of continental material)	Balanced cross-sections		35 - 21	Martin et al. (2023)
Central New Guinea					
	190 km shortening of the Australian margin underneath the ophiolite	Balanced cross-sections		21 - 9	Martin et al. (2023)
Central New Guinea					
	100 km shortening in the Papuan and Irian Jaya Fold-and-thrust belt	Balanced cross-sections		9 - 0	Hobson (1986); Hill (1991); Martin et al. (2023)
Central New Guinea					
	Counterclockwise rotation New Guinea obduction front	Avoid overlap with SE Asian Tethysides		30 - 15	This study
New Guinea ophiolites					
	Northward subduction initiation	Metamorphic sole age of the Papuan Ultra Mafic Belt and global plate circuit		62	Lus et al. (2004); This study
Melanesian Borderlands					
Bismarck Sea	Back-arc extension	Marine magnetic anomalies	C2A - present-day	3.5 - 0	Taylor (1979)
Solomon Sea	Back-arc extension	Marine magnetic anomalies	C19n o - C16n. In y	41.18 - 35.58	Gaina and Müller (2007)
Solomon Sea	End of spreading	New Guinea ophiolite obduction		30	This study
Woodlark Basin	Subducting plate spreading	Marine magnetic anomalies	C3A - present-day	6.3 - 0	Weissel et al. (1982); Taylor et al. (1990)

Santa Cruz Basin/South Rennell Trough	Subducting plate spreading	Marine magnetic anomalies	C19n o - C13n o	40.07 - 30	Seton et al. (2016)
Coral Sea Basin	Marginal basin formation	Marine magnetic anomalies	C27n o - C24n o	63 - 52	Gaina et al. (1999)
Louisiade Trough	Marginal basin formation	Marine magnetic anomalies		63 - 52	Gaina et al. (1999); Seton et al. (2016)
Solomon - Vitiaz - Tonga arc	Southward subduction initiation	Ages of Solomon and Pentecost Islands ophiolites		45	Neef and McDougall (1976); Crawford et al. (2003)
Townsville Basin	Marginal basin formation	Stratigraphy		157 - 110	Falvey and Taylor (1974); Struckmeyer and Symonds (1996); This study
SW Pacific					
Lau Basin	Back-arc extension	Marine magnetic anomalies	C3A - present-day	7 - 0	Yan and Kroenke (1993)
Havre Trough	Back-arc extension	In tandem with Lau Basin		7 - 0	Yan and Kroenke (1993); Chapter 1
North Fiji Basin	Back-arc extension	Marine magnetic anomalies	C4 - present-day	10 - 0	Yan and Kroenke (1993)
South Fiji Basin	Back-arc extension	Marine magnetic anomalies	C9n o - C6n o	27.44 - 15	Sdrolias et al. (2003); Herzer et al. (2009, 2011); Chapter 1
Norfolk Basin	Back-arc extension	In tandem with South Fiji Basin		30 - 15	Sdrolias et al. (2003); Herzer et al. (2009, 2011); Chapter 1
North Loyalty Basin	Back-arc extension	Marine magnetic anomalies	C20n o - C16n o	43.45 - 35	Sdrolias et al. (2003)
South Loyalty Basin	Marginal basin formation	Misfit North and South Zealandia		79 - 62	Chapter 3
Fairway-Aorea and New Caledonia basins	Marginal basin formation	Crustal thickness estimates		92 - 84	Grobys et al. (2008); Chapter 3
Tasman Sea	Marginal basin formation	Marine magnetic anomalies	C33n o - C24n o	95 - 52	Gaina et al. (1998); Grobys et al. (2008); Chapter 3
New Caledonia	Subduction initiation	Metamorphic sole age of the Peridotite Nappe and global plate circuit			Cluzel et al. (2012b); This study

reconstruction to global plate reconstructions or the reconstruction of Seton and Müller (2008), as these lack detail in the description of the Junction Region, and the global plate reconstructions generally incorporate one of the regional reconstructions.

5.1.0 – 15 Ma

The first key interpretation step in our reconstruction coincides with the onset of opening of the Ayu Trough, estimated to have started sometime between 25 and 15 Ma (Weissel and Anderson, 1978; Fujiwara et al., 1995). Since that opening, the Philippine Sea Plate was connected to the Caroline Plate. Before that time, arc rocks dredged from the margins of the Ayu Trough suggest that it was a subduction zone (Kumagai et al., 1996). The youngest of these (c. 20 Ma) shows that subduction must have continued to at least 20 Ma, and our reconstruction assumed that the Ayu Trough's opening started on the young end of the estimated range, around 15 Ma (Figures 9 – 11). This age corresponds to the oldest ages of arc magmatism of the Luzon arc that are related to westward subduction at the Manila Trench (c. 14 Ma; Maleterre et al., 1988; Defant et al., 1990). We initially assumed that the Sorol Trough and Mussau Trench/Lyra Trough that bound the Caroline Plate from the Pacific Plate did not accommodate motion in the last 15 Ma and use the resulting reconstruction to re-evaluate that assumption below.

The reconstruction of the Ayu Trough restores a $\sim 25^\circ$ clockwise rotation of the Palau Basin (the southernmost basin of the Philippine Sea Plate) relative to the Caroline Plate (Figures 9 – 11). Just north of the Ayu Trough Euler pole, this rotation reconstructs sufficient convergence at the Yap trench to restore an amount of lithosphere that is large enough to contain the eastern conjugate lithosphere that formed during formation of the Parece Vela Basin, of which only the western part remains west of Yap Island (Figures 9 – 11). Our reconstruction thus infers that the onset of extensional opening of the Ayu Trough, in combination with oblique opening of the Parece Vela basin after c. 20 Ma, initiated subduction at the Yap trench at the southernmost end of the Parece Vela ridge, locally consuming the forearc lithosphere.

In the northwest, subduction of the Philippine Sea Plate oceanic basins is restored at the Nankai and Ryukyu trenches and the extensional opening in the Mariana Trough, active in the last 6 Ma (Yamazaki et al., 2003), as well as subduction of the West Philippine Basin below the Philippine Mobile Belt, since 4 Ma (Figures 9 and 10). The amount of convergence accommodated by this subduction zone decreases both northwards and southwards, as subduction did not occur to the north of Luzon or to the east of Halmahera. Reconstructing this lateral gradient in convergence led us to reconstruct a small ($\sim 3^\circ$) clockwise rotation of eastern Mindanao and the Palau Basin relative to the West Philippine Basin, accommodated along the Philippine Fault and Mindanao Fracture Zone. Within the Philippines, we restore left-lateral strike slip faulting of 100-200 km since 4 Ma along the Philippine Fault, East Luzon Transform Fault, and Sibuyan Sea Fault in line with geological estimates (Aurelio et al. 1991; Barrier et al., 1991; Mitchell et al., 1986; Cole et al., 1989). The reconstructed



strike-slip faulting ensures that subduction at the Philippine Trench decreased both north and southward.



Figure 10. Snapshot of the kinematic reconstruction at 5 Ma.

front of the Papuan ophiolites, interpreted as a transform fault. To test whether the west Philippine/Halmahera trenches continued into New Guinea before 6 Ma, we initially connected the Philippine Sea Plate to the Papuan ophiolites at this time and restored the New Guinea obduction since ~30 Ma according to kinematic constraints provided by Martin et al. (2023). However, this leads to large overlap between the western Philippine Sea Plate domain and the SE Asian Tethysides before 6 Ma, which is clearly inconsistent with the geological record. This overlap is avoided when the Philippine Sea Plate and the western trenches are reconstructed with the westward moving Pacific Plate, generating 1200 km of left-lateral transform motion along the northern margin of New Guinea, presently occupied by the New Guinea and Manus trenches, between 6 and 15 Ma. This transform motion reconstructs a 1900 km wide Molucca Sea basin at 15 Ma, which reconstructs as a triangular basin between the southward obducting Papuan ophiolites and the westward

moving southern Philippines/Halmahera ophiolites (Figure 11).

Within New Guinea, we reconstruct 100 km of shortening in the New Guinea fold-and-thrust belt since 9 Ma following the balanced cross-sections of Hill (1991) and Hobson (1986). The Sorong-Fault-Bewani-Torricelli fault zone is reconstructed as part of the North Bismarck Microplate and the relative motion at the transform fault system thus follows from the marine magnetic anomaly constraints in the Manus Basin (Figure 9 and 10). This leads to c. 300 km of left-lateral transform motion within northern New Guinea since 3.5 Ma, in line with geological data (Dow and Sukanto, 1984; Webb et al., 2019). The Woodlark Basin opening since 6.5 Ma is reconstructed, which is balanced by resurfacing the northern conjugate oceanic lithosphere of the Solomon Sea that was consumed by subduction at the San Cristobal Trench. Restoring the western propagation of the Woodlark Basin buries the upper Neogene core complexes of the D'Entrecasteaux Islands back to their UHP conditions as part of the down-going Australian lithosphere below the obducting Papuan Ultramafic Belt. In addition, we restore southeastward roll-back of the New Britain trench, which infers ~225 km of right-lateral strike-slip faulting at the Ramu-Markham fault zone (Figure 9 and 10). The amount of roll-back follows from the constraint that motion of the North Bismarck Plate relative to the Papuan ophiolites is pure strike-slip.

Whereas restoring the westward motion of the Philippine Sea Plate in the last 15 Ma together with the Pacific Plate avoids overlaps between the western Philippine Sea Plate and the SE Asian Tethysides, assuming that there was no relative motion between the Pacific and Caroline Plates back to 15 Ma introduces two other kinematic problems. Firstly, an underlap (gap) of about 350 km forms between the Caroline Plate and the New Guinea and Manus trenches along northern New Guinea. This requires that a south-dipping slab should be present below the northern New Guinea margin, and while this boundary is accommodating some thrusting alongside dominantly transform motion, there is no evidence for a tomographically resolvable slab. Secondly, this scenario predicts paleolatitudes for the Philippine Sea Plate that systematically offset to the north compared to paleolatitude data obtained from igneous rocks of the Philippine Sea Plate. This problem may be overcome by restoring the Philippine Sea Plate ~3–4° southwards at 15 Ma relative to the Pacific Plate, which is permitted by, and actually improves, the paleomagnetically predicted paleolatitudes for the Philippine Sea Plate. Candidate structures to accommodate this motion are the margin between the Philippine Sea Plate and the Caroline Plate east of the Ayu Trough, and the Izu-Bonin-Marianas trenches farther to the north, or the Sorol Trough-Lyra Trough boundaries between the Caroline Plate and the Pacific Plate. The first option would require N-S extension between the Pacific Plate and the Philippine Sea Plate on the E-W trending segments of the Philippine Sea Plate-Pacific plate boundary, e.g., connecting the Mariana Trough and the Yap Trench, that should be still present today, whereas it is not. In addition, while this scenario does resolve the underlap at the New Guinea trench, the gap north of the Manus Trench remains and this scenario leads to overlap between the Philippine Sea Plate and SE Asian Tethysides after 15 Ma. Hence, we favor the second



Figure 11. Snapshot of the kinematic reconstruction at 10 Ma.

option, which infers a short-lived south-dipping subduction zone at the Sorol Trough, since 15 Ma, with the Lyra Trough acting as a transform plate boundary between the Caroline and Pacific plates during this time (Figures 11 and 12). The asymmetric, southward deepening Sorol Trough was previously interpreted as a rift (Weissel and Anderson, 1978; Altis, 1999), even though its morphology is highly asymmetric and normal faults are only found on the southern part of the rift (Weissel and Anderson, 1978; Dong et al., 2018). We tentatively infer that these normal faults may instead result from plate bending. There is currently no subducting slab connected to the Pacific Plate at the Sorol Trough, but a subducted slab has long been interpreted from tomography below the Caroline Plate (the Caroline Slab; Hall and Spakman, 2002; Van der Meer et al. 2018), which may represent (part of) this subducted lithosphere. If subduction occurred, it must thus have ceased sufficiently long ago for the slab to sink to the mantle transition zone, and we model the cessation of subduction at 7



Figure 12. Snapshot of the kinematic reconstruction at 15 Ma.

Ma, although this could be a few million years earlier or later.

The largest difference between our reconstructions and previous ones in this time interval is that we reconstruct subduction at the Sorol Trough to avoid major convergence along the northern margin of New Guinea. Gaina and Müller (2007), Zahirovic et al. (2014), and Wu et al. (2016) reconstruct up to c. 1000 km of convergence within New Guinea between the ophiolites and arcs, since 15 Ma. Hall (2002) accommodates the convergence between the southern margin of the Caroline Plate and the New Guinea arcs (without drawing a subduction zone plate boundary), while Liu et al. (2023) divide the convergence between a subduction zone in between the ophiolites and the arc and between the arc and the southern margin of the Caroline Plate. In addition, Hall (2002) reconstructs major strike slip motion within New Guinea.

5.2. 15 – 30 Ma

From 15 Ma back in time, we reconstructed the (northern) Caroline Plate as part of the Pacific Plate. The Philippine Sea plate motion chain (i.e., the collection of the Philippine Sea microplates that are reconstructed relative to each other with preserved magnetic anomalies) is prior to 15 Ma disconnected from the Caroline (Pacific) Plate, accommodated by subduction below the eastern margin of the Ayu Trough (Figures 12 – 15), where arc rocks of early Miocene have been dredged (Kumagai et al., 1996). Instead, we reconstructed the Philippine Sea Plate as connected to the ophiolites that were overthrusting the northern Australian margin of New Guinea since 30 Ma (Martin et al., 2023) and evaluated whether that assumption led to configurations and plate motions elsewhere that conflict with data. With this logic, the relative motion between the Philippine Sea Plate and the surrounding major plates is constrained back to the start of ophiolite obduction on New Guinea, which is estimated to have occurred around 30 Ma based on metamorphic ages of continent-derived rocks (Weiland, 1999; Martin et al., 2023).

The reconstruction at 30 Ma displays westward subduction of the Caroline/Pacific plates along a subduction system that spans from the Izu-Bonin-Mariana trench and its triple junction with the Japan and Nankai Trenches, via the Ayu Trench, to the North Solomon and Vitiaz Trenches, and from there to the Tonga-Kermadec-Hikurangi subduction zone (Figure 15). At 30 Ma, the south Caroline Plate is a separate plate that is spreading relative to the Pacific Plate in the north (Gaina and Müller, 2007), bounded by the Lyra Trough in the east, the North Solomon Trench in the south, and the Ayu Trench in the west (Figure 15). Geological data from New Zealand's North Island show that the Hikurangi subduction zone initiated around 30 Ma, or shortly thereafter (Appendix 2), and from that moment onwards, the west Pacific plate boundary transitioned through the Alpine Fault transform to the Puysegur plate boundary (Kamp, 1986; Le Brun et al., 2000) that ends in a triple junction in the Southern Ocean (Figure 9 - 15).

At 30 Ma, the c. 400 km of shortening related to ophiolite obduction onto the Australian continental margin of northern New Guinea (Martin et al., 2023) is fully restored (Figure 15). The exact shortening direction of the New Guinea obduction is not well constrained. We initially assumed N-S, margin-perpendicular shortening, and kept Halmahera, connected to the Philippine Sea Plate, fixed relative to the Papuan ophiolites. This led to overlap of the Philippines with the SE Asian Tethysides, showing that the Philippines must have undergone a westward motion component between 15 and 30 Ma. We therefore reconstructed the ophiolite obduction with a NNE-SSW shortening direction, and restored westward-increasing shortening, leading to a small counterclockwise rotation relative to Australia of the Papua ophiolites and the Philippine Sea Plate between 30 and 21 Ma (Figures 13 – 15). This satisfies all available structural evidence, avoids overlaps, and predicts mostly transform motion and some minor extension along the western margin of Luzon, which accommodates relative motion between the Philippine Mobile Belt and the SE Asian Tethysides.



Figure 13. Snapshot of the kinematic reconstruction at 20 Ma.

The limited convergence between the Philippine Sea Plate and the Australian Plate, which was restricted to the shortening documented on New Guinea, is in line with the paleolatitudes predicted from paleomagnetic data of the Philippine Sea Plate (Figure 8; Chapter 5). The bulk oceanic crust consumed by post-30 Ma subduction is thus restored to the north of the Philippine Sea Plate, where it was subducted at the Nankai and Ryukyu trenches. Within the Philippine Sea Plate, opening of the Shikoku and Parece Vela Basins is restored (Sdrolias et al., 2004b), which results in a much smaller Philippine Sea Plate mosaic by 30 Ma (Figure 15).

A key difference between our reconstruction and others in the 15–30 Ma interval is that we treat the Philippine Mobile belt as a rigid terrane, while other reconstructions incorporate relative motions between different parts of the Philippines, except for Zahirovic et al. (2014). Wu et al. (2016) and Liu et al. (2023) reconstruct relative convergence between the east and



Figure 14. Snapshot of the kinematic reconstruction at 25 Ma.

west Philippines, accommodated at the location of the present-day Philippine Fault. Hall (2002) and Gaina and Müller (2007), on the other hand, reconstruct relative convergence between the north and south Philippines already before c. 10 Ma, accommodated to the south of Luzon.

Further differences between the existing reconstructions in the 15–30 Ma interval are the configuration and polarity of subduction zone plate boundaries in the New Guinea–Melanesian region. Hall (2002) and Gaina and Müller (2007) reconstruct a similar northward-dipping subduction zone below the Papuan ophiolites, but in their models, the Australian margin enters the trench around 25 Ma, and no convergence is reconstructed in the 15–25 Ma interval. Moreover, in their models, this subduction zone does not connect with the New Caledonia subduction zone, as this trench does not exist, or only until 45 Ma. In the model of Zahirovic et al. (2014), the New Caledonia trench does exist, but is



Figure 15. Snapshot of the kinematic reconstruction at 30 Ma.

connected to the New Guinea trench through extensional plate boundaries. In contrast to the other reconstructions, including ours, the reconstructions of Wu et al. (2016) and Liu et al. (2023) include southward subduction. Liu et al. (2023) incorporate southward subduction of oceanic crust below the entire northern margin of New Guinea, while Wu et al. (2016) reconstruct southward intra-oceanic subduction between New Guinea and the Philippine Sea Plate as well as southward subduction to the east of New Guinea, at the Trobriand Trough and farther to the east. While the Trobriand Trough has been interpreted as the site of southward subduction by others (Joshima et al., 1987), we interpreted the bathymetric depression as a scarp that represents the northern margin of underthrust continental lithosphere below the Papuan ophiolites.

5.3. 30 – 45 Ma

There is in the circum-Junction Region that we reviewed no evidence for continental underthrusting below oceanic or continental lithosphere before 30 Ma. Instead, all accretionary orogenic records reveal oceanic subduction. In addition to subduction below Japan, these restore to two main subduction systems: northward subduction of Australian Plate oceanic lithosphere, and westward subduction of the Pacific Plate, which both occurred contemporaneously below a plate system that includes the precursors of the Philippine Sea Plate, the Papuan ophiolites and Molucca Sea basin, and the Melanesian arcs and marginal basins (including the Solomon Sea basin). This pre-30 Ma plate configuration formed around 45 Ma, which marks the time that westward subduction of the Pacific Plate started at the North Solomon and Vitiaz trenches as inferred from metamorphic sole age estimates on the Solomon and Vanuatu ophiolites (Neef and McDougall, 1976, Richards et al., 1966; Crawford et al., 2003).

Despite the lack of kinematic data that demonstrate relative plate motion amount and direction at the Junction Region trenches in the 30-45 Ma interval, there is enough geological data for a well-constrained reconstruction (Figures 15 – 18). At first, we assumed a simplest-case scenario in which a single plate intervened the Pacific and Australian plate in the Junction Region, bounded on either side by trenches. This plate includes the Philippine Sea Plate, the Papuan ophiolites and the Molucca Sea lithosphere that was reconstructed between the Papuan ophiolites and the southern Philippines and Halmahera at 15 Ma, the eastern continuations of the Papuan ophiolites in the form of the Louisiade and New Caledonia ophiolites, and the eastern Philippine Sea Plate arcs (Izu-Bonin-Mariana) and Melanesian arcs (Solomon, Vitiaz/New Hebrides, Tonga), as well as intervening oceanic basins (Solomon Sea and North Loyalty Basin) (Figure 12). We restored the available marine magnetic anomaly evidence for opening of oceanic basins, but there is no direct field evidence for a plate boundary that cut through this composite series of arcs and basins during this time interval.

First, we reconstructed where the system of two opposing subduction zones must have terminated. There is positive evidence for subduction below the Solomon Sea ophiolites since 45 Ma (Neef and McDougall, 1976, Richards et al., 1966) and the oldest dated arc rocks on Fiji are 39 Ma (Rickard and Williams, 2013), showing that the Pacific trench must have continued beyond Fiji southwards, to the Tonga Trench. However, farther south, subduction at the Hikurangi trench did not start before c. 28-30 Ma (Appendix 2), and at the Alpine Fault there is also no evidence for significant pre-30 Ma dextral motion (Kamp, 1986; Furlong and Kamp, 2013). Instead, at the longitude of the Hikurangi trench, relative plate motion between the Australian and Pacific plates was only accommodated through eastward subduction of the Australian Plate before c. 30 Ma, at the subduction zone below the New Caledonia-Northland ophiolites (Chapter 1). We thus infer that the Solomon-Fiji-Tonga trench ended against a transform fault to the south of the North Loyalty Basin, which we tentatively connect to the Cook transform fault that bounded the Norfolk Basin during



Figure 16. Snapshot of the kinematic reconstruction at 35 Ma.

its opening (Figure 16-18); Sdrolias et al., 2004a; Chapter 1), which is still present in the Tasman Sea, to the north of New Zealand (Figure 4).

Our reconstruction thus implies that to the south of the Cook Fault, there was only one subduction zone (the Three Kings Ridge trench segment of the New Caledonia subduction zone) before 30 Ma, and that the oceanic lithosphere that obducted onto Zealandia, including the Northland Ophiolite, moved as part of the Pacific Plate. The position of this plate boundary therefore follows directly from Pacific-Australia motion before the moment of obduction (which we model at 30 Ma following Chapter 1). We reconstruct the Solomon-Vitiaz arc at 45 Ma to a position that lines up the Papuan Peninsula-Louiside trench with the New Caledonia trench (Figure 18). This position of the Melanesian arc requires that we restore some clockwise rotation of the Tonga trench segment to avoid overlap with the New Caledonia trench at 45 Ma.

In the northwest of the Junction Region, our reconstruction ensures that there is convergence and thus subduction of both the Pacific and Australian plates with the Philippine Sea Plate and Melanesian arcs. The reconstruction positions the entire Philippine-Melanesian plate system from the Tonga-New Caledonia region in the southeast to the northwest Philippines in the northwest such that there is no major convergence between the Philippine Sea Plate and the SE Asian Tethysides after ~40 Ma because there is little geological evidence for significant subduction on the northern Philippines after this time in this region. This reconstruction is in correspondence with paleomagnetic data from the Philippine Sea Plate (Figure 8), and allows for the opening of the Solomon Sea basin, as dictated by the preserved magnetic anomalies (Gaina and Müller, 2007) between the two major bounding subduction zones (Figures 15 - 18).

Within the above-described tectonic framework, we reconstructed the Molucca Sea as a back-arc basin behind the Papuan ophiolites and arcs between 45 and 30 Ma (Figures 15 - 18). As the Molucca Sea has been completely consumed after 15 Ma, there are no preserved marine magnetic anomalies that corroborate this reconstruction, but a 45-30 Ma age of formation is in line with Eocene radiolarian chert that is preserved in the tectonic mélange of Talaud Island (Moore et al., 1981) and the Talaud Ophiolite which was interpreted to have a back-arc basin geochemical signature (Evans et al., 1983). The Eocene oceanic crust of the Zambales, Angat, and Antique ophiolites in Luzon and possibly the Polanco ophiolite on Mindanao (Figure 5; Encarnación et al., 1993; Yumul et al., 2000a; Marcelles et al., 2018) reconstructs as part of this same back-arc basin. Molucca Sea back-arc basin is reconstructed as a larger, westward equivalent of the Solomon Sea basin (Figures 15 - 18).

In our reconstruction, the closure of the Molucca Sea reconstructs the Papuan ophiolites and the arc rocks of northern New Guinea adjacent to the Cretaceous crust and arc remnants of the southern Philippine Mobile Belt (Figure 18). The reconstruction of the Molucca Sea in this way solves and explains several issues: First, it reconstructs sufficient oceanic crust north of the Australian continental margin for a subduction zone to have existed from 45-30 Ma. Second, this scenario explains why there are no late Eocene arc volcanics preserved in the southern Philippines, while they are present in the north: this southern continuation of the arc rifted off during opening of the Molucca Sea and remained active but is now found on New Guinea. Third, the reconstruction of the Molucca Sea in this way provides an explanation for the origin of the Cyclops Ophiolite of New Guinea, from which ages between 43 and 30 Ma were obtained (Monnier et al., 1999). The reconstruction also explains the abrupt termination of the Papuan ophiolites just east of the Bird's Head as a transform (STEP) fault (Figures 15 - 18) and infers that Miocene subduction initiation of the Halmahera subduction zone occurred on the northeastern margin of the Molucca Sea back-arc basin (Figure 12).

By 45 Ma, opening of the West Philippine Basin is largely restored (Hilde and Lee, 1984), which leads to a much smaller Philippine Sea Plate and the N-S length of the Kyushu-Palau ridge west of the Izu-Bonin Mariana-Palau subduction zone is also significantly reduced



Figure 17. Snapshot of the kinematic reconstruction at 40 Ma.

(Figure 18). The extension of the Kyushu-Palau intra-oceanic arc towards the north at 45 Ma is unknown, but we reconstruct a limited northwestward continuation of the Izu-Bonin Mariana-Palau trench. We infer that the Pacific Plate was subducting below Japan at the Nankai and Ryukyu trenches and that the Izu-Bonin Mariana trench ended in a triple junction with transform faults with perhaps minor convergent components between the Philippine Sea Plate and the SE Asian Tethysides to the south, and the Pacific Plate and the Proto-South China Sea embayment to the north.

At 45 Ma, the main difference between existing reconstructions is the amount of restored clockwise vertical-axis rotation of the Philippine Sea Plate. All reconstructions, including ours, restore a rotation of the Philippine Sea Plate at 45 Ma, but to a variable extent. Gaina and Müller (2007), Wu et al. (2016), and Liu et al. (2023) all restore c. 90° rotation, to the extent that spreading in the West Philippine Basin occurs in a NW-SE direction. In

the reconstruction of Hall (2002) the amount of restored rotation at 45° is about 60°, but additional clockwise rotation is restored between 45 and 52 Ma, so that the total amount of restored vertical axis rotation is also around 90° at 52 Ma. In our reconstruction and that of Zahirovic et al. (2014), on the other hand, the amount of vertical axis rotation restored for most of the Philippine Sea Plate is only ~30°. Unlike us, Zahirovic et al. (2014) restored additional rotation of the Philippine Mobile Belt relative to the rest of the Philippine Sea Plate, between 14 and 6 Ma, which results in the restoration of a total of 50° clockwise rotation of the Philippine Mobile Belt at 45 Ma, where it is 30° in our reconstruction.

Another key difference between our reconstruction and the others is the location of (south)westward subduction initiation at the Solomon-Vitiaz-Tonga trench. All previous models reconstruct this subduction zone close to the continental margin at subduction initiation, and subsequently reconstruct trench-roll back and the formation of a back-arc basin, i.e., the Solomon Sea. Our reconstruction is the only one that reconstructs this subduction zone to start intra-oceanic (Figure 18) and model the opening of the Solomon Sea in between two opposing subduction zones. Wu et al. (2016), in addition to their subduction zone that forms along the New Guinea continental margin, also reconstruct a west-dipping intra-oceanic subduction zone, which is subsequently consumed when the subduction zone that hosts the Solomon Arc rolls back.

5.4. 45 – 62 Ma

The logical next step in our reconstruction would be 52 Ma, which corresponds to the age of the oldest supra-subduction oceanic lithosphere of the Izu-Bonin-Mariana forearc and is the widely inferred age for the onset of subduction at the Izu-Bonin Mariana trench (Ishizuka et al., 2011a; Stern et al., 2012; Reagan et al., 2013, 2019). However, as geological data from the Solomon Islands, Vanuatu, Fiji, and Tonga suggest that southwestward subduction of the Pacific Plate beneath these arcs did not start before c. 45 Ma (Neef and McDougall, 1976; Richards et al., 1966; Bloomer et al., 1995; Crawford et al., 2003), it is not straightforward where the Izu-Bonin Mariana plate boundary continued, or where and why it would have ended. Therefore, we chose as next step in our reconstruction 62 Ma. North- and eastward subduction of the Australian Plate at the New Caledonia-New Guinea trench started around 60 Ma as revealed by metamorphic sole ages of the Papuan and New Caledonia ophiolites (Lus et al., 2004; Cluzel et al., 2012b). We incorporate a 62 Ma subduction initiation age at the southwestern Philippine Sea Plate/Melanesian (New Caledonia-New Guinea) subduction zone because at this time a small change in relative plate motion between the Pacific and Australian plates occurred that follows from the global plate circuit. We use the constraints from the Papuan and New Caledonia ophiolites to restore relative motions at the Izu-Bonin Mariana trench from this perspective (Figures 18 – 22).

As (south)westward subduction of the Pacific Plate south of the Philippine Sea Plate (Halmahera) did not start before 45 Ma, we reconstruct the Solomon Islands, Vanuatu,



Figure 18. Snapshot of the kinematic reconstruction at 45 Ma.

and Tonga, as well as intra-oceanic highs and basins east of the Louisiade-New Caledonia trench, such as the Three Kings Ridge (Figures 18 - 22), as part of the Pacific Plate. The New Guinea-New Caledonia subduction zone ended in a zone of diffuse and distributed deformation around New Zealand, close to the Pacific-Australia Euler pole, and around 40 Ma connected with the Emerald Basin spreading center (Chapter 1).

To the north of the Solomon Islands, the Philippine Mobile Belt formed the overriding plate to the New Guinea-New Caledonia subduction, which was not part of the Pacific Plate before 45 Ma, as the Izu-Bonin Mariana subduction zone accommodated subduction of the Pacific Plate below the Philippine Sea Plate. There is no evidence for a discrete plate boundary between the Philippine Mobile Belt (south of Halmahera) and the Solomon arc that may have accommodated the inevitable relative motion between the two. We therefore reconstruct that between 62 and 45 Ma, the Philippines acted as a major relay ramp between



Figure 19. Snapshot of the kinematic reconstruction at 50 Ma.

two subduction systems that laterally decreased convergence in opposite direction. The Izu-Bonin Mariana subduction zone accommodated all Pacific-Australia convergence at the position of the northern Philippines. The amount of convergence accommodated by this subduction zone decreased southwards towards Halmahera, and to the southeast, all Australian-Pacific convergence was accommodated by the New Caledonia-New Guinea subduction zone. We accommodate this evolution by reconstructing a clockwise rotation of the Philippine Mobile Belt relative to the Solomon Islands between 62 and 52 Ma that avoids relative convergence between southern Halmahera and the Pacific Plate. Our restoration of clockwise rotation of the Philippines also ensures that the amount of convergence accommodated by the New Caledonia-New Guinea subduction zone decreased northwards and transitioned into a transform fault with both the Australian Plate and farther north with the SE Asian Tethysides (Figure 19 - 21). This explains the absence of evidence of



Figure 20. Snapshot of the kinematic reconstruction at 55 Ma.

subduction beyond the Papuan ophiolites. After 52 Ma, subduction of the Pacific Plate at the Izu-Bonin-Mariana subduction zone is sustained through opening of the West Philippine and Palau Basins (Hilde and Lee, 1984; Sasaki et al., 2014). Our reconstruction thus infers that the Izu-Bonin Mariana subduction zone was already forming by 62 Ma, at a time that the Philippine Sea Plate only consisted of Cretaceous and latest Jurassic oceanic crust and arc rocks of the small Huatung Basin (Dechamps et al., 2000) and the Philippine Mobile Belt (e.g., Geary et al., 1988; Suerte et al., 2005; Dimalanta et al., 2020). We will return to this element of our reconstruction in the discussion section.

Subduction of the Pacific-Izanagi Ridge below Japan is restored to have occurred at 50 Ma following e.g., Wu and Wu (2019), and at 62 Ma, the Izanagi Plate was subducting below the Eurasian continental margin of Japan (Figures 19 and 21). We reconstruct the western termination of this subduction zone along the continental margin around the Kerama Gap



Figure 21. Snapshot of the kinematic reconstruction at 60 Ma.

in the central Ryukyu Islands, corresponding to the Qingdao line of Wu et al. (2022), to the west of which there is no evidence for post-85 Ma subduction or accretion (see also Chapter 4). Instead, the plate boundary continued southwards along the eastern margin of the Proto-South China Sea embayment (Figures 19 - 22). Wu et al. (2022) postulated that the Qingdao Line may have been a transform fault, but relative plate motions that follow from the global plate circuit combined with the reconstructed orientation of the plate boundary rather suggests that this plate boundary accommodated oblique subduction of the Izanagi and later Pacific plates below the Proto-South China Sea. This oblique trench ended in the triple junction with the northern extension of the Izu-Bonin Mariana subduction zone and the western Philippine transform-dominated plate boundary (Figures 19 - 22).



Figure 22. Snapshot of the kinematic reconstruction at 65 Ma.

5.5. 62 – 85 Ma

Whereas there are records of subduction that accommodated the convergence of the Pacific plate system and the Tethyan plate system after 62 Ma and before 85 Ma (e.g., East Gondwana subduction in New Zealand and New Caledonia (Chapter 3), and the arcs of the Philippines and the circum-Proto-South China Sea embayment (section 3; see also Chapter 4)), evidence for subduction in the Junction Region in the intervening period is sparse. The next step in our reconstruction is therefore 85 Ma.

The global plate circuit straightforwardly explains the tectonic quiescence in the 62-85 Ma interval (Figures 22 - 24). This time interval is bracketed between two major plate motion changes, around 85 Ma and ~50 Ma (as explained, the 62-50 Ma interval accommodated only minor convergence), and relative motions between the major plates were limited. Australia moved only ~600 km to the NE relative to Eurasia. Relative motion between the



Figure 23. Snapshot of the kinematic reconstruction at 70 Ma.

Pacific and Australian plates was slow, and divergent in the south, accommodated at the Tasman Ridge (Figures 23 - 25). The northward decrease in extension at the Tasman Ridge indicates that the Euler Pole of Australia-Pacific motion was located around the northeast corner of the Australian continental margin, around the Coral Sea. To the north, the Pacific Plate moved in the 85-62 Ma time interval some ~700 km to the northwest. Prior to the initiation of subduction of the Australian Plate below the Philippine Sea Plate at the New Caledonia-New Guinea trench at 62 Ma, we reconstruct the Philippine Mobile Belt as part of the Australian Plate (Figures 23 - 25). Because this reconstruction predicts a NW-SE trend of the Philippine Mobile Belt at 62 Ma, the boundary between the Philippine Mobile Belt and the Pacific Plate in the 62-85 Ma interval was predominantly a transform fault with perhaps some obliquely subduction of the Pacific Plate below the Australian Plate. This oblique subduction may explain the sparse Campanian accretionary prism rocks identified



Figure 24. Snapshot of the kinematic reconstruction at 80 Ma.

on Halmahera (Hall et al., 1988) and the 77 Ma diorite intrusion into the Rapu-Rapu ophiolite in the Philippines (David et al., 1997).

With limited Australia-Eurasia motion, the transform-dominated plate boundary east of the Philippine Mobile Belt, which eventually develops into the Izu-Bonin Mariana trench, aligned with the Qingdao Line, where oblique subduction was accommodated. To the east, the Izanagi-Pacific ridge migrated towards the eastern Eurasian margin and formed a triple junction that moved along the east-Philippine Mobile Belt and Qingdao Line (Figure 19 - 25).

The model of Zahirovic et al. (2014) is the only previous regional reconstruction that extends this far back in time. In our model, the Philippine Mobile Belt still acts as a rigid plate, now part of the Australian Plate, whereas the model of Zahirovic et al. (2014) connects the northernmost Cretaceous arc of the Philippine Sea Plate (the Amami Plateau) to the

Pacific Plate at 65 Ma and reconstruct extension between the Cretaceous arcs between 65 and 85 Ma, which we restored during the Eocene based on the age constraints in the intervening basins (Hickey-Vargas, 1998; Ishizuka et al., 2013, 2018). The reconstruction of Zahirovic et al. (2014) suggests that subduction of the Australian Plate below the Papuan ophiolites already started at 85 Ma, while the ophiolites of New Guinea and New Caledonia suggest a c. 60 Ma onset of subduction.

5.6. Before 85 Ma, back to the Permian

Prior to 85 Ma, the western Panthalassa Ocean was surrounded by subduction zones, from Antarctica to Japan (Figures 25 – 32). Along the east Gondwana margins of New Zealand and New Caledonia, accretionary prisms formed during subduction of the Phoenix Plate and its daughter plates that broke up during emplacement of the Ontong-Java-Nui large igneous province (Chapter 3, and references therein). Some marginal basin development may have affected the New Zealand margin in the Triassic-Jurassic (Howell, 1980; Roser et al., 2002; Appendix 1), but this is not of consequence for the reconstruction of the Junction Region. For the Japan margin, major back-arc basin opening, and closure has recently been postulated for Jurassic and Cretaceous time based on combining marine magnetic anomaly reconstructions of the northwestern Pacific Plate with analyses of OPS sequences (Boschman et al., 2021a). However, subduction and arc magmatism along the eastern Eurasian margins of Indochina and South China west of the Qingdao Line was continuous from the Jurassic until ~85 Ma and upper plate deformation remained restricted to Basin and Range-style extension, and prior to that Andean-style orogenesis in the South China Block (Jahn et al., 1990; Lapierre et al., 1997; Li et al., 2012; J. Li et al., 2014). Finally, to the west, the SE Asian Tethysides experienced a northward journey from the northwest Australian margin to the Indochina margin from middle Jurassic to ~85 Ma, accommodated by the closure and opening of Neotethyan oceanic basins (Hall, 2012; Advokaat and Van Hinsbergen, 2023). The plate reconstruction of the Junction Region thus hinges on interpretations of the geology from the Philippines and New Guinea, and the remains of the Proto-South China Sea lithosphere.

5.6.1. Philippine Mobile Belt

The pre-85 Ma geological record of the Philippine Mobile Belt reveals supra-subduction zone oceanic lithosphere of Late Cretaceous age (~100-85 Ma) overlain by arc volcanic rocks of similar age (Dimalanta et al., 2020), and fragments of older oceanic lithosphere of Early Cretaceous (e.g., the Huatung Basin; Deschamps et al., 2000; Ghong et al., 2021) and Late Jurassic age (the Lagonoy and Tacloban ophiolites; Geary et al., 1988; Suerte et al., 2005; Dimalanta et al., 2020). Moreover, the Cebu arc and associated accretionary prisms demonstrate that the northern and southern Philippine Mobile Belt were part of two separate plates that converged parallel to the trend of the Philippine Mobile Belt between ~135 and ~110 Ma, accommodated at the proto-SE Bohol Trench (Faustino et al., 2003; Deng et al.,



Figure 25. Snapshot of the kinematic reconstruction at 90 Ma.

2015, 2019; Gong et al., 2021). The accretionary prisms below the Papua ophiolites reveal that the ocean basin that separated the Philippine Mobile Belt from Australia contained Upper Jurassic oceanic crust (Permana, 1995; Weiland, 1999) that formed after extension affected the northern Australian margin of the Fry and Arafura plateaus (Home et al., 1990; Pigram and Symonds, 1991; Davies, 2012), during which time small microcontinental blocks may have locally separated from this margin (Davies, 2012). Prior to the Late Jurassic, the oceanic crust of the Philippine Mobile Belt did not exist yet, and a volcanic arc was located in Permian and Triassic time on the northern Australian continental margin of south New Guinea (Amiruddin, 2009; Crowhurst et al., 2011; Webb and White, 2016; Jost et al., 2018). This Permian and Triassic arc magmatism is also known from the SW Borneo Block of the SE Asian Tethysides (Burton-Johnson et al., 2020; Wang et al., 2023) which was reconstructed to the west of New Guinea (Advokaat and Van Hinsbergen, 2023) and



Figure 26. Snapshot of the kinematic reconstruction at 100 Ma. Note the more southerly projection compared to the previous figures.

which we infer was the continuation of the pre-Jurassic north Gondwana arc. We used these constraints to propose the following reconstruction.

We consider the Philippine Mobile Belt as the arc and forearc crust that formed above a southwest-dipping subduction zone that consumed oceanic crust of the Panthalassa Ocean (Figures 25 – 32). We refer to this ‘proto-Izu-Bonin Mariana’ subduction zone as the Lagonoy subduction zone, after the oldest ophiolite exposed in the Philippines. In Permian to Triassic time this subduction zone was located along the north Australian margin (Figure 32), but in Late Jurassic time it started to roll back, opening a forearc basin that developed into a back-arc basin, with some trench-parallel convergence accommodated at the SE Bohol trench (Figures 27 – 32). After 110 Ma, extension jumped back to the forearc. This may either have occurred because of trench-parallel extension above an oblique subduction



Figure 27. Snapshot of the kinematic reconstruction at 110 Ma.

zone, such as documented for the Andaman Sea (Curry, 2005) or the Jurassic Californian ophiolites (Arkula et al., 2023), or trench-normal, analogous to the ridge jump from the Parece Vela Basin to the Mariana Trough, or from the South Fiji Basin to the Lau Basin. The Upper Cretaceous crust of the eastern Philippine Mobile Belt formed shortly after the jump in extension and was subsequently overlain by arcs. Trench-parallel extension may have played a role at 135 Ma as suggested by the E-W trending magnetic anomalies of the Huatung Basin (Deschamps et al., 2000), although this basin may also have opened as a back-arc basin above the proto-SE Bohol Trench. In our reconstruction, we model a ‘Mariana Trough style’ ridge jump around 110 Ma, inferring trench-normal extension between 110 and 85 Ma for the Philippine Mobile Belt (Figures 25 – 27), which may be tested in the future with paleomagnetic data from sheeted dyke sequences (see e.g., Maffione et al., 2017). This extension and roll-back ceased when the Pacific changed plate motion at

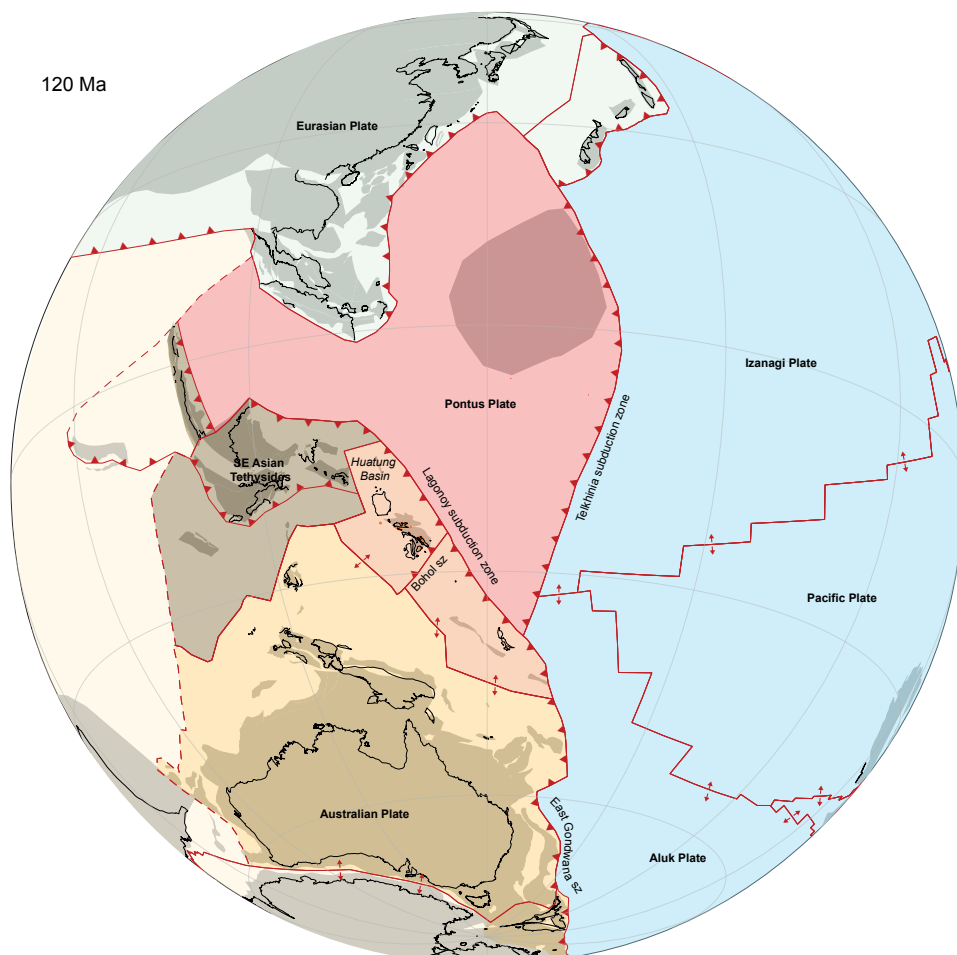


Figure 28. Snapshot of the kinematic reconstruction at 120 Ma.

85 Ma, and the margin became transform dominated (Figure 24).

In our reconstruction of 110 Ma, the opening of a Mariana-style forearc basin is reconstructed, and of the Philippine Mobile Belt and the Molucca Islands, only the pre-110 Ma crust is left. Before 110 Ma, the northward (or in reconstructed coordinates, northwestward) subduction at the proto-SE Bohol Trench is reconstructed by connecting the upper plate of the SE Bohol subduction zone, including the northern Philippine Mobile Belt, to the SW Borneo Block as reconstructed by Advokaat and Van Hinsbergen (2023). This connection infers that the Late Jurassic-Cretaceous Lagonoy subduction zone was continuous with the subduction zone of NW Borneo, which formed the Kuching Zone (Figures 27 - 32). Restoring these in tandem reconstructs the northern Philippines adjacent to the Australian continental margin of west New Guinea and the Bird's Head at 156 Ma (Figure 32), when the SW Borneo Block, as part of the greater Argoland microcontinental Archipelago, was



Figure 29. Snapshot of the kinematic reconstruction at 130 Ma.

separated from the NW Australian margin (Veevers et al., 1991; Hall, 2002; Advokaat and Van Hinsbergen, 2023). Reconstructing the Philippines as an oceanic part of the Argoland Plate thus straightforwardly explains the latest Jurassic ages of the Lagonoy and Tacloban ophiolites (Geary et al., 1988; Suerte et al., 2005) and the oceanic crustal remains below the Papuan ophiolites (Permana, 1995; Weiland, 1999). We reconstruct the south-eastern, down-going plate of the SE Bohol subduction zone, including Mindanao and Halmahera, as an independent plate against the northeastern point of the Australian continental margin at 156 Ma. Applying a constant rotation rate whereby we keep the trench lined up with the northwestern continuation, a small change in plate motion of the SW Borneo Block in the reconstruction of Advokaat and Van Hinsbergen (2023) generates relative convergence across the SE Bohol Trench at 130 Ma, satisfying the geological constraints from the Cebu arc and accretionary prism.



Figure 30. Snapshot of the kinematic reconstruction at 140 Ma.

5.6.2. Proto-South China Sea lithosphere

Prior to the arrest of subduction of Proto-South China Sea lithosphere around 85 Ma, convergence between the Panthalassic plates, and the Eurasian and the ‘Tethyan’ plates was at least in part accommodated by subduction at the trenches surrounding the later Proto-South China Sea, below Borneo, Indochina, and South China. Paleomagnetic data from 135 Ma old pillow lavas from OPS units of NW Borneo that accreted just prior to ~85 Ma subduction cessation (Chapter 4) show that this Proto-South China Sea lithosphere cannot have been part of the Izanagi Plate. Predicting the paleolatitude of the Proto-South China Sea lithosphere by reconstructing it as part of the Izanagi Plate before 85 Ma predicts paleolatitudes of ~30°S at 135 Ma, ~15–25° south of the measured paleolatitude (Chapter 4). The Proto-South China Sea lithosphere must therefore have been part of a plate that was subducting below the Eurasian and Tethyan plates, but that was not the Izanagi Plate.



Figure 31. Snapshot of the kinematic reconstruction at 150 Ma.

Paleomagnetic data show that this plate moved $\sim 15^\circ$ northward between 135 and 85 Ma, and it must have had a westward motion component to have been able to subduct below the Tethyan and Eurasian plates. The plate boundary with the Izanagi Plate must have been a subduction zone with the Proto-South China Sea lithosphere as upper plate. Remains of an arc on the eastern Proto-South China Sea lithosphere have been reported from undated rocks in the accretionary prism of Luzon, and 100 Ma old volcanic rocks in the accretionary prism below the Palawan ophiolite (Pasco et al., 2019; Dycoco et al., 2021; see Chapter 4). Such a configuration of subduction zones surrounding a lithospheric domain between the major Pacific realm and the Tethyan realm was previously inferred from lower mantle seismic tomographic images of anomalies of deeply subducted slabs, imaged at a depth of >2000 km in the mantle below the west-central Pacific Ocean (Van der Meer et al., 2012). At shallower depths, their tomographic model had no resolution, but they inferred from

the slab remnants at >2000 km depth that an intra-oceanic subduction system must have been active in at least Triassic-Jurassic time, separating the Panthalassa realm into two plate systems. Those authors named the western lithospheric system enclosed by these subduction zones the ‘Pontus Ocean’ and Chapter 4 therefore referred to the plate carrying the Proto-South China Sea lithosphere as the ‘Pontus Plate’. We refer to the subduction zone of the Izanagi Plate below the Pontus Plate as the ‘Telkhinia’ subduction zone, following Van der Meer et al. (2012).

Our reconstruction at 110 Ma illustrates that the Pontus Plate must have been a major plate (or, farther back in time, plate system) in the Mesozoic (Figure 27). The Telkhinia subduction zone ended in the south at a trench-trench-trench triple junction with the Lagonoy subduction zone (proto-Izu-Bonin Mariana subduction zone), with the Pontus Plate in a downgoing plate position (Figure 25 - 32). In the north, the Telkhinia subduction zone must have had a triple junction with the subduction zones along the South China Block, and we model a triple junction location around the Kerama Gap/Qingdao Line.

For times back to 156 Ma, we reconstruct the motion of the Pontus Plate as such that we avoid extension with the Izanagi Plate. The Telkhinia trench that accommodated subduction of the Izanagi Plate restores farther into the Panthalassa Ocean back in time, and as a result, its north-south extent becomes longer in older reconstruction slices (Figure 25 - 32). The triple junction at e.g., 135 Ma was located farther southeastwards along the East Gondwana margin, and the Telkhinia subduction zone likely also accommodated the subduction of the Izanagi-Phoenix ridge, or even part of the Pacific Plate (Figure 27 - 32).

The age of the oldest lithosphere in the Pontus Plate, and hence the maximum age of the Telkhinia subduction zone, is unknown. Accreted units below the eastern margin of the Pontus Plate have likely all been lost to subduction. The accreted seamount in the South China margin with an age of ~154 Ma (Xu et al., 2022) show that the plate contained lithosphere of at least Late Jurassic age. For ages older than 135 Ma, we have no direct kinematic constraints left from rocks of the Pontus Plate, and it is possible that the Pontus ‘Ocean’ sensu Van der Meer et al. (2012) contained multiple plates, separated by ridges. In our reconstruction prior to 135 Ma, we keep the Telkhinia subduction zone more or less mantle stationary, following the tomography-based interpretations of the lower mantle below the Pacific Ocean of Van der Meer et al. (2012).

The Pontus Plate (or further back in time, probably plate system) thus formed a Junction Region in between the Panthalassa and Tethys domains. The westernmost plate boundary of the Panthalassa Ocean (or the ‘Thalassa Ocean’ sensu Van der Meer et al., 2012) was formed by the Telkhinia subduction zone, that connected the subduction zone below Japan with the subduction zone below East Gondwana. To the west, the subduction zones along the Philippine Mobile Belt (Lagonoy subduction zone) and the Kuching Zone adjacent to the SW Borneo Block must have connected through an intra-oceanic trench system to the trenches along Sundaland and South China. Such trenches were also inferred for Jurassic and older times based on seismic tomographic images of the lowermost mantle



Figure 32. Snapshot of the kinematic reconstruction at 160 Ma.

by Van der Meer et al. (2012), but geological relics of these trenches have not been identified yet. Such relics would have been consumed by subduction below the SW Borneo Block in the south, the West Sulawesi and Sibumasu terranes of Sundaland, and depending on how far this subduction zone reached westwards, perhaps even in de Bangong-Nujiang suture zone between the Lhasa and Qiangtang terranes of western Burma. Future analysis of accretionary prisms in SE Asia may identify further constraints on the intra-oceanic subduction systems that must have existed between the Pontus and Neotethys oceans. The reconstruction at 160 Ma (Figure 32) satisfies all presently available geological constraints on intra-oceanic subduction that we are aware of from the Junction Region.

The key difference with the reconstruction of Zahirovic et al. (2014) in the oldest part of our reconstruction is the location of the plate boundary that separates the Panthalassa plates from the Junction. Where we follow the constraints of Wu et al. (2022) and Chapter 4 to

infer a subduction zone that extends from the East Gondwana northwards to the Qingdao Line, and the subduction of the Pontus Plate below the SE China and Indochina margins, Zahirovic et al. (2014) incorporate the widely held view that the Izanagi Plate subducted below the entire Eurasian margin. Moreover, their model opens the Proto-South China Sea as a back-arc basin between c. 65 and 35 Ma, while geological data from surrounding regions indicate that the oceanic lithosphere of this basin was of Cretaceous age (Dycoco et al., 2021; Xu et al., 2022; Wang et al., 2023; Chapter 4).

6. Discussion: Geodynamic implications

Our kinematic reconstruction is based on the modern geological architecture of the Junction Region, in which we assumed a simplest plate model with the least amount of plate boundaries necessary to explain the present-day geology. In this section we briefly discuss the geodynamic implications that follow from our reconstruction, and how they may contribute to a better understanding of geodynamics.

6.1. Small oceanic basins opening in the downgoing plate close to trenches

An interesting finding of our plate reconstruction is that the Junction Region hosts several examples of relatively small oceanic basins that opened within a down-going plate, in the proximity of and at ridges parallel to a subduction zone. Opening of oceanic basins above subduction zones is a common phenomenon, as illustrated by the numerous forearc and back-arc basins of the West and Southwest Pacific realms, such as the Mariana Trough, Ogasawara Trough, Parece-Vela Basin, South Fiji Basin, or Lau Basin (Figure 1). Examples of oceanic basins that opened in a down-going plate are the South China Sea basin, the Santa Cruz Basin, and the Woodlark Basin (Figure 33). We speculate that there may be causal relationships between opening of these basins and the nearby subduction zones. The South China Sea basin opened from the late Eocene to mid-Miocene, during southward subduction of the Proto-South China Sea, partly contemporaneous with the Sulu Sea that started opening as back-arc basin in the upper plate (e.g., Advokaat and Van Hinsbergen, 2023). It was recently suggested that the Proto-South China Sea may have been underlain by an oceanic plateau that initially stopped subduction in the Mesozoic (Chapter 4). Those authors tentatively suggested that when this oceanic plateau was eventually forced to subduct during counterclockwise vertical-axis rotation of Borneo, the eclogitization of thickened oceanic crust may have caused an especially strong slab pull, that resulted in the extension and eventual break-up of the down-going plate and the formation of the South China Sea.

The Santa Cruz Basin formed in the Eocene during eastward subduction at the New Caledonia subduction zone, while the North Loyalty back-arc basin opened contemporaneously and in a parallel orientation in the overriding plate (Seton et al., 2016; Chapter 1). The eastern margin of the Santa Cruz Basin is flanked by the West Torres Plateau. In the case of the Santa Cruz Basin, however, extension in the down-going plate

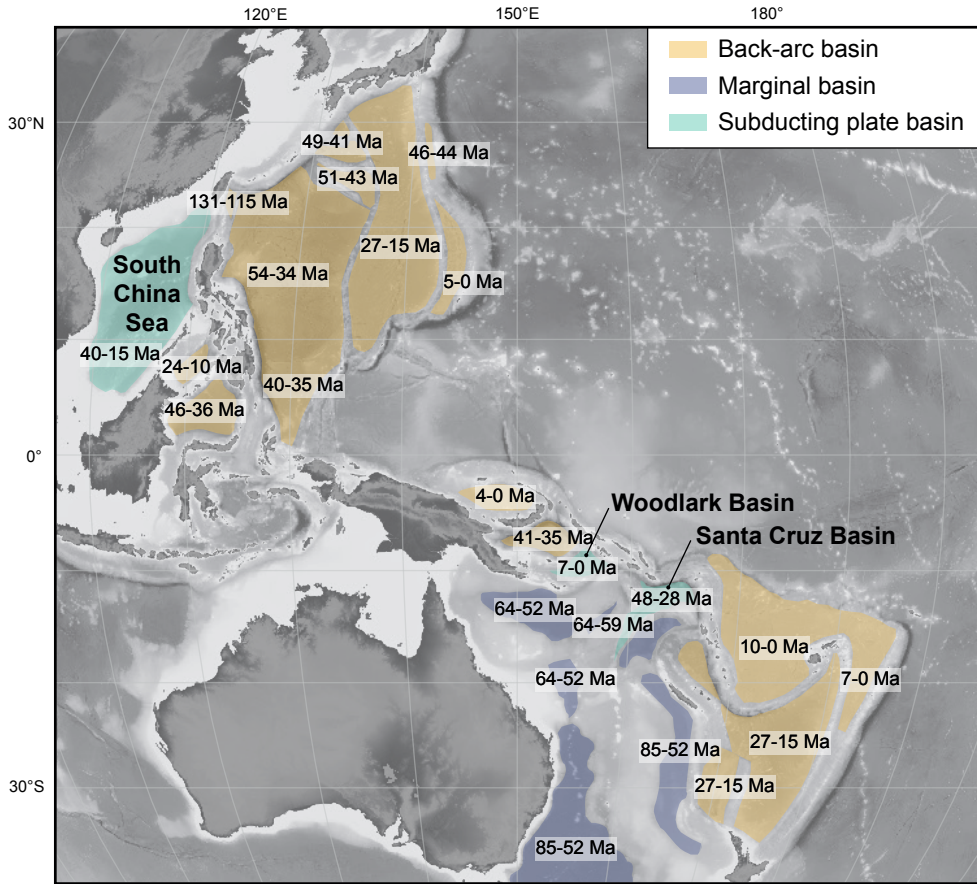


Figure 33. Map of the oceanic basins in the Junction Region colored by their tectonic setting. Back-arc basins formed above active subduction zones. Marginal basins formed by breaking of a continental margin in absence of a subduction zone. The subducting plate basins formed at ridges that were created within a downgoing plate close to a subduction zone.

ceased in the early Oligocene, while subduction of the plateau is presently occurring at the New Hebrides trench. Moreover, it is unknown whether the West Torres Plateau was being subducted during opening of the Santa Cruz Basin, because its original eastward extension is unknown.

The Woodlark Basin also recently started forming in the down-going Australian Plate, but at a higher angle to the subduction zone owing to rotational opening around an Euler pole not far west of the d'Entrecasteaux Islands. In this basin, there is no evidence of the presence of an oceanic plateau, but it is attached to older, Eocene, oceanic crust of the Solomon Sea. Similar to the tectonic settings of the South China Sea and Santa Cruz basins, there is also a back-arc basin in the northwest (the Manus Basin) that forms in an overriding plate position to the Woodlark Basin. However, in the case of the South China

Sea and Santa Cruz Basin, their opening was preceded a few Ma by the opening of the back-arc basin, while in the case of the Woodlark Basin, the back-arc basin is younger than the subducting plate basin. Moreover, where the back-arc and subducting plate basins opened roughly parallel in the case of the South China Sea and Santa Cruz basins, the orientation of the Manus Basin is at a higher angle with the Woodlark Basin.

Other than the fact that all these basins formed in a down-going plate in the proximity and roughly parallel to a subduction zone, the most striking resemblance between the South China Sea and Santa Cruz basins is that both formed parallel to a back-arc basin in the overriding plate that started forming a few Ma earlier, but this similarity is not shared with the Woodlark Basin. The basins that opened in subducting plates all formed in pre-existing weak zones of that plate; the South China Sea formed within the South China margin accretionary prism, and the Santa Cruz and Woodlark basin formed at an obducted continent-ocean transition zone of the Australian Plate.

The consequence of back-arc basins that form during slab roll-back is that subduction rates exceed the convergence rates between the plates that were originally interacting at the plate boundary, an effect that is in these cases caused or enhanced by the formation of subducting plate basins. The reason behind this effect related to the formation of subducting-plate basins and its connection to subduction zone dynamics are topics that may be explored further through geodynamic modeling.

Finally, the Coral Sea and Caroline Plate basins also opened in a down-going plate position, and roughly parallel to the San Cristobal North Solomon subduction zone, respectively, but at a far larger distance and at a larger scale than the aforementioned basins. A causal relationship between the opening of the basin and the subduction zone may therefore be less straightforward. We consider the Coral Sea Basin as a northward extension of the Tasman Sea, which formed as a marginal basin during continental break-up. Previously, the Caroline Plate was considered a back-arc basin (e.g., Weissel and Anderson, 1978; Gaina and Müller, 2007; Wu et al., 2016), but in our reconstruction the plate is separated from the north-dipping New Guinea subduction zone by the south-dipping North Solomon-Vitiaz subduction zone and the basin is therefore not in a back-arc position. As the large igneous provinces on the Caroline Plate clearly indicate its interaction with a mantle plume, we suspect that the formation of Caroline Plate basins may be related to weakening by a mantle plume, with spreading driven by slab pull of the already subducting slab.

6.2. Absolute plate and slab motion

Placing our reconstruction in a mantle reference frame provides insight into the absolute motions of plates and subducted slabs (known as ‘slab dragging’; Spakman et al., 2018), during subduction and after slab break-off. Chapter 1 showed that the Tonga-Kermadec slab was dragged northward, laterally through the mantle over about 1200 km since 30 Ma, resulting from the northward, trench-parallel component of the absolute motion of Pacific Plate. Our reconstruction now assigns an earlier age of subduction initiation of the

Tonga segment of the subduction zone of 45 Ma, which increases the amount of Tonga slab dragging since subduction initiation to 1600 km (~ 3.5 cm/yr). The accompanying northward motion of the Australian Plate resulted in also northward motion of the Tonga-Kermadec trench and upper plate (Figure 34). Slab dragging is not restricted to trenches that accommodate subduction between two plates that also share a trench-parallel absolute plate motion component. Slab dragging also occurs during highly oblique subduction below near-mantle-stationary upper plates, e.g., the northward dragging of the Burma slab as part of the Indian Plate (Le Dain et al., 1984; Parsons et al., 2021). In addition to trench-parallel slab dragging, slab dragging also occurs during trench-perpendicular absolute motion; the motion of upper plates (and hence trenches) relative to the mantle may result in slab retreat or slab advance, which causes flat-lying and steep (or even overturned) slabs, respectively (e.g., Qayyum et al., 2022). We here assess the motion of trenches and slabs relative to the mantle as the result of absolute plate motion, and how this may have influenced slab geometry, by placing our reconstruction of the Junction Region in the global moving hotspot reference frame of Doubrovine et al. (2012).

The rapid Australian absolute plate motion must mean that the New Hebrides slab, which has been subducting and rolling back below Vanuatu, has experienced northward slab dragging since its formation (c. 10 Ma ago, Yan and Kroenke, 1993). The clockwise rotation of the trench has resulted in a larger amount of absolute trench motion in the south than in the north, and a larger northward component of the northern part of the trench. This slab dragging component may provide a straightforward explanation for the incipient subduction at the Hunter fracture zone that started in the Plio-Pleistocene (Patriat et al., 2015; 2019; Lallemand and Arcay, 2021). This transform formed as a STEP fault accommodating New Hebrides trench roll-back. We foresee that the resistance of the New Hebrides slab against northward slab dragging, which is known to cause trench-parallel shortening in the downgoing plate (Spakman et al., 2018), may contribute to the incipient subduction at the Hunter fracture zone.

The Tonga-Kermadec trench was connected northwards with the Solomon-Vitiaz trench, which also accommodated Pacific-Australia relative motion. The motion of the Pacific Plate relative to the mantle since 45 Ma is roughly towards the WNW, similar to the orientation of the North Solomon trench. The subduction of the Pacific Plate at the North Solomon trench is thus purely the result of the 2200 km (~ 4.9 cm/yr) northward motion of the North Solomon trench since 45 Ma, as part of the Australian Plate (Figure 34). The northward motion of the North Solomon trench leads to slab retreat.

Farther north, the Izu-Bonin Mariana subduction zone also has a N-S orientation. The Philippine Sea Plate underwent a strong northward motion component (see section 5; also Chapter 5). Like the Tonga-Kermadec slab, the Izu-Bonin Mariana slab is located due west of the present-day trench (Miller et al., 2004; Wu et al., 2016; Van der Meer et al., 2018), but the subduction zone originated much farther southward (Figure 34). Slab dragging at the Mariana trench was c. 3000 km (~ 6.6 cm/yr), i.e., almost twice as fast as

the Tonga-Kermadec subduction zone since 45 Ma. We suggest that the N-S opening of the West Philippine Basin and the NE-SW opening of the Parece Vela Basin accommodated additional slab dragging of the Izu-Bonin section driven by absolute motion of the Pacific Plate. Moreover, as subduction here initiated earlier than in the Tonga-Kermadec case, the total amount of slab dragging is much larger, in the order of ~4000 km for the northernmost Izu-Bonin trench since 52 Ma (~7.7 cm/yr) and ~3000 km for the central Mariana trench (~5.8 cm/yr). The recent clockwise rotation of the Philippine Sea Plate accommodated by extensional motion in the Ayu Trough since 15 M, has resulted in slab advance of the southern portion of the trench, which explains the steep nature of the Mariana slab (e.g., Spakman et al., 1989; Van der Hilst, 1991; Miller et al., 2004). This also suggests that the Mariana Trough back-arc did not open because of slab roll-back, but rather due to slab resistance against overriding plate retreat.

In the north of the Philippine Sea Plate, the position of the trenches along the Eurasian margin have been comparatively stable relative to the mantle since the Late Cretaceous. The total amount of trench retreat of the Ryukyu arc since 70 Ma is about 750 km (~1.1 cm/yr). However, the opening of the Shikoku Basin in the Philippine Sea Plate, which was accompanied by trench retreat of the Izu-Bonin trench, has resulted in large-scale (~1600 km since 30 Ma) trench-parallel slab dragging at the Nankai trench, analogous to the Burma slab.

The Manila and the Halmahera trenches that form the western plate boundary of the Philippine Sea Plate have experienced large absolute trench motions since subduction initiation around 15 Ma. In this case, however, the position of the down-going plate relative to the mantle has been almost stationary throughout the subduction history. So even though the Manila trench's upper plate underwent large scale northward, trench-parallel, motion, lateral slab dragging is minimal here.

In addition to the presently active subduction zones, we may also analyze former trenches in our reconstruction and make inferences about where we may find slab remnants in the mantle. The north- and eastward dipping New Guinea-New Caledonia subduction zones have been subject to slab dragging (Figure 34). Like most trenches in the Junction Region, these trenches and slabs underwent northward absolute motion, which resulted in trench-parallel dragging at the New Caledonia trench. Chapter 1 showed that the South Loyalty Slab, identified by Schellart et al. (2009), is in a position that is just north of the reconstructed 30 Ma location of the New Caledonia trench, at which time northward subduction ceased and the slab likely detached. After the end of subduction, the slab sank vertically into the mantle, and the inactive trench subsequently overrode the slab during northward motion of the Australian Plate. The change in orientation from roughly N-S at the New Caledonia trench to roughly E-W at the New Guinea trench resulted in slab advance rather than lateral dragging of the slab at the New Guinea trench (Figure 34). During the Eocene, however, slab advance in the New Guinea sector was largely cancelled by roll-back such that the trench remained in a more or less mantle-stationary position.

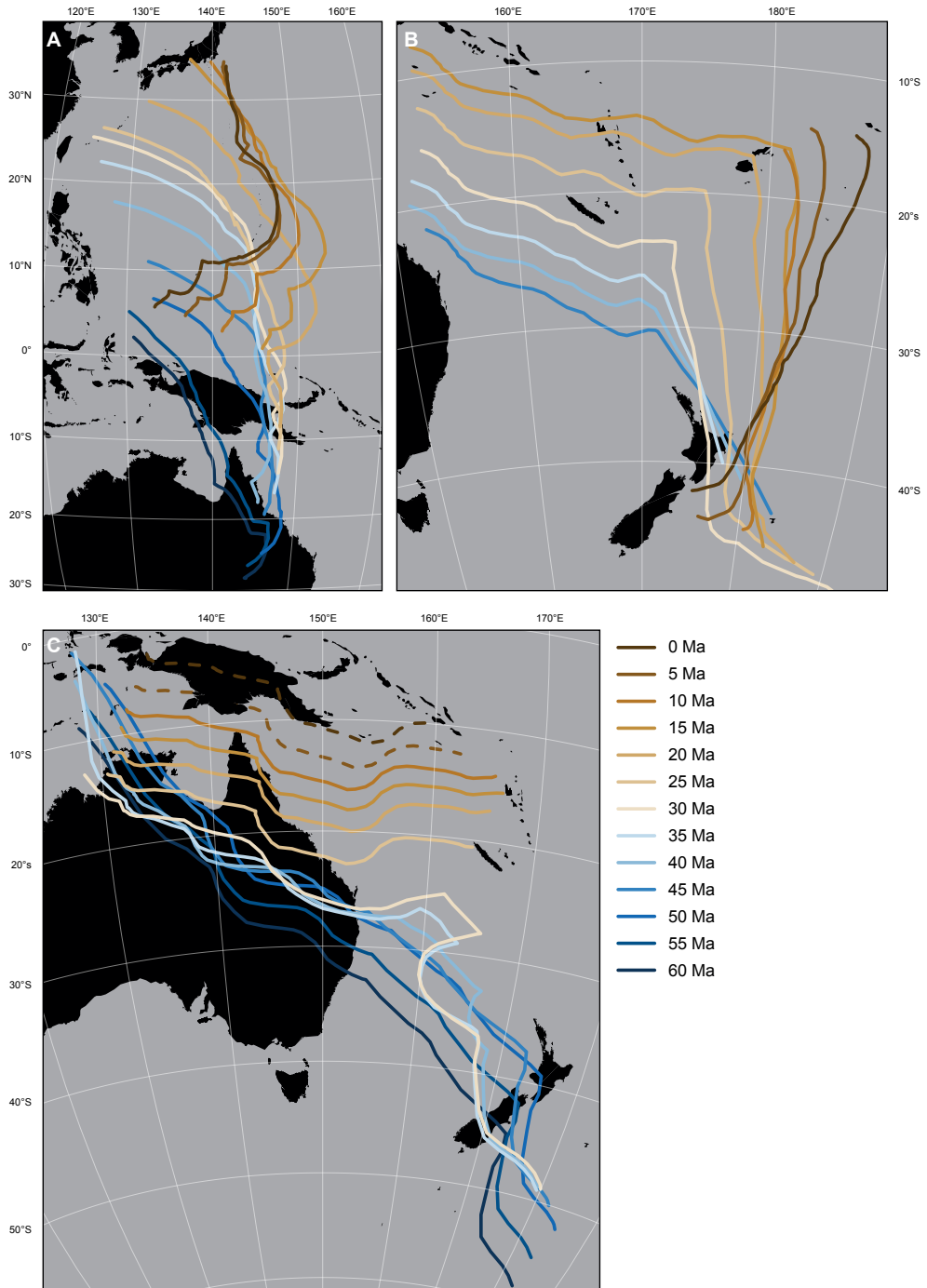


Figure 34. Maps showing the locations of subduction zones through time in the mantle reference frame of Doubrovine et al. (2012). A) Izu-Bonin Mariana subduction zone; B) Tonga-Kermadec(-Vitiāz-Solomon) subduction zone; C) New Guinea-New Caledonia subduction zone.

The opening of the Molucca Sea and Solomon Sea back-arc basins occurred mostly due to northward absolute motion components of the Philippine Sea Plate relative to this mantle-stationary trench. Subsequent slab advance during northward motion of the New Guinea trench may have resulted in a steeply dipping or overturned slab. Depending on how the geometry of the slab was affected by slab advance, both the Arafura and Carpentaria slabs of Van der Meer et al. (2018) may be correlated to the New Guinea subduction zone. Following slab break-off, Australia overrode these slabs, and their mantle wedges. Previously, Van Hinsbergen et al. (2020b) inferred that Australia overriding a former mantle wedge above the Arafura slab led to the enigmatic arc-signature in the Pliocene Ertsberg and Grasberg magmatic centers in Central New Guinea, close to the obduction front. Those authors used the reconstructions of Hall (2002) and Zahirovic et al. (2014) who suggested that the Arafura slab formed entirely at an intra-oceanic subduction zone far north of Australia, prior to ~30 Ma. Our reconstruction instead suggests that the only candidate to have formed the Arafura slab is the subduction zone that led to the obduction of the Papuan ophiolite. The timing of its break-off may have occurred anytime after 30 Ma, but the position of the slab suggests that this occurred around 10 Ma, and that the time delay between mantle wedge formation and plowing of the Australian margin through the mantle is shorter than interpreted by Van Hinsbergen et al. (2020b).

In the Cretaceous, the Lagonoy subduction zone underwent trench retreat, as well as northward trench-parallel slab dragging. Slab dragging at the Telkhinia trench was dominated by slab advance. During roll-back of the Lagonoy subduction zone, the Telkhinia subduction zone was progressively consumed by the Lagonoy subduction zone, and we therefore expect that the Telkhinia slab may have broken in several instances. This may explain some of the slab remnants that are present in the mantle below the eastern margin of eastern Australia. One of the slab remnants below Australia is the Lake Eyre slab, which is in the lower mantle below Lake Eyre, Australia. This slab was previously interpreted using the reconstruction of Hall (2002) as the detached slab that formed during northward subduction of the Australian Plate below the Papuan ophiolites (Schellart and Spakman, 2015). In their interpretation subduction there ceased around 50 Ma, based on the c. 54 Ma age of the metamorphic sole below the Papuan Ultramafic Belt (Lus et al., 2004). However, as the metamorphic sole forms during subduction initiation rather than subduction termination, this age does not represent the end of subduction but the start, and the geology of New Guinea indicates that oceanic subduction continued into the Oligocene and obduction until the late Miocene. In light of our reconstruction, it is unlikely that the Lake Eyre slab is correlated to a 60-30 Ma New Guinea subduction zone. Instead, when putting our reconstruction in the slab references frame of Van der Meer et al. (2010), the Lake Eyre slab is in a location that could correspond to the location of the Lagonoy subduction zone around 85 Ma, just prior to when this plate boundary became dominated by transform motion owing to the change in absolute motion of the Pacific plate from west to north (Figure 35). The change in relative plate motion at the plate boundary may have resulted

in slab detachment which subsequently sank vertically into the mantle. This interpretation would suggest that the Lake Eyre slab is much older than previously thought.

Our analysis of slab dragging in the west Pacific region shows that lateral slab dragging such as previously shown for the Tonga-Kermadec (Chapter 1) is a rule rather than an exception. Lateral slab dragging is a common phenomenon that occurs in all subduction zones where the down-going plate has a trench-parallel component. In addition, the absolute motion of upper plates relative to slabs is a key driver of upper plate deformation (Van Hinsbergen and Schouten, 2021). Slab dragging can only be correctly analyzed in an absolute plate motion frame, because the absolute plate motion of both the upper plate and down-going plate as well as their interaction at the trench determine the amount and type of slab dragging. In addition, as illustrated by the example of the Lake Eyre slab, our reconstruction sheds a new light on the plate boundary evolution in the Junction Region that requires a reinterpretation of the geological history of upper and especially lower mantle slabs, such as those listed in the Atlas of the Underworld (Van der Meer et al., 2018).

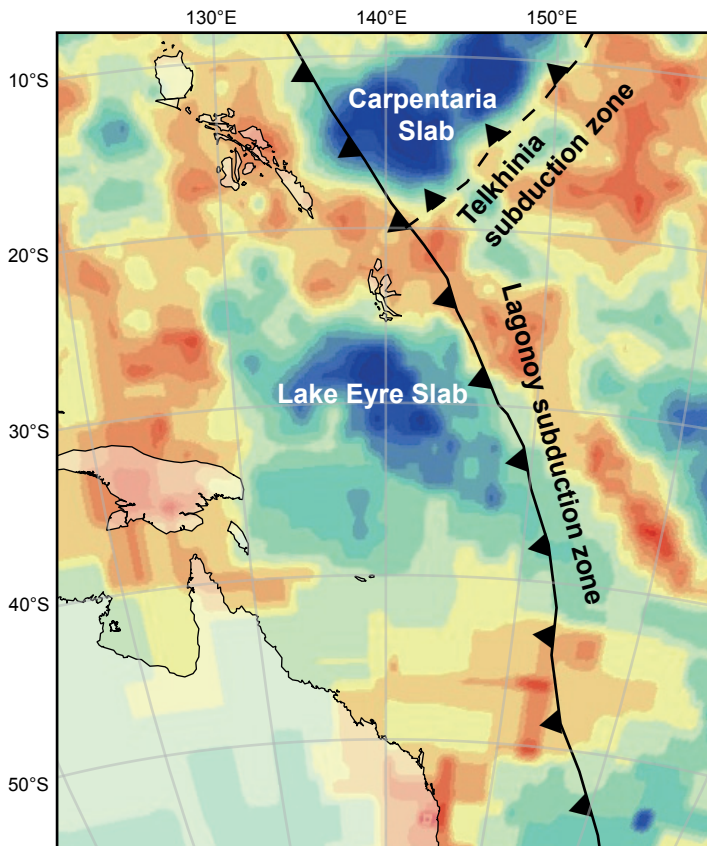


Figure 35. Reconstructed position of the Lagonoy subduction zone at 85 Ma in the slab reference frame of Van der Meer et al. (2010) projected on a seismic tomographic image of present-day mantle structure at a depth of 1050 km, based on the UU-P07 tomographic model (Amaru, 2007).

6.3. Subduction initiation

The Izu-Bonin Mariana subduction zone is one of the best-studied subduction zones on Earth, particularly to understand subduction initiation (e.g., Stern and Bloomer, 1992; Stern et al., 2003, 2012; Reagan et al., 2010; Ishizuka et al., 2011a; Arculus et al., 2015). The age of subduction initiation at the Izu-Bonin Mariana trench is generally inferred from the oldest supra-subduction zone gabbros and basalts recovered from the Izu-Bonin-Mariana forearc, which are ~52 Ma old (Ishizuka et al., 2011a; Reagan et al., 2010, 2013, 2019). This inference assumes that the catastrophic extension that led to the overriding plate spreading centers at which these basalts and gabbros formed along the strike of the Izu-Bonin-Mariana forearc signals spontaneous subduction initiation. In such a setting, the area consumed by initial subduction resulting from the gravitationally driven lithospheric collapse of the down-going plate must be instantaneously compensated by upper plate extension, and the magmatic rocks formed during that extension must thus be synchronous with subduction initiation (e.g., Stern and Bloomer; Stern, 2004; Arculus et al., 2015). However, the Semail Ophiolite of Oman comprises similar forearc crust that formed through catastrophic extension because of lithospheric collapse, but there, rocks that formed at the incipient subduction plate boundary are exhumed as metamorphic sole rocks, which are about 8 Ma older than the age of forearc basalts (Guilmette et al., 2018). Similar and even larger time delays between the formation of the metamorphic sole and the formation of forearc crust have been shown since for the Coast Range Ophiolite in California (Mulcahy et al., 2018), the Halilbağı Complex in Turkey (Pourteau et al., 2019) and the Xigaze Ophiolite in Tibet (Guilmette et al., 2023). These time lags between metamorphic sole and subsequent forearc crust formation can only exist in subduction zones that formed due to far-field-forced convergence, as the subduction interface formed before lithospheric collapse occurred (Guilmette et al., 2018). The metamorphic sole of the Izu-Bonin Mariana subduction zone remains buried below the Izu-Bonin Mariana forearc and it is therefore impossible to determine its age that would directly resolve the debate of whether subduction initiation occurred spontaneously or was forced. In this case, a kinematic reconstruction provides the next best insight into the question of whether subduction initiation at the Izu-Bonin Mariana trench must have been spontaneous or may have been induced.

Based on our reconstruction, we find that there is no need to assume that subduction initiation at the Izu-Bonin Mariana trench must have been spontaneous. Instead, our reconstruction shows that it is more likely that subduction initiation at the Izu-Bonin Mariana trench was forced and occurred around 62 Ma linked to the slow Pacific-Australian plate convergence that also led to the formation of the New Guinea-New Caledonia subduction zone. If correct, subduction initiation occurred about 10 Ma before lithospheric collapse and extension in the Izu-Bonin Mariana forearc, a similar delay as in the Tethyan and Californian examples. This is based on the reconstructed 62-52 Ma clockwise rotation of the Philippine Mobile Belt that is required for the northward decrease of convergence to avoid subduction of the Australian Plate beyond the Papuan ophiolite belt.

In addition to the cause of subduction initiation, also the nature of the Izu-Bonin Mariana plate boundary before it became a subduction zone has been subject of debate. The most common suggestion is that subduction initiated along a transform fault between two mid-ocean ridge segments (e.g., Casey and Dewey, 1984; Dewey and Casey, 2011), whether it be spontaneous or induced (e.g., Stern and Bloomer, 1992; Hall et al., 2003). This suggestion was mostly based on the interpretation that extension and spreading in the West Philippine Basin predated subduction initiation, but it did not explain the presence of oceanic crust in the overriding Philippine Sea Plate that is up to 100 Ma older (the Lagonoy Ophiolite) at time of subduction initiation. Our reconstruction shows that the Izu-Bonin Mariana trench initiated along a pre-existing weakness zone indeed, which had accommodated mostly transform motion for about 20 Ma resulting from relative plate motion changes around 85 Ma, but that was a subduction zone before that time: our ‘Lagonoy’ subduction zone that was active in the Mesozoic.

If the Izu-Bonin Mariana trench formed through forced subduction initiation that resulted from a small change in Australia-Pacific relative plate motion at 62 Ma together with the New Guinea-New Caledonia subduction zone, the 52 Ma lithospheric collapse may signal the effective onset of slab pull, and thus may have been a trigger for the Eocene change in Pacific Plate motion that resulted in the formation of the Hawaii-Emperor Bend (Torsvik et al., 2017). Izu-Bonin Mariana subduction initiation as driver for the change in absolute plate motion of the Pacific Plate was previously suggested based on geodynamic modelling (Faccenna et al., 2012). Moreover, the possibility that the initiation of effective slab pull that is reflected in lithospheric collapse following subduction initiation may cause absolute plate motion changes was tested and shown for the forced subduction initiation event below the Oman and Anatolia ophiolites that caused a change in African plate motion (Gürer et al., 2022). Our reconstruction shows that it is feasible that the sequence of events from forced subduction initiation to lithospheric collapse and a subsequent change in absolute plate motion applies to the Izu-Bonin Mariana trench and Pacific Plate. To what extent the subduction initiation at the Izu-Bonin Mariana trench was responsible for the change in absolute plate motion of the Pacific Plate is uncertain, as the NW Pacific was the location of other drastic plate tectonic changes, including subduction of the Izanagi-Pacific Ridge that led to the first demonstrable subduction of Pacific Plate lithosphere (Seton et al., 2015; Wu and Wu, 2019) and a subduction polarity reversal after the collision of the Olyutorsky arc with Kamchatka (Domeier et al., 2017; Vaes et al., 2019). Based on the reconstructed 45 Ma age of the Solomon-Vitiaz-Tonga subduction zone, we find it most likely that subduction initiation there was a result of the change in absolute plate motion change of the Pacific Plate rather than a cause, but after it happened, it will have contributed to a more westerly course of absolute Pacific Plate motion. However, if future age constraints provide evidence for an older age of subduction initiation there, it may have played an active role in changing the absolute motion of the Pacific Plate.

7. Conclusions

We developed a kinematic restoration of the Junction Region back to the Jurassic, based on the present-day orogenic record of the circum-Philippine Sea Plate and Australasian region. We presented a comprehensive review of the orogens of southwestern Japan, Taiwan, the Philippines and northern Molucca Islands, New Guinea, and the Solomon Islands and adjacent archipelagoes and ocean basins. Our reconstruction is based on a systematic restoration of the tectonic motions that are inferred from these orogenic and marine geophysical records, cast in context of relative motions of the Australian, Eurasian, and Pacific plates, and in context of a recent restoration of orogenesis in the Tethyan belts of SE Asia. We present our reconstruction in a series of maps from the present back to the Jurassic and provide GPlates reconstruction files that can be placed in mantle or paleomagnetic reference frames as basis for geodynamic or paleoclimatic analysis, respectively. Our conclusions are plentiful, but include the following:

1. The Molucca Sea as well as the Eocene ophiolites of the Philippines and the Cyclops Ophiolite in New Guinea formed as part of an Eocene back-arc basin above a northward dipping subduction zone that consumed the Australian Plate. Subduction at this trench initiated around 62 Ma, was contiguous with the New Caledonia subduction zone, and ended in the Oligocene.
2. The latest Jurassic oceanic crust that is preserved in the Philippines originated from the northern margin of the Australian Plate where continental margin subduction was active during the Permian and Triassic. The formation of the ophiolites records the onset of oceanic spreading and the formation of an Early Cretaceous back-arc basin behind a proto-Izu-Bonin Mariana subduction zone which we refer to as the Lagonoy subduction zone. The Late Cretaceous ophiolites formed when extension relocated to the forearc.
3. Trench-parallel slab dragging as well as slab retreat and advance are common features of subduction zones. The previously identified Lake Eyre slab is not related to the New Guinea subduction zone, but instead may be related to slab break-off at the Lagonoy subduction zone around 85 Ma, when this plate boundary became a transform fault. Instead, the Arafura or possibly the Carpentaria slabs may have formed at the New Guinea subduction zone. A careful re-evaluation of modern mantle structure of the western Pacific in light of our reconstruction is timely.
4. There is no necessity for spontaneous subduction initiation at the Izu-Bonin Mariana trench. Our reconstruction predicts forced subduction initiation around 62 Ma, which subsequently resulted in lithospheric collapse and the formation of the Izu-Bonin Mariana forearc around 52 Ma. The lithospheric collapse may have been a trigger of the change in absolute plate motion of the Pacific Plate that caused the formation of the Hawaii-Emperor Bend.



Upper Triassic siltstones at Kiritehere Beach, New Zealand

Appendix I

Post-remagnetisation vertical axis rotation and tilting of the Murihiku Terrane (North Island, New Zealand)

This appendix has been published as:

Van de Lagemaat, S. H. A., Boschman, L. M., Kamp, P. J. J., Langereis, C. G., & Van Hinsbergen, D. J. J. (2018). Post-remagnetisation vertical axis rotation and tilting of the Murihiku Terrane (North Island, New Zealand). *New Zealand Journal of Geology and Geophysics*, 61(1), 9-25.

Abstract

We collected palaeomagnetic sample sets from Murihiku Terrane, North Island to constrain its palaeolatitude during the Late Triassic–Jurassic. The majority of the sample host rocks were remagnetised. However, a few samples show a magnetic signal that possibly recorded a primary remanent magnetisation. These samples preliminarily indicate that Murihiku Terrane was located at c. 63°S during the Early Jurassic. The remagnetised samples reveal significant post-remagnetisation tectonic rotation and tilting of the host rocks. We estimated an 83 ± 5 Ma timing of remagnetisation by plotting the palaeolatitude data on the apparent polar wander path of northern Zealandia. Samples from southernmost sites have lower inclination, which we interpret as reflecting eastward post-remagnetisation tilt of this region by 20°. In addition, declination data indicate large-scale post-remagnetisation rotation of Port Waikato and Awakino Gorge areas. This study contributes to the ongoing debate on the age and tectonic origin of oroclines in New Zealand basement.

1. Introduction

The New Zealand continent (Zealandia) separated from Gondwana during the Late Cretaceous following continental rifting and sea floor spreading in Tasman Sea and between Campbell Plateau and Marie Byrd Land (MacKinnon 1983; Haston and Luyendyk 1991; Mortimer 2004). The majority of basement on land in New Zealand, the so-called Eastern Province, consists of volcanic arc (Brook Street Terrane), ocean floor (Dun Mountain Terrane), forearc (Murihiku Terrane) and accretionary wedge elements (Torlesse complex), interpreted to have formed at one or more intra-oceanic subduction zones (Mortimer et al. 2014). This allochthonous assemblage is separated from Gondwana-derived units in western New Zealand (Northwest Nelson, Westland, Fiordland) by the Median Batholith (c. 375 and 110 Ma), which represents a long-lived magmatic arc along the Gondwana margin (Mortimer 2004).

The Murihiku Terrane, noted above is one of the Eastern Province elements, is structurally separate from adjacent terranes, forming a simple yet long syncline, known in the North Island as the Kawhia syncline and in the South Island as the Southland syncline. This terrane has long been regarded as a Triassic–Jurassic forearc basin based on its simple structure, its well-bedded and fossil-rich character and its volcanic arc provenance (Briggs et al. 2004).

Here, we present the results of a paleomagnetic study of rocks within the Kawhia syncline in an attempt to constrain the paleolatitude of the Murihiku Terrane during the Jurassic, and hence to assess the amount of probable Early Cretaceous convergence between it and Paleozoic terranes comprising eastern Gondwana. We are aware that previous paleomagnetic studies have concluded widespread remagnetisation of the Eastern Province basement of New Zealand (Haston and Luyendyk 1991), including within the Kawhia syncline (Oliver 1994; Kodama et al. 2007). Nevertheless, we hypothesise that the analysis of samples from different facies and localities within the Murihiku Terrane may

identify some that retain a detrital remanent magnetisation from which the paleolatitude can be calculated. Even if the rocks drilled at all sampled sites turn out to be remagnetised, these paleomagnetic data may be useful to help constrain the post-remagnetisation tectonic history of the terrane.

2. Geological setting

The Murihiku Terrane mostly comprises Triassic to Upper Jurassic marine and non-marine sediments (Ballance and Campbell 1993) consisting mainly of volcanoclastic sandstone and siltstone with conglomerate in places and frequent tuff layers (Aita and Spörli 1992). These strata span c. 90 Ma and have thicknesses of up to 10 km or more (Coombs et al. 1992; Roser et al. 2002). Zeolite facies have formed through low-grade burial metamorphism (Coombs 1954; Ballance et al. 1980; Roser et al. 2002).

Petrographic and geochemical studies of Murihiku Terrane samples show that they derived from direct volcanic eruptive materials and mainly from erosion of a volcanic arc terrane (Roser et al. 2002; Briggs et al. 2004). The sediments and tuff accumulated within a forearc basin probably underlain by oceanic crust (Spörli 1987; Aita and Spörli 1992). However, an origin as an intra-arc or back-arc basin has also been suggested (Howell 1980; Coombs et al. 1992). A paleomagnetically determined paleolatitude for Murihiku basin strata would help constrain the intra-Panthalassa Ocean location where the volcanic arc may have formed.

A previous paleomagnetic study of Lower Jurassic Murihiku Terrane volcanic rocks in the Southland syncline suggested that the basin was located at a high paleolatitude, close to the eastern Gondwana margin (Grindley et al. 1980). The similarity between Triassic plant fossils in Murihiku Terrane strata and from nearby coastal regions of Gondwana has also been used to suggest that the origin of the Murihiku basin must have been close to the Gondwana margin (Retallack 1987). However, the presence of two synchronous magmatic/volcanic arcs of the Median Batholith and the Brook Street Terrane in particular, has been used to suggest that a subduction plate boundary must have existed between the intra-oceanic arc and Gondwana during the Permian prior to accumulation of sediments now exposed in the Murihiku Terrane (Bradshaw 1994; Mortimer 2004). Whether the Murihiku Terrane basin originated adjacent to or at a distance from the eastern Gondwana margin thus remains uncertain, but all tectonostratigraphic terranes were sutured along that margin by the end of the Early Cretaceous (Howell 1980).

At present, the Murihiku Terrane is exposed in both North and South Islands as a broad synclinorium. From south to north, the synclinorium consists of the Southland, Key Summit and Nelson synclines in the South Island and the Kawhia syncline in the North Island (Campbell et al. 2003). The Murihiku Terrane synclinorium is dextrally offset by c. 460 km along the Alpine Fault (e.g. Edbrooke et al. 2015). Regional strikes of Murihiku and other basement bends towards the Alpine Fault and form large oroclines on either side of this fault. The age of oroclinal bending within these terranes as well as its relation to Alpine

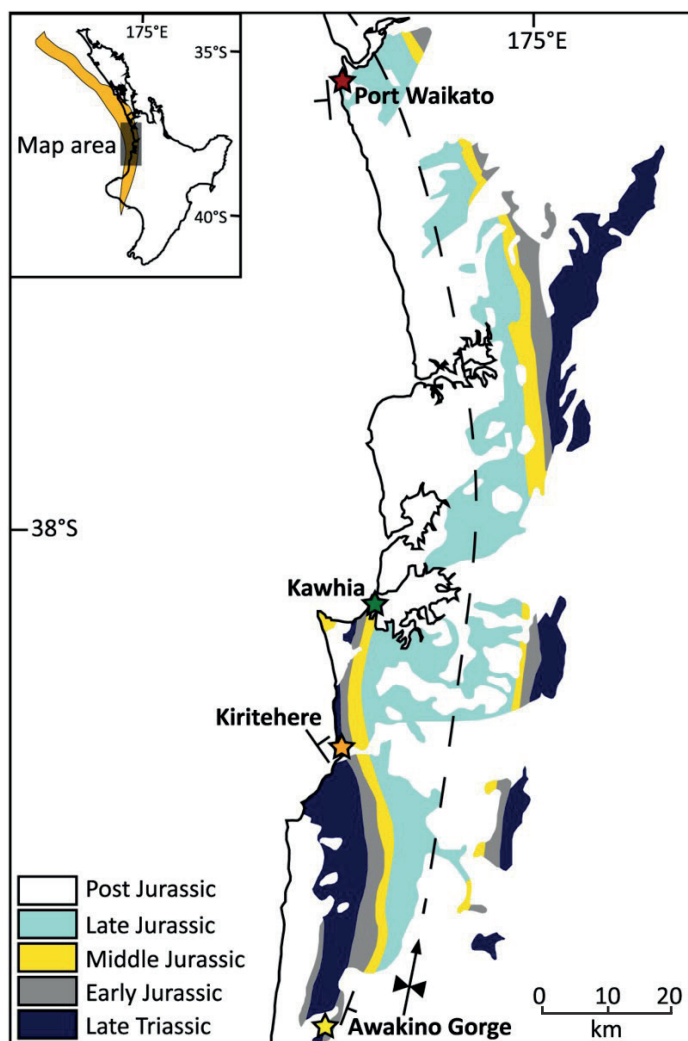


Figure I. Simplified geological map of Murihiku Terrane exposed within Kawhia syncline (based on Edbrooke 2001, 2005). Note the change in strike of the fold axis (dashed line) of the syncline from north–northeast in the south to north–northwest in the north. Stars indicate sample localities. Inset, Map of North Island showing the distribution of Murihiku Terrane (orange colour) (based on Mortimer 2004).

Fault deformation remains uncertain. A widely held view is that Cenozoic plate motion within New Zealand was accommodated across the Alpine Fault as well as in a broad zone of deformation, leading to bending of basement terranes as a result of large-scale drag (Kamp 1987; Sutherland 1999b; Mortimer 2014). An alternative view is that the basement terranes were bent pre-Cenozoic and that the curvature of the terranes remained unchanged in the Cenozoic because Neogene dextral displacement on Alpine Fault occurred in a very narrow zone (Lamb et al. 2016).

In the Kawhia syncline, the location of our paleomagnetic sampling, the Murihiku Terrane is exposed along the west coast of the central–western North Island between Port Waikato in the north and Awakino Gorge in the south as well as inland. The Kawhia syncline is c. 40 km wide and the strike of its fold axis varies from north–northeast in the south to north–northwest in the north (Figure 1). The age of Murihiku Terrane strata within the Kawhia syncline varies from Late Triassic (Norian) to Late Jurassic (Tithonian) (Roser et al. 2002).

3. Methods

Rock samples from Murihiku Terrane were obtained from three locations (Figure 1) using a petrol-powered drill with a drill bit having an internal diameter of 25 mm. We always sampled over a sufficiently long interval (10–20 m) per site, enough to average out paleosecular variation (see A95 parameter in and explanation below). The cores were oriented in the field using a Brunton magnetic compass with an inclinometer attached. Cores were cut into subsamples 22 mm long using a double-blade circular saw.

Laboratory analyses were carried out at the paleomagnetic laboratory, Fort Hoofddijk, at Utrecht University, the Netherlands. The natural remanent magnetisation of samples was measured on a 2G DC-SQUID magnetometer and further investigated using thermal as well as alternating field (AF) stepwise demagnetisation. Thermal demagnetisation was carried out using successively higher temperatures (in °C): 20, 100, 150, 180, 210, 240, 270, 300, 330, 360, 390, 420, 450, 480, 500, 520, 540, 560 and 580. During AF demagnetisation we used the following field strengths (in mT): 0, 4, 8, 12, 16, 20, 25, 30, 35, 40, 45, 50, 60, 70, (80, 90, 100). Thermomagnetic analyses to determine the nature of magnetic carriers were performed on representative samples for each locality using a horizontal translation-type Curie balance with cycling applied magnetic field, usually 150–300 mT (Mullender et al. 1993). We used (finely crushed) bulk material, usually 50–80 mg. A number of heating–cooling cycles was applied to detect magneto-mineralogical alterations during heating. We used the following temperature scheme (in °C): 20–150, 100–250, 150–350, 250–400, 350–500 and 400–700.

Statistical analysis and interpretation were performed using the online, platform independent portal: www.paleomagnetism.org (Koymans et al. 2016). Demagnetisation diagrams are plotted as orthogonal vector diagrams (Zijderveld 1967). Interpretation of demagnetisation diagrams was performed by determining a characteristic remanent magnetisation (ChRM) for components decaying towards the origin. We determined great circles if we found no clear ChRM decaying towards the origin because of a pervasive (low temperature or low coercive) overprint causing overlapping blocking temperatures or coercivity. Lines (ChRM, denoted as ‘setpoints’) and planes (great circles) were determined following an eigenvector approach (Kirschvink 1980). If we have both setpoints and great circles in a site, we use the method of McFadden and McElhinny (1988) to determine great circle solutions. We applied a 45° cut-off to the virtual geomagnetic pole (VGP) distribution

Table I. Information about GPS location of the site, measured bedding plane (strike/dip) and their age plus reference and the number of demagnetised samples per site

Site	GPS coordinates					No. of samples demagnetised	
	Strike/Dip (°)	Latitude (°N)	Longitude (°E)	Age (stage)	Age (Ma)	Th.	AF
AG1	302/63	-38.6739	174.6876	Middle Rhaetian	207–204	Hay (1967)	5 12
AG2	026/70	-38.6737	174.7108	Middle Toarcian	181–176	Hay (1967)	7 22
AG3	022/54	-38.6270	174.7309	Bajocian	170–168	Hay (1967)	5 28
AG4	021/60	-38.6370	174.7275	Bajocian	170–168	Hay (1967)	3 10
K11	327/33	-38.3268	174.7041	Lower Rhaetian	209–207	Kear (1960)	8 26
K12	328/37	-38.3168	174.7108	Upper Rhaetian	204–201	Kear (1960)	5 17
K13	310/29	-38.3201	174.7075	Middle Rhaetian	207–204	Kear (1960)	3 14
K14	336/29	-38.3201	174.7075	Middle Rhaetian	207–204	Kear (1960)	3 13
K15	323/29	-38.3201	174.7075	Middle Rhaetian	207–204	Kear (1960)	6 26
PW1	175/36	-37.3993	174.7108	Late Tithonian	147–145	Challinor (2001)	8 40

of a set of directions (following Johnson et al. 2008; Deenen et al. 2011). This is an arbitrary fixed angle cut-off meant to remove outliers due to excursions or transitional directions, or to remove outliers due to (assumed, possible) errors in sampling and orientation measurement. Mean directions were determined using Fisher (1953), whereas directional statistics were derived from the corresponding VGP distribution (Deenen et al. 2011), and errors in declination (ΔD_x) and inclination (ΔI_x) were calculated from the cone of confidence (A95) of the mean VGP following Butler (1992). We applied the reliability criteria of Deenen et al. (2011) by determining A95 of the VGP distribution and calculate the N-dependent values of A95min and A95max (recalculated by Deenen et al. 2014). Values plotting within this envelope can be explained by paleosecular variation. Values of $A95 > A95_{max}$ may indicate additional sources of scatter, while values of $A95 < A95_{min}$ represent low dispersion (high k-values, as with lavas) and cannot reliably represent paleosecular variation. To test the primary origin of the ChRM and if the data permit, we perform field tests. The fold test follows an eigenvector approach (Tauxe and Watson 1994) or the reversal test using the coordinate bootstrap test (Tauxe et al. 2010). The results are compared with the expected directions for a reference locality from the Global Apparent Polar Wander Path of Torsvik et al. (2012). All methods used (and more) are available at www.paleomagnetism.org. In the online supplementary information, we provide all the demagnetisation results and interpretations as a .dir file that can be easily imported into www.paleomagnetism.org. Similarly, all statistical results are provided as a .pmag file.

3.1. Location descriptions

Awakino Gorge

The southernmost area we sampled was a road section exposed in Awakino Gorge (AG), (Figure 1, Table 1). The oldest rocks (Site AG1) we drilled are of Middle Rhaetian age (207–204 Ma, Otapirian New Zealand Stage) followed upwards by Middle Toarcian Site AG2 (181–176 Ma, upper Ururoan to lower Te Temaikian New Zealand Stage) and then Bajocian Sites AG3 and AG4 (170–168 Ma, mid-Temaikian New Zealand Stage) (Hay 1967). Stage boundary ages are based on the geological time scale of Gradstein et al. (2012). The 94 samples collected include both sandstone and siltstone (mudstone) facies. Cores from AG1 are mostly quite weathered. At AG2, some cores comprise very fine bluish-grey siltstone and some comprise sandstone. Cores from AG3 comprise bluish-grey siltstone of which the top 0.5 cm is weathered to a brownish colour. The cores taken from AG4 are from two turbidite units comprising silty sandstone.

Kiritehere

Some 87 cores were collected from five sites at Kiritehere Beach (KI) (Figure 1), these sites being accessible only during low tide. One drill site (KI1) is located on the shore platform south of Rararimu Stream, and the four other sites (KI2–5) lie on the shore platform north of this stream. The cores comprise bluish-grey siltstone that was easy to drill. The age of the

cores obtained from Kiritehere range from lowermost Rhaetian (209–207 Ma, Otapirian New Zealand stage, Site KI1) to Middle Rhaetian (207–204 Ma, Site KI3-5) and Upper Rhaetian (204–201 Ma, Site KI2) (Kear 1960). After cutting, 116 specimens were available for paleomagnetic analysis.

Port Waikato

The most northerly area sampled within the Kawhia syncline was along the rocky coast immediately south of Port Waikato (PW), which is mainly accessible during low tide. This section comprises central parts of the Kawhia syncline and some of the youngest beds preserved within it (Late Tithonian, c. 147–145 Ma; Puaroan New Zealand Stage) (Challinor 2001) (Figure 1, Table 1). At Port Waikato, the sedimentary succession comprises Coleman Conglomerate (a formational unit), which consists of siltstone, sandstone and minor conglomerate (Challinor 2001). The 24 cores we drilled comprise mainly silty sandstone, yielding 48 specimens for paleomagnetic analysis.

4. Results

4.1. Magnetic carriers

We carried out thermomagnetic analyses on selected samples at each locality and present representative examples in Figure 3. From Awakino Gorge, sample AG1.2 (Figure 2A) shows magnetisation that has an almost reversible decrease until 580 °C (Figure 2A), indicating magnetite as the main magnetic carrier. At temperatures above 350 °C, however, there is a slight decrease in the cooling curves, which suggests some contribution of maghemite that inverts to hematite at c. 350 °C (Dankers 1978). The final cooling curve is lower on the figure indicating that at least part of the magnetite/maghemite has been oxidised. Sample AG3.5 (Figure 2B) shows similar behaviour, but above 420 °C there is a small increase followed by a higher cooling curve. This indicates the new formation of magnetite from (a small amount of) pyrite that inverts to magnetite at temperatures above 390–420 °C, which subsequently oxidises to maghemite and finally to haematite, causing the increase and subsequent decrease in magnetisation (Passier et al. 2001). This is visible in thermomagnetic curves. In thermal demagnetization, the newly formed magnetite may produce spurious demagnetisation behaviour at higher temperatures. Samples from Kiritehere show a significant increase in magnetisation above c. 420 °C, which is caused by the transformation of pyrite into magnetite. The newly formed magnetite is subsequently demagnetised at temperatures above 500 °C. In sample KI1.21 (Figure 2C) there is again a slight loss of magnetisation in the cooling curves after heating to 350 °C, indicating the presence of maghemite. The final cooling curve is lower, meaning that the available maghemite and magnetite have been oxidised. In sample KI2.10 (Figure 2D), the newly formed magnetite from pyrite is (nearly) fully demagnetised. There is no notable contribution of maghemite considering the final cooling curve, which is only marginally higher than the heating curves, meaning that there are some traces left of the newly formed magnetite.

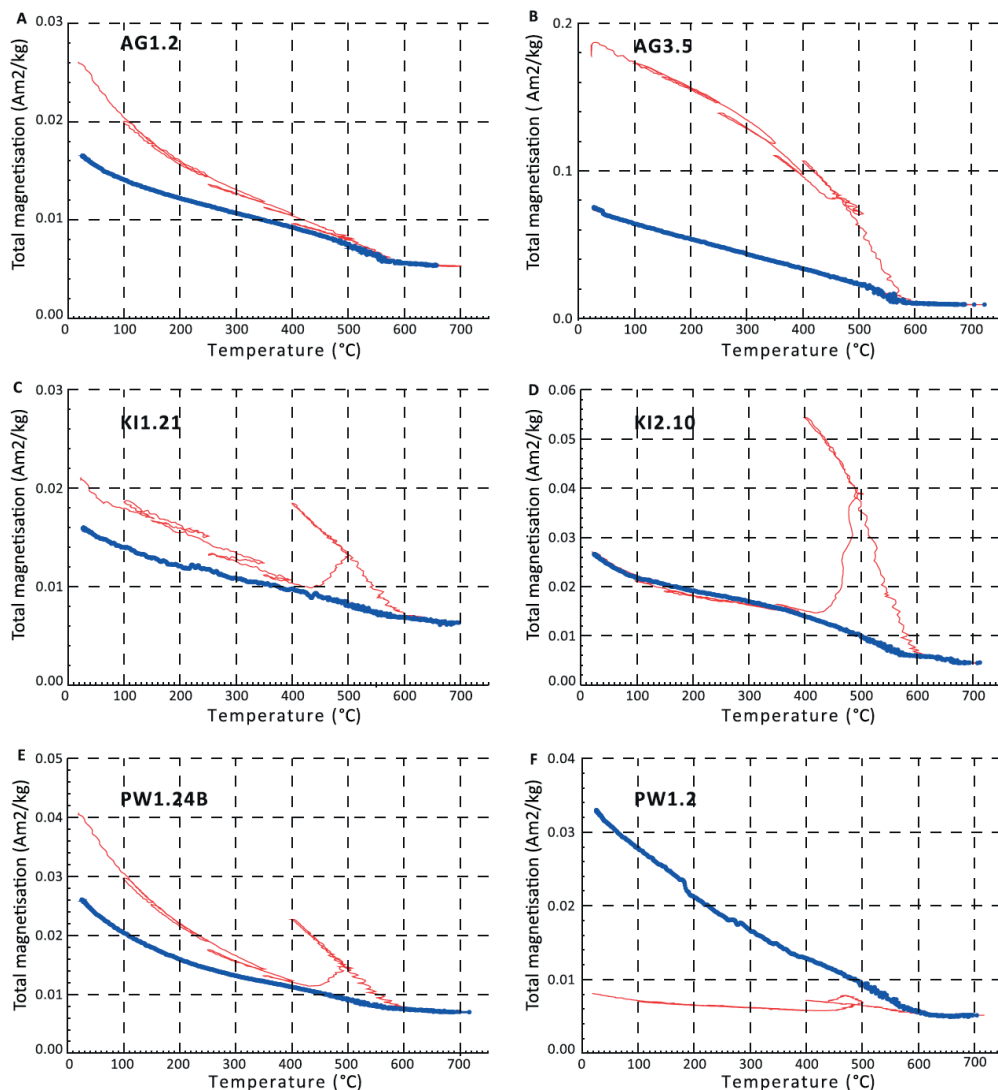


Figure 2. Representative thermomagnetic curves from a Curie balance using a cycling field between 50 and 300 mT (Mullender et al. 1993). Heating is applied to a maximum temperature of 700 °C in a number of heating-cooling cycles (thin red lines) with the final cooling curve as a thick blue line. Samples are from Awakino Gorge (AG), Kiritehere (KI) and Port Waikato (PW). We used crushed bulk material (typically 50–80 mg). Interpretations are described in the text.

4.2. Demagnetisation behaviour and paleomagnetic directions

Samples from Awakino Gorge that were thermally demagnetised generally show the removal of a low-temperature or low-coercive component, followed by a remanent magnetisation component that is stable and decays linearly to the origin above 180–210 °C or above 12 mT. This component is completely removed in most samples at 500 °C (Figure 3A), or at c. 60 mT (Figure 3B), which we interpret as the ChRM.

Samples from Port Waikato generally show behaviour similar to those of Kiritehere (PW1.24B, Figure 2E). In sample PW1.2 (Figure 2F) there is a different behaviour; above 450 °C some new magnetite is formed but it is again demagnetised at c. 500 °C. Yet the final cooling curve is significantly higher than the heating curves, and new magnetic material is probably formed at temperatures up to 700 °C. This is possibly magnetite, judged from the breakdown of clay minerals at the highest temperature reached (700 °C).

Mean paleomagnetic directions for all sites are listed in Table 2. ChRMs interpreted from Awakino Gorge samples show variation in mean declination from 81.0° (AG4) to 130.3° (AG1) (Table 2). In geographic coordinates, mean inclinations vary between –49.7° (AG2) and –63.8° (AG1) (Table 2). When all AG sites are grouped together, 14 of 93 directions are rejected by the 45° cut-off (Figure 4A,B). All samples indicate normal polarity and give a mean direction with $D = 101.9 \pm 5.0^\circ$ and $I = -58.5 \pm 3.5^\circ$ (where D = declination, I = inclination). After tilt correction, the mean direction is $D = 310.5 \pm 4.9^\circ$; $I = -59.7 \pm 3.3^\circ$ (Figure 4A,B, Table 2).

Remarkably, eight samples form a separate cluster with very low inclinations before bedding tilt correction (see yellow symbols, Figure 4). These samples were all taken at Toarcian site AG2. These samples do not show characteristic differences in composition compared to the other samples taken at AG2. Two of these samples were thermally demagnetised and both have a stable natural remanent magnetisation component between 300 and 500 °C. The stable natural remanent magnetisation component during AF demagnetisation is obtained between 30 and 60 mT (Figure 5). The mean in situ direction of these samples (AG2*) is $D = 301.3 \pm 5.4^\circ$ and $I = 5.8 \pm 10.7^\circ$, and a tilt-corrected direction $D = 316.8 \pm 27.0^\circ$ and $I = 74.9 \pm 7.5^\circ$ (Table 2).

Thermal demagnetisation behaviour in Kiritehere samples generally shows a stable natural magnetisation component between 300 and 500 °C, and occasionally between 180 and 500 °C (Figure 3C). AF demagnetisation diagrams show linear trends and the magnetisation component is generally removed at 60–80 mT (Figure 3D).

Because of the relatively small stratigraphic range from which the sites (KI1–5) were taken at Kiritehere, directions from all 116 measured specimens were grouped and treated as a single set for statistical analysis (Figure 4C,D, Table 2). Only five samples are rejected by the 45° cut-off. All sites indicate normal polarity and give a direction $D = 26.8 \pm 6.9^\circ$ and $I = -74.4 \pm 2.0^\circ$, and a tilt-corrected direction $D = 257.3 \pm 5.5^\circ$; $I = -70.3 \pm 2.1^\circ$.

The Port Waikato samples show very consistent behaviour, with linear decay for both thermal and AF demagnetisation above 180–210 °C and 10–12 mT, respectively (Figure

Table 2. Geomagnetic directions per site

Site	Ns	Na	D (°)	ΔDx (°)	I (°)	ΔIx (°)	K	A95min	A95	A95max	λ (°)
Geographic coordinates											
AG1	17	16	130.3	12.3	-63.8	6.8	19.5	4.0	8.6	14.3	-45.5
AG2	29	21	103.4	5.6	-49.7	5.4	44.6	3.6	4.8	12.0	-30.5
AG3	34	31	98.3	8.4	-62.4	5.0	19.2	3.0	6.0	9.4	-43.8
AG4	13	13	81.0	9.0	-55.0	7.2	33.4	4.3	7.3	16.3	-35.5
AG all	93	79	101.9	5.0	-58.5	3.5	17.7	2.1	3.9	5.2	-39.2
AG E20	85	77	121.0	12.0	-77.0	2.9	11.4	2.1	5.0	5.3	-65.3
AG2*	8	8	301.3	5.4	5.8	10.7	106.6	5.2	5.4	22.1	2.9
AG2* E20	8	8	304.1	6.2	22.7	10.9	83.3	5.2	6.1	22.1	11.8
KI1	33	30	37.3	18.1	-78.6	3.7	16.6	3.1	6.7	9.6	-68.0
KI2	22	20	60.5	11.3	-70.0	4.5	25.4	3.6	6.6	12.4	-54.0
KI3	17	17	356.2	12.5	-74.0	3.8	34.1	3.9	6.2	13.8	-60.1
KI4	16	15	17.3	10.7	-71.7	3.8	43.6	4.1	5.9	14.9	-56.5
KI5	32	30	14.9	8.1	-69.9	3.3	30.6	3.1	4.8	9.6	-53.1
KI all	121	116	26.8	6.9	-74.4	2.0	16.3	1.8	3.4	4.1	-60.7
PW1	48	44	346.2	9.5	-74.1	2.9	22.2	2.6	4.7	7.6	-60.3
Tectonic coordinates											
AG1	17	17	184.9	8.1	-36.4	13.4	21.5	3.9	7.9	13.8	-13.9

Ns=total number of measured samples, Na=number of samples after 45° cut-off

Declination/inclination (D, I), their respective errors (ΔDx, ΔIx) and paleolatitude (λ) in degrees

AG2 includes samples taken at AG2, excluding AG2*, which is the sample set that has a deviating magnetic signal and is listed separately. Values given in bold are used for our paleomagnetic analysis and interpretation. AG E20 refers to the Awakino Gorge sample set corrected for the 20° eastward dip.

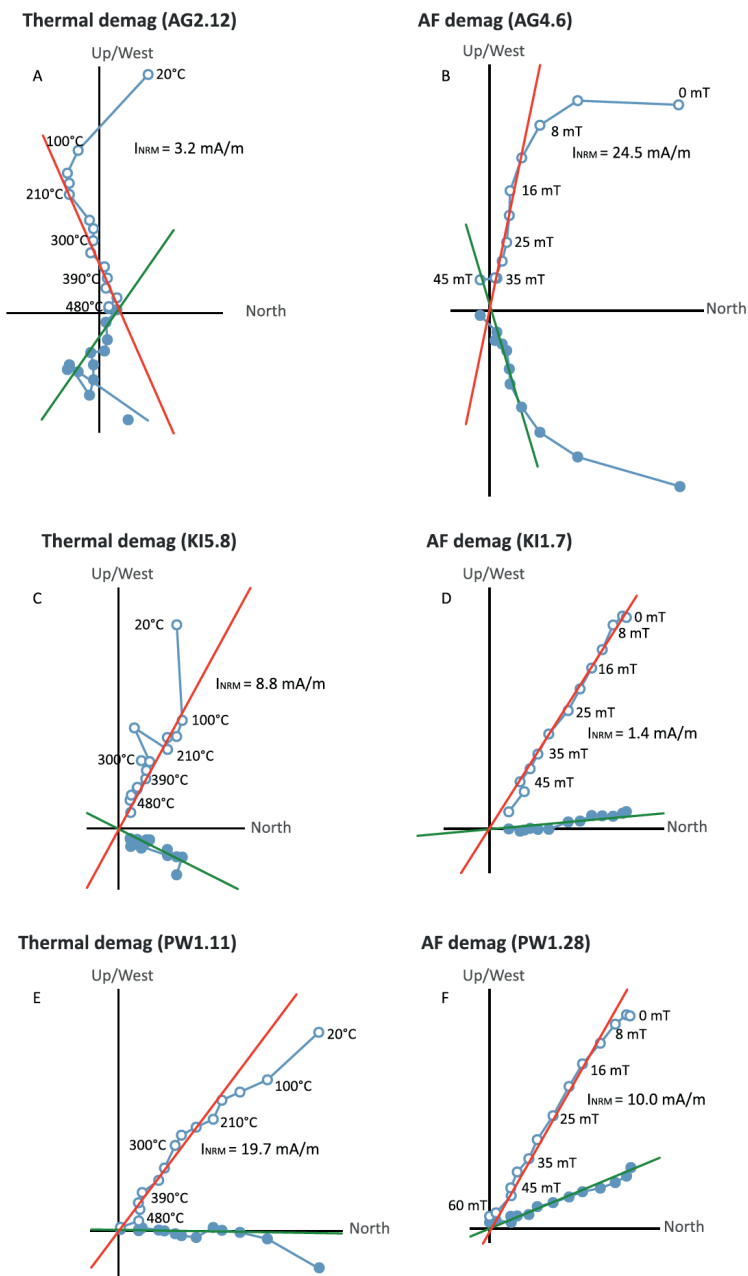


Figure 3. Representative examples of demagnetisation diagrams (Zijderveld 1967) in geographic coordinates from our three sample localities (AG, KI and PW). I_{NRM} indicates the initial natural remanent magnetisation, closed (open) symbols are projections on the horizontal (vertical) plane, and the respective projections (green, red lines) denote the interpreted characteristic remanent magnetisation (ChRM). Numbers refer to temperature ($^{\circ}\text{C}$) or AF field (mT) steps. The initial natural remanent magnetisation intensities (I_{NRM}) are given in mA/m.

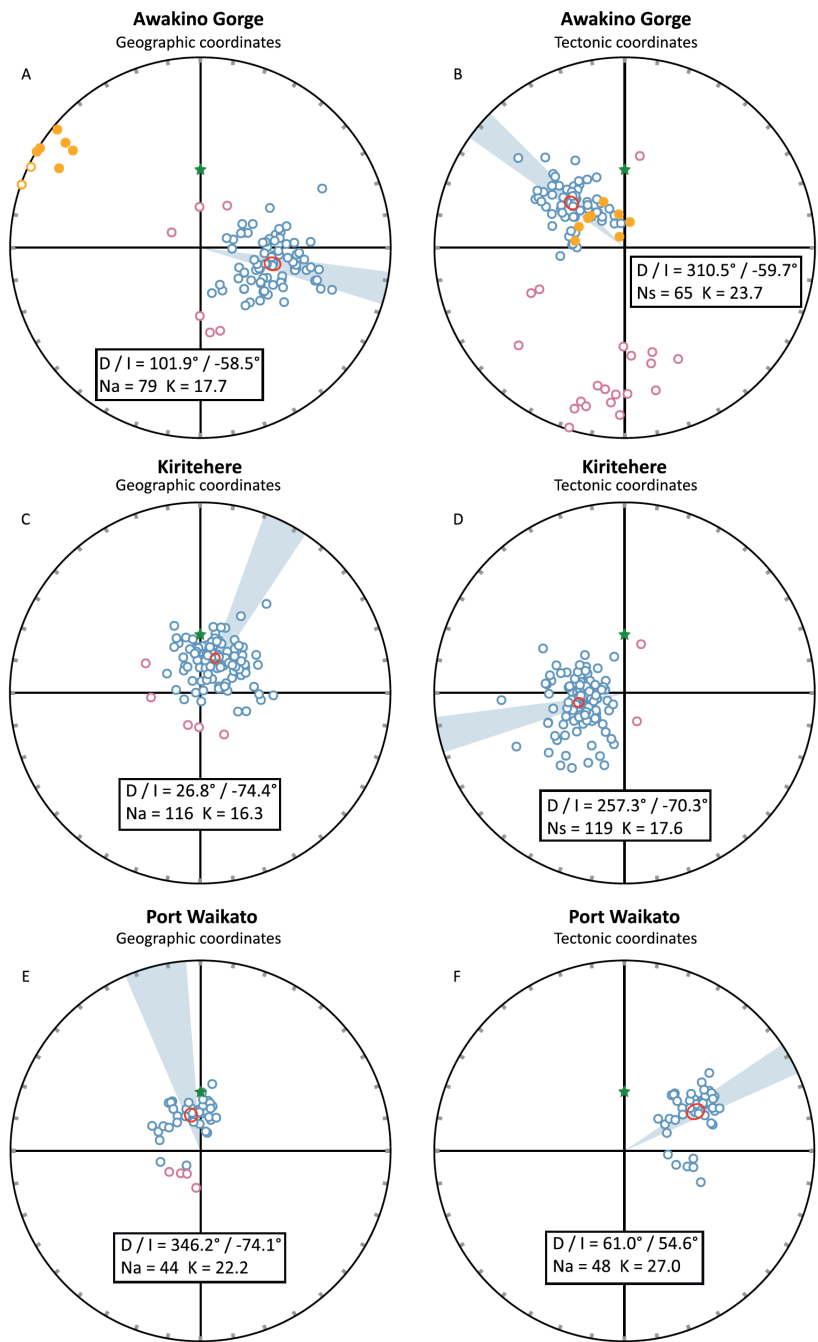


Figure 4. Equal area projections of characteristic remanent magnetisation (ChRM) directions per site. Closed (open) circles indicate lower (upper) hemisphere projection. Boxes give the mean with D/I as declination/inclination, K is the precision parameter of the VGP distribution, Na is the number of accepted samples accepted by the 45° cut-off.

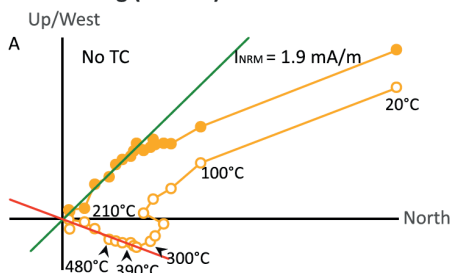
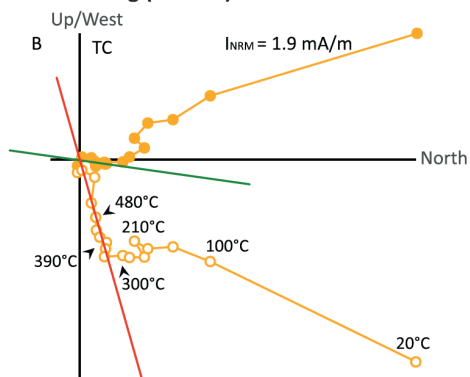
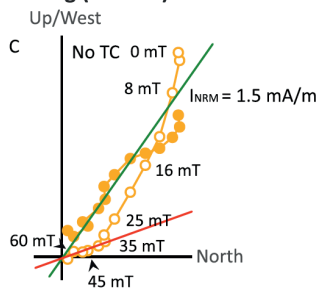
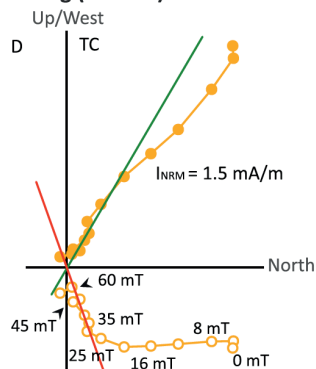
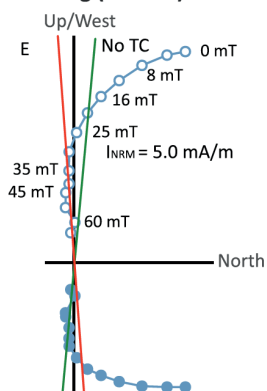
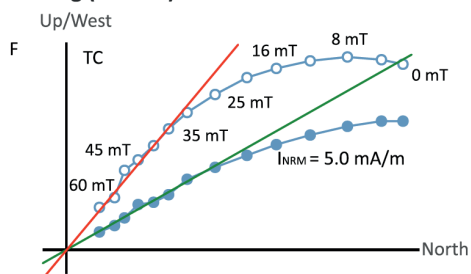
Thermal demag (AG2.18)**Thermal demag (AG2.18)****AF demag (AG2.22)****AF demag (AG2.22)****AF demag (AG2.10)****AF demag (AG2.10)**

Figure 5. Examples of demagnetisation diagrams in both geographic (no TC, left column) and tectonic (TC, right column) coordinates for samples from sites AG2* (yellow) and AG2 (blue). For symbols, refer to caption to Figure 3.

3E,F, Table 2). The stable remanent magnetisation component is removed at 480–510 °C or at 60–80 mT. The 48 specimens from Port Waikato yield a mean direction $D = 346.2 \pm 9.5^\circ$ and $I = -74.1 \pm 2.9^\circ$, and a tilt-corrected direction $D = 61.0 \pm 4.9^\circ$ and $I = -54.6 \pm 4.0^\circ$ (Figure 4E,F, Table 2). Four samples are rejected by the 45° cut-off and, again, all samples indicate normal polarity.

All sites have an A95 value between A95min and A95max (Table 2), which suggests that the scatter in the individual datasets can be simply explained by paleosecular variation (Deenen et al. 2011).

Thermal demagnetisation behaviour in Kiritehere samples generally shows a stable natural magnetisation component between 300 and 500 °C, and occasionally between 180 and 500 °C (Figure 3C). AF demagnetisation diagrams show linear trends and the magnetisation component is generally removed at 60–80 mT (Figure 3D).

Because of the relatively small stratigraphic range from which the sites (KI1–5) were taken at Kiritehere, directions from all 116 measured specimens were grouped and treated as a single set for statistical analysis (Figure 4C,D, Table 2). Only five samples are rejected by the 45° cut-off. All sites indicate normal polarity and give a direction $D = 26.8 \pm 6.9^\circ$ and $I = -74.4 \pm 2.0^\circ$, and a tilt-corrected direction $D = 257.3 \pm 5.5^\circ$; $I = -70.3 \pm 2.1^\circ$.

The Port Waikato samples show very consistent behaviour, with linear decay for both thermal and AF demagnetisation above 180–210 °C and 10–12 mT, respectively (Figure 3E,F, Table 2). The stable remanent magnetisation component is removed at 480–510 °C or at 60–80 mT. The 48 specimens from Port Waikato yield a mean direction $D = 346.2 \pm 9.5^\circ$ and $I = -74.1 \pm 2.9^\circ$, and a tilt-corrected direction $D = 61.0 \pm 4.9^\circ$ and $I = -54.6 \pm 4.0^\circ$ (Figure 4E,F, Table 2). Four samples are rejected by the 45° cut-off and, again, all samples indicate normal polarity.

All sites have an A95 value between A95min and A95max (Table 2), which suggests that the scatter in the individual datasets can be simply explained by paleosecular variation (Deenen et al. 2011).

4.3. Fold test

We performed a fold test for all three localities, following the eigenvector bootstrap approach of Tauxe and Watson (1994) in www.paleomagnetism.org. The eight samples of AG2* that form a separate cluster (Figure 4A,B) are not taken into account in the Awakino Gorge fold test in the absence of significant bedding tilt differences. The remaining Awakino Gorge directions clearly fail the fold test, with highest clustering around 0% unfolding, ranging [−8%, +6%] at the 95% level (Figure 6A).

The fold test performed on Kiritehere samples shows a less straightforward result, and highest clustering is found around an unfolding percentage of 44%, ranging [15–73%] (Figure 6B). This may be the result of remagnetisation during folding, but it may also be the result of a new phase of folding after a first post-folding remagnetisation occurred (Tauxe and Watson 1994). Therefore, the data fail the fold test and tectonically corrected directions

for Kiritehere sample sites cannot be used for tectonic analysis.

The Port Waikato samples were all taken at one site at an outcrop with a very constant bedding orientation and consequently a fold test cannot be performed on the directions of the Port Waikato locality.

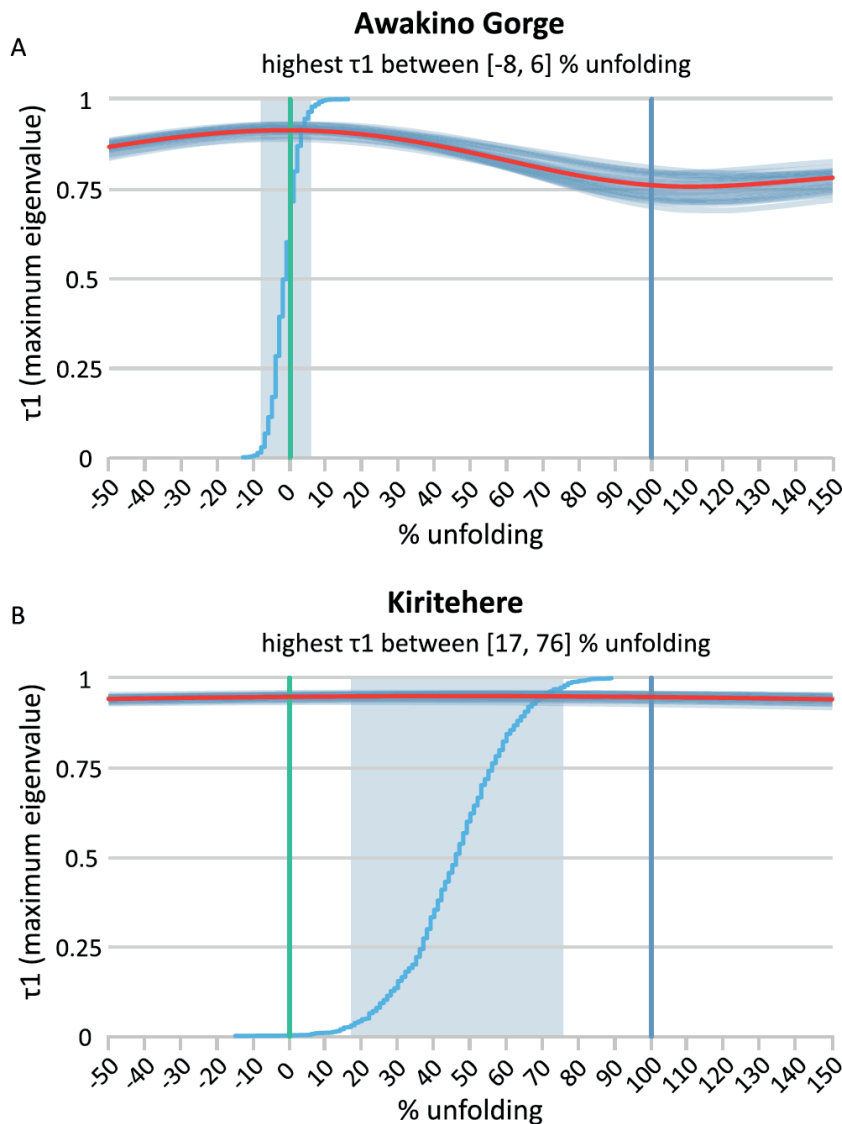


Figure 6. Results of the eigenvector bootstrap (Nb=1000) fold test according to Tauxe and Watson (1994) performed on the Awakino (A) and Kiritehere (B) data sets. Shaded area shows the cumulative distribution function of the maximum unfolding at the 95% bootstrap confidence level. The first 25 bootstraps are shown.

5. Discussion

The most striking result from our paleomagnetic analysis is the almost exclusively normal polarity held within samples from all three localities, despite the large stratigraphic age range (c. 209–145 Ma) sampled. During accumulation of Murihiku sediments, many polarity reversals took place (Gradstein et al. 2012). Therefore, the almost complete absence of samples with reversed polarity, with the possible exception of AG2*, implies widespread remagnetisation. The negative fold test of Awakino Gorge demonstrates that the remanent magnetisation signal was acquired after folding of the succession. The outcome of the fold test performed on Kiritehere data demonstrates that these samples do not carry their original (or at least pre-folding) magnetisation, but the exact timing of the magnetisation relative to the deformation history is more difficult to assess. Therefore, we conclude that most of the sample host rocks have been remagnetised. As a result, the bulk of our data cannot help constrain the Mesozoic paleolatitude of the Murihiku Terrane. However, as the paleomagnetic directions do not correspond to a recent geocentric axial dipole (GAD) direction (Figure 4), we explore their value in identifying a tectonic signal since remagnetisation. This implies that we need an estimate of the age of remagnetisation. The meaning of the small set of directions in AG2* that show a different paleomagnetic result are also discussed.

5.1. Remagnetisation event

The occurrence of widespread remagnetisation in New Zealand has been demonstrated previously by Haston and Luyendyk (1991), Oliver (1994) and Kodama et al. (2007). The age and origin of the remagnetisation event remains unclear, but is of importance for understanding New Zealand's tectonic history. Some suggestions of the age and origin have been made, but none has been conclusive. Haston and Luyendyk (1991) undertook a paleomagnetic study of samples from the Waipapa Terrane and compared their computed paleomagnetic pole (69.7°S, 150.7°E) to a synthetic apparent polar wander path of New Zealand. They concluded that the remagnetisation event most likely occurred between 12 Ma and 58 Ma. They prefer a 25 Ma age of remagnetisation, caused by a major change in the tectonic regime. The change in tectonic regime has been associated with: (i) emplacement of ophiolites across northern Northland Peninsula at that time (Ballance and Spörli 1979), (ii) inception of subduction along the Hikurangi margin (e.g. Cole and Lewis 1981; Kamp 1999) and (iii) initiation of arc volcanism (e.g. Mortimer et al. 2010). Remagnetisation in the Waipapa Terrane may be due to fluid migration associated with those events. Oliver (1994) undertook a paleomagnetic study of rocks from the Kawhia and Marokopa areas within the Murihiku Terrane north of Kiritehere. He acquired exclusively normal polarity magnetic directions, in agreement with our findings. He obtained a paleomagnetic pole from the remagnetised directions (57.2°S, 163.2°E), which is consistent with the c. 80–90 Ma position predicted by the apparent polar wander path of Australia, as well as a Cretaceous pole determined for Marie Byrd Land (West Antarctica) by Grindley and Oliver (1983).

Oliver (1994) thus suggested that remagnetisation took place around 85 Ma, possibly linked to onset of Tasman Sea spreading around that time (Weissel et al. 1977; Weissel and Hayes 1977; Gaina et al. 1998). Kodama et al. (2007) concluded that remagnetisation must have occurred no later than Late Paleocene–Eocene, since they argued for a primary magnetic signal in Late Paleocene–Eocene sedimentary rocks in Kaiwhata Stream.

The timing of folding of the Kawhia syncline and its parasitic smaller-scale folds, has been constrained from thermal history modelling of apatite fission track data obtained from samples collected from the Port Waikato area (Kamp and Liddell 2000). These data indicate cooling of 110–120 °C along the eastern limb of the syncline by c. 100 Ma, indicating that folding occurred during the early Cretaceous.

Furthermore, the remagnetisation of strata within the Kawhia syncline probably occurred before uplift and erosion of the Kawhia syncline succession, which accompanied or followed deformation of the succession. This can be reasoned from the requirement that remagnetisation is thought to require burial temperatures higher than those in the near subsurface following the bulk of the erosion. The timing of uplift and erosion of Murihiku Terrane is constrained stratigraphically to lie between: (i) the latest Jurassic, which is the age of the Huriwai Group, forming the youngest strata involved in the syncline and hence giving a maximum age when peak burial heating was experienced by the strata; and (ii) the Late Eocene, which is the age of the overlying Te Kuiti Group (Nelson 1978; Edbrooke 2005; Kamp et al. 2014). From this, we conclude that remagnetisation most probably occurred after 100 Ma and before 40 Ma.

We confined the estimated age of remagnetisation further by plotting our obtained geomagnetic directions on the apparent polar wander path of New Zealand. To this end, we calculated the Global Apparent Polar Wander Path of Torsvik et al. (2012) in the coordinates of New Zealand north of the Alpine Fault (northern Zealandia), using the Euler rotations provided in the plate reconstruction of Müller et al. (2016). We used the thereto designed tool at www.paleomagnetism.org as described in Li et al. (2017). Comparison between the paleolatitudes of reference location (38.359°S, 174.802°E) calculated from the directions in geographic coordinates for both Port Waikato and Kiritehere and the predicted Apparent Polar Wander Path for northern Zealandia, suggests an age of remagnetisation of 80 ± 8 Ma (Figure 7, black bar on horizontal axis). Because all our samples carry a normal polarity signal, resetting of the magnetic signal must have taken place during a normal polarity interval. Based on the 80 ± 8 Ma fit, remagnetisation then likely occurred during the Cretaceous Normal Superchron (126–83.6 Ma), or possibly during younger chrons such as 33n (79.9–74.3 Ma) (Gradstein et al. 2012). Because of its shallower inclination ($I = -58.2^\circ$) compared with our other sites, the corresponding paleolatitude of Awakino Gorge differs considerably from those of Port Waikato and Kiritehere, and would be close to the present-day latitude of New Zealand (Figure 7). This could indicate that the remagnetisation is a relatively young (Eocene) to very recent field overprint. However, if the samples of Awakino Gorge were overprinted by a recent field, a declination of 0° would be expected, which is not

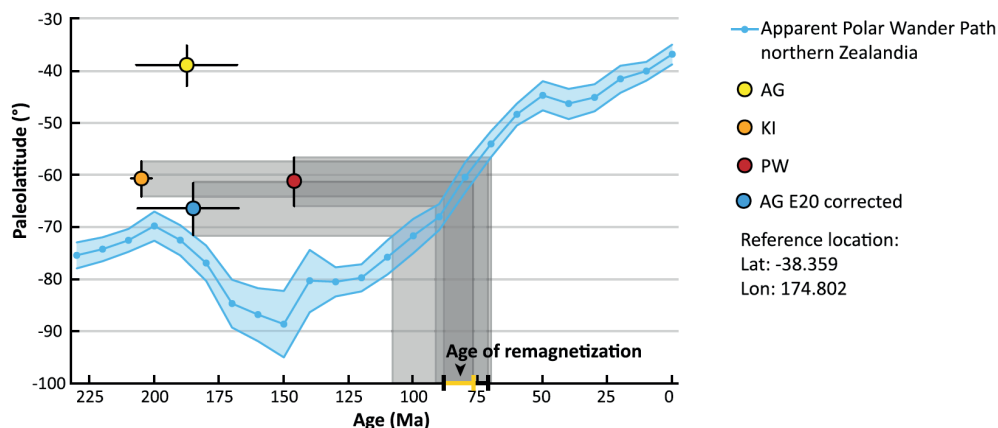


Figure 7. Diagram of the paleolatitudes (geographic coordinates) of sampling localities AG, KI, PW and the AG locality corrected for a 20° dip towards the east vs. the Apparent Polar Wander Path (APWP) of northern Zealandia. From the uncertainties in paleolatitude we deduce an age of remagnetisation of c. 83 ± 5 Ma. The paleolatitude of Awakino Gorge significantly deviates from the paleolatitudes of Kiritehere and Port Waikato, but becomes very similar after the E-dip correction.

observed (Figure 4). We consider a possible explanation for this discrepancy below.

We note that an c. 80 Ma age of remagnetisation coincides with the early stages of seafloor spreading in the Tasman Sea (Gaina et al. 1998), as previously noted by Oliver (1994). Additionally, remagnetisation may be related to the end of subduction along the Gondwana margin of New Zealand. The timing of the end of subduction is subject to debate and is generally thought to have occurred around 105–100 Ma (Bradshaw 1989; Luyendyk 1995; Davy et al. 2008; Matthews et al. 2012), but ages around 85 Ma have been proposed (Mazengarb and Harris 1994; Kamp and Liddell 2000; Vry et al. 2004), for example based on zircon fission track analysis of the youngest rocks in the toe of the Torlesse Complex (Kamp 1999, 2000).

5.2. Post-remagnetisation tectonics affecting the Awakino Gorge area?

Given the evidence above for pervasive and widespread remagnetisation in the Kawhia syncline, as well as by previous studies in the North Island and Marlborough, South Island (Haston and Luyendyk 1991; Oliver 1994; Kodama et al. 2007), it is remarkable that in situ directions for samples from Awakino Gorge differ significantly from those obtained from the Port Waikato and Kiritehere sections. As we have already identified, if the in situ direction in AG samples is an overprint direction, it must have been acquired sometime between the Eocene and present day (Figure 7). This is very unlikely, however, given the large difference of $> 100^\circ$ between the GAD declination and the declination observed at Awakino Gorge (Figure 4). We therefore seek an alternative explanation for the lower inclination and the declination of Awakino Gorge data.

An inferred Late Cretaceous overprint would yield an observed inclination of around

-74° at the reference location (38.359°S , 174.802°E), identical within error to the values reported here for the Port Waikato and Kiritehere sample sites (Table 2). Because the average observed inclination for the Awakino Gorge samples is $-58.2 \pm 3.6^\circ$, the sample host strata have been subject to inclination lowering of c. 15° .

The western limb of the syncline in the Awakino Gorge area has been accentuated by Late Oligocene and Early Miocene reverse displacement on the Manganui Fault (Kamp et al. 2004). Because this fault lies to the west of the Awakino Gorge paleomagnetic sampling sites, it probably increased the eastward dip of the beds we sampled by 20° as they lie in the hanging wall of the fault. This post-remagnetisation deformation may have contributed to the inclination shallowing of the magnetisation in these rocks compared with those at the Kiritehere and Port Waikato sample sites.

Because the 20° eastward tilting occurred after remagnetisation, we have to apply a $000/20$ bedding tilt correction to our data from Awakino Gorge. This leads to $I = -77 \pm 2.9^\circ$ and $D = 121.0 \pm 12.0^\circ$ (for full parameters see Table 2). The newly obtained inclination is far more consistent with the data of Kiritehere and Port Waikato. We can now also use the Awakino Gorge data to obtain the age of remagnetisation, which is now constrained to 83 ± 5 Ma (Figure 7, yellow bar on horizontal axis).

5.3. Rotation of Murihiku Terrane

Another interesting feature is that the declination of the Kiritehere data set corresponds well to the 80 Ma declination of New Zealand, whereas the declinations of both Port Waikato and Awakino Gorge deviate (Figure 8). This suggests that parts of Murihiku Terrane have been rotated since the widespread remagnetisation. Because our Kiritehere data record a declination very similar to the declination of New Zealand at 80 Ma, it suggests that this part of the Murihiku Terrane has not been rotated relative to New Zealand since remagnetisation. Other paleomagnetic studies of Murihiku Terrane strata in the Kawhia area north of Kiritehere also suggested that the Murihiku Terrane did not experience significant amounts of vertical axis rotation since remagnetisation (Oliver 1994; Kodama et al. 2007) (Figure 9).

By contrast, our results suggest that the basement in Awakino Gorge rotated about $77.3 \pm 5.0^\circ$ clockwise, whereas the basement in the Port Waikato area has rotated c. $39.4 \pm 9.5^\circ$ counterclockwise since remagnetisation (Figure 9). After correcting the site data from Awakino Gorge for the 20° eastward dip, the rotation of the basement succession in Awakino Gorge increases to c. $95.8 \pm 12.0^\circ$.

Previous paleomagnetic studies do indicate large-scale Neogene clockwise rotation along the Hikurangi margin, related to deformation considered to be associated with active subduction to the east of New Zealand (Wright and Walcott 1986; Rowan et al. 2005; Lamb 2011). These rotations may have affected the southern part of the Murihiku Terrane (i.e. Awakino Gorge) as well. However, previous paleomagnetic studies carried out on Oligocene calcareous siltstone (Whaingaroa Formation) exposed at the entrance to Bexley Station in Awakino Gorge (Lamb 2011, figure 4), record clockwise rotations up to 30° that had ceased

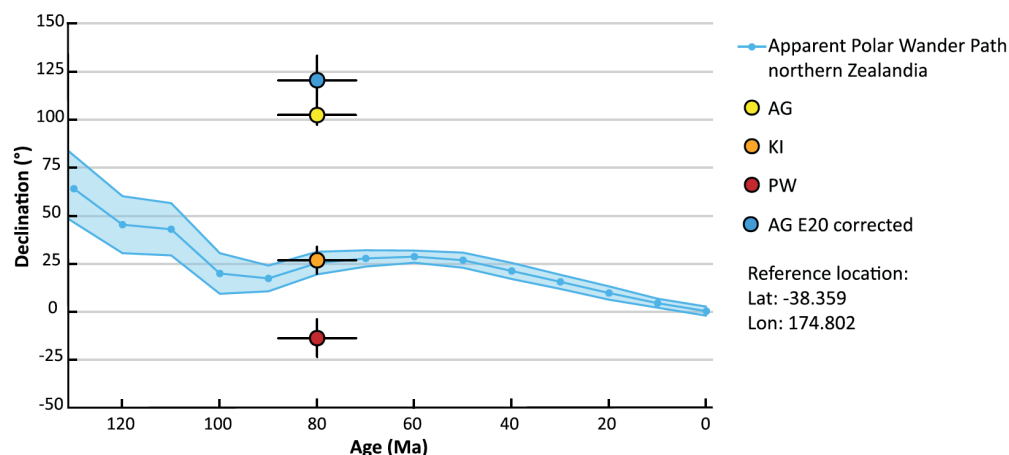


Figure 8. Diagram of declinations (geographic coordinates) of our sampling sites and the Apparent Polar Wander Path (APWP) of northern Zealandia. The declination of Kiritehere fits well with our inferred age of remagnetisation of 83 ± 5 Ma, but declinations of Port Waikato and Awakino Gorge deviate, indicating respectively $39.4 \pm 9.5^\circ$ counterclockwise and $77.3 \pm 5.0^\circ$ (uncorrected for 20° eastward dip) and $95.8 \pm 12.0^\circ$ (corrected for 20° eastward dip) clockwise rotations for these areas.

by the Early Miocene (Mumme and Walcott 1985, cited in Lamb 2011). No paleomagnetic evidence exists for later rotations in this area.

We propose that rotation of the Murihiku Terrane in the Kawhia syncline is not directly related to modern Australia–Pacific plate boundary zone deformation. Clockwise rotation in the Awakino Gorge area is thought to have ceased before the c. 30–25 Ma inception of the Alpine Fault (Kamp 1986; Lamb 2011), and it would also fail to explain the counterclockwise rotation at Port Waikato. We suggest that the observed rotation may have been related to Cretaceous bending of basement terranes expressed in the New Zealand orocline, the origin of which remains unknown. The timing of bending is also subject to debate. Essentially, there are three scenarios regarding the age of the New Zealand orocline (Bradshaw et al. 1996, see also Lamb et al. 2016): (i) oroclinal bending is older than Late Cretaceous; (ii) large-scale bending occurred exclusively during the Cenozoic; and (iii) the basement terranes of New Zealand were partially bent before the Cenozoic, but a substantial amount of rotation occurred during the Cenozoic.

Our results suggest that considerable rotation occurred since the Late Cretaceous (83 ± 5 Ma), which would argue against the first option given above. Because we cannot rule out the possibility of partially bent terranes before c. 83 Ma, suggestions (ii) and (iii) are both considered possible. There is no paleomagnetic evidence for any rotations that occurred in this area since the Miocene, therefore the bulk of bending occurred between 83 ± 5 Ma and c. 20 Ma.

The rotation of Port Waikato with respect to Kiritehere is fairly consistent with the overall strike of the Kawhia syncline. The difference in the general strike of the Kawhia

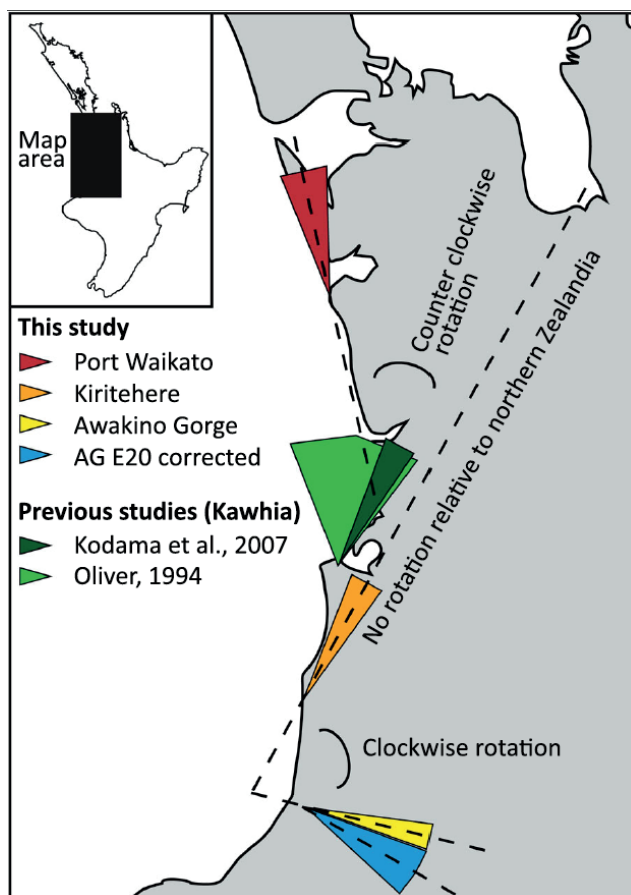


Figure 9. Map showing declinations of our sites and those of Oliver (1994) and Kodama et al. (2007) with respective confidence parachutes (ΔD_x). Declinations of Oliver (1994) and Kodama et al. (2007) have been acquired by recalculating their published data using www.paleomagnetism.org.

syncline at Kiritehere (c. 10°) and Port Waikato (c. 335°) is c. 35° (see Figure 1, based on eastern limb), which corresponds well to our inferred rotation (c. 40°). However, the large rotation of the basement succession in Awakino Gorge with respect to Kiritehere cannot be explained in the same way. Therefore, a substantial part of the rotation at Awakino Gorge must be a local phenomenon. At this point we cannot explain the origin of the rotation at Awakino Gorge, but our data clearly indicate its occurrence.

Additional paleomagnetic studies can usefully be carried out to place tighter constraints on the origin and timing of rotation of the Murihiku Terrane in the Kawhia syncline, and the possible relation to bending of basement terranes. Comparing the amount of rotation predicted from the declination of Cenozoic rocks from the Port Waikato and Awakino Gorge areas with the declinations of this study allows estimation of the timing of rotation. When the age of rotation is more tightly constrained, a hypothesis can be formulated about

the origin of rotation in sample host rocks in both the Awakino Gorge and Port Waikato areas, and the possible relation to bending of the basement terranes can be investigated more completely. Importantly, our study shows that remagnetised Murihiku Terrane sedimentary rocks widely exposed in the central-western North Island, are excellent recorders of a Cretaceous paleomagnetic field yet to be completely defined, but which can nevertheless be used to deduce post-Late Cretaceous regional vertical axis rotation and horizontal-axis tilt histories.

5.4. A primary, Jurassic magnetisation at Awakino Gorge?

As mentioned previously, eight samples collected from site AG2 (Early Jurassic, Toarcian age, 181–176 Ma) in Awakino Gorge record a magnetic component that is distinct from all other samples. This is a high-temperature component that provides an *in situ* inclination of only 5.8° . If acquired after bedding tilt, as with the regional ChRM interpreted from all other samples, this would require a latitude of magnetisation close to the equator. However, New Zealand has not been close to the equator since the Toarcian. Rather, it was located very close to the South Pole. It is therefore highly unlikely that these samples acquired their magnetisation after tilting.

We therefore tentatively assume that these samples have retained their pre-tilt magnetisation and escaped complete remagnetisation. We thus correct the AG2* directions for bedding tilt to obtain the original inclination. This gives a direction $D = 316 \pm 27.0^\circ$ and $I = 74.9 \pm 7.5^\circ$ (Figure 4, Table 2). This would imply that Murihiku Basin was located at a paleolatitude of 61.6°N during the Toarcian, which is not possible. Therefore, we assume that these rocks record a reversed magnetic signal and that the Murihiku forearc basin was located at $61.6 \pm 12^\circ\text{S}$ during the Toarcian.

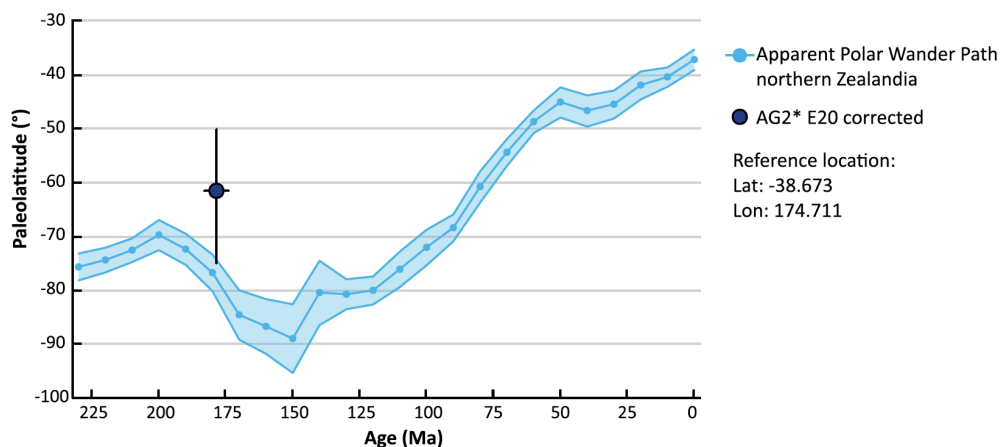


Figure 10. Apparent Polar Wander Path (APWP) of northern Zealandia and the paleolatitude of site AG2*, first corrected for the eastward dip of 20° (plunge correction), and subsequently tilt corrected with the plunge corrected bedding plane.

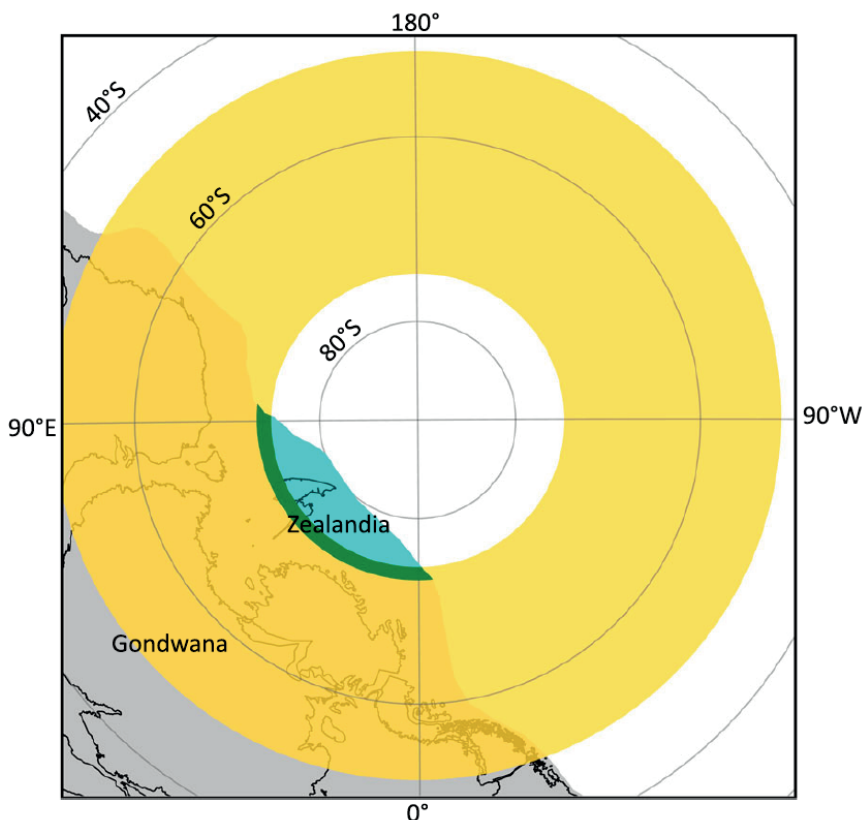


Figure 11. Map showing the possible locations (yellow disc, latitudes 50°S–75°S) of the Murihiku forearc basin based on site AG2* (reference location 38.373°S, 174.711°E). The grey area is the position of Gondwana based on the reconstruction of Müller et al. (2016) in the paleomagnetic reference frame of Torsvik et al. (2012). Present-day coastlines are for reference only. The blue zone indicates the uncertainty of the position of northern Zealandia within Gondwana. The overlap between the paleolatitude belt and the blue zone (green belt) indicates the possible locations of Murihiku forearc basin if it was part of the Gondwana margin.

Because we previously inferred that Awakino Gorge has been subject to a Late Oligocene to Early Miocene 20° tilt, we have to apply an additional bedding tilt correction. The corrected geomagnetic directions are $D = 308.3 \pm 27.6^\circ$ and $I = 75.2 \pm 7.5^\circ$, corresponding to a paleolatitude of $62.1 \pm 12^\circ\text{S}$ (Table 2).

This paleolatitude is in agreement with that of Grindley et al. (1980), which is the only other paleomagnetic study that may have found a paleolatitude from a primary magnetic signal of Murihiku Terrane rocks. They obtained a paleolatitude of 66°S for the Glenham Porphyry of Early Jurassic (c. 190 Ma) age in the Southland syncline part of the Murihiku Terrane. Both studies therefore imply that the Murihiku Terrane was located in the vicinity of the New Zealand sector of the eastern Gondwana margin during sediment accumulation.

When compared with the apparent polar wander path of northern Zealandia, our

calculated paleolatitude is located within c. 20° expected for Zealandia in the Toarcian (Figure 10). This would thus provide a first-order estimate that the intra-oceanic arc to which the Murihiku forearc basin was paired, was probably located within 1000–2000 km, but possibly up to 3500 km, north of the contemporary Gondwana margin (Figure 11).

The similarity in paleolatitude from our small dataset and the one of Grindley et al. (1980) is promising, but the results of both studies are subject to uncertainties. The findings of Grindley et al. (1980) have been called doubtful due to uncertainty in tilt-corrections for volcanic rocks (Kodama et al. 2007), while our data set is very small and lacks independent field tests. Therefore, we emphasise the tentative nature of our interpretation, and a larger data set is needed to put better constraints on the original paleolatitude of the Murihiku forearc basin.

Finding the original signal has proven to be extremely difficult due to the widespread magnetic overprint. Nevertheless, our data show that such an effort is not futile and provides a lead to identify primary magnetisations in Murihiku rocks. It would be worthwhile to carry out extensive sampling of the rock succession exposed in Awakino Gorge and in Glenham Porphyry to increase the data set and quantitatively constrain the Mesozoic plate kinematic history of the Gondwana margin and adjacent intra-oceanic arcs of New Zealand.

6. Conclusions

To aid kinematic restoration of the Mesozoic and Cenozoic plate tectonic and orogenic history of part of New Zealand, we performed a paleomagnetic study on rocks from the Upper Triassic to Lower Jurassic of the Murihiku forearc basin in the central-western North Island, New Zealand. Our results confirm previous interpretations of widespread pervasive remagnetisation throughout the North Island in the form of exclusively normal polarities – despite accumulation of the rocks during times of high reversal frequency – and negative fold tests. We show demagnetisation results for 248 samples from three localities at Awakino Gorge, Port Waikato, and Kiritehere Beach. The latter two record similar in situ inclinations of c. –74°, corresponding to a latitude of 61°S during post-tilt remagnetisation. Based on comparison of the expected paleolatitude of these samples with the apparent polar wander path of New Zealand, we estimate remagnetisation to have occurred around 83 ± 5 Ma.

We show that remagnetised directions in Murihiku Terrane sediments provide an excellent datum for post-remagnetisation studies of regional tilt and vertical axis rotation. We show that the lower inclinations in Awakino Gorge paleomagnetic data compared with data for the more northern sample localities are consistent with a regional eastward tilt of c. 20° as a result of reverse displacement on Manganui Fault.

The Murihiku Terrane has, in addition, been subjected to significant rotation since remagnetisation. Port Waikato has been rotated $39.4 \pm 9.5^\circ$ counterclockwise and Awakino Gorge has been rotated $77.3 \pm 5.0^\circ$ clockwise ($95.8 \pm 12.0^\circ$ when corrected for eastward tilt), whereas Kiritehere rocks have remained stable with respect to Zealandia. We suggest that

these rotations can be used to reconstruct the tectonic bending of basement terranes, which must have occurred, at least in part, after the remagnetisation event estimated at 83 ± 5 Ma.

Only 8 of the 93 demagnetised Awakino Gorge samples, all at the Awakino Gorge 2 site, retain a high-temperature, high-coercivity magnetic component that may represent a primary magnetisation. In situ inclinations of only 5° would require equatorial latitudes of magnetisation, which is not possible considering plate reconstruction constraints. A primary magnetisation cannot be confirmed by independent field tests, but pre-bedding tilt directions of these eight samples suggest a paleolatitude for Murihiku Terrane of $62.1 \pm 12^\circ\text{S}$ during the Early Jurassic (Toarcian), c. 15° north of the New Zealand sector of the contemporary eastern Gondwana Margin.



Upper Cretaceous turbidites in Waihau Bay, New Zealand

Appendix 2

Geochemistry of syntectonic carbonate veins within Late Cretaceous turbidites, Hikurangi margin (New Zealand): Implications for a mid-Oligocene age of subduction initiation

This appendix has been published as:

Van de Lagemaat, S. H. A., Mering, J. A., & Kamp, P. J. J. (2022). Geochemistry of syntectonic carbonate veins within Late Cretaceous turbidites, Hikurangi margin (New Zealand): Implications for a mid-Oligocene age of subduction initiation. *Geochemistry, Geophysics, Geosystems*, 23(5), e2021GC010125.

Abstract

We document the geochemistry of calcite veins in the Late Cretaceous Tikiore Formation (Raukumara Peninsula, New Zealand) to characterize their fluid composition and source and to help establish the age of subduction initiation at the Hikurangi margin of the Australia-Pacific plate boundary. The calcite veins occur within normal faults offsetting turbidites that accumulated in a lower slope basin. Vein calcite trace metal content and rare earth element patterns are consistent with a seawater-derived brine composition. Oxygen isotope ($\delta^{18}\text{O}$) values range from -6.1 to $+8.4\text{‰}$ and are -0.2‰ VPDB on average; positive $\delta^{13}\text{C}$ values of up to $+28\text{‰}$ VDPB reflect methanogenesis. Oxygen isotope temperature data indicate that calcite vein mineralization occurred at temperatures in the range of 29°C – 48°C . This is markedly less than the maximum burial temperature experienced by the host rocks, which we estimate to be $104 \pm 10^{\circ}\text{C}$ at 30–27 Ma from the inverse modeling of apatite fission track data. The vein calcite has a 28.5 ± 4.9 Ma U-Pb age. From these data, we infer that the succession above Tikiore Formation was removed by slumping, thereby resulting in fluid overpressure in the reservoir, followed by hydraulic fracturing and the precipitation of the vein calcite. Ultimately, the data presented here from the Tikiore veins are consistent with subduction initiation at 30–27 Ma, based on the U-Pb age of the vein calcite and modeling of apatite fission track data for the host sandstone, corroborated by the 30–27 Ma timing of back thrusting on the Taranaki Fault and related foredeep development in eastern Taranaki Basin.

1. Introduction

The Hikurangi subduction zone is the sector of the modern Australia-Pacific plate boundary east of North Island and northernmost South Island (New Zealand), where the oceanic Pacific Plate subducts beneath the continental Australia Plate (Figure 1). Early studies concluded that the modern plate boundary including the Alpine Fault sector in South Island formed at about 23 Ma (Oligocene-Miocene boundary) (e.g., Carter and Norris, 1976; Cooper et al., 1987; Field et al., 1997; Kamp, 1986). This age is based on geologic features, such as a stratigraphic change from carbonate to terrigenous sedimentation in Oligocene-Miocene sedimentary basins in New Zealand (e.g., Ballance, 1993; Carter and Norris, 1976; Field et al., 1997; Nelson and Hume, 1977), and the early Miocene start of arc volcanism in northern North Island (e.g., Ballance, 1976; Ballance et al., 1985; Hayward et al., 2001; Isaac et al., 1994). These manifestations are, however, likely to provide minimum estimates of the timing of initiation of the current plate boundary because substantial rock uplift is required for a wholesale change from carbonate to terrigenous sediment input to basins, and a considerable distance of subduction is needed before arc magma is typically generated. More recently, Furlong and Kamp (2013) showed from analysis of plate motions coupled with analysis of the stratigraphy in multiple basins across New Zealand that crustal extension transitioned to crustal shortening between 29 Ma at the latitude of the northern Hikurangi margin and 26 Ma in the more southerly Fordland region of southwestern South

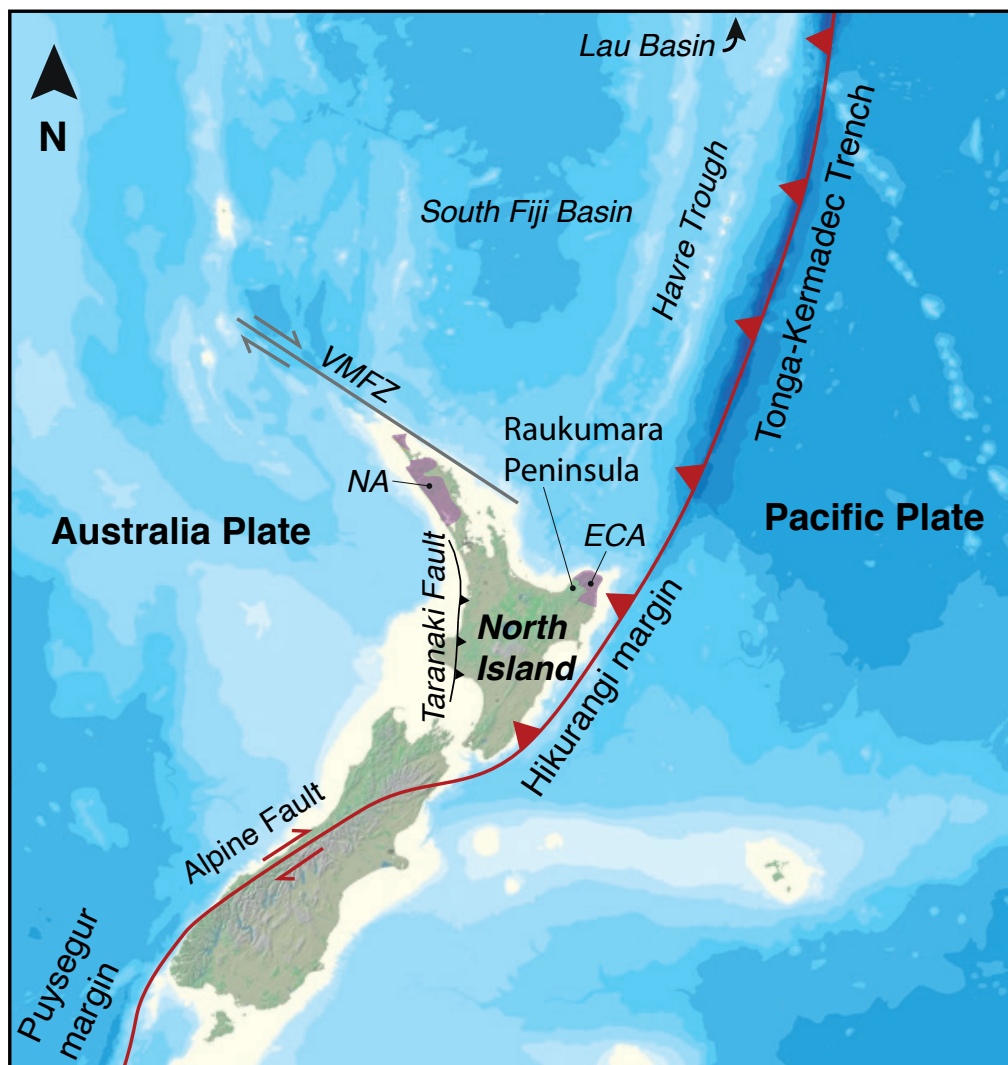


Figure 1. Tectonic Map of the New Zealand region showing the Tonga-Kermadec arc-trench system, which passes south to the ocean-continent Hikurangi margin along eastern North Island, both part of the Australia-Pacific plate boundary. Note the general distribution in pink of the Northland Allochthon (NA) and the East Coast Allochthon (ECA), and the location of the Vening Meinesz Fracture Zone (VMFZ). Background image obtained from NIWA (CANZ, 2008).

Island. This suggests that initial subduction at the Hikurangi Margin might have started at about 29 Ma but no geological confirmation of this has yet been demonstrated.

Subduction initiation at the Hikurangi Margin has previously been associated with emplacement of the East Coast Allochthon (ECA) (Brothers and Delaloye, 1982; Rait et al., 1991). The ECA is a widespread allochthon exposed in Raukumara Peninsula in eastern North Island within the forearc region of the Hikurangi margin (Figures 1 and 2). It

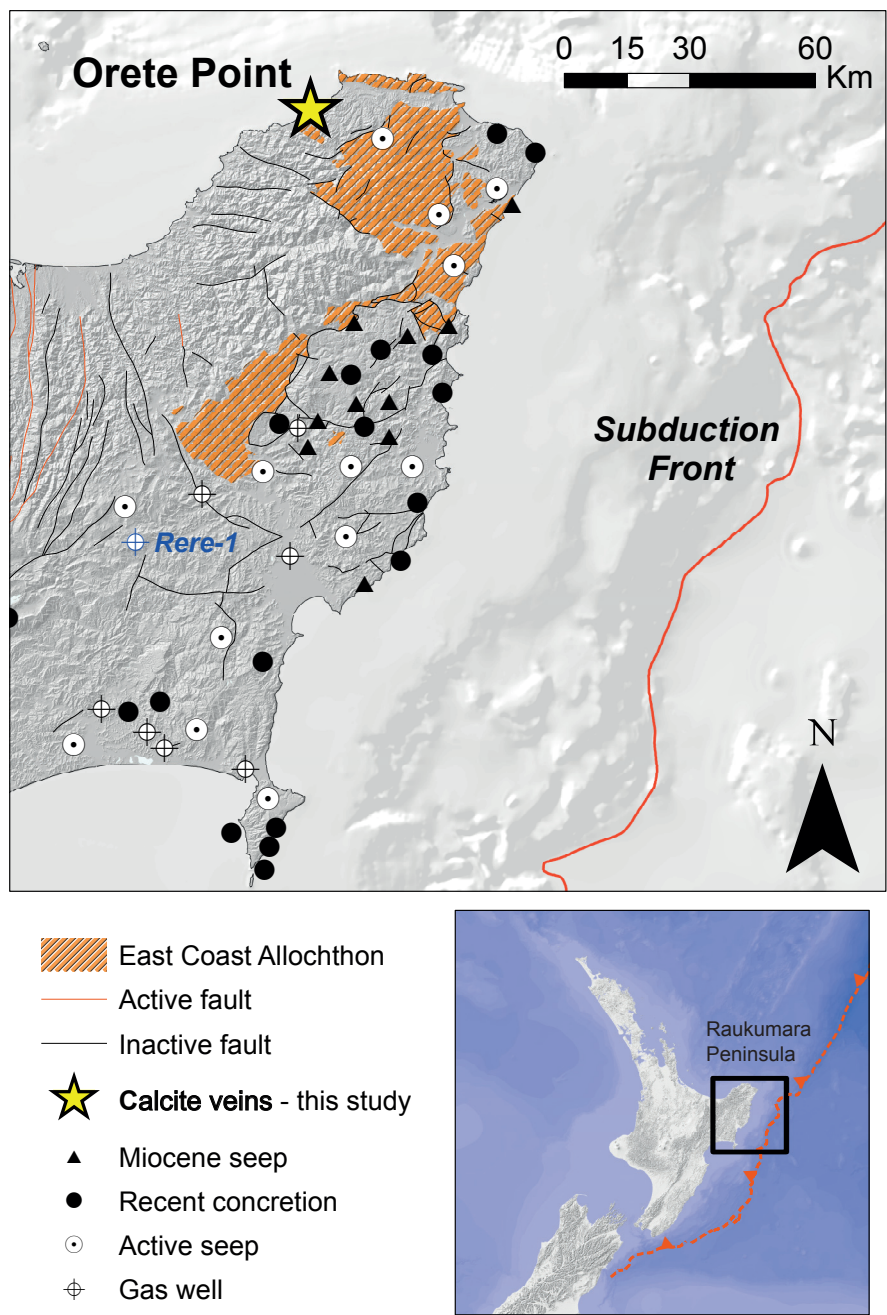


Figure 2. Raukumara Peninsula in Eastern North Island, New Zealand, in relation to the modern subduction front of the Hikurangi margin. Note the distribution of the East Coast Allochthon. Orete Point is the location of this study. The distribution of Miocene cold seep carbonate occurrences and active seeps and springs in the northern part of the Hikurangi margin are also shown (from Nyman et al., 2010).

comprises several thrust sheets of sedimentary rocks and one sheet of ocean floor lavas and is considered to have been gravitationally emplaced from offshore northeast of Raukumara Peninsula to the southwest during the latest Oligocene and earliest Miocene and into an inboard position on the Australia Plate within the principal forearc basin (Mazengarb and Speden, 2000; Rait, 1992; Stoneley, 1968). To better constrain the timing of subduction initiation at the Hikurangi margin, we report the results of geochemical analysis and U-Pb dating of calcite veins sampled from Tikiore Formation, the lowermost sedimentary formation in the ECA, exposed at Waihou Bay at the northern end of the Raukumara Peninsula (Figures 2 and 3). We then compare our geological results with predictions from plate tectonic analysis (Furlong and Kamp, 2013) about the timing of subduction initiation at the Hikurangi margin.

Our approach to analysis and interpretation of the carbonate veins in the Tikiore Formation follows that of prior studies of syntectonic vein carbonates and fluid flow through accretionary margins within the Cascadia Margin (e.g., Ritger et al., 1987; Sample et al., 1993), the Californian Margin (Campbell et al., 2002), and the Nankai Trough (e.g., Sakai et al., 1992; Sample et al., 2017). We also draw upon a body of work on the chemistry of active fluid seeps within the Hikurangi Margin (Figure 1), including saline springs on land (e.g., Barnes et al., 2019; Giggenbach et al., 1995) and cold seeps at sites offshore (Lewis and Marshall, 1996). In addition, we draw upon published work on fossil seafloor cold seep limestone formed atop fluid vents that were buried by ongoing Miocene and Pliocene sedimentation within the East Coast forearc basin (Campbell et al., 2008; Nelson et al., 2019; Nyman and Nelson, 2011; Nyman et al., 2010).

The precipitation of carbonate in accretionary and other settings involves dissolved carbon species (e.g., CH_4 and CO_2) and cations (e.g., Ca^{2+} , Mg^{2+} , and Fe^{2+}) (e.g., Campbell et al., 2002, 2008; Sample, 1996; Vrolijk and Sheppard, 1991). Rapid burial in accretionary wedges traps pore water and organic matter, which later contributes to the fluids from which vein calcite precipitates (Farsang et al., 2021). Oxidation of organic matter generates CO_2 , whereas reduction generates CH_4 (e.g., Campbell et al., 2008; Saffer, 2007). For mineralization to take place, fluid must reach and exceed carbonate saturation. Where fluid pressure exceeds lithostatic pressure at depth in a rock succession, hydraulic fracturing can result, possibly associated with a change in the stress regime (Barker et al., 2006; Beach, 1980; Brown et al., 1994; Oliver and Bons, 2001; Saffer, 2007). Fluid pulsing through fractures can cause CO_2 degassing, which increases pH and enables carbonate precipitation (Uysal et al., 2011). In methane-rich fluids, anaerobic oxidation of methane (AOM), associated with sulfate reduction, can also lead to an increase in alkalinity, enabling carbonate formation (Lloyd et al., 2016):



AOM-style carbonate mineralization has been widely documented within Miocene cold

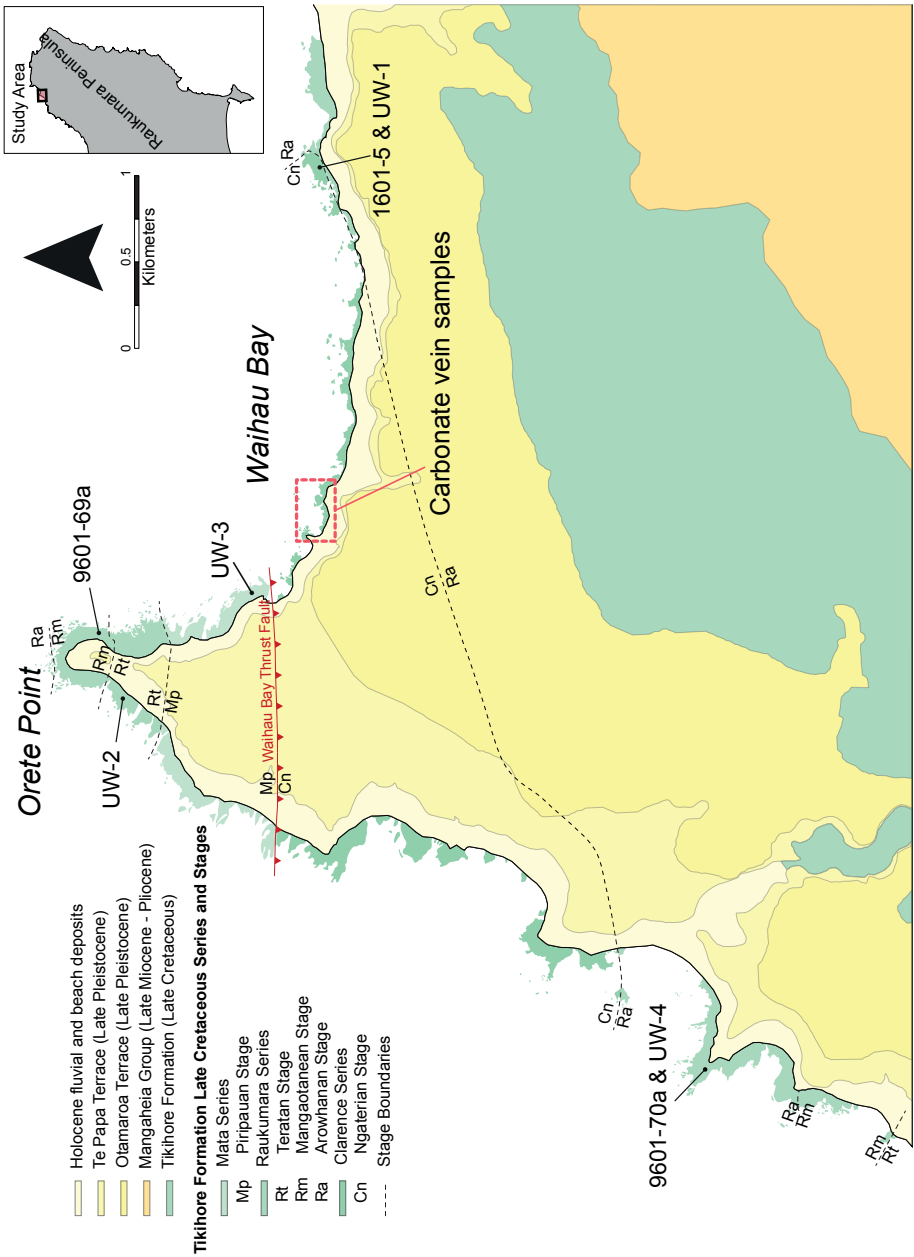


Figure 3. Geological map showing the calcite vein locations and the distribution of Tikhore Formation, including its rocky shore platform outcrop, northern Raukumara Peninsula. The distribution of New Zealand Late Cretaceous stages within Tikhore Formation and the fission track and vitrinite reflectance sample locations are also shown.

seep carbonates in the eastern Raukumara Peninsula (Campbell et al., 2008; Nelson et al., 2019), in tubular concretions within a late Miocene succession resulting from fluid migration tens of meters beneath the contemporary seafloor (Nyman et al., 2010), and in Late Cretaceous concretions (Kiel et al., 2013). There are numerous examples of modern gas seeps and saline springs on land and offshore Raukumara Peninsula, conveying aqueous fluids and dissolved gases to the surface (Barnes et al., 2019; Francis, 1995; Nyman et al., 2010).

We describe the field relations, texture, major element and trace metal composition, and stable-isotope composition of vein samples in Tikiore Formation to reconstruct the composition and temperature of the fluid reservoir from which the veins formed. We utilize U-Pb dating to quantitatively constrain the timing of vein carbonate mineralization. In addition, we apply apatite fission track and vitrinite reflectance methods to the vein host sandstone to constrain the thermal history of the Tikiore Formation. Together with the carbonate vein information, this enables us to reconstruct the sequence of events that led to the formation of the calcite veins and to interpret the timing of subduction initiation at the Hikurangi margin.

2. Tectonic and geological settings

The East Coast region of North Island lies inboard of the Hikurangi Trough (trench) and currently has a NE-SW trend (Figure 1). Prior to the early Miocene, its orientation was NW-SE, colinear with the east coast of Northland (e.g., Bradshaw, 1989; King, 2000). The sedimentary basement underlying this whole margin is formed by subduction accretion processes during the Cretaceous (Mazengarb and Harris, 1994). During the latest Cretaceous to Oligocene, this margin accumulated a passive margin sedimentary drape of mainly terrigenous siltstone (Tinui, Mangatu, and Ruatoria groups; Figure 4). Since the early Miocene, the part of the East Coast of North Island south of Raukumara Peninsula has been tectonically rotated clockwise to be now oriented NE-SW as demonstrated by analysis of paleomagnetic data (Lamb, 2011; Rowan et al., 2005; Walcott et al., 1981). Prior to the start of this rotation, the Australia-Pacific plate boundary developed along the eastern Northland (northern North Island) continental margin possibly as a transform fault, part of which still exists, known as the Vening Meinesz Fracture Zone (VMFZ) (Figure 1).

Two very large allochthons, the Northland Allochthon and the East Coast Allochthon (ECA; Figure 1), were emplaced onto the Australia Plate from the vicinity of the new Hikurangi Subduction Zone during the latest Oligocene and early Miocene (Ballance and Spörli, 1979; Field et al., 1997; Isaac et al., 1994; Mazengarb and Speden, 2000; Rait, 1992). Both the Northland and East Coast allochthons have similar stratigraphy, lithology, and structure, reflecting mobilization of the same Late Cretaceous and Paleogene passive margin sedimentary succession and seafloor basalt. Our study is exclusively focused on Tikiore Formation at Waihou Bay, which occurs within the ECA.

Stoneley (1968) first mapped (part of) the ECA and inferred its emplacement by

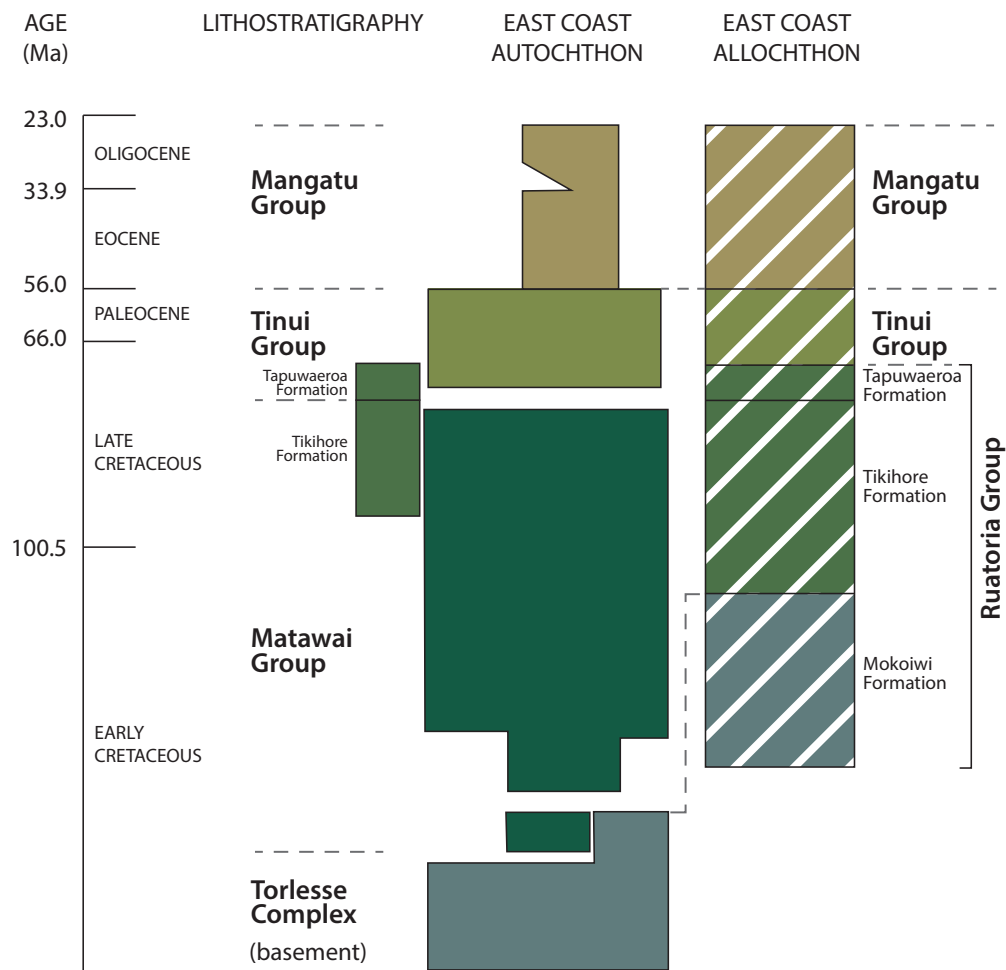


Figure 4. Stratigraphic legend for Cretaceous–Oligocene strata in the East Coast of North Island (New Zealand), following the geological mapping by Mazengarb and Speden (2000). The similar succession of lithologies for both the autochthonous and allochthonous strata reflects the late Oligocene and early Miocene emplacement of the East Coast Allochthon to the southwest and inboard of its former lower slope position on the Australia Plate continental margin. The Mokoikiwi Formation is the youngest and most outboard part of the Cretaceous accretionary wedge, now displaced inboard as part of the East Coast Allochthon; the Torlesse Complex is an older part of the same wedge. Tikihore Formation has been mapped both in the autochthon and allochthon although having differences in their duration of sediment accumulation. The calcite veins characterized in this study were collected from allochthonous Tikihore Formation at Waihou Bay.

gravitational sliding to the south-southwest off a structural high located offshore to the northeast of Raukumara Peninsula. Subsequent mapping has established the full extent of the ECA (Figure 2; Rait, 1992; Mazengarb and Speden, 2000) and confirmed its south-southwestward direction of emplacement as a series of gravitationally driven thrust sheets (Rait, 1992). The final phase of emplacement of the ECA into the East Coast forearc basin was accompanied by supra-allochthon accumulation of early Miocene bathyal mudstone in piggy-back basins on some of the thrust sheets (Mazengarb and Speden, 2000).

The Tikiore Formation comprises the oldest sedimentary rocks that were incorporated into the ECA and was deposited during the late Cenomanian–early mid-Santonian (c. 96–83 Ma (Crampton, 1996); upper Ngaterian–Piripauan stages of the New Zealand geological time scale; Raine et al., 2015). The Tikiore Formation is inferred to have accumulated within an accretionary slope basin atop the outer edge of the Cretaceous accretionary wedge (Mazengarb and Harris, 1994), known as the Torlesse Complex (Edbrooke et al., 2015; Mortimer, 2004). The Tikiore Formation is one of several units within the Ruatoria Group (Figure 4), which includes all accretionary shelf and slope basin units within the ECA (Mazengarb and Speden, 2000).

The Tikiore Formation comprises mainly mass-emplaced terrigenous sandstone (turbidites) and associated hemipelagic mudstone beds. This succession is continuously exposed on the shore platform around Orete Point and part of Waihou Bay (Mazengarb and Speden, 2000) (Figures 2 and 3). The beds dip moderately to steeply and are mostly overturned. The Waihou Bay Thrust Fault (Figure 3) is a steeply dipping late reverse fault that significantly offsets the succession and juxtaposes beds of Ngaterian age (99.5–95.2 Ma) against beds of Piripauan age (86.5–83.6 Ma) (Crampton, 1996). Otherwise, the beds are offset by normal faults with up to a few meters of displacement and by subsequent bedding-parallel thrust faults with tens of meters of offset. In a few instances, thrust faults demonstrably offset normal faults.

3. Analytical methodology

3.1. Petrographic observations

Vein samples were collected for analysis at four in situ sites from shore platform exposures in Waihou Bay (Figures 3 and 5). Vein samples ($n = 10$) were cut perpendicular to vein orientations, polished, and imaged under reflected light, cathodoluminescence light (CL), and ultraviolet (UV) light (Figures 6 and 7, and S1 in Supporting Information S1). Cathodoluminescence (CL) imaging was carried out using a CITL Mk5-1 cathodoluminescence stage attached to an optical microscope. The CL microscope was operated with an acceleration voltage of ~15 kV and a gun current of 200–240 μ A.



Figure 5. Photos of typical occurrences of calcite veining and breccia in Tikiore Formation at Waihau Bay. Veins occur within zones of brecciated sandstone within and adjacent to normal faults. (a) Calcite veins and breccia in a normal fault trace marked with a red-dashed line. (b) Calcite veins orthogonal to bedding without evidence of a fault trace.

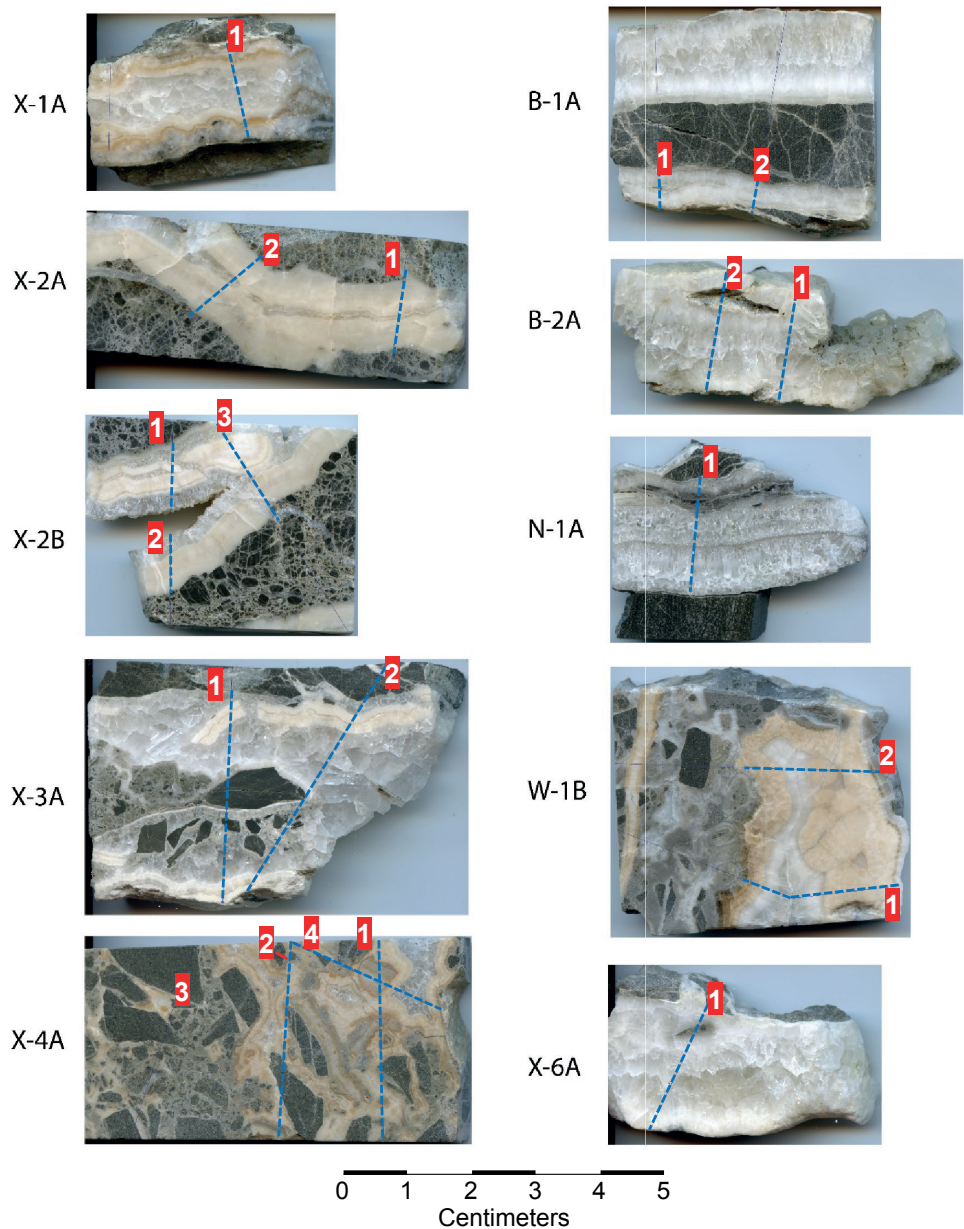


Figure 6. Photos of polished slabs evaluated in this study. These samples record evidence of hydraulic fracturing, focused fluid flow and calcite mineralization, with disruption and secondary infilling in and around earlier vein material. Blue-dashed lines denote ICP-MS transects referenced in the text. Red-highlighted number indicates the starting point of an ICP-MS transect. Samples exhibit deformation and veining events in three phases: (i) brecciation of the sandstone host rock and pervasive calcite cementation, (ii) infilling of fractures and breccia zones with a milky white to orange (plain light) laminar calcite, and (iii) disruption of milky and orange calcite and infilling of blocky white-clear calcite in the vein centers, leaving some vugs.

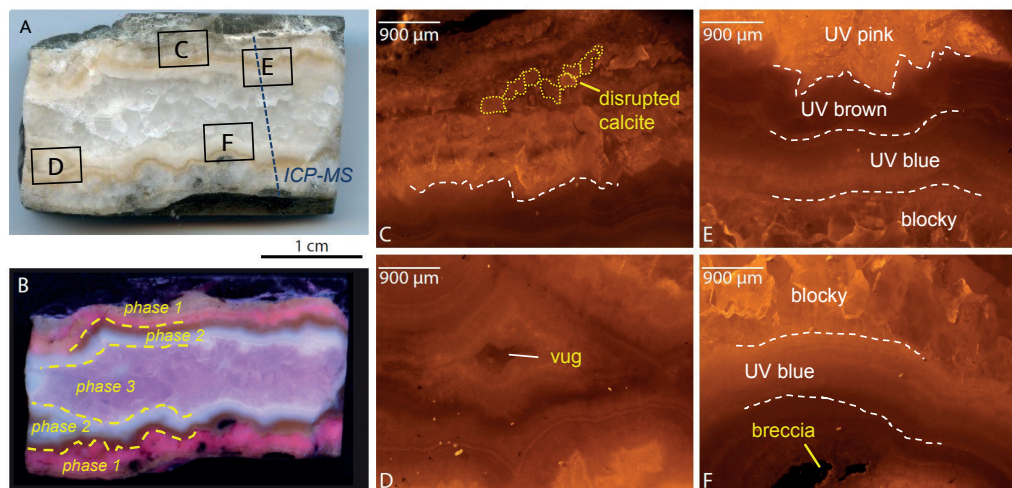


Figure 7. Polished slab of vein XI in reflected light (a), ultraviolet (UV) light (b), and Cathodoluminescence (CL) light (c–f), highlighting carbonate textures. The blue line in panel A depicts the LA-ICPMS transect. Panel (b). UV light reveals four distinct zones. The rim zone, in contact with wall rock, is pink. This is followed by a thin band of brown laminated microcrystalline calcite, followed by a zone of very pale blue microcrystalline banded calcite. The vein center is infilled with a blocky white-clear calcite that is pale purple under UV. CL images (c–f) highlight crystal morphology within zones. Laminations within the blue and orange microcrystalline calcite are visible in all four CL images. For reference, the color boundaries on the UV image are drawn with a dashed white line between the pink and brown zones (c, e), brown and blue (e), and blue to blocky (e, f). Images of other samples in reflected light, UV light, and CL are provided in Figure S1 in Supporting Information S1.

3.2. Elemental analysis and U-Pb dating

The elemental geochemistry of vein samples was determined by Laser Ablation Induction Coupled Plasma Mass Spectrometry (LA-ICP-MS) at the University of Waikato. Analyses were carried out using an Agilent 8900 Triple Quadrupole ICP-MS, coupled with a Laurus Technik S155 SE ablation cell and a RESOLUTION 193 nm ArF excimer laser. Transects were measured across veins at a rate of 50 μm/s. All operating conditions are provided in Table S1 in Supporting Information S1. Elemental results were processed using *ioGAS*TM software and are reported in the analytical results section. Raw data are provided in the data repository.

Rare earth element patterns are used here to understand fluid source, fluid-rock interaction, and the oxidation state of fluids. Rare earth elements have been normalized to post Archean Australian Shale (PAAS) abundances (Taylor and McLennan, 1985). Anomalies were computed by comparing the shale-normalized value of a given element to the PAAS values of immediate neighbor elements on the REY spider diagram (Figure 8). For example, the shale normalized Eu anomaly is computed in the following:

$$\text{Eu}/\text{Eu}^*_{\text{SN}} = 2[\text{Eu}]_{\text{SN}}/[\text{Sm}]_{\text{SN}} + [\text{Gd}]_{\text{SN}}$$

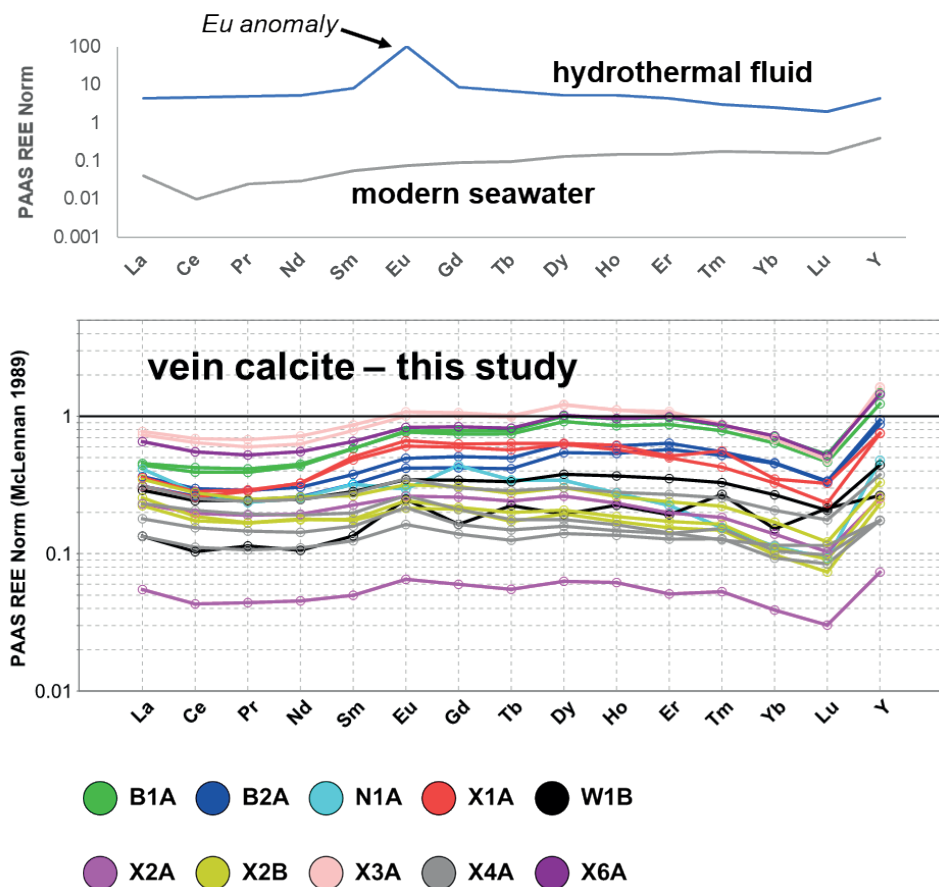


Figure 8. Representative spider diagram of rare earth elements plus Y (REY) abundances, normalized to post-Archaeon Australian Shale (PAAS) (Taylor and McLennan, 1985), derived from La-ICPMS spot analyses along the laser transects across 10 vein calcite samples (Figure 5). All values presented are mean values. The absence of a positive Eu anomaly suggests that there was no hydrothermal fluid source for the vein calcite. A positive Y excursion is a characteristic of a seawater-derived fluid source.

U-Pb measurements of calcite veins were carried out by LA-ICP-MS as spot analyses. Within a given paragenetic zone, 20–60 spots were taken on transects along particular veins at 80–100 μm intervals. Spot analyses were taken at 30-s intervals with a pulse repetition rate of 10 Hz, a spot diameter of 100 μm , and a fluence of 7 J cm^{-2} . Data processing was carried out using the *Iolite*® software package (Paton et al., 2010). The SRM NIST 612 standard was used as a primary reference material. The calcite standard WC-1 with a reported age of 254.4 ± 6.4 Ma (Roberts et al., 2017) was used for U-Pb normalization.

3.3. Stable isotope analysis

Carbon and oxygen stable isotope measurements in calcite were carried out using a continuous flow laser spectroscopy approach modified from an analytical setup described by Barker et al. (2011) and Beinlich et al. (2017) at the University of Waikato. Samples were digested in 102% orthophosphoric acid at 72°C in exetainer vials for a minimum of 2 hr prior to measurement. Sample CO₂ liberated from vein calcite was flushed from vials using a dual needle continuous flow system and passed through an ethanol-dry ice slush trap to remove water. Instrument operation parameters, reference materials, and raw analytical data are provided in Table S2 in Supporting Information S1 and the data repository. The typical precision of measurement for $\delta^{13}\text{C}$ ($\pm 0.3\text{‰}$ VPDB) and $\delta^{18}\text{O}$ ($\pm 0.2\text{‰}$ VPDB) was computed from the standard deviations of carbonate reference materials (RMs), which were run in duplicate.

3.4. Apatite fission track analysis and vitrinite reflectance analysis

Apatite fission track analysis (AFT) was applied to three samples (see Figure 3 for sample locations). The methods used for mineral separation and AFT dating of sample 1601-5 were the same as those described in Kamp (1999). The analyses and modeling were undertaken in the University of Waikato fission track laboratory. The age data for two of the samples (9601-69a and 9601-70a) have previously been reported together with apatite chlorine compositions (Kamp, 1999). Track lengths were remeasured. New AFT data are presented for one sample (1601-5), which together with the others help constrain the thermal history of the particular part of the Tikiore Formation containing the calcite veins. Inverse modeling methods using HeFTy software v. 1.9.1 (Ketcham, 2005) were undertaken for all three sample AFT data sets. Stratigraphic constraints as described in Section 5.5 have been incorporated in the inverse models. The chlorine content of apatites in samples 9601-69a and -70 has been established by microprobe analysis as reported in Kamp (1999). For sample 9601-69a, the average wt.% Cl is 0.380 (range: 0.002–1.337) and for 9601-70a, it is 0.088 (range: 0.000–0.437). The AFT data have been modeled using a Durango Apatite Cl value of 0.4%. The graphical output for the thermal history modeling of the AFT data for sample (1601-5) is shown in Figure 9.

Vitrinite Reflectance (VIRF; vitrinite inertinite reflectance and fluorescence) was undertaken on plant-sourced macerals in each of four Tikiore Formation sandstone samples by Newman Energy Research Ltd under contract to University of Waikato. In the VIRF methodology, paired reflectance and fluorescence measurements were obtained on both vitrinite and inertinite (Newman, 1997). This method allows indigenous vitrinite of orthohydrous (“normal”) composition, which provides reliable reflectance data, to be distinguished from lower reflectance perhydrous vitrinite, which may have been altered during burial or oxidized (weathered) in the outcrop setting. Coals are the reference standards for VIRF measurements in terrigenous sediment samples (Newman et al., 2000). Rock samples for VIRF were crushed to <1 mm and mounted in polyester as 25-mm-

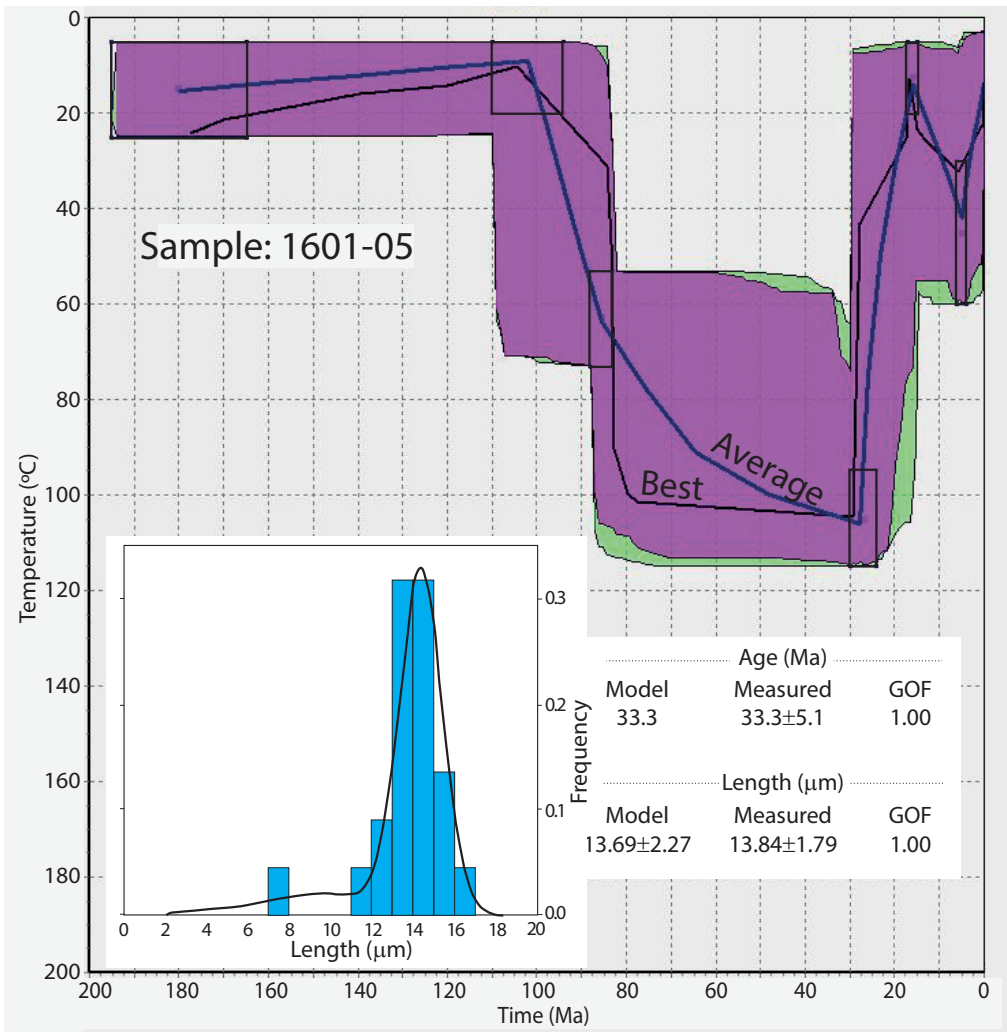


Figure 9. Apatite fission track thermal history model for sample 1601-5 from the Late Cretaceous Tikiore Formation (N.Z. Ngaterian Stage, 99.5–95.2 Ma) is produced with HeFTy software (Ketcham, 2005). This model and those of 9601-69a and 9601-70a (Figure S3 in Supporting Information S1) start with considerable provenance age, and sedimentation prior to 95 Ma. Maximum burial heating is constrained between 30 and 24 Ma, but the temperature is unconstrained. Exhumation of the sample host rock to the surface is constrained by the 16–15 Ma stratigraphic age of Clifdenian (15.9–15.1 Ma) neretic marine sediments west of outcrops of Tikiore Formation (Mazengarb and Speden, 2000). The late Miocene burial heating is broadly constrained to lie between 7.5 and 4 Ma, the age of inner shelf Mangaheia Group sediments overlying Tikiore Formation (Figure 3). The goodness of fit (GOF) is optimal at 1.0 for both age and length and the average and best model paths of 100,000 monte trax simulations are very similar. The purple zone represents good model results and the green margin represents acceptable model paths.

diameter disks and then polished using a LECO (AP-60/VP150) polisher with the final polish attained with colloidal silica on a silk-covered bronze lap.

4. Description of Tikiore Formation carbonate veins

Carbonate veins occur in the lowermost part of the Tikiore Formation at Waihou Bay within normal fault zones, which displace highly indurated sandstone beds of Ngaterian and Arowhanan age (99.5–93.7 Ma) (Figure 3). Four examples of carbonate veins within normal faults (Figure 5) occur along a limited part of the rocky shore platform outlined in Figure 3.

The fault-hosted veins are exposed over distances of 2–3 m with up to 100 m of separation between occurrences. Veins are typically 0.5–2 cm in diameter. Larger brecciated zones, containing anastomosing carbonate veins, occur over thicknesses of up to 30 cm. The veins in their field setting typically exhibit macroscopically zoned growth, including white to orange microcrystalline carbonate. In many cases, veins also contain a white to clear blocky textured carbonate in the vein centers, which does not always completely infill them.

4.1. Textural observations and phases of vein growth

Vein textures are described within three paragenetic phases of fracturing, dilation, and mineralization within the Tikiore Formation. Textural variations occur within these Phases 1–3, which are defined as subphases in Table 1. These subphases reflect the multistage history of deformation, fluid migration, and mineralization recorded by the Tikiore Formation. Table S3 in Table S1 provides more petrographic and textural details from both plane and UV light observations. However, for the purposes of placing the deformation and geochemical information recorded by the Tikiore veins into a regional tectonic context, we primarily refer to Phases 1–3. The ICP-MS transects and stable isotope data (i.e., $\delta^{13}\text{C}$ and $\delta^{18}\text{O}$) presented in the following sections encompass the opaque white and orange calcite material in Phase 2 and the blocky coarse calcite in Phase 3. Geochemical interpretations of these data are not made at the subphase level.

All vein phases are bright orange under CL (Figures 7 and S1 in Supporting Information S1), which is indicative of Mn^{2+} activation in calcite (e.g., Götze, 2012). When exposed to shortwave UV light, the vein infilling calcite exhibits a range of colors (Figures 7 and S1 in Supporting Information S1). XRD scans show that calcite is the only carbonate species present in all of the samples analyzed (Figure S2 in Supporting Information S1).

Phase 1 describes initial brecciation of the sandstone host rock and early cementation, typically composed of numerous thin anastomosing veinlets, giving the sandstone within, and immediately adjacent to normal fault zones, a distinctive pale gray color (Figures 5 and 6). The angular clasts produced during this initial phase of fracturing can also be internally calcite cemented although this is not always the case. The Phase 1 breccia and vein material is displaced by secondary brecciation, accompanied by episodic dilation and vein infilling with milky white and orange calcite (Phase 2). Phase 2 calcite is frequently microcrystalline

Table 1. Textures present in calcite veins

	Phase	Sub-phase	Texture	X1	X2	X3	X4	X6	B1	B2	N1	W1
Vein chemistry assessed	1	1	Initial brecciation									
		2	White milky calcite									
	2	3	Brecciation									
		4	White milky calcite									
		5	Orange milky calcite									
		6	White milky calcite									
	3	7	Blocky white-clear calcite									
		8	Late veinlets									

and finely laminated. This vein phase is pink, brown, and blue under UV light. Typically, Phase 2 calcite is present on both sides of veins as observed in cross section, and the outermost part in contact with the wall rock is commonly pink under UV light (Figures 7 and S1 in Supporting Information S1). Phase 3 encompasses vein mineralization of blocky white-clear calcite. This blocky calcite disrupts earlier milky white microcrystalline calcite and infills most vein centers although infilling is incomplete in some cases. The coarseness of these drusy calcite crystals and their incomplete infilling of vein cavities suggests that Phase 3 vein material represents the final significant period of fluid transmission through vein conduits. Minor and very thin late veinlets crosscut intact vein and breccia zones in some cases. In the following sections, we present the geochemistry of the primary vein infilling Phase 2 and 3 materials.

5. Results

5.1. Mineral chemistry of calcite veins

Select major and trace elemental abundances as obtained from LA-ICP-MS analyses are reported in Table 2. ICP-MS transects across veins through the main infilling calcite of Phases 2 and 3 indicate that elemental concentrations vary from vein rim to center and in many cases are symmetrically zoned. A representative set of elemental transect data are presented for sample X1A in Figure 10, which shows that concentrations of Mg, Sr, and Ba increase in the orange band within the opaque microcrystalline calcite of Phase 2. Concentrations of Mn are elevated in the outer opaque white subphase of Phase 2, which is in contact with wall rock (>8,000 ppm), but strongly depleted in the subsequent orange and milky white microcrystalline subphases (<2,000 ppm), and in the blocky calcite of Phase 3 (~2,000–3,000 ppm) in the vein interior. Rare earth element abundance is lowest in the orange microcrystalline subphase in the center of Phase 2 and in the center of the blocky calcite of Phase 3 at the vein interior.

Table 2. Select major and trace elemental abundances in calcite veins

Transect	Mg	Mn	Fe	Sr	Ba	Na	K	ΣREE
ALL	2587	580	79	576	18	114	66	29
-	1565	373	27	407	10	63	37	7
+	3852	917	161	702	30	224	125	85
B1A-1	1151	448	150	599	13	109	56	72
-	863	394	65	478	8	52	24	16
+	1733	612	310	733	20	304	133	128
B1A-2	1610	499	189	498	15	160	77	68
-	1251	446	95	383	10	73	35	18
+	2077	563	267	600	19	298	147	123
B2A-1	2396	422	77	543	16	81	74	29
-	1519	385	23	469	10	44	40	5
+	4749	513	223	606	26	167	157	74
B2A-2	2092	529	113	477	14	81	50	32
-	1529	413	37	397	10	39	29	11
+	2703	633	218	596	18	169	121	77
N1A-1	558	3306	167	368	3	41	24	26
-	437	2917	130	173	1	23	14	5
+	994	4052	309	584	6	71	72	89
W1B-1	2691	211	82	655	18	140	64	5
-	2197	141	55	511	13	92	45	2
+	3038	350	113	813	23	209	87	18
W1B-2	2791	258	91	581	19	100	77	6
-	2523	149	65	468	17	83	63	2
+	3109	404	138	685	21	121	107	53
X1A-1	3355	1944	52	626	31	71	43	49
-	2379	707	21	457	19	41	24	13
+	4688	3251	115	796	65	111	66	86
X1A-2	3104	2203	120	540	27	91	86	40
-	2192	1500	51	453	18	67	57	7
+	4024	4641	180	730	38	177	137	92
X2A-1	4369	267	14	359	11	55	40	3
-	3674	242	10	330	5	34	24	1
+	5511	321	21	390	18	79	51	16
X2A-2	3713	308	23	349	10	39	50	29
-	3024	272	10	323	6	28	34	17
+	4381	400	74	378	18	59	95	45

Table 2 (*continued*)

X2B-1	1356	463	54	342	8	283	102	27
-	1165	345	40	303	5	198	69	13
+	1901	682	94	419	12	504	164	45
X2B-2	2411	372	40	397	9	68	19	22
-	902	304	15	322	7	47	7	7
+	3055	569	107	513	13	103	47	91
X2B-3	1862	456	52	340	8	166	83	21
-	1418	373	26	309	7	116	63	7
+	2818	679	90	400	12	247	137	55
X3A-1	1482	809	155	554	14	199	60	116
-	1036	630	99	415	9	58	23	62
+	1955	941	242	677	18	637	180	179
X3A-2	2032	774	144	599	15	171	48	94
-	1555	537	74	442	9	60	25	48
+	2746	1010	226	767	20	432	102	184
X4A-1	4765	860	18	734	43	115	66	7
-	3959	727	8	663	36	69	39	3
+	5954	974	35	834	61	220	112	21
X4A-2	4986	853	27	664	39	181	137	9
-	4366	732	17	621	34	127	73	5
+	5522	1017	52	713	49	229	213	24
X4A-3	4124	923	47	681	35	156	117	34
-	3798	785	27	619	28	114	60	23
+	4512	1035	141	737	42	225	160	60
X4A-4	3244	1072	33	655	39	124	72	35
-	2436	879	23	581	31	78	44	12
+	3817	1429	77	797	55	217	132	66
X6A-1	1600	475	146	502	10	82	53	73
-	1231	414	54	376	6	44	28	33
+	2124	642	245	593	17	201	109	152

Concentrations in parts per million (ppm)

Values are median results for each transect

Ranges reflect 25 percentile (-) to 75 percentile (+)

Elements in a given transect are normalised to the calcium concentration, assuming a Ca value of 40.3 weight percent

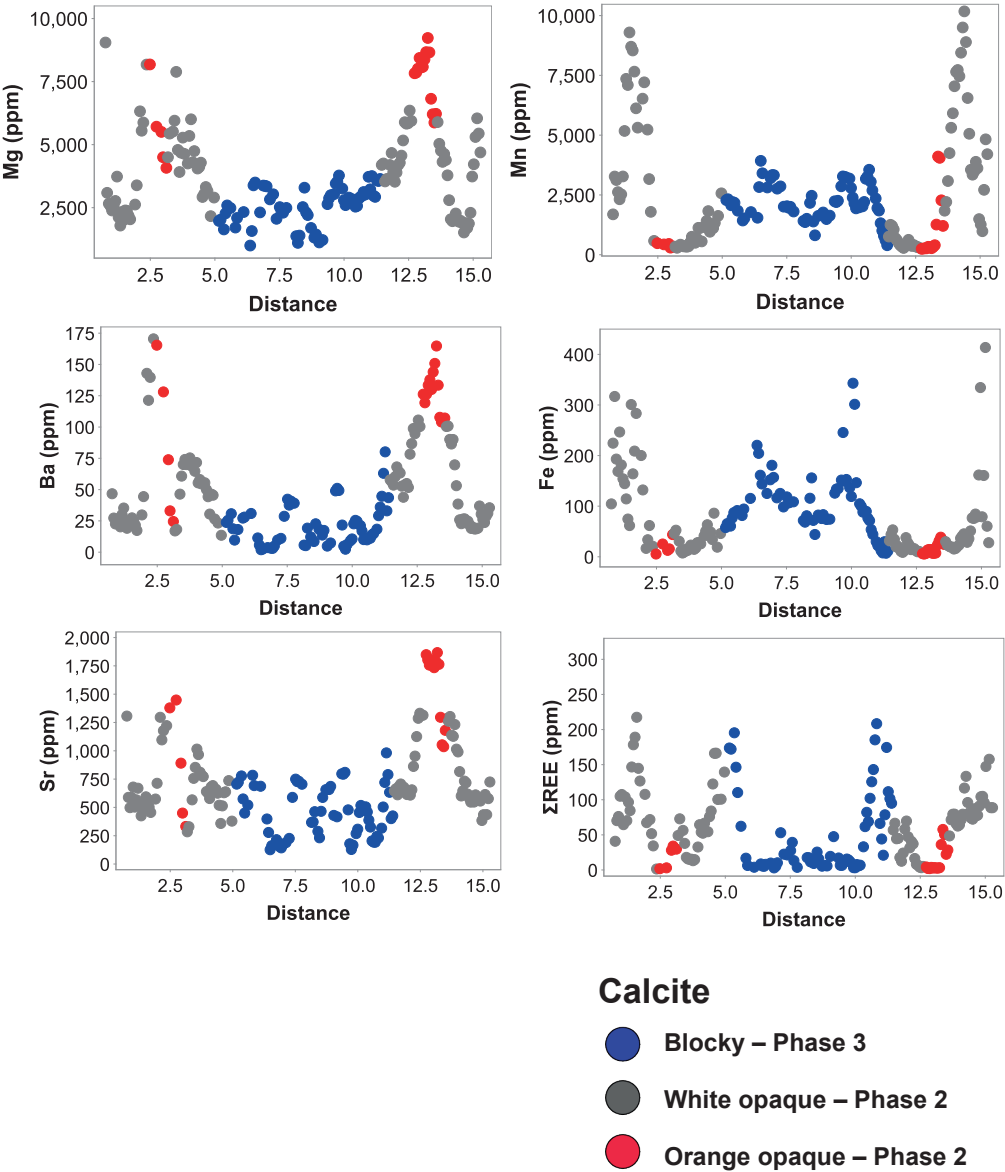


Figure 10. Abundance of major (Mg, Ba, Mn, Sr, and Fe) and trace elements (as sum of REE) for spot analyses by La-ICPMS along a line scan (Figure 6) of sample XIA (XIA-I). For each element, the spot data points are colored to distinguish the white and orange color zones (plain light) in Phase 2 calcite and the Phase 3 blocky calcite.

Spider diagram plots of calcite veins exhibit consistent patterns of relative enrichment or depletion for all samples (Figure 8). Median transect values of computed rare earth anomalies were near 1 for $[\text{Eu}/\text{Eu}^*]_{\text{PAAS}}$ (0.75–1.27), $[\text{Ce}/\text{Ce}^*]_{\text{PAAS}}$ (0.77–0.95), $[\text{Gd}/\text{Gd}^*]_{\text{PAAS}}$ (0.62–1.42), and $[\text{Er}/\text{Er}^*]_{\text{PAAS}}$ (0.85–1.11). REE concentrations do not vary significantly across the measured calcite veins (i.e., Phases 2–3). Here, values are computed for $[\text{Ce}/\text{Ce}^*]_{\text{PAAS}}$, $[\text{Gd}/\text{Gd}^*]_{\text{PAAS}}$, $[\text{Er}/\text{Er}^*]_{\text{PAAS}}$, and $[\text{Eu}/\text{Eu}^*]_{\text{PAAS}}$. Eu typically occurs in a 3+ oxidation state, but in reducing environments may attain 2+ valence. Strong positive Eu anomalies are indicative of mixing with hydrothermal fluids (e.g., German et al., 1993; Meyer et al., 2012; Tostevin et al., 2016). Small positive Eu anomalies of up to 1.5 are typical in fluids derived from seawater. The median Eu anomaly across all Tikiore Formation calcite transect measurements is 1.23, while the 25–75 percentile range is 1.02–1.23. The computed Eu anomaly exceeded 1.5 in less than 5% of transect measurements. Positive outliers for single measurements along transects either reflect local sample heterogeneity or counting statistics, given the relatively short integration time for spots along transects. The median Y/Ho value for all calcite vein transects is 39, while individual transects exhibited median values between 29 and 55 (Table 3). Y/Ho ratios are extremely consistent across paragenetic Phases 2 and 3. Modern seawater exhibits a strongly positive Y/Ho signature for calcite, typically greater than 36 (De Baar et al., 1985; Tostevin et al., 2016). Hence, both the Eu anomaly and Y/Ho ratio (Table 3; Figure S4 in Supporting Information S1) are consistent with a seawater-derived brine composition from which the calcite veins precipitated.

5.2. Stable isotope composition of calcite veins

Oxygen and carbon stable isotope results are documented in Table 4 and are plotted in Figure 11. Raw data are available from the data repository. Oxygen isotope values ($\delta^{18}\text{O}$) range from -6.1 to $+8.4$ ‰ and are -0.2 ‰ VPDB on average. Carbon isotope values ($\delta^{13}\text{C}$) exhibit considerably greater variability across veins with values ranging between -28.0 and $+27.5$ ‰ and are -11.8 ‰ VPDB on average.

5.3. U-Pb age of calcite veins

The U-Pb age of the Tikiore Formation calcite veins was calculated, following the method described in Parrish et al. (2018). In this approach, common ^{208}Pb is calculated by subtracting radiogenic ^{208}Pb from $^{208}\text{Pb}_{\text{total}}$. The amount of ^{208}Pb radiogenic is calculated from the measured ^{232}Th , assuming closed-system behavior for ^{232}Th - ^{208}Pb radiogenic decay. Subsequently, the $^{208}\text{Pb}_{\text{common}}/^{206}\text{Pb}$ is plotted against $^{238}\text{U}/^{206}\text{Pb}$. In this method, the x-intercept is the common Pb-corrected $^{238}\text{U}/^{206}\text{Pb}$ ratio. Multiple spot ages are plotted in an array of data for linear regression and intercept calculation using Isoplot (Ludwig, 2013). Parrish et al. (2018) demonstrated that this method results in smaller uncertainties and less regression scatter than in ^{207}Pb -corrected methods (e.g., Tera and Wasserburg, 1972). Lead ratio compositions at 0 and 85 Ma (Stacey and Kramers, 1975) have been applied to calculate the common Pb for each spot analysis. Common Pb ratios vary insignificantly

Table 3. Select REE results

Transect	Y/Ho	Eu*	Ce*	Gd*	Er*
ALL	39.26	1.11	0.89	1.01	1.05
-	31.64	1.02	0.82	0.90	0.95
+	48.68	1.23	0.96	1.11	1.12
B1A-1	42.40	1.13	0.93	1.00	1.09
-	36.48	1.06	0.86	0.91	1.04
+	49.79	1.20	0.99	1.09	1.14
B1A-2	42.53	1.12	0.94	1.00	1.08
-	35.17	1.05	0.89	0.94	1.03
+	50.81	1.19	1.00	1.08	1.13
B2A-1	46.04	1.09	0.89	1.02	1.08
-	36.76	1.01	0.80	0.96	1.02
+	61.10	1.19	0.98	1.10	1.15
B2A-2	45.91	1.10	0.88	1.04	1.11
-	35.96	1.02	0.80	0.93	1.05
+	59.14	1.19	0.94	1.12	1.18
N1A-1	53.57	0.75	0.82	1.42	1.07
-	40.68	0.69	0.68	1.25	0.99
+	65.28	0.85	0.94	1.60	1.14
W1B-1	37.52	1.25	0.77	0.62	0.85
-	23.98	0.99	0.48	0.20	0.36
+	51.53	4.79	0.89	1.00	1.09
W1B-2	37.95	1.10	0.89	1.00	1.02
-	31.07	1.01	0.83	0.90	0.96
+	46.47	1.22	0.93	1.07	1.09
X1A-1	34.17	1.08	0.85	1.01	0.96
-	28.58	1.00	0.78	0.84	0.80
+	44.54	1.27	0.90	1.10	1.03
X1A-2	37.30	1.07	0.87	1.04	1.00
-	32.48	1.01	0.81	0.98	0.98
+	54.13	1.12	0.91	1.11	1.05
X2A-1	39.30	1.06	0.83	1.04	0.98
-	29.37	0.93	0.77	0.87	0.82
+	48.89	1.33	0.88	1.22	1.06
X2A-2	30.96	1.07	0.91	1.03	0.97
-	25.59	1.01	0.88	0.96	0.91
+	38.41	1.15	0.94	1.11	1.02

Table 3 (continued)

X2B-1	37.19	1.10	0.88	1.06	1.04
-	30.07	0.99	0.80	0.97	0.96
+	48.79	1.22	0.92	1.20	1.15
X2B-2	36.79	1.10	0.91	1.04	1.03
-	30.15	1.02	0.86	0.96	0.96
+	43.90	1.21	0.99	1.11	1.10
X2B-3	37.88	1.09	0.87	1.08	1.03
-	29.42	0.98	0.82	0.98	0.94
+	48.42	1.22	0.95	1.21	1.13
X3A-1	40.00	1.10	0.93	1.03	1.06
-	34.21	1.05	0.85	0.98	1.02
+	45.42	1.15	1.01	1.09	1.10
X3A-2	42.06	1.09	0.94	1.04	1.10
-	35.25	1.05	0.88	0.98	1.06
+	46.88	1.15	1.00	1.11	1.13
X4A-1	41.93	1.14	0.87	1.00	1.05
-	32.83	0.98	0.81	0.81	0.80
+	52.48	1.38	0.93	1.14	1.17
X4A-2	36.66	1.27	0.88	0.92	1.01
-	29.73	1.10	0.81	0.65	0.78
+	45.91	1.64	0.95	1.06	1.16
X4A-3	28.76	1.22	0.95	0.96	1.03
-	22.48	1.11	0.90	0.81	0.88
+	35.00	1.37	1.00	1.09	1.09
X4A-4	37.04	1.16	0.91	0.97	1.02
-	31.16	1.07	0.85	0.88	0.90
+	43.49	1.30	0.95	1.05	1.10
X6A-1	40.74	1.10	0.91	1.03	1.09
-	34.81	1.05	0.87	0.97	1.05
+	48.03	1.15	0.96	1.09	1.12

Rare Earth Element anomalies are calculated relative to shale normalised abundances (PAAS)

Values are median results for each transect

Ranges reflect 25 percentile (-) to 75 percentile (+)

Table 4. Calcite vein isotope results

Sample	$\delta^{13}\text{C}$ (‰ VPDB)	$\delta^{18}\text{O}$ (‰ VPDB)	Inferred temperature range (°C)		
			T at 0‰ VSMOW	T at 3.5‰ VSMOW	T at 6‰ VSMOW
NIB					
NIB.1	7	8.4	-23	-10	0
NIB.2	-21.5	-0.1	12	29	42
XIB					
XIB.1	-21.9	1.8	3	19	31
XIB.2	-14.2	-0.2	12	29	42
XIB.3	-6.6	1.4	5	21	34
XIB.4	14.3	-1.2	17	35	48
X2C					
X2C.1	-19.9	-0.9	16	33	47
X2C.2	-20.9	-1.8	20	38	52
X2C.3	-21.2	-3	26	45	59
X2C.4	-10.4	-2.8	25	43	58
X2D					
X2D.1	-2.8	-0.1	12	29	42
X2D.2	-19.1	-0.3	13	30	43
X2D.3	-18.1	-1.4	18	36	49
X2D.3rep	-18.2	0.3	10	27	40
X2D.4	-11.2	0.1	11	28	41
X2D.5	-6.1	-0.9	16	33	47
X2D.6	-6.2	3	-2	13	25
X3B					
X3B.1	-3	1.7	4	20	32
X3B.2	-19.7	-6.1	43	64	80
X3B.3	-12.9	-3.1	27	45	60
X3B.3rep	-13.9	-2.4	23	41	56
X3B.4	-12.7	0.6	9	25	38
X3B.5	-18.2	-1.8	20	38	52
X3B.6	-21.1	-0.4	13	30	44
X4B					
X4B.1	0.2	-3.5	29	48	62
X4B.2	-13.5	-2.3	23	41	55
X4B.3	-14.6	-2.3	23	41	55

Table 4 (continued)

X4B.4	-19.3	-1.8	20	38	52
X4B.5	-11.6	-0.7	15	32	45
WIA					
WIA.1	-17.7	-2.3	23	41	55
WIA.2	22.2	4.9	-9	5	16
WIA.3	-26	1.2	6	22	35
WIA.3rep	-27.7	2.3	1	17	29
WIA.4	-28	-0.6	14	31	45
WIA.5	-23.5	1.1	7	23	35
BIB					
BIB.1	-6.8	3.1	-2	13	25
BIB.2	-13.2	4.4	-7	7	18
BIB.3	-6.2	-0.3	13	30	43
BIB.4	27.5	5.5	-12	2	13
B2B					
B2B.1	-9.8	-0.3	13	30	43
B2B.2	-16.6	-5.2	38	58	74

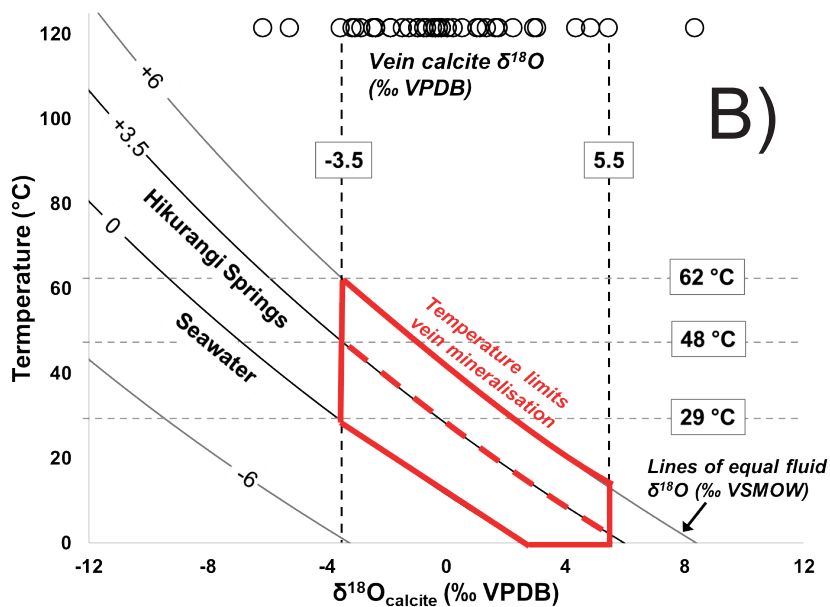
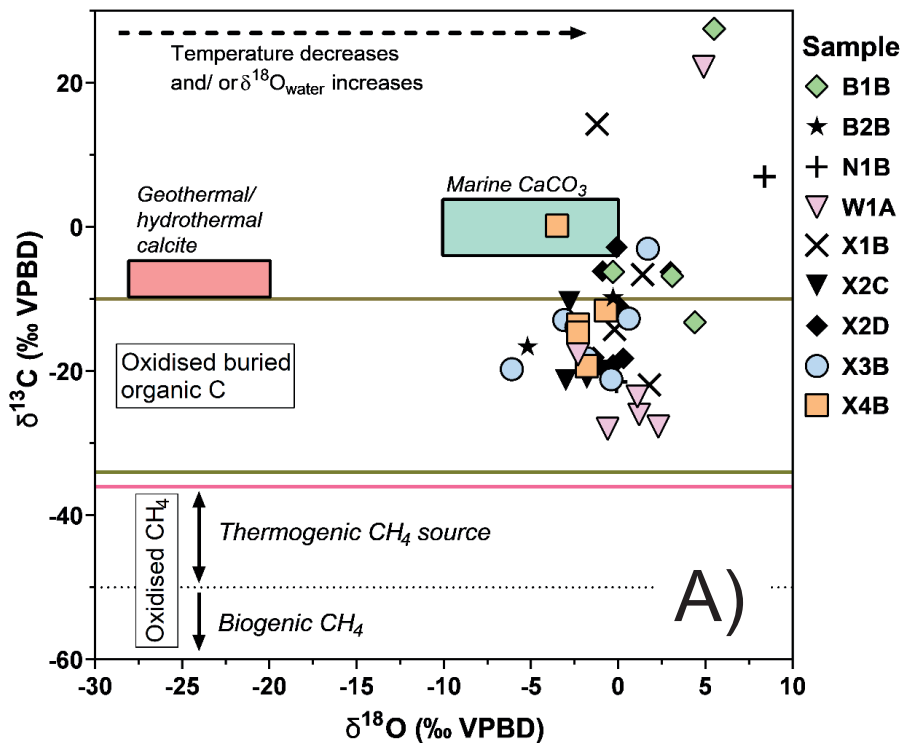
Average 1σ of $\delta^{13}\text{C}$ and $\delta^{18}\text{O}$ are 0.3 ‰ and 0.2 ‰, respectively

Vein temperatures determined using fractionation factor in Kim and O'Neil, 1997

within the 0–85 Ma period. We used common Pb ratios of 2.07 ± 0.02 for $^{208}\text{Pb}/^{206}\text{Pb}$ and 0.838 ± 0.02 for $^{207}\text{Pb}/^{206}\text{Pb}$ to anchor single spot analyses and to make the comparison between anchored and unanchored regression ages.

For quality control, $^{206}\text{Pb}_{\text{common}}$ was calculated from $^{208}\text{Pb}_{\text{common}}$ using the common Pb ratio described above. The value of $^{206}\text{Pb}_{\text{common}}$ was subsequently subtracted from $^{206}\text{Pb}_{\text{total}}$ to calculate $^{206}\text{Pb}_{\text{radiogenic}}$. If the value of $^{206}\text{Pb}_{\text{radiogenic}}$ was less than or equal to zero, a spot analysis was deemed unreliable and discarded. Analyses with $^{238}\text{U}/^{206}\text{Pb}$ uncertainty ellipses larger than 40% were also discarded. These cut-off criteria resulted in rejection of a large number of spot analyses. To derive a meaningful result, an aggregate age was calculated from all sample spot analyses for which the uncertainty ellipses were smaller than 40%. This approach assumes that vein mineralization was a transient phenomenon. Some 48 spot analyses across three samples were used to calculate a weighted mean. A table with the measured and calculated values and calculated single spot ages for these 48 spots is provided in the data repository. The weighted mean age of the single spot analyses is 28.5 ± 4.9 Ma. Three of the spot analyses fell outside the error range of the weighted mean and these analyses were therefore regarded as outliers.

Forty-five spot analyses were used to calculate the regression age using the 86T-W plot. Figure 12 illustrates the single spot age results on the Parrish et al. (2018) 86T-W plot.



◀ **Figure 11.** Carbon and oxygen isotope results for Tikiore Formation calcite vein analyses. Panel (a) $\delta^{18}\text{O}$ – $\delta^{13}\text{C}$ results plotted alongside the values of major terrestrial reservoirs. The brown lines bound the typical $\delta^{13}\text{C}$ values of oxidized terrestrial organic matter. The red horizontal line denotes the upper limit of $\delta^{13}\text{C}$ in methane. The horizontal dashed line within the methane $\delta^{13}\text{C}$ domain defines the boundary between thermogenic and biogenic formation processes. The red box defines the range of values for high-temperature calcite in modern North Island geothermal systems (Simmons and Christenson, 1994). The green box defines the range of calcite and aragonite precipitating from ocean water. In general, a move to the right for $\delta^{18}\text{O}$ reflects decreasing mineralization temperature or increases in the oxygen isotope values of fluids. The carbon isotope value ranges are from Wagner et al. (2018). Panel (b) Illustration of Tikiore Formation vein calcite fluid-mineral oxygen isotope temperature relationships. Contours of equal fluid $\delta^{18}\text{O}$ contours are plotted. The red polygon denotes the range of fluid $\delta^{18}\text{O}$ (‰ VSMOW) and temperature conditions consistent with the oxygen isotope results for calcite (‰ VPDB) reported here. The fluid-calcite $\delta^{18}\text{O}$ fractionation factor in Kim and O'Neil (1997) was used to generate fluid-temperature outcomes.

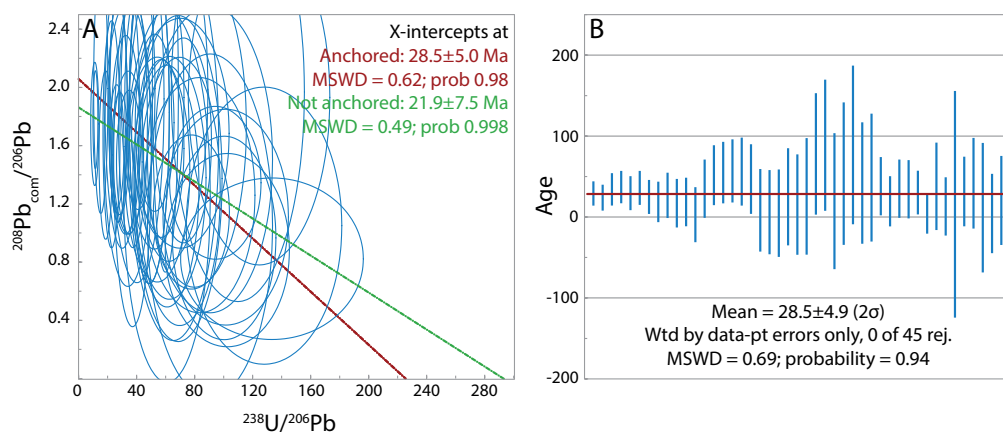


Figure 12. U-Pb age relationships determined for calcite veins from Tikiore Formation. Uncertainty ellipses and error bars are 2σ of the mean. (a) 86T-W plot determined using the method described in Parrish et al. (2018). The red line is the regression line with common Pb anchored, while the green line is the unanchored regression line. (b) Weighted mean plot of single spot ages corrected using the 208Pb method described in Parrish et al. (2018).

This results in a common Pb anchored regression age of 28.5 ± 4.9 Ma (MSWD = 0.62; probability = 0.98), whereas the unanchored regression age is 21.9 ± 7.5 Ma (MSWD = 0.49; probability = 0.998). We have adopted the Pb-anchored regression age for interpretation, given its smaller error and larger MSWD values. Also, the unanchored regression age at face value is younger than the biostratigraphic age inferred for emplacement of the ECA (Mazengarb and Speden, 2000; Rait, 1992). The ages measured on the WC-1 standard are 258.8 ± 2.7 (MSWD = 0.94) using the 86T-W regression age and 251.7 ± 4.1 (MSWD = 1.08) using the conventional T-W regression age. Both are within error of the 254.4 ± 6.4 Ma age as reported by Roberts et al. (2017).

5.4. Maximum burial temperature of Tikiore Formation and timing of cooling

To help constrain the host rock's maximum burial temperature(s) and the timing of the start of cooling, we obtained apatite fission track (AFT) and vitrinite reflectance data for a suite of sandstone samples from Tikiore Formation. Both methods are regarded as standard approaches for assessing the thermal history of sedimentary rocks. The AFT results are given in Table 5 and the VIRF results are given in Table 6.

As the ECA has a disrupted stratigraphy, constraints on the depth of burial of Tikiore Formation for use in the HeFTy thermal history modeling of AFT data can only be estimated from the Late Cretaceous–late Oligocene stratigraphy in deep drill hole Rere-1 (Figure 2), drilled into autochthonous strata immediately south of the ECA (Field et al., 1997). This drill hole intersected 1,920 m of 100–86 Ma section, overlapping in age with the Tikiore Formation exposed at Waihou Bay, and 1,680 m of 85–23 Ma section that accumulated post subduction as an overlying passive margin succession (Tinui and Maungatu groups; Figure 4). We use the two Rere-1 stratigraphic packets and their ages to constrain the Late Cretaceous–Oligocene heating in our HeFTy models (Figure 9 and S3 in Supporting Information S1).

The timing of the start of cooling of the Tikiore Formation is constrained between 30 and 24 Ma. The older limit is older than any suggestions in the literature about the timing of the start of the modern plate boundary in New Zealand and ECA emplacement; the younger limit is close to the Oligocene–Miocene boundary, which was previously regarded as when the modern plate boundary formed (e.g., Carter and Norris, 1976; Cooper et al., 1987; Field et al., 1997; Kamp, 1986). The end of the early Miocene cooling phase is constrained to be c. 14 Ma based on the unconformable accumulation of neretic mid-Miocene (Lillburnian Stage, 15.10–13.05 Ma) strata over Cretaceous accretionary wedge rocks (Pahau Terrane) located immediately east of Waihou Bay (Mazengarb and Speden, 2000). The amount of middle and late Miocene burial heating (Figure 9) is not prescribed, but the timing of its peak is constrained to be within 7.5–4 Ma, based on the timing of the start of regional uplift and erosion of Raukumara Peninsula (Mazengarb and Speden, 2000), which led to the current exposure of Tikiore Formation at Waihou Bay. Sample 1601-5 is from a location immediately east of the vein calcite occurrences (Figure 3). The measured AFT age for this sample is 33.0 ± 5.0 Ma, much younger than the stratigraphic age (99.5–95.2 Ma; Ngaterian Stage) of the sample host sandstone, but only about 5 m.y. older than its likely cooling age prior to incorporation into the ECA. This age, together with a measured mean track length around 13.8 microns, and the occurrence of some short tracks (7–8 microns), suggests qualitatively that the fission tracks were not fully annealed at the point of maximum burial; that is, the maximum burial temperature did not reach the total resetting temperature of about 110°C for fission tracks in apatite of Durango composition. The HeFTy thermal history model for sample 1601-5 indicates a maximum burial temperature of about 105°C and a start of cooling at around 28 Ma. We adopt the average path in the HeFTy model to read the maximum temperature and the timing of the start of cooling. The middle to late

Table 5. Apatite fission track results

Sample number	Number of crystals	Spontaneous			Induced		P(χ^2) %	ps/pi	pd	Nd	Age (Ma)	Mean Track Length $\pm 1\sigma$ (μm)	Standard Deviation (μm)	Number of lengths
		ps	Ns	pi	Ni									
1601-5	30	0.487	230	2.364	1117	98.18	-	0.929	2203	33.3 \pm 2.6	13.84 \pm 1.79	1.51	100	
9601-69a	20	0.458	448	1.699	1662	<0.1	0.230 \pm 0.023	0.873	4315	40.3 \pm 4.6	14.22 \pm 1.79	1.70	56	
9601-70a	15	0.227	56	1.904	469	63.2	-	0.873	4315	17.9 \pm 2.3	12.21 \pm 1.57	1.67	8	

Track densities (ρ) are $\times 106$ tracks cm^{-2} . All analyses are by the External Detector Method using 0.5 for the $4\pi/2\pi$ geometry correction factor. Apatite ages calculated using dosimeter glass SRM 612 and zeta-612 = 343.5 ± 4.5 ($\pm 1\sigma$) is the probability of obtaining χ^2 value for v degrees of freedom (where v is the number of crystals - 1) (Galbraith, 1981); pooled ps/pi ratio is used to calculate age and uncertainty where $P(\chi^2) > 5\%$; mean ps/pi ratio is reported for samples where $P(\chi^2) < 5\%$ and for which Central ages (Galbraith and Green, 1990) are calculated.

Table 6. VRIF results

Sample ID	Ro (normal) %	s.d.	Range %	Confidence	Criteria for confidence ratings
UW-1	1.42 (n=18)	0.123	1.17-1.56	Good	multiple vitrinite populations, inertinite support
UW-2	0.72 (n=11)	0.112	0.58-0.90	Good+	well defined VIRF curve including inertinite support
UW-3	0.72 (n=11)	0.138	0.56-0.93	Good+	well defined VIRF curve including inertinite support
UW-4a	1.32 (n=19)	0.092	1.17-1.44	Good+	well defined VIRF curve including inertinite support

Miocene burial heating peaked at about 45°C at 5 Ma, prior to cooling of the host rock to the surface. The goodness-of-fit (GOF) values for this HeFTy model are 1.0 for both age and length, and the “Average” and “Best” paths of 100,000 Monte Carlo simulations are similar, giving a high level of confidence in the peak burial temperature reached and the timing of the 28 Ma start of cooling (Figure 9).

Sample 9601-69a has statistically similar AFT parameters of age and track length with those for sample 1601-5 and they were not reset at the time of peak burial heating. The HeFTy model result indicates a peak burial temperature of about 104°C compared with 105°C for 1601-5 (Figure S3 in Supporting Information S1). The constraint box for 9601-69a was set at 32–25 Ma with the modeled average path cooling starting at c. 30 Ma. The GOF values are 0.92 for age and 0.70 for track length.

Sample 9601-70a was collected from a site on the western side of Orete Point more distant from the calcite vein locations than the other two AFT samples within the Arowhanan part of Tikiore Formation (Figure 3). The measured fission track age is 17.9 ± 5.1 Ma with a mean track length of 12.21 ± 1.57 microns. The measured age indicates that the AFT parameters were reset leading up to the peak of burial heating, suggesting that the formation temperature at that point exceeded 110°C. As the measured age is younger than the likely late Oligocene age of peak heating, the AFT data cannot resolve the amount and timing of peak heating. The HeFTy model (Figure S3 in Supporting Information S1) does however show middle and late Miocene burial heating to 82°C at about 4 Ma, which shortened the track lengths to 12.21 ± 1.57 microns. The GOF for the 9601-70a model is 1.00 for both age and track length.

We now consider vitrinite reflectance data (Table 6) for each of four samples. Sample UW-1 is from a thick-bedded turbidite at the same outcrop as AFT sample 1601-5 (Figure 3). Parts of sample UW-1 are heavily iron stained with framboidal pyrite altered to iron

oxide, indicative of recent weathering. The VIRF chart for UW-1 features both oxidized and unoxidized organic assemblages. Normal vitrinite in sample UW-1 of 1.42% Ro (normal) clusters toward the high reflectance end of the normal vitrinite compositional range and is consequently considered to have a high bias as some oxidized vitrinite grains are probably included in this Ro (normal) value. Thermal history modeling using HeFTy and the burial history shown for 1601-5, but varying the input maximum temperature at 28 Ma, gives a peak of about 140°C well in excess of that estimated from modeling of the AFT data for 1601-5 (c. 105°C).

Sample UW-4 is a moderately carbonaceous siltstone that exhibits considerable iron staining on weathered surfaces, but internal surfaces are unaffected and most pyrite is unaltered. This sample was collected from the same site as sample 9601-70a (Figure 3). The Ro (normal) value for this sample is 1.32%. The HeFTy modeling of this vitrinite data using the same burial history for 9601-70a, but varying the input temperature at 27 Ma, gives a maximum burial temperature of 125°C.

Sample UW-2 was taken from a turbidite sandstone bed on the shore platform close to Orete Point (Figure 3) and lies in the Teratan (90.5–86.5 Ma) part of Tikiore Formation; that is, at a stratigraphic level above the vein calcite occurrences. The measured vitrinite reflectance Ro (normal) is 0.72%, and together with inertinite data, forms a well-defined curve. The thermal history modeling using a similar burial history as for AFT sample 9601-69a, but varying the input maximum burial temperature at 30 Ma, results in a paleotemperature of about 110°C for UW-2. This is a slightly higher paleotemperature value than expected, given its higher stratigraphic position in Tikiore Formation compared with samples 9601-69a and 1,601-5 of 105°C and 104°C, respectively.

Sample UW-3 is from the highest stratigraphic level (Piripauan, 86.5–83.6 Ma) in Tikiore Formation exposed at Waihou Bay. This sandstone sample is from a turbidite with obvious plant material aligned with parallel laminations. It has unaltered pyrite and the Ro (normal) VR value is 0.72% based on an unbiased normal vitrinite assemblage. With the same measured Ro value as for sample UW-2, the maximum temperature estimate would be about 110°C, also higher by 5°C than would be expected from the AFT modeling of samples 1601-5 and 9601-69a.

6. Discussion

6.1. Isotopic constraints upon vein mineralization environment

Carbon isotope values reflect source material and the redox conditions in the fluid that precipitated vein calcite. A number of terrestrial carbon sources overlap with the $\delta^{13}\text{C}$ results for veins measured here (Figure 11). Overall, the results reflect two distinct processes common in sedimentary environments. More negative carbon isotope values (less than -10‰ VPDB) are consistent with sourcing from microbially mediated oxidized buried organic matter (approximately -30 to -10‰ VPDB) or, potentially, thermogenic methane (-50 to -20‰ VPDB) (e.g., Budai et al., 2002; Drake et al., 2015). The positive $\delta^{13}\text{C}$ values

measured, in excess of +20‰ VPDB, in several vein samples are significantly more enriched than marine and geothermal-hydrothermal CO₂ (Figure 11). The most extremely positive $\delta^{13}\text{C}$ values in the Tikiore Formation veins reflect mineralization from a highly enriched dissolved inorganic carbon (DIC) pool, resulting from bacterial methanogenesis (Budai et al., 2002; Drake et al., 2015). The enriched DIC was either sourced locally in vug spaces in vein interiors or flowed from elsewhere in the reservoir. Under semi or fully closed-system conditions within vug spaces in vein interiors, microbial processing of isotopically lighter carbon may have progressively enriched the $\delta^{13}\text{C}$ of the residual DIC.

The oxygen isotope composition of calcite reflects the isotope composition of source fluids as well as the fluid temperature at the time of vein mineralization. We apply three fluid $\delta^{18}\text{O}$ composition scenarios to the data set reported here (Figure 11). In the first scenario, fluids involved in hydraulic fracturing and vein mineralization in the Tikiore Formation were likely trapped marine pore waters that migrated through the upper part of the evolving wedge and did not undergo any isotopic enrichment. Second, present-day saline spring fluids within the Hikurangi margin that exhibit $\delta^{18}\text{O}$ values of +3.5‰ VSMOW on average (Barnes et al., 2019; Giggenbach et al., 1995; Reyes et al., 2010) are plotted. We also consider the possibility that the veins formed from a more enriched sedimentary brine of +6‰ VSMOW, analogous to deep continental fluids (Kharaka and Hanor, 2003). Some degree of enrichment above 0‰ VSMOW would not be atypical. We apply these three fluid compositional ranges (i.e., ~0 to +3.5‰ or 0 to +6 ‰ VSMOW) to establish the likely fluid temperature range at the time of vein mineralization shown in red in Figure 11. Based on this analysis, we derive the following upper bounds for fluid temperature: 29°C if we assume the fluid is an unevolved seawater at 0‰ VSMOW, 48°C assuming mineralization from average Hikurangi saline springs with a $\delta^{18}\text{O}$ value of +3.5‰ VSMOW, or 62°C assuming an evolved continental sedimentary brine at +6‰ VSMOW. From this, we infer that the fluid temperature during mineralization of the calcite veins in Tikiore Formation most likely lay between 29°C and 48°C, but may have been as high as 62°C if the fluid were isotopically enriched.

6.2. Degree of cooling of Tikiore Formation before vein formation

One purpose of estimating the burial temperatures for selected horizons in Tikiore Formation was to better characterize the degree of cooling that must have preceded the formation of the carbonate veins described here and the peak burial temperature of Tikiore Formation. AFT samples 1601-5 and 9601-69a stratigraphically and geographically bracket the exposures where the calcite veins were described and sampled and we use the modeled peak burial temperature of the more conservative slightly lower value ($104 \pm 10^\circ\text{C}$; cf., $105 \pm 10^\circ\text{C}$) to calculate the maximum burial temperature of Tikiore Formation and the difference between it and the vein calcite fluid temperature range at the time of calcite precipitation. The VRIF results provide an upper bound on the maximum burial temperature but they are consistently higher and more variable than those estimated from modeling of

the apatite fission track data. Therefore, we adopt the fission track temperatures ($104 \pm 10^\circ\text{C}$) as more realistic. For the vein mineralization temperature, rather than taking the fluid temperature values (29°C , 48°C , and 62°C) marked on Figure 11b, we have computed the mean and standard deviation temperature values at 0‰ VSMOW, +3.5‰ VSMOW, and +6‰ VSMOW from each of the sample calcite $\delta^{18}\text{O}$ results (‰ VPDB); that is, using all of the data (see data repository). The computed mean and SD temperature values are $13 \pm 13^\circ\text{C}$ at 0‰ VSMOW, $30 \pm 14^\circ\text{C}$ at +3.5‰ VSMOW, and $43 \pm 16^\circ\text{C}$ at +6‰ VSMOW. These temperature ranges are lower than those marked in Figure 11b because they use all of the isotope data as opposed to the upper temperature bound of the red box in Figure 11b. The important observation is that the computed mean temperature values and their ranges are low compared with the maximum burial temperature estimate ($104 \pm 10^\circ\text{C}$) for Tikiore Formation, indicating that most of the exhumation of Tikiore Formation must have preceded vein mineralization.

The matrix offset temperature between the conservative peak burial temperature ($104 \pm 10^\circ\text{C}$), taking account of the associated error range, and the vein mineralization temperature and its range for the +3.5‰ VSMOW estimate ($30 \pm 14^\circ\text{C}$; adopted for this calculation as it is based on the average $\delta^{18}\text{O}$ value composition of modern saline spring fluids in the Raukumara region) is 114°C – 16°C and 94°C – $44^\circ\text{C} = 98^\circ\text{C}$ – 50°C . This offset temperature range for a geothermal gradient of 25°C indicates 2.0–3.9 km of erosion of rock section from above the structural level of Tikiore Formation before the vein mineralization occurred. This compares with a total amount of 3.8–4.6 km of exhumation of Tikiore Formation based on its peak burial temperature of $104 \pm 10^\circ\text{C}$. Hence, only about 0.1–1.8 km of exhumation of Tikiore Formation postdated the calcite vein mineralization. As the U-Pb age of the vein calcite overlaps with the modeled AFT age of exhumation (30–27 Ma), the early unloading of rock section and the subsequent hydraulic fracturing and vein mineralization occurred in quick succession within the age range we can resolve for these events.

6.3. Triggering mechanisms for calcite vein growth

Field and petrographic observations, and geochemical analyses, indicate that the formation of calcite veins in Tikiore Formation involved hydraulic fracturing within normal fault zones, fluid migration, and calcite mineralization. The symmetric UV fluorescence patterns and elemental zonation across veins imply isotropic mineral growth that initiated at the outer margins of fractures and grew inward with blocky calcite partially to fully infilling vein centers during Phase 3. These patterns are consistent with a crack-seal formation mechanism (e.g., Oliver and Bons, 2001; Ramsay, 1980), where fracturing and dilation are followed by rapid infilling and mineral growth.

Some degree of fluid pumping through the fractures may also explain the development of the vein infilling textures in Tikiore Formation. Multiple brecciation and fluid events are inferred from Tikiore Formation vein samples that show deformation of early phase

infills (Table 1; Figure 6). The so-called valve model (e.g., Lee and Morse, 1999; Sibson, 1990) holds that the greatest vein growth rates occur during rapid fluid flow events along fractured channels. Given the relatively large diameter (>1 cm) of many veins in Tikiore Formation, it is likely that fluid flow and mineral infilling occurred during multiple short-lived events. Episodic pulses enable rapid migration of fluids at, or near, calcite saturation (Lee and Morse, 1999).

6.4. Exhumation and associated uplift within the Hikurangi margin

The location of the convergent plate boundary at the Late Cretaceous termination of subduction along the New Zealand sector of East Gondwana has been mapped by seismic reflection methods at depth along parts of the Hikurangi margin (Barnes et al., 2010). It lies inboard of the Hikurangi Trough (trench), reflecting subsequent Neogene outbuilding of the modern subduction margin. Tikiore Formation accumulated in an accretionary slope basin located immediately inboard of the Late Cretaceous Gondwana plate edge (Mazengarb and Harris, 1994). We interpret the vein calcite U-Pb age and the AFT modeled age range of 30–27 as dating the start of exhumation of Tikiore Formation, related to uplift of the edge of the plate at that time. Exhumation of Tikiore Formation was probably achieved by slumping of the weakly to moderately consolidated overlying sedimentary succession (Tinui and Ruatoria groups; Figure 4) off the Tikiore Formation as originally envisaged by Stoneley (1968). Figure 13 is a schematic representation of this succession of events. The early slumping process markedly reduced the lithostatic load on the fluid reservoir (either in the Tikiore Formation or in the underlying accretionary wedge), which reduced the effective stress such that the already existing fluid pressure in the reservoir was able to fracture (hydraulic fracturing) the Tikiore Formation. Our observation that calcite veins with zones of brecciation lie within normal fault zones suggests that hydraulic fracturing exploited normal faults probably associated with slumping of cover rocks from above the Tikiore Formation.

Prior work has established that the ECA was emplaced from the NE (offshore) to the SW (Rait, 1992; Stoneley, 1968) into a forearc basin, inboard, and higher up on the Australia Plate than the elevation of the lower slope position where its sediment content accumulated. Based on its mapped extent (Mazengarb and Speden, 2000), the ECA has a length of 150 km, a width of 60 km, and a thickness of about 2 km, amounting to an approximate 18,000 km³ volume. These factors require considerable uplift near the mid-Oligocene edge of the Australia Plate. We speculate that this uplift was driven by the start of subduction of the oceanic Pacific Plate beneath the outer edge of the continental Australia Plate (Figure 13).

Geodynamic models of subduction initiation involving oblique convergence predict the uplift of the overriding plate followed by its subsidence (Gurnis et al., 2004; Toth and Gurnis, 1998). Shuck et al. (2022) have recently demonstrated this sequence of events for initiation of the Puysegur subduction margin, which is the subduction zone at the southern end of the Alpine Fault (Figure 3). It has opposite polarity to the Hikurangi margin. We suggest

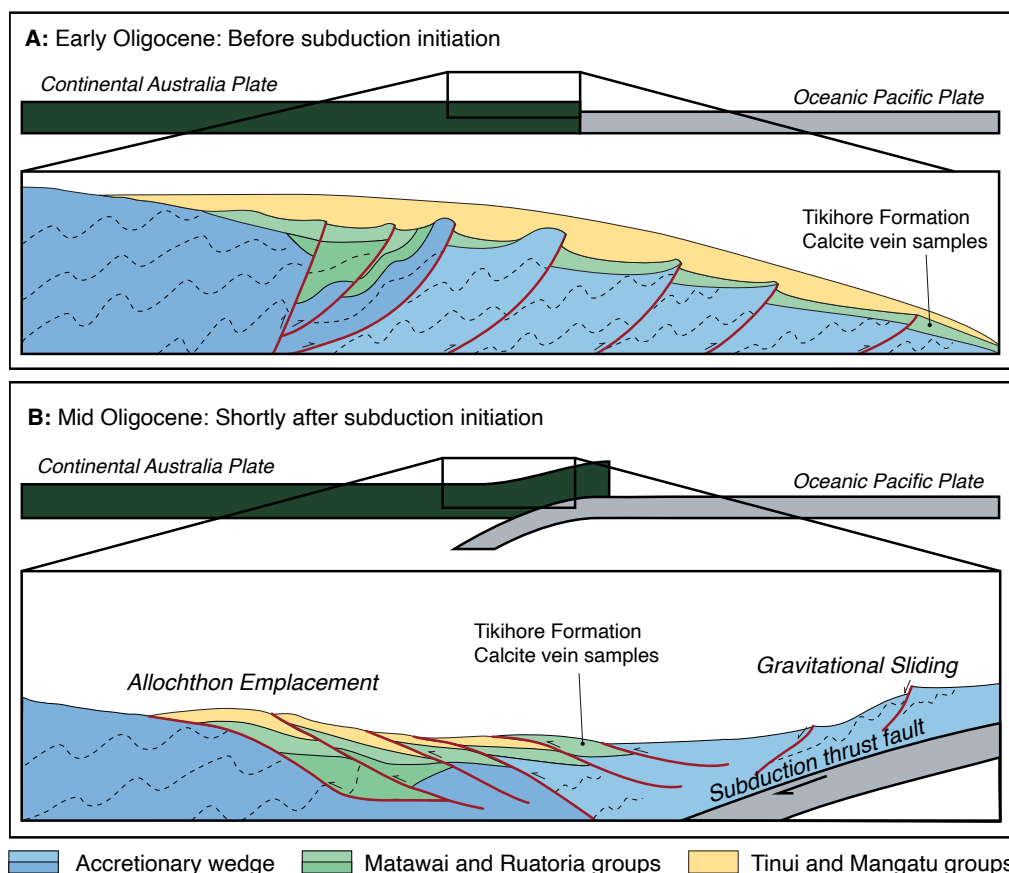


Figure 13. Schematic illustration showing in Panel A the continent-ocean juxtaposition during the early Oligocene before initiation of Pacific Plate subduction. The Torlesse Complex accretionary wedge including its basins (Matawai Group) formed during the Cretaceous involving Phoenix Plate subduction below East Gondwana. The Tinui and Mangatu groups accumulated during the latest Cretaceous and Paleogene as passive margin sediments. Panel B shows mid-Oligocene initiation of Pacific Plate subduction with uplift of the leading edge of Australia Plate, leading to gravitational sliding of the sedimentary section and part of the accretionary wedge (Mokoiwi Formation) off the structural high, forming the East Coast Allochthon on the Australia Plate.

that the Shuck et al. (2022) geological model for subduction initiation at the Puysegur margin also applies to the Hikurangi margin, in particular the uplift of the leading edge of the overriding plate as the first manifestation of subduction initiation and subsidence of the margin as the second manifestation. A difference however is that the Puysegur margin appears to have evolved out of a fault, whereas the Hikurangi margin involved subduction initiation at a continental margin that was formerly the outer edge of the upper plate of a Cretaceous subduction zone.

6.5. Supporting evidence for Hikurangi margin subduction initiation during the mid-Oligocene?

Here we discuss other geological evidence in support of our 30–27 Ma age range of subduction initiation at the Hikurangi margin. Figure 14 is a map of Zealandia at 27 Ma with the Australia Plate fixed and 800 km of late Oligocene and Neogene displacement and deformation through New Zealand restored, consistent with reconstructions by Bradshaw (1989) and King (2000). The development of the Australia-Pacific plate boundary through New Zealand occurred during two phases. The first, from 43 to 30 Ma, involved a diverse plate boundary system from south to north through western New Zealand that linked spreading in the Emerald Basin and South Tasman Sea (Cande and Stock, 2004b; Keller, 2005; Weissel et al., 1977) to a continental rift in western South Island (the Challenger Rift System; Kamp, 1986), to a foreland basin (Taranaki Foreland Basin; King and Thrasher, 1996), to a zone of structural inversion (Reinga Basin; Bache et al., 2012), and to a subduction zone immediately west of New Caledonia (Schellart et al., 2006; Chapter 1). The change in tectonic character northward along this plate boundary zone is reflected in the central New Zealand location of finite rotation poles for 40–35 and 34–30 Ma (Figure 14). These poles lie within the uncertainty ellipses derived by Keller (2005) from small circles to transform faults offsetting the Macquarie Spreading Centre in the Emerald Basin.

The second tectonic phase started with the 30–28 Ma end of east-dipping subduction in the New Caledonia margin and the start of west-dipping subduction along the new Tonga-Kermadec subduction zone (Chapter 1). The Tonga-Kermadec subduction zone rolled back to its present position northeast of Raukumara Peninsula during the early Miocene accompanied by back-arc spreading in the South Fiji Basin (Herzer et al., 2011; Mortimer et al., 2007; Chapter 1) and post 7 Ma spreading in the Lau-Havre Trough (Anderson et al., 2021) (Figure 1).

During 30–27 Ma, the Tonga-Kermadec subduction zone linked southward to the Hikurangi margin, which formed along the continent-ocean boundary of northeastern North Island (Figure 14). By 26 Ma, the Hikurangi margin had linked to the Alpine Fault, which cut obliquely across the more northerly trend of the former Challenger Rift System (Kamp, 1986). A set of finite rotation poles describing the 26 Ma onward relative motion between the Australia and Pacific plates along this second plate boundary zone are reported in Cande and Stock (2004). Furlong and Kamp (2009) derived stage poles at 1 m.y. intervals from these finite rotation poles. It is difficult to derive definitive stage poles for the interval 30–26 Ma because of the increasingly oblique deformation that occurred during the late stages of spreading along the Macquarie Spreading Center (Cande and Stock, 2004b) and also because of post-spreading deformation that distorted the transform faults offsetting the spreading ridge along the modern plate boundary zone (Hayes et al., 2009; Keller, 2005). Nevertheless, Furlong and Kamp (2009, 2013) did report them for this interval, but we adopt here a parsimonious pole route for the interval of 30–26 Ma (Figure 14). After 26 Ma, the stage poles rapidly migrated to the southeast toward the Present-day Euler pole

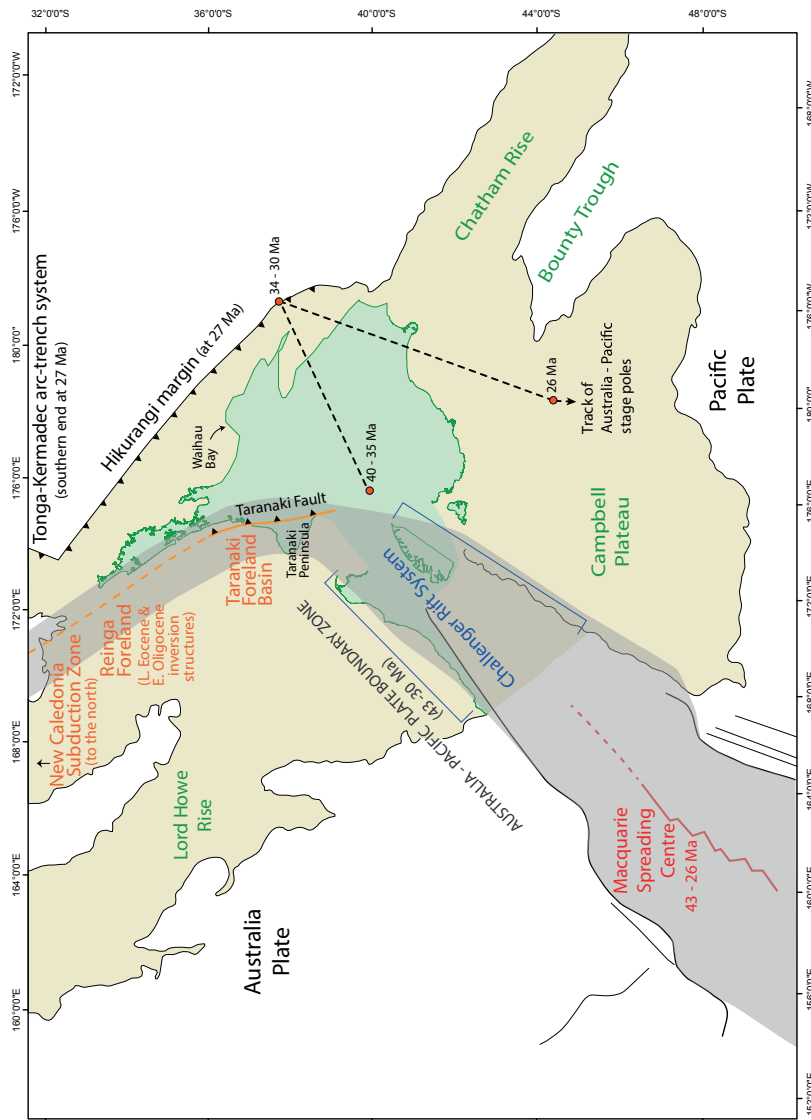


Figure 14. In this map, the Australia Plate is fixed relative to the Pacific Plate, and the continental crust of Zealandia, shown in light brown, is referenced to the current latitude and longitude as though it is all Australia Plate. The deformation taken up within the modern Australia-Pacific plate boundary zone has been restored with the conservation of area of the onland extent of New Zealand, shown in green, at 27 Ma. The map shows in a gray swath the western New Zealand extent and tectonic character of the initial (45–30 Ma) Australia-Pacific plate boundary zone through New Zealand. After 30 Ma, the Hikurangi margin formed part of a second plate boundary zone, which linked to the Alpine Fault and Puysegur Subduction Zone (neither shown here). See the text for discussion about the poles of rotation.

(Furlong and Kamp, 2009).

At 30 Ma, the finite rotation pole lay on or near what would become part of the Hikurangi margin. Our study area at Waihou Bay and the likely position of the sedimentary and volcanic succession that became the ECA lay to the north of that pole position (Figure 14). During 30–26 Ma, the direction of the pole track implies increasing rates of convergence at the Hikurangi margin. This margin also lengthened southward during this interval (Figure 14). It is reasonable therefore that sometime after 30 Ma and by 27 Ma, convergent relative plate motion would have been expressed as subduction initiation along the Hikurangi Margin.

Taranaki Basin (Figure 14), located immediately west of Taranaki Fault (King and Thrasher, 1996), carries a stratigraphic and structural record of both phases of plate boundary development through New Zealand. During 43–30 Ma, Taranaki Basin lay within the plate boundary zone and a foredeep developed along its eastern part beneath northern Taranaki Peninsula and the part of the basin farther north (King and Thrasher, 1996). This foredeep was loaded by basement beneath the Tongaporutu-Herangi High to its east, this structural high forming from upper crustal thickening within the Taranaki Fault Zone (Stagpoole and Nicol, 2008). After 30 Ma, Taranaki Fault was well oriented to accommodate displacement as a backthrust to the Hikurangi Margin (Figure 14).

Strogen et al. (2019) have recently reported the development of a new foredeep during c. 30–27 Ma, centered over the southern part of the peninsula and immediately south of it. They relate this new phase of subsidence to an unconformity developed within a piggy-back basin succession immediately east of the Herangi High (Kamp et al., 2014). We consider that the development of this second foredeep in Taranaki Basin, related to renewed thrusting within the Taranaki Fault Zone, reflects strain transferred through the crust of North Island from shortening at the nascent Hikurangi subduction zone.

7. Conclusions

1. Syntectonic vein calcite within normal fault zones that offset turbidite beds in Tikiore Formation on the rocky shore platform at Waihou Bay, northern Raukumara Peninsula, precipitated during rapid fluid flow associated with hydraulic fracturing.
2. The trace metal content and rare earth element patterns established for the calcite veins are consistent with a seawater-derived brine composition with no evidence of hydrothermal conditions.
3. The positive $\delta^{13}\text{C}$ values of the calcite veins of up to +28‰ VDPB reflect contemporary methanogenesis and preferential processing of isotopically lighter carbon remaining in the vein reservoir following the early phases of vein precipitation, which depleted its original more negative $\delta^{13}\text{C}$ content.
4. Oxygen isotope ($\delta^{18}\text{O}$) values of the vein calcite range from –6.1 to +8.4‰ and are –0.2‰ VPDB on average. Reasoning that the $\delta^{18}\text{O}$ composition of the fluids at the time of calcite mineralization likely lay between ~0 and +3.5 $\delta^{18}\text{O}$ ‰ VSMOW on

average (based on the composition of modern sea water vs. saline spring fluids, respectively, in the Raukumara region) the upper bound of mineralization likely occurred at temperatures between 29°C and 48°C. Alternatively, using all of the sample calcite $\delta^{18}\text{O}\text{‰}$ VPDB results, the mean and SD calcite fluid temperature values at mineralization are calculated to have been $13 \pm 13^\circ\text{C}$ at 0‰ VSMOW and $30 \pm 14^\circ\text{C}$ at +3.5‰ VSMOW. Both methods of deriving mineralization temperature estimates are markedly less than the maximum burial temperatures experienced by the host rocks, which we estimate to be $104 \pm 10^\circ\text{C}$ from the inverse modeling of apatite fission track data, supported by the results of vitrinite reflectance data.

5. A calcite vein has been U-Pb dated by LA-ICP-MS, yielding an age of 28.5 ± 4.9 Ma (MSWD = 0.62; probability = 0.98), using a common Pb-anchored regression.
6. We attribute fracturing and fluid migration to rapid decompression of the fluid reservoir due to the removal by submarine slumping of several km of stratigraphic section above Tikiore Formation and associated normal faulting, the slump material then contributing to the East Coast Allochthon, ultimately emplaced in a more inboard part (forearc basin) of the Australia Plate.
7. We infer the start of subduction at the Hikurangi margin to lie in the range of 30–27 Ma, consistent with the 30–28 Ma age of formation of the Tonga-Kermadec arc-trench system immediately to the north and the 30–27 Ma timing of a new phase of shortening across the Taranaki Fault Zone and related foredeep development in eastern Taranaki Basin.

Data Availability Statement

All raw LA-ICP-MS and stable isotope data are available from the data repository associated with this manuscript (Van de Lagemaat et al., 2021; <http://doi.org/10.17632/tjhzpdkvmp.1>).

Supplementary information

Supplementary information related to each chapter of this thesis can be accessed through a Google Drive folder using the following link:

<https://drive.google.com/drive/folders/1DvlHwRssdEZW8J7ST9-E9NqWcaFDAZY1>

Or by scanning the following QR code:



References

- Abbott, L. D. (1995). Neogene tectonic reconstruction of the Adelbert-Finisterre-New Britain collision, northern Papua New Guinea. *Journal of Southeast Asian Earth Sciences*, 11(1), 33-51.
- Adams, C.J., Campbell, H.J., & Griffin, W.L. (2007). Provenance comparisons of Permian to Jurassic tectonostratigraphic terranes in New Zealand: perspectives from detrital zircon age patterns. *Geological Magazine*, 144(4), 701-729.
- Adams, C.J., Campbell, H.J., Graham, I.J., & Mortimer, N. (1998). Torlesse, Waipapa and Caples suspect terranes of New Zealand: integrated studies of their geological history in relation to neighbouring terranes. *Episodes*, 21, 235-240.
- Adams, C.J., Mortimer, N., Campbell, H.J., & Griffin, W.L. (2013). The mid-cretaceous transition from basement to cover within sedimentary rocks in eastern New Zealand: evidence from detrital zircon age patterns. *Geological Magazine*, 150(3), 455-478.
- Advokaat, E. L., Hall, R., White, L. T., Watkinson, I. M., Rudyawan, A., & BouDagher-Fadel, M. K. (2017). Miocene to recent extension in NW Sulawesi, Indonesia. *Journal of Asian Earth Sciences*, 147, 378-401.
- Advokaat, E. L., Marshall, N. T., Li, S., Spakman, W., Krijgsman, W., & van Hinsbergen, D. J. (2018). Cenozoic rotation history of Borneo and Sundaland, SE Asia revealed by paleomagnetism, seismic tomography, and kinematic reconstruction. *Tectonics*, 37(8), 2486-2512.
- Advokaat, E. L., Marshall, N. T., Li, S., Spakman, W., Krijgsman, W., & van Hinsbergen, D. J. (2018). Cenozoic rotation history of Borneo and Sundaland, SE Asia revealed by paleomagnetism, seismic tomography, and kinematic reconstruction. *Tectonics*, 37(8), 2486-2512.
- Advokaat, E. L. & Van Hinsbergen, D. J. J., submitted. Finding Argoland: reconstructing a lost continent in SE Asia. *Gondwana Research*. Submitted article available via: https://drive.google.com/drive/folders/1DvIHwRssdEZW8j7ST9-E9NqWcaFDAZY1?usp=share_link
- Aita, Y., & Spörli, K. B. (1992). Tectonic and paleobiogeographic significance of radiolarian microfaunas in the Permian to Mesozoic basement rocks of the North Island, New Zealand. *Palaeogeography, Palaeoclimatology, Palaeoecology*, 96, 103-125.
- Almasco, J. N., Rodolfo, K., Fuller, M., & Frost, G. (2000). Paleomagnetism of Palawan, Philippines. *Journal of Asian Earth Sciences*, 18(3), 369-389.
- Altis, S. (1999). Origin and tectonic evolution of the Caroline Ridge and the Sorol Trough, western tropical Pacific, from admittance and a tectonic modeling analysis. *Tectonophysics*, 313(3), 271-292.
- Alvarez-Marrón, J., McClay, K. R., Harambour, S., Rojas, L., & Skarmeta, J. (1993). Geometry and evolution of the frontal part of the Magallanes foreland thrust and fold belt (Vicuña area), Tierra del Fuego, southern Chile. *AAPG bulletin*, 77(11), 1904-1921.
- Alvarez-Marron, J., Brown, D., Camanni, G., Wu, Y. M., & Kuo-Chen, H. (2014). Structural complexities in a foreland thrust belt inherited from the shelf-slope transition: Insights from the Alishan area of Taiwan. *Tectonics*, 33(7), 1322-1339.
- Amante, C., & Eakins, B. W. (2009). ETOPO1 1 arc-minute global relief model: Procedures, data sources and analysis. In NOAA technical memorandum NESDIS NGDC-24 (pp. 1- 19). National Geophysical Data Center: NOAA.
- Amaru, M. L. (2007). Global travel time tomography with 3-D reference models. Ph. D thesis, Utrecht University, the Netherlands.
- Amiruddin, A. (2009). A review on Permian to triassic active or convergent margin in southeasternmost gondwanaland: possibility of exploration target for tin and hydrocarbon deposits in the Eastern Indonesia. *Indonesian Journal on Geoscience*, 4(1), 31-41.
- An, M., Wiens, D.A., Zhao, Y., Feng, M., Nyblade, A.A., Kanao, M., Li, Y., Maggi, A., & Lévêque, J.J. (2015). S-velocity model and inferred Moho topography beneath the Antarctic Plate from Rayleigh waves. *Journal of Geophysical Research: Solid Earth*, 120(1), 359-383.
- Andal, E. S., Arai, S., & Yumul Jr, G. P. (2005). Complete mantle section of a slow-spreading ridge-derived ophiolite: An example from the Isabela ophiolite in the Philippines. *Island Arc*, 14(3), 272-294.
- Anderson, M. O., Norris-Julseth, C., Rubin, K. H., Haase, K., Hannington, M. D., Baxter, A. T., & Stewart, M. S. (2021). Geologic and structural evolution of the NE Lau Basin, Tonga: Morphotectonic analysis and classification of structures using shallow seismicity. *Frontiers in Earth Sciences*, 9, 665185.
- Arai, R., Kodaira, S., Yuka, K., Takahashi, T., Miura, S., & Kaneda, Y. (2017). Crustal structure of the southern Okinawa Trough: Symmetrical rifting, submarine volcano, and potential mantle accretion in the continental back-arc basin. *Journal of Geophysical Research: Solid Earth*, 122(1), 622-641.
- Arcilla, C. A., Ruelo, H. B., & Umbal, J. (1989). The Angat ophiolite, Luzon, Philippines: lithology, structure,

- and problems in age interpretation. *Tectonophysics*, 168(1-3), 127-135.
- Arculus, R. J., Ishizuka, O., Bogus, K. A., Gurnis, M., Hickey-Vargas, R., Aljahdali, M. H., ... & Zhang, Z. (2015). A record of spontaneous subduction initiation in the Izu–Bonin–Mariana arc. *Nature Geoscience*, 8(9), 728-733.
- Arkula, C., Lom, N., Wakabayashi, J., Rea-Downing, G., Qayyum, A., Dekkers, M. J., ... & van Hinsbergen, D. J. (2023). The forearc ophiolites of California formed during trench-parallel spreading: Kinematic reconstruction of the western USA Cordillera since the Jurassic. *Earth-Science Reviews*, 237, 104275.
- Atwater, T., & Severinghaus, J. (1989). Tectonic maps of the northeast Pacific. In E.L. Winterer, D.M. Hussong, & R.W. Decker (Eds.), *The Eastern Pacific Ocean and Hawaii*. Geological Society of America.
- Atwater, T., 1989. Plate tectonic history of the northeast Pacific and western North America. *The eastern Pacific Ocean and Hawaii*: Boulder, Colorado, Geological Society of America, *Geology of North America*, v. N: 21-72.
- Aurelio, M. A. (2000). Shear partitioning in the Philippines: constraints from Philippine Fault and global positioning system data. *Island Arc*, 9(4), 584-597.
- Aurelio, M. A., Barrier, E., Rangin, C., & Müller, C. (1991). The Philippine Fault in the late Cenozoic tectonic evolution of the Bondoc-Masbate-N. Leyte area, central Philippines. *Journal of Southeast Asian Earth Sciences*, 6(3-4), 221-238.
- Aurelio, M. A., Forbes, M. T., Taguibao, K. J. L., Savella, R. B., Bacud, J. A., Franke, D., ... & Carranza, C. D. (2014). Middle to Late Cenozoic tectonic events in south and central Palawan (Philippines) and their implications to the evolution of the south-eastern margin of South China Sea: Evidence from onshore structural and offshore seismic data. *Marine and Petroleum Geology*, 58, 658-673.
- Auzemery, A., Willingshofer, E., Yamato, P., Duretz, T., & Sokoutis, D. (2020). Strain localization mechanisms for subduction initiation at passive margins. *Global and Planetary Change*, 195, 103323.
- Auzende, J.-M., Pelletier B., Eissen, J. Ph., (1995). The North Fiji Basin, geology structure and geodynamic evolution. In: *Back-arc Basins: Tectonics and magmatism*, edited by Brian Taylor, Plenum Press, New York. 139– 175.
- Auzende, J.M., Pelletier, B., & Eissen, J.P. (1995). The North Fiji Basin geology, structure, and geodynamic evolution. In *Backarc Basins* (pp. 139-175). Springer.
- Bache, F., Sutherland, R., Stagpoole, V., Herzer, R., Collot, J., & Rouillard, P. (2012). Stratigraphy of the southern Norfolk Ridge and the Reinga Basin: A record of initiation of Tonga-Kermadec-Northland subduction in the southwest Pacific. *Earth and Planetary Science Letters*, 321–322, 41– 53.
- Bailly, V., Pubellier, M., Ringenbach, J. C., De Sigoyer, J., & Sapin, F. (2009). Deformation zone ‘jumps’ in a young convergent setting; the Lengguru fold-and-thrust belt, New Guinea Island. *Lithos*, 113(1-2), 306-317.
- Baker, P. E., Coltorti, M., Briquieu, L., Hasenaka, T., Condcliffe, E., & Crawford, A. J. (1994). Petrology and composition of the volcanic basement of Bougainville Guyot, Site 831. *Proceeding of the Ocean Drilling Program, Scientific Results*, 134, 363– 373.
- Baker, S., & Malaihollo, J. (1996). Dating of Neogene igneous rocks in the Halmahera region: arc initiation and development. *Geological Society, London, Special Publications*, 106(1), 499-509.
- Bakhmutov, V., & Shpyra, V. (2011). Palaeomagnetism of Late Cretaceous-Paleocene igneous rocks from the western part of the Antarctic Peninsula (Argentine Islands Archipelago). *Geological Quarterly*, 55, 285-300.
- Baldwin, S. L., Fitzgerald, P. G., & Webb, L. E. (2012). Tectonics of the New Guinea region. *Annual Review of Earth and Planetary Sciences*, 40, 495-520.
- Baldwin, S. L., Lister, G. S., Hill, E. J., Foster, D. A., & McDougall, I. (1993). Thermochronologic constraints on the tectonic evolution of active metamorphic core complexes, D'Entrecasteaux Islands, Papua New Guinea. *Tectonics*, 12(3), 611-628.
- Baldwin, S. L., Monteleone, B. D., Webb, L. E., Fitzgerald, P. G., Grove, M., & June Hill, E. (2004). Pliocene eclogite exhumation at plate tectonic rates in eastern Papua New Guinea. *Nature*, 431(7006), 263-267.
- Baldwin, S. L., Webb, L. E., & Monteleone, B. D. (2008). Late Miocene coesite-eclogite exhumed in the Woodlark Rift. *Geology*, 36(9), 735-738.
- Ballance, P. F. (1976). Evolution of the upper Cenozoic magmatic arc and plate boundary in northern New Zealand. *Earth and Planetary Science Letters*, 28(3), 356– 370.
- Ballance, P. F. (1993). South Pacific sedimentary basins (p. 143). Elsevier.
- Ballance, P. F., & Campbell, J. D. (1993). A murihiku arc-related basin of New Zealand (Triassic–Jurassic). In P. F. Ballance (Ed.), *South Pacific sedimentary basins* (pp. 21–33). Amsterdam: Elsevier.
- Ballance, P. F., & Spörl, K. B. (1979). Northland allochthon. *Journal of the Royal Society of New Zealand*, 9(2), 259-275.

- Ballance, P. F., Hayward, B. W., & Brook, F. J. (1985). Subduction regression of volcanism in New Zealand. *Nature*, 313(6005), 820.
- Ballance, P. F., Heming, R. F., & Sameshima, T. (1980). Petrography of the youngest known Murihiku Supergroup, New Zealand: latest Jurassic arc volcanism on the southern margin of Gondwana. In M. M. Cresswell & P. Vella (Eds.), *Gondwana five* (pp. 161–165). Rotterdam: Balkema.
- Ballantyne, P. (1991). Petrological constraints upon the provenance and genesis of the East Halmahera ophiolite. *Journal of Southeast Asian Earth Sciences*, 6(3-4), 259–269.
- Ballantyne, P. D.; (1990). The petrology of the ophiolitic rocks of the Halmahera region, Indonesia. Doctoral thesis (Ph.D), UCL (University College London).
- Balmater, H. G., Manalo, P. C., Faustino-Eslava, D. V., Queaño, K. L., Dimalanta, C. B., Guotana, J. M. R., Ramos, N. T., Payot, B. D., & Yumul Jr, G. P. (2015). Paleomagnetism of the Samar Ophiolite: Implications for the Cretaceous sub-equatorial position of the Philippine island arc. *Tectonophysics*, 664, 214–224.
- Balmater, H. G., Manalo, P. C., Faustino-Eslava, D. V., Queaño, K. L., Dimalanta, C. B., Guotana, J. M. R., ... & Yumul Jr, G. P. (2015). Paleomagnetism of the Samar Ophiolite: Implications for the Cretaceous sub-equatorial position of the Philippine island arc. *Tectonophysics*, 664, 214–224.
- Barckhausen, U., Ranero, C.R., Cande, S.C., Engels, M., & Weinrebe, W. (2008). Birth of an intraoceanic spreading center. *Geology*, 36(10), 767–770.
- Barckhausen, U., Ranero, C.R., von Huene, R., Cande, S.C., & Roeser, H.A. (2001). Revised tectonic boundaries in the Cocos Plate off Costa Rica: Implications for the segmentation of the convergent margin and for plate tectonic models. *Journal of Geophysical Research: Solid Earth*, 106(B9), 19207–19220.
- Barker, P. F. (1970). Plate tectonics of the Scotia Sea region. *Nature*, 228, 1293–1296.
- Barker, P. F. (1991). Tectonic development of the Scotia Arc region. *Geology of Antarctica*, 6, 215–248.
- Barker, P. F. (1995). Tectonic framework of the east Scotia Sea. *Backarc Basins: Tectonics and Magmatism*, 281–314.
- Barker, P. F. (2001). Scotia Sea regional tectonic evolution: implications for mantle flow and palaeocirculation. *Earth-Science Reviews*, 55(1–2), 1–39.
- Barker, P. F., & Jahn, R. A. (1980). A marine geophysical reconnaissance of the Weddell Sea. *Geophysical Journal International*, 63(1), 271–283.
- Barker, P. F., & Lawver, L. A. (1988). South American–Antarctic plate motion over the past 50 Myr, and the evolution of the South American–Antarctic Ridge. *Geophysical Journal International*, 94(3), 377–386.
- Barker, P. F., Barber, P. L., & King, E. C. (1984). An early Miocene ridge crest–trench collision on the South Scotia Ridge near 36°W. *Tectonophysics*, 102(1–4), 315–332.
- Barker, P. F., Hill, I. A., Weaver, S. D., & Pankhurst, R. J. (1982). The origin of the eastern South Scotia Ridge as an intraoceanic island arc.
- Barker, P.F. (1982). The Cenozoic subduction history of the Pacific margin of the Antarctic Peninsula: ridge crest–trench interactions. *Journal of the Geological Society*, 139(6), 787–801.
- Barker, S. L., Cox, S. F., Eggins, S. M., & Gagan, M. K. (2006). Microchemical evidence for episodic growth of antitaxial veins during fracture-controlled fluid flow. *Earth and Planetary Science Letters*, 250(1–2), 331–344.
- Barker, S. L., Dipple, G. M., Dong, F., & Baer, D. S. (2011). Use of laser spectroscopy to measure the $^{13}\text{C}/^{12}\text{C}$ and $^{18}\text{O}/^{16}\text{O}$ compositions of carbonate minerals. *Analytical Chemistry*, 83(6), 2220–2226.
- Barnes, J. D., Cullen, J., Barker, S., Agostini, S., Penniston-Dorland, S., Lassiter, J. C., et al. (2019). The role of the upper plate in controlling fluid-mobile element (Cl, Li, B) cycling through subduction zones: Hikurangi forearc, New Zealand. *Geosphere*, 15(3), 642–658.
- Barnes, P. M., Lamarche, G., Bialas, J., Henrys, S., Pecher, I., Netzeband, G. L., et al. (2010). Tectonic and geological framework for gas hydrates and cold seeps on the Hikurangi subduction margin, New Zealand. *Marine Geology*, 272(1–4), 26–48.
- Barrier, A., Nicol, A., Browne, G.H., & Bassett, K.N. (2020). Late Cretaceous coeval multi-directional extension in South Zealandia: Implications for eastern Gondwana breakup. *Marine and Petroleum Geology*, 118, 104383.
- Barrier, E., Huchon, P., & Aurelio, M. (1991). Philippine fault: A key for Philippine kinematics. *Geology*, 19(1), 32–35.
- Bas, M. L., Maitre, R. L., Streckeisen, A., Zanettin, B., & IUGS Subcommittee on the Systematics of Igneous Rocks. (1986). A chemical classification of volcanic rocks based on the total alkali–silica diagram. *Journal of Petrology*, 27(3), 745–750.
- Batara, B., & Xu, C. (2022). Evolved magmatic arcs of South Borneo: Insights into Cretaceous slab subduction. *Gondwana Research*, 111, 142–164.
- Battan, R., Chung, S. L., Komiya, T., Maruyama, S., Lin, A. T., Lee, H. Y., & Iizuka, Y. (2022, December).

- Zircon U-Pb Ages and Geochemical Characteristics of Magmatic Rocks from Choiseul and Santa Isabel, Solomon Islands: Implications for the Magmatic and Tectonic Evolution in SW Pacific. In AGU Fall Meeting Abstracts (Vol. 2022, pp. V12C-0058).
- Beach, A. (1980). Numerical models of hydraulic fracturing and the interpretation of syntectonic veins. *Journal of Structural Geology*, 2(4), 425–438.
- Behrendt, J.C. (1999). Crustal and lithospheric structure of the West Antarctic Rift System from geophysical investigations—a review. *Global and Planetary Change*, 23(1-4), 25-44.
- Beiersdorf, H., Bach, W., Delisle, G., Faber, E., Gerling, P., Hinz, K., & Dheeradilok, P. (1997). Age and possible modes of formation of the Celebes Sea basement, and thermal regimes within the accretionary complexes off SW Mindanao and N Sulawesi. In *Proceedings of the International Conference on Stratigraphy and Tectonic Evolution of Southeast Asia and the South Pacific* (pp. 369-387).
- Beinlich, A., Barker, S. L., Dipple, G. M., Gupta, M., & Baer, D. S. (2017). Stable isotope ($\delta^{13}\text{C}$, $\delta^{18}\text{O}$) analysis of sulfide-bearing carbonate samples using laser absorption spectrometry. *Economic Geology*, 112(3), 693–700.
- Bellon, H. & Rangin, C. (1991). Geochemistry and isotopic dating of Cenozoic volcanic arc sequences around the Celebes and Sulu Seas. *Proceedings of the Ocean Drilling Program Scientific Results*, 124, 321-338.
- Bellon, H., & Yumul Jr, G. P. (2000). Mio-Pliocene magmatism in the Baguio Mining District (Luzon, Philippines): age clues to its geodynamic setting. *Comptes Rendus de l'Académie des Sciences-Series IIA-Earth and Planetary Science*, 331(4), 295-302.
- Beniest, A., & Schellart, W. P. (2020). A geological map of the Scotia Sea area constrained by bathymetry, geological data, geophysical data and seismic tomography models from the deep mantle. *Earth-Science Reviews*, 210, 103391.
- Benyshek, E. K., & Taylor, B. (2021). Tectonics of the Papua-Woodlark Region. *Geochemistry, Geophysics, Geosystems*, 22(1), e2020GC009209.
- Benyshek, E.K., Wessel, P., & Taylor, B. (2019). Tectonic Reconstruction of the Ellice Basin. *Tectonics*, 38(11), 3854-3865.
- Bergman, S. C., Hutchison, C. S., Swauger, D. A., & Graves, J. E. (2000). K: Ar ages and geochemistry of the Sabah Cenozoic volcanic rocks. *Geological society of Malaysia Bulletin* 44, 165-171.
- Berly, T. (2005). Ultramafic and mafic rock types from Choiseul, Santa Isabel and Santa Jorge (Northeastern Solomon Islands): origins and significance (Doctoral dissertation, Université Joseph-Fourier-Grenoble I).
- Berly, T. J., Hermann, J., Arculus, R. J., & Lapierre, H. (2006). Supra-subduction zone pyroxenites from San Jorge and Santa Isabel (Solomon Islands). *Journal of Petrology*, 47(8), 1531-1555.
- Bernard, A., Munschy, M., Rotstein, Y., & Sauter, D. (2005). Refined spreading history at the Southwest Indian Ridge for the last 96 Ma, with the aid of satellite gravity data. *Geophysical Journal International*, 162(3), 765-778.
- Bernardel, G., Carson, L., Meffre, S., Symonds, P., & Mauffret, A. (2002). Geological and morphological framework of the Norfolk Ridge to Three Kings Ridge region (p. 76). Canberra: Geoscience Australia.
- Betka, P. (2013). Structure of the Patagonian Fold-Thrust Belt in the Magallanes Region of Chile, 53–55 Degrees S Lat (Ph. D. dissertation): Austin, Texas, University of Texas at Austin.
- Betka, P., Klepeis, K., & Mosher, S. (2015). Along-strike variation in crustal shortening and kinematic evolution of the base of a retroarc fold-and-thrust belt: Magallanes, Chile 53° S–54° S. *Bulletin*, 127(7-8), 1108-1134.
- Betka, P., Klepeis, K., & Mosher, S. (2016). Fault kinematics of the Magallanes-Fagnano fault system, southern Chile; an example of diffuse strain and sinistral transtension along a continental transform margin. *Journal of Structural Geology*, 85, 130-153.
- Bevis, M., Taylor, F. W., Schutz, B. E., Recy, J., Isacks, B. L., Helu, S., et al. (1995). Geodetic observations of very rapid convergence and back-arc extension at the Tonga arc. *Nature*, 374(6519), 249–251.
- Biddle, K. T., Uliana, M. A., Mitchum Jr, R. M., Fitzgerald, M. G., & Wright, R. C. (1986). The stratigraphic and structural evolution of the central and eastern Magallanes Basin, southern South America. *Foreland basins*, 41-61.
- Bijl, P. K., Bendle, J. A., Bohaty, S. M., Pross, J., Schouten, S., Tauxe, L., ... & Yamane, M. (2013). Eocene cooling linked to early flow across the Tasmanian Gateway. *Proceedings of the National Academy of Sciences*, 110(24), 9645-9650.
- Bijl, P. K., Houben, A. J., Hartman, J. D., Pross, J., Salabarnada, A., Escutia, C., & Sangiorgi, F. (2018). Paleooceanography and ice sheet variability offshore Wilkes Land, Antarctica—Part 2: Insights from Oligocene–Miocene dinoflagellate cyst assemblages. *Climate of the Past*, 14(7), 1015-1033.
- Bijwaard, H., Spakman, W., & Engdahl, E. R. (1998). Closing the gap between regional and global travel time tomography. *Journal of Geophysical Research*, 103(B12), 30,055–30,078.

- Billedo, E. B. (1996). The pre-Tertiary ophiolitic complex of northeastern Luzon and the Polillo group of islands, Philippines. *Journal of the Geological Society of the Philippines*, 51, 95-114.
- Billedo, E. B., Stephan, J. F., Delteilt, J., Bellon, H., Sajona, F., Feraud, G. (1996). The pre-Tertiary ophiolitic complex of northeastern Luzon and the Polillo group of islands, Philippines. *Journal of the Geological Society of the Philippines*, 51, 95-114.
- Billen, M.I., & Stock, J. (2000). Morphology and origin of the Osbourn Trough. *Journal of Geophysical Research: Solid Earth*, 105(B6), 13481-13489.
- Bingham, R. G., Ferraccioli, F., King, E. C., Larter, R. D., Pritchard, H. D., Smith, A. M., & Vaughan, D. G. (2012). Inland thinning of West Antarctic Ice Sheet steered along subglacial rifts. *Nature*, 487(7408), 468-471.
- Bird, P. (2003). An updated digital model of plate boundaries. *Geochemistry, Geophysics, Geosystems*, 4(3).
- Bladon, G. M. (1988). Catalogue, appraisal and significance of K-Ar isotopic ages determined for igneous and metamorphic rocks in Irian Jaya. Geological Research and Development Centre, Bandung, Indonesia. Preliminary Geological Report, 86.
- Blail, U. (1982). Paleomagnetism of Deep Sea Drilling Project Leg 60 Sediments and Igneous Rocks from the Mariana Region. *Deep Sea Drill. Proj.* 60, 855-873.
- Bloomer, S. H., Taylor, B., MacLeod, C. J., Stern, R. J., Fryer, P., Hawkins, J. W., & Johnson, L. (1995). Early arc volcanism and the ophiolite problem: A perspective from drilling in the western Pacific. In B. Taylor, & J. Natland (Eds.), *Active Margins and Marginal Basins of the Western Pacific*, American Geophysical Union Geophysical Monograph (Vol. 88, pp. 1–30). Washington, DC: American Geophysical Union.
- Bohoyo, F., Galindo-Zaldívar, J., Maldonado, A., Schreider, A. A., & Surinach, E. (2002). Basin development subsequent to ridge-trench collision: the Jane Basin, Antarctica. *Marine Geophysical Researches*, 23, 413-421.
- Boschman, L. M., van Hinsbergen, D. J., & Spakman, W. (2021a). Reconstructing Jurassic-Cretaceous Intra-Oceanic Subduction Evolution in the Northwestern Panthalassa Ocean Using Ocean Plate Stratigraphy From Hokkaido, Japan. *Tectonics*, 40(8), e2019TC005673.
- Boschman, L. M., Van Hinsbergen, D. J., Langereis, C. G., Flores, K. E., Kamp, P. J., Kimbrough, D. L., ... & Spakman, W. (2021b). Reconstructing lost plates of the Panthalassa Ocean through paleomagnetic data from circum-Pacific accretionary orogens. *American Journal of Science*, 321(6), 907-954.
- Boschman, L. M., van Hinsbergen, D. J., Torsvik, T. H., Spakman, W., & Pindell, J. L. (2014). Kinematic reconstruction of the Caribbean region since the Early Jurassic. *Earth-Science Reviews*, 138, 102-136.
- Boschman, L.M., & Van Hinsbergen, D.J.J. (2016). On the enigmatic birth of the Pacific Plate within the Panthalassa Ocean. *Science Advances*, 2(7), e1600022.
- Boschman, L.M., Van der Wiel, E., Flores, K.E., Langereis, C.G., & Van Hinsbergen, D.J.J. (2019). The Caribbean and Farallon plates connected: Constraints from stratigraphy and paleomagnetism of the Nicoya Peninsula,
- Boyden, J. A., Müller, R. D., Gurnis, M., Torsvik, T. H., Clark, J. A., Turner, M., ... & Cannon, J. S. (2011). Next-generation plate-tectonic reconstructions using GPlates. *Geoinformatics: Cyberinfrastructure for the Solid Earth Sciences*, Cambridge University Press, Cambridge (2011), pp. 95-113
- Boyden, J., Müller, R. D., Gurnis, M., Torsvik, T. H., Clark, J., Turner, M., et al. (2011). Next-generation plate-tectonic reconstructions using GPlates. In R. Keller, & C. Baru (Eds.), *Geoinformatics: Cyberinfrastructure for the solid earth sciences* (pp. 95–113). Cambridge: Cambridge University Press.
- Bradshaw, J. D. (1989). Cretaceous geotectonic patterns in the New Zealand region. *Tectonics*, 8(4), 803–820.
- Bradshaw, J. D. (1994). Brook street and Murihiku terranes of New Zealand in the context of a mobile south pacific Gondwana margin. *Journal of South American Earth Sciences*, 7, 325–332.
- Bradshaw, J. D., Weaver, S. D., & Muir, R. J. (1996). Mid-Cretaceous oroclinal bending of New Zealand terranes. *New Zealand Journal of Geology and Geophysics*, 39, 461–468.
- Breitfeld, H. T., Davies, L., Hall, R., Armstrong, R., Forster, M., Lister, G., Thirlwall, M., Grassineau, N., Hennig-Breitfeld, J. & van Hattum, M. W. (2020). Mesozoic paleo-Pacific subduction beneath SW Borneo: U-Pb geochronology of the Schwaner granitoids and the Pinoh metamorphic group. *Frontiers in Earth Science*, 8, 568715.
- Breitfeld, H. T., Hall, R., Galin, T., & BouDagher-Fadel, M. K. (2018). Unravelling the stratigraphy and sedimentation history of the uppermost Cretaceous to Eocene sediments of the Kuching Zone in West Sarawak (Malaysia), Borneo. *Journal of Asian Earth Sciences*, 160, 200-223.
- Breitfeld, H. T., Hall, R., Galin, T., Forster, M. A., & BouDagher-Fadel, M. K. (2017). A Triassic to Cretaceous Sundaland–Pacific subduction margin in West Sarawak, Borneo. *Tectonophysics*, 694, 35-56.
- Briais, A., Patriat, P., & Tapponnier, P. (1993). Updated interpretation of magnetic anomalies and seafloor

- spreading stages in the South China Sea: Implications for the Tertiary tectonics of Southeast Asia. *Journal of Geophysical Research: Solid Earth*, 98(B4), 6299–6328.
- Briggs, R. M., Middleton, M. P., & Nelson, C. S. (2004). Provenance history of a late Triassic-Jurassic Gondwana margin forearc basin, Murihiku Terrane, North Island, New Zealand: petrographic and geochemical constraints. *New Zealand Journal of Geology and Geophysics*, 47, 589–602.
- Brocher, T. M. (1985). On the formation of the Vitiaz Trench lineament and North Fiji Basin. *Geological investigations of the Northern Melanesian Borerland*, Circum-Pacific Council for Energy and Mineral Resources Earth Science Series 3, 13–33.
- Brothers, R. N., & Delaloye, M. (1982). Obducted ophiolites of North Island: Origin, age, emplacement and tectonic implications for tertiary and quaternary volcanicity. *New Zealand Journal of Geology and Geophysics*, 25(3), 257–274.
- Brown, D., Alvarez-Marron, J., Camanni, G., Biete, C., Kuo-Chen, H., & Wu, Y. M. (2022). Structure of the south-central Taiwan fold-and-thrust belt: Testing the viability of the model. *Earth-Science Reviews*, 231, 104094.
- Brown, D., Alvarez-Marron, J., Biete, C., Kuo-Chen, H., Camanni, G., & Ho, C. W. (2017). How the structural architecture of the Eurasian continental margin affects the structure, seismicity, and topography of the south central Taiwan fold-and-thrust belt. *Tectonics*, 36(7), 1275–1294.
- Brown, D., Ryan, P. D., Byrne, T., Chan, Y. C., Rau, R. J., Lu, C. Y., ... & Wang, Y. J. (2011). The arc–continent collision in Taiwan. *Arc-continent collision*, 213–245.
- Brown, K. M., Bekins, B., Clennell, B., Dewhurst, D., & Westbrook, G. (1994). Heterogeneous hydrofracture development and accretionary fault dynamics. *Geology*, 22(3), 259–262.
- Budai, J. M., Martini, A. M., Walter, L. M., & Ku, T. C. W. (2002). Fracture-fill calcite as a record of microbial methanogenesis and fluid migration: A case study from the Devonian Antrim Shale, Michigan basin. *Geofluids*, 2(3), 163–183.
- Burns, K. L., Rickard, M. J., Belbin, L., & Chamalaun, F. (1980). Further palaeomagnetic confirmation of the Magellanes orocline. *Tectonophysics*, 63(1–4), 75–90.
- Burton-Johnson, A., & Riley, T.R. (2015). Autochthonous v. Accreted terrane development of continental margins: a revised in situ tectonic history of the Antarctic Peninsula. *Journal of the Geological Society*, 172(6), 822–835.
- Burton-Johnson, A., Macpherson, C. G., Millar, I. L., Whitehouse, M. J., Ottley, C. J., & Nowell, G. M. (2020). A Triassic to Jurassic arc in north Borneo: Geochronology, geochemistry, and genesis of the Segama Valley Felsic Intrusions and the Sabah ophiolite. *Gondwana Research*, 84, 229–244.
- Butler, R. F. (1992). *Paleomagnetism: magnetic domains to geologic terrains*. Boston, MA: Backwell Scientific Publications.
- Butterworth, P. J., Crame, J. A., Howlett, P. J., & Macdonald, D. I. M. (1988). Lithostratigraphy of upper jurassic-lower cretaceous strata of eastern Alexander Island, Antarctica. *Cretaceous Research*, 9(3), 249–264.
- Buys, J., Spandler, C., Holm, R. J., & Richards, S. W. (2014). Remnants of ancient Australia in Vanuatu: Implications for crustal evolution in island arcs and tectonic development of the southwest Pacific. *Geology*, 42(11), 939–942.
- Calderon, M., Fildani, A., Hervé, F., Fanning, C. M., Weislogel, A., & Cordani, U. (2007). Late Jurassic bimodal magmatism in the northern sea-floor remnant of the Rocas Verdes basin, southern Patagonian Andes. *Journal of the Geological Society*, 164(5), 1011–1022.
- Camanni, G., & Ye, Q. (2022). The significance of fault reactivation on the Wilson cycle undergone by the northern South China Sea area in the last 60 Myr. *Earth-Science Reviews*, 225, 103893.
- Campbell, H. J., Mortimer, N., & Turnbull, I. M. (2003). Murihiku Supergroup, New Zealand: redefined. *Journal of the Royal Society of New Zealand*, 33, 85–95.
- Campbell, K. A., Farmer, J. D., & Des Marais, D. (2002). Ancient hydrocarbon seeps from the Mesozoic convergent margin of California: Carbonate geochemistry, fluids and palaeoenvironments. *Geofluids*, 2(2), 63–94.
- Campbell, K. A., Francis, D. A., Collins, M., Gregory, M. R., Nelson, C. S., Greinert, J., & Aharon, P. (2008). Hydrocarbon seep-carbonates of a Miocene forearc (East Coast basin), North Island, New Zealand. *Sedimentary Geology*, 204(3–4), 83–105.
- Campbell, M.J., Rosenbaum, G., Allen, C.M., & Mortimer, N. (2020). Origin of dispersed Permian-Triassic fore-arc basin terranes in New Zealand: Insights from zircon petrochronology. *Gondwana Research*, 78, 210–227.
- Cande, S. C., & Stock, J. M. (2004). Cenozoic reconstructions of the Australia-New Zealand-South Pacific sector of Antarctica. In N. F. Exon, J. P. Kennet, & M. J. Malone (Eds.), *The Cenozoic Southern Ocean: Tectonics, sedimentation, and climate change between Australia and Antarctica*, Geophysical Monograph

- Series 151 (pp. 5–17). Washington, DC.: American Geophysical Union.
- Cande, S. C., & Stock, J. M. (2004). Pacific—Antarctic—Australia motion and the formation of the Macquarie Plate. *Geophysical Journal International*, 157(1), 399–414.
- Cande, S. C., Patriat, P., & Dymant, J. (2010). Motion between the Indian, Antarctic and African plates in the early Cenozoic. *Geophysical Journal International*, 183(1), 127–149.
- Cande, S. C., Stock, J. M., Müller, R. D., & Ishihara, T. (2000). Cenozoic motion between east and West Antarctica. *Nature*, 404(6774), 145–150.
- Cande, S.C., & Stock, J.M. (2004a). Cenozoic Reconstructions of the Australia-New Zealand-South Pacific Sector of Antarctica. In *The Cenozoic Southern Ocean: Tectonics, Sedimentation, and Climate Change between Australia and Antarctica*. Geophysical Monograph 151 (pp. 5-17). American Geophysical Union.
- Cande, S.C., & Stock, J.M. (2004b). Pacific-Antarctic-Australia motion and the formation of the Macquarie Plate. *Geophysical Journal International*, 157(1), 399–414.
- Cande, S.C., Herron, E.M., & Hall, B.R. (1982). The early Cenozoic tectonic history of the Southeast Pacific. *Earth and Planetary Science Letters*, 57(1), 63–74.
- Cande, S.C., Patriat, P., & Dymant, J. (2010). Motion between the Indian, Antarctic, and African plates in the early Cenozoic. *Geophysical Journal International*, 183(1), 127–149.
- Cande, S.C., Raymond, C.A., Stock, J.M., & Haxby, W.F. (1995). Geophysics of the Pitman Fracture Zone and Pacific-Antarctic plate motions during the Cenozoic. *Science*, 270(5238), 947–953.
- CANZ (2008). New Zealand region Bathymetry, 1:4 000 000 (2nd ed.). NIWA Chart, Miscellaneous Series No. 85.
- Cao, L., Shao, L., Qiao, P., Cui, Y., Zhang, G., & Zhang, X. (2021). Formation and paleogeographic evolution of the Palawan continental terrane along the Southeast Asian margin revealed by detrital fingerprints. *Bulletin*, 133(5-6), 1167–1193.
- Cao, L., Shao, L., van Hinsbergen, D. J., Jiang, T., Xu, D., & Cui, Y. (2023). Provenance and evolution of East Asian large rivers recorded in the East and South China Seas: A review. *Geological Society of America Bulletin*.
- Cao, X., Flament, N., Li, S., & Müller, R. D. (2021). Spatio-temporal evolution and dynamic origin of Jurassic-Cretaceous magmatism in the South China Block. *Earth-Science Reviews*, 217, 103605.
- Capitanio, F. A., Morra, G., Goes, S., Weinberg, R. F., & Moresi, L. (2010). India–Asia convergence driven by the subduction of the Greater Indian continent. *Nature Geoscience*, 3(2), 136–139.
- Carey, S. W. (1955). The orocline concept in geotectonics-Part I. In *Papers and proceedings of the Royal Society of Tasmania* (Vol. 89, pp. 255–288).
- Carter, A., Curtis, M., & Schwanethal, J. (2014). Cenozoic tectonic history of the South Georgia microcontinent and potential as a barrier to Pacific-Atlantic through flow. *Geology*, 42(4), 299–302.
- Carter, R. T., & Norris, R. J. (1976). Cainozoic history of southern New Zealand: An accord between geological observations and plate-tectonic predictions. *Earth and Planetary Science Letters*, 31(1), 85–94.
- Casey, J. F., & Dewey, J. F. (1984). Initiation of subduction zones along transform and accreting plate boundaries, triple-junction evolution, and forearc spreading centres—implications for ophiolitic geology and obduction. *Geological Society, London, Special Publications*, 13(1), 269–290.
- Cawood, P. A., Hawkesworth, C. J., Dhuime, B., (2012). Detrital zircon record and tectonic setting. *Geology* 40, 875–878.
- Challinor, A. B. (2001). Stratigraphy of Tithonian (Ohauan-Puaroan) marine beds near Port Waikato, New Zealand, and a redescription of *Belemnopsis aucklandica* (Hochstetter). *New Zealand Journal of Geology and Geophysics*, 44, 219–242.
- Chambers, L. M., Pringle, M. S., & Fitton, J. G. (2004). Phreatomagmatic eruptions on the Ontong Java Plateau: an Aptian 40Ar/39Ar age for volcanoclastic rocks at ODP Site 1184. *Geological Society, London, Special Publications*, 229(1), 325–331.
- Chandler, M. T., Wessel, P., Taylor, B., Seton, M., Kim, S. S., & Hyeong, K. (2012). Reconstructing Ontong Java Nui: Implications for Pacific absolute plate motion, hotspot drift and true polar wander. *Earth and Planetary Science Letters*, 331, 140–151.
- Chang, S.-J., Ferreira, A. M. G., & Faccenda, M. (2016). Upper- and mid-mantle interaction between the Samoan plume and the Tonga-Kermadec slabs. *Nature Communications*, 7, 10799.
- Charlton, T. R., Hall, R., & Partoyo, E. (1991). The geology and tectonic evolution of Waigeo Island, NE Indonesia. *Journal of Southeast Asian Earth Sciences*, 6(3-4), 289–297.
- Chen, W. S., Chung, S. L., Chou, H. Y., Zugerbai, Z., Shao, W. Y., & Lee, Y. H. (2017). A reinterpretation of the metamorphic Yuli belt: Evidence for a middle-late Miocene accretionary prism in eastern Taiwan. *Tectonics*, 36(2), 188–206.
- Chen, W. S., Huang, Y. C., Liu, C. H., Feng, H. T., Chung, S. L., & Lee, Y. H. (2016). UPb zircon geochronology

- constraints on the ages of the Tananao Schist Belt and timing of orogenic events in Taiwan: Implications for a new tectonic evolution of the South China Block during the Mesozoic. *Tectonophysics*, 686, 68–81.
- Chertova, M. V., Spakman, W., & Steinberger, B. (2018). Mantle flow influence on subduction evolution. *Earth and Planetary Science Letters*, 489, 258–266.
- Chertova, M. V., Spakman, W., Geenen, T., Van Den Berg, A. P., & Van Hinsbergen, D. J. J. (2014). Underpinning tectonic reconstructions of the western Mediterranean region with dynamic slab evolution from 3-D numerical modeling. *Journal of Geophysical Research: Solid Earth*, 119(7), 5876–5902.
- Chertova, M. V., Spakman, W., Van den Berg, A. P., & Van Hinsbergen, D. J. J. (2014). Absolute plate motions and regional subduction evolution. *Geochemistry, Geophysics, Geosystems*, 15, 3780–3792.
- Chivas, A. R., & McDougall, I. (1978). Geochronology of the Koloula porphyry copper prospect, Guadalcanal, Solomon Islands. *Economic Geology*, 73(5), 678–689.
- Choi, H., Kim, S.S., Dymant, J., Granot, R., Park, S.H., & Hong, J.K. (2017). The kinematic evolution of the Macquarie Plate: a case study for the fragmentation of oceanic lithosphere. *Earth and Planetary Science Letters*, 478, 132–142.
- Chung, S. L., & Sun, S. S. (1992). A new genetic model for the East Taiwan Ophiolite and its implications for Dupal domains in the Northern Hemisphere. *Earth and Planetary Science Letters*, 109(1–2), 133–145.
- Civile, D., Lodolo, E., Vuan, A., & Loreto, M. F. (2012). Tectonics of the Scotia–Antarctica plate boundary constrained from seismic and seismological data. *Tectonophysics*, 550, 17–34.
- Clennett, E. J., Sigloch, K., Mihalynuk, M. G., Seton, M., Henderson, M. A., Hosseini, K., ... & Müller, R. D. (2020). A quantitative tomotectonic plate reconstruction of western North America and the eastern Pacific basin. *Geochemistry, Geophysics, Geosystems*, 21(8), e2020GC009117.
- Cloos, M., Sapiie, B., van Ufford, A. Q., Weiland, R. J., Warren, P. Q., & McMahon, T. P. (2005). Collisional delamination in New Guinea: The geotectonics of subducting slab breakoff. *GSA Special Papers*.
- Cluzel, D., & Meffre, S. (2002). The Boghen terrane (New Caledonia, SW Pacific): a Jurassic accretionary complex. Preliminary U–Pb radiochronological data on detrital zircon. *Comptes Rendus Geosciences*, 334(11), 867–874.
- Cluzel, D., & Meffre, S. (2019). In search of Gondwana heritage in the Outer Melanesian Arc: no pre-upper Eocene detrital zircons in Viti Levu river sands (Fiji Islands). *Australian Journal of Earth Sciences*, 66(2), 265–277.
- Cluzel, D., Adams, C.J., Meffre, S., Campbell, H., & Maurizot, P. (2010). Discovery of early Cretaceous rocks in New Caledonia: New geochemical and U–Pb zircon age constraints on the transition from subduction to marginal breakup in the Southwest Pacific. *Journal of Geology*, 118(4), 381–397.
- Cluzel, D., Aitchison, J. C., & Picard, C. (2001). Tectonic accretion and underplating mafic terranes in the late Eocene intraoceanic fore-arc of New Caledonia (Southwest Pacific): Geodynamic implications. *Tectonophysics*, 240, 23–59.
- Cluzel, D., Jourdan, F., Meffre, S., Maurizot, P., & Lesimple, S. (2012b). The metamorphic sole of New Caledonia ophiolite: 40Ar/39Ar, U–Pb, and geochemical evidence for subduction inception at a spreading ridge. *Tectonics*, 31(3).
- Cluzel, D., Maurizot, P., Collot, J., & Sevin, B. (2012a). An outline of the Geology of New Caledonia; from Permian–Mesozoic Southeast Gondwanaland active margin to Cenozoic obduction and supergene evolution. *Episodes Journal of International Geoscience*, 35(1), 72–86.
- Cluzel, D., Meffre, S., Maurizot, P., & Crawford, A. J. (2006). Earliest Eocene (53 ma) convergence in the Southwest Pacific: Evidence from pre-obduction dikes in the ophiolite of New Caledonia. *Terra Nova*, 18(6), 395–402.
- Cluzel, D., Whitten, M., Meffre, S., Aitchison, J. C., & Maurizot, P. (2018). A Reappraisal of the Poya Terrane (New Caledonia): Accreted Late Cretaceous–Paleocene Marginal Basin Upper Crust, Passive Margin Sediments, and Early Eocene E–MORB Sill Complex. *Tectonics*, 37(1), 48–70.
- Cogné, J. P., Kravchinsky, V. A., Halim, N., & Hankard, F. (2005). Late Jurassic–Early Cretaceous closure of the Mongol–Okhotsk Ocean demonstrated by new Mesozoic palaeomagnetic results from the Trans-Baikal area (SE Siberia). *Geophysical Journal International*, 163(2), 813–832.
- Cole, J. W., & Lewis, K. B. (1981). Evolution of the Taupo–Hikurangi subduction system. *Tectonophysics*, 72, 1–21.
- Cole, J., McCabe, R., Moriarty, T., Malicse, J. A., Delfin, F. G., Tebar, H., & Ferrer, H. P. (1989). A preliminary Neogene paleomagnetic data set from Leyte and its relation to motion on the Philippine fault. *Tectonophysics*, 168(1–3), 205–220.
- Cole, W. S. (1950). Larger foraminifers from the Palau Islands. *US Geological Survey Professional Paper*, B, 221, 21–26.
- Collot, J.-Y., Herzer, R., Lafoy, Y., & Géli, L. (2009). Mesozoic history of the Fairway–Aotea Basin: Implications

- for the early stages of Gondwana fragmentation. *Geochemistry, Geophysics, Geosystems*, 10, Q12019.
- Collot, J.-Y., Lallemand, S., Pelletier, B., Eissen, J.-P., Glaçon, G., Fisher, M. A., et al. (1992). Geology of the d'Entrecasteaux-New Hebrides arc collision zone: Results from a deep submersible survey. *Tectonophysics*, 212(3-4), 213–241.
- Collot, J.-Y., Malahoff, A., Recy, J., Latham, G., & Missegue, F. (1987). Overthrust emplacement of New Caledonia ophiolite: Geophysical evidence. *Tectonics*, 6(3), 215–232.
- Collot, J.-Y., Vendé-Leclerc, M., Rouillard, P., Lafoy, Y., & Géli, L. (2012). Map helps unravel complexities of the southwestern Pacific Ocean. *Eos, Transactions American Geophysical Union*, 93(1), 1-2.
- Collot, J.-Y., & Davy, B. (1998). Forearc structures and tectonic regimes at the oblique subduction zone between the Hikurangi Plateau and the southern Kermadec margin. *Journal of Geophysical Research: Solid Earth*, 103(B1), 623-650.
- Collot, J.-Y., Lamarche, G., Wood, R. A., Delteil, J., Sosson, M., Lebrun, J. F., & Coffin, M. F. (1995). Morphostructure of an incipient subduction zone along a transform plate boundary: Puysegur Ridge and Trench. *Geology*, 23(6), 519-522.
- Conand, C., Mouthereau, F., Ganne, J., Lin, A. T. S., Lahfid, A., Daudet, M., Mesalles, L., Giletycz, S., & Bonzani, M. (2020). Strain partitioning and exhumation in oblique Taiwan collision: Role of rift architecture and plate kinematics. *Tectonics*, 39(4), e2019TC005798.
- Conrad, C.P., and Lithgow-Bertelloni, C., 2002. How slabs drive plate tectonics: *Science* 298, 207–209.
- Coombs, D. S. (1954). The nature and alteration of some Triassic sediments from Southland, New Zealand. *Transactions of the Royal Society of New Zealand*, 82, 65–109.
- Coombs, D. S., Cook, N. D. J., & Campbell, J. D. (1992). The Park Volcanics Group: Field relations of an igneous suite emplaced in the Triassic-Jurassic Murihiku Terrane, South Island, New Zealand. *New Zealand Journal of Geology and Geophysics*, 35, 337–351.
- Cooper, A. F., Barreiro, B. A., Kimbrough, D. L., & Mattinson, J. M. (1987). Lamprophyre dike intrusion and the age of the Alpine fault, New Zealand. *Geology*, 15(10), 941–944.
- Cosca, M., Arculus, R., Pearce, J., & Mitchell, J. (1998). $^{40}\text{Ar}/^{39}\text{Ar}$ and $\text{K}-\text{Ar}$ geochronological age constraints for the inception and early evolution of the Izu–Bonin–Mariana arc system. *Island Arc*, 7(3), 579-595.
- Coulson, F. I., & Vedder, J. G. (1986). Geology of the central and western Solomon Islands. *Geology and Offshore Resources of Pacific Island Arcs—central and western Solomon Islands*, 4, 59-87.
- Coutts, D. S., Matthews, W. A., & Hubbard, S. M. (2019). Assessment of widely used methods to derive depositional ages from detrital zircon populations. *Geoscience Frontiers*, 10(4), 1421-1435.
- Cowley, S., Mann, P., Coffin, M. F., & Shipley, T. H. (2004). Oligocene to Recent tectonic history of the Central Solomon intra-arc basin as determined from marine seismic reflection data and compilation of onland geology. *Tectonophysics*, 389(3-4), 267-307.
- Cox, A., & Hart, R. B. (1986). *Plate Tectonics: How It Works*. Blackwell Scientific Publications. Inc, Boston. 392 pp.
- Crameri, F. (2018). Scientific colour maps. Zenodo. <https://doi.org/10.5281/zenodo.1243862>
- Crameri, F., Magni, V., Domeier, M., Shephard, G. E., Chotalia, K., Cooper, G., ... & Thielmann, M. (2020). A transdisciplinary and community-driven database to unravel subduction zone initiation. *Nature communications*, 11(1), 3750.
- Crameri, F., Shephard, G.E., & Heron, P.J. (2020). The misuse of colour in science communication. *Nature Communications*, 11, 5444.
- Crampton, J. S. (1996). Inoceramid bivalves from the Late Cretaceous of New Zealand (Vol. 14, pp. 74–165). Institute of Geological and Nuclear Sciences Monograph.
- Crampton, J.S., Mortimer, N., Bland, K.J., Strogen, D.P., Sagar, M., Hines, B.R., King, P.R., & Seebeck, H. (2019). Cretaceous termination of subduction at the Zealandia margin of Gondwana: the view from the paleo-trench. *Gondwana Research*, 70, 222-242.
- Cramwinckel, M. J., Huber, M., Kocken, I. J., Agnini, C., Bijl, P. K., Bohaty, S. M., ... & Sluijs, A. (2018). Synchronous tropical and polar temperature evolution in the Eocene. *Nature*, 559(7714), 382-386.
- Crawford, A. J., Meffre, S., & Symonds, P. A. (2003). 120 to 0 Ma tectonic evolution of the southwest Pacific and analogous geological evolution of the 600 to 220 Ma Tasman Fold Belt System. *Geological Society of Australia Special Publication*, 22, 377–397.
- Croon, M. B., Cande, S. C., & Stock, J. M. (2008). Revised Pacific-Antarctic plate motions and geophysics of the Menard Fracture Zone. *Geochemistry, Geophysics, Geosystems*, 9, Q07001.
- Crowhurst, P. V., Maas, R., Hill, K. C., Foster, D. A., & Fanning, C. M. (2004). Isotopic constraints on crustal architecture and Permo-Triassic tectonics in New Guinea: Possible links with eastern Australia. *Australian Journal of Earth Sciences*, 51(1), 107-122.
- Cui, Y., Shao, L., Li, Z.X., Zhu, W., Qiao, P., & Zhang, X. (2021). A Mesozoic Andean-type active continental

- margin along coastal South China: New geological records from the basement of the northern South China Sea. *Gondwana Research*, 99, 36-52.
- Cunningham, W. D. (1993). Strike-slip faults in the southernmost Andes and the development of the Patagonian orocline. *Tectonics*, 12(1), 169-186.
- Cunningham, W. D. (1994). Uplifted ophiolitic rocks on Isla Gordon, southernmost Chile: implications for the closure history of the Rocas Verdes marginal basin and the tectonic evolution of the Beagle Channel region. *Journal of South American Earth Sciences*, 7(2), 135-147.
- Cunningham, W. D. (1995). Orogenesis at the southern tip of the Americas: the structural evolution of the Cordillera Darwin metamorphic complex, southernmost Chile. *Tectonophysics*, 244(4), 197-229.
- Cunningham, W. D., Klepeis, K. A., Gose, W. A., & Dalziel, I. W. (1991). The Patagonian Orocline: New paleomagnetic data from the Andean magmatic arc in Tierra del Fuego, Chile. *Journal of Geophysical Research: Solid Earth*, 96(B10), 16061-16067.
- Curry, J. R. (2005). Tectonics and history of the Andaman Sea region. *Journal of Asian Earth Sciences*, 25(1), 187-232.
- Dalziel, I. W. D. (1981). Back-arc extension in the southern Andes: a review and critical reappraisal. *Philosophical Transactions of the Royal Society of London. Series A, Mathematical and Physical Sciences*, 300(1454), 319-335.
- Dalziel, I. W. D. (1986). Collision and Cordilleran orogenesis: an Andean perspective. *Geological Society, London, Special Publications*, 19(1), 389-404.
- Dalziel, I. W. D. (2006). On the extent of the active West Antarctic rift system. *Terra Antarctica Reports*, 12, 193-202.
- Dalziel, I. W. D., Dott Jr, R. H., Winn Jr, R. D., & Bruhn, R. L. (1975). Tectonic relations of South Georgia Island to the southernmost Andes. *Geological Society of America Bulletin*, 86(7), 1034-1040.
- Dalziel, I. W., & Elliot, D. H. (1982). West Antarctica: problem child of Gondwanaland. *Tectonics*, 1(1), 3-19.
- Dalziel, I. W., de Wit, M. J., & Palmer, K. F. (1974). Fossil marginal basin in the southern Andes. *Nature*, 250(5464), 291-294.
- Dalziel, I. W., Lawver, L. A., & Murphy, J. B. (2000). Plumes, orogenesis, and supercontinental fragmentation. *Earth and Planetary Science Letters*, 178(1-2), 1-11.
- Dalziel, I. W., Lawver, L. A., Norton, I. O., & Gahagan, L. M. (2013). The Scotia Arc: genesis, evolution, global significance. *Annual Review of Earth and Planetary Sciences*, 41, 767-793.
- Dankers, P. H. M. (1978). Magnetic properties of dispersed natural iron-oxides of known grain-size [PhD Thesis, University of Utrecht]. Utrecht, Netherlands: University of Utrecht.
- Dankers, P. H. M., & Zijdeveld, J. D. A. (1981). Alternating field demagnetization of rocks, and the problem of gyromagnetic remanence. *Earth and Planetary Science Letters*, 53(1), 89-92.
- Davey, F. J. (1982). The structure of the South Fiji Basin. *Tectonophysics*, 87(1-4), 185-241.
- David Jr, S., Stephan, J. F., Delteil, J., Müller, C., Butterlin, J., Bellon, H., & Billedo, E. (1997). Geology and tectonic history of Southeastern Luzon, Philippines. *Journal of Asian Earth Sciences*, 15(4-5), 435-452.
- Davies, H. L. (1980a). Aitape-Vanimo - 1:250,000 Geological Series. Geological Survey of Papua New Guinea, Dept. of Minerals and Energy, Port Moresby.
- Davies, H. L. (1980b). Folded thrust fault and associated metamorphism in the Suckling-Dayman massif, Papua New Guinea. *American Journal of Science*, 280A, 171-191.
- Davies, H. L. (2005). The geology of Bougainville. Bougainville before the conflict (eds AJ Regan & HM Griffin), 20-30.
- Davies, H. L. (2012). The geology of New Guinea-the cordilleran margin of the Australian continent. *Episodes Journal of International Geoscience*, 35(1), 87-102.
- Davies, H. L., & Jaques, A. L. (1984). Emplacement of ophiolite in Papua New Guinea. *Geological Society, London, Special Publications*, 13(1), 341-349.
- Davies, H. L., & Smith, I. E. (1971). Geology of eastern Papua. *Geological Society of America Bulletin*, 82(12), 3299-3312.
- Davies, H. L., & Warren, R. G. (1988). Origin of eclogite-bearing, domed, layered metamorphic complexes ("core complexes") in the D'Entrecasteaux islands, Papua New Guinea. *Tectonics*, 7(1), 1-21.
- Davies, H. L. (1982). Mianmin - 1 : 250 000 geological series. Geological Survey of Papua New Guinea, Dept. of Minerals and Energy, Port Moresby.
- Davies, L., Hall, R., & Armstrong, R. (2014). Cretaceous crust in SW Borneo: petrological, geochemical and geochronological constraints from the Schwaner Mountains.
- Davy, B. (2014). Rotation and offset of the Gondwana convergent margin in the New Zealand region following Cretaceous jamming of Hikurangi Plateau large igneous province subduction. *Tectonics*, 33(8), 1577-1595.

- Davy, B., Hoernle, K., & Werner, R. (2008). Hikurangi plateau: Crustal structure, rifted formation, and Gondwana subduction history. *Geochemistry, Geophysics, Geosystems*, 9, Q07004.
- De Baar, H. J. W., Bacon, M. P., Brewer, P. G., & Bruland, K. W. (1985). Rare Earth elements in the Pacific and Atlantic Oceans. *Geochimica et Cosmochimica Acta*, 49(9), 1943–1959.
- De Boer, C. B., & Dekkers, M. J. (1998). Thermomagnetic behaviour of haematite and goethite as a function of grain size in various non-saturating magnetic fields. *Geophysical Journal International*, 133(3), 541–552.
- De Jesus, J. V., Yumul, G. P., & Faustino, D. V. (2000). The Cansiwang Melange of southeast Bohol (central Philippines): origin and tectonic implications. *Island Arc*, 9(4), 565–574.
- De Wit, M. J. (1977). The evolution of the Scotia Arc as a key to the reconstruction of southwestern Gondwanaland. *Tectonophysics*, 37(1-3), 53–81.
- de Wit, M. J., & Stern, C. R. (1981). Variations in the degree of crustal extension during formation of a back-arc basin. *Tectonophysics*, 72(3-4), 229–260.
- Decker, J., Ferdian, F., Morton, A., Fanning, M., & White, L. T. (2017). New geochronology data from eastern Indonesia—An aid to understanding sedimentary provenance in a frontier region.
- Deenen, M. H. L., Langereis, C. G., van Hinsbergen, D. J. J., & Biggin, A. J. (2011). Geomagnetic secular variation and the statistics of paleomagnetic directions. *Geophysical Journal International*, 186, 509–520.
- Deenen, M. H. L., Langereis, C. G., Van Hinsbergen, D. J. J., & Biggin, A. J. (2014). Erratum: Geomagnetic secular variation and the statistics of paleomagnetic directions. *Geophysical Journal International*, 197, 643.
- Defant, M. J., Jacques, D., Maury, R. C., de Boer, J., & Joron, J. L. (1989). Geochemistry and tectonic setting of the Luzon arc, Philippines. *Geological Society of America Bulletin*, 101(5), 663–672.
- Defant, M. J., Maury, R., Joron, J. L., Feigenson, M. D., Leterrier, J., Bellon, H., ... & Richard, M. (1990). The geochemistry and tectonic setting of the northern section of the Luzon arc (the Philippines and Taiwan). *Tectonophysics*, 183(1-4), 187–205.
- DeMets, C., Gordon, R. G., & Argus, D. F. (2010). Geologically current plate motions. *Geophysical journal international*, 181(1), 1–80.
- DeMets, C., Iaffaldano, G., & Merkouriev, S. (2015). High-resolution Neogene and quaternary estimates of Nubia-Eurasia-North America plate motion. *Geophysical Journal International*, 203(1), 416–427.
- DeMets, C., Merkouriev, S., & Sauter, D. (2021). High resolution reconstructions of the Southwest Indian Ridge, 52 Ma to present: implications for the breakup and absolute motion of the Africa plate. *Geophysical Journal International*, 226(3), 1461–1497.
- Deng, J., Yang, X., Qi, H., Zhang, Z. F., Mastoi, A. S., & Sun, W. (2017). Early Cretaceous high-Mg adakites associated with Cu-Au mineralization in the Cebu Island, Central Philippines: Implication for partial melting of the paleo-Pacific Plate. *Ore Geology Reviews*, 88, 251–269.
- Deng, J., Yang, X., Qi, H., Zhang, Z. F., Mastoi, A. S., Al Emil, G. B., & Sun, W. (2019). Early Cretaceous adakite from the Atlas porphyry Cu-Au deposit in Cebu Island, Central Philippines: Partial melting of subducted oceanic crust. *Ore Geology Reviews*, 110, 102937.
- Deng, J., Yang, X., Zhang, L. P., Duan, L., Mastoi, A. S., & Liu, H. (2020). An overview on the origin of adakites/adakitic rocks and related porphyry Cu-Au mineralization, Northern Luzon, Philippines. *Ore Geology Reviews*, 124, 103610.
- Deng, J., Yang, X., Zhang, Z. F., & Santosh, M. (2015). Early Cretaceous arc volcanic suite in Cebu Island, Central Philippines and its implications on paleo-Pacific plate subduction: Constraints from geochemistry, zircon U–Pb geochronology and Lu–Hf isotopes. *Lithos*, 230, 166–179.
- Deschamps, A., & Lallemand, S. (2002). The West Philippine Basin: An Eocene to early Oligocene back arc basin opened between two opposed subduction zones. *Journal of Geophysical Research: Solid Earth*, 107(B12), EPM-1.
- Deschamps, A., Monié, P., Lallemand, S., Hsu, S. K., & Yeh, K. Y. (2000). Evidence for Early Cretaceous oceanic crust trapped in the Philippine Sea Plate. *Earth and Planetary Science Letters*, 179(3-4), 503–516.
- Dewey, J. F., & Casey, J. F. (2011). The origin of obducted large-slab ophiolite complexes. *Arc-continent collision*, 431–444.
- Dickinson, W.R., Gehrels, G.E., (2009). Use of U-Pb ages of detrital zircons to infer maximum depositional ages of strata: A test against a Colorado Plateau Mesozoic database. *Earth Planet Sc Lett* 288, 115–125.
- Diegor, W. G. (1996). The ophiolitic basement complex of Cebu. *Journal of the Geological Society of the Philippines*, 51, 48–60.
- Dimalanta, C. B., Faustino-Eslava, D. V., Gabo-Ratio, J. A. S., Marquez, E. J., Padrones, J. T., Payot, B. D., ... & Yumul Jr, G. P. (2020). Characterization of the proto-Philippine Sea Plate: Evidence from the emplaced oceanic lithospheric fragments along eastern Philippines. *Geoscience Frontiers*, 11(1), 3–21.

- Dimalanta, C. B., Ramos, E. G. L., Yumul Jr, G. P., & Bellon, H. (2009). New features from the Romblon Island Group: Key to understanding the arc–continent collision in Central Philippines. *Tectonophysics*, 479(1-2), 120-129.
- Dimalanta, C. B., Suerte, L. O., Yumul, G. P., Tamayo, R. A., & Ramos, E. G. L. (2006). A Cretaceous supra-subduction oceanic basin source for Central Philippine ophiolitic basement complexes: Geological and geophysical constraints. *Geosciences Journal*, 10, 305-320.
- Domeier, M., Shephard, G. E., Jakob, J., Gaina, C., Doubrovine, P. V., & Torsvik, T. H. (2017). Intraoceanic subduction spanned the Pacific in the Late Cretaceous–Paleocene. *Science Advances*, 3(11), eaao2303.
- Dong, D., Zhang, Z., Bai, Y., Fan, J., & Zhang, G. (2018). Topographic and sedimentary features in the Yap subduction zone and their implications for the Caroline Ridge subduction. *Tectonophysics*, 722, 410-421.
- Doo, W. B., Hsu, S. K., Yeh, Y. C., Tsai, C. H., & Chang, C. M. (2015). Age and tectonic evolution of the northwest corner of the West Philippine Basin. *Marine Geophysical Research*, 36, 113-125.
- Dott Jr, R. H., Winn Jr, R. D., Dewit, M. J., & Bruhn, R. L. (1977). Tectonic and sedimentary significance of Cretaceous Tekenika Beds of Tierra del Fuego. *Nature*, 266(5603), 620-622.
- Doubleday, P. A., Macdonald, D. I. M., & Nell, P. A. R. (1993). Sedimentology and structure of the trench-slope to forearc basin transition in the Mesozoic of Alexander Island, Antarctica. *Geological Magazine*, 130(6), 737-754.
- Doubrovine, P. V., & Tarduno, J. A. (2008a). Linking the Late Cretaceous to Paleogene Pacific plate and the Atlantic bordering continents using plate circuits and paleomagnetic data. *Journal of Geophysical Research*, 113, B07104.
- Doubrovine, P. V., & Tarduno, J. A. (2008b). A revised kinematic model for the relative motion between Pacific oceanic plates and North America since the Late Cretaceous. *Journal of Geophysical Research*, 113, B12101.
- Doubrovine, P. V., Steinberger, B., & Torsvik, T. H. (2012). Absolute plate motions in a reference frame defined by moving hot spots in the Pacific, Atlantic, and Indian oceans. *Journal of Geophysical Research*, 117, B09101.
- Doust, H. (1990). Geology of the Sepik basin, Papua New Guinea. Papua New Guinea (PNG) Proceedings of the First PNG Petroleum Convention, 461-478.
- Dow, D. B., & Sukanto, R. (1984). Western Irian Jaya: the end-product of oblique plate convergence in the late Tertiary. *Tectonophysics*, 106(1-2), 109-139.
- Downey, N.J., Stock, J.M., Clayton, R.W., & Cande, S.C. (2007). History of the Cretaceous Osborn spreading center. *Journal of Geophysical Research: Solid Earth*, 112(B4).
- Drake, H., Åström, M. E., Heim, C., Broman, C., Åström, J., Whitehouse, M., et al. (2015). Extreme 13 C depletion of carbonates formed during oxidation of biogenic methane in fractured granite. *Nature Communications*, 6(1), 1– 9.
- Druken, K. A., Kincaid, C., Griffiths, R. W., Stegman, D. R., & Hart, S. R. (2014). Plume-slab interaction: The Samoa-Tonga system. *Physics of the Earth and Planetary Interiors*, 232, 1– 14.
- Durret, T., Gerya, T.V., & Spakman, W. (2014). Slab detachment in laterally varying subduction zones: 3-D numerical modeling. *Geophysical Research Letters*, 41(6), 1951-1956.
- Dycoco, J. M. A., Payot, B. D., Valera, G. T. V., Labis, F. A. C., Pasco, J. A., Perez, A. D., & Tani, K. (2021). Juxtaposition of Cenozoic and Mesozoic ophiolites in Palawan island, Philippines: New insights on the evolution of the Proto-South China Sea. *Tectonophysics*, 819, 229085.
- Eagles, G. (2004). Tectonic evolution of the Antarctic-Phoenix plate system since 15 Ma. *Earth and Planetary Science Letters*, 217(1-2), 97-109.
- Eagles, G. (2010). The age and origin of the central Scotia Sea. *Geophysical Journal International*, 183(2), 587-600.
- Eagles, G. (2016a). Plate kinematics of the Rocas Verdes Basin and Patagonian orocline. *Gondwana Research*, 37, 98-109.
- Eagles, G. (2016b). Tectonic reconstructions of the Southernmost Andes and the Scotia Sea during the opening of the Drake Passage. *Geodynamic Evolution of the Southernmost Andes: Connections with the Scotia Arc*, 75-108.
- Eagles, G., & Jokat, W. (2014). Tectonic reconstructions for paleobathymetry in Drake Passage. *Tectonophysics*, 611, 28-50.
- Eagles, G., & Livermore, R. A. (2002). Opening history of Powell Basin, Antarctic Peninsula. *Marine Geology*, 185(3-4), 195-205.
- Eagles, G., & Scott, B.G. (2014). Plate convergence west of Patagonia and the Antarctic Peninsula since 61 Ma. *Global and Planetary Change*, 123, 189-198.
- Eagles, G., Gohl, K., & Larter, R.D. (2004a). High-resolution animated tectonic reconstruction of the South

- Pacific and West Antarctic margin. *Geochemistry, Geophysics, Geosystems*, 5(7).
- Eagles, G., Gohl, K., & Larter, R.D. (2004b). Life of the Bellingshausen plate. *Geophysical Research Letters*, 31(7).
- Eagles, G., Larter, R. D., Gohl, K., & Vaughan, A. P. (2009). West Antarctic rift system in the Antarctic Peninsula. *Geophysical Research Letters*, 36(21).
- Eagles, G., Livermore, R. A., Fairhead, J. D., & Morris, P. (2005). Tectonic evolution of the west Scotia Sea. *Journal of Geophysical Research: Solid Earth*, 110(B2).
- Eagles, G., Livermore, R., & Morris, P. (2006). Small basins in the Scotia Sea: the Eocene Drake passage gateway. *Earth and Planetary Science Letters*, 242(3-4), 343-353.
- Eakins, B.W., & Lonsdale, P.F. (2003). Structural patterns and tectonic history of the Bauer microplate, Eastern Tropical Pacific. *Marine Geophysical Research*, 24(3), 171-205.
- Edbrooke, S. W. (compiler). (2001). *Geology of the Auckland area: Scale 1:250,000*. Lower Hutt: Institute of Geological & Nuclear Sciences Limited. Institute of Geological & Nuclear Sciences 1:250,000 geological map 3. 74 p. + 1 folded map.
- Edbrooke, S. W. (compiler). (2005). *Geology of the Waikato area: Scale 1:250,000*. Lower Hutt: Institute of Geological & Nuclear Sciences Limited. Institute of Geological & Nuclear Sciences 1:250,000 geological map 3. 74 p. + 1 folded map.
- Edbrooke, S. W., Heron, D. W., Forsyth, P. J., & Jongens, R. (2015). *Geology map of New Zealand 1:1,000,000*. GNS Science Map, 2.
- Eissen, J.-P., Crawford, A. J., Cotten, J., Meffre, S., Bellon, H., & Delaune, M. (1998). Geochemistry and tectonic significance of basalts in the Poya Terrane, New Caledonia. *Tectonophysics*, 284(3-4), 203- 219.
- Encarnación, J. (2004). Multiple ophiolite generation preserved in the northern Philippines and the growth of an island arc complex. *Tectonophysics*, 392(1-4), 103-130.
- Encarnación, J. P., Mukasa, S. B., & Obille Jr, E. C. (1993). Zircon U-Pb geochronology of the Zambales and Angat Ophiolites, Luzon, Philippines: Evidence for an Eocene arc-back arc pair. *Journal of Geophysical Research: Solid Earth*, 98(B11), 19991-20004.
- Engelbreton, D.C., Cox, A., & Gordon, R.G. (1985). Relative motions between oceanic and continental plates in the Pacific basin. *Geological Society of America Special Papers*, 206.
- Esteban, F. D., Ormazabal, J. P., Palma, F., Cayo, L. E., Lodolo, E., & Tassone, A. (2020). Strike-slip related folding within the Malvinas/Falkland Trough (south-western Atlantic ocean). *Journal of South American Earth Sciences*, 98, 102452.
- Evangelinos, D., Escutia, C., Etourneau, J., Hoem, F., Bijl, P., Boterblom, W., ... & López-Quirós, A. (2020). Late oligocene-miocene proto-antarctic circumpolar current dynamics off the Wilkes Land margin, East Antarctica. *Global and Planetary Change*, 191, 103221.
- Evans, C. A., Hawkins, J. W., & Moore, G. F. (1983). Petrology and geochemistry of ophiolitic and associated volcanic rocks on the Talaud Islands, Molucca Sea Collision Zone, northeast Indonesia. *Geodynamics of the Western Pacific-Indonesian Region*, 11, 159-172.
- Ewart, A., Brother, R. N., & Mateen, A. (1977). An outline of the geology and geochemistry, and the possible petrogenetic evolution of the volcanic rocks of the Tonga-Kermadec-New Zealand island arc. *Journal of Volcanology and Geothermal Research*, 2(3), 205- 250.
- Ewing, J. I., Ludwig, W. J., Ewing, M., & Eittreim, S. L. (1971). Structure of the Scotia sea and Falkland plateau. *Journal of Geophysical Research*, 76(29), 7118-7137.
- Fabbri, O., Monié, P., & Fournier, M. (2004). Transtensional deformation at the junction between the Okinawa trough back-arc basin and the SW Japan island arc. *Geological Society, London, Special Publications*, 227(1), 297-312.
- Faccenna, C., Becker, T. W., Lallemand, S., & Steinberger, B. (2012). On the role of slab pull in the Cenozoic motion of the Pacific plate. *Geophysical Research Letters*, 39(3), L03305.
- Faccenna, C., Oncken, O., Holt, A. F., & Becker, T. W. (2017). Initiation of the Andean orogeny by lower mantle subduction. *Earth and Planetary Science Letters*, 463, 189-201.
- Fairbridge, R. W., & Stewart Jr, H. B. (1960). Alexa Bank, a drowned atoll on the Melanesian Border Plateau. *Deep Sea Research* (1953), 7(2), 100-116.
- Falvey, D. A., & Taylor, L. W. (1974). Queensland Plateau and Coral Sea Basin: structural and time-stratigraphic patterns. *Exploration Geophysics*, 5(4), 123-126.
- Farsang, S., Louvel, M., Zhao, C., Mezouar, M., Rosa, A. D., Widmer, R. N., et al. (2021). Deep carbon cycle constrained by carbonate solubility. *Nature Communications*, 12(1), 1- 9.
- Faure, M., & Ishida, K. (1990). The Mid-Upper Jurassic olistostrome of the west Philippines: a distinctive key-marker for the North Palawan block. *Journal of Southeast Asian Earth Sciences*, 4(1), 61-67.
- Faustino, D. V., Yumul, G. P., De Jesus, J. V., Dimalanta, C. B., Aitchison, J. C., Zhou, M. F., ... & De Leon, M.

- M. (2003). Geology of southeast Bohol, central Philippines: accretion and sedimentation in a marginal basin. *Australian Journal of Earth Sciences*, 50(4), 571–583.
- Field, B. D., & Uruski, C. I. (1997). Cretaceous-Cenozoic geology and petroleum systems of the East Coast region, New Zealand (Vol. 1). Institute of Geological & Nuclear Sciences.
- Fildani, A., Cope, T. D., Graham, S. A., & Wooden, J. L. (2003). Initiation of the Magallanes foreland basin: Timing of the southernmost Patagonian Andes orogeny revised by detrital zircon provenance analysis. *Geology*, 31(12), 1081–1084.
- Fisher, D. M., Lu, C.-Y., & Chu, H.-T. (2002). Taiwan slate belt: Insights into the ductile interior of an arc-continent collision. *Geological Society of America: Special Paper*, 358, 93–106.
- Fisher, R. A. (1953). Dispersion on a sphere. *Proceedings of the Royal Society of London. Series A. Mathematical and Physical Sciences*, 217(1130), 295–305.
- Fitton, J. G., Mahoney, J. J., Wallace, P. J., & Saunders, A. D. (2004). Origin and evolution of the Ontong Java Plateau: introduction. *Geological Society, London, Special Publications*, 229(1), 1–8.
- Fitzgerald, P. (2002). Tectonics and landscape evolution of the Antarctic plate since the breakup of Gondwana, with an emphasis on the West Antarctic Rift System and the Transantarctic Mountains. *Royal Society of New Zealand Bulletin*, 35, 453–469.
- Fitzgerald, P. G., & Baldwin, S. (1997). Detachment fault model for the evolution of the Ross Embayment. *The Antarctic region: Geological evolution and processes*, 555–564.
- Fitzsimons, I. C. W. (2000). Grenville-age basement provinces in East Antarctica: evidence for three separate collisional orogens. *Geology*, 28(10), 879–882.
- Floyd, P. A., & Leveridge, B. E. (1987). Tectonic environment of the Devonian Gramscatho basin, south Cornwall: framework mode and geochemical evidence from turbiditic sandstones. *Journal of the Geological Society* 144, 531–542.
- Fosdick, J. C., Grove, M., Hourigan, J. K., & Calderon, M. (2013). Retroarc deformation and exhumation near the end of the Andes, southern Patagonia. *Earth and Planetary Science Letters*, 361, 504–517.
- Fosdick, J. C., Romans, B. W., Fildani, A., Bernhardt, A., Calderón, M., & Graham, S. A. (2011). Kinematic evolution of the Patagonian retroarc fold-and-thrust belt and Magallanes foreland basin, Chile and Argentina, 51 30 S. *Bulletin*, 123(9–10), 1679–1698.
- Francis, D. A. (1995). Oil and gas seeps of northern and central East Coast Basin. *Petroleum Exploration in New Zealand News*, 44, 21–27.
- Francis, G. (1988). Stratigraphy of Manus Island, Western New Ireland Basin, Papua New Guinea. *Geology and Offshore Resources of Pacific Island Arcs—New Ireland and Manus Region, Papua New Guinea*, 9, 31–40.
- Fujiwara, T., Tamaki, K., Fujimoto, H., Ishii, T., Seama, N., Toh, H., ... & Kinoshita, H. (1995). Morphological studies of the Ayu trough, Philippine sea–Caroline plate boundary. *Geophysical Research Letters*, 22(2), 109–112.
- Fukao, Y., & Obayashi, M. (2013). Subducted slabs stagnant above, penetrating through, and trapped below the 660 km discontinuity. *Journal of Geophysical Research: Solid Earth*, 118, 5920–5938.
- Fukao, Y., Widiyantoro, S., & Obayashi, M. (2001). Stagnant slabs in the upper and lower mantle transition region. *Reviews of Geophysics*, 39(3), 291–323.
- Fuller, M., Haston, R., & Almasco, J. (1989). Paleomagnetism of the Zambales ophiolite, Luzon, northern Philippines. *Tectonophysics*, 168(1–3), 171–203.
- Fuller, M., Haston, R., Lin, J. L., Richter, B., Schmidtke, E., & Almasco, J. (1991). Tertiary paleomagnetism of regions around the South China Sea. *Journal of Southeast Asian Earth Sciences*, 6(3–4), 161–184.
- Furlong, K. P., & Govers, R. (1999). Ephemeral crustal thickening at a triple junction: The Mendocino crustal conveyor. *Geology*, 27(2), 127–130.
- Furlong, K. P., & Kamp, P. J. (2009). The lithospheric geodynamics of plate boundary transpression in New Zealand: Initiating and emplacing subduction along the Hikurangi margin, and the tectonic evolution of the Alpine Fault system. *Tectonophysics*, 474(3–4), 449–462.
- Furlong, K. P., & Kamp, P. J. (2013). Changes in plate boundary kinematics: Punctuated or smoothly varying—Evidence from the Mid-Cenozoic transition from lithospheric extension to shortening in New Zealand. *Tectonophysics*, 608, 1328–1342.
- Furlong, K. P., & Kamp, P. J. (2009). The lithospheric geodynamics of plate boundary transpression in New Zealand: Initiating and emplacing subduction along the Hikurangi margin, and the tectonic evolution of the Alpine Fault system. *Tectonophysics*, 474(3–4), 449–462.
- Gaina, C., & Müller, R. D. (2007). Cenozoic tectonic and depth/age evolution of the Indonesian gateway and associated back-arc basins. *Earth-Science Reviews*, 83(3–4), 177–203.
- Gaina, C., Müller, R. D., Royer, J. Y., Stock, J., Hardebeck, J., & Symonds, P. (1998). The tectonic history of the

- Tasman Sea: a puzzle with 13 pieces. *Journal of Geophysical Research: Solid Earth*, 103(B6), 12413-12433.
- Gaina, C., Müller, R. D., Royer, J. Y., & Symonds, P. (1999). Evolution of the Louisiade triple junction. *Journal of Geophysical Research: Solid Earth*, 104(B6), 12927-12939.
- Gaina, C., Torsvik, T. H., van Hinsbergen, D. J., Medvedev, S., Werner, S. C., & Labails, C. (2013). The African Plate: A history of oceanic crust accretion and subduction since the Jurassic. *Tectonophysics*, 604, 4-25.
- Galbraith, R. F. (1981). On statistical models for fission track counts. *Journal of the International Association for Mathematical Geology*, 13(6), 471- 478.
- Galbraith, R. F., & Green, P. F. (1990). Estimating the component ages in a finite mixture. *International Journal of Radiation Applications and Instrumentation. Part D. Nuclear Tracks and Radiation Measurements*, 17(3), 197- 206.
- Galindo-Zaldívar, J., Bohoyo, F., Maldonado, A., Schreider, A., Surinach, E., & Vázquez, J. T. (2006). Propagating rift during the opening of a small oceanic basin: the Protector Basin (Scotia Arc, Antarctica). *Earth and Planetary Science Letters*, 241(3-4), 398-412.
- Galindo-Zaldívar, J., Gamboa, L., Maldonado, A., Nakao, S., & Bochu, Y. (2004). Tectonic development of the Bransfield Basin and its prolongation to the South Scotia Ridge, northern Antarctic Peninsula. *Marine Geology*, 206(1-4), 267-282.
- Galindo-Zaldívar, J., Puga, E., Bohoyo, F., González, F. J., Maldonado, A., Martos, Y. M., ... & de Federico Antonio, D. (2014). Magmatism, structure and age of Dove Basin (Antarctica): A key to understanding South Scotia Arc development. *Global and Planetary Change*, 123, 249-268.
- Gao, L., Zhao, Y., Yang, Z., Liu, J., Liu, X., Zhang, S. H., & Pei, J. (2018). New paleomagnetic and $^{40}\text{Ar}/^{39}\text{Ar}$ geochronological results for the South Shetland Islands, West Antarctica, and their tectonic implications. *Journal of Geophysical Research: Solid Earth*, 123(1), 4-30.
- Gardiner, N.P., & Hall, M. (2021). Discordant forearc deposition and volcanism preceding late-Cretaceous subduction shutdown in Marlborough, north-eastern South Island, New Zealand. *Earth-Science Reviews*, 214, 103530.
- Gardiner, N.P., Hall, M., Frears, B.T., & Lovell, R.W. (2022). A stratigraphic record from syn to post subduction sedimentation in Marlborough, New Zealand, and implications for Gondwana breakup. *Marine and Petroleum Geology*, 136, 105472.
- Gardiner, N.P., Hall, M.W., & Cawood, P.A. (2021). A forearc stratigraphic response to Cretaceous plateau collision and slab detachment, South Island, New Zealand. *Tectonics*, 40(10), e2021TC006806.
- Garrison, R. E., Espiritu, E., Horan, L. J., & Mack, L. E. (1979). Petrology, sedimentology, and diagenesis of hemipelagic limestone and tuffaceous turbidities in the Aksitero Formation, central Luzon, Philippines. *U.S. Geological Survey Professional Papers* 1112, 1-16
- Geary, E. E., & Kay, R. W. (1989). Identification of an early Cretaceous ophiolite in the Camarines Norte-Calaguas Islands basement complex, eastern Luzon, Philippines. *Tectonophysics*, 168(1-3), 109-126.
- Geary, E. E., Harrison, T. M., & Heizler, M. (1988). Diverse ages and origins of basement complexes, Luzon, Philippines. *Geology*, 16(4), 341-344.
- Geary, E.E. (1986) Tectonic significance of basement complexes and ophiolites in the northern Philippines: Results of geological, geochronological and geochemical investigations (Ph.D. thesis). Ithaca, New York, Cornell University, 221 p.
- German, C. R., Higgs, N. C., Thomson, J., Mills, R., Elderfield, H., Blusztajn, J., et al. (1993). A geochemical study of metalliferous sediment from the TAG hydrothermal Mound, 26°08' N, mid-Atlantic Ridge. *Journal of Geophysical Research*, 98(B6), 9683- 9692.
- Gerritsen, D., Vaes, B., & van Hinsbergen, D. J. (2022). Influence of data filters on the position and precision of paleomagnetic poles: what is the optimal sampling strategy?. *Geochemistry, Geophysics, Geosystems*, 23(4), e2021GC010269.
- Ghidella, M. E., Yáñez, G., & LaBrecque, J. L. (2002). Revised tectonic implications for the magnetic anomalies of the western Weddell Sea. *Tectonophysics*, 347(1-3), 65-86.
- Ghiglione, M. C., & Ramos, V. A. (2005). Progression of deformation and sedimentation in the southernmost Andes. *Tectonophysics*, 405(1-4), 25-46.
- Ghiglione, M. C., Likierman, J., Barberón, V., Beatriz Giambiagi, L., Aguirre-Urreta, B., & Suarez, F. (2014). Geodynamic context for the deposition of coarse-grained deep-water axial channel systems in the Patagonian Andes. *Basin Research*, 26(6), 726-745.
- Ghiglione, M. C., Quinteros, J., Yagupsky, D., Bonillo-Martínez, P., Hlebszevtich, J., Ramos, V. A., ... & Quesada, S. (2010). Structure and tectonic history of the foreland basins of southernmost South America. *Journal of South American Earth Sciences*, 29(2), 262-277.
- Ghiglione, M. C., Suarez, F., Ambrosio, A., Da Poian, G., Cristallini, E. O., Pizzio, M. F., & Reinoso, R. M. (2009). Structure and evolution of the Austral Basin fold-thrust belt, southern Patagonian Andes. *Revista*

- de la Asociación Geológica Argentina, 65(1), 215–226.
- Giardini, D., & Woodhouse, J. H. (1986). Horizontal shear flow in the mantle beneath the Tonga arc. *Nature*, 319(6054), 551–555.
- Gibaga, C. R. L., Arcilla, C. A., & Hoang, N. (2020). Volcanic rocks from the Central and Southern Palawan Ophiolites, Philippines: tectonic and mantle heterogeneity constraints. *Journal of Asian Earth Sciences*: X, 4, 100038.
- Gibbons, A.D., Barckhausen, U., Van Den Bogaard, P., Hoernle, K., Werner, R., Whittaker, J.M., & Müller, R.D. (2012). Constraining the Jurassic extent of Greater India: Tectonic evolution of the West Australian margin. *Geochemistry, Geophysics, Geosystems*, 13(5).
- Giggenbach, W. F., Stewart, M. K., Lyon, G. L., Sano, Y., & Goguel, R. L. (1995). Isotopic and chemical composition of solutions and gases from the East Coast accretionary prism, New Zealand. In *Isotope and geochemical techniques applied to geothermal investigations* (pp. 209–231). IAEA.
- Gill, J., Todd, E., Hoernle, K., Hauff, F., Price, A. A., & Jackson, M. G. (2022). Breaking up is hard to do: Magmatism during oceanic arc breakup, subduction reversal, and cessation. *Geochemistry, Geophysics, Geosystems*, 23(12), e2022GC010663.
- Goes, S., Cammarano, F., & Hansen, U. (2004). Synthetic seismic signature of thermal mantle plumes. *Earth and Planetary Science Letters*, 218(3–4), 403–419.
- Goes, S., Capitanio, F. A., Morra, G., Seton, M., & Giardini, D. (2011). Signatures of downgoing plate-buoyancy driven subduction in Cenozoic plate motions. *Physics of the Earth and Planetary Interiors*, 184(1–2), 1–13.
- Gohl, K., Teterin, D., Eagles, G., Netzeband, G., Grobys, J., Parsiegla, N., ... & Udintsev, G. B. (2007). Geophysical survey reveals tectonic structures in the Amundsen Sea embayment, West Antarctica. US Geological Survey Open-File Report, 2007-1047.
- Gong, L., Hollings, P., Zhang, Y., Tian, J., Li, D., & Chen, H. (2021). Contribution of an Eastern Indochina-derived fragment to the formation of island arc systems in the Philippine Mobile Belt. *GSA Bulletin*, 133(9–10), 1979–1995.
- González, V. R., Puigdomenech, C. G., Zaffarana, C. B., Vizán, H., & Somoza, R. (2020). Paleomagnetic evidence of the brittle deformation of the Central Patagonian Batholith at Gastre area (Chubut Province, Argentina). *Journal of South American Earth Sciences*, 98, 102442.
- Goodge, J. W. (2020). Geological and tectonic evolution of the Transantarctic Mountains, from ancient craton to recent enigma. *Gondwana Research*, 80, 50–122.
- Gorbatov, A., & Kennett, B. L. N. (2003). Joint bulk-sound and shear tomography for Western Pacific subduction zones. *Earth and Planetary Science Letters*, 210, 527–543.
- Götze, J. (2012). Application of cathodoluminescence microscopy and spectroscopy in geosciences. *Microscopy and Microanalysis*, 18(6), 1270–1284.
- Govers, R., & Wortel, M. J. R. (2005). Lithosphere tearing at STEP faults: Response to edges of subduction zones. *Earth and Planetary Science Letters*, 236(1–2), 505–523.
- Gradstein, F. M., Ogg, J. G., Schmitz, M., & Ogg, G. (Eds.). (2012). *The geologic time scale 2012*. Elsevier.
- Granot, R., & Dymant, J. (2018). Late Cenozoic unification of East and West Antarctica. *Nature Communications*, 9(1), 3189.
- Granot, R., Cande, S. C., Stock, J. M., & Damaske, D. (2013). Revised Eocene-Oligocene kinematics for the West Antarctic rift system. *Geophysical Research Letters*, 40(2), 279–284.
- Granot, R., Cande, S. C., Stock, J. M., & Damaske, D. (2013b). Correction to “Revised Eocene-Oligocene kinematics for the West Antarctic rift system”. *Geophysical Research Letters*, 40, 4625.
- Griffin, T. J., & Moresby, P. (1983). Granitoids of the Tertiary continent-island arc collision zone, Papua New Guinea. *Geological Society of America, Memoir* 159, 61–76.
- Grindley, G. W., & Oliver, P. J. (1983). Paleomagnetism of Cretaceous volcanic rocks from Marie Byrd Land, Antarctica. In R. L. Oliver, P. R. James, & J. B. Jago (Eds.), *Antarctic earth science: Proceedings of the 4th International Symposium on Antarctic Earth Sciences* (pp. 573–578). Canberra: Australian Academy of Science.
- Grindley, G. W., Oliver, P. J., & Sukroo, J. C. (1980). Lower Mesozoic position of southern New Zealand determined from paleomagnetism of the Glenham Porphyry, Murihiku Terrane, Eastern Southland. In M. M. Cresswell & P. Vella (Eds.), *Gondwana five* (pp. 319–326). Rotterdam: Balkema.
- Grobys, J. W., Gohl, K., & Eagles, G. (2008). Quantitative tectonic reconstructions of Zealandia based on crustal thickness estimates. *Geochemistry, Geophysics, Geosystems*, 9(1).
- Grommé, C. S., Wright, T. L., & Peck, D. L. (1969). Magnetic properties and oxidation of iron-titanium oxide minerals in Alae and Makaopuhi lava lakes, Hawaii. *Journal of Geophysical Research*, 74(22), 5277–5293.
- Grunow, A. M. (1993). New paleomagnetic data from the Antarctic Peninsula and their tectonic implications.

- Journal of Geophysical Research: Solid Earth, 98(B8), 13815-13833.
- Guillot, M. G. (2016). Magmatic evolution of the southernmost Andes and its relation with subduction processes. *Geodynamic Evolution of the Southernmost Andes: Connections with the Scotia Arc*, 37-74.
- Guilmette, C., Smit, M. A., van Hinsbergen, D. J., Gürer, D., Corfu, F., Charette, B., ... & Savard, D. (2018). Forced subduction initiation recorded in the sole and crust of the Semail Ophiolite of Oman. *Nature Geoscience*, 11(9), 688-695.
- Guilmette, C., van Hinsbergen, D., Smit, M., Godet, A., Fournier-Roy, F., Butler, J., ... & Hodges, K. (2023). Formation of the Xigaze Metamorphic Sole under the Tibetan continental margin reveals generic characteristics of the subduction initiation process. Preprint available via: <https://doi.org/10.21203/rs.3.rs-2621281/v1>
- Gungor, A., Lee, G. H., Kim, H. J., Han, H. C., Kang, M. H., Kim, J., & Sunwoo, D. (2012). Structural characteristics of the northern Okinawa Trough and adjacent areas from regional seismic reflection data: geologic and tectonic implications. *Tectonophysics*, 522, 198-207.
- Guotana, J. M. R., Payot, B. D., Dimalanta, C. B., Ramos, N. T., Faustino-Eslava, D. V., Queaño, K. L., & Yumul Jr, G. P. (2017). Arc and backarc geochemical signatures of the proto-Philippine Sea Plate: Insights from the petrography and geochemistry of the Samar Ophiolite volcanic section. *Journal of Asian Earth Sciences*, 142, 77-92.
- Guotana, J. M. R., Payot, B. D., Dimalanta, C. B., Ramos, N. T., Faustino-Eslava, D. V., Queaño, K. L., & Yumul Jr, G. P. (2018). Petrological and geochemical characteristics of the Samar Ophiolite ultramafic section: implications on the origins of the ophiolites in Samar and Leyte islands, Philippines. *International Geology Review*, 60(4), 401-417.
- Gürer, D., Granot, R., & van Hinsbergen, D. J. (2022). Plate tectonic chain reaction revealed by noise in the Cretaceous quiet zone. *Nature Geoscience*, 15(3), 233-239.
- Gurnis, M., Hall, C., & Lavier, L. (2004). Evolving force balance during incipient subduction. *Geochemistry, Geophysics, Geosystems*, 5(7).
- Gurnis, M., Van Avendonk, H., Gulick, S.P., Stock, J., Sutherland, R., Hightower, E., Shuck, B., Patel, J., Williams, E., Kardell, D., Herzig, E., Idini, B., Graham, K., Estep, J., & Carrington, L. (2019). Incipient subduction at the contact with stretched continental crust: the Puysegur Trench. *Earth and Planetary Science Letters*, 520, 212-219.
- Hafkenscheid, E., Wortel, M. J. R., & Spakman, W. (2006). Subduction history of the Tethyan region derived from seismic tomography and tectonic reconstructions. *Journal of Geophysical Research*, 111, B08401.
- Hall, C. E., Gurnis, M., Sdrolias, M., Lavier, L. L., & Müller, R. D. (2003). Catastrophic initiation of subduction following forced convergence across fracture zones. *Earth and Planetary Science Letters*, 212(1-2), 15-30.
- Hall, R. (1996). Reconstructing Cenozoic SE Asia. *Geological Society, London, Special Publications*, 106(1), 153-184.
- Hall, R. (2002). Cenozoic geological and plate tectonic evolution of SE Asia and the SW Pacific: computer-based reconstructions, model and animations. *Journal of Asian earth sciences*, 20(4), 353-431.
- Hall, R. (2012). Late Jurassic–Cenozoic reconstructions of the Indonesian region and the Indian Ocean. *Tectonophysics*, 570, 1-41.
- Hall, R., & Breitfeld, H. T. (2017). Nature and demise of the proto-South China Sea. *Bulleting of the Geological Society of Malaysia*, 63, 61-76.
- Hall, R., & Spakman, W. (2002). Subducted slabs beneath the eastern Indonesia–Tonga region: insights from tomography. *Earth and Planetary Science Letters*, 201(2), 321-336.
- Hall, R., & Spakman, W. (2003). Mantle structure and tectonic evolution of the region north and east of Australia. *Geological Society of Australia Special Publication*, 22, 361– 381.
- Hall, R., Ali, J. R., Anderson, C. D., & Baker, S. J. (1995a). Origin and motion history of the Philippine Sea Plate. *Tectonophysics*, 251(1-4), 229-250.
- Hall, R., Audley-Charles, M. G., Banner, F. T., Hidayat, S., & Tobing, S. L. (1988). Basement rocks of the Halmahera region, eastern Indonesia: a Late Cretaceous–Early Tertiary arc and fore-arc. *Journal of the Geological Society*, 145(1), 65-84.
- Hall, R., Fuller, M., Ali, J. R., & Anderson, C. D. (1995b). The Philippine Sea plate: magnetism and reconstructions. *Active margins and marginal basins of the Western Pacific*, 88, 371-404.
- Hall, R., van Hattum, M. W., & Spakman, W. (2008). Impact of India–Asia collision on SE Asia: the record in Borneo. *Tectonophysics*, 451(1-4), 366-389.
- Handschumacher, D.W. (1976). Post-Eocene plate tectonics of the eastern Pacific. *Geophysical Pacific Ocean Basin Margin*, 19, 177-202.
- Handy, M. R., Schmid, S. M., Bousquet, R., Kissling, E., & Bernoulli, D. (2010). Reconciling plate-tectonic reconstructions of Alpine Tethys with the geological–geophysical record of spreading and subduction in

- the Alps. *Earth-Science Reviews*, 102(3-4), 121-158.
- Harley, S. (2003). Archaean-Cambrian crustal development of East Antarctica: metamorphic characteristics and tectonic implications. *Geological Society, London, Special Publications*, 206(1), 203-230.
- Hartman, J.D., Sangiorgi, F., & Escutia Dotti, C. (2018). Paleooceanography and Ice Sheet Variability Offshore Wilkes Land, Antarctica—Part 3: Insights from Oligocene–Miocene TEX86-Based Sea Surface Temperature Reconstructions.
- Haston, R. B., & Fuller, M. (1991). Paleomagnetic data from the Philippine Sea plate and their tectonic significance. *Journal of Geophysical Research: Solid Earth*, 96(B4), 6073-6098.
- Haston, R. B., & Luyendyk, B. P. (1991). Paleomagnetic results from the Waipapa Terrane, Northland Peninsula, North Island, New Zealand: Tectonic implications from widespread remagnetizations. *Tectonics*, 10, 986-994.
- Haston, R. B., Stokking, L. B., & Ali, J. (1992). 31. Paleomagnetic data from holes 782A, 784A, and 786A, Leg 125. *Proceedings of Ocean Drilling Program, Scientific Results* (125), 535-545.
- Haston, R., Fuller, M., & Schmidtke, E. (1988). Paleomagnetic results from Palau, West Caroline Islands: a constraint on Philippine Sea plate motion. *Geology*, 16(7), 654-657.
- Hathway, B. (2000). Continental rift to back-arc basin: Jurassic–cretaceous stratigraphical and structural evolution of the Larsen Basin, Antarctic Peninsula. *Journal of the Geological Society*, 157(2), 417-432.
- Hawkins, J. W. (1985). Geology of the composite terranes of east and central Mindanao. *Circum Pacific Council Publications, Earth Science Series* 1, 437-463.
- Hawkins, J. W., & Evans, C. A. (1983). Geology of the Zambales Range, Luzon, Philippine Islands: Ophiolite derived from an island arc-back arc basin pair. *Washington DC American Geophysical Union Geophysical Monograph Series*, 27, 95-123.
- Hawkins, J. W., & Ishizuka, O. (2009). Petrologic evolution of Palau, a nascent island arc. *Island Arc*, 18(4), 599-641.
- Hawkins, J., & Batiza, R. (1977). Metamorphic rocks of the Yap arc-trench system. *Earth and Planetary Science Letters*, 37(2), 216-229.
- Hay, R. F. (1967). Sheet 7, Taranaki, 'Geological map of New Zealand 1:250,000'. DSIR Wellington.
- Hayes, G. P., Furlong, K. P., & Ammon, C. J. (2009). Intraplate deformation adjacent to the Macquarie ridge south of New Zealand—The tectonic evolution of a complex plate boundary. *Tectonophysics*, 463(1-4), 1-14.
- Hayes, G. P., Furlong, K. P., & Ammon, C. J. (2009). Intraplate deformation adjacent to the Macquarie Ridge south of New Zealand—The tectonic evolution of a complex plate boundary. *Tectonophysics*, 463(1-4), 1-14.
- Hayward, B. W., Black, P. M., Smith, I. E., Ballance, P. F., Itaya, T., Doi, M., et al. (2001). K-Ar ages of early Miocene arc-type volcanoes in northern New Zealand. *New Zealand Journal of Geology and Geophysics*, 44(2), 285-311.
- He, Z. Y., & Xu, X. S. (2012). Petrogenesis of the Late Yanshanian mantle-derived intrusions in southeastern China: response to the geodynamics of paleo-Pacific plate subduction. *Chemical Geology*, 328, 208-221.
- Hegarty, K. A., Weissel, J. K., & Hayes, D. E. (1983). Convergence at the Caroline-Pacific plate boundary: collision and subduction. *Washington DC American Geophysical Union Geophysical Monograph Series*, 27, 326-348.
- Heine, C., Zoethout, J., & Müller, R.D. (2013). Kinematics of the South Atlantic rift. *Solid Earth*, 4(2), 215-253.
- Hennig-Breitfeld, J., Breitfeld, H. T., Hall, R., BouDagher-Fadel, M., & Thirlwall, M. (2019). A new upper Paleogene to Neogene stratigraphy for Sarawak and Labuan in northwestern Borneo: Paleogeography of the eastern Sundaland margin. *Earth-science reviews*, 190, 1-32.
- Hennig, J., Breitfeld, H. T., Hall, R., & Nugraha, A. S. (2017). The Mesozoic tectono-magmatic evolution at the Paleo-Pacific subduction zone in West Borneo. *Gondwana Research*, 48, 292-310.
- Herron, E.M., & Tucholke, B.E. (1976). Sea-floor magnetic patterns and basement structure in the southeastern Pacific. In C.D. Hollister & C. Craddock (Eds.), *Initial Reports of the Deep Sea Drilling Project*, 35, 263-278.
- Herve, F., Pankhurst, R.J., Fanning, C., Calderón, M., & Yaxley, G. (2007). The south Patagonian batholith: 150 my of granite magmatism on a plate margin. *Lithos*, 97(3-4), 373-394.
- Hervé, M., Suárez, M., & Puig, A. (1984). The Patagonian Batholith S of Tierra del Fuego, Chile: timing and tectonic implications. *Journal of the Geological Society*, 141(5), 909-917.
- Herzer, R. H., & Mascle, J. (1996). Anatomy of a continent-backarc transform—The Vening Meinesz Fracture Zone northwest of New Zealand. *Marine Geophysical Researches*, 18(2-4), 401-427.
- Herzer, R. H., Barker, D. H. N., Roest, W. R., & Mortimer, N. (2011). Oligocene-Miocene spreading history

- of the northern South Fiji Basin and implications for the evolution of the New Zealand plate boundary. *Geochemistry, Geophysics, Geosystems*, 12, Q02004.
- Herzer, R. H., Davy, B. W., Mortimer, N., Quilty, P. G., Chaproniere, G. C. H., Jones, C. M., et al. (2009). Seismic stratigraphy and structure of the Northland Plateau and the development of the Vening Meinesz transform margin, SW Pacific Ocean. *Marine Geophysical Researches*, 30(1), 21–60.
- Heuret, A., & Lallemand, S. (2005). Plate motions, slab dynamics and back-arc deformations. *Physics of the Earth and Planetary Interiors*, 149, 31–51.
- Hickey-Vargas, R., Ishizuka, O., & Bizimis, M. (2013). Age and geochemistry of volcanic clasts from DSDP Site 445, Daito Ridge and relationship to Minami-Daito Basin and early Izu-Bonin arc magmatism. *Journal of Asian Earth Sciences*, 70, 193–208.
- Hickey-Vargas, R., Yogodzinski, G. M., Ishizuka, O., McCarthy, A., Bizimis, M., Kusano, Y., ... & Arculus, R. (2018). Origin of depleted basalts during subduction initiation and early development of the Izu-Bonin-Mariana island arc: Evidence from IODP expedition 351 site U1438, Amami-Sankaku basin. *Geochimica et Cosmochimica Acta*, 229, 85–111.
- Hickey-Vargas, R. (1998). Origin of the Indian Ocean-type isotopic signature in basalts from Philippine Sea plate spreading centers: An assessment of local versus large-scale processes. *Journal of Geophysical Research: Solid Earth*, 103(B9), 20963–20979.
- Hickey-Vargas, R. (2005). Basalt and tonalite from the Amami Plateau, northern West Philippine Basin: New Early Cretaceous ages and geochemical results, and their petrologic and tectonic implications. *Island Arc*, 14(4), 653–665.
- Hilde, T. W., & Chao-Shing, L. (1984). Origin and evolution of the West Philippine Basin: a new interpretation. *Tectonophysics*, 102(1–4), 85–104.
- Hill, D. J., Haywood, A. M., Valdes, P. J., Francis, J. E., Lunt, D. J., Wade, B. S., & Bowman, V. C. (2013). Paleogeographic controls on the onset of the Antarctic circumpolar current. *Geophysical Research Letters*, 40(19), 5199–5204.
- Hill, E. J. (1994). Geometry and kinematics of shear zones formed during continental extension in eastern Papua New Guinea. *Journal of Structural Geology*, 16(8), 1093–1105.
- Hill, E. J., & Baldwin, S. L. (1993). Exhumation of high-pressure metamorphic rocks during crustal extension in the D'Entrecasteaux region, Papua New Guinea. *Journal of Metamorphic Geology*, 11(2), 261–277.
- Hill, I. A., & Barker, P. F. (1980). Evidence for Miocene back-arc spreading in the central Scotia Sea. *Geophysical Journal International*, 63(2), 427–440.
- Hill, K. C. (1991). Structure of the Papuan fold belt, Papua New Guinea. *AAPG bulletin*, 75(5), 857–872.
- Hill, K. C., & Gleadow, A. J. W. (1989). Uplift and thermal history of the Papuan Fold Belt, Papua New Guinea: Apatite fission track analysis. *Australian Journal of Earth Sciences*, 36(4), 515–539.
- Hill, K. C., & Hall, R. (2002). Mesozoic–Cainozoic evolution of Australia's New Guinea margin in a West Pacific context. *Defining Australia: the Australian Plate as Part of Planet Earth*: Geological Society of America and Geological Society of Australia, joint publication, special paper, 1–43.
- Hill, K. C., & Raza, A. (1999). Arc-continent collision in Papua Guinea: Constraints from fission track thermochronology. *Tectonics*, 18(6), 950–966.
- Hinz, K., Block, M., Kudrass, H. R., & Meyer, H. (1991). Structural elements of the Sulu Sea, Philippines. *AAPG Bulletin* 78.
- Hinz, K., Block, M., Kudrass, H. R., & Meyer, H. (1994). Structural elements of the Sulu Sea, Philippines. *AAPG Bulletin (American Association of Petroleum Geologists)*, 78(CONF-940803-).
- Ho, C. S. (1969). Geological significance of potassium-argon ages of the Chimei igneous complex in eastern Taiwan. *Bull. Geol. Surv. Taiwan*, 20, 63–74.
- Ho, C. S. (1986). A synthesis of the geologic evolution of Taiwan. *Tectonophysics*, 125(1–3), 1–16.
- Hobson, D. M. (1986). A thin skinned model for the Papuan thrust belt and some implications for hydrocarbon exploration. *The APPEA Journal*, 26(1), 214–225.
- Hochmuth, K., & Gohl, K. (2017). Collision of Manihiki Plateau fragments to accretional margins of northern Andes and Antarctic Peninsula. *Tectonics*, 36(2), 229–240.
- Hochmuth, K., Gohl, K., & Uenzelmann-Neben, G. (2015). Playing jigsaw with large igneous provinces—A plate tectonic reconstruction of Ontong Java Nui, West Pacific. *Geochemistry, Geophysics, Geosystems*, 16(11), 3789–3807.
- Hoernle, K., Gill, J., Timm, C., Hauff, F., Werner, R., Garbe-Schönberg, D., & Gutjahr, M. (2021). Hikurangi Plateau subduction a trigger for Vitiaz arc splitting and Havre Trough opening (southwestern Pacific). *Geology*, 49(5), 536–540.
- Hoernle, K., Hauff, F., Van den Bogaard, P., Werner, R., Mortimer, N., Geldmacher, J., Garbe-Schönberg, D., & Davy, B. (2010). Age and geochemistry of volcanic rocks from the Hikurangi and Manihiki oceanic

- plateaus. *Geochimica et Cosmochimica Acta*, 74(24), 7196-7219.
- Hollings, P., Wolfe, R., Cooke, D. R., & Waters, P. J. (2011). Geochemistry of Tertiary igneous rocks of northern Luzon, Philippines: Evidence for a back-arc setting for alkalic porphyry copper-gold deposits and a case for slab roll-back?. *Economic Geology*, 106(8), 1257-1277.
- Hollis, C. J., & Hanson, J. A. (1991). Well-preserved late Paleocene Radiolaria from Tangihua Complex, Camp Bay, eastern Northland. *Tane*, 33, 65-76.
- Holloway, N. H. (1982). North Palawan block, Philippines—its relation to Asian mainland and role in evolution of South China Sea. *AAPG Bulletin*, 66(9), 1355-1383.
- Holm, R. J., Rosenbaum, G., & Richards, S. W. (2016). Post 8 Ma reconstruction of Papua New Guinea and Solomon Islands: Microplate tectonics in a convergent plate boundary setting. *Earth-Science Reviews*, 156, 66-81.
- Holm, R. J., Spandler, C., & Richards, S. W. (2015). Continental collision, orogenesis and arc magmatism of the Miocene Maramuni arc, Papua New Guinea. *Gondwana Research*, 28(3), 1117-1136.
- Holt, J.W., Blankenship, D.D., Morse, D.L., Young, D.A., Peters, M.E., Kempf, S.D., Richter, T.G., Vaughan, D.G., & Corr, H.F. (2006). New boundary conditions for the West Antarctic Ice Sheet: Subglacial topography of the Thwaites and Smith glacier catchments. *Geophysical Research Letters*, 33(9).
- Home, P. C., Dalton, D. G., & Brannan, J. (1990). Geological evolution of the western Papuan basin. *Proceedings of the First PNG Petroleum Convention*, 107-117.
- Honza, E., & Fujioka, K. (2004). Formation of arcs and backarc basins inferred from the tectonic evolution of Southeast Asia since the Late Cretaceous. *Tectonophysics*, 384(1-4), 23-53.
- Hou, Y., Shao, L., Cui, Y., Allen, M. B., Zhu, W., Qiao, P., ... & Goh, T. L. (2022). Sediment features and provenance analysis of the late Mesozoic–early Cenozoic strata of the Ryukyu Islands: Implications for palaeogeography of East China Sea. *Marine and Petroleum Geology*, 145, 105840.
- Houben, A.J., Bijl, P.K., Sluijs, A., Schouten, S., & Brinkhuis, H. (2019). Late Eocene Southern Ocean cooling and invigoration of circulation preconditioned Antarctica for full-scale glaciation. *Geochemistry, Geophysics, Geosystems*, 20(5), 2214-2234.
- House, M.A., Gurnis, M., Kamp, P.J., & Sutherland, R. (2002). Uplift in the Fiordland region, New Zealand: Implications for incipient subduction. *Science*, 297(5589), 2038-2041.
- Howell, D. G. (1980). Mesozoic accretion of exotic terranes along the New Zealand segment of Gondwanaland. *Geology*, 8(10), 487-491.
- Huang, C. Y., Chen, W. H., Wang, M. H., Lin, C. T., Yang, S., Li, X., ... & Harris, R. (2018). Juxtaposed sequence stratigraphy, temporal-spatial variations of sedimentation and development of modern-forming forearc Lichi Mélange in North Luzon Trough forearc basin onshore and offshore eastern Taiwan: An overview. *Earth-science reviews*, 182, 102-140.
- Huang, C. Y., Wang, P., Yu, M., You, C. F., Liu, C. S., Zhao, X., ... & Yumul Jr, G. P. (2019). Potential role of strike-slip faults in opening up the South China Sea. *National Science Review*, 6(5), 891-901.
- Huang, C. Y., Yuan, P. B., & Tsao, S. J. (2006). Temporal and spatial records of active arc-continent collision in Taiwan: A synthesis. *Geological Society of America Bulletin*, 118(3-4), 274-288.
- Hutchison, C. S. (1996). The 'Rajang accretionary prism' and 'Lupar Line' problem of Borneo. *Geological Society, London, Special Publications*, 106(1), 247-261.
- Hutchison, C. S., Bergman, S. C., Swauger, D. A., & Graves, J. E. (2000). A Miocene collisional belt in north Borneo: uplift mechanism and isostatic adjustment quantified by thermochronology. *Journal of the Geological Society*, 157(4), 783-793.
- Hutchison, D. S. (1975). Basement geology of the North Sepik region, Papua New Guinea. *Bureau of Mineral Resources, Australia, Record*, 162.
- Hutchison, D. S., & Norvick, M. (1978). Wewak, Papua New Guinea 1: 250,000 geological series. *Geological Survey of Papua New Guinea, Dept. of Minerals and Energy, Port Moresby*.
- Hutchison, D. S., & Norvick, M. (1980). *Geology of the North Sepik region, Papua New Guinea. Bureau of Mineral Resources*.
- Iaffaldano, G., Bodin, T., & Sambridge, M. (2012). Reconstructing plate-motion changes in the presence of finite-rotations noise. *Nature Communications*, 3(1), 1-6.
- Imai, A. (2001). Generation and evolution of ore fluids for porphyry Cu-Au mineralization of the Santo Tomas II (Philex) deposit, Philippines. *Resource Geology*, 51(2), 71-96.
- Isaac, M. J., Herzer, R. H., Brook, F. J., & Hayward, B. W. (1994). Cretaceous and Cenozoic sedimentary basins of Northland, New Zealand. *Institute of Geological & Nuclear Sciences monograph 8. Institute of Geological & Nuclear Sciences, Lower Hutt*.
- Ishizuka, O., Hickey-Vargas, R., Arculus, R. J., Yagodinski, G. M., Savov, I. P., Kusano, Y., ... & Sudo, M. (2018). Age of Izu–Bonin–Mariana arc basement. *Earth and Planetary Science Letters*, 481, 80-90.

- Ishizuka, O., Kimura, J. I., Li, Y. B., Stern, R. J., Reagan, M. K., Taylor, R. N., ... & Haraguchi, S. (2006). Early stages in the evolution of Izu-Bonin arc volcanism: New age, chemical, and isotopic constraints. *Earth and Planetary Science Letters*, 250(1-2), 385-401.
- Ishizuka, O., Tani, K., Harigane, Y., Yamazaki, T., & Ohara, Y. (2015). Geologic and geochronological constraints on the Philippines Sea tectonics around 50 Ma. *JpGU 2015 Abstract*.
- Ishizuka, O., Tani, K., Reagan, M. K., Kanayama, K., Umino, S., Harigane, Y., ... & Dunkley, D. J. (2011a). The timescales of subduction initiation and subsequent evolution of an oceanic island arc. *Earth and Planetary Science Letters*, 306(3-4), 229-240.
- Ishizuka, O., Tani, K., Taylor, R. N., Umino, S., Sakamoto, I., Yokoyama, Y., ... & Sekimoto, S. (2022). Origin and age of magmatism in the northern Philippine Sea basins. *Geochemistry, Geophysics, Geosystems*, 23(4).
- Ishizuka, O., Taylor, R. N., Ohara, Y., & Yuasa, M. (2013). Upwelling, rifting, and age-progressive magmatism from the Oki-Daito mantle plume. *Geology*, 41(9), 1011-1014.
- Ishizuka, O., Taylor, R. N., Yuasa, M., & Ohara, Y. (2011b). Making and breaking an island arc: A new perspective from the Oligocene Kyushu-Palau arc, Philippine Sea. *Geochemistry, Geophysics, Geosystems*, 12(5).
- Ishizuka, O., Yuasa, M., Tamura, Y., Shukuno, H., Stern, R. J., Naka, J., ... & Taylor, R. N. (2010). Migrating shoshonitic magmatism tracks Izu-Bonin-Mariana intra-oceanic arc rift propagation. *Earth and Planetary Science Letters*, 294(1-2), 111-122.
- Isozaki, Y., Aoki, K., Nakama, T., & Yanai, S. (2010). New insight into a subduction-related orogen: A reappraisal of the geotectonic framework and evolution of the Japanese Islands. *Gondwana Research*, 18(1), 82-105.
- Isozaki, Y., Maruyama, S., & Furuoka, F. (1990). Accreted oceanic materials in Japan. *Tectonophysics*, 181(1-4), 179-205.
- Ito, T., Kojima, Y., Kodaira, S., Sato, H., Kaneda, Y., Iwasaki, T., ... & Ikawa, T. (2009). Crustal structure of southwest Japan, revealed by the integrated seismic experiment Southwest Japan 2002. *Tectonophysics*, 472(1-4), 124-134.
- Jackson, M. G., Hart, S. R., Konter, J. G., Koppers, A. A., Staudigel, H., Kurz, M. D., Blusztajn, J., & Sinton, J. M. (2010). Samoan hot spot track on a "hot spot highway": Implications for mantle plumes and a deep Samoan mantle source. *Geochemistry, Geophysics, Geosystems*, 11(12).
- Jahn, B. M. (1986). Mid-ocean ridge or marginal basin origin of the East Taiwan Ophiolite: chemical and isotopic evidence. *Contributions to Mineralogy and Petrology*, 92(2), 194-206.
- Jahn, B. M., Chen, P. Y., & Yen, T. P. (1976). Rb-Sr ages of granitic rocks in southeastern China and their tectonic significance. *Geological Society of America Bulletin*, 87(5), 763-776.
- Jahn, B. M., Chi, W. R., & Yui, T. F. (1992). A late Permian formation of Taiwan (marbles from Chia-Li well no. 1): Pb-Pb isochron and Sr isotopic evidence, and its regional geological significance. *J. Geol. Soc. China*, 35(2), 193-218.
- Jahn, B. M., Martineau, F. & Comichet, J. (1984). Chronological significance of Sr isotopic compositions in the crystalline limestones of the Central Range, Taiwan. *Memoirs of Geological Society China* 6, 295-301.
- Jahn, B. M., Zhou, X. H., & Li, J. L. (1990). Formation and tectonic evolution of southeastern China and Taiwan: isotopic and geochemical constraints. *Tectonophysics*, 183(1-4), 145-160.
- Jakes, A. L. (1976). High-K₂O island-arc volcanic rocks from the Finisterre and Adelbert Ranges, northern Papua New Guinea. *Geological Society of America Bulletin*, 87(6), 861-867.
- Jakes, A. L. (1981). Petrology and petrogenesis of cumulate peridotites and gabbros from the Marum ophiolite complex, northern Papua New Guinea. *Journal of Petrology*, 22(1), 1-40.
- Jakes, A. L., & BW, C. (1978). Geochemistry of LIL-element enriched tholeiites from the Marum ophiolite complex, northern Papua New Guinea. *Australian Journal of Geology and Geophysics* 3(4), 297-310.
- Jakes, A. L., & Chappell, B. W. (1980). Petrology and trace element geochemistry of the Papuan ultramafic belt. *Contributions to Mineralogy and Petrology*, 75(1), 55-70.
- Jakes, A. L., & Robinson, G.P. (1976). Madang - Papua New Guinea 1: 250,000 geological series. Geological Survey of Papua New Guinea, Dept. of Minerals and Energy, Port Moresby.
- Jakes, A. L., & Robinson, G.P. (1980). Bogia - Papua New Guinea 1: 250,000 geological series. Geological Survey of Papua New Guinea, Dept. of Minerals and Energy, Port Moresby.
- Jakes, A. L., Chappell, B. W., & Taylor, S. R. (1983). Geochemistry of cumulus peridotites and gabbros from the Marum Ophiolite Complex, northern Papua New Guinea. *Contributions to Mineralogy and Petrology*, 82, 154-164.
- Jarboe, N., Koppers, A., Tauxe, L., Minnett, R. and Constable, C. (2012). The online MagIC Database: data archiving, compilation, and visualization for the geomagnetic, paleomagnetic and rock magnetic

- communities, AGU Fall Meeting Abstracts, pp. GP31A-1063.
- Jasin, B. (2000). Significance of Mesozoic radiolarian chert in Sabah and Sarawak. In *Proceedings Geological Society of Malaysia Annual Conference* (pp. 123-130).
- Jasin, B. (2018). Radiolarian biostratigraphy of Malaysia. *Bulletin of the Geological Society of Malaysia*, 65, 45-58.
- Jasin, B., & Said, U. (1999). Significance of Early Jurassic Radiolaria from West Sarawak, Malaysia. *Proceedings Geological Society of Malaysia Annual Conference* (pp. 491-502).
- Jasin, B., & Tongkul, F. (2013). Cretaceous radiolarians from Baliojong ophiolite sequence, Sabah, Malaysia. *Journal of Asian Earth Sciences*, 76, 258-265.
- Ji, W., Lin, W., Faure, M., Chen, Y., Chu, Y., & Xue, Z. (2017). Origin of the Late Jurassic to Early Cretaceous peraluminous granitoids in the northeastern Hunan province (middle Yangtze region), South China: Geodynamic implications for the Paleo-Pacific subduction. *Journal of Asian Earth Sciences*, 141, 174-193.
- Jiang, X. Y., & Li, X. H. (2014). In situ zircon U-Pb and Hf-O isotopic results for ca. 73 Ma granite in Hainan Island: Implications for the termination of an Andean-type active continental margin in southeast China. *Journal of Asian Earth Sciences*, 82, 32-46.
- Jiang, Y. H., Wang, G. C., Liu, Z., Ni, C. Y., Qing, L., & Zhang, Q. (2015). Repeated slab advance-retreat of the Palaeo-Pacific plate underneath SE China. *International Geology Review*, 57(4), 472-491.
- Jochum, K.P., Nohl, U., Herwig, K., Lammel, E., Stoll, B. and Hofmann, A.W., (2005). GeoReM: a new geochemical database for reference materials and isotopic standards. *Geostandards and Geoanalytical Research*, 29(3): 333-338.
- Johnson, C. L., Constable, C. G., Tauxe, L., Barendregt, R., Brown, L. L., Coe, R. S., Layer, P., Mejia, V., Opdyke, N. D., Singer, B. S., et al. (2008). Recent investigations of the 0-5 Ma geomagnetic field recorded by lava flows. *Geochemistry, Geophysics, Geosystems*, 9, Q04032.
- Johnson, T. L. (1979). Alternative model for emplacement of the Papuan ophiolite, Papua New Guinea. *Geology*, 7(10), 495-498.
- Jokat, W., Boebel, T., König, M., & Meyer, U. (2003). Timing and geometry of early Gondwana breakup. *Journal of Geophysical Research: Solid Earth*, 108(B9).
- Jolivet, L., Tamaki, K., & Fournier, M. (1994). Japan Sea, opening history and mechanism: A synthesis. *Journal of Geophysical Research: Solid Earth*, 99(B11), 22237-22259.
- Jones, P.C., Johnson, A.C., von Frese, R.R., & Corr, H. (2002). Detecting rift basins in the Evans Ice Stream region of West Antarctica using airborne gravity data. *Tectonophysics*, 347(1-3), 25-41.
- Jordan, T., Ferraccioli, F., Vaughan, D., Holt, J., Corr, H., Blankenship, D., & Diehl, T. (2010). Aerogravity evidence for major crustal thinning under the Pine Island Glacier region (West Antarctica). *Bulletin*, 122(5-6), 714-726.
- Jordan, T.A., Riley, T.R., & Siddoway, C.S. (2020). The geological history and evolution of West Antarctica. *Nature Reviews Earth & Environment*, 1(2), 117-133.
- Joseph, L. E., & Finlayson, E. J. (1991). A revised stratigraphy of Muyua (Woodlark Island). *Geological Survey of Papua New Guinea*.
- Joshima, M., Okuda, Y., Murakami, F., Kishimoto, K., & Honza, E. (1986). Age of the Solomon Sea Basin from magnetic lineations. *Geo-Marine Letters*, 6, 229-234.
- Jost, B. M., Webb, M., & White, L. T. (2018). The Mesozoic and Palaeozoic granitoids of north-western New Guinea. *Lithos*, 312, 223-243.
- Kakizaki, Y., Weissert, H., Hasegawa, T., Ishikawa, T., Matsuoka, J., & Kano, A. (2013). Strontium and carbon isotope stratigraphy of the Late Jurassic shallow marine limestone in western Palaeo-Pacific, northwest Borneo. *Journal of Asian Earth Sciences*, 73, 57-67.
- Kamp, P. J. J. (1986). The mid-Cenozoic challenger rift system of western New Zealand and its implications for the age of alpine fault inception. *Geological Society of America Bulletin*, 97(3), 255-281.
- Kamp, P. J. J. (1986). The mid-Cenozoic Challenger Rift System of western New Zealand and its implications for the age of Alpine fault inception. *The Geological Society of America Bulletin*, 97(3), 255-281.
- Kamp, P. J. J. (1987). Age and origin of the New Zealand orocline in relation to Alpine Fault movement. *Journal of the Geological Society*, 144, 641-652.
- Kamp, P. J. J. (1999). Tracking crustal processes by FT thermochronology in a forearc high (Hikurangi margin, New Zealand) involving Cretaceous subduction termination and mid-Cenozoic subduction initiation. *Tectonophysics*, 307, 313-343.
- Kamp, P. J. J. (2000). Thermochronology of the Torlesse accretionary complex, Wellington region, New Zealand. *Journal of Geophysical Research: Solid Earth*, 105, 19253-19272.
- Kamp, P. J. J., & Liddell, I. J. (2000). Thermochronology of northern Murihiku Terrane, New Zealand, derived

- from apatite FT analysis. *Journal of the Geological Society*, 157, 345–354.
- Kamp, P. J. J., Tripathi, A. R. P., & Nelson, C. S. (2014). Paleogeography of late Eocene to earliest Miocene Te Kuiti Group, central-western North Island, New Zealand. *New Zealand Journal of Geology and Geophysics*, 57, 128–148.
- Kamp, P. J. J., van der Wiel, L., Lyon, Z., van de Lagemaat, S. H. A., Boschman, L. M., & van Hinsbergen, D. J. J. (2017). From Global plate kinematics (GPlates) to basin-scale strain expressed in stratigraphy and structure: An application to Taranaki Basin, New Zealand. *New Zealand Petroleum Conference 2017*, 21–23 March, New Plymouth. Download at: <http://www.petroleumconference.nz/past-conferences/2017-presentations/>
- Kamp, P. J. J., Vonk, A. J., Nelson, C. S., Hansen, R. J., Tripathi, A., Hood, S., Ngatai, M., & Hendy, A. J. W. (2004). Constraints on the evolution of Taranaki Fault from thermochronology and basin analysis: Implications for the Taranaki Fault play. *2004 New Zealand Petroleum Conference Proceedings*; 7–10th March 2004; Auckland. Crown Minerals. Ministry of Economic Development, Wellington. 25pp.
- Karig, D. E. (1971). Structural history of the Mariana island arc system. *Geological Society of America Bulletin*, 82(2), 323–344.
- Karig, D. E. (1983). Accreted terranes in the northern part of the Philippine archipelago. *Tectonics*, 2(2), 211–236.
- Karsli, O., Caran, Ş., Dokuz, A., Çoban, H., Chen, B., & Kandemir, R. (2012). A-type granitoids from the Eastern Pontides, NE Turkey: Records for generation of hybrid A-type rocks in a subduction-related environment. *Tectonophysics*, 530, 208–224.
- Kear, D. (1960). Sheet 4, Hamilton, 'Geological map of NZ 1:250,000'. DSIR Wellington.
- Keating, B. (1980). Paleomagnetic study of sediments from deep sea drilling project leg 59. Kroenke, L., Scott, R., et al., Init. Repts. DSDP, 59, 523–532.
- Keating, B. H., & Helsley, C. E. (1985). Implications of island arc rotations to the studies of marginal terranes. *Journal of geodynamics*, 2(2–3), 159–181.
- Keating, B. H., & Herrero, E. (1980). Palcomagnetic studies of basalts and andesites from DSDP Leg 59, Initial Rep. Deep Sea Drill. Proj, 59, 533–544.
- Keenan, T. E. (2016). Rapid conversion from spreading to subduction: Structural, geochemical, and geochronological studies in Palawan, Philippines (PhD Thesis, Saint Louis University).
- Keenan, T. E., Encarnación, J., Buchwaldt, R., Fernandez, D., Mattinson, J., Rasoazanamparany, C., & Luetkemeyer, P. B. (2016). Rapid conversion of an oceanic spreading center to a subduction zone inferred from high-precision geochronology. *Proceedings of the National Academy of Sciences*, 113(47), E7359–E7366.
- Keller, W.R., 2004. Cenozoic plate tectonic reconstructions and plate boundary processes in the Southwest Pacific, Ph. D Thesis, California Institute of Technology, Pasadena, CA, 139 pp.
- Ketcham, R. A. (2005). Forward and inverse modeling of low-temperature thermochronometry data. *Reviews in Mineralogy and Geochemistry*, 58(1), 275–314.
- Kharaka, Y. K., & Hanor, J. S. (2003). Deep fluids in the continents. I. Sedimentary basins. *Treatise on geochemistry* (Vol. 5, p. 605).
- Kiel, S., Birgel, D., Campbell, K. A., Crampton, J. S., Schiøler, P., & Peckmann, J. (2013). Cretaceous methane-seep deposits from New Zealand and their fauna. *Palaeogeography, Palaeoclimatology, Palaeoecology*, 390, 17–34.
- Kim, S. T., & O'Neil, J. R. (1997). Equilibrium and nonequilibrium oxygen isotope effects in synthetic carbonates. *Geochimica et Cosmochimica Acta*, 61(16), 3461–3475.
- Kiminami, K., Miyashita, S., & Kawabata, K. (1994). Ridge collision and in situ greenstones in accretionary complexes: An example from the Late Cretaceous Ryukyu Islands and southwest Japan margin. *Island Arc*, 3(2), 103–111.
- Kimura, G., Hashimoto, Y., Kitamura, Y., Yamaguchi, A., & Koge, H. (2014). Middle Miocene swift migration of the TTT triple junction and rapid crustal growth in southwest Japan: A review. *Tectonics*, 33(7), 1219–1238.
- King, P. R. (2000). Tectonic reconstructions of New Zealand: 40 Ma to the present. *New Zealand Journal of Geology and Geophysics*, 43(4), 611–638.
- King, P. R., & Thrasher, G. P. (1996). Cretaceous-Cenozoic geology and petroleum systems of the Taranaki Basin, New Zealand. *Institute of Geological & Nuclear Sciences monograph 13* (p. 244). Institute of Geological & Nuclear Sciences, Lower Hutt.
- King, R. (1955). The remanent magnetism of artificially deposited sediments. *Geophysical Supplements to Monthly Notices of the Royal Astronomical Society*, 7(3), 115–134.
- Kinoshita, H. (1980). Paleomagnetism of sediment cores from Deep Sea Drilling Project Leg 58, Philippine

- Sea. Init. Rept., DSDP, 58, 765-768.
- Kirschvink, J. (1980). The least-squares line and plane and the analysis of palaeomagnetic data. *Geophysical Journal International*, 62(3), 699-718.
- Kizaki, K. (1986). Geology and tectonics of the Ryukyu Islands. *Tectonophysics*, 125(1-3), 193-207.
- Klepeis, K., Betka, P., Clarke, G., Fanning, M., Hervé, F., Rojas, L., Mpodozis, C., & Thomson, S. (2010). Continental underthrusting and obduction during the Cretaceous closure of the Rocas Verdes rift basin, Cordillera Darwin, Patagonian Andes. *Tectonics*, 29(3).
- Klepeis, K.A. (1994a). The Magallanes and Deseado fault zones: Major segments of the South American-Scotia transform plate boundary in southernmost South America, Tierra del Fuego. *Journal of Geophysical Research: Solid Earth*, 99(B11), 22001-22014.
- Klepeis, K.A. (1994b). Relationship between uplift of the metamorphic core of the southernmost Andes and shortening in the Magallanes foreland fold and thrust belt, Tierra del Fuego, Chile. *Tectonics*, 13(4), 882-904.
- Klepeis, K.A., & Austin Jr, J.A. (1997). Contrasting styles of superposed deformation in the southernmost Andes. *Tectonics*, 16(5), 755-776.
- Kley, J., Monaldi, C., & Salfity, J. (1999). Along-strike segmentation of the Andean foreland: causes and consequences. *Tectonophysics*, 301(1-2), 75-94.
- Klimetz, M. P. (1987). The Mesozoic Tectonostratigraphic Terranes and Accretionary Heritage of South-Eastern Mainland Asia. *Terrane Accretion and Orogenic Belts*, 19, 221-234.
- Klingelhofer, F., Lafoy, Y., Collot, J.-Y., Cosquer, E., Géli, L., Nouzé, H., & Vially, R. (2007). Crustal structure of the basin and ridge system west of New Caledonia (southwest Pacific) from wide-angle and reflection seismic data. *Journal of Geophysical Research*, 112, B11102.
- Knesel, K.M., Cohen, B.E., Vasconcelos, P.M., & Thiede, D.S. (2008). Rapid change in drift of the Australian plate records collision with Ontong Java Plateau. *Nature*, 454(7205), 754-757.
- Knittel, U. (1983). Age of the Cordon Syenite Complex and its implication on the Mid-Tertiary history of North Luzon. *Philippine Geol*, 37(2), 22-31.
- Knittel, U., Walia, M., Suzuki, S., Dimalanta, C. B., Tamayo, R., Yang, T. F., & Yumul Jr, G. P. (2017). Diverse protolith ages for the Mindoro and Romblon Metamorphics (Philippines): Evidence from single zircon U-Pb dating. *Island Arc*, 26(1), e12160.
- Kobayashi, K., Fujioka, K., Fujiwara, T., Iwabuchi, Y., & Kitazato, H. (1997). Why is the Palau Trench so deep? Deep-sea trench without plate convergence. *Proceedings of the Japan Academy, Series B*, 73(6), 89-94.
- Kodama, K., Fukuoka, M., Aita, Y., Sakai, T., Hori, R. S., Takemura, A., Campbell, H. J., Hollis, C. J., Grant-Mackie, J. A., & Spörli, K. B. (2007). Paleomagnetic results from Arrow Rocks in the framework of paleomagnetism in pre-Neogene rocks from New Zealand. In B. Spörli, A. Takemura, & R. S. Hori (Eds.), *The oceanic Permian/Triassic boundary sequence at Arrow Rocks (Oruatuemanu), Northland, New Zealand* (pp. 177-196). Wellington: GNS Science Monograph.
- König, M., & Jokat, W. (2006). The Mesozoic breakup of the Weddell Sea. *Journal of Geophysical Research: Solid Earth*, 111(B12).
- Konstantinovskaia, E.A. (2001). Arc-continent collision and subduction reversal in the Cenozoic evolution of the Northwest Pacific: an example from Kamchatka (NE Russia). *Tectonophysics*, 333(1-2), 75-94.
- Korenaga, J. (2005). Why did not the Ontong Java Plateau form subaerially?. *Earth and Planetary Science Letters*, 234(3-4), 385-399.
- Koulali, A., Tregoning, P., McClusky, S., Stanaway, R., Wallace, L., & Lister, G. (2015). New Insights into the present-day kinematics of the central and western Papua New Guinea from GPS. *Geophysical Journal International*, 202(2), 993-1004.
- Koymans, M. R., Langereis, C. G., Pastor-Galán, D., & van Hinsbergen, D. J. J. (2016). Paleomagnetism.org: An online multi-platform open source environment for paleomagnetic data analysis. *Computers and Geosciences*, 93, 127-137.
- Koymans, M., van Hinsbergen, D. J. J., Pastor-Galan, D., Vaes, B., & Langereis, C. (2020). Towards FAIR paleomagnetic data management through Paleomagnetism.org 2.0. *Geochemistry, Geophysics, Geosystems*, 21(2), e2019GC008838.
- Kraemer, P.E. (1998). Structure of the Patagonian Andes: Regional balanced cross section at 50 S, Argentina. *International Geology Review*, 40(10), 896-915.
- Kraemer, P.E. (2003). Orogenic shortening and the origin of the Patagonian orocline (56 S. Lat). *Journal of South American Earth Sciences*, 15(7), 731-748.
- Kravchinsky, V. A., Cogné, J. P., Harbert, W. P., & Kuzmin, M. I. (2002). Evolution of the Mongol-Okhotsk Ocean as constrained by new palaeomagnetic data from the Mongol-Okhotsk suture zone, Siberia. *Geophysical Journal International*, 148(1), 34-57.

- Kroenke, L. (1981). Site 451: East edge of the West Mariana Ridge. Initial Report of the Deep Sea Drilling Project, 59, 405-483.
- Kroenke, L. W., & Eade, J. V. (1982). Three Kings Ridge: A west-facing arc. *Geo-Marine Letters*, 2(1-2), 5–10.
- Kroenke, L. W., Resig, J. M., & Cooper, P. A. (1986). Tectonics of the Southeastern Solomon Islands: Formation of the Malaita Anticlinorium. *Geology and Offshore Resources of Pacific Island Arcs—central and western Solomon Islands*, 4, 109-116.
- Kumagai, H., Kaneoka, I., & Ishii, T. (1996). The active period of the Ayu Trough estimated from K-Ar ages: The southeastern spreading center of Philippine Sea Plate. *Geochemical Journal*, 30(2), 81-87.
- Kump, L.R., Brantley, S.L., & Arthur, M.A. (2000). Chemical weathering, atmospheric CO₂, and climate. *Annual Review of Earth and Planetary Sciences*, 28, 611-667.
- Labis, F. A. C., Payot, B. D., Valera, G. T. V., Pasco, J. A., Dycoco, J. M. A., Tamura, A., Morishita, T., & Arai, S. (2021). Melt-rock interaction in the subarc mantle: records from the plagioclase peridotites of the southern Palawan Ophiolite, Philippines. *International Geology Review*, 63(9), 1067-1089.
- LaBrecque, J.L., & Barker, P. (1981). The age of the Weddell basin. *Nature*, 290(5806), 489-492.
- Lafoy, Y., Géli, L., Klingelhoefer, F., Vially, R., Sichler, B., & Nouzé, H. (2005). Discovery of continental stretching and oceanic spreading in the Tasman Sea. *Eos, Transactions American Geophysical Union*, 86(10), 101-105.
- Lafoy, Y., Missegue, F., Cluzel, D., & Le Sauve, R. (1996). The Loyalty-New Hebrides Arc collision: Effects on the Loyalty Ridge and basin system, Southwest Pacific (first results of the ZoNéCo programme). *Marine Geophysical Researches*, 18(2-4), 337–356.
- Lagabriele, Y., Goddérès, Y., Donnadieu, Y., Malavieille, J., & Suarez, M. (2009). The tectonic history of Drake Passage and its possible impacts on global climate. *Earth and Planetary Science Letters*, 279(3-4), 197-211.
- Lagabriele, Y., Ruellan, E., Tanahashi, M., Bourgois, J., Buffet, G., de Alteriis, G., et al. (1996). Active oceanic spreading in the Northern North Fiji Basin: Results of the NOFI cruise of R/V L'Atalante (Newstarmer Project). *Marine Geophysical Researches*, 18(2-4), 225–247.
- Lai, Y. M., Song, S. R., Lo, C. H., Lin, T. H., Chu, M. F., & Chung, S. L. (2017). Age, geochemical and isotopic variations in volcanic rocks from the Coastal Range of Taiwan: Implications for magma generation in the Northern Luzon Arc. *Lithos*, 272, 92-115.
- Laird, M.G., & Bradshaw, J.D. (2004). The break-up of a long-term relationship: the Cretaceous separation of New Zealand from Gondwana. *Gondwana Research*, 7(1), 273-286.
- Lallemant, S., & Arcay, D. (2021). Subduction initiation from the earliest stages to self-sustained subduction: Insights from the analysis of 70 Cenozoic sites. *Earth-Science Reviews*, 221, 103779.
- Lallemant, S., Heuret, A., & Boutelier, D. (2005). On the relationships between slab dip, back-arc stress, upper plate absolute motion, and crustal nature in subduction zones. *Geochemistry, Geophysics, Geosystems*, 6(9).
- Lallemant, S., Heuret, A., Faccenna, C., & Funiciello, F. (2008). Subduction dynamics as revealed by trench migration. *Tectonics*, 27, TC3014.
- Lamb, S. (2011). Cenozoic tectonic evolution of the New Zealand plate-boundary zone: A paleomagnetic perspective. *Tectonophysics*, 509(3-4), 135–164.
- Lamb, S., Mortimer, N., Smith, E., & Turner, G. (2016). Focusing of relative plate motion at a continental transform fault: Cenozoic dextral displacement >700 km on New Zealand's Alpine Fault, reversing >225 km of late Cretaceous sinistral motion. *Geochemistry, Geophysics, Geosystems*, 17, 1197–1213.
- Lambiase, J. J., Tzong, T. Y., William, A. G., Bidgood, M. D., Brenac, P., & Cullen, A. B. (2008). The West Crocker formation of northwest Borneo: A Paleogene accretionary prism. In: *Formation and Applications of the Sedimentary Record in Arc Collision Zones*, Amy E. Draut, Peter. D. Clift, David W. Scholl (Eds). GSA Special Papers.
- Lambiase, J. J., Tzong, T. Y., William, A. G., Bidgood, M. D., Brenac, P., & Cullen, A. B. (2008). The West Crocker formation of northwest Borneo: A Paleogene accretionary prism.
- Landmesser, C., Andrews, J. & Packham, G. (1973). Aspects of the geology of the eastern Coral Sea and the western New Hebrides Basin. *Initial Reports of the Deep Sea Drilling Project*, 30, 647-662
- Lapierre, H., Jahn, B. M., Charvet, J., & Yu, Y. W. (1997). Mesozoic felsic arc magmatism and continental olivine tholeiites in Zhejiang Province and their relationship with the tectonic activity in southeastern China. *Tectonophysics*, 274(4), 321-338.
- Lapierre, H., Jahn, B. M., Charvet, J., & Yu, Y. W. (1997). Mesozoic felsic arc magmatism and continental olivine tholeiites in Zhejiang Province and their relationship with the tectonic activity in southeastern China. *Tectonophysics*, 274(4), 321-338.
- Lapouille, A. (1982). Etude des bassins marginaux fossiles du Sud-Ouest Pacifique: bassin Nord

- d'Entrecasteaux, bassin Nord-Loyaute, bassin Sud-Fidjien, Contribution a l'etude geodynamique du Sud-Ouest Pacifique, Travaux et Documents de l'ORSTOM, 147, 409-438.
- Larsen, H. C., Mohn, G., Nirrengarten, M., Sun, Z., Stock, J., Jian, Z., ... & Zhong, L. (2018). Rapid transition from continental breakup to igneous oceanic crust in the South China Sea. *Nature Geoscience*, 11(10), 782-789.
- Larson, R. L., & Chase, C. G. (1972). Late Mesozoic evolution of the western Pacific Ocean. *Geological Society of America Bulletin*, 83(12), 3627-3644.
- Larson, R.L. (1997). Superplumes and ridge interactions between Ontong Java and Manihiki plateaus and the Nova-Canton trough. *Geology*, 25(9), 779-782.
- Larson, R.L., Pockalny, R.A., Viso, R.F., Erba, E., Abrams, L.J., Luyendyk, B.P., Stock, J.M., & Clayton, R.W. (2002). Mid-Cretaceous tectonic evolution of the Tongareva triple junction in the southwestern Pacific Basin. *Geology*, 30(1), 67-70.
- Larter, R. D., Cunningham, A. P., Barker, P. F., Gohl, K., & Nitsche, F. O. (2002). Tectonic evolution of the Pacific margin of Antarctica I. Late Cretaceous tectonic reconstructions. *Journal of Geophysical Research*, 107(B12), 2345.
- Larter, R.D., Barker, P.F., & Lawver, L.M. (1991). Effects of ridge crest-trench interaction on Antarctic-Phoenix spreading: forces on a young subducting plate. *Journal of Geophysical Research: Solid Earth*, 96(B12), 19583-19607.
- Larter, R. D., Vanneste, L.E., Morris, P., & Smythe, D.K. (2003). Structure and tectonic evolution of the South Sandwich arc. *Geological Society, London, Special Publications*, 219(1), 255-284.
- Launay, J., Dupont, J., & Lapouille, A. (1982). The Three Kings Ridge and the Norfolk Basin (southwest Pacific): An attempt at structural interpretation. *South Pacific Marine Geological Notes*, 2, 121- 130.
- Lawver, L.A., & Gahagan, L.M. (1994). Constraints on timing of extension in the Ross Sea region. *Terra Antarctica*, 1(3), 545-552.
- Le Dain, A. Y., Taponnier, P., & Molnar, P. (1984). Active faulting and tectonics of Burma and surrounding regions. *Journal of Geophysical Research: Solid Earth*, 89(B1), 453-472.
- Lebrun, J. F., Lamarche, G., Collet, J. Y., & Delteil, J. (2000). Abrupt strike-slip fault to subduction transition: The Alpine fault-Puysegur trench connection, New Zealand. *Tectonics*, 19(4), 688-706.
- Lee, C. S., Shor Jr, G. G., Bibee, L. D., Lu, R. S., & Hilde, T. W. (1980). Okinawa Trough: Origin of a back-arc basin. *Marine Geology*, 35(1-3), 219-241.
- Lee, T. Y., & Lawver, L. A. (1995). Cenozoic plate reconstruction of Southeast Asia. *Tectonophysics*, 251(1-4), 85-138.
- Lee, Y. J., & Morse, J. W. (1999). Calcite precipitation in synthetic veins: Implications for the time and fluid volume necessary for vein filling. *Chemical Geology*, 156(1-4), 151- 170.
- LeMasurier, W.E. (2008). Neogene extension and basin deepening in the West Antarctic rift inferred from comparisons with the East African rift and other analogs. *Geology*, 36(3), 247-250.
- Letouzey, J., & Kimura, M. (1986). The Okinawa Trough: genesis of a back-arc basin developing along a continental margin. *Tectonophysics*, 125(1-3), 209-230.
- Lewis, K. B., & Marshall, B. A. (1996). Seep faunas and other indicators of methane-rich dewatering on New Zealand convergent margins. *New Zealand Journal of Geology and Geophysics*, 39(2), 181- 200.
- Li, C. F., Xu, X., Lin, J., Sun, Z., Zhu, J., Yao, Y., ... & Zhang, G. L. (2014). Ages and magnetic structures of the South China Sea constrained by deep tow magnetic surveys and IODP Expedition 349. *Geochemistry, Geophysics, Geosystems*, 15(12), 4958-4983.
- Li, H., Ling, M. X., Li, C. Y., Zhang, H., Ding, X., Yang, X. Y., Fan, W. M., Li, Y. L., & Sun, W. D. (2012). A-type granite belts of two chemical subgroups in central eastern China: Indication of ridge subduction. *Lithos*, 150, 26-36.
- Li, H., Ling, M.X., Li, C.Y., Zhang, H., Ding, X., Yang, X.Y., Sun, W.D., et al. (2012). A-type granite belts of two chemical subgroups in central eastern China: Indication of ridge subduction. *Lithos*, 150, 26-36.
- Li, J., Zhang, Y., Dong, S., & Johnston, S. T. (2014). Cretaceous tectonic evolution of South China: A preliminary synthesis. *Earth-Science Reviews*, 134, 98-136.
- Li, S., Advokaat, E.L., Van Hinsbergen, D.J., Koymans, M., Deng, C., & Zhu, R. (2017). Paleomagnetic constraints on the Mesozoic-Cenozoic paleolatitudinal and rotational history of Indochina and South China: Review and updated kinematic reconstruction. *Earth-Science Reviews*, 171, 58-77.
- Li, X., Li, J., Yu, X., Wang, C., & Jourdan, F. (2015). ⁴⁰Ar/³⁹Ar ages of seamount trachytes from the South China Sea and implications for the evolution of the northwestern sub-basin. *Geoscience Frontiers*, 6(4), 571-577.
- Li, Z. X., & Li, X. H. (2007). Formation of the 1300-km-wide intracontinental orogen and postorogenic magmatic province in Mesozoic South China: A flat-slab subduction model. *Geology*, 35(2), 179-182.

- Li, Z. X., Li, X. H., Chung, S. L., Lo, C. H., Xu, X., & Li, W. X. (2012). Magmatic switch-on and switch-off along the South China continental margin since the Permian: Transition from an Andean-type to a Western Pacific-type plate boundary. *Tectonophysics*, 532, 271-290.
- Li, Z., Qiu, J. S., & Yang, X. M. (2014). A review of the geochronology and geochemistry of Late Yanshanian (Cretaceous) plutons along the Fujian coastal area of southeastern China: Implications for magma evolution related to slab break-off and rollback in the Cretaceous. *Earth-Science Reviews*, 128, 232-248.
- Lin, C. T., Harris, R., Sun, W. D., & Zhang, G. L. (2019). Geochemical and geochronological constraints on the origin and emplacement of the East Taiwan Ophiolite. *Geochemistry, Geophysics, Geosystems*, 20(4), 2110-2133.
- Lindley, D. (1988). Early Cainozoic stratigraphy and structure of the Gazelle Peninsula, east New Britain: An example of extensional tectonics in the New Britain arc-trench complex. *Journal of the Geological Society of Australia*, 35(2), 231-244.
- Lindley, I. D. (2006). New Britain Trench, Papua New Guinea: An extensional element in a regional sinistral strike-slip system. *New Concepts in Global Tectonics Newsletter*, 41, 15-27.
- Lindley, I. D. (2016). Plate flexure and volcanism: late cenozoic tectonics of the tabar–lihir–tanga–feni alkaline province, new Ireland basin, Papua New Guinea. *Tectonophysics*, 677, 312-323.
- Lindley, I. D. (2021). Cenozoic volcanism, tectonics and mineralisation of Woodlark Island (Muyuw), eastern Papua. *Australian Journal of Earth Sciences*, 68(5), 609-627.
- Ling, H. Y., Hall, R., & Nichols, G. J. (1991). Early Eocene Radiolaria from Waigeo Island, Eastern Indonesia. *Journal of Southeast Asian Earth Sciences*, 6(3-4), 299-305.
- Lippert, P. C., Van Hinsbergen, D. J., & Dupont-Nivet, G. (2014). Early Cretaceous to present latitude of the central proto-Tibetan Plateau: A paleomagnetic synthesis with implications for Cenozoic tectonics, paleogeography, and climate of Asia. *Geological Society of America Special Papers*, 507, 1-21.
- Little, T. A., Hacker, B. R., Gordon, S. M., Baldwin, S. L., Fitzgerald, P. G., Ellis, S., & Korchinski, M. (2011). Diapiric exhumation of Earth's youngest (UHP) eclogites in the gneiss domes of the D'Entrecasteaux Islands, Papua New Guinea. *Tectonophysics*, 510(1-2), 39-68.
- Liu, B., Li, S. Z., Suo, Y. H., Li, G. X., Dai, L. M., Somerville, I. D., ... & Yu, S. (2016). The geological nature and geodynamics of the Okinawa Trough, Western Pacific. *Geological Journal*, 51, 416-428.
- Liu, B., Wu, J. H., Li, H., Wu, Q. H., Evans, N. J., Kong, H., & Xi, X. S. (2020). Geochronology, geochemistry and petrogenesis of the Dengfuxian lamprophyres: Implications for the early Cretaceous tectonic evolution of the South China Block. *Geochemistry*, 80(2), 125598.
- Liu, J. X., Wang, S., Wang, X. L., Du, D. H., Xing, G. F., Fu, J. M., Chen, X., & Sun, Z. M. (2020). Refining the spatio-temporal distributions of Mesozoic granitoids and volcanic rocks in SE China. *Journal of Asian Earth Sciences*, 201, 104503.
- Liu, J., Li, S., Cao, X., Dong, H., Suo, Y., Jiang, Z., ... & Foulger, G. R. (2023). Back-Arc Tectonics and Plate Reconstruction of the Philippine Sea-South China Sea Region Since the Eocene. *Geophysical Research Letters*, 50(5), e2022GL102154.
- Liu, L., Zhang, Z., Cheng, Z., Santosh, M., Liu, B., & Li, H. (2021). Ultramafic xenoliths from aillikites in the Tarim large igneous province: Implications for Alaskan-type affinity and role of subduction. *Lithos*, 380, 105902.
- Liu, W., Gai, C., Feng, W., Cao, W., Guo, L., Zhong, Y., ... & Liu, Q. (2021). Coeval evolution of the eastern Philippine Sea Plate and the South China Sea in the Early Miocene: paleomagnetic and provenance constraints from ODP site 1177. *Geophysical Research Letters*, 48(14), e2021GL093916.
- Livermore, R. A., & Woollett, R. W. (1993). Seafloor spreading in the Weddell Sea and southwest Atlantic since the Late Cretaceous. *Earth and Planetary Science Letters*, 117(3-4), 475-495.
- Livermore, R., Hillenbrand, C. D., Meredith, M., & Eagles, G. (2007). Drake Passage and Cenozoic climate: an open and shut case? *Geochemistry, Geophysics, Geosystems*, 8(1).
- Livermore, R., Nankivell, A., Eagles, G., & Morris, P. (2005). Paleogene opening of Drake Passage. *Earth and Planetary Science Letters*, 236(1-2), 459-470.
- Llubes, M., Seoane, L., Bruinsma, S., & Rémy, F. (2018). Crustal thickness of Antarctica estimated using data from gravimetric satellites. *Solid Earth*, 9(2), 457-467.
- Lo, C. H., Onstott, T. C., Chen, C. H., & Lee, T. (1994). An assessment of $^{40}\text{Ar}/^{39}\text{Ar}$ dating for the whole-rock volcanic samples from the Luzon Arc near Taiwan. *Chemical Geology*, 114(1-2), 157-178.
- Lo, Y. C., Chih-Tung, C., Lo, C. H., & Sun-Lin, C. (2020). Ages of ophiolitic rocks along plate suture in Taiwan orogen: Fate of the South China Sea from subduction to collision. *TAO: Terrestrial, Atmospheric and Oceanic Sciences*, 31(4), 3.
- Lodolo, E., Civile, D., Vuan, A., Tassone, A., & Geletti, R. (2010). The Scotia-Antarctica plate boundary from 35°W to 45°W. *Earth and Planetary Science Letters*, 293(1-2), 200-215.

- Lodolo, E., Donda, F., & Tassone, A. (2006). Western Scotia Sea margins: improved constraints on the opening of the Drake Passage. *Journal of Geophysical Research: Solid Earth*, 111(B6).
- Lodolo, E., Menichetti, M., Bartole, R., Ben-Avraham, Z., Tassone, A., & Lippai, H. (2003). Magallanes-Fagnano continental transform fault (Tierra del Fuego, southernmost South America). *Tectonics*, 22(6).
- Loiselle, M.C., & Wones, D.R. (1979). Characteristics and origin of anorogenic granites. *Geological Society of America Abstracts with Programs*, 11, 468.
- Longerich, H. P., Jackson, S. E., & Günther, D. (1996). Inter-laboratory note. Laser ablation inductively coupled plasma mass spectrometric transient signal data acquisition and analyte concentration calculation. *Journal of analytical atomic spectrometry*, 11(9), 899-904.
- Longshaw, S., & Griffiths, D. (1983). A palaeomagnetic study of Jurassic rocks from the Antarctic Peninsula and its implications. *Journal of the Geological Society*, 140(6), 945-954.
- Louden, K. E. (1977). Paleomagnetism of DSDP sediments, phase shifting of magnetic anomalies, and rotations of the West Philippine Basin. *Journal of Geophysical Research*, 82(20), 2989-3002.
- Loyd, S. J., Sample, J., Tripathi, R. E., Defliese, W. F., Brooks, K., Hovland, M., et al. (2016). Methane seep carbonates yield clumped isotope signatures out of equilibrium with formation temperatures. *Nature Communications*, 7(1), 1– 12.
- Ludwig, K. R. (2003). User's manual for isoplot 3.00, a geochronological toolkit for microsoft excel. Berkeley Geochronol. Cent. Spec. Publ., 4, 25-32.
- Ludwig, K. R. (2013). Isoplot 4.13. Berkeley Geochronology Center Special Publication, (Vol. 4).
- Lus, W. Y., McDougall, I., & Davies, H. L. (2004). Age of the metamorphic sole of the Papuan Ultramafic Belt ophiolite, Papua New Guinea. *Tectonophysics*, 392(1-4), 85-101.
- Luyendyk, B. P. (1995). Hypothesis for Cretaceous rifting of east Gondwana caused by subducted slab capture. *Geology*, 23, 373–376.
- Luyendyk, B. P., Sorlien, C. C., Wilson, D. S., Bartek, L. R., & Siddoway, C. S. (2001). Structural and tectonic evolution of the Ross Sea rift in the Cape Colbeck region, Eastern Ross Sea, Antarctica. *Tectonics*, 20(6), 933-958.
- Maac, Y. O., & Ylade, E. D. (1988). Stratigraphic and paleontologic studies of Tablas, Romblon. Report of Research and Development Cooperation ITIT Project, (8319), 44-67.
- Macdonald, D., Gomez-Perez, I., Franzese, J., Spalletti, L., Lawver, L., Gahagan, L., ... & Hole, M. (2003). Mesozoic break-up of SW Gondwana: implications for regional hydrocarbon potential of the southern South Atlantic. *Marine and Petroleum Geology*, 20(3-4), 287-308.
- MacKinnon, T. C. (1983). Origin of the Torlesse terrane and coeval rocks, South Island, New Zealand. *Geological Society of America Bulletin*, 94, 967–985.
- Maffione, M. (2016). Kinematic evolution of the Southern Andean orogenic arc. In *Geodynamic Evolution of the Southernmost Andes* (pp. 173-200). Springer.
- Maffione, M., Speranza, F., Faccenna, C., & Rossello, E. (2010). Paleomagnetic evidence for a pre-early Eocene (~50 Ma) bending of the Patagonian orocline (Tierra del Fuego, Argentina): Paleogeographic and tectonic implications. *Earth and Planetary Science Letters*, 289(1-2), 273-286.
- Maffione, M., Thieulot, C., Van Hinsbergen, D. J., Morris, A., Plümper, O., & Spakman, W. (2015). Dynamics of intraoceanic subduction initiation: 1. Oceanic detachment fault inversion and the formation of supra-subduction zone ophiolites. *Geochemistry, Geophysics, Geosystems*, 16(6), 1753-1770.
- Maffione, M., van Hinsbergen, D. J., de Gelder, G. I., van der Goes, F. C., & Morris, A. (2017). Kinematics of Late Cretaceous subduction initiation in the Neo-Tethys Ocean reconstructed from ophiolites of Turkey, Cyprus, and Syria. *Journal of Geophysical Research: Solid Earth*, 122(5), 3953-3976.
- Mahoney, J. J., Storey, M., Duncan, R. A., Spencer, K. J., & Pringle, M. (1993). Geochemistry and age of the Ontong Java Plateau. *The Mesozoic Pacific: Geology, Tectonics, and Volcanism. Geophysical Monograph Series*, 77, 233-261.
- Maillet, P., Monzier, M., Selo, M., & Storzer, D. (1983). The D'Entrecasteaux Zone (Southwest Pacific). A petrological and geochronological reappraisal. *Marine Geology*, 53(3), 179– 197.
- Malahoff, A., Feden, R. H., & Fleming, H. S. (1982). Magnetic anomalies and tectonic fabric of marginal basins north of New Zealand. *Journal of Geophysical Research*, 87(B5), 4109– 4125.
- Malahoff, A., Kroenke, L. W., Cherkis, N., & Brozena, J. (1994). Magnetic and tectonic fabric in the North Fiji Basin and Lau Basin. In L. W. Kroenke, & J. V. Eade (Eds.), *Basin formation, ridge crest processes and metalogenesis in the North Fiji Basin, Circum Pacific Council for Energy and Mineral Resources, Earth Science Series* (Vol. 15, pp. 49– 63). Berlin, Heidelberg: Springer.
- Malaihollo, J. F., & Hall, R. (1996). The geology and tectonic evolution of the Bacan region, east Indonesia. *Geological Society, London, Special Publications*, 106(1), 483-497.
- Maletterre, P. (1988). The Southern Central Cordillera of Luzon; a multistage Upper Eocene to Pleistocene

- arc-deformed on the northern end of the Philippine strike-slip fault. In International Symposium on the Geodynamic Evolution of Eastern Eurasian Margin (Abstracts), Paris 13-20 September 1988.
- Maloney, K., Clarke, G., Klepeis, K., Fanning, C., & Wang, W. (2011). Crustal growth during back-arc closure: Cretaceous exhumation history of Cordillera Darwin, southern Patagonia. *Journal of Metamorphic Geology*, 29(6), 649-672.
- Malpas, J., Spörli, K. B., Black, P. M., & Smith, I. E. M. (1992). Northland ophiolite, New Zealand, and implications for plate-tectonic evolution of the Southwest Pacific. *Geology*, 20(2), 149– 152.
- Manalo, P. C., Dimalanta, C. B., Faustino-Eslava, D. V., Payot, B. D., Ramos, N. T., Queaño, K. L., ... & Yumul Jr, G. P. (2015). Geochemical and Geophysical Characteristics of the Balud Ophiolitic Complex (BOC), Masbate Island, Philippines: Implications for its Generation, Evolution and Emplacement. *Terrestrial, Atmospheric & Oceanic Sciences*, 26(6).
- Mao, S., & Mohr, B. (1995). Middle Eocene dinocysts from Bruce Bank (Scotia Sea, Antarctica) and their paleoenvironmental and paleogeographic implications. *Review of Palaeobotany and Palynology*, 86(3-4), 235-263.
- Marchadier, Y., & Rangin, C. (1990). Polyphase tectonics at the southern tip of the Manila trench, Mindoro-Tablas Islands, Philippines. *Tectonophysics*, 183(1-4), 273-287.
- Marchesi, C., Garrido, C. J., Godard, M., Belley, F., & Ferre, E. (2009). Migration and accumulation of ultra-depleted subduction related melts in the Massif du Sud ophiolite (New Caledonia). *Chemical Geology*, 266, 180– 195.
- Marshak, S. (1988). Kinematics of orocline and arc formation in thin-skinned orogens. *Tectonics*, 7(1), 73-86.
- Martin, A. K. (2011). Double saloon door tectonics in the Japan Sea, Fossa magna, and the Japanese Island arc. *Tectonophysics*, 498(1-4), 45-65.
- Martin, P. E., Macdonald, F. A., McQuarrie, N., Flowers, R. M., Weiland, R. J., Maffre, P. J. Y. (2023). The rise of New Guinea and the fall of Neogene global temperatures. *Proceedings of the National Academy of Sciences*.
- Matthews, D. H., & Maling, D. H. (1967). The geology of the South Orkney Islands: I. Signy Island. *FIDS Scientific Reports*, 25, 1-32.
- Matthews, K. J., Hale, A. J., Gurnis, M., Müller, R. D., & DiCaprio, L. (2011). Dynamic subsidence of Eastern Australia during the Cretaceous. *Gondwana Research*, 19(2), 372– 383.
- Matthews, K. J., Müller, R. D., Wessel, P., & Whittaker, J. M. (2011). The tectonic fabric of the ocean basins. *Journal of Geophysical Research: Solid Earth*, 116(B12).
- Matthews, K. J., Seton, M., & Müller, R. D. (2012). A global-scale plate reorganization event at 105–100 Ma. *Earth and Planetary Science Letters*, 355–356, 283– 298.
- Matthews, K. J., Williams, S. E., Whittaker, J. M., Müller, R. D., Seton, M., & Clarke, G. L. (2015). Geologic and kinematic constraints on Late Cretaceous to mid Eocene plate boundaries in the southwest Pacific. *Earth-Science Reviews*, 140, 72– 107.
- Matthews, K. J., Maloney, K.T., Zahirovic, S., Williams, S.E., Seton, M., Mueller, R.D. (2016). Global plate boundary evolution and kinematics since the late Paleozoic. *Global and Planetary Change*, 146, 226-250.
- Maurizot, P. (2011). First sedimentary record of the pre-obduction convergence in New Caledonia: formation of an Early Eocene accretionary complex in the north of Grande Terre and emplacement of the 'Montagnes Blanches' nappe. *Bulletin de la Société Géologique de France*, 182(6), 479-491.
- Maurizot, P., Cluzel, D., Meffre, S., Campbell, H.J., Collot, J., Sevin, B. (2020b). Pre-late Cretaceous basement terranes of the Gondwana active margin of New Caledonia. *Geological Society, London, Memoirs*, 51(1), 27-52.
- Maurizot, P., Cluzel, D., Patriat, M., Collot, J., Iseppi, M., Lesimple, S., Sechiari, A., Bosch, D., Montanini, A., Macera, P., Davies, H.L. (2020a). The Eocene subduction-obduction complex of New Caledonia. *Geological Society, London, Memoirs*, 51(1), 93-130.
- Mazengarb, C., & Harris, D. H. M. (1994). Cretaceous stratigraphic and structural relations of Raukumara Peninsula, New Zealand: Stratigraphic patterns associated with the migration of a thrust system. *Annales Tectonicae*, 8, 100–118.
- Mazengarb, C., & Speden, I. G. (2000). Geology of the Raukumara area. Institute of Geological & Nuclear Sciences 1:250 000 Geological Map 6.1 Sheet + 60 p. Lower Hutt, New Zealand. Institute of Geological & Nuclear Sciences Limited.
- McAtamney, J., Klepeis, K., Mehrtens, C., Thomson, S., Betka, P., Rojas, L., & Snyder, S. (2011). Along-strike variability of back-arc basin collapse and the initiation of sedimentation in the Magallanes foreland basin, southernmost Andes (53-54.5° S). *Tectonics*, 30(5).
- McCabe, R., & Uyeda, S. (1983). Hypothetical model for the bending of the Mariana Arc. Washington DC

- American Geophysical Union Geophysical Monograph Series, 27, 281-293.
- McCabe, R., Almasco, J., & Diegor, W. (1982). Geologic and paleomagnetic evidence for a possible Miocene collision in western Panay, central Philippines. *Geology*, 10(6), 325-329.
- McCaffrey, R., Silver, E. A., & Raitt, R. W. (1980). Crustal structure of the Molucca Sea collision zone, Indonesia. In *The tectonic and geologic evolution of Southeast Asian seas and islands*, Geophysical Monograph 23, 161-177.
- McCarron, J.J., Larter, R.D. (1998). Late Cretaceous to early Tertiary subduction history of the Antarctic Peninsula. *Journal of the Geological Society*, 155(2), 255-268.
- McCarthy, A., Magri, L., Sauermilch, I., Fox, J., Seton, M., Mohn, G., ... & Whittaker, J. M. (2022). The Louisiade ophiolite: a missing link in the western Pacific. *Terra Nova*, 34(2), 146-154.
- McFadden, P. L., & McElhinny, M. W. (1988). The combined analysis of remagnetization circles and direct observations in palaeomagnetism. *Earth and Planetary Science Letters*, 87(1-2), 161-172.
- McKenzie, D. P., & Parker, R. L. (1967). The North Pacific: an example of tectonics on a sphere. *Nature*, 216(5122), 1276-1280.
- McLennan, S.M., Hemming, S., McDaniel, D.K., Hanson, G.N., (1993). Geochemical approaches to sedimentation, provenance, and tectonics, in: Johnsson, M.J., Basu, A. (Eds.), *Processes Controlling the Composition of Clastic Sediments*, Geological Society of America Special Paper. Geological Society of America, Colorado, pp. 21-40.
- Meert, J. G., Pivarunas, A. F., Evans, D. A., Pisarevsky, S. A., Pesonen, L. J., Li, Z. X., ... & Salminen, J. M. (2020). The magnificent seven: a proposal for modest revision of the quality index. *Tectonophysics*, 790, 228549.
- Meffre, S., Symonds, P., Bernardel, G., Carson, L., & Mauffret, A. (2001). Basalts, sedimentary rocks and peridotites of the Three Kings Ridge: Implications for the initiation of convergence along the Tonga-Kermadec Arc, in paper presented at Fifth Australian Marine Geoscience Conference, Consortium for Ocean Geosciences of Australian Universities, Hobart, Australia.
- Meijer, A., Reagan, M., Ellis, H., Shafiquallah, M., Sutter, J., Damon, P., & Kling, S. (1983). Chronology of volcanic events in the eastern Philippine Sea. Washington DC American Geophysical Union Geophysical Monograph Series, 27, 349-359.
- Mesalles, L., Walia, M., Lee, H., & Lee, Y. H. (2018, December). Cenozoic evolution of the Panay Island, Philippines: magmatic chronology and arc-continent collision. In *AGU Fall Meeting Abstracts* (Vol. 2018, pp. T23A-0343).
- Metcalf, I. (1985). Lower Permian conodonts from the Terbat formation, Sarawak. *Warta Geologi* 11, 1-4.
- Metcalf, I. (2011). Tectonic framework and Phanerozoic evolution of Sundaland. *Gondwana Research*, 19(1), 3-21.
- Metcalf, I. (2013). Gondwana dispersion and Asian accretion: Tectonic and palaeogeographic evolution of eastern Tethys. *Journal of Asian Earth Sciences*, 66, 1-33.
- Metcalf, I. (2017). Tectonic evolution of Sundaland. *Bulletin of the Geological Society of Malaysia*, 63, 27-60.
- Meyer, E. E., Quicksall, A. N., Landis, J. D., Link, P. K., & Bostick, B. C. (2012). Trace and rare Earth elemental investigation of a Sturtian cap carbonate, Pocatello, Idaho: Evidence for ocean redox conditions before and during carbonate deposition. *Precambrian Research*, 192, 89-106.
- Miki, M. (1995). Two-phase opening model for the Okinawa Trough inferred from paleomagnetic study of the Ryukyu arc. *Journal of Geophysical Research: Solid Earth*, 100(B5), 8169-8184.
- Milanese, F. N., Olivero, E. B., Kirschvink, J. L., & Rapalini, A. E. (2017). Magnetostratigraphy of the Rabot formation, upper Cretaceous, James Ross Basin, Antarctic Peninsula. *Cretaceous Research*, 72, 172-187.
- Milanese, F., Rapalini, A., Slotznick, S. P., Tobin, T. S., Kirschvink, J., & Olivero, E. (2019). Late Cretaceous paleogeography of the Antarctic Peninsula: New paleomagnetic pole from the James Ross Basin. *Journal of South American Earth Sciences*, 91, 131-143.
- Miller, M. S., Kennett, B. L. N., & Lister, G. S. (2004). Imaging changes in morphology, geometry, and physical properties of the subducting Pacific plate along the Izu-Bonin-Mariana arc. *Earth and Planetary Science Letters*, 224(3-4), 363-370.
- Mitchell, A. H. G., & Warden, A. J. (1971). Geological evolution of the New Hebrides island arc. *Journal of the Geological Society*, 127(5), 501-529.
- Mitchell, A. H. G., Hernandez, F. T., & Dela Cruz, A. P. (1986). Cenozoic evolution of the Philippine Archipelago. *Journal of Southeast Asian Earth Sciences*, 1(1), 3-22.
- MMAJ-JICA (1977). Report on geological survey of northeastern Luzon. Phase III: Metal Mining Agency of Japan and Japan International Cooperation Agency, Tokyo.
- MMAJ-JICA. (1986). Report on Mineral Exploration, Mineral Deposits and Tectonics of Two Contrasting

- Geologic Environments in the Republic of the Philippines, Phase II (Masbate and Leyte Areas). MMAJ-JICA. (1987). Report on the mineral exploration, mineral deposits and tectonics of two contrasting geological environments in the Philippines, Phase 3 (part1), northern Sierra Madre area. Government of Japan, 403.
- Molnar, P., Atwater, T., Mammerickx, J., Smith, S.M. (1975). Magnetic anomalies, bathymetry and the tectonic evolution of the South Pacific since the late Cretaceous. *Geophysical Journal International*, 40(3), 383-420.
- Monnier, C., Girardeau, J., Maury, R. C., & Cotten, J. (1995). Back-arc basin origin for the East Sulawesi ophiolite (eastern Indonesia). *Geology*, 23(9), 851-854.
- Monnier, C., Girardeau, J., Pubellier, M., Polvé, M., Permana, H., & Bellon, H. (1999). Petrology and geochemistry of the Cyclops ophiolites (Irian Jaya, East Indonesia): consequences for the Cenozoic evolution of the north Australian margin. *Mineralogy and Petrology*, 65(1-2), 1-28.
- Monteleone, B. D., Baldwin, S. L., Ireland, T. R., & Fitzgerald, P. G. (2001). Thermochronologic constraints for the tectonic evolution of the Moresby seamount, Woodlark Basin, Papua New Guinea. In *Proc. ODP, Sci. Results* (Vol. 180, pp. 1-34). Ocean Drilling Program.
- Monteleone, B. D., Baldwin, S. L., Webb, L. E., Fitzgerald, P. G., Grove, M., & Schmitt, A. K. (2007). Late Miocene–Pliocene eclogite facies metamorphism, D'Entrecasteaux Islands, SE Papua New Guinea. *Journal of Metamorphic Geology*, 25(2), 245-265.
- Montes, C., Rodriguez-Corcho, A. F., Bayona, G., Hoyos, N., Zapata, S., & Cardona, A. (2019). Continental margin response to multiple arc-continent collisions: The northern Andes-Caribbean margin. *Earth-Science Reviews*, 198, 102903.
- Moore, G. F., Kadarisman, D., Evans, C. A., & Hawkins, J. W. (1981). Geology of the Talaud islands, Molucca sea collision zone, northeast Indonesia. *Journal of Structural Geology*, 3(4), 467-475.
- Morishita, T., Tani, K. I., Soda, Y., Tamura, A., Mizukami, T., & Ghosh, B. (2018). The uppermost mantle section below a remnant proto-Philippine Sea island arc: Insights from the peridotite fragments from the Daito Ridge. *American Mineralogist: Journal of Earth and Planetary Materials*, 103(7), 1151-1160.
- Morley, C. K. (2016). Major unconformities/termination of extension events and associated surfaces in the South China Seas: Review and implications for tectonic development. *Journal of Asian Earth Sciences*, 120, 62-86.
- Morrice, M. G., Jezek, P. A., Gill, J. B., Whitford, D. J., & Monoarfa, M. (1983). An introduction to the Sangihe arc: Volcanism accompanying arc—arc collision in the Molucca Sea, Indonesia. *Journal of Volcanology and Geothermal Research*, 19(1-2), 135-165.
- Mortimer, N. (2004). New Zealand's geological foundations. *Gondwana Research*, 7(1), 261-272.
- Mortimer, N. (2014). The oroclinal bend in the South Island, New Zealand. *Journal of Structural Geology*, 64, 32–38.
- Mortimer, N., Campbell, H. J., Tulloch, A. J., King, P. R., Stagpoole, V. M., Wood, R. A., ... & Seton, M. (2017). Zealandia: Earth's hidden continent. *GSA today*, 27(3), 27-35.
- Mortimer, N., Gans, P. B., Palin, J. M., Herzer, R. H., Pelletier, B., & Monzier, M. (2014b). Eocene and Oligocene basins and ridges of the Coral Sea-New Caledonia region: Tectonic link between Melanesia, Fiji, and Zealandia. *Tectonics*, 33(7), 1386-1407.
- Mortimer, N., Gans, P. B., Palin, J. M., Meffre, S., Herzer, R. H., & Skinner, D. N. B. (2010). Location and migration of Miocene–Quaternary volcanic arcs in the SW Pacific region. *Journal of Volcanology and Geothermal Research*, 190, 1–10.
- Mortimer, N., Herzer, R. H., Gans, P. B., Laporte-Magoni, C., Calvert, A. T., & Bosch, D. (2007). Oligocene–Miocene tectonic evolution of the South Fiji Basin and Northland Plateau, SW Pacific Ocean: Evidence from petrology and dating of dredged rocks. *Marine Geology*, 237(1-2), 1–24.
- Mortimer, N., Herzer, R. H., Gans, P. B., Parkinson, D. L., & Seward, D. (1998). Basement geology from Three Kings Ridge to West Norfolk Ridge, southwest Pacific Ocean: evidence from petrology, geochemistry and isotopic dating of dredge samples. *Marine Geology*, 148(3-4), 135-162.
- Mortimer, N., Hoernle, K., Hauff, F., Palin, J.M., Dunlap, W.J., Werner, R., Faure, K. (2006). New constraints on the age and evolution of the Wishbone Ridge, Southwest Pacific cretaceous microplates, and Zealandia-West Antarctica breakup. *Geology*, 34(3), 185-188.
- Mortimer, N., Rattenbury, M. S., King, P. R., Bland, K. J., Barrell, D. J. A., Bache, F., ... & Turnbull, R. E. (2014a). High-level stratigraphic scheme for New Zealand rocks. *New Zealand Journal of Geology and Geophysics*, 57(4), 402-419.
- Mortimer, N., van den Bogaard, P., Hoernle, K., Timm, C., Gans, P.B., Werner, R., Riefstahl, F. (2019). Late Cretaceous oceanic plate reorganization and the breakup of Zealandia and Gondwana. *Gondwana Research*, 65, 31-42.

- Moss, S. J. (1998). Embaluh Group turbidites in Kalimantan: evolution of a remnant oceanic basin in Borneo during the Late Cretaceous to Palaeogene. *Journal of the Geological Society*, 155(3), 509-524.
- Moulin, M., Aslanian, D., & Unternehr, P. (2010). A new starting point for the South and Equatorial Atlantic Ocean. *Earth Science Reviews*, 98(1-2), 1-37.
- Mouthereau, F., & Lacombe, O. (2006). Inversion of the Paleogene Chinese continental margin and thick-skinned deformation in the Western Foreland of Taiwan. *Journal of Structural Geology*, 28(11), 1977-1993.
- Mouthereau, F., Lacombe, O., Deffontaines, B., Angelier, J., & Brusset, S. (2001). Deformation history of the southwestern Taiwan foreland thrust belt: insights from tectono-sedimentary analyses and balanced cross-sections. *Tectonophysics*, 333(1-2), 293-322.
- Mueller, C. O., & Jokat, W. (2019). The initial Gondwana break-up: A synthesis based on new potential field data of the Africa-Antarctica Corridor. *Tectonophysics*, 750, 301-328.
- Muir, R.J., Ireland, T.R., Weaver, S.D., Bradshaw, J.D., Waight, T.E., Jongens, R., Eby, G.N. (1997). SHRIMP U-Pb geochronology of Cretaceous magmatism in Northwest Nelson-Westland, South Island, New Zealand. *New Zealand Journal of Geology and Geophysics*, 40(4), 453-463.
- Mukasa, S. B., & Dalziel, I. W. (1996). Southernmost Andes and South Georgia Island, North Scotia Ridge: Zircon U-Pb and muscovite $^{40}\text{Ar}/^{39}\text{Ar}$ age constraints on tectonic evolution of southwestern Gondwanaland. *Journal of South American Earth Sciences*, 9(5-6), 349-365.
- Mulcahy, S. R., Starnes, J. K., Day, H. W., Coble, M. A., & Vervoort, J. D. (2018). Early onset of Franciscan subduction. *Tectonics*, 37(5), 1194-1209.
- Mullender, T. A. T., Van Velzen, A. J., & Dekkers, M. J. (1993). Continuous drift correction and separate identification of ferrimagnetic and paramagnetic contributions in thermomagnetic runs. *Geophysical Journal International*, 114(3), 663-672.
- Mullender, T. A., Frederichs, T., Hilgenfeldt, C., de Groot, L. V., Fabian, K., & Dekkers, M. J. (2016). Automated paleomagnetic and rock magnetic data acquisition with an in-line horizontal "2 G" system. *Geochemistry, Geophysics, Geosystems*, 17(9), 3546-3559.
- Muller, C. (1991). Biostratigraphy and geological evolution of the Sulu Sea and surrounding area. In *Proceedings of the Ocean Drilling Program, Scientific Results (Vol. 124, pp. 121-131)*. Ocean Drilling Program.
- Müller, R. D., Cannon, J., Qin, X., Watson, R. J., Gurnis, M., Williams, S., ... & Zahirovic, S. (2018). GPlates: building a virtual Earth through deep time. *Geochemistry, Geophysics, Geosystems*, 19(7), 2243-2261.
- Müller, R. D., Royer, J. Y., Cande, S. C., Roest, W. R., & Maschenkov, S. (1999). New constraints on the Late Cretaceous/Tertiary plate tectonic evolution of the Caribbean. *Sedimentary basins of the world*, 4, 33-59.
- Müller, R. D., Seton, M., Zahirovic, S., Williams, S. E., Matthews, K. J., Wright, N. M., ... & Cannon, J. (2016). Ocean basin evolution and global-scale plate reorganization events since Pangea breakup. *Annual Review of Earth and Planetary Sciences*, 44, 107-138.
- Müller, R. D., Zahirovic, S., Williams, S. E., Cannon, J., Seton, M., Bower, D. J., ... & Gurnis, M. (2019). A global plate model including lithospheric deformation along major rifts and orogens since the Triassic. *Tectonics*, 38(6), 1884-1907.
- Müller, R., Gohl, K., Cande, S., Goncharov, A., & Golynsky, A. (2007). Eocene to Miocene geometry of the West Antarctic rift system. *Australian Journal of Earth Sciences*, 54(8), 1033-1045.
- Mumme, T. C., & Walcott, R. I. (1985). Paleomagnetic studies at geophysics division, 1980-1983. *Geophysics Division, Department of Scientific and Industrial Research* 204.
- Musgrave, R. J. (1990). Paleomagnetism and tectonics of Malaita, Solomon Islands. *Tectonics*, 9(4), 735-759.
- Nakanishi, M., & Winterer, E. L. (1998). Tectonic history of the Pacific-Farallon-Phoenix triple junction from Late Jurassic to Early Cretaceous: an abandoned Mesozoic spreading system in the central Pacific basin. *Journal of Geophysical Research: Solid Earth*, 103(B6), 12453-12468.
- Nakanishi, M., Tamaki, K., & Kobayashi, K. (1992). Magnetic anomaly lineations from Late Jurassic to Early Cretaceous in the west-central Pacific Ocean. *Geophysical Journal International*, 109(3), 701-719.
- Nakanishi, M., Winterer, E.L. (1998). Tectonic history of the Pacific-Farallon-Phoenix triple junction from late Jurassic to early Cretaceous: an abandoned Mesozoic spreading system in the Central Pacific basin. *Journal of Geophysical Research: Solid Earth*, 103(B6), 12453-12468.
- Navarrete, C., Gianni, G., Encinas, A., Márquez, M., Kamerbeek, Y., Valle, M., & Folguera, A. (2019). Triassic to Middle Jurassic geodynamic evolution of southwestern Gondwana: from a large flat-slab to mantle plume suction in a rollback subduction setting. *Earth Science Reviews*, 194, 125-159.
- Neef, G. & McDougall I. (1976) Potassium-argon ages on rocks from Small Nggela Island, British Solomon Islands, SW Pacific, *Pacific Geology* (11), 81-86.
- Nelson, C. S. (1978). Stratigraphy and paleontology of the Oligocene Te Kuiti group, Waitomo county, South

- Auckland, New Zealand. *New Zealand Journal of Geology and Geophysics*, 21, 553–594.
- Nelson, C. S., & Hume, T. M. (1977). Relative intensity of tectonic events revealed by the tertiary sedimentary record in the North Wanganui Basin and adjacent areas, New Zealand. *New Zealand Journal of Geology and Geophysics*, 20(2), 369–392.
- Nelson, C. S., Campbell, K. A., Nyman, S. L., Greinert, J., Francis, D. A., & Hood, S. D. (2019). Genetic link between Miocene seafloor methane seep limestones and underlying carbonate conduit concretions at Rocky Knob, Gisborne, New Zealand. *New Zealand Journal of Geology and Geophysics*, 62(3), 318–340.
- Nerlich, R., Clark, S. R., & Bunge, H.-P. (2013). The Scotia Sea gateway: no outlet for Pacific mantle. *Tectonophysics*, 604, 41–50.
- Newman, J. (1997). New approaches to detection and correction of suppressed vitrinite reflectance. *The APPEA Journal*, 37(1), 524–535.
- Newman, J., Eckersley, K. M., Francis, D. A., & Moore, N. A. (2000). Application of vitrinite–inertinite reflectance and fluorescence (VIRF) to maturity assessment in the East Coast and Canterbury Basins of New Zealand. *New Zealand Petroleum Conference Proceedings*, 314, 333.
- Nguyen, T. T. B., Satir, M., Siebel, W., & Chen, F. (2004). Granitoids in the Dalat zone, southern Vietnam: age constraints on magmatism and regional geological implications. *International Journal of Earth Sciences*, 93, 329–340.
- Nichols, G., & Hall, R. (1999). History of the Celebes Sea Basin based on its stratigraphic and sedimentological record. *Journal of Asian Earth Sciences*, 17(1–2), 47–59.
- Nicholson, K. N., Black, P. M., & Picard, C. (2000a). Geochemistry and tectonic significance of the Tangihua Ophiolite Complex, New Zealand. *Tectonophysics*, 321(1), 1–15.
- Nicholson, K. N., Black, P. M., Picard, C., Cooper, P., Hall, C. M., & Itaya, T. (2007). Alteration, age, and emplacement of the Tangihua Complex Ophiolite, New Zealand. *New Zealand Journal of Geology and Geophysics*, 50(2), 151–164.
- Nicholson, K. N., Picard, C., & Black, P. M. (2000b). A comparative study of Late Cretaceous ophiolitic basalts from New Zealand and New Caledonia: Implications for the tectonic evolution of the SW Pacific. *Tectonophysics*, 327(3–4), 157–171.
- Nishimura, T. (2011). Back-arc spreading of the northern Izu–Ogasawara (Bonin) Islands arc clarified by GPS data. *Tectonophysics*, 512(1–4), 60–67.
- Niu, Y., Liu, Y., Xue, Q., Shao, F., Chen, S., Duan, M., Guo, P., Gong, H., Hu, Y., Hu, Z., Kong, J., Li, J., Liu, J., Sun, P., Sun, W., Ye, L., Xiao, Y., & Zhang, Y. (2015). Exotic origin of the Chinese continental shelf: new insights into the tectonic evolution of the western Pacific and eastern China since the Mesozoic. *Science Bulletin*, 60(18), 1598–1616.
- NOAA National Centers for Environmental Information. 2022: ETOPO 2022 15 Arc-Second Global Relief Model. NOAA National Centers for Environmental Information.
- NOAA National Geophysical Data Center. (2009). ETOPO1 1 Arc-Minute Global Relief Model.
- Nong, A. T., Hauzenberger, C. A., Gallhofer, D., & Dinh, S. Q. (2021). Geochemistry and zircon UPb geochronology of Late Mesozoic igneous rocks from SW Vietnam–SE Cambodia: Implications for episodic magmatism in the context of the Paleo-Pacific subduction. *Lithos*, 390, 106101.
- Nong, A. T., Hauzenberger, C. A., Gallhofer, D., Skrzypek, E., & Dinh, S. Q. (2022). Geochemical and zircon U–Pb geochronological constraints on late mesozoic Paleo-Pacific subduction-related volcanism in southern Vietnam. *Mineralogy and Petrology*, 116(5), 349–368.
- Nyman, S. L., & Nelson, C. S. (2011). The place of tubular concretions in hydrocarbon cold seep systems: Late Miocene Urenui Formation, Taranaki Basin, New Zealand. *AAPG Bulletin*, 95(9), 1495–1524.
- Nyman, S. L., Nelson, C. S., & Campbell, K. A. (2010). Miocene tubular concretions in East Coast basin, New Zealand: Analogue for the subsurface plumbing of cold seeps. *Marine Geology*, 272(1–4), 319–336.
- O'Neill, C. J., Müller, R. D., & Steinberger, B. (2005). On the uncertainties in hotspot reconstructions and the significance of moving hotspot reference frames. *Geochemistry, Geophysics, Geosystems*, 6, Q04003.
- O'Dogherty, L. 1994. Biochronology and Palaeontology of Mid-Cretaceous Radiolarians from Northern Apennines (Italy) and Betic Cordillera (Spain). *Memoires de Geologie (Lausanne)*. 21, 1–413.
- Obayashi, M., Yoshimitsu, J., Nolet, G., Fukao, Y., Shiobara, H., Sugioka, H., et al. (2013). Finite frequency whole mantle P wave tomography: Improvement of subducted slab images. *Geophysical Research Letters*, 40, 5652–5657.
- Ogg, J. G. (2012). Chapter 5—Geomagnetic polarity time scale. In F. M. Gradstein, J. G. Ogg, M. Schmitz, & G. Ogg (Eds.), *The geologic time scale* (pp. 85–113). Boston: Elsevier.
- Ogg, J. G. (2020). Geomagnetic polarity time scale. In F. M. Gradstein, J. G. Ogg, M. D. Schmitz, G. M. Ogg (Eds.), *Geologic Time Scale 2020* (pp. 159–192). Elsevier.
- Okada, A. (1973). On the quaternary faulting along the median tectonic line. *The Median Tectonic Line*, 46,

- 49–86.
- Olfindo, V. S. V., Payot, B. D., Valera, G. T. V., Gadot Jr, E. G., Villaplaza, B. R. B., Tani, K., ... & Yumul Jr, G. P. (2019). Petrographic and geochemical characterization of the crustal section of the Pujada Ophiolite, southeastern Mindanao, Philippines: Insights to the tectonic evolution of the northern Molucca Sea Collision Complex. *Journal of Asian Earth Sciences*, 184, 103994.
- Oliver, N. H., & Bons, P. D. (2001). Mechanisms of fluid flow and fluid–rock interaction in fossil metamorphic hydrothermal systems inferred from vein–wallrock patterns, geometry and microstructure. *Geofluids*, 1(2), 137–162.
- Oliver, P. J. (1994). The tectonic significance of paleomagnetic results from the Triassic and Jurassic Murihiku sedimentary rocks of the Kawhia region, North Island, New Zealand. In G. J. Van der Lingen, K. M. Swanson, & R. J. Muir (Eds.), *Evolution of the Tasman Sea basin: Proceedings of the Tasman Sea conference* (pp. 67–82). Rotterdam: Balkema.
- Olivero, E. B., & Malumíán, N. (2008). Mesozoic–Cenozoic stratigraphy of the Fuegian Andes, Argentina. *Geologica Acta*, 6(1), 5–18.
- Österle, J. E., Little, T. A., Seward, D., Stockli, D. F., & Gamble, J. (2020). The petrology, geochronology and tectono-magmatic setting of igneous rocks in the Suckling–Dayman metamorphic core complex, Papua New Guinea. *Gondwana Research*, 83, 390–414.
- Ott, B., & Mann, P. (2015). Late Miocene to Recent formation of the Aure–Moresby fold-thrust belt and foreland basin as a consequence of Woodlark microplate rotation, Papua New Guinea. *Geochemistry, Geophysics, Geosystems*, 16(6), 1988–2004.
- Owen-Smith, T. M., Ganerød, M., van Hinsbergen, D. J., Gaina, C., Ashwal, L. D., & Torsvik, T. H. (2019). Testing early Cretaceous Africa–South America fits with new paleomagnetic data from the Etendeka Magmatic Province (Namibia). *Tectonophysics*, 760, 23–35.
- Packham, G. H., & Terrill, A. (1975). Submarine geology of the South Fiji basin. Initial Reports of the Deep Sea Drilling Project, 30, 617–645.
- Pacle, N. A. D., Dimalanta, C. B., Ramos, N. T., Payot, B. D., Faustino-Eslava, D. V., Queaño, K. L., & Yumul Jr, G. P. (2017). Petrography and geochemistry of Cenozoic sedimentary sequences of the southern Samar Island, Philippines: clues to the unroofing history of an ancient subduction zone. *Journal of Asian Earth Sciences*, 142, 3–19.
- Page, R. W. (1976). *Geochronology of Igneous and Metamorphic Rocks in the New Guinea Highlands*. Bureau of Mineral Resources, Canberra, Australia.
- Pain, C. F. (1983). Volcanic rocks and surfaces as indicators of landform age: The Astrolabe Agglomerate, Papua New Guinea. *Australian Geographer*, 15(6), 376–381.
- Pandey, A., Parson, L., & Milton, A. (2010). Geochemistry of the Davis and Aurora banks: possible implications on evolution of the North Scotia Ridge. *Marine Geology*, 268(1–4), 106–114.
- Pankhurst, R., Riley, T., Fanning, C., & Kelley, S. (2000). Episodic silicic volcanism in Patagonia and the Antarctic Peninsula: chronology of magmatism associated with the break-up of Gondwana. *Journal of Petrology*, 41(5), 605–625.
- Paquette, J.-L., & Cluzel, D. (2007). U–Pb zircon dating of post-obduction volcanic-arc granitoids and a granulite-facies xenolith from New Caledonia. Inference on Southwest Pacific geodynamic models. *International Journal of Earth Sciences*, 96, 613–622.
- Parrish, R. R., Parrish, C. M., & Lasalle, S. (2018). Vein calcite dating reveals Pyrenean orogen as cause of Paleogene deformation in southern England. *Journal of the Geological Society*, 175(3), 425–442.
- Parrot, J. F., & Dugas, F. (1980). The disrupted ophiolitic belt of the Southwest Pacific: evidence of an Eocene subduction zone. *Tectonophysics*, 66(4), 349–372.
- Parson, L. M., & Wright, I. C. (1996). The Lau–Havre–Taupo back-arc basin: A southward-propagating, multi-stage evolution from rifting to spreading. *Tectonophysics*, 263(1–4), 1–22.
- Parsons, A. J., Sigloch, K., & Hosseini, K. (2021). Australian Plate Subduction is Responsible for Northward Motion of the India–Asia Collision Zone and 1,000 km Lateral Migration of the Indian Slab. *Geophysical Research Letters*, 48(18), e2021GL094904.
- Pasco, J. A., Dycoco, J. M. A., Valera, G. T. V., Payot, B. D., Pillejera, J. D. B., Uy, F. A. A. E., ... & Dimalanta, C. B. (2019). Petrogenesis of ultramafic–mafic clasts in the Dos Hermanos Mélange, Ilocos Norte: insights to the evolution of western Luzon, Philippines. *Journal of Asian Earth Sciences*, 184, 104004.
- Passier, H. F., de Lange, G. J., & Dekkers, M. J. (2001). Rock-magnetic properties and geochemistry of the active oxidation front and the youngest sapropel in the Mediterranean. *Geophysical Journal International*, 145, 604–614.
- Paton, C., Woodhead, J. D., Hellstrom, J. C., Hergt, J. M., Greig, A., & Maas, R. (2010). Improved laser ablation U–Pb zircon geochronology through robust downhole fractionation correction. *Geochemistry, Geophysics, Geosystems*, 11(3).

- Patriat, M., Collot, J., Danyushevsky, L., Fabre, M., Meffre, S., Falloon, T., ... & Fournier, M. (2015). Propagation of back-arc extension into the arc lithosphere in the southern New Hebrides volcanic arc. *Geochemistry, Geophysics, Geosystems*, 16(9), 3142-3159.
- Patriat, M., Collot, J., Etienne, S., Poli, S., Clerc, C., Mortimer, N., ... & VESPA scientific voyage team. (2018). New Caledonia obducted Peridotite Nappe: offshore extent and implications for obduction and postobduction processes. *Tectonics*, 37(4), 1077-1096.
- Patriat, M., Falloon, T., Danyushevsky, L., Collot, J., Jean, M. M., Hoernle, K., ... & Feig, S. T. (2019). Subduction initiation terranes exposed at the front of a 2 Ma volcanically-active subduction zone. *Earth and Planetary Science Letters*, 508, 30-40.
- Pearce, J. A. (2008). Geochemical fingerprinting of oceanic basalts with applications to ophiolite classification and the search for Archean oceanic crust. *Lithos*, 100(1-4), 14-48.
- Pearce, J., Hastie, A., Leat, P., Dalziel, I., Lawver, L., Barker, P., Millar, I., Barry, T., & Bevins, R. (2014). Composition and evolution of the Ancestral South Sandwich Arc: Implications for the flow of deep ocean water and mantle through the Drake Passage Gateway. *Global and Planetary Change*, 123, 298-322.
- Pelayo, A. M., & Wiens, D. A. (1989). Seismotectonics and relative plate motions in the Scotia Sea region. *Journal of Geophysical Research: Solid Earth*, 94(B6), 7293-7320.
- Pelletier, B., & Auzende, J. M. (1996). Geometry and structure of the Vitiaz trench lineament (SW Pacific). *Marine Geophysical Researches*, 18, 305-335.
- Pepper, M., Gehrels, G., Pullen, A., Ibanez-Mejia, M., Ward, K. M., & Kapp, P. (2016). Magmatic history and crustal genesis of western South America: Constraints from U-Pb ages and Hf isotopes of detrital zircons in modern rivers. *Geosphere*, 12(5), 1532-1555.
- Pérez-Díaz, L., & Eagles, G. (2014). Constraining South Atlantic growth with seafloor spreading data. *Tectonics*, 33(9), 1848-1873.
- Permana, H. (1995). Etude des ophiolites des Weylands (Irian Jaya): origine et âge de mise en place. Comparaison avec celles de la Haute Chaîne centrale. Mémoire DEA, Université de Brest, France.
- Pessagno, E.A. & Newport, R.L. (1972). A technique for extracting Radiolaria from Radiolarian chert. *Micropaleontology* 18(2), 231-234.
- Petterson, M. G., Babbs, T., Neal, C. R., Mahoney, J. J., Saunders, A. D., Duncan, R. A., ... & Natogga, D. (1999). Geological-tectonic framework of Solomon Islands, SW Pacific: crustal accretion and growth within an intra-oceanic setting. *Tectonophysics*, 301(1-2), 35-60.
- Petterson, M. G., Coleman, P. J., Tolia, D., Mahoa, H., & Magu, R. (2009). Application of terrain modelling of the Solomon Islands, Southwest Pacific, to the metallogenesis and mineral exploration in composite arc-ocean floor terrain collages. *Pacific Minerals in the New Millennium: Science, Exploration, Mining, and Community*, 99-120.
- Petterson, M. G., Neal, C. R., Mahoney, J. J., Kroenke, L. W., Saunders, A. D., Babbs, T. L., ... & McGrail, B. (1997). Structure and deformation of north and central Malaita, Solomon Islands: tectonic implications for the Ontong Java Plateau-Solomon arc collision, and for the fate of oceanic plateaus. *Tectonophysics*, 283(1-4), 1-33.
- Philippon, M., & Corti, G. (2016). Obliquity along plate boundaries. *Tectonophysics*, 693, 171- 182.
- Phinney, E. J., Mann, P., Coffin, M. F., & Shipley, T. H. (1999). Sequence stratigraphy, structure, and tectonic history of the southwestern Ontong Java Plateau adjacent to the North Solomon Trench and Solomon Islands arc. *Journal of Geophysical Research: Solid Earth*, 104(B9), 20449-20466.
- Phinney, E. J., Mann, P., Coffin, M. F., & Shipley, T. H. (2004). Sequence stratigraphy, structural style, and age of deformation of the Malaita accretionary prism (Solomon arc-Ontong Java Plateau convergent zone). *Tectonophysics*, 389(3-4), 221-246.
- Pieters, P. E. (1976). Port Moresby-Kalo-Aroa - Papua New Guinea 1: 250,000 geological series. Geological Survey of Papua New Guinea, Dept. of Minerals and Energy, Port Moresby.
- Pieters, P. E., Hartono, U., & Amri, C. (1989). Geology of the Mar sheet area, Irian Jaya. Geological Research and Development Centre, Bandung (62pp.).
- Pieters, P. E., Pigram, C. J., Trail, D. S., Dow, D. B., Ratman, N., & Sukanto, R. (1983). The stratigraphy of western Irian Jaya. *Proceedings Indonesian Petroleum Association, Twelfth Annual Convention*. 229-261.
- Pigram, C. J., & Symonds, P. A. (1991). A review of the timing of the major tectonic events in the New Guinea Orogen. *Journal of Southeast Asian Earth Sciences*, 6(3-4), 307-318.
- Pikser, J. E., Forsyth, D. W., & Hirth, G. (2012). Along-strike translation of a fossil slab. *Earth and Planetary Science Letters*, 331-332, 315- 321.
- Pindell, J. L., & Kennan, L. (2009). Tectonic evolution of the Gulf of Mexico, Caribbean and northern South America in the mantle reference frame: An update. Geological Society, London, Special Publications,

- 328(1), 1.1-55.
- Poblete, F., Arriagada, C., Roperch, P., Astudillo, N., Hervé, F., Kraus, S., & Le Roux, J. (2011). Paleomagnetism and tectonics of the South Shetland Islands and the northern Antarctic Peninsula. *Earth and Planetary Science Letters*, 302(3-4), 299-313.
- Poblete, F., Roperch, P., Arriagada, C., Ruffet, G., de Arellano, C. R., Hervé, F., & Poujol, M. (2016). Late Cretaceous-early Eocene counter-clockwise rotation of the Fuegian Andes and evolution of the Patagonia-Antarctic Peninsula system. *Tectonophysics*, 668, 15-34.
- Porth H., Muller C. & Daniels C.H. von (1989). The sedimentary formations of the Visayan Basin, Philippines. In: PORTH H. & DANIELS C.H. (eds.), *On the Geology and Hydrocarbon Prospects of the Visayan Basin, Philippines*. - Geologisches Jahrbuch, Stuttgart, Heft 70, p. 29-87.
- Pourteau, A., Scherer, E. E., Schorn, S., Bast, R., Schmidt, A., & Ebert, L. (2019). Thermal evolution of an ancient subduction interface revealed by Lu-Hf garnet geochronology, Halilbağı Complex (Anatolia). *Geoscience Frontiers*, 10(1), 127-148.
- Prinzhofer, A. (1981). *Structure et pétrologie d'un cortège ophiolitique: Le massif du sud (Nouvelle Calédonie)*, Ph. D Thesis. École Nationale Supérieure des Mines de Paris, France.
- Pubellier, M., Bader, A. G., Rangin, C., Deffontaines, B., & Quebral, R. (1999). Upper plate deformation induced by subduction of a volcanic arc: the Snellius Plateau (Molucca Sea, Indonesia and Mindanao, Philippines). *Tectonophysics*, 304(4), 345-368.
- Pubellier, M., Monnier, C., Maury, R., & Tamayo, R. (2004). Plate kinematics, origin and tectonic emplacement of supra-subduction ophiolites in SE Asia. *Tectonophysics*, 392(1-4), 9-36.
- Pubellier, M., Quebral, R., Rangin, C., Deffontaines, B., Muller, C., Butterlin, J., & Manzano, J. (1991). The Mindanao collision zone: a soft collision event within a continuous Neogene strike-slip setting. *Journal of Southeast Asian Earth Sciences*, 6(3-4), 239-248.
- Qayyum, A., Lom, N., Advokaat, E. L., Spakman, W., Van Der Meer, D. G., & van Hinsbergen, D. J. (2022). Subduction and Slab Detachment Under Moving Trenches During Ongoing India-Asia Convergence. *Geochemistry, Geophysics, Geosystems*, 23(11), e2022GC010336.
- Qian, S., Zhang, X., Wu, J., Lallemand, S., Nichols, A. R., Huang, C., ... & Zhou, H. (2021). First identification of a Cathaysian continental fragment beneath the Gagua Ridge, Philippine Sea, and its tectonic implications. *Geology*, 49(11), 1332-1336.
- Qian, X., Yu, Y., Wang, Y., Gan, C., Zhang, Y., & Asis, J. B. (2022). Late Cretaceous Nature of SW Borneo and Paleo-Pacific Subduction: New Insights from the Granitoids in the Schwaner Mountains. *Lithosphere*, 2022(1), 8483732.
- Quarles van Ufford, A., & Cloos, M. (2005). Cenozoic tectonics of New Guinea. *AAPG Bulletin*, 89(1), 119-140.
- Queaño, K. L. (2005). Upper Miocene to Lower Pliocene Sigaboy formation turbidites, on the Pujada Peninsula, Mindanao, Philippines: internal structures, composition, depositional elements and reservoir characteristics. *Journal of Asian Earth Sciences*, 25(3), 387-402.
- Queaño, K. L., Ali, J. R., Aitchison, J. C., Yumul, G. P., Pubellier, M., & Dimalanta, C. B. (2008). Geochemistry of Cretaceous to Eocene ophiolitic rocks of the Central Cordillera: Implications for Mesozoic-early Cenozoic evolution of the northern Philippines. *International Geology Review*, 50(4), 407-421.
- Queaño, K. L., Ali, J. R., Milsom, J., Aitchison, J. C., & Pubellier, M. (2007). North Luzon and the Philippine Sea Plate motion model: Insights following paleomagnetic, structural, and age-dating investigations. *Journal of Geophysical Research: Solid Earth*, 112(B5).
- Queaño, K. L., Ali, J. R., Pubellier, M., Yumul Jr, G. P., & Dimalanta, C. B. (2009). Reconstructing the Mesozoic-early Cenozoic evolution of northern Philippines: Clues from palaeomagnetic studies on the ophiolitic basement of the Central Cordillera. *Geophysical Journal International*, 178(3), 1317-1326.
- Queaño, K. L., Dimalanta, C. B., Yumul Jr, G. P., Marquez, E. J., Faustino-Eslava, D. V., Suzuki, S., & Ishida, K. (2017b). Stratigraphic units overlying the Zambales Ophiolite Complex (ZOC) in Luzon, (Philippines): Tectonostratigraphic significance and regional implications. *Journal of Asian Earth Sciences*, 142, 20-31.
- Queaño, K. L., Marquez, E. J., Aitchison, J. C., & Ali, J. R. (2013). Radiolarian biostratigraphic data from the Casiguran Ophiolite, northern Sierra Madre, Luzon, Philippines: stratigraphic and tectonic implications. *Journal of Asian Earth Sciences*, 65, 131-142.
- Queaño, K. L., Marquez, E. J., Dimalanta, C. B., Aitchison, J. C., Ali, J. R., & Yumul Jr, G. P. (2017a). Mesozoic radiolarian faunas from the northwest Ilocos Region, Luzon, Philippines and their tectonic significance. *Island Arc*, 26(4), e12195.
- Queaño, K. L., Yumul Jr, G. P., Marquez, E. J., Gabo-Ratio, J. A., Payot, B. D., & Dimalanta, C. B. (2020). Consumed tectonic plates in Southeast Asia: Markers from the Mesozoic to early Cenozoic stratigraphic units in the northern and central Philippines. *Journal of Asian Earth Sciences*, X, 4, 100033.
- Quebral, R. (1994). *Tectonique du segment méridional de la faille Philippine, Mindanao oriental, Philippines*:

- passage d'une zone de collision à une zone de décrochement (Doctoral dissertation, Paris 6).
- Quebral, R. D., Pubellier, M., & Rangin, C. (1996). The onset of movement on the Philippine Fault in eastern Mindanao: A transition from a collision to a strike-slip environment. *Tectonics*, 15(4), 713-726.
- Quesnel, B., Gautier, P., Cathelineau, M., Boulvais, P., Couteau, C., & Drouillet, M. (2016). The internal deformation of the Peridotite Nappe of New Caledonia: A structural study of serpentine-bearing faults and shear zones in the Koniombo Massif. *Journal of Structural Geology*, 85, 51- 67.
- Rahim, A. R., Konjing, Z., Asis, J., Jalil, N. A., Muhamad, A. J., Ibrahim, N., Munif Koraini, A., Che Kob, R., Mazlan, H., & Tjia, H. D. (2017). Tectonostratigraphic terranes of Kudat Peninsula, Sabah.
- Raimbourg, H., Augier, R., Famin, V., Gadenne, L., Palazzin, G., Yamaguchi, A., & Kimura, G. (2014). Long-term evolution of an accretionary prism: The case study of the Shimanto Belt, Kyushu, Japan. *Tectonics*, 33(6), 936-959.
- Raine, J. I., Beu, A. G., Boyes, A. F., Campbell, H. J., Cooper, R. A., Crampton, J. S., et al. (2015). New Zealand geological timescale NZGT 2015/1. *New Zealand Journal of Geology and Geophysics*, 58(4), 398- 403.
- Rait, G. J. (1992). Early Miocene thrust tectonics on Raukumara peninsula, Northeastern New Zealand. PhD thesis. Victoria University of Wellington. Retrieved from Victoria University of Wellington Research Archive <http://hdl.handle.net/10063/700>
- Rait, G. J., Chanier, F., & Waters, D. W. (1991). Landward-and seaward-directed thrusting accompanying the onset of subduction beneath New Zealand. *Geology*, 19(3), 230- 233.
- Ramsay, J. G. (1980). The crack-seal mechanism of rock deformation. *Nature*, 284(5752), 135- 139.
- Rangin, C. (1991). The Philippine Mobile Belt: a complex plate boundary. *Journal of Southeast Asian Earth Sciences*, 6(3-4), 209-220.
- Rangin, C., Bellon, H., Benard, F., Letouzey, J., Muller, C., & Sanudin, T. A. H. I. R. (1990). Neogene arc-continent collision in Sabah, northern Borneo (Malaysia). *Tectonophysics*, 183(1-4), 305-319.
- Rangin, C., Dahrin, D., Quebral, R., & Modéc Scientific Party. (1996). Collision and strike-slip faulting in the northern Molucca Sea (Philippines and Indonesia): preliminary results of a morphotectonic study. Geological Society, London, Special Publications, 106(1), 29-46.
- Rangin, C., Spakman, W., Pubellier, M., & Bijwaard, H. (1999). Tomographic and geological constraints on subduction along the eastern Sundaland continental margin (South-East Asia). *Bulletin de la Société géologique de France*, 170(6), 775-788.
- Rangin, C., Stephan, J. F., & Muller, C. (1985). Middle Oligocene oceanic crust of South China Sea jammed into Mindoro collision zone (Philippines). *Geology*, 13(6), 425-428.
- Rangin, C., Stephan, J. F., Butterlin, J., Bellon, H., Muller, C., Chorowicz, J., & Baladad, D. (1991). Collision néogène d'arcs volcaniques dans le centre des Philippines: stratigraphie et structure de la chaîne d'Antique (île de Panay). *Bulletin Societe Géologique du France*, 162(3), 465-477.
- Rapalini, A. E., Tohver, E., Bettucci, L. S., Lossada, A. C., Barcelona, H., & Pérez, C. (2015). The late Neoproterozoic Sierra de las Ánimas Magmatic complex and Playa Hermosa Formation, southern Uruguay, revisited: Paleogeographic implications of new paleomagnetic and precise geochronologic data. *Precambrian Research*, 259, 143-155.
- Rapela, C., & Pankhurst, R. (1992). The granites of northern Patagonia and the Gastre Fault System in relation to the break-up of Gondwana. Geological Society, London, Special Publications, 68(1), 209-220.
- Raza, A., Hill, K. C., & Korsch, R. J. (2009). Mid-Cretaceous uplift and denudation of the Bowen and Surat Basins, eastern Australia: Relationship to Tasman Sea rifting from apatite fission-track and vitrinite-reflectance data. *Australian Journal of Earth Sciences*, 56(3), 501-531.
- Reagan, M. K., & Meijer, A. (1984). Geology and geochemistry of early arc-volcanic rocks from Guam. *Geological Society of America Bulletin*, 95(6), 701-713.
- Reagan, M. K., Hanan, B. B., Heizler, M. T., Hartman, B. S., & Hickey-Vargas, R. (2008). Petrogenesis of volcanic rocks from Saipan and Rota, Mariana Islands, and implications for the evolution of nascent island arcs. *Journal of Petrology*, 49(3), 441-464.
- Reagan, M. K., Heaton, D. E., Schmitz, M. D., Pearce, J. A., Shervais, J. W., & Koppers, A. A. (2019). Forearc ages reveal extensive short-lived and rapid seafloor spreading following subduction initiation. *Earth and Planetary Science Letters*, 506, 520-529.
- Reagan, M. K., Ishizuka, O., Stern, R. J., Kelley, K. A., Ohara, Y., Blichert-Toft, J., ... & Woods, M. (2010). Fore-arc basalts and subduction initiation in the Izu-Bonin-Mariana system. *Geochemistry, Geophysics, Geosystems*, 11(3).
- Reagan, M. K., McClelland, W. C., Girard, G., Goff, K. R., Peate, D. W., Ohara, Y., & Stern, R. J. (2013). The geology of the southern Mariana fore-arc crust: Implications for the scale of Eocene volcanism in the western Pacific. *Earth and Planetary Science Letters*, 380, 41-51.
- Récy, J. (1977). Fossil subduction zones: examples in the South West Pacific, International Symposium

- Geodynamics in S.W. Pacific, 345-356.
- Ren, J., Niu, B., Wang, J., Jin, X., Zhao, L., & Liu, R. (2013). Advances in research of Asian geology—A summary of 1: 5M International Geological Map of Asia project. *Journal of Asian Earth Sciences*, 72, 3-11.
- Retallack, G. J. (1987). Triassic vegetation and geography of the New Zealand portion of the Gondwana supercontinent. In E. D. McKenzie (Ed.), *Gondwana six: stratigraphy, sedimentology and paleontology* (pp. 29-39). Washington, DC: American Geophysical Union
- Rey, P., & Müller, R. (2010). Fragmentation of active continental plate margins owing to the buoyancy of the mantle wedge. *Nature Geoscience*, 3, 257-261.
- Reyes, A. G., Christenson, B. W., & Faure, K. (2010). Sources of solutes and heat in low-enthalpy mineral waters and their relation to tectonic setting, New Zealand. *Journal of Volcanology and Geothermal Research*, 192(3-4), 117- 141.
- Reyners, M., Eberhart-Phillips, D., & Bannister, S. (2011). Tracking repeated subduction of the Hikurangi Plateau beneath New Zealand. *Earth and Planetary Science Letters*, 311(1-2), 165-171.
- Reyners, M., Eberhart-Phillips, D., Upton, P., & Gubbins, D. (2017). Three-dimensional imaging of impact of a large igneous province with a subduction zone. *Earth and Planetary Science Letters*, 460, 143-151.
- Richard, M., Bellon, H., Maury, R., Barrier, E., & Wen-Shing, J. (1986). Miocene to recent calc-alkalic volcanism in eastern Taiwan: K-Ar ages and petrography. *Tectonophysics*, 125(1-3), 87-102.
- Richards, J. R., Cooper, J. A., Webb, A. W., & Coleman, P. J. (1966). Potassium-Argon Measurements of the Age of Basal Schists in the British Solomon Islands. *Nature*, 211, 1251-1252.
- Richter, C., & Ali, J. R. (2015). Philippine sea plate motion history: Eocene-Recent record from ODP Site 1201, central West Philippine basin. *Earth and Planetary Science Letters*, 410, 165-173.
- Rickard, M. J., & Williams, I. S. (2013). No zircon U-Pb evidence for a Precambrian component in the Late Eocene Yavuna trondhjemite, Fiji. *Australian Journal of Earth Sciences*, 60(4), 521-525.
- Ridgway, J., & Coulson, F. I. E. (1987). *The Geology of Choiseul and the Shortland Islands, Solomon Islands* (Vol. 8). HM Stationery Office.
- Ridley, W. I., Rhodes, J. M., REID, A. M., Jakes, P., Shih, C. Y., & Bass, M. N. (1974). Basalts from leg 6 of the deep-sea drilling project. *Journal of petrology*, 15(1), 140-159.
- Riefstahl, F., Gohl, K., Davy, B., Hoernle, K., Mortimer, N., Timm, C., Werner, R., & Hochmuth, K. (2020). Cretaceous intracontinental rifting at the southern Chatham Rise margin and initialization of seafloor spreading between Zealandia and Antarctica. *Tectonophysics*, 776, 228298.
- Riley, T. R., & Knight, K. B. (2001). Age of pre-break-up Gondwana magmatism. *Antarctic Science*, 13(2), 99-110.
- Riley, T. R., Carter, A., Leat, P. T., Burton-Johnson, A., Bastias, J., Spikings, R. A., ... & Bristow, C. S. (2019). Geochronology and geochemistry of the northern Scotia Sea: a revised interpretation of the North and West Scotia Ridge junction. *Earth and Planetary Science Letters*, 518, 136-147.
- Ringenbach, J. C., Stephan, J. F., Maletterre, P., & Bellon, H. (1990). Structure and geological history of the Lepanto-Cervantes releasing bend on the Abra River fault, Luzon Central Cordillera, Philippines. *Tectonophysics*, 183(1-4), 225-241.
- Rinke-Hardekopf, L., Dashtgard, S.E., Huang, C., Gibson, H.D., (2021). Application of grouped detrital zircon analyses to determine provenance and closely approximate true depositional age: Early Cretaceous McMurray-Clearwater succession, Canada. *Geoscience Frontiers* 12, 877-892.
- Ritger, S., Carson, B., & Suess, E. (1987). Methane-derived authigenic carbonates formed by subduction-induced pore-water expulsion along the Oregon/Washington margin. *The Geological Society of America Bulletin*, 98(2), 147- 156.
- Roberts, N. M., Rasbury, E. T., Parrish, R. R., Smith, C. J., Horstwood, M. S., & Condon, D. J. (2017). A calcite reference material for LA-ICP-MS U-Pb geochronology. *Geochemistry, Geophysics, Geosystems*, 18(7), 2807- 2814.
- Rodrigo, J. D., Gabo-Ratio, J. A. S., Queaño, K. L., Fernando, A. G. S., de Silva Jr, L. P., Yonezu, K., & Zhang, Y. (2020). Geochemistry of the Late Cretaceous Pandan Formation in Cebu Island, Central Philippines: sediment contributions from the Australian plate margin during the Mesozoic. *The Depositional Record*, 6(2), 309-330.
- Rodrigo, J., & Schlagintweit, F. (2022). The Lower Cretaceous Tuburan Limestone of Cebu Island, Philippines: Microfacies, micropalaeontology, biostratigraphy, and palaeogeographic perspectives. *Carnets Geol.*, 22(14), 661-679.
- Rodrigo, J., Tsutsumi, Y., Tani, K., Haga, T., & Aira, J. (2021). Tectonostratigraphy of the basement complex of Cebu Island, central Philippines: New constraints from petrography, micropaleontology and geochronology. In *The Second International Symposium of the International Geoscience Programme*

- Project 679, 19.
- Rodriguez-Roa, F. A., & Wiltschko, D. V. (2010). Thrust belt architecture of the central and southern Western Foothills of Taiwan. *Geological Society, London, Special Publications*, 348(1), 137-168.
- Roeser, H. A. (1991). Age of the crust of the southeast Sulu Sea basin based on magnetic anomalies and age determined at site 768. In *Proceedings of the Ocean Drilling Program, Scientific Results* 124, 339-343.
- Rogerson, R. (1987). The geology and mineral resources of the Sepik headwaters region, Papua New Guinea (Vol. 12). Geological Survey of Papua New Guinea.
- Rogerson, R. J., & Hilyard, D. B. (1990). Scrapland: a suspect composite terrane in Papua New Guinea. *Papua New Guinea (PNG) Petroleum Convention Proceedings*.
- Rollinson, H. R., Rollinson, H., & Pease, V. (2021). Using geochemical data: To understand geological processes. Cambridge University Press.
- Roser, B. P., Coombs, D. S., Korsch, R. J., & Campbell, J. D. (2002). Whole-rock geochemical variations and evolution of the arc-derived Murihiku Terrane, New Zealand. *Geological Magazine*, 139(6), 665-685.
- Roser, B., Korsch, R., (1988). Provenance signatures of sandstone-mudstone suites determined using discriminant function analysis of major-element data. *Chemical Geology* 67, 119-139.
- Rouillard, P., Collot, J., Sutherland, R., Bache, F., Patriat, M., Etienne, S., & Maurizot, P. (2017). Seismic stratigraphy and paleogeographic evolution of Fairway Basin, Northern Zealandia, Southwest Pacific: From Cretaceous Gondwana breakup to Cenozoic Tonga-Kermadec subduction. *Basin Research*, 29, 189-212.
- Rowan, C. J., Roberts, A. P., & Rait, G. J. (2005). Relocation of the tectonic boundary between the Raukumara and Wairoa domains (East Coast, North Island, New Zealand): Implications for the rotation history of the Hikurangi margin. *New Zealand Journal of Geology and Geophysics*, 48(1), 185-196.
- Royer, J. Y., & Chang, T. (1991). Evidence for relative motions between the Indian and Australian plates during the last 20 my from plate tectonic reconstructions: Implications for the deformation of the Indo-Australian plate. *Journal of Geophysical Research: Solid Earth*, 96(B7), 11779-11802.
- Rudnick, R. L., Gao, S., (2003). Composition of the continental crust, in: Rudnick, Roberta L. (Ed.), *Treatise in Geochemistry* Vol. 3, The Crust. Elsevier, Oxford, pp. 1-64.
- Ruellan, E., Delteil, J., Wright, I., & Matsumoto, T. (2003). From rifting to active spreading in the Lau Basin-Havre Trough backarc system (SW Pacific): Locking/unlocking induced by seamount chain subduction. *Geochemistry, Geophysics, Geosystems*, 4(5), 8909.
- Ryburn, R. J. (1980). Blueschists and associated rocks in the south Sepik region, Papua New Guinea; field relations, petrology, mineralogy, metamorphism and tectonic setting. Doctoral dissertation, University of Auckland.
- Rytuba, J. J., & Miller, W. R. (1990). Geology and geochemistry of epithermal precious metal vein systems in the intra-oceanic arcs of Palau and Yap, western Pacific. *Journal of Geochemical Exploration*, 35(1-3), 413-447.
- Saffer, D. M. (2007). 7. Pore Pressure within underthrust sediment in subduction zones. In *The seismogenic zone of subduction thrust faults* (pp. 171-209). Columbia University Press.
- Sager, W. W., & Carvallo, C. (2022). Paleomagnetism and paleolatitude of igneous drill core samples from the Izu-Bonin forearc and implications for Philippine Sea plate motion. *Tectonophysics*, 841, 229573.
- Saito, M. (2008). Rapid evolution of the Eocene accretionary complex (Hyuga Group) of the Shimanto terrane in southeastern Kyushu, southwestern Japan. *Island Arc*, 17(2), 242-260.
- Sajona, F. G., Bellon, H., Maury, R. C., Pubellier, M., Quebral, R. D., Cotten, J., ... & Pamatian, P. (1997). Tertiary and quaternary magmatism in Mindanao and Leyte (Philippines): geochronology, geochemistry and tectonic setting. *Journal of Asian Earth Sciences*, 15(2-3), 121-153.
- Sakai, H., Gamo, T., Ogawa, Y., & Boulegue, J. (1992). Stable isotopic ratios and origins of the carbonates associated with cold seepage at the eastern Nankai Trough. *Earth and Planetary Science Letters*, 109(3-4), 391-404.
- Salabarnada, A., Escutia, C., Röhl, U., Nelson, C. H., McKay, R., Jiménez-Espejo, F., ... & Salzmann, U. (2018). Paleooceanography and ice sheet variability offshore Wilkes Land, Antarctica—Part 1: Insights from late Oligocene astronomically paced contourite sedimentation. *Climate of the Past*, 14(7), 991-1014.
- Sample, J. C. (1996). Isotopic evidence from authigenic carbonates for rapid upward fluid flow in accretionary wedges. *Geology*, 24(10), 897-900.
- Sample, J. C., Reid, M. R., Tols, H. J., & Moore, J. C. (1993). Carbonate cements indicate channeled fluid flow along a zone of vertical faults at the deformation front of the Cascadia accretionary wedge (northwest US coast). *Geology*, 21(6), 507-510.
- Sample, J. C., Torres, M. E., Fisher, A., Hong, W. L., Destigneville, C., Defliese, W. F., & Tripathi, A. E. (2017). Geochemical constraints on the temperature and timing of carbonate formation and lithification in the

- Nankai Trough, NanTroSEIZE transect. *Geochimica et Cosmochimica Acta*, 198, 92–114.
- Sandmann, S., Nagel, T. J., Froitzheim, N., Ustaszewski, K., & Münker, C. (2015). Late Miocene to Early Pliocene blueschist from Taiwan and its exhumation via forearc extraction. *Terra Nova*, 27(4), 285–291.
- Sanfilippo, A. & Riedel, W.R. (1985). Cretaceous Radiolaria. In: Bolli, H.M., Saunders, J.B. & Perch-Nielsen, K. (Ed.). *Plankton Stratigraphy*, 631–712. New York: Cambridge University Press.
- Sangiorgi, F., Bijl, P. K., Passchier, S., Salzmann, U., Schouten, S., McKay, R., ... & Bohaty, S. M. (2018). Southern Ocean warming and Wilkes Land ice sheet retreat during the mid-Miocene. *Nature Communications*, 9(1), 1–11.
- Santos, R. A. (2014). Mineral Resource Estimate Report of the Islands of Nonoc, Awasan, and Hanigad and Part of South Dinagat for Pacific Nickel Philippines Inc. (PNPI). MPSA No. 072-1997-XIII.
- Saputra, A., Hall, R., & White, L. T. (2014). Development of the Sorong Fault Zone North of Misool, Eastern Indonesia. Indonesian Petroleum Association, 38th Annual Convention Proceedings, IPA 14-G-086.
- Saragih, R. Y., Sunan, H. L., Slameto, E., & Nurdiana, I. (2020, December). Rifting and Lifting Neogene Age in Biak-Yapen Basin Based on Structural Trajectory Analogy in Biak and Supiori Island. In IOP Conference Series: Materials Science and Engineering (Vol. 982, No. 1, p. 012042). IOP Publishing.
- Sarewitz, D. R., & Karig, D. E. (1986). Processes of allochthonous terrane evolution, Mindoro Island, Philippines. *Tectonics*, 5(4), 525–552.
- Sasaki, T., Yamazaki, T., & Ishizuka, O. (2014). A revised spreading model of the West Philippine Basin. *Earth, Planets and Space*, 66, 1–9.
- Sato, T., Kasahara, J., Katao, H., Tomiyama, N., Mochizuki, K., & Koresawa, S. (1997). Seismic observations at the Yap Islands and the northern Yap Trench. *Tectonophysics*, 271(3–4), 285–294.
- Schellart, W. P. (2005). Influence of the subducting plate velocity on the geometry of the slab and migration of the subduction hinge. *Earth and Planetary Science Letters*, 231(3–4), 197–219.
- Schellart, W. P. (2007). North-eastward subduction followed by slab detachment to explain ophiolite obduction and Early Miocene volcanism in Northland, New Zealand. *Terra Nova*, 19(3), 211–218.
- Schellart, W. P. (2017). Andean mountain building and magmatic arc migration driven by subduction-induced whole mantle flow. *Nature Communications*, 8, 2010.
- Schellart, W. P., & Spakman, W. (2012). Mantle constraints on the plate tectonic evolution of the Tonga–Kermadec–Hikurangi subduction zone and the South Fiji Basin region. *Australian Journal of Earth Sciences*, 59(6), 933–952.
- Schellart, W. P., & Spakman, W. (2015). Australian plate motion and topography linked to fossil New Guinea slab below Lake Eyre. *Earth and Planetary Science Letters*, 421, 107–116.
- Schellart, W. P., Kennett, B. L. N., Spakman, W., & Amaru, M. (2009). Plate reconstructions and tomography reveal a fossil lower mantle slab below the Tasman Sea. *Earth and Planetary Science Letters*, 278(3–4), 143–151.
- Schellart, W. P., Lister, G. S., & Toy, V. G. (2006). A Late Cretaceous and Cenozoic reconstruction of the Southwest Pacific region: tectonics controlled by subduction and slab rollback processes. *Earth-Science Reviews*, 76(3–4), 191–233.
- Schellart, W. P., Stegman, D. R., & Freeman, J. (2008). Global trench migration velocities and slab migration induced upper mantle volume fluxes: Constraints to find an Earth reference frame based on minimizing viscous dissipation. *Earth-Science Reviews*, 88, 118–144.
- Schepers, G., Van Hinsbergen, D. J., Spakman, W., Kesters, M. E., Boschman, L. M., & McQuarrie, N. (2017). South-American plate advance and forced Andean trench retreat as drivers for transient flat subduction episodes. *Nature Communications*, 8, 15249.
- Scher, H. D., & Martin, E. E. (2006). Timing and climatic consequences of the opening of Drake Passage. *Science*, 312(5772), 428–430.
- Schimschal, C. M., & Jokat, W. (2018). The crustal structure of the continental margin east of the Falkland Islands. *Tectonophysics*, 724, 234–253.
- Schimschal, C. M., & Jokat, W. (2019). The Falkland Plateau in the context of Gondwana breakup. *Gondwana Research*, 68, 108–115.
- Schlüter, H. U., HINz, K., & Block, M. (1996). Tectono-stratigraphic terranes and detachment faulting of the South China Sea and Sulu Sea. *Marine Geology*, 130(1–2), 39–78.
- Schmidtke, E. A., Fuller, M. D., & Haston, R. B. (1990). Paleomagnetic data from Sarawak, Malaysian Borneo, and the late Mesozoic and Cenozoic tectonics of Sundaland. *Tectonics*, 9(1), 123–140.
- Schreider, A. A., Schreider, A., Galindo-Zaldivar, J., Maldonado, A., Sazhneva, A., & Evsenko, E. (2017). Age of the scan basin (Scotia Sea). *Oceanology*, 57(2), 328–336.
- Schreider, A. A., Schreider, A., Galindo-Zaldivar, J., Maldonado, A., Sazhneva, A., & Evsenko, E. (2018). Age of the floors of the protector and dove basins (Scotia Sea). *Oceanology*, 58(3), 447–458.

- Schweller, W. J., Karig, D. E., & Bachman, S. D. (1983). The Tectonic and Geologic Evolution of Southeast Asian Seas and Islands: Part 2. American Geophysical Union Geophysical Monograph Series 27, 95-123.
- Scotese, C. R. (2021). An atlas of Phanerozoic paleogeographic maps: the seas come in and the seas go out. *Annual Review of Earth and Planetary Sciences*, 49, 679-728.
- Scott, K. M. (1966). Sedimentology and dispersal pattern of a cretaceous flysch sequence, Patagonian Andes, southern Chile. *AAPG Bulletin*, 50(1), 72-107.
- Sdrolias, M., & Müller, R. D. (2006). Controls on back-arc basin formation. *Geochemistry, Geophysics, Geosystems*, 7, Q04016.
- Sdrolias, M., Müller, R. D., & Gaina, C. (2001). Plate tectonic evolution of eastern Australian marginal ocean basins. In K. C. Hill & T. Bernecker (Eds.), *Eastern Australian Basins Symposium* (pp. 227-237). Melbourne: Petroleum Exploration Society of Australia Special Publication.
- Sdrolias, M., Müller, R. D., & Gaina, C. (2003). Tectonic evolution of the southwest Pacific using constraints from backarc basins. *Geological Society of America Special Papers*, 372, 343-359.
- Sdrolias, M., Müller, R. D., Mauffret, A., & Bernardel, G. (2004a). Enigmatic formation of the Norfolk Basin, SW Pacific: A plume influence on back-arc extension. *Geochemistry, Geophysics, Geosystems*, 5, Q06005.
- Sdrolias, M., Roest, W. R., & Müller, R. D. (2004b). An expression of Philippine Sea plate rotation: the Parece Vela and Shikoku basins. *Tectonophysics*, 394(1-2), 69-86.
- Seno, T., & Maruyama, S. (1984). Paleogeographic reconstruction and origin of the Philippine Sea. *Tectonophysics*, 102(1-4), 53-84.
- Seton, M., & Müller, R. D. (2008). Reconstructing the junction between Panthalassa and Tethys since the Early Cretaceous. *PESA Eastern Australian Basin Symposium III abstract*, 263-266.
- Seton, M., Flament, N., Whittaker, J., Müller, R. D., Gurnis, M., & Bower, D. J. (2015). Ridge subduction sparked reorganization of the Pacific plate-mantle system 60-50 million years ago. *Geophysical Research Letters*, 42(6), 1732-1740.
- Seton, M., Mortimer, N., Williams, S., Quilty, P., Gans, P., Meffre, S., ... & Matthews, K. J. (2016). Melanesian back-arc basin and arc development: Constraints from the eastern Coral Sea. *Gondwana Research*, 39, 77-95.
- Seton, M., Müller, R. D., Zahirovic, S., Gaina, C., Torsvik, T., Shephard, G., ... & Chandler, M. (2012). Global continental and ocean basin reconstructions since 200 Ma. *Earth-Science Reviews*, 113(3-4), 212-270.
- Seton, M., Whittaker, J.M., Wessel, P., Müller, R.D., DeMets, C., Merkouriev, S., ... Williams, S.E. (2014). Community infrastructure and repository for marine magnetic identifications. *Geochemistry, Geophysics, Geosystems*, 15(4), 1629-1641.
- Seton, M., Williams, S. E., Domeier, M., Collins, A. S., & Sigloch, K. (2023). Deconstructing plate tectonic reconstructions. *Nature Reviews Earth & Environment*, 4(3), 185-204.
- Sevin, B., Cluzel, D., Maurizot, P., Quesnel, F., Ricordel-Prognon, C., Chapronniere, G., et al. (2014). A drastic Lower Miocene regolith evolution triggered by post obduction slab break-off and uplift in New Caledonia. *Tectonics*, 33, 1787-1801.
- Sevin, B., Maurizot, P., Cluzel, D., Tournadour, E., Etienne, S., Folcher, N., ... & Patriat, M. (2020). Post-obduction evolution of New Caledonia. *Geological Society, London, Memoirs*, 51(1), 147-188.
- Shao, L., Cao, L., Qiao, P., Zhang, X., Li, Q., & van Hinsbergen, D. J. (2017). Cretaceous-Eocene provenance connections between the Palawan Continental Terrane and the northern South China Sea margin. *Earth and Planetary Science Letters*, 477, 97-107.
- Shapiro, M.N., & Solov'ev, A.V. (2009). Formation of the Olyutorsky-Kamchatka foldbelt: A kinematic model. *Russian Geology and Geophysics*, 50(8), 668-681.
- Shellnutt, J. G., Lan, C. Y., Van Long, T., Usuki, T., Yang, H. J., Mertzman, S. A., Iizuka, Y., Chung, S.L., Wang, K.L., & Hsu, W. Y. (2013). Formation of Cretaceous Cordilleran and post-orogenic granites and their microgranular enclaves from the Dalat zone, southern Vietnam: Tectonic implications for the evolution of Southeast Asia. *Lithos*, 182, 229-241.
- Shen, W., Wiens, D.A., Anandakrishnan, S., Aster, R.C., Gerstoft, P., Bromirski, P.D., ... Winberry, J.P. (2018). The crust and upper mantle structure of central and West Antarctica from Bayesian inversion of Rayleigh wave and receiver functions. *Journal of Geophysical Research: Solid Earth*, 123(9), 7824-7849.
- Shiraki, K. (1971). Metamorphic basement rocks of Yap Islands, western Pacific: Possible oceanic crust beneath an island arc. *Earth and Planetary Science Letters*, 13(1), 167-174.
- Shuck, B., Gulick, S. P., Van Avendonk, H. J., Gurnis, M., Sutherland, R., Stock, J., & Hightower, E. (2022). Stress transition from horizontal to vertical forces during subduction initiation. *Nature Geoscience*, 15(2), 149-155.
- Sibson, R. H. (1990). Conditions for fault-valve behaviour. *Geological Society, London, Special*
- Sibuet, J. C., Hsu, S. K., Shyu, C. T., & Liu, C. S. (1995). Structural and kinematic evolutions of the Okinawa

- Trough backarc basin. Backarc Basins: Tectonics and Magmatism, 343-379.
- Sibuet, J. C., Letouzey, J., Barbier, F., Charvet, J., Foucher, J. P., Hilde, T. W., ... & Stéphan, J. F. (1987). Back arc extension in the Okinawa Trough. *Journal of Geophysical Research: Solid Earth*, 92(B13), 14041-14063.
- Siegrist, H. G., Reagan, M. K., RH, R., & JW, J. (2008). *Geologic Map and Sections of Guam. Mariana Islands (1: 50,000), Revision of original map from USGS Professional Report A, 403, 1964.*
- Sigloch, K., & Mihalynuk, M. G. (2013). Intra-oceanic subduction shaped the assembly of Cordilleran North America. *Nature*, 496(7443), 50-56.
- Sijp, W. P., Anna, S., Dijkstra, H. A., Flögel, S., Douglas, P. M., & Bijl, P. K. (2014). The role of ocean gateways on cooling climate on long time scales. *Global and Planetary Change*, 119, 1-22.
- Silver, E. A., & Moore, J. C. (1978). The Molucca sea collision zone, Indonesia. *Journal of Geophysical Research: Solid Earth*, 83(B4), 1681-1691.
- Silver, E. A., & Rangin, C. (1991). Leg 124 Tectonic synthesis. In *Proceedings of the Ocean Drilling Program*, 124, 3-9.
- Simmons, S. F., & Christenson, B. W. (1994). Origins of calcite in a boiling geothermal system. *American Journal of Science*, 294(3), 361– 400.
- Sliter, W. V., Ishizaki, K., & Saito, T. (1992). Cretaceous planktonic foraminiferal biostratigraphy and paleoceanographic events in the Pacific Ocean with emphasis on indurated sediment. *Centenary of Japanese Micropaleontology*, 281-99.
- Smalley Jr, R., Dalziel, I. W., Lawver, L. A., Gómez, D., Teferle, F. N., Sastrup, S., & Hunegnaw, A. (2019). The current tectonic setting of South Georgia Island based on GPS geodetic and marine seismic reflection data. *AGUFM*, 2019, G34A-01.
- Smalley Jr, R., Dalziel, I., Bevis, M., Kendrick, E., Stamps, D., King, E., ... & Parra, H. (2007). Scotia arc kinematics from GPS geodesy. *Geophysical Research Letters*, 34(21).
- Smalley Jr, R., Kendrick, E., Bevis, M., Dalziel, I., Taylor, F., Lauria, E., ... & Piana, E. (2003). Geodetic determination of relative plate motion and crustal deformation across the Scotia-South America plate boundary in eastern Tierra del Fuego. *Geochemistry, Geophysics, Geosystems*, 4(9).
- Smith, I. E. (2013). The chemical characterization and tectonic significance of ophiolite terrains in southeastern Papua New Guinea. *Tectonics*, 32(2), 159-170.
- Smith, R. B., Betzler, C., Brass, G. W., Huang, Z., Linsley, B. K., Menill, D., ... & Spadea, P. (1990). Depositional history of the Celebes Sea from ODP Sites 767 and 770. *Geophysical Research Letters*, 17(11), 2061-2064.
- Smith, T.R., & Cole, J.W. (1997). Somers ignimbrite formation: Cretaceous high-grade ignimbrites from South Island, New Zealand. *Journal of Volcanology and Geothermal Research*, 75(1-2), 39-57.
- Spakman, W., & Hall, R. (2010). Surface deformation and slab-mantle interaction during Banda arc subduction rollback. *Nature Geoscience*, 3(8), 562-566.
- Spakman, W., Chertova, M. V., van den Berg, A., & van Hinsbergen, D. J. (2018). Puzzling features of western Mediterranean tectonics explained by slab dragging. *Nature Geoscience*, 11(3), 211-216.
- Spakman, W., Stein, S., van der Hilst, R., & Wortel, R. (1989). Resolution experiments for NW Pacific subduction zone tomography. *Geophysical Research Letters*, 16(10), 1097-1100.
- Spiegel, C., Lindow, J., Kamp, P.J., Meisel, O., Mukasa, S., Lisker, F., ... Gohl, K. (2016). Tectonomorphic evolution of Marie Byrd Land-Implications for Cenozoic rifting activity and onset of West Antarctic glaciation. *Global and Planetary Change*, 145, 98-115.
- Spörli, K. B. (1987). Development of the New Zealand microcontinent. In J. W. H. Monger & J. Francheteau (Eds.), *Circum-pacific orogenic belts and evolution of the Pacific Ocean basin (Geodynamic Series 18)* (pp. 115–132). Washington, DC: American Geophysical Union
- Srivastava, S. P., & Roest, W. R. (1996). Comment on “Porcupine plate hypothesis” by MF Gerstell and JM Stock (*Marine Geophysical Researches* 16, pp. 315–323, 1994). *Marine Geophysical Researches*, 18(5), 589-593.
- Stacey, J. T., & Kramers, J. S. (1975). Approximation of terrestrial lead isotope evolution by a two-stage model. *Earth and Planetary Science Letters*, 26(2), 207– 221.
- Stagpoole, V., & Nicol, A. (2008). Regional structure and kinematic history of a large subduction back thrust: Taranaki Fault, New Zealand. *Journal of Geophysical Research*, 113(B1), B01403.
- Stampfli, G. M., & Borel, G. D. (2002). A plate tectonic model for the Paleozoic and Mesozoic constrained by dynamic plate boundaries and restored synthetic oceanic isochrons. *Earth and Planetary science letters*, 196(1-2), 17-33.
- Steinberger, B., Sutherland, R., & O'Connell, R.J. (2004). Prediction of Emperor-Hawaii seamount locations from a revised model of global plate motion and mantle flow. *Nature*, 430(6996), 167-173.
- Stern, C.R., & De Wit, M.J. (2003). Rocas Verdes ophiolites, southernmost South America: Remnants of progressive stages of development of oceanic-type crust in a continental margin back-arc basin.

- Geological Society, London, Special Publications, 218(1), 665-683.
- Stern, C.R., Mukasa, S.B., & Fuenzalida, R.H. (1992). Age and petrogenesis of the Sarmienot ophiolite complex of southern Chile. *Journal of South American Earth Sciences*, 6(1-2), 97-104.
- Stern, R. J. (2004). Subduction initiation: spontaneous and induced. *Earth and Planetary Science Letters*, 226(3-4), 275-292.
- Stern, R. J., & Bloomer, S. H. (1992). Subduction zone infancy: examples from the Eocene Izu-Bonin-Mariana and Jurassic California arcs. *Geological Society of America Bulletin*, 104(12), 1621-1636.
- Stern, R. J., & Gerya, T. (2018). Subduction initiation in nature and models: A review. *Tectonophysics*, 746, 173-198.
- Stern, R. J., Fouch, M. J., & Klemperer, S. L. (2003). An overview of the Izu-Bonin-Mariana subduction factory. *Geophysical Monograph, American Geophysical Union*, 138, 175-222.
- Stern, R. J., Reagan, M., Ishizuka, O., Ohara, Y., & Whattam, S. (2012). To understand subduction initiation, study forearc crust: To understand forearc crust, study ophiolites. *Lithosphere*, 4(6), 469-483.
- Stern, R.J. (2004). Subduction initiation: spontaneous and induced. *Earth and Planetary Science Letters*, 226(3-4), 275-292.
- Steuer, S., Franke, D., Meresse, F., Savva, D., Pubellier, M., Auxietre, J. L., & Aurelio, M. (2013). Time constraints on the evolution of southern Palawan Island, Philippines from onshore and offshore correlation of Miocene limestones. *Journal of Asian Earth Sciences*, 76, 412-427.
- Stewart, W. D., & Sandy, M. J. (1988). *Geology of New Ireland and Djaul Islands, northeastern Papua New Guinea. Geology and Offshore Resources of Pacific Island Arcs-New Ireland and Manus Region, Papua New Guinea*, 9, 13-30.
- Stock, J., & Molnar, P. (1987). Revised history of early Tertiary plate motion in the south-West Pacific. *Nature*, 325(6104), 495-499.
- Stock, J.M., & Cande, S.C. (2002). Tectonic history of Antarctic seafloor in the Australia-New Zealand-South Pacific sector: Implications for Antarctic continental tectonics.
- Stoneley, R. (1968). A lower tertiary decollement on the East Coast, North Island, New Zealand. *New Zealand Journal of Geology and Geophysics*, 11(1), 128- 156.
- Storey, B., & Mair, B. (1982). The composite floor of the cretaceous back-arc basin of South Georgia. *Journal of the Geological Society*, 139(6), 729-737.
- Storey, B., Mair, B., & Bell, C. (1977). The occurrence of Mesozoic oceanic floor and ancient continental crust on South Georgia. *Geological Magazine*, 114(3), 203-208.
- Storey, B.C., Vaughan, A.P., & Millar, I.L. (1996). Geodynamic evolution of the Antarctic Peninsula during Mesozoic times and its bearing on Weddell Sea history. *Geological Society, London, Special Publications*, 108(1), 87-103.
- Strogen, D. P., Higgs, K. E., Griffin, A. G., & Morgans, H. E. (2019). Late Eocene-early Miocene facies and stratigraphic development, Taranaki Basin, New Zealand: The transition to plate boundary tectonics during regional transgression. *Geological Magazine*, 156(10), 1751- 1770.
- Struckmeyer, H. I. M., & Symonds, P. A. (1997). Tectonostratigraphic evolution of the Townsville Basin, Townsville Trough, offshore northeastern Australia. *Australian Journal of Earth Sciences*, 44(6), 799-817.
- Suárez, M. (1976). Plate-tectonic model for southern Antarctic Peninsula and its relation to southern Andes. *Geology*, 4(4), 211-214.
- Suerte, L. O., Yumul, G. P., Tamayo, R. A., Dimalanta, C. B., Zhou, M. F., Maury, R. C., ... & Balce, C. L. (2005). *Geology, geochemistry and U-Pb SHRIMP age of the Tacloban Ophiolite Complex, Leyte Island (Central Philippines): Implications for the existence and extent of the proto-Philippine Sea Plate*. *Resource Geology*, 55(3), 207-216.
- Suggate, S. M., Cottam, M. A., Hall, R., Sevastjanova, I., Forster, M. A., White, L. T., Armstrong, R. A., Carter, A., & Mojares, E. (2014). South China continental margin signature for sandstones and granites from Palawan, Philippines. *Gondwana Research*, 26(2), 699-718.
- Sugiyama, Y. (1994). Neotectonics of Southwest Japan due to the right-oblique subduction of the Philippine Sea plate. *Geofisica International*, 33(1), 53-76.
- Sun, P., Guo, P., & Niu, Y. (2021). Eastern China continental lithosphere thinning is a consequence of paleo-Pacific plate subduction: A review and new perspectives. *Earth-Science Reviews*, 218, 103680.
- Sun, S.-S., McDonough, W.F., (1989). Chemical and isotopic systematics of oceanic basalts: implications for mantle composition and processes. *Geological Society, London, Special Publications* 42, 313-345.
- Suppe, J. & Chi, W. R. (1985). Tectonic implications of Miocene sediments of Lan-Hsu island, northern Luzon arc. *Petroleum Geology of Taiwan*, 21, 93-106.
- Suppe, J. O. H. N. (1980). A retrodeformable cross section of northern Taiwan. In *Proc. Geol. Soc. China*, 23, 46-55.

- Sutherland, R. (1999a). Basement geology and tectonic development of the greater New Zealand region: An interpretation from regional magnetic data. *Tectonophysics*, 308(3), 341–362.
- Sutherland, R. (1999b). Cenozoic bending of New Zealand basement terranes and alpine fault displacement: A brief review. *New Zealand Journal of Geology and Geophysics*, 42, 295–301.
- Sutherland, R., & Hollis, C. (2001). Cretaceous demise of the Moa Plate and strike-slip motion at the Gondwana margin. *Geology*, 29(3), 279–282.
- Sutherland, R., Collot, J., Bache, F., Henrys, S., Barker, D., Browne, G. H., et al. (2017). Widespread compression associated with Eocene Tonga-Kermadec subduction initiation. *Geology*, 45(4), 355–358.
- Taira, A. (1988). The Shimanto belt in Shikoku, Japan-evolution of Cretaceous to Miocene accretionary prism. The Shimanto belt, Southwest Japan-Studies on the evolution of an accretionary prism.
- Taira, A., Mann, P., & Rahardiawan, R. (2004). Incipient subduction of the Ontong Java Plateau along the North Solomon trench. *Tectonophysics*, 389(3-4), 247–266.
- Taira, A., Okada, H., Whitaker, J. H., & Smith, A. J. (1982). The Shimanto Belt of Japan: Cretaceous-lower Miocene active-margin sedimentation. Geological Society, London, Special Publications, 10(1), 5–26.
- Tamayo Jr, R. A., Maury, R. C., Yumul Jr, G. P., Polvé, M., Cotten, J., Dimantala, C. B., & Olaguera, F. O. (2004). Subduction-related magmatic imprint of most Philippine ophiolites: implications on the early geodynamic evolution of the Philippine archipelago. *Bulletin de la Société Géologique de France*, 175(5), 443–460.
- Tamayo Jr, R. A., Yumul Jr, G. P., Maury, R. C., Polvé, M., Cotten, J., & Bohn, M. (2001). Petrochemical investigation of the Antique Ophiolite (Philippines): Implications on volcanogenic massive sulfide and podiform chromitite deposits. *Resource Geology*, 51(2), 145–164.
- Tamayo, R. A., Yumul, G. P., Maury, R. C., Bellon, H., Cotten, J., Polvé, M., ... & Querubin, C. (2000). Complex origin for the south-western Zamboanga metamorphic basement complex, Western Mindanao, Philippines. *Island Arc*, 9(4), 638–652.
- Tamayo, R. J., Yumul Jr, G. P., Santos, R. A., Jumawan, F., Rodolfo, K. S. (1998). Petrology and mineral chemistry of a back-arc upper mantle suite: Example from the Camarines Norte Ophiolite complex, South Luzon. *Journal of the Geological Society of the Philippines*, 51, 1–23.
- Tanaka, G., & Nomura, S. I. (2009). Late Miocene and Pliocene Ostracoda from the Shimajiri Group, Kume-jima Island, Japan: Biogeographical significance of the timing of the formation of back-arc basin (Okinawa Trough). *Palaeogeography, Palaeoclimatology, Palaeoecology*, 276(1-4), 56–68.
- Tankard, A.J., Martin, M., Eriksson, K., Hobday, D., Hunter, D., & Minter, W. (2012). *Crustal Evolution of Southern Africa: 3.8 Billion Years of Earth History*. Springer Science & Business Media.
- Tanner, P., Pankhurst, R., & Hyden, G. (1982). Radiometric evidence for the age of the subduction complex in the South Orkney and South Shetland Islands, West Antarctica. *Journal of the Geological Society*, 139(6), 683–690.
- Tapster, S., Roberts, N. M. W., Petterson, M. G., Saunders, A. D., & Naden, J. (2014). From continent to intra-oceanic arc: Zircon xenocrysts record the crustal evolution of the Solomon island arc. *Geology*, 42(12), 1087–1090.
- Tauxe, L., & Kent, D. V. (2004). A simplified statistical model for the geomagnetic field and the detection of shallow bias in paleomagnetic inclinations: was the ancient magnetic field dipolar?. *Geophysical Monograph Series*, 145, 101–115.
- Tauxe, L., & Watson, G. S. (1994). The fold test: an eigen analysis approach. *Earth and Planetary Science Letters*, 122(3-4), 331–341.
- Tauxe, L., with contributions from Butler, R.F., Van der Voo, R., and Banerjee, S.K., (2010). *Essentials of Paleomagnetism*, University of California Press
- Taylor, B. (1979). Bismarck Sea: evolution of a back-arc basin. *Geology*, 7(4), 171–174.
- Taylor, B. (2006). The single largest oceanic plateau: Ontong Java–Manihiki–Hikurangi. *Earth and Planetary Science Letters*, 241(3-4), 372–380.
- Taylor, B., Goodliffe, A. M., & Martinez, F. (1999). How continents break up: insights from Papua New Guinea. *Journal of Geophysical Research: Solid Earth*, 104(B4), 7497–751
- Taylor, F. W., Jouannic, C., & Bloom, A. L. (1985). Quaternary uplift of the Torres Islands, northern New Hebrides frontal arc: Comparison with Santo and Malekula Islands, central New Hebrides frontal arc. *The Journal of Geology*, 93(4), 419–438.
- Taylor, G. K., Gascoyne, J., & Colley, H. (2000). Rapid rotation of Fiji: Paleomagnetic evidence and tectonic implications. *Journal of Geophysical Research*, 105(B3), 5771–5781.
- Taylor, S. R., & McLennan, S. M. (1985). *The continental crust: Its composition and evolution* (p. 312). Blackwell.
- Tebbens, S. F., & Cande, S. C. (1997). Southeast Pacific tectonic evolution from early Oligocene to present.

- Journal of Geophysical Research: Solid Earth, 102(B6), 12061-12084.
- Tebbens, S. F., Cande, S. C., Kovacs, L., Parra, J. C., LaBrecque, J. L., & Vergara, H. (1997). The Chile ridge: a tectonic framework. *Journal of Geophysical Research: Solid Earth*, 102(B6), 12035-12059.
- Tejada, M. L. G., & Castillo, P. R. (2002). In search of a common ground: Geochemical study of ancient oceanic crust in eastern Luzon, Philippines. *Geochimica et Cosmochimica Acta* 56(66), 767.
- Tejada, M. L. G., Mahoney, J. J., Duncan, R. A., & Hawkins, M. P. (1996). Age and geochemistry of basement and alkalic rocks of Malaita and Santa Isabel, Solomon Islands, southern margin of Ontong Java Plateau. *Journal of Petrology*, 37(2), 361-394.
- Tejada, M. L. G., Mahoney, J. J., Neal, C. R., Duncan, R. A., & Petterson, M. G. (2002). Basement geochemistry and geochronology of Central Malaita, Solomon Islands, with implications for the origin and evolution of the Ontong Java Plateau. *Journal of Petrology*, 43(3), 449-484.
- Tera, F., & Wasserburg, G. J. (1972). U-Th-Pb systematics in three Apollo 14 basalts and the problem of initial Pb in lunar rocks. *Earth and Planetary Science Letters*, 14(3), 281-304.
- Thomas, C., Livermore, R., & Pollitz, F. (2003). Motion of the Scotia Sea plates. *Geophysical Journal International*, 155, 789-804.
- Thurrow, J. (1988). Cretaceous radiolarians of the North Atlantic Ocean: ODP Leg 103 (Site 638, 640 and 641) and DSDP Legs 93 (Site 603) and 47B (Site 398). In: Boillot, G., Winterer, E.L. et al. (Ed.). *Proceedings of the Ocean Drilling Program, Scientific Result 103*, 379-418. Texas, College Station.
- Thuy, N. T. B., Satir, M., Siebel, W., Vennemann, T., & Van Long, T. (2004). Geochemical and isotopic constraints on the petrogenesis of granitoids from the Dalat zone, southern Vietnam. *Journal of Asian Earth Sciences*, 23(4), 467-482.
- Tikku, A. A., & Cande, S. C. (1999). The oldest magnetic anomalies in the Australian-Antarctic Basin: Are they isochrons? *Journal of Geophysical Research*, 104(B1), 661-677.
- Tikku, A. A., & Cande, S. C. (2000). On the fit of Broken Ridge and Kerguelen Plateau. *Earth and Planetary Science Letters*, 180(1-2), 117-132.
- Timm, C., Davy, B., Haase, K., Hoernle, K. A., Graham, I. J., De Ronde, C. E., ... & Gamble, J. A. (2014). Subduction of the oceanic Hikurangi Plateau and its impact on the Kermadec arc. *Nature Communications*, 5(1), 4923.
- Timm, C., Hoernle, K., Werner, R., Hauff, F., van den Bogaard, P., Michael, P., ... & Koppers, A. (2011). Age and geochemistry of the oceanic Manihiki Plateau, SW Pacific: New evidence for a plume origin. *Earth and Planetary Science Letters*, 304(1-2), 135-146.
- Tingey, R.J. (1991). *The Geology of Antarctica*. Oxford University Press.
- Torres-Carbonell, P. J., Dimieri, L. V., & Martinioni, D. R. (2013). Early foreland deformation of the Fuegian Andes (Argentina): Constraints from the strain analysis of Upper Cretaceous-Danian sedimentary rocks. *Journal of Structural Geology*, 48, 14-32.
- Torres-Carbonell, P. J., Dimieri, L. V., & Olivero, E. B. (2011). Progressive deformation of a Coulomb thrust wedge: the eastern Fuegian Andes thrust-fold belt. *Geological Society, London, Special Publications*, 349(1), 123-147.
- Torres-Carbonell, P. J., Dimieri, L. V., Olivero, E. B., Bohoyo, F., & Galindo-Zaldívar, J. (2014). Structure and tectonic evolution of the Fuegian Andes (southernmost South America) in the framework of the Scotia Arc development. *Global and Planetary Change*, 123, 174-188.
- Torres-Carbonell, P. J., Olivero, E. B., & Dimieri, L. V. (2008). Structure and evolution of the Fuegian Andes foreland thrust-fold belt, Tierra del Fuego, Argentina: Paleogeographic implications. *Journal of South American Earth Sciences*, 25(4), 417-439.
- Torres-Carbonell, P. J., Olivero, E. B., & Dimieri, L. V. (2008a). Control en la magnitud de desplazamiento de rumbo del Sistema Transformante Fagnano, Tierra del Fuego, Argentina. *Revista geológica de Chile*, 35(1), 63-77.
- Torres-Carbonell, P.J., & Dimieri, L.V. (2013). Cenozoic contractional tectonics in the Fuegian Andes, southernmost South America: a model for the transference of orogenic shortening to the foreland. *Geologica Acta*, 11(3), 331-357.
- Torres-Carbonell, P.J., & Olivero, E.B. (2012). Sand dispersal in the southeastern Austral Basin, Tierra del Fuego, Argentina: Outcrop insights from Eocene channeled turbidite systems. *Journal of South American Earth Sciences*, 33(1), 80-101.
- Torres-Carbonell, P.J., Rodríguez Arias, L., & Atencio, M.R. (2017). Geometry and kinematics of the Fuegian thrust-fold belt, southernmost Andes. *Tectonics*, 36(1), 33-50.
- Torsvik, T. H., Doubrovine, P. V., Steinberger, B., Gaina, C., Spakman, W., & Domeier, M. (2017). Pacific plate motion change caused the Hawaiian-Emperor Bend. *Nature Communications*, 8(1), 15660.
- Torsvik, T. H., Müller, R. D., Van der Voo, R., Steinberger, B., & Gaina, C. (2008). Global plate motion frames:

- Toward a unified model. *Reviews of Geophysics*, 46, RG3004.
- Torsvik, T. H., Rouse, S., Labails, C., & Smethurst, M. A. (2009). A new scheme for the opening of the South Atlantic Ocean and the dissection of an Aptian salt basin. *Geophysical Journal International*, 177(3), 1315-1333.
- Torsvik, T. H., Steinberger, B., Shephard, G. E., Doubrovine, P. V., Gaina, C., Domeier, M., ... & Sager, W. W. (2019). Pacific-Panthalassic reconstructions: Overview, errata and the way forward. *Geochemistry, Geophysics, Geosystems*, 20(7), 3659-3689.
- Torsvik, T. H., Van der Voo, R., Preeden, U., Mac Niocaill, C., Steinberger, B., Doubrovine, P. V., ... & Cocks, L. R. M. (2012). Phanerozoic polar wander, palaeogeography and dynamics. *Earth-Science Reviews*, 114(3-4), 325-368.
- Torsvik, T., & Cocks, L. (2017). *Earth History and Palaeogeography*. Cambridge: Cambridge University Press.
- Tostevin, R., Shields, G. A., Tarbuck, G. M., He, T., Clarkson, M. O., & Wood, R. A. (2016). Effective use of cerium anomalies as a redox proxy in carbonate-dominated marine settings. *Chemical Geology*, 438, 146-162.
- Toth, J., & Gurnis, M. (1998). Dynamics of subduction initiation at preexisting fault zones. *Journal of Geophysical Research*, 103(B8), 18053-18067.
- Tracey Jr, J. I., Schlanger, S. O., Stark, J. T., Doan, D. B., & May, H. G. (1964). General geology of Guam (No. 403-A).
- Tregoning, P., Tan, F., Gilliland, J., McQueen, H., & Lambeck, K. (1998). Present-day crustal motion in the Solomon Islands from GPS observations. *Geophysical research letters*, 25(19), 3627-3630.
- Tulloch, A. J., & Kimbrough, D. L. (1989). The Paparoa metamorphic core complex, New Zealand: Cretaceous extension associated with fragmentation of the Pacific margin of Gondwana. *Tectonics*, 8(6), 1217-1234.
- Tulloch, A. J., & Kimbrough, D. L. (2003). Tectonic Evolution of Northwestern Mexico and the Southwestern USA, Paired plutonic belts in convergent margins and the development of high Sr/Y magmatism: Peninsular Ranges batholith of Baja-California and Median batholith of New Zealand. In S. E. Johnson, S. R. Paterson, J. M. Fletcher, G. H. Girty, D. L. Kimbrough, & A. Martín-Barajas (Eds.), *Geological Society of America Special Papers* (Vol. 374, pp. 275-295). Geological Society of America.
- Tulloch, A. J., & Rabone, S.D.C. (1993). Mo-bearing granodiorite porphyry plutons of the early Cretaceous Separation Point Suite, West Nelson, New Zealand. *New Zealand Journal of Geology and Geophysics*, 36(4), 401-408.
- Tulloch, A. J., Kimbrough, D.L., Landis, C.A., Mortimer, N., & Johnston, M.R. (1999). Relationships between the Brook Street terrane and median Tectonic Zone (Median batholith): evidence from Jurassic conglomerates. *New Zealand Journal of Geology and Geophysics*, 42(2), 279-293.
- Tulloch, A. J., Ramezani, J., Mortimer, N., Mortensen, J., van den Bogaard, P., & Maas, R. (2009). Cretaceous felsic volcanism in New Zealand and Lord Howe rise (Zealandia) as a precursor to final Gondwana breakup. *Geological Society, London, Special Publications*, 321(1), 89-118.
- Turcotte, D. L., & Schubert, G. (2002). *Geodynamics* (456 pp.). Cambridge, UK: Cambridge University Press.
- Udintsev, G., Kurentsova, N., Beresnev, A., Kol'tsova, A., Domoratskaya, L., Schenke, G., Bakhmutov, V., & Solov'ev, V. (2012). Tectonics of the Drake Passage-Scotia Sea Zone in the Southern Ocean. *Doklady Earth Sciences*, 445(2), 1029-1035.
- Ujiie, K. (1997). Off-scraping accretionary process under the subduction of young oceanic crust: The Shimanto Belt of Okinawa Island, Ryukyu Arc. *Tectonics*, 16(2), 305-322.
- Ujiie, K. (2002). Evolution and kinematics of an ancient décollement zone, mélange in the Shimanto accretionary complex of Okinawa Island, Ryukyu Arc. *Journal of Structural Geology*, 24(5), 937-952.
- Ulrich, M., Picard, C., Guillot, S., Chauvel, C., Cluzel, D., & Meffre, S. (2010). Multiple melting stages and refertilization as indicators for ridge to subduction formation: The New Caledonia ophiolite. *Lithos*, 115(1-4), 223-236.
- Uysal, I. T., Feng, Y. X., Zhao, J. X., Bolhar, R., Işik, V., Baublys, K. A., et al. (2011). Seismic cycles recorded in late Quaternary calcite veins: Geochronological, geochemical and microstructural evidence. *Earth and Planetary Science Letters*, 303(1-2), 84-96.
- Vaes, B., Gallo, L. C., & van Hinsbergen, D. J. (2022). On pole position: causes of dispersion of the paleomagnetic poles behind apparent polar wander paths. *Journal of Geophysical Research: Solid Earth*, 127(4), e2022JB023953.
- Vaes, B., Li, S., Langereis, C. G., & van Hinsbergen, D. J. (2021). Reliability of palaeomagnetic poles from sedimentary rocks. *Geophysical Journal International*, 225(2), 1281-1303.
- Vaes, B., Van Hinsbergen, D. J. J., Van de Lagemaat, S. H. A., Van der Wiel, E., Lom, N., Advokaat, E., ... & Langereis, C., (2023). A global apparent polar wander path for the last 320 Ma calculated from site-level paleomagnetic data. *Earth-Science Reviews* 244, 104547.

- Vaes, B., Van Hinsbergen, D.J.J., & Boschman, L.M. (2019). Reconstruction of subduction and back-arc spreading in the NW Pacific and Aleutian Basin: Clues to causes of Cretaceous and Eocene plate reorganizations. *Tectonics*, 38(4), 1367–1413.
- Van de Beuke, S., Stagg, H. M. J., Sayers, J., Willcox, J. B., & Symonds, P. A. (2003). Geological framework of the Northern Lord Howe Rise and adjacent areas. *Geoscience Australia Record*, 2003, 1–116.
- Van de Lagemaat, S. H. A., Mering, J. A., & Kamp, P. J. J. (2021). LA-ICP-MS and stable isotope data of Waihu Bay (North Island, New Zealand) carbonate veins [Dataset]. Mendeley Data, V1. stl
- Van den Broek, J. M., & Gaina, C. (2020). Microcontinents and continental fragments associated with subduction systems. *Tectonics*, 39(8), e2020TC006063.
- Van der Hilst, R. D. (1995). Complex morphology of subducted lithosphere in the mantle beneath the Tonga trench. *Nature*, 374(6518), 154–157.
- Van der Hilst, R., Engdahl, R., Spakman, W., & Nolet, G. (1991). Tomographic imaging of subducted lithosphere below northwest Pacific island arcs. *Nature*, 353(6339), 37–43.
- Van der Meer, D. G., Spakman, W., Van Hinsbergen, D. J., Amaru, M. L., & Torsvik, T. H. (2010). Towards absolute plate motions constrained by lower-mantle slab remnants. *Nature Geoscience*, 3(1), 36–40.
- Van der Meer, D. G., Torsvik, T. H., Spakman, W., Van Hinsbergen, D. J. J., & Amaru, M. L. (2012). Intra-Panthalassa Ocean subduction zones revealed by fossil arcs and mantle structure. *Nature Geoscience*, 5(3), 215–219.
- Van der Meer, D. G., van Hinsbergen, D. J. J., & Spakman, W. (2018). The Atlas of the Underworld: A catalogue of slab remnants in the mantle imaged by seismic tomography, and their geological interpretation. *Tectonophysics*, 723, 309–448.
- Van der Meer, Q. H. A., Waight, T. E., Scott, J. M., & Münker, C. (2017). Variable sources for Cretaceous to recent HIMU and HIMU-like intraplate magmatism in New Zealand. *Earth and Planetary Science Letters*, 469, 27–41.
- Van Der Meer, Q. H. A., Waight, T. E., Tulloch, A. J., Whitehouse, M. J., & Andersen, T. (2018). Magmatic evolution during the Cretaceous transition from subduction to continental break-up of the Eastern Gondwana margin (New Zealand) documented by in-situ zircon O–Hf isotopes and bulk-rock Sr–Nd isotopes. *Journal of Petrology*, 59(5), 849–880.
- Van der Meer, Q. H., Storey, M., Scott, J. M., & Waight, T. E. (2016). Abrupt spatial and geochemical changes in lamprophyre magmatism related to Gondwana fragmentation prior, during and after opening of the Tasman Sea. *Gondwana Research*, 36, 142–156.
- Van der Voo, R., van Hinsbergen, D. J., Domeier, M., Spakman, W., & Torsvik, T. H. (2015). Latest Jurassic–earliest Cretaceous closure of the Mongol–Okhotsk Ocean: A paleomagnetic and seismological-tomographic analysis. *Geological Society of America Special Papers*, 513, 589–606.
- Van Hattum, M. W. A., Hall, R., Pickard, A. L., & Nichols, G. J. (2013). Provenance and geochronology of Cenozoic
- Van Hattum, M. W., Hall, R., Pickard, A. L., & Nichols, G. J. (2006). Southeast Asian sediments not from Asia: Provenance and geochronology of north Borneo sandstones. *Geology*, 34(7), 589–592. sandstones of northern Borneo. *Journal of Asian Earth Sciences*, 76, 266–282.
- Van Hinsbergen, D. J. J., & Schouten, T. L. A. (2021). Deciphering paleogeography from orogenic architecture: constructing orogens in a future supercontinent as a thought experiment. *American Journal of Science*, 321(4–5), 507–537.
- Van Hinsbergen, D. J. J., Dekkers, M. J., Bozkurt, E., & Koopman, M. (2010). Exhumation with a twist: Paleomagnetic constraints on the evolution of the Menderes metamorphic core complex, western Turkey. *Tectonics*, 29(3).
- Van Hinsbergen, D. J. J., Hafkenscheid, E., Spakman, W., Meulenkamp, J., & Wortel, R. (2005). Nappe stacking resulting from subduction of oceanic and continental lithosphere below Greece. *Geology*, 33(4), 325–328.
- Van Hinsbergen, D. J. J., Lippert, P. C., Li, S., Huang, W., Advokaat, E. L., & Spakman, W. (2019). Reconstructing Greater India: Paleogeographic, kinematic, and geodynamic perspectives. *Tectonophysics*, 760, 69–94.
- Van Hinsbergen, D. J. J., Peters, K., Maffione, M., Spakman, W., Guilmette, C., Thieulot, C., ... & Kaymakci, N. (2015). Dynamics of intraoceanic subduction initiation: 2. Suprasubduction zone ophiolite formation and metamorphic sole exhumation in context of absolute plate motions. *Geochemistry, Geophysics, Geosystems*, 16(6), 1771–1785.
- Van Hinsbergen, D. J. J., Steinberger, B., Guilmette, C., Maffione, M., Gürer, D., Peters, K., ... & Spakman, W. (2021). A record of plume-induced plate rotation triggering subduction initiation. *Nature Geoscience*, 14(8), 626–630.
- Van Hinsbergen, D. J. J., Torsvik, T. H., Schmid, S. M., Mañenco, L. C., Maffione, M., Vissers, R. L., ... & Spakman, W. (2020). Orogenic architecture of the Mediterranean region and kinematic reconstruction of its tectonic evolution since the Triassic. *Gondwana Research*, 81, 79–229.

- Van Hinsbergen, D. J., J. Spakman, W., de Boorder, H., Van Dongen, M., Jowitt, S. M., & Mason, P. R. (2020b). Arc-type magmatism due to continental-edge plowing through ancient subduction-enriched mantle. *Geophysical Research Letters*, 47(9), e2020GL087484.
- Van Horne, A., Sato, H., & Ishiyama, T. (2017). Evolution of the Sea of Japan back-arc and some unsolved issues. *Tectonophysics*, 710, 6–20.
- Van Hunen, J., & Allen, M.B. (2011). Continental collision and slab break-off: a comparison of 3D-numerical models with observations. *Earth and Planetary Science Letters*, 302(1–2), 27–37.
- Vanneste, L.E., & Larter, R.D. (2002). Sediment subduction, subduction erosion, and strain regime in the northern South Sandwich forearc. *Journal of Geophysical Research: Solid Earth*, 107(B7), EPM 5-1-EPM 5-24.
- Veivers, J. J. (2012). Reconstructions before rifting and drifting reveal the geological connections between Antarctica and its conjugates in Gondwanaland. *Earth-Science Reviews*, 111(3–4), 249–318.
- Veivers, J. J., Powell, C. M., & Roots, S. R. (1991). Review of seafloor spreading around Australia. I. Synthesis of the patterns of spreading. *Australian journal of earth sciences*, 38(4), 373–389.
- Vérard, C., Flores, K., & Stampfli, G. (2012). Geodynamic reconstructions of the South America–Antarctica plate system. *Journal of Geodynamics*, 53, 43–60.
- Vermeesch, P. (2021). Maximum depositional age estimation revisited. *Geoscience Frontiers*, 12(2), 843–850.
- Villamor, P., & Berryman, K. (2001). A late Quaternary extension rate in the Taupo Volcanic Zone, New Zealand, derived from fault slip data. *New Zealand Journal of Geology and Geophysics*, 44(2), 243–269.
- Vishnevskaya, V.S. (1993). Jurassic and Cretaceous radiolarian biostratigraphy in Russia. In: Blueford, J. & Murchey, B. (Eds.). *Radiolarian of giant and subgiant fields in Asia*, 175–200. *Micropaleontology special publ.* 6.
- Viso, R. F., Larson, R. L., & Pockalny, R. A. (2005). Tectonic evolution of the Pacific–Phoenix–Farallon triple junction in the South Pacific Ocean. *Earth and Planetary Science Letters*, 233(1–2), 179–194.
- Vissers, R. L. M., & Meijer, P. T. (2012a). Mesozoic rotation of Iberia: Subduction in the Pyrenees?. *Earth-Science Reviews*, 110(1–4), 93–110.
- Vissers, R. L. M., & Meijer, P. T. (2012b). Iberian plate kinematics and Alpine collision in the Pyrenees. *Earth-Science Reviews*, 114(1–2), 61–83.
- Von Gosen, W., & Loske, W. (2004). Tectonic history of the Calcatapul Formation, Chubut province, Argentina, and the "Gastre fault system." *Journal of South American Earth Sciences*, 18(1), 73–88.
- Vrolijk, P., & Sheppard, S. M. (1991). Syntectonic carbonate veins from the Barbados accretionary prism (ODP Leg 110): Record of palaeohydrology. *Sedimentology*, 38(4), 671–690.
- Vry, J. K., Baker, J., Maas, R., Little, T. A., Grapes, R., & Dixon, M. (2004). Zoned (Cretaceous and Cenozoic) garnet and the timing of high grade metamorphism, Southern Alps, New Zealand. *Journal of Metamorphic Geology*, 22(3), 137–157.
- Vuan, A., Lodolo, E., Panza, G., & Sauli, C. (2005). Crustal structure beneath Discovery Bank in the Scotia Sea from group velocity tomography and seismic reflection data. *Antarctic Science*, 17(1), 97–106.
- Wagner, T., Magill, C. R., & Herrle, J. O. (2018). Carbon isotopes. In W. M. White (Ed.), *Encyclopedia of geochemistry. Encyclopedia of earth sciences series*. Springer.
- Wai, K. M., Abbott, M. J., & Grady, A. E. (1994). The Sadowa Igneous Complex, Eastern Papua New Guinea: Ophiolite or not?. *Goldschmidt Conference Edinburgh*, 949–950.
- Waight, T. E., Weaver, S. D., & Muir, R. J. (1998). Mid-Cretaceous granitic magmatism during the transition from subduction to extension in southern New Zealand: a chemical and tectonic synthesis. *Lithos*, 45(1–4), 469–482.
- Wakita, K. (2015). OPS mélange: A new term for mélanges of convergent margins of the world. *International Geology Review*, 57(5–8), 529–539.
- Wakita, K., & Metcalfe, I. (2005). Ocean plate stratigraphy in East and Southeast Asia. *Journal of Asian Earth Sciences*, 24(6), 679–702.
- Walcott, R. I., Christoffel, D. A., & Mumme, T. C. (1981). Bending within the axial tectonic belt of New Zealand in the last 9 Myr from paleomagnetic data. *Earth and Planetary Science Letters*, 52(2), 427–434.
- Walker, D. A., & McDougall, I. (1982). ⁴⁰Ar/³⁹Ar and K–Ar dating of altered glassy volcanic rocks: the Dabi Volcanics, PNG. *Geochimica et Cosmochimica Acta*, 46(11), 2181–2190.
- Wallis, S. R., Yamaoka, K., Mori, H., Ishiwatari, A., Miyazaki, K., & Ueda, H. (2020). The basement geology of Japan from A to Z. *Island Arc*, 29(1), e12339.
- Walther, H. W. (1981). Early Cretaceous porphyry copper mineralization on Cebu Island, Philippines, dated with K–Ar and R–Sr methods. *Geologisches Jahrbuch*, 48, 21–35.
- Wang, K. L., Lo, Y. M., Chung, S. L., Lo, C. H., Hsu, S. K., Yang, H. J., & Shinjo, R. (2012). Age and Geochemical Features of Dredged Basalts from Offshore SW Taiwan: The Coincidence of Intra-Plate Magmatism with

- the Spreading South China Sea. *Terrestrial, Atmospheric & Oceanic Sciences*, 23(6).
- Wang, X., Cao, L., Zhao, M., Cheng, J., & He, X. (2022). What conditions promote atypical subduction: Insights from the Mussau Trench, the Hjort Trench, and the Gagua Ridge. *Gondwana Research*.
- Wang, Y., Forsyth, D. W., Rau, C. J., Carriero, N., Schmandt, B., Gaherty, J. B., & Savage, B. (2013). Fossil slabs attached to unsubducted fragments of the Farallon plate. *Proceedings of the National Academy of Sciences*, 110, 5342–5346.
- Wang, Y., Qian, X., Asis, J. B., Cawood, P. A., Wu, S., Zhang, Y., Wu, S., Zhang, Y., Feng, Q., & Lu, X. (2023). “Where, when and why” for the arc-trench gap from Mesozoic Paleo-Pacific subduction zone: Sabah Triassic-Cretaceous igneous records in East Borneo. *Gondwana Research*, 117, 117–138.
- Wang, Y., Zhang, A., Qian, X., Asis, J. B., Feng, Q., Gan, C., Zhang, Y., Cawood, P. A., Wang, W., & Zhang, P. (2021). Cretaceous Kuching accretionary orogenesis in Malaysia Sarawak: Geochronological and geochemical constraints from mafic and sedimentary rocks. *Lithos*, 400, 106425.
- Warren, P. Q., & Cloos, M. (2007). Petrology and tectonics of the Derewo metamorphic belt, west New Guinea. *International Geology Review*, 49(6), 520–553.
- Waters, P. J., Cooke, D. R., Gonzales, R. I., & Phillips, D. (2011). Porphyry and epithermal deposits and 40Ar/39Ar geochronology of the Baguio district, Philippines. *Economic Geology*, 106(8), 1335–1363.
- Watts, A. B., Weissel, J. K., & Larson, L. R. (1977). Sea-floor spreading in marginal basins of the western Pacific. *Tectonophysics*, 37(1-3), 167–181.
- Watts, D.R., Watts, G.C., & Bramall, A. (1984). Cretaceous and early Tertiary paleomagnetic results from the Antarctic Peninsula. *Tectonics*, 3(3), 333–346.
- Webb, A. A. G., Guo, H., Clift, P. D., Husson, L., Müller, T., Costantino, D., ... & Wang, Q. (2017). The Himalaya in 3D: Slab dynamics controlled mountain building and monsoon intensification. *Lithosphere*, 9(4), 637–651.
- Webb, L. E., Baldwin, S. L., & Fitzgerald, P. G. (2014). The Early-Middle Miocene subduction complex of the Louisiade Archipelago, southern margin of the Woodlark Rift. *Geochemistry, Geophysics, Geosystems*, 15(10), 4024–4046.
- Webb, M., & White, L. T. (2016). Age and nature of Triassic magmatism in the Netoni Intrusive Complex, West Papua, Indonesia. *Journal of Asian Earth Sciences*, 132, 58–74.
- Webb, M., White, L. T., Jost, B. M., & Tiranda, H. (2019). The Tamrau Block of NW New Guinea records late Miocene–Pliocene collision at the northern tip of the Australian Plate. *Journal of Asian Earth Sciences*, 179, 238–260.
- Webb, M., White, L. T., Jost, B. M., Tiranda, H., & BouDagher-Fadel, M. (2020). The history of Cenozoic magmatism and collision in NW New Guinea—New insights into the tectonic evolution of the northernmost margin of the Australian Plate. *Gondwana Research*, 82, 12–38.
- Wegener, A. L. (1912). Die Entstehung der Kontinente. *Geologische Rundschau* 3, 276–292
- Weiland Jr, R. J. (1999). Emplacement of the Irian ophiolite and unroofing of the Ruffaer metamorphic belt of Irian Jaya, Indonesia. PhD Thesis. The University of Texas at Austin.
- Weissel, J. K. (1980). Evidence for Eocene oceanic crust in the Celebes Basin. Washington DC American Geophysical Union Geophysical Monograph Series, 23, 37–47.
- Weissel, J. K., & Anderson, R. N. (1978). Is there a Caroline plate?. *Earth and Planetary Science Letters*, 41(2), 143–158.
- Weissel, J. K., & Hayes, D. E. (1977). Evolution of the Tasman Sea reappraised. *Earth and Planetary Science Letters*, 36, 77–84
- Weissel, J. K., & Watts, A. B. (1979). Tectonic evolution of the Coral Sea basin. *Journal of Geophysical Research: Solid Earth*, 84(B9), 4572–4582.
- Weissel, J. K., Hayes, D. E., & Herron, E. M. (1977). Plate tectonic synthesis: The displacements between Australia, New Zealand and Antarctica since the Late Cretaceous. *Marine Geology*, 25(1–3), 231–227.
- Weissel, J. K., Taylor, B., & Karner, G. D. (1982). The opening of the Woodlark Basin, subduction of the Woodlark spreading system, and the evolution of northern Melanesia since mid-Pliocene time. *Tectonophysics*, 87(1-4), 253–277.
- Weissel, J. K., Watts, A. B., & Lapouille, A. (1982). Evidence for Late Paleocene to Late Eocene seafloor spreading in the Southern New Hebrides Basin. *Tectonophysics*, 87(1-4), 243–251.
- Wessel, P., & Kroenke, L.W. (2008). Pacific absolute plate motion since 145 Ma: An assessment of the fixed hot spot hypothesis. *Journal of Geophysical Research: Solid Earth*, 113(B6).
- Wessel, P., Matthews, K.J., Müller, R.D., Mazzoni, A., Whittaker, J.M., Myhill, R., & Chandler, M.T. (2015). Semiautomatic fracture zone tracking. *Geochemistry, Geophysics, Geosystems*, 16(7), 2462–2472.
- Whattam, S. A. (2009). Arc-continent collisional orogenesis in the SW Pacific and the nature, source and correlation of emplaced ophiolitic nappe components. *Lithos*, 113(1-2), 88–114.

- Whattam, S. A., Malpas, J. G., Ali, J. R., Smith, I. E., & Lo, C. H. (2004). Origin of the Northland Ophiolite, northern New Zealand: discussion of new data and reassessment of the model. *New Zealand Journal of Geology and Geophysics*, 47(3), 383-389.
- Whattam, S. A., Malpas, J., Ali, J. R., & Smith, I. E. M. (2008). New SW Pacific tectonic model: Cyclical intraoceanic magmatic arc construction and near-coeval emplacement along the Australia-Pacific margin in the Cenozoic. *Geochemistry, Geophysics, Geosystems*, 9, Q03021.
- Whattam, S. A., Malpas, J., Ali, J. R., Lo, C. H., & Smith, I. E. (2005). Formation and emplacement of the Northland ophiolite, northern New Zealand: SW Pacific tectonic implications. *Journal of the Geological Society*, 162(2), 225-241.
- Whattam, S. A., Malpas, J., Smith, I. E. M., & Ali, J. R. (2006). Link between SSZ ophiolite formation, emplacement and arc inception, Northland, New Zealand: U-Pb SHRIMP constraints; Cenozoic SW Pacific tectonic implications. *Earth and Planetary Science Letters*, 250(3-4), 606-632.
- Whattam, S. A., & Stern, R. J. (2015). Late Cretaceous plume-induced subduction initiation along the southern margin of the Caribbean and NW South America: The first documented example with implications for the onset of plate tectonics. *Gondwana Research*, 27(1), 38-63.
- White, R.V., Tarney, J., Kerr, A.C., Saunders, A.D., Kempton, P.D., Pringle, M.S., & Klaver, G.T. (1999). Modification of an oceanic plateau, Aruba, Dutch Caribbean: Implications for the generation of continental crust. *Lithos*, 46(1), 43-68.
- Whittaker, J. M., Goncharov, A., Williams, S. E., Müller, R. D., & Leitchnikov, G. (2013). Global sediment thickness data set updated for the Australian-Antarctic Southern Ocean. *Geochemistry, Geophysics, Geosystems*, 14(8), 3297-3305.
- Whittaker, J. M., Muller, R. D., Leitchnikov, G., Stagg, H., Sdrolias, M., Gaina, C., & Goncharov, A. (2007). Major Australian-Antarctic plate reorganization at Hawaiian-Emperor bend time. *Science*, 318(5847), 83-86.
- Whittaker, J.M., Williams, S.E., & Müller, R.D. (2013). Revised tectonic evolution of the Eastern Indian Ocean. *Geochemistry, Geophysics, Geosystems*, 14(6), 1891-1909.
- Wilder, D.T. (2003). Relative Motion History of the Pacific-Nazca (Farallon) Plates since 30 Million Years Ago (Doctoral dissertation, USF Tampa Graduate Theses and Dissertations).
- Willan, R.C., & Hunter, M.A. (2005). Basin evolution during the transition from continental rifting to subduction: evidence from the lithofacies and modal petrology of the Jurassic Latady Group, Antarctic Peninsula. *Journal of South American Earth Sciences*, 20(3), 171-191.
- Williams, S.E., Whittaker, J.M., & Müller, R.D. (2011). Full-fit, palinspastic reconstruction of the conjugate Australian-Antarctic margins. *Tectonics*, 30(6), TC6017.
- Wilson, T.J. (1991). Transition from back-arc to foreland basin development in the southernmost Andes: Stratigraphic record from the Ultima Esperanza District, Chile. *Geological Society of America Bulletin*, 103(1), 98-111.
- Winn Jr, R. (1978). Upper Mesozoic flysch of Tierra del Fuego and South Georgia Island: a sedimentologic approach to lithosphere plate restoration. *Geological Society of America Bulletin*, 89(4), 533-547.
- Winterer, E.L., Lonsdale, P.F., Matthews, J.L., & Rosendahl, B.R. (1974, October). Structure and acoustic stratigraphy of the Manihiki Plateau. *Deep Sea Research and Oceanographic Abstracts*, 21(10), 793-813.
- Wintsch, R. P., & Li, X. H. (2014). Hf and O isotopic evidence for metamorphic crystallization of zircon during contact metamorphism of Fenniaolin metabasalts, Tananao complex, Taiwan. *Lithos*, 205, 142-147.
- Wintsch, R. P., Yang, H. J., Li, X. H., & Tung, K. A. (2011). Geochronologic evidence for a cold arc-continent collision: The Taiwan orogeny. *Lithos*, 125(1-2), 236-248.
- Wobbe, F., Gohl, K., Chambord, A., & Sutherland, R. (2012). Structure and breakup history of the rifted margin of West Antarctica in relation to Cretaceous separation from Zealandia and Bellingshausen plate motion. *Geochemistry, Geophysics, Geosystems*, 13(4), Q04W10.
- Wolfart, R., Čeppek, P., Gramann, F., Kemper, E., & Porth, H. (1986). Stratigraphy of Palawan Island, Philippines. *Newsletters on Stratigraphy*, 19-48.
- Wood, R., & Woodward, D. (2002). Sediment thickness and crustal structure of offshore western New Zealand from 3D gravity modelling. *New Zealand Journal of Geology and Geophysics*, 45(2), 243-255.
- Woodhead, J., Hergt, J., Sandiford, M., & Johnson, W. (2010). The big crunch: Physical and chemical expressions of arc/continent collision in the Western Bismarck arc. *Journal of Volcanology and Geothermal Research*, 190(1-2), 11-24.
- Wortel, M.J.R., & Spakman, W. (2000). Subduction and slab detachment in the Mediterranean-Carpathian region. *Science*, 290(5498), 1910-1917.
- Worthing, M. A., & Crawford, A. J. (1996). The igneous geochemistry and tectonic setting of metabasites

- from the Emo Metamorphics, Papua New Guinea; a record of the evolution and destruction of a backarc basin. *Mineralogy and Petrology*, 58(1-2), 79-100.
- Worthington, T. J., Hekinian, R., Stoffers, P., Kuhn, T., & Hauff, F. (2006). Osbourn Trough: Structure, geochemistry and implications of a mid-Cretaceous paleosspreading ridge in the South Pacific. *Earth and Planetary Science Letters*, 245(3-4), 685-701.
- Wright, I. C. (1993). Pre-spread rifting and heterogeneous volcanism in the southern Havre Trough back-arc basin. *Marine Geology*, 113(3-4), 179-200.
- Wright, I. C., & Walcott, R. I. (1986). Large tectonic rotation of part of New Zealand in the last 5 Ma. *Earth and Planetary Science Letters*, 80, 348-352.
- Wright, N. M., Müller, R. D., Seton, M., & Williams, S. E. (2015). Revision of Paleogene plate motions in the Pacific and implications for the Hawaiian-Emperor bend. *Geology*, 43(5), 455-458.
- Wright, N. M., Seton, M., Williams, S. E., & Mueller, R. D. (2016). The Late Cretaceous to recent tectonic history of the Pacific Ocean basin. *Earth-Science Reviews*, 154, 138-173.
- Wu, J. T. J., & Wu, J. (2019). Izanagi-Pacific ridge subduction revealed by a 56 to 46 Ma magmatic gap along the northeast Asian margin. *Geology*, 47(10), 953-957.
- Wu, J., Lin, Y. A., Flament, N., Wu, J. T. J., & Liu, Y. (2022). Northwest Pacific-Izanagi plate tectonics since Cretaceous times from western Pacific mantle structure. *Earth and Planetary Science Letters*, 583, 117445.
- Wu, J., Suppe, J., Lu, R., & Kanda, R. (2016). Philippine Sea and East Asian plate tectonics since 52 Ma constrained by new subducted slab reconstruction methods. *Journal of Geophysical Research: Solid Earth*, 121(6), 4670-4741.
- Wu, Z., Zhu, W., Shao, L., & Xu, C. (2016). Sedimentary facies and the rifting process during the late Cretaceous to early Oligocene in the northern continental margin, South China Sea. *Interpretation*, 4(3), SP33-SP45.
- Wysoczanski, R. J., Todd, E., Wright, I. C., Leybourne, M. I., Hergt, J. M., Adam, C., & Mackay, K. (2010). Backarc rifting, constructional volcanism and nascent disorganised spreading in the southern Havre Trough backarc rifts (SW Pacific). *Journal of Volcanology and Geothermal Research*, 190(1-2), 39-57.
- Xia, L., & Li, X. (2019). Basalt geochemistry as a diagnostic indicator of tectonic setting. *Gondwana Research*, 65, 43-67.
- Xu, J., Ben-Avraham, Z., Kelty, T., & Yu, H. S. (2014). Origin of marginal basins of the NW Pacific and their plate tectonic reconstructions. *Earth-Science Reviews*, 130, 154-196.
- Xu, X., Dong, C., Li, W., & Zhou, X. (1999). Late Mesozoic intrusive complexes in the coastal area of Fujian, SE China: the significance of the gabbro-diorite-granite association. *Lithos*, 46(2), 299-315.
- Xu, Y., Yan, Q., Shi, X., Jichao, Y., Deng, X., Xu, W., & Jing, C. (2022). Discovery of Late Mesozoic volcanic seamounts at the ocean-continent transition zone in the Northeastern margin of South China Sea and its tectonic implication. *Gondwana Research*.
- Xu, Y., Yang, Y., Yu, H., Gao, W., Gao, X., Liu, B., Tian, C., Yang, J., & Zhang, W. (2020). Geochemistry and petrogenesis of volcanic rocks from the continent-ocean transition zone in northern South China Sea and their tectonic implications. *Journal of Ocean University of China*, 19(5), 1051-1061.
- Yamazaki, T., Chiyonobu, S., Ishizuka, O., Tajima, F., Uto, N., & Takagawa, S. (2021). Rotation of the Philippine Sea plate inferred from paleomagnetism of oriented cores taken with an ROV-based coring apparatus. *Earth, Planets and Space*, 73(1), 1-10.
- Yamazaki, T., Seama, N., Okino, K., Kitada, K., Joshima, M., Oda, H., & Naka, J. (2003). Spreading process of the northern Mariana Trough: Rifting-spreading transition at 22 N. *Geochemistry, Geophysics, Geosystems*, 4(9).
- Yamazaki, T., Takahashi, M., Iryu, Y., Sato, T., Oda, M., Takayanagi, H., Chiyonobu, S., Nishimura, A., Nakazawa, T., & Ooka, T. (2010). Philippine Sea Plate motion since the Eocene estimated from paleomagnetism of seafloor drill cores and gravity cores. *Earth, Planets and Space*, 62(6), 495-502.
- Yan, C. Y. & Kroenke, L. W. (1993). A plate reconstruction of the southwest Pacific 0-100 Ma. In *Proceedings of Ocean Drilling Program, Scientific Results*, 130, 697-709.
- Yan, Q., Metcalfe, I., & Shi, X. (2017). U-Pb isotope geochronology and geochemistry of granites from Hainan Island (northern South China Sea margin): Constraints on late Paleozoic-Mesozoic tectonic evolution. *Gondwana Research*, 49, 333-349.
- Yan, S., Yan, Q., Shi, X., Yuan, L., Liu, Y., Yang, G., & Ye, X. (2022). The dynamics of the Sorol Trough magmatic system: Insights from bulk-rock chemistry and mineral geochemistry of basaltic rocks. *Geological Journal*, 57(10), 4074-4089.
- Yang, K. M., Huang, S. T., Jong-Chang, W., Ting, H. H., Wen-Wei, M., Lee, M., ... & Chang-Jie, L. (2007). 3D geometry of the Chelungpu thrust system in central Taiwan: Its implications for active tectonics. *TAO: Terrestrial, Atmospheric and Oceanic Sciences*, 18(2), 143.

- Yang, K. M., Rau, R. J., Chang, H. Y., Hsieh, C. Y., Ting, H. H., Huang, S. T., ... & Tang, Y. J. (2016). The role of basement-involved normal faults in the recent tectonics of western Taiwan. *Geological Magazine*, 153(5-6), 1166-1191.
- Yang, T. F., Tien, J. L., Chen, C. H., Lee, T., & Punongbayan, R. S. (1995). Fission-track dating of volcanics in the northern part of the Taiwan-Luzon Arc: eruption ages and evidence for crustal contamination. *Journal of Southeast Asian Earth Sciences*, 11(2), 81-93.
- Yang, T., Liu, S., Guo, P., Leng, W., & Yang, A. (2020). Yanshanian orogeny during North China's drifting away from the trench: Implications of numerical models. *Tectonics*, 39(12), e2020TC006350.
- Ye, Q., Mei, L., Shi, H., Camanni, G., Shu, Y., Wu, J., Yu, L., Deng, P. & Li, G. (2018). The Late Cretaceous tectonic evolution of the South China Sea area: An overview, and new perspectives from 3D seismic reflection data. *Earth-science reviews*, 187, 186-204.
- Yeh, K. Y., & Cheng, Y. N. (2001). The first finding of early Cretaceous radiolarians from Lanyu, the Philippine Sea Plate. *Collection and Research*, (13), 111-145.
- Yu, M., Dilek, Y., Yumul Jr, G. P., Yan, Y., Dimalanta, C. B., & Huang, C. Y. (2020). Slab-controlled elemental-isotopic enrichments during subduction initiation magmatism and variations in forearc chemostratigraphy. *Earth and Planetary Science Letters*, 538, 116217.
- Yui, T. F., Maki, K., Lan, C. Y., Hirata, T., Chu, H. T., Kon, Y., Yokoyama, T. D., Jahn, B. M., & Ernst, W. G. (2012). Detrital zircons from the Tananao metamorphic complex of Taiwan: Implications for sediment provenance and Mesozoic tectonics. *Tectonophysics*, 541, 31-42.
- Yui, T. F., Okamoto, K., Usuki, T., Lan, C. Y., Chu, H. T., & Liou, J. G. (2009). Late Triassic–Late Cretaceous accretion/subduction in the Taiwan region along the eastern margin of South China—evidence from zircon SHRIMP dating. *International Geology Review*, 51(4), 304-328.
- Yumul Jr, G. P. (1993). Angat Ophiolitic Complex, Luzon, Philippines: a Cretaceous dismembered marginal basin ophiolitic complex. *Journal of Southeast Asian Earth Sciences*, 8(1-4), 529-537.
- Yumul Jr, G. P. (1997). Distribution, geochemistry and mineralization potentials of Philippine ophiolite and ophiolitic sequences. *Ofoliti*, 22, 47-56.
- Yumul Jr, G. P. (2007). Westward younging disposition of Philippine ophiolites and its implication for arc evolution. *Island Arc*, 16(2), 306-317.
- Yumul Jr, G. P., Dimalanta, C. B., & Jumawan, F. T. (2000a). Geology of the southern Zambales ophiolite complex, Luzon, Philippines. *Island Arc*, 9(4), 542-555.
- Yumul Jr, G. P., Dimalanta, C. B., Gabo-Ratio, J. A. S., Queaño, K. L., Armada, L. T., Padrones, J. T., Faustino-Eslava, D. V., Payot, B. D., & Marquez, E. J. (2020). Mesozoic rock suites along western Philippines: Exposed Proto-South China Sea fragments?. *Journal of Asian Earth Sciences*: X, 4, 100031.
- Yumul Jr, G. P., Dimalanta, C. B., Maglambayan, V. B., & Tamayo Jr, R. A. (2003). Mineralization controls in island arc settings: Insights from Philippine metallic deposits. *Gondwana Research*, 6(4), 767-776.
- Yumul Jr, G. P., Dimalanta, C. B., Tamayo Jr, R. A., & Faustino-Eslava, D. V. (2013). Geological features of a collision zone marker: the Antique Ophiolite Complex (Western Panay, Philippines). *Journal of Asian Earth Sciences*, 65, 53-63.
- Yumul Jr, G. P., Dimalanta, C. B., Tamayo Jr, R. A., & Zhou, M. F. (2006). Geology and geochemistry of the Rapu-Rapu ophiolite complex, eastern Philippines: possible fragment of the proto-Philippine Sea Plate. *International Geology Review*, 48(4), 329-348.
- Yumul Jr, G. P., Dimalanta, C. B., Tamayo Jr, R. A., Maury, R. C., Bellon, H., Polvé, M., ... & Cotten, J. (2004). Geology of the Zamboanga Peninsula, Mindanao, Philippines: An enigmatic South China continental fragment? *Geological Society, London, Special Publications*, 226(1), 289-312.
- Yumul Jr, G. P., Dimalanta, C. B., Tamayo, R. A., & Barretto, J. A. L. (2000b). Contrasting morphological trends of islands in Central Philippines: speculation on their origin. *Island Arc*, 9(4), 627-637.
- Yumul Jr, G. P., Jumawan, F. T., & Dimalanta, C. B. (2009). Geology, geochemistry and chromite mineralization potential of the Amnay Ophiolitic Complex, Mindoro, Philippines. *Resource geology*, 59(3), 263-281.
- Yumul Jr, G. R. (1989). Petrological characterization of the residual-cumulate sequences of the Zambales ophiolite complex, Luzon, Philippines. *Ofoliti* 14, (253-291).
- Zaffarana, C., Somoza, R., Mercader, R., Giacosa, R., & Martino, R. (2010). Anisotropy of magnetic susceptibility study in two classical localities of the Gastre Fault System, Central Patagonia. *Journal of South American Earth Sciences*, 30(3-4), 151-166.
- Zaffarana, C.B., Somoza, R., Orts, D.L., Mercader, R., Boltshauser, B., González, V.R., & Puigdomenech, C. (2017). Internal structure of the late Triassic Central Patagonian batholith at Gastre, southern Argentina: Implications for pluton emplacement and the Gastre fault system. *Geosphere*, 13(6), 1973-1992.
- Zahirovic, S., Seton, M., & Müller, R. D. (2014). The Cretaceous and Cenozoic tectonic evolution of Southeast Asia. *Solid Earth*, 5(1), 227-273.

- Zamoras, L. R., & Matsuoka, A. (2001). The Malampaya Sound Group in the Calamian Islands, North Palawan Block (Philippines). *The Journal of the Geological Society of Japan*, 107(5), XI-XII.
- Zamoras, L. R., & Matsuoka, A. (2004). Accretion and postaccretion tectonics of the Calamian Islands, North Palawan block, Philippines. *Island Arc*, 13(4), 506-519.
- Zamoras, L. R., Montes, M. G. A., Queano, K. L., Marquez, E. J., Dimalanta, C. B., Gabo, J. A. S., & Yumul Jr, G. P. (2008). Buruanga peninsula and Antique Range: two contrasting terranes in Northwest Panay, Philippines featuring an arc-continent collision zone. *Island Arc*, 17(4), 443-457.
- Zglinicki, K., Szamalek, K., & Górska, I. (2020). The Cyclops Ophiolite as a Source of High-Cr Spinel from Marine Sediments on the Jayapura Regency Coast (New Guinea, Indonesia). *Minerals*, 10(9), 735.
- Zhang, A., Asis, J. B., Fang, X., Li, H., Omang, S. A., Chen, M., Fang, Q., Li, D., & Peng, T. (2022). Late Cretaceous fore-arc spreading in the northern Kuching Zone of West Borneo, SE Asia: Constraints from the Pakong Mafic Complex. *Journal of Asian Earth Sciences*, 230, 105189.
- Zhang, B., Guo, F., Zhang, X., Wu, Y., Wang, G., & Zhao, L. (2019). Early Cretaceous subduction of Paleo-Pacific Ocean in the coastal region of SE China: Petrological and geochemical constraints from the mafic intrusions. *Lithos*, 334, 8-24.
- Zhang, G., Zhang, J., Wang, S., & Zhao, J. (2020). Geochemical and chronological constraints on the mantle plume origin of the Caroline Plateau. *Chemical Geology*, 540, 119566.
- Zhang, G.L., & Li, C. (2016). Interactions of the Greater Ontong Java mantle plume component with the Osborn Trough. *Scientific Reports*, 6(1), 22407.
- Zhang, J., & Zhang, G. (2020). Geochemical and chronological evidence for collision of proto-Yap arc/Caroline plateau and rejuvenated plate subduction at Yap trench. *Lithos*, 370, 105616.
- Zhang, X., Pease, V., Skogseid, J., Wohlgemuth-Ueberwasser, C. (2015). Reconstruction of tectonic events on the northern Eurasia margin of the Arctic, from U-Pb detrital zircon provenance investigations of late Paleozoic to Mesozoic sandstones in southern Taimyr Peninsula. *Geological Society of America Bulletin* B31241.1.
- Zhao, Q., Yan, Y., Zhu, Z., Carter, A., Clift, P. D., Hassan, M. H. A., Yao, D., & Aziz, J. H. A. (2021). Provenance study of the Lubok Antu Melange from the Lupar valley, West Sarawak, Borneo: Implications for the closure of eastern Meso-Tethys?. *Chemical Geology*, 581, 120415.
- Zhao, X.F., Zhou, M.F., Li, J.W., & Wu, F.Y. (2008). Association of Neoproterozoic A- and I-type granites in South China: Implications for the generation of A-type granites in a subduction-related environment. *Chemical Geology*, 257(1-2), 1-15.
- Zheng, H., Sun, X., Wang, P., Chen, W., & Yue, J. (2019). Mesozoic tectonic evolution of the Proto-South China Sea: A perspective from radiolarian paleobiogeography. *Journal of Asian Earth Sciences*, 179, 37-55.
- Zhou, D., Wang, W., Wang, J., Pang, X., Cai, D., & Sun, Z. (2006). Mesozoic subduction-accretion zone in northeastern South China Sea inferred from geophysical interpretations. *Science China. Earth Sciences*, 49(5), 471.
- Zhou, X. M., & Li, W. X. (2000). Origin of Late Mesozoic igneous rocks in Southeastern China: implications for lithosphere subduction and underplating of mafic magmas. *Tectonophysics*, 326(3-4), 269-287.
- Zhou, X., Sun, T., Shen, W., Shu, L., & Niu, Y. (2006). Petrogenesis of Mesozoic granitoids and volcanic rocks in South China: a response to tectonic evolution. *Episodes Journal of International Geoscience*, 29(1), 26-33.
- Zhu, J., Li, S., Jia, Y., Zhang, S., Chen, X., Chen, R., Suo, Y., Cao, X., Jia, Z., Ou, X., Liu, J., Wang, P., & Zhou, J. (2022). Links of high velocity anomalies in the mantle to the Proto-South China Sea slabs: Tomography-based review and perspective. *Earth-Science Reviews*, 231, 104074.
- Zhu, W., Xie, X., Wang, Z., Zhang, D., Zhang, C., Cao, L., & Shao, L. (2017). New insights on the origin of the basement of the Xisha Uplift, South China Sea. *Science China Earth Sciences*, 60, 2214-2222.
- Zijderveld, J.D.A. (1967): A.C. demagnetization of rocks: analysis of results. In D.W. Collinson, K.M. Crees and S.K. Runcorn (Eds.) *Methods in Paleomagnetism* (pp. 254-286). Elsevier, Amsterdam.
- Zirakparvar, N. A., Baldwin, S. L., & Vervoort, J. D. (2011). Lu-Hf garnet geochronology applied to plate boundary zones: Insights from the (U) HP terrane exhumed within the Woodlark Rift. *Earth and Planetary Science Letters*, 309(1-2), 56-66.
- Zirakparvar, N. A., Baldwin, S. L., & Vervoort, J. D. (2013). The origin and geochemical evolution of the Woodlark Rift of Papua New Guinea. *Gondwana Research*, 23(3), 931-943.

Samenvatting

Het reconstrueren van de vroegere beweging van de tektonische platen is essentieel voor het begrijpen van de geologische geschiedenis van de aarde, want dit heeft implicaties voor geodynamica, paleogeografie, paleoklimatologie en mijnbouw. Het reconstrueren van gesubduceerde platen brengt echter veel uitdagingen met zich mee. Terwijl de ontstaansgeschiedenis van bestaande oceaanbekkens gereconstrueerd kan worden met behulp van afwijkingen in het magnetisme in gesteente onder de oceanen en van breukzones, ontbrak er tot nu toe een duidelijk kader voor de reconstructie van ondergeschoven platen omdat er verschillende interpretaties in omloop zijn van geologische en geochemische gegevens. Onlangs is er een reconstructieprotocol ontwikkeld waarbij de input voor een reconstructie beperkt wordt tot kwantitatieve geologische gegevens. Deze aanpak vermijdt geodynamische interpretaties en leidt tot transparante, reproduceerbare reconstructies, die makkelijk zijn aan te passen wanneer nieuwe data worden vergaard. In dit proefschrift wordt dit nieuwe reconstructieprotocol toegepast op het zuidwesten en westen van het Panthalassa-domein. Dit heeft geresulteerd in kinematische reconstructies van Patagonië, via Antarctica en Australië, tot aan Japan, uitmondend in de complexe reconstructie van het Kruispuntgebied tussen de Panthalassa- en Tethys-domeinen.

De nieuwe reconstructies die in dit proefschrift worden gepresenteerd, hebben implicaties op het gebied van zowel regionale als mondiale tektoniek en geodynamica. De Cenozoïsche reconstructie van de Zuidwest-Pacifische regio op het niveau van de aardmantel laat zien dat sinds het begin van de subductie bij de Tonga-Kermadec subductiezone, het gesubduceerde deel van de Pacifische Plaat lateraal door de mantel werd getrokken over een afstand van meer dan 1200 km, inclusief het deel in de ondermantel. Het belangrijkste resultaat van de Mesozoïsche reconstructie van de Zuidwest-Pacifische regio is dat subductie langs de Oost-Gondwana-marge doorging tot minstens 90 miljoen jaar geleden, en mogelijk tot 79 miljoen jaar geleden. Dit betekent dat subductie hier 10 tot 25 miljoen jaar langer doorging dan over het algemeen werd aangenomen.

In het zuidoosten van het Panthalassa-domein laat de reconstructie van het Scotia Zeegebied zien dat de subductiezone van de Zuidelijke Sandwicheilanden ontstond uit subductie die begon in het Laat-Krijt (~80 miljoen jaar geleden) onder de continentale korst van Zuid-Orkney, dat deel uitmaakt van Antarctica. Vervolgens bewoog deze subductiezone zich verder naar het noorden door het uiteenvallen van de Zuid-Amerikaanse lithosfeer, waarbij de korst naar de bovenliggende plaat werd overgebracht, terwijl de mantel-lithosfeer subduceerde. De Straat Drake begon rond 50 miljoen jaar geleden open te gaan, toen Zuid-Amerika naar het westen begon te bewegen, en het begin van opengaan hing dus samen met het wegbewegen van de bovenliggende plaat. Oceanische spreidingscentra ontstonden ongeveer 35-25 miljoen jaar geleden in de Scotia Zee, wat de koppeling van de beweging tussen de subducerende plaat en de bovenliggende plaat verminderde. Daardoor kon het terugrollen van de gesubduceerde plaat bijdragen aan back-arc-extensie.

In het noordwesten van het Panthalassa-gebied werden nieuwe paleomagnetische, biostratigrafische, geochemische en geochronologische gegevens verkregen in het noorden van Sabah, Borneo. Deze gegevens suggereren dat de plaat die in het Laat-Krijt onder Borneo subduceerde, een nieuw te onderscheiden plaat was (de Pontus Plaat) die gescheiden was van de overige paleo-Pacifische platen door een subductiezone. Bovendien suggereren de nieuwe gegevens dat het stoppen van de subductie in het Mesozoïcum in het Proto-Zuid-Chinese Zeegebied mogelijk het gevolg was van een verstopte trog, waarschijnlijk veroorzaakt doordat daar verdikte oceanische lithosfeer terechtkwam.

De reconstructie van het Kruispuntgebied tussen het Panthalassa- en Tethys-gebied suggereert dat de bewaard gebleven oceanische korst uit het Jura tijdperk op de Filipijnen afkomstig was van de noordelijke rand van de Australische Plaat, waarlangs subductie langs de rand van dat continent actief was in het Perm en het Trias. Bovendien toont de reconstructie aan dat er geen noodzaak is voor spontaan beginnende subductie bij de Izu-Bonin Mariana-trog, die begon langs de reeds bestaande Mesozoïsche subductiezone.



Pohutukawa in Waihau Bay, New Zealand

Acknowledgements

This dissertation would have never existed without the involvement of many colleagues, friends, and family, to whom I owe a great deal of gratitude. First and foremost, I would like to thank my promotor **Douwe**. I am very fortunate to have approached you as a student for an MSc thesis project. At that time, I could never have imagined that it would eventually lead to this dissertation, and that both my projects would be part of it. Thank you for being a great supervisor when I was as a master student, because it has greatly contributed to me wanting to do a PhD - with you. Thank you for giving me the opportunity to develop myself as a scientist and for continuing your great supervision during my PhD. Your guidance, your dedication, your passion for our field, and your lightning-fast feedback have been of immeasurable value. It made these past years not only a valuable learning experience but also a lot of fun.

I owe a great deal of thanks to **Lydian**. I got to know you as a great co-supervisor for my master thesis and guided research, but when we went to New Zealand on fieldwork it felt like I was there with a friend. Your enthusiasm for plate reconstructions has definitely contributed to my passion for the field. Thank you for demonstrating that it is possible to pursue a PhD without working crazy hours. Many thanks for the opportunity to accompany you to New Caledonia, which turned out to be another fantastic fieldwork experience.

I am greatly indebted to **Peter Kamp**. I feel very lucky that I got to know you through our New Zealand fieldwork during my master. I am forever grateful that you gave me the opportunity to work with you, because the only thing I wanted to do after graduation was go back to my beloved New Zealand for more than just a few weeks. Combining my love for New Zealand with my love for geology turned out to be the best first job. Learning from you and working with you has been very fulfilling.

Throughout my PhD, I have greatly enjoyed the company of my office mates, fellow PhD students within the TRIGGER project, paranymphs, and now friends: **Bram** and **Erik**. Without you two, this journey would have been nearly impossible, and I am incredibly grateful that we've been able to share both joys and challenges. The walks through the botanical gardens to blow off some steam, the cakes to celebrate our achievements, and the brainstorming sessions when I was feeling lost have all been invaluable over the past years.

I would also like to thank the rest of the TRIGGER team and Mantle Dynamics group. **Wim** and **Cedric**, thank you for coming to lunch when Douwe wouldn't. **Abdul** and **Nalan**, it was great to have two other teammates doing plate reconstructions, and to share the sorrow over canceled fieldworks plans due to covid. **Thomas**, thank you for teaching me the basics of programming. **Eldert**, thank you for all the discussions on SE Asia plate tectonics and thank you for coming to Borneo with me. **Goran**, thank you for our time on Vancouver

Island. Despite the rain, the cold, and the flat tyres, I have fond memories of the beautiful island, the sections that we turned into Swiss cheese, and of course the black bears. **Kalijn**, it has been great to have someone in the group that shares my love for the mountains. Talking with you about our adventures was a nice distraction from all the science talk.

Despite covid being around for much of my PhD, which resulted in the cancellation of some fieldwork projects, I was lucky enough to go on two fieldworks for my project. **Junaidi Asis** and **Licheng Cao**, thank you for our time in Borneo and for teaching me some basics about radiolarians and zircons. For my time in Guam, I am greatly indebted to **John Jenson** who made this fieldwork possible. Many thanks to **Jonie**, **Fagan**, and **CJ**. You provided some very welcome extra hands during sampling. And special thanks to Jonie, who made sure we also enjoyed some of the fun things Guam has to offer. **Raymond**, **Melchor**, and **Mina**, thank you for making our experience in Guam extra special by inviting us into your home. **Mike**, thank you for being extremely helpful with arranging our drilling equipment, and for laughing just mildly at us when we put gasoline in the wrong container.

I am also very grateful to colleagues that helped me make sense of the data that was collected during these fieldworks. Thank you **Daniel Pastor-Galán** for all our sessions on paleomagnetism of Guam. I really hope we get to go to Ogasawara one day. Thanks to **Paul Mason** for your patience when helping me interpreting the geochemical data from Borneo and thank you **Mark Dekkers** for your very last-minute help with the geomagnetic analysis and interpretation.

Many thanks to my colleagues that made coffee breaks, conferences, and supervision of the first-year fieldwork much more enjoyable: **Annemijn**, **Rûna**, **Hen**, **Janneke**, **Frenk**, **Rosa**, **Liz**, **Romy**, **Martha**, **Renato**, **Remco**, **Bas**, **Joris**, **Wout**, **Mariette**. Thanks to **Marlow** for the fun during our fieldwork in New Caledonia. Thank you, **Frida**, for involving me in your project and giving me the opportunity to learn something about paleoceanography.

Supervising students has also enriched my PhD experience, and for that, thanks to **Merel**, **Daan**, **Raf**, and **Harini**. Special thanks to **Bas Zanderink**. I am very happy that after two years, we were able to replace our canceled fieldwork in the Philippines with our fieldwork in Guam. Thank you very much for your hard work and your fantastic sense of humor.

Buiten alle hulp en gezelligheid van collega's heb ik ook veel gehad aan mijn vriendschappen. Als eerste veel dank aan **Awesome**. Het is heel fijn om vrienden te hebben die tenminste nog enigszins snappen wat je aan het doen bent. **Maarten**, bedankt dat we samen zo hard kunnen lachen en bedankt voor onze gezamenlijke interesse in bepaalde praatjes. **Jorieke**, dankjewel voor je oprechte interesse en je eerlijkheid, en een twijfelachtige dankjewel voor de baco's bij voetbal. **Noortje**, bedankt voor het zijn van de beste veldwerkpartner en dat je mij inspireert om te genieten van de kleine dingen.

Lieve **Anne, Camille, Carlijn, Dorien, Esther, Hester, Manouk, Nicky, Saskia** en **Lisanne**. Ondanks dat jullie allemaal totaal ander soort werk doen, zijn jullie wel altijd super betrokken en geïnteresseerd in wat ik doe. Bedankt voor jullie support, maar bovenal bedankt voor de fijne vriendschap die ik met jullie heb. De wintersporten en huttentochten, maar ook de borrels, diners en vooral de goede gesprekken met jullie waren heerlijke momenten om even te ontsnappen aan het proefschrift.

Ook veel dank aan Odysseus bestuur XXV: **Karina, Joost, Michael, Paul, Roos, Rudie** en **Stef**. Bedankt voor het verrijken van mijn studentenleven en het overnemen van mijn taken toen ik op veldwerk in Nieuw-Zeeland was, waar de basis voor dit proefschrift is gelegd. Dankjewel **Femke, Miriam, Nadia, Nina, Zorana** en **Senne** dat we al twintig jaar vrienden zijn.

Heel veel dank aan mijn grootste supporter **Leonie**. Bedankt dat je er al zolang voor me bent, dat ik zo goed kan voelen hoe trots je op me bent, en dat ik zo goed met je kan praten.

Lieve **papa** en **mama**, ik kan niet in woorden uitdrukken hoe dankbaar ik ben met jullie als mijn ouders. Dankjewel dat ik met alles bij jullie terecht kan, dat jullie mij altijd steunen en dat jullie altijd in mij geloven. Papa, heel erg bedankt dat jij mijn hele proefschrift hebt doorgelezen op zoek naar spel- en typfouten, en dat ik dankzij jou mijn proefschrift precies op tijd kon inleveren. Mama, heel erg bedankt voor de keren dat jij mij wist over te halen om hulp te vragen wanneer ik dat moeilijk vond.

Lieve **Bastiaan, Charlotte** en **Rutger**, wat ben ik rijk met mijn drie geweldige brussen. Dankjewel Bastiaan dat je mij inspireert om het beste uit mezelf te halen, zowel op werk als op persoonlijk vlak. Dankjewel Charlotte dat je de beste zus bent die er bestaat en dat het zó vanzelfsprekend is tussen ons. Dankjewel Rutger dat je mij leert om het leven niet altijd serieus te nemen. Ik ben ook erg dankbaar voor de Lagematenverrijking: **Gitte, Emiliano** en **Paloma**. Jullie verrijken het leven van mijn brussen, maar ook zeker dat van mij. Daarnaast ben ik oneindig dankbaar voor de kleine **Mateo**, bij wie ik gewoon even op bezoek moest gaan als de stress in het laatste jaar me te veel werd.

Lieve **Hanneke, Henk, Mark** en **Arlaine**. Ik mag van geluk spreken dat ik zo'n lieve schoonfamilie heb. Heel veel dank voor alle leuke vakanties, voor de gezellige etentjes, de wandelingen en voor jullie interesse in mijn werk.

Liefste **Merijn**. Wat een geluk dat wij elkaar leerden kennen in Aliaga. Wat een geluk dat jij al zo lang in mijn leven bent en dat ik al zo lang op je kan bouwen. Dankjewel voor je liefde, voor je support, voor je oneindige geduld, voor je zorgzaamheid. Jij weet vaak beter wat ik nodig heb dan ik zelf. Bedankt voor alle dingen die we al samen beleefd hebben. Bedankt dat je me altijd uitdaagt om mijn grenzen te verleggen. Ik kijk er enorm naar uit om samen nieuwe avonturen aan te gaan. Dankjewel dat ik met jou het leven mag vieren.



Curriculum Vitae

14 January 1991	Born in Utrecht, The Netherlands
2003 - 2009	Secondary school Christelijk Gymnasium Utrecht
2009 - 2010	Exchange year (<i>Liberal arts and sciences</i>) The College of Wooster, USA
2010 - 2014	BSc Earth Sciences Utrecht University, The Netherlands
2014 - 2017	MSc Earth Structure and Dynamics (<i>cum laude</i>) Utrecht University, The Netherlands
2018	Research Officer University of Waikato, New Zealand
2019 - 2023	PhD Candidate Utrecht University, The Netherlands



Bibliography

Included in this thesis (Chapters 1 – 6 and Appendices 1 and 2):

1. **Van de Lagemaat, S.H.A.**, Van Hinsbergen, D.J.J., Boschman, L.M., Kamp, P.J.J. & Spakman, W. (2018). Southwest Pacific absolute plate kinematic reconstruction reveals major mid- to Late Cenozoic Tonga-Kermadec slab dragging, *Tectonics* 37(8), 2647-2674.
2. **Van de Lagemaat, S.H.A.**, Swart, M.L.A., Vaes, B., Kusters, M.E., Boschman, L.M., Burton-Johnson, A., Bijl, P.K., Spakman, W. & Van Hinsbergen, D.J.J. (2021). Subduction initiation in the Scotia Sea region and opening of the Drake Passage: when and why?, *Earth-Science Reviews* 215, 103551.
3. **Van de Lagemaat, S.H.A.**, Kamp, P.J.J., Boschman, L.M. & Van Hinsbergen, D.J.J. (2023). Reconciling the Cretaceous breakup and demise of the Phoenix Plate with East Gondwana orogenesis in New Zealand, *Earth-Science Reviews* 236, 104276.
4. **Van de Lagemaat, S.H.A.**, Cao, L., Asis, J., Advokaat, E.L., Mason, P.R.D., Dekkers, M.J. & Van Hinsbergen, D.J.J. (submitted). Causes of Cretaceous subduction termination below South China and Borneo: Was the Proto-South China Sea underlain by an oceanic plateau? *Geoscience Frontiers*.
5. **Van de Lagemaat, S.H.A.**, Pastor-Galán, D., Zanderink, B.B.G., Villareal, M.J.Z., Jenson, J.W., Dekkers, M.J. & Van Hinsbergen, D.J.J. (2023). A critical reappraisal of paleomagnetic evidence for Philippine Sea Plate Rotation. *Tectonophysics* 863, 230010.
6. **Van de Lagemaat, S.H.A.** & Van Hinsbergen, D.J.J. (submitted). Plate tectonic cross-roads: Reconstructing the Panthalassa-Neotethys Junction Region from Philippine Sea Plate and Australasian oceans and orogens. *Gondwana Research*.
7. **Van de Lagemaat, S.H.A.**, Boschman, L.M., Kamp, P.J.J., Langereis, C.R. & Van Hinsbergen, D.J.J. (2018). Vertical axis rotation and tilting after remagnetisation of the Murihiku Terrane (North Island, New Zealand), *New Zealand Journal of Geology and Geophysics* 61(1), 9-25.
8. **Van de Lagemaat, S.H.A.**, Mering, J.A. & Kamp, P.J.J. (2022). Geochemistry of syntectonic carbonate veins within Late Cretaceous turbidites, Hikurangi margin (New Zealand): Implications for a mid-Oligocene age of subduction initiation, *Geochemistry, Geophysics, Geosystems* 23(5), e2021GC010125.

Not included in this thesis:

9. Boschman, L.M., Van Hinsbergen, D.J.J., Langereis, C.G., Flores, K.E., Kamp, P.J.J., Kimbrough, D.L., Ueda, H., **Van de Lagemaat, S.H.A.**, Van der Wiel, E. & Spakman, W. (2021). Reconstructing lost plates of the Panthalassa Ocean through paleomagnetic data from circum-Pacific accretionary orogens, *American Journal of Science* 321(6), 907-954.
10. Vaes, B., Van Hinsbergen, D.J.J., **Van de Lagemaat, S.H.A.**, Van der Wiel, E., Lom, N., Advokaat, E.L., Boschman, L.M., Gallo, L.C., Greve, A., Guilmette, C., Li, S., Lippert, P.C., Montheil, L., Qayyum, A. & Langereis, C.G. (2023). A global apparent polar wander path since 320 Ma calculated from site-level paleomagnetic data, *Earth-Science Reviews* 244, 104547.
11. Hoem, F.S., López-Quirós A., **Van de Lagemaat, S.H.A.**, Etourneau, J., Sicre, M.-A., Escutia, C., Brinkhuis, H., Peterse, F., Sangiorgi, F. & Bijl, P.K. (2023). Late Cenozoic Temperature evolution of the South Atlantic Ocean, *Climate of the Past* 19(9).
12. Hoem, F.S., Van den Broek, K., López-Quirós A., **Van de Lagemaat, S.H.A.**, Bohaty, S.M., Hillenbrand, C.-H., Larter, R., Van Peer, T.E., Brinkhuis, H., Sangiorgi, F., Bijl, P.K. (submitted). Stepwise Oligocene-Miocene breakdown of sub-polar gyres and strengthening of the Antarctic Circumpolar Current. *Journal of Micropaleontology*.
13. Andjić, G., Vaes, B., **Van de Lagemaat, S.H.A.**, Boschman, L., Dekkers, M.A., Johnston, S.T. & Van Hinsbergen, D.J.J. (submitted). Mesozoic drift of the Wrangellia superterrane revisited: the way forward from paleomagnetic data, *Tectonics*.

